Functional Characterization of Histone Deacetylase 2 and Histone Deacetylase 3 in *Candida albicans*

A thesis submitted to the University of Kent for the degree of

Doctor of Philosophy

in the School of Biosciences

April 9, 2019

Misty R. Peterson

Word Count: 74,425/ Pages: 226

Abstract

C. albicans is an opportunistic fungal pathogen which causes infections in humans and contributes significantly to world mortality rates. The phenotypic plasticity of this yeast supports its virulence and different morphologies are triggered by specific environmental cues including temperature, nutritional deprivation and pH. Development of hyphae facilitates the translocation of cells through human tissue and white or opaque forms of this yeast have the tendency to form hypha and mate, respectively. Switching between forms is regulated in many ways for example by transcription factors and hypotheses suggest that these may occur though changes to the packaging of DNA. This would be facilitated by modification of the histone proteins that contribute to the condensation of DNA into various chromatin states. It has been shown that deletion of the histone deacetylase *HDA1* of *C. albicans* stunts the yeast to hyphae transition and increases white to opaque switching. In the common model yeast, *S. cerevisiae*, Hda1 forms a complex with 'Histone deacetylase' proteins Hda2 and Hda3. Whether this complex forms in *C. albicans* is unknown.

This thesis evaluates *C. albicans* Hda1, Hda2 and Hda3 proteins through their expression and separately by *in vivo* functional analyses. The results offer a plan for soluble expression of full length Hda1 protein as well as a construct for soluble expression of its Arb2 domain. Expression of full length Hda2 and Hda3 yielded insoluble protein. *In vivo* co-immunoprecipitation experiments unveil an interaction between Hda1 and Hda2 as well as Hda1 and Hda3. Homozygous mutants in these proteins have common and unique phenotypes which are hypothesized to be environmentally dependent. Specifically, the *hda2*ΔΔ and *hda3*ΔΔ homozygous mutants are sensitive to respiratory stressors sodium nitroprusside (SNP) and salicylhydroxamic acid (SHAM), copper and oxidative stress by NaCl but resistant to rapamycin. The *hda2*ΔΔ mutant is resistant to caspofungin and fluconazole while *hda3*ΔΔ is sensitive to zinc. Phenotypes for rapamycin and fluconazole are diminished or not evident in hyphae inducing media (RPMI). Whole protein extractions show decreased expression of Hda1 and likely Hda3 in hyphae induction conditions. This suggests that changes in protein abundance and environmental conditions lead to different roles, and potentially arrangements, of these proteins in complex. RNAseq results support the observed phenotypes as well as the hypothesis that these proteins form a complex. In summary, this thesis includes evidence of several functional roles for *C. albicans* Hda2 and Hda3 proteins including in white-opaque and yeast-hypha morphological switching and gives proof of their interaction with Hda1.

Acknowledgements

I would like to thank Dr. Alessia Buscaino for the introduction to *C. albicans* research, her supervision and guidance throughout this project. Also, Dr. R. Jordan Price for assisting with portions of the RNAseq analysis and all the members of the Buscaino lab for their support and contributions. Thanks to Dr. Campbell Gourlay for his role on the thesis supervisory team and willingness to provide input during the final stages of this thesis. To Tobias von der Haar for attending supervisory meetings and advice on experiments. Thanks to my scientist friends at Kent Fungal Group and external labs (as noted in this text) for helping with strains, plasmids, protocols and advice. Great appreciation to the University of Kent for providing a 50-year Anniversary scholarship and assistance with the tuition of my PhD studies.

I would like to show appreciation for the supervision of Dr. Abhimanyu K. Singh and to Dr. Susanne Schroeder (Brown Lab, University of Kent, Canterbury), for training in protein biochemistry and crystallization. My appreciation to Microscope Facilities and Ian Brown for advice toward developing a strategy for biofilm imaging and for microscope training. Thanks to Biosciences Facilities and Kevin Howland for supervising the protein identification of by mass spectrometry. Thanks to the larger network of department members in Stacey building, Argenta/Charles River Laboratory and the School of Biosciences for support.

I would like to express my gratitude to earlier supervisors that prepared me for this PhD project. To Professor Rohinton Kamakaka (University of California Santa Cruz) for supporting my learning, assisting with revisions and encouraging me to pursue a role in science. To Professor Shannon Bros Seeman (San Jose State University) for teaching that *viva voce* examinations are a celebration of learning. To Dr. Paul Wolber (Agilent, San Jose) and Dr. Joshua Mackie (San Jose State University) for the training on Next Generation Sequencing analysis. To Dr. Angelos Evangelou for encouragement and extensive help with editing. To the Roussopoulos family for their support of my early postgraduate studies. Finally, to my friends, family and Mom for supporting my academic exploration.

Table of Contents

Table of Figures

List of Abbreviations

aa	amino acids
ALS	Agglutinin-Like Sequence
Amp	Ampicillin
APS	Ammonium Persulfate
Arb	Argonaute binding (protein)
ATP	Adenosine Triphosphate
BirA- (Avi tag)	B-mercaptoethanol
BME	2-Mercaptoethanol
BSI	BloodStream Infection
CAI	Codon Adaptation Index
cAMP	cyclic adenosine monophosphate
CCD	Coiled Coil Domain
cDNA	complementary DNA
ChIP	Chromatin Immunoprecipitation
CoIP	Co-Immunoprecipitation
Clox	Cre-lox
Cm	Chloramphenicol
CV	Column Volume
Da	Daltons
DAC	Deacetylase (Domain)
DBD	DNA Binding Domain
DNA	deoxyribonucleic acid
DTT	1,4-dithiothreitol
DMEM	Dulbecco's Modified Eagle Media
DSF	Differential scanning fluorimetry
EDTA	Ethylenediaminetetraacetic acid
FPLC	Fast protein liquid chromatography
EtBr	Ethidium Bromide
FCS/FBS	Fetal calf/bovine serum
FDR	False Discovery Rate
g	grams
xg	units of times gravity
GFP	Green Fluorescent Protein
GSEA	Gene Set Enrichment Analysis
GST	Glutathione S-transferase
H	Histone
HA	Human influenza hemagglutinin
HU	Hydroxyurea/Hydroxycarbamide
HAT	Histone Acetyltransferase
HDAC	Histone Deacetylase
IEC	Ion Exchange Column
IPTG	Isopropyl β-D-1-thiogalactopyranoside
L	liters
LIP	Lipase

K	Lysine
M	Molar
MALDI-TOF	Matrix Assisted Laser Desorption Ionization-Time of Flight
APK	mitogen-activated protein kinase
MAT/MTL	Mating Type Locus
mM	milli Molar
MeOH	Methanol
MES	2-(N-morpholino) ethane sulfonic acid
MIC	Minimum Inhibitory Concentration
ml	milliliter
MQ	MilliQ Water
MRS	Major Repeat Sequence
MW	Molecular Weight
Nat	Nourseothricin
NES	Normalized Enrichment Score
Ni-NTA	Nickel-nitrolotriacetic acid
Orf	Open reading frame
PAGE	Polyacrylamide gel
PBS	Phosphate-buffered saline
PCA	Principle Component Analysis
PCR	Polymerase Chain Reaction
PDB	Protein Data Dank
PKA	Protein Kinase A
PTM	Post Translational Modification
PVDF	polyvinylidene difluoride
qRT	quantitative Reverse Transcriptase
RNAseq	RNA sequencing
RPMI	Roswell Park Memorial Institute (Media)
SAP	Secretion of aspartic proteases
SAT	streptothricin acetyltransferase
SDS	Sodium dodecyl sulfate/sodium lauryl sulfate
SEC	Size Exclusion Column
SHAM	Salicylhydroxamic acid
SNP	Sodium nitroprusside
TBST	Tris-buffered saline (with 0.1 %) Tween 20 (Polysorbate 20)
TEV	Tobacco Etch Virus
TET (pTET)	Tetracycline
U	Units (of restriction enzyme)
YPD	Yeast Extract Peptone Dextrose
V	volts
v/v	volume per volume
w/v	weight per volume

CHAPTER 1. Introduction

1.1 Human fungal pathogens

Fungal colonization of human tissue is a natural course for many species in the fungal kingdom that pursue survival through a saprophytic approach. Given that there are likely 2.2-3.8 million species of fungi on this planet with only 3-8% currently named, it is certain that the field of recognition for these type of human pathogens will continue to grow with time (Hawksworth & Lucking 2017). Currently over three hundred types of pathogenic fungi are known (Taylor et al. 2001). The field of medical mycology recognizes the impact of conditions with varying levels of severity that develop in humans due to pathogenic fungi (Gow & Netea 2016). In addition to skin and mucosal membrane disorders, these pathogens can cause lung disease and damage major organs. These infections are found to be concomitant with a range of diseases including cancer, AIDS, rheumatoid arthritis, cystic fibrosis and other conditions (Denning 2015).

Fungal infections lead to over 1.5 million deaths and more than a billion infections in the world each year. Contributing to this, many countries have limited access for fungal diagnostic technology and medications for treating these conditions (Denning 2015; Bongomin et al. 2017; Gow & Netea 2016). Currently world mortality rates for fungal infections are high, but it is difficult to account for since due to the concomitant nature of these conditions death is often attributed to other factors. This is compounded by the fact that fungal infections are commonly not detectable by blood sample (Lamoth et al. 2018). For a fungus to be able to infect humans it must be introduced to the host, endure the increased temperature of the body, be able to engage move through tissue and evade the immune system, consequently, these infections are more efficient in immune compromised individuals. Still, several hundreds of pathogenic fungal species have been shown to take humans as their hosts (Kohler et al. 2014).

While there are hundreds of pathogenic species, a portion of these commonly infect humans (*Candida*, *Aspergillus*, *Cryptococcus* and others) (Underhill & Pearlman 2015). Many pathogenic fungi which infect humans occur more commonly in certain locations in the world, their prevalence varies by country and climate (Bongomin et al. 2017). Pathogens are found on certain plants, in soil, in air and commonly on both the outside and inside of the human body. For example, *Blastomyces* is a soil dwelling fungus which when inhaled can cause respiratory distress and failure and the condition is called Blastomycosis. It occurs mostly in North America, Canada and South Africa (Lemos et

al. 2001; Kohler et al. 2014; Saccente & Woods 2010). Fungi exist in environmental situations that allow their survival needs to be met. Likewise, when they act as pathogens in the human body these fungi are often found in distinct locations particularly in early stages of disease, such as mucosal membranes and on the skin. Infections can be localized to their entry point as in the case of ringworm or athlete's foot (Centers for Disease Control and Prevention 2018). More serious infections spread throughout the system by moving via the blood stream. The blood stream infection, Candidemia caused by *Candida* species, has been shown to contribute crude mortality rates of 62 % in sampled hospital populations (n = 108) and it is known that faster treatment improves this outcome (i.e. treatment started less than 12 hours from diagnosis) (Garey et al. 2006; Gudlaugsson et al. 2003). In general, there is an over 50 % mortality rate for individuals with invasive fungal infections (Brown et al. 2012).

The symptoms and severity of these infections are wide ranging. Fungal pathogens use a variety of effective physiological strategies to find the way into various niches of the human body and this makes it very difficult to combat later stage infections.

1.1.1 Primary and opportunistic fungal pathogens

There are hundreds of known fungal pathogens, and many are dangerous to humans. Common fungal pathogens are mostly opportunistic while others can infect despite a healthy immune state (van Burik & Magee 2001; Kohler et al. 2014). The National Institute of Health's book of Medical Microbiology cites three classes of primary fungal pathogens and close to ten opportunistic types but more continue to be identified (Walsh & Dixon 1996; Jones et al. 2008). Opportunistic fungal infections arise from fungi that live normally in a non-invasive state within the host and become invasive due to a change in the host-environment or immune system. Primary fungal pathogens can attack a healthy human system whereas opportunistic pathogens flourish in an immune compromised state.

Mortality rates due to primary fungal infections which effect immunocompetent individuals vary more widely: Blastomycosis : (Midwest and Atlantic US: 2-68 %), Coccidiomomycosis (Southwestern US: 1-70 %), Histoplasmosis (Midwestern US: 28-50 %), Paracoccidioidomycosis (Brazil: 5-27 %), and Talaromycosis (Southeast Asia: 2-75 %) (Brown et al. 2012; Revankar 2017; Walsh & Dixon 1996; Centers for Disease Control and Prevention 2017).

Perhaps the most well-known primary fungal pathogens are *Cryptococci* (*C. gattii*), though species of the pathogens are found to be opportunistic (*C. neoformans*) (Won et al. 2006; Kohler et al. 2014).

Opportunistic pathogens are normally benign and infect only upon immune system compromise, examples include: (1) *Candida* which causes thrush and other infections (Singh et al. 2014); and (2) *Aspergillus* which causes infection that takes the form of allergic response, sinusitis or pneumonia this may complicate asthma which can lead to more acute infection (Natarajan & Subramanian 2014; Kohler et al. 2014). Infections by other opportunistic fungi such as *non-Fumigatus aspergilli*, *Fusarium* and *Pseudoallescheria*, and uncommon molds which are often lethal due to drug resistance (Torres et al. 2003; Nucci & Anaissie 2007; Quan & Spellberg 2010; Kohler et al. 2014).

Estimates based on infected populations worldwide show mortality rates for common opportunistic fungi to be very high in populations infected with the diseases: Aspergillosis (30-95 %), Candidiasis (46-75 %), Cryptococcosis (20-70 %), Mucormycosis (30-90 %) and Pneumocystis (30-80 %). Invasive fungal infections are much less common than superficial infections and yet still these fungal pathogens are implicated in 10,000-1,000,000 life threatening infections per year worldwide (Bongomin et al. 2017).

1.1.2 The impact of *C. albicans* species in human fungal infections

While other types of yeast contribute to human fungal infections, *C. albicans* is documented as the most prevalently observed culprit (J. Guinea 2014). In a population-based survey of three California based counties during the years of 1992-1993 (Alameda, Contra Costa and San Francisco: population 2.94 million), the most common cause among the ~1,600 cases of the invasive fungal infections per year was *Candida* species 50.9 % of the isolates obtained were *Candida albicans* (henceforth: *C. albicans*) and 33.9 % of first time infections turned out to be fatal (Rees et al. 1998). Many of these invasive *Candida* infections were found to be concomitant with other conditions that contribute to an immunocompromised host state including cancerous malignancies (18.2 %; n = 78), HIV (15.3 %; n = 61), diabetes (13.6 %; n = 58) and lung disease (13.6 %; n = 56). Likewise, recent surgery on the abdomen or heart was also found to be a contributing factor (17.9 %; n = 284; abdominal or cardiac surgeries).

C. albicans is by far the most prevalent type of *Candida* found to cause infections worldwide although these rates are decreasing. This may be accounted for by use of drugs

that target these species while allowing others to flourish or gain immunity (J. Guinea 2014). In a survey with samples from 127 medical centers in 39 countries between 1997-2007 called the ARTEMIS Disk Global Antifungal Surveillance study program, yearly collections of clinical isolates tested were 61-73 % *C. albicans* (~12-33,000 cases reported each year) (Pfaller & Diekema 2007; J Guinea 2014). The *C. albicans* species is a common culprit of mucosal disease where other fungi are blamed for more respiratory oriented effects (Bongomin et al. 2017).

While *C. albicans* often survives in a commensal state keeping balance with other bacteria and fungi in the human flora, infections do occur and often result in lengthy hospital stays with significant costs for care. A decade long census carried out in the United States showed that ~5% of a population of 100,000 people are hospitalized annually for invasive candidiasis (survey of 33 US states; Strollo et al. 2016). These numbers do not account for the chronic recurring nature of these conditions; for example, Candidemia (Pfaller & Diekema 2010). As an opportunistic fungal pathogen, *C. albicans* is very successful in the human host system.

1.2 The pathogen *C. albicans*

C. albicans is found in many people with normal immune function without creating any harm. In fact, a recent study found *C. albicans* to be the most common yeast species in the intestinal microbiota and it was found in specimens from ~40 % of 111 healthy individuals tested (Strati et al. 2016). *C. albicans* is also normally found on human skin, mucosal membranes and in the genitourinary tract. It has the potential to infect mucosal cavities, nails, and deeper systems of the body like the blood stream and organs (Nobile & Johnson 2015). These infections are problematic for certain individuals, disproportionately affecting infants and the elderly (Pfaller & Diekema 2007). Likewise, those suffering from chronic viral conditions and cancer, or individuals with otherwise compromised immune response have higher vulnerability and conditions impacting white blood cell levels are a predisposing factor for these infections (Wisplinghoff et al. 2004).

In a large multi-center study: Surveillance and Control of Pathogens of Epidemiological Importance (SCOPE), approximately 24,000 cases of BloodStream Infections (BSI) were monitored at sites across the United States from 1995-2002. Among these cases, *C. albicans* was found to account for 54 % of infections but the species

brought the lowest mortality rate (which was still 37 %). Of these infections, 15 % were pediatric.

In a more detailed evaluation of data embedded in the SCOPE study, a group of 2000 BSI within one university medical center from 1998-2002 was examined. It was found that 197 of the infections were caused by *Candida* species and 63 % of these by *C. albicans*. In survivors of these *C. albicans* infections, the inflammatory response lasted approximately 9 days before their systems returned to normal. Among the cases reviewed, there was an overall mortality for *C. albicans* BSI of 42 % with 27 % of patients experiencing septic shock and 35 % displaying end organ disfunction. Approximately half of these patients received drug treatment within 24 hours and about a quarter of the *Candida* samples surveyed were resistant to fluconazole (10 % of the *C. albicans* isolates were resistant) (Wisplinghoff et al. 2006).

Cuts or breaks in the skin or mucosal membranes can contribute to development of *Candida* infections (Pfaller & Diekema 2007) while BSI are often acquired in hospital settings. Invasive candidiasis is a yeast infection of the bloodstream, tissues and organs. The capacity to adapt to different environmental conditions facilitates quick and insidious penetrance by *Candida* which uses morphological changes as a strategy to disperse widely in a host before embedding deeply into tissue and organ systems. Phenotypes that allow for the virulence of *C. albicans* infection include: the development of hyphae which allows the yeast to pierce through some types of tissue and the formation of biofilm with structuring that resists disruption by antifungals. The structural strength and embedded penetrance of this pathogen during infection make treatment difficult (Yang et al. 2014; Dalle et al. 2010; Taff et al. 2013).

To study this, models for mucosal infection have been constructed with organ cell cultures that mimic human tonsil and cervical tissues; the different surfaces of these organs are of contrasting makeup. Tonsil surfaces are dynamic, they contribute a surface with many layers of cells that are constantly replaced and proliferating while invaginations of the tonsils offer crypts lined with a single cell layer. Likewise, cervical cells are lined with a single cell layer that is distinct in its secretion of mucous, which forms a protective physical barrier that is continuously changing with hormonal signals. Very different efficiencies and dynamics of colonization by *C. albicans* are observed in these models. For example, colonization is much easier in the more external layers of the tonsil surface but given that these cells have a short life cycle invasion is less likely to occur. Also,

colonization is more successful in external layers of cervical cells when they are cut, damaged or slightly disturbed (Southern et al. 2008).

In humans that are immune compromised, fungal infections have an advantage. For example, often the first symptoms of HIV infections are opportunistic infections like oral candidiasis and it is even used as an indicator to screen for the virus (Damery et al. 2013; de Repentigny et al. 2004). It is notable that populations of particularly adhesive yeast strains are observed with infections of HIV positive hosts and the virus itself contributes proteins which help the yeast escape from phagocytosis by macrophages (Torre et al. 1999). In general, factors that bring susceptibility include decreased digestive secretions, nutrient deficiencies, liver disease, the demographics of the gut microbial community and use of medications. Symptoms do not always include an obvious display of colonization; they can vary and present like those typical of other flus or infections. Diagnosis can be made by stool, blood or biochemical analysis (as reviewed by Martins et al. 2014).

1.2.1 Interactions of *C. albicans* with its host

Immune responses to *C. albicans* do occur yet still the organism manages to establish infections in a variety of niches in the human body (see Section 1.2). In the face of antibodies, antimicrobial peptides, phagocytes, neutrophils, macrophages and many other immune defenses, the yeast must quickly adjust its physiology to survive by responding to the challenging situations mounted by the host immune response (see Fig. 1.1).

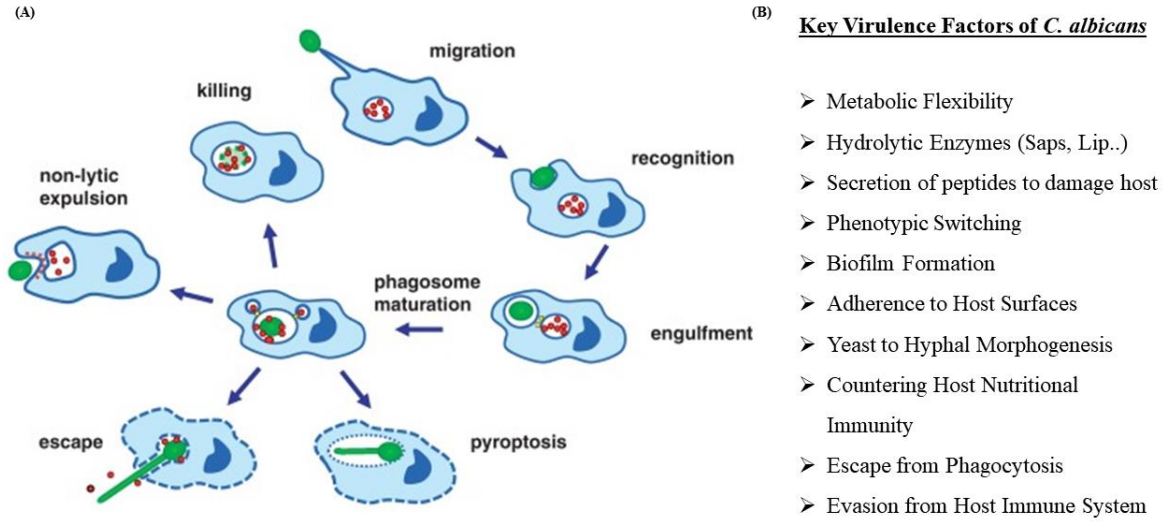

Figure 1.1 Aspects of interaction between *C. albicans* and a host immune agent
Interactions and virulence of *C. albicans*: (A) Stages of interactions between *C. albicans* and macrophages (B) List of *C. albicans* key virulence factors; [Adapted from Figures 1 and 2 of da Silva Dantas et al. 2016]

There are many strategies used by *C. albicans* to resist the host immune system. These include white-opaque switching, yeast-hyphae transition, adaptation to metal, biofilm formation, chromosome remodeling and gene silencing. Additional strategies to survive in the host immune system include: (1) Secretion of Aspartic Proteases (Sap) to cleave host 'complement' immune response proteins and to degrade system response components (Gropp et al. 2009); (2) use of alternative carbon source pathways (gluconeogenesis and glyoxylate cycle) to adapt to different nutrient conditions (Lorenz et al. 2004); (3) Release of ammonia from amino acid degradation to alkalize the nearby area and adapt to changes in pH (Vylkova & Lorenz 2014); (4) use of heat shock proteins (automatic negative regulatory loop involving Heat Shock transcription Factor (Hsf1) and Heat Shock Protein 90 (Hsp90)) to keep high temperatures from causing protein unfolding (Leach 2012). *C. albicans* uses these and other techniques to respond to the many physical and chemical barriers put up by the human host (Dühring et al. 2015).

For example, macrophages (a first line immune defense) recognize *C. albicans* hyphae and can kill the yeast cells by phagocytosis and other toxic defenses that include secretion of: antimicrobials, degrading enzymes and oxidative compounds (van de Veerdonk et al. 2015; Krysan et al. 2014; da Silva Dantas et al. 2016; Dühring et al. 2015). The *C. albicans* cell can in turn kill the macrophage through a programmed lytic

inflammatory cell death pathway, which may require filamentation (Noble et al. 2010; Tyc et al. 2016).

1.2.2 Molecular mechanisms of *C. albicans* pathogenicity

The pathogenicity of *C. albicans* is facilitated through several known mechanisms including interaction with host cells through adhesion, invasion and biofilm formation (Mayer et al. 2013). Specific gene families linked to virulence of this pathogen are LIPases (*LIP*), *SAP*s and Agglutinin Like Sequence (*ALS*) (Anderson et al. 2014; Hube et al. 2000; Hoyer 2001; Magee et al. 1993).

Adhesion describes the interaction and actual adherence of *C. albicans* cells to host cell surfaces; although interactions also happen between yeast cells and inanimate barriers like medical silicone (Thomson et al. 2015; Mayer et al. 2013) Adhesion genes include *ALS* proteins and hypha-associated GPI-linked protein (*HWP1*) and several other proteins which reside at the cell surface and bind to other cells or surfaces that are encountered. Als proteins also have roles in biofilm formation which are discussed in more detail in Section 1.2.3. Adhesin protein Hwp1 functions downstream of negative regulators of the hyphae transition, including: Enhanced Filamentous Growth (Efg1), dTMP-UPtake (Tup1) and Reduced Filamentous Growth 1 (Rfg1) (Sharkey et al. 1999). These proteins are also involved in biofilm formation and while these processes (adhesion, invasion, hyphal development and biofilm formation) are investigated as separate traits in the literature, their interplay is intricately intertwined when this pathogen infects a host system (Liu & Filler 2011; Phan et al. 2007; Almeida et al. 2008; Mayer et al. 2013; Nobile et al. 2008).

Adhesion ability of the yeast cell and the composition of the encountered surface contribute to the navigation of hyphae during invasion (Thomson et al. 2015). Invasion is the ability of *C. albicans* to pierce through cell membranes which allows the pathogen to move through obstacles including host tissue (Thomson et al. 2015). Invasion by *C. albicans* occurs differently in different tissue types. For example, invasion of oral tissues can occur both through endocytosis by host cells and active penetration while only the latter is utilized for invasion of intestinal tissues (Dalle et al. 2010). Surface invasion by this fungi is facilitated by Als3, Heat Shock Protein 70 (HSP70) and Stress-seventy subfamily Ssa1 (both also function as an adhesins) (Sun et al. 2010; Phan et al. 2007; Mayer et al. 2013).

Finally, several traits related to fitness contribute to virulence, including: adaptions to a variety of stressors by heat shock proteins, regulation of pH levels by excretion of ammonia and sequestering of nutrients including: carbon, nitrogen, iron, zinc, copper and manganese (Mayer et al. 2013).

1.2.3 Biofilm formation

Donlan et al., 2002 contributes the "new definition of a biofilm" as: "a microbially derived sessile community characterized by cells that are irreversibly attached to a substratum or interface or to each other, are embedded in a matrix of extracellular polymeric substances that they have produced and exhibit an altered phenotype with respect to growth rate and gene transcription." It is proposed that this is the most 'natural' growth state for microorganisms (Nobile & Johnson 2015).

Biofilms allow *C. albicans* to form multidimensional architecture which provides an insulated environment within which the yeast can thrive. *C. albicans* biofilms are made up of densely packed yeast and hyphae cells. The biofilm matrix is made of a variety of components, including proteins (enzymes), glycoproteins (polysaccharides), carbohydrates, lipids and nucleic acids. The expression of hundreds of genes change when *C. albicans* cells are growing in a biofilm rather than in a free culture (Nobile & Johnson 2015; Finkel & Mitchell 2011; Fox & Nobile 2012; Nobile et al. 2012; García-Sánchez et al. 2004).

The formation of biofilm allows for cohabitation of different species, a factor that can increase the mortality of hosts. For example, a study of infections of mice with *C. albicans* and the pathogenic bacteria *Staphylococcus aureus* showed a synergistic effect when both infectious agents were introduced at low levels for which they were individually not lethal and biofilm-like features were observed in the animals small intestines (Carlson 1982; Desai et al. 2014). While research on species interface within *C. albicans* biofilms often focuses on *Staphylococcus* species, other fungi and bacteria are also found in these environments. Both gram negative and gram positive bacteria are found in biofilms with *C. albicans* and the architectures of the biofilms can vary tremendously due to of the type of cohabiting bacteria and the ratios of the two organism types (Soll & Daniels 2016; Nett et al. 2010; McAlester et al. 2008). *C. albicans* is also found to interact in biofilms with other types of *Candida* including *C. glabrata, C. rugosa* and *C. dubliniensis* (Alves et al. 2014; Martins et al. 2016; Kirkpatrick et al. 2000; Al-Fattani & Douglas 2006).

While biofilms are found on surfaces of the human body, they are also very inclined to develop on implanted devices such as central venous catheters, implanted tubes, on voice prosthetic and joint prosthetic devices (Andes et al. 2004; Ramage et al. 2006; Donlan & Costerton 2002; Kojic & Darouiche 2004). They also occur and are difficult to dislodge on more common everyday items like contact lens and dentures (LA et al. 1991; Daniluk et al. 2006; Nett et al. 2010).

Biofilm development requires a combined effort between several morphological aspects of *C. albicans* cells as they function to adhere to a surface and layer upon each other creating the microenvironments of a mature biofilm. The stages of biofilm development are: adherence, initiation, maturation and dispersion (Richard et al. 2005; Uppuluri et al. 2010; Fox & Nobile 2012). Once the yeast cells adhere, the cells divide to become further established creating a first layer (initiation) of cells which is added upon as the biofilm matures to a more complex form featuring layers and matrix (Fig. 1.2) (Lee et al. 2016). Mature biofilms develop until they are bulging with yeast, hyphae and extracellular matrix to the point that they eventually start to shed cells which disperse from the biofilm to new locations on the host surface (Gulati & Nobile 2016; Ramage et al. 2004; Uppuluri et al. 2010). Drugs targeted at disrupting biofilms are currently in the discovery stages of development and trialed treatments use azole and echinocandin drugs in combination with *HSP90* inhibitors as a way of disrupting dispersal of biofilms (Hnisz et al. 2012; Nobile & Johnson 2015; Robbins et al. 2011; Cowen et al. 2009).

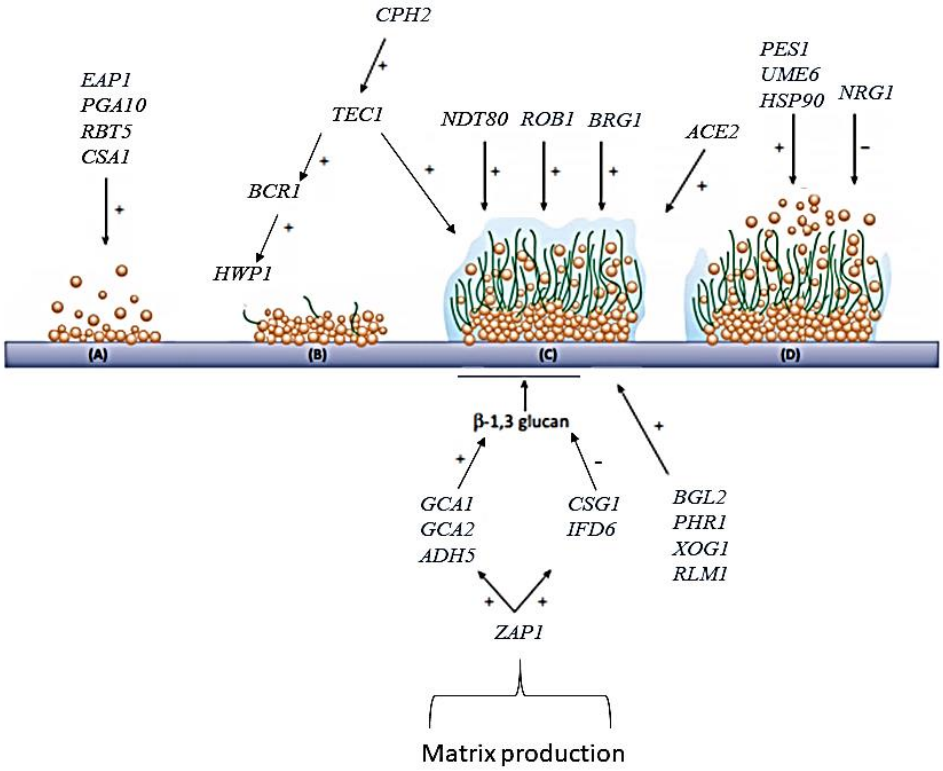

Figure 1.2 Stages of biofilm development and regulatory network genes of *C. albicans*
Left to right: (A) adhesion (B) formation of basal microcolony layers (C) mature biofilm including cells with multiple morphologies and (D) detachment and dispersion; [Adapted from Figure 1 Araujo 2017]

There are at least six major transcriptional regulators which are engaged during biofilm formation: Bcr1, Tec1, Efg1, Non-DiTyrosine 80 (Ndt80), Regulator of Biofilm 1 (Rob1) and Biofilm ReGulator 1(Brg1) and 44 other essential transcriptional regulators are involved. These regulators have roles in adherence, hyphal growth in liquid, extracellular matrix and cell dispersal. Additionally, specific genes related to drug resistance (MultiDrug Resistance 1 (*MDR1*), *Candida* Drug Resistance genes *CDR1* and *CDR2*) are upregulated in the adherence stage of biofilms (Nobile & Johnson 2015). This upregulation may be due to the multi-microbial make-up of biofilms (other *Candida* species, yeasts and bacteria) and to the antagonism of their emitted small molecule defenses. Likewise, cell wall related protein regulation is upregulated (beta-1,3-Glucan Synthase Catalytic subunit 1 (*FKS1*), Beta-GLucanase 2 (*BGL2*), eXO-1,3-beta-Glucanase 1 (*XOG1*), PH Responsive (*PHR1*) and *RLM1*) (Nobile & Johnson 2015).

The genetic and functional properties of biofilms vary with the mating type of the cell population from which they are constructed. For example, the size of molecule that can enter the matrix of biofilms made from mating type a/α *C. albicans* is restricted which

makes them less susceptible to immune agents and antifungals. They are regulated by the Ras1/cAMP pathway rather than the MAPK pathway (mating pheromone related) which differentially lead into Tec1 regulation of biofilm formation (Yi et al. 2011).

1.2.4 The dynamic genome of *C. albicans*

While *C. albicans* generally resides as a diploid organism, haploid cells occur in populations as a result of spontaneous chromosome loss (Hickman et al. 2013; Olaiya & Sogin 1979; Riggsby et al. 1982). The diploid genome has been sequenced and it is made up of eight chromosomes (1-7 and R with rDNA) (Jones et al. 2004; van het Hoog et al. 2007). The telomeres have distinct sub-telomeric repeat sequences. The chromosomes also have a Major Repeat Sequences (MRS) which expand and contract during growth phases and play a role in translocations and chromosome loss. Recombination events including reciprocal translocations, substitutions, single nucleotide polymorphisms, insertions, deletions and changes to ploidy, have been observed (Ene et al. 2018).

1.2.4.1 Chromosome remodeling in *C. albicans*

Chromosome remodeling is a strategy used by pathogens to adapt, evade, repair DNA and survive. The chromatin maintenance proteins that are utilized by *C. albicans* to impact pathogenicity include HATs and HAT complexes, HDACs and HDAC complexes, DNA damage and cell cycle progression proteins and complexes, chromatin remodeling and nucleosome repositioning proteins and complexes in addition to transcriptional activators and repressors (Lopes da Rosa & Kaufman 2012).

1.2.4.2 Gene silencing in *C. albicans*

Silencing is used to create stability in the genome, particularly to package away problematic repetitive elements (Iglesias & Moazed 2017). While silencing has not been studied extensively in *C. albicans* the amount of repetitive DNA in its genome is considerable and falls into three major classes: (1) rDNA locus on chromosome R; (2) Major Repeat Sequences (MRS) which occur at nine sites in the genome; (3) telomeric and subtelomeric repetitive regions including a telomere like region in the middle of Chromosome 1. Silencing in these regions involves the Silent Information Regulator 2 (Sir2) protein and distinct histone modified heterochromatin is allocated into these regions (Freire-Benéitez et al. 2016a; van het Hoog et al. 2007). The heterochromatin state at telomeres is shown to be temperature dependent (Freire-Benéitez et al. 2016). The variability of telomere gene expression is decreased when environmental conditions are

more stable, and this aspect of subtelomeric genes expression is increased with proximity to the telomere (Anderson et al. 2014).

1.2.5 Mating in *C. albicans*

While it was initially difficult to discover mating in *C. albicans*, evidence of the MTL locus was found in 2000 (Hull & Johnson 1999). It is 1.4x larger than the *Saccharomyces cerevisiae* (henceforth: *S. cerevisiae*) MAT locus with three additional open reading frames. Both the *MTLa* and two *MTL*α sequences are present in an individual strain of *C. albicans* and the organization of open reading frames (orfs) (a and α on separate chromosomes) and the ordering of introns in the *MTL* regions are conserved relative to *S. cerevisiae* (Hull & Johnson 1999). Mating was initially observed in two separate laboratories which each used different strategies to manipulate strains. They created a single mating type (either the *MTLa* or *MTL*α) by either direct deletion of one loci or using a specific method of sorbose selection that encouraged loss of one copy of Chromosome 5 where the mating type loci are found (Magee 2000; Hull et al. 2000). Mating was shown based upon prototrophic markers acquired from both parental strains and mating products were tetraploid with one nucleus (Christophe d'. Enfert 2007; Bennett & Johnson 2005).

1.2.6 Translation in *C. albicans*

C. albicans yeast has a special protein synthesis feature in which their genetic code is distinct from most other organisms. In most organisms, CUG codons within the mRNA transcript are met in a ribosome by a tRNA charged by the leucine amino acid $tRNA_{CUG}^{leu}$ and the amino acid leucine is added to construct the nascent chain. In contrast, for *C. albicans* and some other organisms, CUG codons are normally translated as serine and less often leucine. This depends on the amino acid charging of the providing tRNA which is variably paired with these amino acids based upon its own sequence (Suzuki et al. 1997). A number of other closely related yeasts share this translational feature and are grouped in the 'CUG clade' (Skrzypek et al. 2017).

The frequency of the incorporation of serine in CUG clade organisms is around 97 % in normal growth conditions but it is suggested that in cases of environmental stress the coding of leucine becomes more frequent (Simões et al. 2016). Studies that artificially encourage this phenomenon have found that complete replacement of the serine amino acids with leucine can be viable and that as levels of replacement increase, growth rate decreases and phenotypic variability rises (Bezerra et al. 2013). Simoes et al., 2016 suggest that *C. albicans* may even utilize this mechanism for variation at other codon sites

and have engineered strains to incorporate different anticodons in a $tRNA^{Ser}$ to cause abnormal incorporation of the serine amino acids during translation and show that the organism tolerates other scenarios of amino acid misincorporation. These strains show uniquely acquired resistance to certain stress medias ($CuSO_4$, $CaCl_2$, sorbitol, urea and others), pH and temperature. Across generations these strains also show a loss of heterozygosity and increase of single nucleotide polymorphisms (Simões et al. 2016).

It has been shown that codon mistranslation can change the makeup of the *C. albicans* cell surface proteins whose coding genes have a relatively large number of CUG codons and that these changes can impact interaction of *C. albicans* cells with agents of the host immune system (Miranda et al. 2013).

Other translational components are at play in these systems as well. For example, it has been shown that in genes which code for stress responses in yeast, codons that recognize modified tRNAs are more common and in yeast tRNA modifying enzymes are known to be upregulated in certain stress situations (such as oxidation and DNA damage response) (Quax et al. 2015; Begley et al. 2007; Chan et al. 2012).

In *C. albicans*, amino acid differences, such as those caused by CUG codons, can change the makeup of proteins based on environmental stress and this may strategically alter protein folding and function. This could potentially impact signaling cascades and contribute to morphological changes. It is suggested that this strategy for development of novel protein functions may allow for adaptation at the level of the organism (Gomes et al. 2007; Selmecki et al. 2010).

The relative populations of tRNAs is just one factor contributing to the rate of amino acid misincorporation. To look more closely at this, one experiment explored the phenotype of cells in a *C. albicans* strain designed to incorporate an unnatural >50 % of Leu translation. In this strain, distinct morphologies including irregular wrinkled and jagged colonies are observed. Additionally, sequencing analysis showed that more single nucleotide polymorphisms (SNPs) were found in genes with higher numbers of CUG codons. While these strains were quite manipulated (with one or two copies of $tRNA_{CAG}^{ser}$ knocked out), this study served as a tool to understand the effect of CUG clade membership on genomic diversification and pathogenesis (Bezerra et al. 2013; Anderson et al. 2014).

It is notable from an evolutionary standpoint that when compared, the CUG codons of *C. albicans* typically align with serine or other codons of *S. cerevisiae*. Similarly, the

CUG leucine codons of *S. cerevisiae* most commonly align with Leu codons of *C. albicans* (Butler et al. 2009).

1.2.7 Environmental sensing and response in *C. albicans*

Adaptation to extreme environments by surviving with scarce or toxic levels of nutrients is just one of the strategies we discuss in this chapter that facilitate the persistence of *C. albicans* within human hosts. Several sensing pathways allow *C. albicans* to detect nutrients including amino acids, ammonium and nitrogen in their environment (Brega et al. 2004; Biswas et al. 2003; Maidan et al. 2005; Biswas & Morschhäuser 2005; Biswas, Dijck, et al. 2007). Major signal transduction pathways are involved in the morphological changes of *C. albicans* including cAMP-PKA through which inhibition of the cAMP phosphodiesterase induces morphological transitions (Biswas, Dijck, et al. 2007; Rocha et al. 2001). This pathway is regulated by Ras1 and allows for carbon dioxide and adenylate cyclase sensing (Feng et al. 1999). It also monitors an important downstream pathway controlled by Efg1 that controls embedded growth, phenotype switching and cell wall dynamics (Giusani et al. 2002; Srikantha et al. 2000; Sohn et al. 2003). In addition, there are mating related MAPK pathways which act through phosphorylation events and influence morphogenesis and virulence (Köhler & Fink 1996; Monge et al. 2006; Ramírez-Zavala et al. 2013; Diez-Orejas et al. 1997).

1.2.8 Accession of metals by *C. albicans*

The ability of *C. albicans* to tolerate metals is a crucial component in their fitness and ability to adapt to a variety of environments. Host environments may present pathogens with starvation for metals that are essential for their normal function such as iron and copper, or even their overabundance. For example, high copper is found in the acidic anaerobic conditions of the human digestive tract (Weissman et al. 2000). Thus, the ability to endure fluctuating levels of metals is considered a feature of competitive fitness for the pathogens (Li et al. 2015).

To support iron uptake, *C. albicans* produce siderophore proteins Siderophore Iron Transport (Sit1) which bind iron. *C. albicans* can also harvest iron from siderophore proteins of bacteria or haem proteins which can be bound by the Repressed By Tup1 5 (Rbt5) protein (Almeida et al. 2009; Heymann et al. 2002; Weissman & Kornitzer 2004). Other Ferric REductase (Fre) and FErrous Transport, (Fet) family proteins oxidize and solubilize the iron before it is brought into the cell by copper and iron transporters. Many

of these proteins are involved in the processing and adaptation to other metals (including copper) which engage the yeast system (Weissman et al. 2000; Mayer et al. 2013).

It is notable that *C. albicans* is much more resistant to copper than *S. cerevisiae* and this is attributed to the Copper Resistance Determinant 1 (*CRP1*) gene which encodes a unique protein that works as an extrusion pump to move copper out of cells. The metallothionein Cup1 protein binds copper in *C. albicans* and the main transport bringing reduced copper into cells is Copper Transport, Ctr1). Preparation of reduced copper is facilitated by Fre1 (Weissman et al. 2000; Mayer et al. 2013).

Assimilation of zinc by *C. albicans* is done through pathways structured similarly to the iron intake mechanism but the zinc scavenger protein pH Regulated Antigen 1 (Pra1) and zinc transporter Zrt1 are employed (Citiulo et al. 2012; Mayer et al. 2013). Pra1 expression (as well as Zinc Regulated Transporters, Zrt1, Zrt2 and Zrt3) is controlled by Zinc Activation Protein 1 (*ZAP1*/*CSR1*), the main controller of zinc homeostasis. Zap1 has far reaching effects and is also involved in biofilm and hyphae formation (Gerwien et al. 2018; Nobile et al. 2009).

1.2.9 Drug Resistance of C. albicans infections

Treatment of *C. albicans* infection is approached by several types of drugs: polyenes, pyrimidine analogues, allylamines, azoles and echinocandins (Perfect 2017).

Current first line anti-fungal treatment for *C. albicans* infections are azole drugs (Fluconazole, Intraconazole, etc.). Azoles target the enzyme 14-α-sterol demethylase, encoded by the *ERG11* gene, disrupting the synthesis of sterols which are components of the fungal cell wall (Whaley et al. 2016). The effectiveness of treatment by azoles varies with the location and severity of an infection. For example, a model that simulated the extent that fluconazole treatment is fungicidal or fungistatic found that these outcomes vary based upon aspects of the microenvironment including cell density, pH and presence of acetic acid (Moosa et al. 2004). One important deficit of this drug class is that it is relatively ineffective at combating other often concomitant invasive fungi (*Candida glabrata*, *Candida krusei*, *Aspergillus spp.* and molds) and bacterial species (Denning & Hope 2010; Montravers et al. 2011).

The effectiveness of fluconazole treatment is commonly overcome by drug resistance. In a test of 5265 patient samples of *C. albicans* from nine different labs worldwide, 4.8 % were found to be resistant to normal treatment levels of fluconazole (at MIC = 0.06 μg/mL is the epidemiological cutoff value established by European

Committee on Antimicrobial Susceptibility Testing (EUCAST) for fluconazole) (Espinel-Ingroff et al. 2014). Resistance to fluconazole is well documented and prevalent relative to resistance to the other drugs (Rex et al. 1994; Denning & Hope 2010). For example, in a study of 348 samples from immunocompromised and AIDS patients the North West of England, of which *C. albicans* infection composed 73 %, resistance (12.5 mg/L) of fluconazole was observed in 17.5 % of the samples (33 % in AIDS patients; 11 % in others). In the same study, pyrimidine analog Flucytosine resistance (16 mg/L) was observed in 3.4 % of the samples (6.5 % of isolates from patients with AIDS) and only one isolate was resistant (4 mg/L) Amphotericin B (Law et al. 1994).

Transcription factors involved in drug resistance often influence the production of proteins that pump drugs out of cells. These transcription factors are also often involved in the pathway which is targeted by fluconazole, ergosterol biosynthesis. Resistance of *C. albicans* to fluconazole has been shown for strains with gain-of-function mutations in the protein Multidrug Resistance Regulator 1 (*MRR1*; gain-of-function mutant has point mutation: P653S) (Christoph et al. 2012; Hiller et al. 2006). *MRR1* is a transcription factor that regulates *MDR1* transcription, it is induced by CCAAT-binding factor-dependent transcription factor (*HAP43*- also called *CAP2*) (Skrzypek et al. 2017). *MDR1* encodes for proteins that act as efflux pumps which eject toxic compounds from the cell (including drugs) and its overexpression has been linked to resistance to two antifungal drugs, cerulenin and Brefeldin A (Hiller et al. 2006). Cerulenin prevents germination in *C. albicans* by inhibiting fatty acid biosynthesis while Brefeldin A impedes transport through the Golgi complex, both are substrates for efflux pumps (Hoberg et al. 1983; Wirsching et al. 2001; Diwischek et al. 2009). Upregulation of *MDR1* based resistance to fluconazole, however, is less straight forward as it is shown to depend on the background strain, resistance is observed in the CA14 *C. albicans* background but not SC5314). The CA14 strain differs from its parent (SC5314) in three aspects: (1) it is auxotrophic for uridine (2) it is delete of the iron utilization gene *iro1*ΔΔ and (3) unless complemented by Ura3 it has lost virulence when tested in a mouse model (Fonzi & Irwin 1993; Garcia et al. 2001; Cole et al. 1995). Additional genes are thought to be upregulated along with *MDR1* which vary in these strains and contribute to the presence or absence of fluconazole resistance (Hiller et al. 2006).

A few microarray studies have explored genes up and down regulated along with overexpression of *MDR1*. The following genes were found consistently across these studies: (1) *Genes de Respuesta a Estres* (Stress Responsive Gene) 2 (*GRP2*) which codes

for a methylglyoxal reductase protein that is found in secretions from biofilm and planktonic cultures and is induced during oxidative stress by transcription factor Cap1; (2) Aldo-keto reductases *IFD6* which is bound by biofilm regulator Zap1 and CR_09100C_A; and (3) SNooZe 1 (*SNZ1*) which is regulated by bZIP transcription factor (Gcn4), it is involved in vitamin B synthesis and induced by the yeast-hyphae switch (Karababa et al. 2004; Cowen et al. 2002; Rogers & Barker 2003; Kusch et al. 2004; Skrzypek et al. 2017; Nobile et al. 2009).

Once resistance to azole drugs has developed there are three next line options: polyenes (i.e. Amphotericin B), pyrimidine analogues (i.e. Flucytosine), and the echinocandins (i.e. caspofungin). Allylamines are used for non-invasive infections, for example those occurring in nails. Polyenes are antifungal agents produced naturally by certain types of bacteria. They function by interacting with sterols in the cell membranes of pathogenic fungi (Ciesielski et al. 2016; Ghannoum & Rice 1999). The pyrimidine like drug Flucytosine enters the fungal cell where it is modified by fungal enzymes. It can then infiltrate the pyrimidine salvage pathway causing the production of toxic precursors that negatively affect the synthesis of DNA and contribute to the formation of dysfunctional RNA. Echinocandins drugs are derived from fungi which function by inhibiting an enzyme necessary for the synthesis of the cell wall protein β-1,3-D-glucan synthase. This leads to cell wall defects (Denning & Hope 2010; Hope 2010; Douglas 2001).

1.2.10 Dimorphism of *C. albicans*

The ability of *C. albicans* to change its physical form is one of the most amazing ways that it adjusts to new environments and facilitates its own survival under a wide range of stressful conditions. Despite the distinct appearance and physical separation of dimorphic shifts that occur in *C. albicans* it is notable that the molecular pathways implicated in these transitions are somewhat linked. This section outlines two types of phenotypic transitions observed in *C. albicans* as well as their triggers and underlying molecular pathways.

C. albicans cells have several forms which are visibly apparent even at the colony level. In the next sections we will discuss in detail phenotypes which include switching between white or grey or opaque cell types and utilization of environmental amino acids to elongate and form hyphae. In addition, we will explore how their underlying molecular pathways relate.

1.2.10.1 White-opaque and opaque-white switching

The switching of *C. albicans* between white and opaque forms is important to the yeasts' ability to filament or to mate. These forms are passed across generations and this reversible transition has many physiological implications. While in the white state the cells tend to form hyphae, the opaque version is competent at mating (Srikantha et al. 2001). Additionally, opaque cells are temperature sensitive and rarely form hyphae (see Section 1.2.10.3) (Slutsky et al. 1987).

Two distinct white and opaque forms are observed in *C. albicans* and differences in these cell types are visible with the naked eye. As can be seen in Figure 1.3 the white form takes a more rounded shape while the opaque form is elongated, 'pimpled', and large. Opaque cells have three times the volume and double the mass of white cells, yet they contain the same amount of DNA. It has been shown that opaque cells have an advantage at evading certain specific immune responses, but commonly the two cell types are equally successful and this depends on the immune cell type and the environment in which it is engaging with the *C. albicans* cells (Sasse et al. 2013). For example, white cells are shown to be preferentially phagocytosed by some hemocyte and macrophage cells of *Drosophila* and mouse origin respectively (Sasse et al. 2013).

Switching between white and opaque (and vice versa) is relatively rare but the frequency can be increased by manipulation of growth conditions and rates can be monitored in an experimental setting as a measured phenotype. Switching can be induced by oxidative stress, temperature, Ultra Violet (UV) damage, genetic alterations to DNA repair related proteins, exposure to chemicals and manipulation of cell cycle (Lohse & Johnson 2009). Switching between white and opaque forms is a way that this pathogen evades host immune systems.

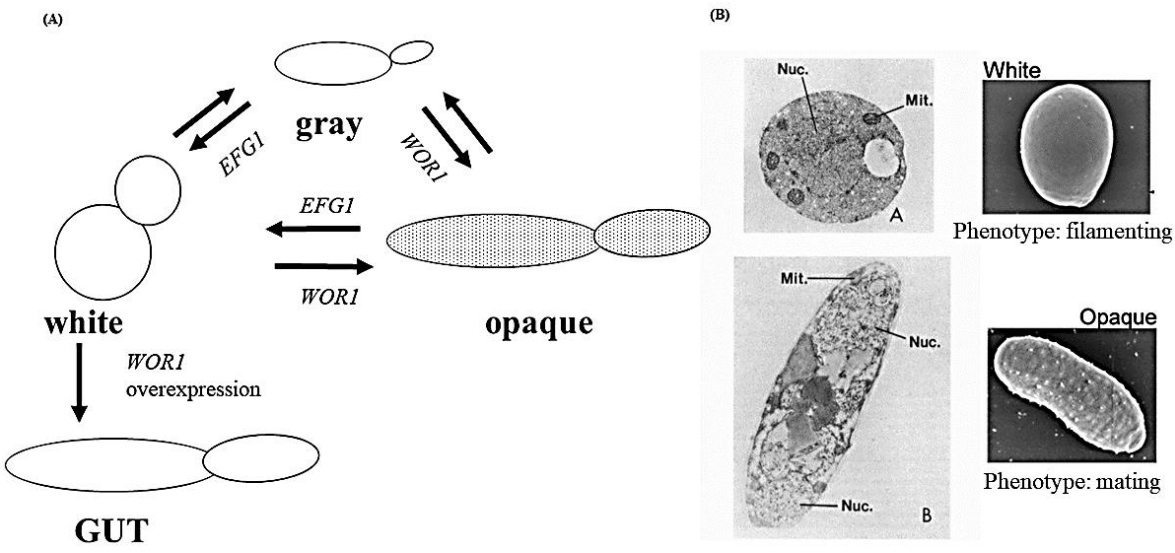

Figure 1.3 White and opaque forms and genes involved in switching of *C. albicans*
(A) Classes of White and Opaque forms and genes involved in switching; [Figure adapted from Scaduto and Bennett 2015 Figure 1] (B) Transmission micrograph images showing white and opaque cell appearance, anatomy and description of noteworthy phenotypes [Figure adapted from Slutsky et al., 1986 and Scanning electron micrograph images from Srikantha et al., 2001]

While once thought to occur exclusively in homozygous mating types, white-opaque switching is now known to occur in both heterozygous and homozygous mating types of *C. albicans* (Lockhart et al. 2002; Slutsky et al. 1987; Xie et al. 2013; Li et al. 2016; Miller & Johnson 2002). White-opaque switching is repressed by combined input from the *MTL*a1 and *MTL*α2 loci (not *MTL*α1) (Miller & Johnson 2002). Opaque cells are 100x more mating competent and it is secretion of pheromones by 'alpha' opaque cells that signal formation of mating projections in 'a' opaque cells during mating (Miller & Johnson 2002). A *MTL*a1 and *MTL*α2 allele are inherited following crosses and both opaque x opaque and opaque x white mating produce offspring cells which are usually white (3-4 % of offspring from experiments with these crosses were opaque) (Miller & Johnson 2002).

The pimpled surface of opaque cells reflects a unique antigen signature similar to that of hyphae (Anderson & Soll 1987).The white-opaque switch is a mechanism that *C. albicans* uses to evade the immune system in some environments. For example, white cells can evade neutrophils except for when they form a germ tube on a glass slide but not in embedded growth conditions (Sasse et al. 2013). Surface antigens (pH regulated Pra1 and others) change based on yeast or hypha form and these likely contribute to the susceptibility to engulfment by immune agents (Bommanavar et al. 2017).

It is also known that opaque cells signal white cells to increase the thickness of biofilms through pheromone secretions that promote white cell interactions (Daniels et al. 2006). The resulting biofilms which are then made up of mostly white cells, provide a protected environment where opaque cells can undergo elongation and mating (Daniels et al. 2006).

The morphological switch to opaque is regulated by the White Opaque Regulator (*WOR1*) and MiniChromosome Maintenance 1 (*MCM1*) gene expression while transition to the white phase is regulated by *EFG1* (see Sections 1.2.2/3).

WOR1 is a transcription regulator that regulates its own expression and may regulate adhesion factors. Experiments show that constitutive expression of *WOR1* converts all cells (a or α) to stable opaque cells and natural expression of *WOR1* is virtually abolished in white cells. *WOR1* expression is thought to be a bi-stable switch modulated by histone modifiers that self-propagates through a positive or double-negative feedback loops resulting in the high level expression observed in opaque cells (Huang et al. 2006; Hnisz, Schwarzmüller, et al. 2009). Mcm1 is a transcriptional regulator linked to master gene circuit regulation in *S. cerevisiae* and other yeasts (Tuch et al. 2008). It is involved in hyphal regulation in *C. albicans* and binds with Wor1 at sites of gene regulators that instigate the white-opaque switch (Tuch et al. 2008). *EFG1* acts as a repressor of white-opaque switching, it allows *RIM101* pathway signaling to cause this switch only under certain pH conditions (Nie et al. 2010).

It has been shown that *EFG1* has both up and downstream roles in relation to *WOR1*. An epigenetic study of deletion mutants showed that *EFG1* acts downstream of *WOR1* for the physiological aspects morphology change but upstream of *WOR1* during phase commitment by gene expression changes (Hnisz, Schwarzmüller, et al. 2009). If both *WOR1* and *EFG1* are deleted the cells take a grey form (see Fig. 1.3) (Lohse & Johnson 2009; Sasse et al. 2013; Scaduto & Bennett 2015; Srikantha et al. 2001). Strains overexpressing *WOR1* in a murine intestinal infection system take a heritable “dark” (GUT) opaque like form or are white cells (gastrointestinal induced transition) and the “dark” form dominates this population (Fig. 1.3). On the other hand, grey cells show an advantage in a mucous membrane (tongue) infection model. The GUT cells have distinct gene expression patterns including downregulation of genes associated with virulence and a subset of the genes with changed regulation that are common with opaque cells (Scaduto

& Bennett 2015; Tao et al. 2014; Pande et al. 2013). Each of these white, grey and opaque forms have distinct gene expression profiles (Tao et al. 2014).

1.2.10.2 Yeast-hyphae and hyphae-yeast transitions

In yeasts, the switch between yeast and hypha forms is known as ‘dimorphic’ switching. While ‘dimorphic’ or yeast-hyphae switching is explored in some detail in other pathogenic yeasts, it is noted that the conservation of pathways between *C. albicans* and other yeasts beyond the level of master regulators is low (Boyce & Andrianopoulos 2015).

Stages of development of the yeast and hyphae phenotypes are evaluated based upon parameters such as the diameter of the hyphal extension, the presence of constrictions, overall roundness or oval shape, extent of branching, the parallel state of cell walls, length, extent of budding and separation of buds, and presence of large vacuoles. The morphological states are categorized as yeast, pseudo-hyphae or hypha, with aspects that include germ tubes (which will form in response to serum), septin rings and actin patches (Fig.1.4) (Sudbery et al. 2004; Sudbery 2011a).

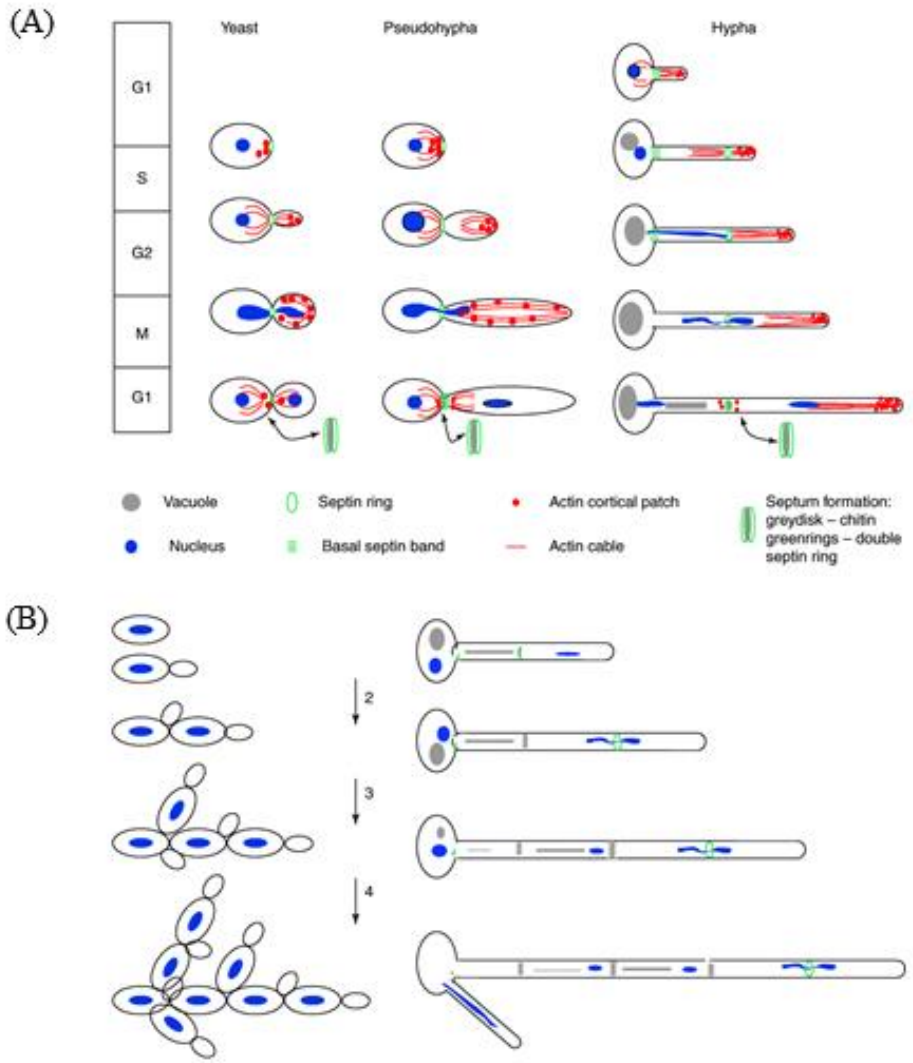

Figure 1.4 Major morphological states of *C. albicans*: yeast, pseudohyphae and hyphae
(A) Yeast to hypha development stages, anatomy and cell cycle (B) Cell cycles 2-4 after re-inoculation of unbudded yeast cells. The structures shown in 3 and 4 are not commonly observed in liquid culture because of they are fragmented by shear forces; [Adapted from Figure 2a, Sudbery et al. 2004]

In *C. albicans*, switching from hyphae to yeast form is important to advance infection. It allows the yeast to move out of the tissues and through the host's fluid systems to reach the more obscured niches including organs (Saville et al. 2003). Filamentation, or development of hyphae is reflexive to environmental factors including serum, temperature, pH, nutritional/starvation, N-acetylglucosamine (GlcNAc), carbon dioxide and adherence (Mitchell 1998; Brown & Gow 1999; Braun & Johnson 2000; Biswas, Dijck, et al. 2007). Most of these stimuli have distinct molecular pathways that feed into regulation of the main regulators for this morphogenic change. For example, changes in

pH encourage the transition through the Rim101 pathway while changes in nutrition, serum GlcNAc affect Efg1 triggering pathways (Biswas, Dijck, et al. 2007).

The transition from invasive hyphae to yeast form is observed by two phenotypes at the colony level: (1) a small number of long rapidly growing single hyphae strands originating at the center of colonies and (2) uniform long hyphae manifesting from the colony center to enclose the original colony (Csank et al. 1998; Pendrak & Roberts 2015). Pseudohyphae are another distinct phase that like hyphae have the ability to invade substrates, yet have irregular thickness (thinner at center) and noted septal separation at the mother cell (where mitosis occurs) and synchronized cell divisions (Sudbery et al. 2004). These occasionally bud axially and in bipolar events of *C. albicans* which contrasts with the solely unipolar budding in *S. cerevisiae* (Veses & Gow 2009). Some genotypic features promote this phenotype and homozygous Tup1 mutants constitutively form pseudohyphae (Murad et al. 2001; Sudbery et al. 2004).

Quorum sensing is a self-regulation mechanism that organisms use to respond to local cell density. It is used by *C. albicans* to determine morphological cell fate (Kruppa 2008). Cells sense the density of the local cell populations through molecules including farnesol, tyrosol and dodecanol which directly manipulate the hyphae-yeast transition. These signaling molecules encourage the cells to take yeast form at high cell densities when they might otherwise form hyphae (Mayer et al. 2013; Chen et al. 2004; Hall et al. 2011; Hornby et al. 2001).

Switching is a strategy used by fungi to avoid engulfment and phagocytosis by immune cells like macrophages and neutrophils. Hyphal development can camouflage detectable cell wall components to keep cells from being recognized by macrophages (McKenzie et al. 2010). *C. albicans* is even able to delay phagosome maturation by taking the hypha form and this is dependent on cell wall makeup as lower levels of the cell wall protein O-mannan allow for the maturation to progress (Bain et al. 2012). Likewise, growth of C. albicans is reduced by the presence of macrophage cells (Marcil et al. 2002). Most of all, it is shown that *C. albicans* hyphae and pseudohyphae can pierce, escape and kill macrophage cells (Marcil et al. 2002). Still, despite the fact that the reversable switch between yeast and hyphae cells is well documented in *C. albicans* there is no conclusion about the link between the occurrence of hyphal state and resulting infection rate of this pathogen. There is, however, evidence that this dimorphism contributes to virulence (Jacobsen et al. 2012; Mayer et al. 2013).

Deletion of genes that stunt the development of hyphae in *C. albicans* can decrease virulence in *C. elegans* models though development of hyphae is not necessary for infection (Pukkila-Worley et al. 2009a; Lo et al. 1997). When considering this and other phenotypes in relation to pathogenicity, it is important to recognize the various stages of infection as these qualify the interactions between host tissues and organ microenvironments (Gow et al. 2002). Some deletion mutants that are unable to form hyphae also have a decreased ability to germinate (Brand 2012; Phan et al. 2000). Microscopy of diseased tissue shows the presence of both yeast and hyphal forms. Hypha forms are also observed in endothelial cells, skin, hair and nails while germinating cells are more commonly endocytosed to the bloodstream than yeast (Brand 2012; Phan et al. 2000).

The regulation of switching between yeast and hypha forms in *C. albicans* has been explored extensively and many genetic pathways are known to contribute to the phenotype (see Fig.1.5).

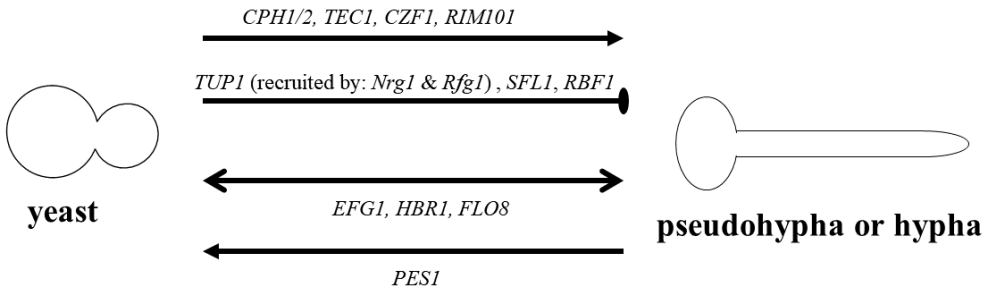

Figure 1.5 Genetic regulation of yeast-hyphae and hyphae-yeast transitions
Genes involved in facilitation or inhibition of yeast-hyphae, hyphae-yeast, and bidirectional switching of *C. albicans* cell morphology: arrow = positive regulation, flat end = negative regulation; [Adapted from Sudbery 2011b]

At least three main independent pathways involving the transcriptional regulators *TUP1*, *CPH1* and *EFG1* contribute in an additive manner toward the phenotype by activating filamentation through individualized responses (rather than a cumulative mass effect) (Braun & Johnson 2000).

The *TUP1* pathway can be triggered by farnesol or Yet Another Kinase 1 (*YAK1*) functions upstream of *TUP1* in this pathway (Goyard et al. 2008; Uppuluri et al. 2007). Negative Regulator of Glucose controlled genes (Nrg1) and Rfg1 are each proposed to recruit Tup1 and Suppressor gene for Flocculation 1 (Sfl1) (see Section 1.22). Sfl1 functions in a similar pathway in both *C. albicans* and *S. cerevisiae* where it is regulated

by Takashi's Protein Kinase 2 (Tpk2) and exerts control over Flo8 which is a transcription factor required for hyphal formation, CO_2 induced white-opaque switching and hyphal virulence in mice models (Skrzypek et al. 2017; Bauer & Wendland 2007). The cAMP-PKA pathway is repressed by Tup1. Efg1 is an important transcriptional regulator in this pathway where it associates with Flo8 to induce hyphal development (Stoldt et al. 1997; Stichternoth & Ernst 2009).

The *Candida* PseudoHyphal regulators 1 (*CPH1*) mediated MAPK pathway can be triggered to induce filamentation by environmental factors including serum, starvation or glucose levels (Biswas, Van Dijck, et al. 2007; Eisman et al. 2006). Expression of *CPH1* is repressed by farnesol (Sato et al. 2004). Under osmotic stress, low temperature, specific pH levels or nitrogen starvation the protein functions to promote hyper-invasive growth (Biswas, Dijck, et al. 2007) These pathways are controlled by different upstream regulators which become active depending on the environmental stimulus (Biswas, Dijck, et al. 2007).

Another pathway is triggered in embedded growth situations. During embedded growth *C. albicans* cells experiences aerobic situations and hypoxia. While several factors are known to be regulators of gene expression in this environmental condition the *C. albicans* Zinc Finger protein 1 (Czf1) pathway is known to positively regulate hyphae specific genes during hypoxia. It also positively regulates hyphal growth in response to farnesol and other cues (Sudbery 2011b). Efg1 and Flo8 also act in embedded growth conditions as negative regulators of Czf1 (Giusani et al. 2002; Stichternoth & Ernst 2009; Cao et al. 2006). Another hyphal development regulator HemogloBin Response 1 (Hbr1), *HBR1* represses the development of hyphae in embedded conditions but promotes agar invasion in aerobic conditions (Pendrak et al. 2004).

Three other main pathways that regulate filamentation in embedded growth conditions involve (Hope et al. 2008; Brown et al. 1999; Pendrak & Roberts 2015):

1. Czf1-Efg1- The Czf-Efg1 pathway responds to farnesol which inhibits filamentation, this pathway has also been implicated in white-opaque switching in response to temperature and also cell death (Langford et al. 2013).
2. Flo8-Mss1- (FLOcculation 8-Mitochondrial splicing system 1); The increased expression of *MSS11* during hyphal formation leads to the cooperative binding of Flo8 and Mss11 to the *HWP1* promoter in embedded conditions at both high (37 °C) and low (24 °C) temperatures (Su et al. 2009).

3. Dck1-Rac1- (DoCKer domain 1-Ras Homolog 1); Dck2 has a DOCKER domain catalytic domain that binds and activates ribosome associated complex protein RAC1 during invasive growth conditions (Hope et al. 2008).

Induction of hyphal growth can happen as a response to pH, this engages a pathway of Rim family proteins that eventually triggers Rim101 which exerts a direct positive regulation on hypha genes. Rim101 also has a second, indirect role in which it serves as an upstream regulator of genes that can induce or repress filamentation (Davis et al. 2000).

Signals from Cph2 and Efg1 converge to regulate Transposon Enhancement Control 1 (Tec1) which has binding sites in the upstream regions of hypha specific and serum induced genes (Lane et al. 2001). These are just some of many examples of pathways converging to promote a morphological phenotype in *C. albicans.* Another example is *EFG1*, *TUP1* and *RBF1* which all contribute to the regulation of hypha-specific *HWP1* (Sharkey et al. 1999). Conversely, RPG-box-binding factor 1 (*RBF1)* is a negative regulator of filamentous growth as it occurs when the gene is deleted (Ishii et al. 1997).

While many genes stunt or inhibit filamentation when deleted, few positive regulators of the hyphae-yeast switch are named. The switch is encouraged by lower temperatures (24-30 °C), farnesol and inhibition of cAMP signaling. One known regulator of the hyphae-yeast switch is Pescadillo homolog *PES1* (Lindsay et al. 2012; Shen et al. 2008). *PES1* homologs are involved in cell cycle control and ribosome biogenesis. It is notable that in *C. albicans* loss of this gene is viable in hyphae but not yeast cells. It has a role in lateral yeast growth in hyphal cells and is also essential for virulence in insect cell and in mice models (Shen et al. 2008; Skrzypek et al. 2017).

1.2.10.3 Molecular links between white-opaque and yeast-hyphae switching in *C. albicans*

While both white and opaque *C. albicans* cells can undergo the yeast-hyphae transition, the environmental triggers for these two cell types are different. A study by Si et al., 2013 compared these factors and found that white cells filament in serum, high temperature, neutral pH, and conditions depleted of nutrients. High temperatures inhibit filamentation in opaque cells which will not cause the shift to hyphal development in white cells. In white cells factors that induce hyphal development include: low phosphate or sorbitol mediums (Si et al. 2013).

Loss of Nrg1, Rfg1 or Tup1 cause white cells to start hyphal growth in what are normally yeast growth conditions; likewise, in opaque cells show loss of Nrg1 or Tup1 causes filamentation in normal conditions. Rfg1 is a bidirectional regulator of filamentation in white cells it only promotes filamentation in opaque cells. Ume6 is the master regulator of hyphal development in both white and opaque cells (Si et al. 2013). This study also found that the MAPK pathway which is activated by various environmental triggers (pheromone, osmotic stress, temperature, etc.) only regulates the white filamentous growth pathway (Si et al. 2013; Monge et al. 2006).

1.3 Chromatin and its modification

Chromatin refers to histone and non-histone proteins in complex with DNA (Alberts B, Johnson A 2002). The structure of these components functions as a gatekeeper for proteins that can activate or repress transcription of genes.

In its first level of packaging, DNA is wrapped around histone proteins to form nucleosomes. Each nucleosome is composed of an octamer of histones. There are two molecules of the histones H2A, H2B, H3 and H4 in each nucleosome (octamer). In addition, there is one molecule of histone H1 in most nucleosomes. The DNA is wrapped twice around each nucleosome (Fig.1.6) (Luger et al. 1997, Richmond et al. 1997).

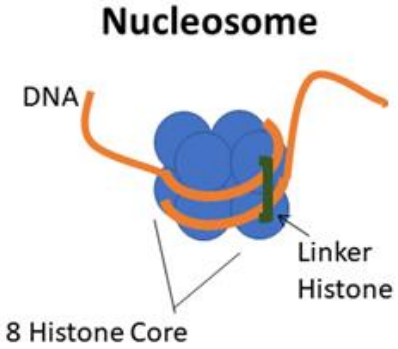

Figure 1.6 Model showing nucleosome in complex with DNA
Model of nucleosome depicting the octamer of histones H2A, H2B, H3 and H4 (each in duplex) wrapped by DNA and linker histone H1 [adapted from Richmond et al. 1997].

The wrapping of a nucleosome encompasses ~200 base pairs of DNA, and nucleosomes connect to adjacent nucleosomes via linker DNA forming a beads on a string structure (Li & Reinberg 2011). In eukaryotic genomes the formation of chromatin condenses the DNA by a factor of 30-40 (Richmond et al. 1997). This wrapping can take

different formations and its organization has implications at the transcriptional level. It is also known that the presence or absence of nucleosomes relates to the level of transcription occurring within a genomic region (Rando & Winston 2012; Clark-Adams et al. 1988).

The beads on a string fiber might be further folded and packaged into a 30 nm fiber though this is currently debatable. At least two models have been proposed for the 30 nm fiber, a one-start helix solenoid or a two-start helix zig-zag/twisted-ribbon (Williams et al. 1986; Robinson et al. 2006; Tremethick 2007; Schalch et al. 2005). The solenoid model suggests a superhelix configuration with nucleosomes connected by bent linker DNA, this contrasts with the straight linker DNA proposed in the zig-zag/twisted-ribbon model. Additionally, long range interactions and looping have been shown (Li & Reinberg 2011; Kan et al. 2007; Kadauke & Blobel 2009). These and other factors, including chromosome location in the nucleus, impact the expression level of the genes (Guelen et al. 2008; Li & Reinberg 2011).

Distinct chromatin types localize in the nucleus to specific "chromatin bodies" with varying levels of transcriptional activity. Two mechanisms of phase-separation have been proposed. The first suggests that bridging proteins link chromatin segments with similar properties causing them to form a liquid globule phase. The second model proposes that soluble binding proteins with multiple binding sites induce nucleation of liquid bodies around the chromatin (Erdel & Rippe 2018; Klosin & Hyman 2017; Larson et al. 2017; Strom et al. 2017).

The level of packing of DNA or 'chromatin' state can span from a relatively open, accessible and expressing chromatin "euchromatin" state to a more tightly packed and repressed configuration called "heterochromatin." Heterochromatin imparts silencing of DNA and contributes to its maintenance. It is classified into one of two forms both characterized by hypoacetylation (Grewal & Elgin 2002). The first, 'constitutive' heterochromatin occurs in distinct regions (telomeric, peri-centromeric) of the chromosome and has characteristics that include repetitive regions with some limited transcription (Saksouk et al. 2015). The second, 'facultative' heterochromatin is marked by distinct histone modification patterns that include methylation and ubiquitination, which facilitate flexing of normally silenced regions of DNA into expressed states under certain cellular conditions (Trojer & Reinberg 2007).

Post-translational modification (PTM) to histone proteins affects the tightness and positioning of various condensed DNA structures. Steric adjustment of nucleosomes and

their DNA regions occur by electrostatic balancing of the charges contributed by histone modifications (Fig.1.7A).

Histone post-translational modifications are chemical additions, which alter the properties of amino acids in proteins and thus modulate the protein function. For example, acetylation neutralizes the positive charge of a lysine while phosphorylation adds a negative group (Verdone et al. 2006). These modifications to the histone proteins alter the properties (charge, adduct, folding) of the histones and result in physical adjustments to the nucleosome. This impacts the overall wrapping of the DNA changing access for transcriptional machinery which may result in transcriptional activation or repression.

In addition to PTMs chromatin remodeling proteins are involved in the creation of chromatin states. For example, the Swi/Snf complex and the Isw complex remodel chromatin by sliding and/or evicting nucleosomes and the presence of these proteins has been shown to be essential for the development of hyphae in *C. albicans* (Mao et al. 2006; Gutiérrez et al. 2007; Skrzypek et al. 2017).

In a 2015 review article, Sharakhov and Sharakhova provide a case for pathogens taking advantage of epigenetic strategies to enhance their virulence by manipulating the packaging of DNA to change gene expression. This is done by changes to modifications on a localized area of histones, changing the local chromatin landscape or through changing the nuclear position of chromosomes (Sharakhov & Sharakhova 2015). In theory, this can happen in two different ways: within the pathogen itself or by impact to the host genome. In terms of fungal pathogenesis, the second scenario has been investigated in plant models. These organisms have conserved systems that propagate histone modifications to their genome (see Section 1.5). The across-organism conservation of histone-modification systems provides an opportunity for molecular manipulation of a host system by the infectious agents. For example, it has been shown that chemicals (HC-toxin and Depudecin) are synthesized and exuded by indwelling fungi (*C. carbonum* and *A. brassicicola*) that can inhibit and induce Histone DeAcetylase (HDAC) responses within plants (maize/*Z. mays* and *A. thaliana*) (Jeon et al. 2014)

1.4 Readers and writers of the ‘Histone Code’

Modifications to histones impact the local packing of DNA as well as the structure of chromosomes and this results in the changed expression of genes. One hypothesis about these modifications is the ‘histone code’ which proposes proteins which contribute

modifications to the landscape of histone marks can be assigned to the simple categories of, ‘writers’, ‘readers’ or ‘erasers’ depending on their function. This grouping separates the proteins that leave a PTM (writers) from those that recognize and respond to modifications (readers) and those that remove them (erasers). It follows that the pattern of chemical residues added to histone tails can be interpreted by researchers as a ‘histone code,’ with the implication being that they function as braille-like instructions (Strahl & Allis 2000). The modifications function locally allowing or excluding interface with other proteins and/or at the larger scale by structuring densely or loosely packed areas of the chromosome. The histone code is written like a ‘language’ onto the histones as chemical additions that obstruct or allow access of the transcriptional machinery to the DNA. The message of modification can have different meanings based on context signaling for: recruitment, regulation, local protein-protein interactions or other nearby histone modifications.

The different types of histone modifications include: acetylation, phosphorylation, ubiquitination, methylation, ADP ribosylation, glycosylation and sumoylation (Strahl & Allis 2000; Shiio & Eisenman 2003). Phosphorylation and acetylation are often associated and are generally activators of transcription (Eberharter & Becker 2002; Rossetto et al. 2012). Phosphorylation normally occurs at serine, threonine and tyrosine residues (Rossetto et al. 2012). Ubiquitination can activate or repress transcription depending on which histone modifying enzyme marks a lysine residue (Cao & Yan 2012). The effects of methylation are site specific and some such as histone H3K9 are repressive while other sites such as histone H3K4 are important for gene activation (Zhang & Reinberg 2001). ADP ribosylation is an activating mark that may compete with acetylation or methylation since they all modify the lysine residues of histone tails (Messner & Hottiger 2011; Eberharter & Becker 2002). O-GlcNAc glycosylation is associated with gene repression (Dehennaut et al. 2014). This glycosylation mark competes with phosphorylation to mark serine or threonine residues (Zhang et al. 2011). Finally, sumoylation is a repressive mark that may interact with the Histone DeAcetylase 1 (Hda1) protein to deacetylate local histones (discussed in detail later in Section 1.5.2) (Shiio & Eisenman 2003). Sumoylation marks modify many *C. albicans* proteins and roles of this modification are found on proteins involved in stress response, growth and virulence (Leach et al. 2011). For example, this mark is added to Wor1 by Wos1 and this regulation is dependent on ambient CO_2 levels (Yan et al. 2015).

To give an example of the histone code, lysine residues of histone tails are recognized by specialized bromo protein domains. Some Histone AcetylTransferase (HAT) proteins are dual function and act as writers and readers (Marmorstein & Zhou 2014). *S. cerevisiae* General Control Nonderepressible (Gcn5) protein is associated with two main roles during times when the yeast undergoes stress: (1) acetylating histones (H3 at lysine 19 (K19)) near transcriptional start sites of stress response genes and (2) localizing to sites of relatively long gene transcripts. The significance of length of gene transcripts relates to the function of RNA polymerase II (Chakalova & Fraser 2010). Areas with long gene transcripts may have relatively more accessible and open chromatin structure, and they may also create more domain boundaries. These regions can function to insulate gene areas creating spatial gaps that affect the typical interactions of loci within chromosomal interaction domains (CID) (Le & Laub 2016). The acetylation of histones by Gcn5 is a way that the protein acts in the capacity of a 'writer' and this can cause changes to the packaging of local DNA which may even result in eviction of nucleosomes (Govind et al. 2007). Likewise, the re-localization of Gcn5 during stress response from genes with shorter open reading frames to those with long open reading frames occurs in conjunction with decreased acetylation at the genes with short open reading frames. This results in the yeast undergoing an increase in the relative transcription of genes with longer open reading frames and this is due to environmental conditions (Xue-Franzén et al. 2013).

Yet another aspect of the 'reader' role of Gcn5 protein is its function as a transcriptional coactivator which may act to recruit other proteins (Sanchez & Zhou 2009). In other cases, writers and readers are on different proteins (Fahrenkrog 2015). In the model yeast, *S. pombe*, Gcn5 has been shown to function in concert with the HDAC Cryptic Loci Regulator 3 (Clr3) to modulate histone (and non-histone protein) acetylation and transcriptional elongation during yeast stress response. This is a unique pairing as the 'eraser' Clr3 is the only HDAC shown to act in this way (Johnsson et al. 2009).

A second hypothesis proposes that there is 'crosstalk' between histone modifications. This suggests the occurrence of dynamic molecular communications between histone modifiers, histones and other related proteins through the post translational histone modifications (Fig.1.7) (Lee et al. 2010).

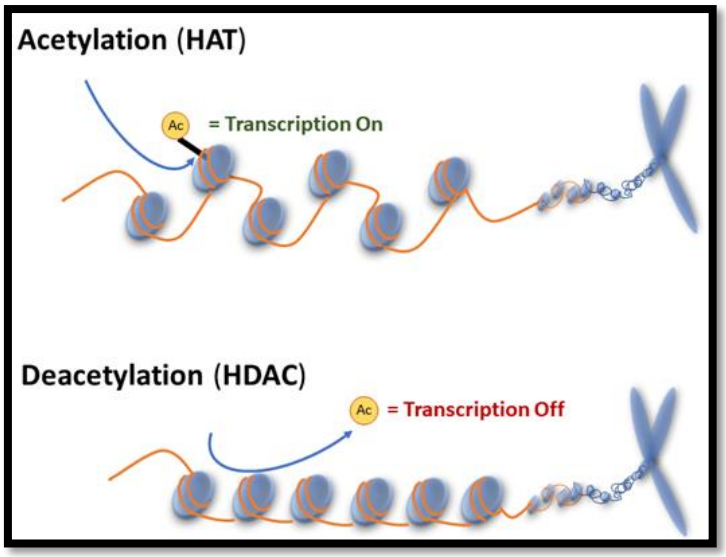

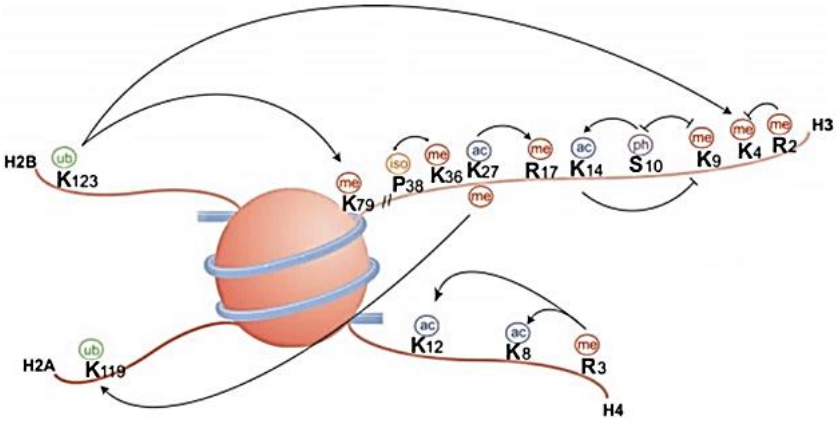

Histone	Modification
H2A	S122 phosphorylation
H2A	S129 phosphorylation
H2B	S10 phosphorylation
H2B	K11 acetylation
H2B	K123 ubiquitination
H3	K4 methylation
H3	K36 methylation
H3	K79 methylation
H3	T45 phosphorylation
H3	K9 acetylation
H3	K14 acetylation
H3	K18 acetylation
H3	K56 acetylation
H4	K16 acetylation

Figure 1.7 Models showing modification of chromatin by histone acetylation state and crosstalk between histone modifications
(Top) The changing chromatin landscape based on histone acetylation: Euchromatic, open DNA conformation in the presence of acetylation and heterochromatic, tightly wound DNA conformation in the absence of acetylation
(Bottom) Schematic of histone modifications and crosstalk; arrow = positive effect, flat head = negative effect [Adapted from Bannister & Kouzarides 2011 modification of originally published figures in Kouzarides 2007] and table of histone modifications involved in aging and apoptotic processes in yeast. [Adapted from (Fahrenkrog 2015)]

Currently, evidence supports at least three strategies by which crosstalk happens: (1) a histone modification influences the activity a histone modifying enzyme, (2) histone modifying enzymes interact while united in a complex or (3) the cleavage of a part of the histone triggers the histone modification status (Suganuma & Workman 2008). An example of the first strategy was shown in a 2008 study by the Berger Lab at the University

of Pennsylvania. They showed that linked dual modifications of *S. cerevisiae* histone H3 (phosphorylation at S10 which promotes acetylation at K14 by Gcn5) leads to the binding of yeast 14-3-3 protein homologs Bmh1 and Bmh2. This type of protein has the propensity to bind other chromatin-modifying proteins (Walter et al. 2008). There are several examples of the second strategy, for example it was shown in *S. pombe* that the Clr4 H3K9 methylase functions in complex with at least two other proteins that complex with chromatin binding factors Clr7 and Clr8 as well as the Cul4 ubiquitin ligase, the activity of which promotes function of Clr4. This is facilitated thanks to the binding of Clr8 (in complex) by H3K4 demethylase Lid2, linking the two modification events (Li et al. 2008;). Finally, proteolytic histone H3 cleavage at the N-terminal tail has been shown in mouse embryonic stem cells and this is likely due to the lysosomal cysteine protease Cathepsin L. It is also shown that specific modifications modulate this protease activity suggesting a mechanism for differentiation of these cells (Duncan et al. 2008).

As an example of 'crosstalk', where several proteins and complexes have functions in both acetylation and ubiquitination pathways. Lysine acetylation competitively excludes ubiquitination when the marks are targeting the same residue (Caron et al. 2005). Other mechanisms for acetylation and ubiquitination crosstalk include the modification of proteins by acetylation which creates a binding site for a ubiquitinase protein or acetylation that leads to complex dissociation of ubiquitinating complexes and their subsequent degradation (Caron et al. 2005).

A similar scenario exists with methylation, however, while a mark of acetylation may block methylation at one location, the same mark can promote methylation at another nearby lysine residue (Lee et al. 2010). An example of this is found in human polycomb group proteins which regulate cell fate decisions and contribute to the development of human tumors. It has been shown that when H3K27 methylation occurs, acetylation at the same histone tail site increases and this specifically occurs at Polycomb Repressive Complex (*PRC2*) target genes. Based on this evidence, Pasini et al., 2010 propose that there is a switch governed by the methylation or acetylation marks that activates polycomb group target genes and that polycomb group proteins repress acetylation by competitive binding at their target genes (Pasini et al. 2010). Similarly, it is reported that methylation can exclude nearby methylation while simultaneously encouraging acetylation (Fischle et al. 2003; Caron et al. 2005). Other marks can be involved as well for example, sumoylation is a more recently discovered modification that is thought to participate in cross talk with acetylation and methylation marks on histone H4 (Nathan et al. 2003). In *S. cerevisiae*,

sumoylation marks inhibit acetylation by HATs and these marks may recruit or activate HDACs to many sites identified in histone H2B and H4 (Lee & Workman 2007; Nathan et al. 2006).

While the hypotheses of a 'histone code' or 'crosstalk' start constructive discussions about potential systems of histone modifications, it is debated whether the categorization of these PTMs as symbols with meaning will confirm this hypothesis. Issues with the hypothesis arise with the realization that the modifications directly affect transcription of genes, blurring the simple separation of symbol and meaning while complicating efforts to decipher. Whether these modifications have specific unique meaning or if they are focused toward consistent patterns that regulate gene expression is highly speculative. It has been accurately suggested that the histone code hypothesis may be a naïve approach to research on the subject (Henikoff & Turner 2006; van Steensel 2005).

1.5 Acetylation: histone acetyl transferase and deacetylase proteins

As discussed in the previous sections, acetylation is a reversible modification propagated or 'written' by Histone Acetyltransferase (HAT) proteins (Zhou et al. 2016). Histone Deacetylase (HDAC/KDAC) proteins remove this mark and are known as an 'eraser' of this mark (Strahl & Allis 2000; Seto & Yoshida 2014). Acetyl groups are added to lysine (K) residues in the protruding tails of nucleosome component histone proteins or other proteins (see Figs. 1.7 and 1.8).

Histone	Modification site: *H. sapiens*	Modification site: *S. cerevisiae*	Modification site: *C. albicans*
H2B	K5, K11, K12, K15, K16, K23	K3, K9, K11, K12, K16, K21, K22	K7, K8, K12, K17, K18, K22, K23, K47, K112
H2A	K5, K9	K4, K7	K6, K11, K13
H3	K9, K14, K18, K23, K27, K56	K9, K14, K18, K23, K27, K56	K10, K15, K19, K24, K28, K37, K57
H4	N-terminus, K5, K8, K12, K16	N-terminus, K5, K8, K12, K16	K8, K11, K15, K19, K62, K94

Figure 1.8 Table comparing the histone acetylation sites of humans and yeasts (*S. cerevisiae* and *C. albicans*)
[Adapted from Table 1 in Xiong et al. 2010 with added *C. albicans* and *H. sapiens* sites from Zhou et al. 2016 and Yuan et al. 2009 (Beck et al. 2006; Garcia et al. 2007)]

In general, acetylation functions to neutralize the positive charge on lysine residues, thus allowing the chromatin to become less compact and more accessible

(Haberland et al. 2009). It is commonly thought that acetylation simply functions to activate gene expression, however, this is not always the case; likewise, mutations in deacetylase proteins can enhance transcription (Strahl & Allis 2000). In fact, deacetylase enzymes are often recruited before HAT complexes and it is suggested that they too may contribute a modification (Strahl & Allis 2000).

Acetylation does not only happen at histones. For example, multiple acetylation sites on the molecular chaperone, Hsp90 are shown to be targets of various deacetylase proteins (including Hda1 discussed below 1.5.2). Hsp90 proteins regulate azole drug resistance (Cowen 2009). Inhibiting both Hsp90 and HDAC proteins can alleviate azole resistance in some clinical isolates (although due to functional redundancy this requires inhibition of several HDAC proteins see Section 1.7.3). It is speculated that the fluctuation of acetylation states is a mechanism that regulates the function of the Hsp90 protein (Li et al. 2017; Lamoth et al. 2014). In fact, there are so many non-histone substrates it is suggested that acetylation may play a role similar to phosphorylation in signaling cascades (Roth et al. 2001; Kouzarides 2000; Cheung et al. 2000). This is supported by the fact that bacterial orthologs of histone deacetylase proteins evolved before histone proteins and consequently the proteins are often more appropriately referred to as lysine deacetylases (Gregoretti et al. 2004).

1.5.1 Histone acetyl transferase proteins

Histone acetyl transferase (HAT) proteins function by transferring an acetyl group from acetyl-CoA to a nitrogen within the lysine residue of a histone tail (Yuan & Marmorstein 2013).

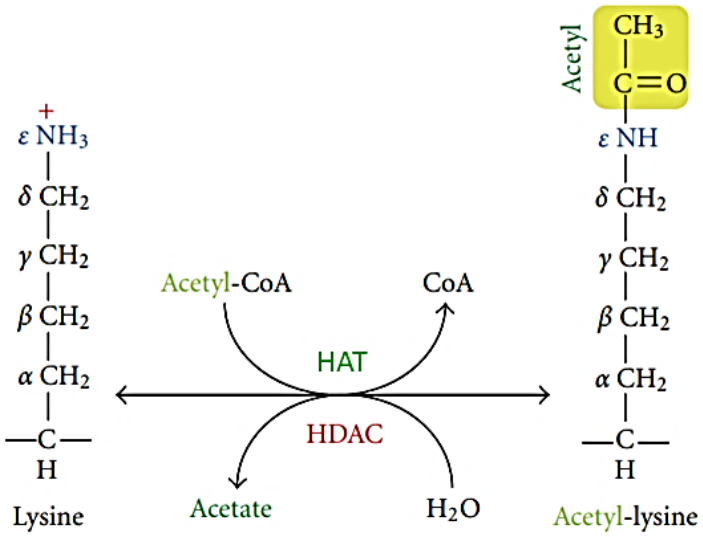

Figure 1.9 Model showing acetylation and deacetylation at a lysine residue
HAT transfers acetyl moiety (yellow) from acetyl-CoA to the lysine residue and HDAC removes the group releasing acetate; [Adapted from Figure 1 Kim et al. 2010]

Acetylation of histones results in charge neutralization of lysine residues and the creation of binding sites for bromodomain proteins which directly interact with acetylated residues (Sanchez & Zhou 2009; Josling et al. 2012; Dhalluin et al. 1999). These proteins are categorized by their targets and localization: B-type HAT proteins are cytoplasmic and mark free histones with acetylation that directs their transport to the nucleus, they do not have bromodomains; A-type HAT proteins function in the nucleus and have a bromodomain. An example of an A-type HAT is Gcn5 (see Section 1.4). HAT proteins can also be grouped by the complexes (ADA, SAGA, PCAF, NuA3, NuA4, MSL, etc.), histones (H2, H3, H4) and other proteins (HATS, coactivators, CRE-Binding Protein (CBP), Gcn5 protein, etc.) with which they associate. HATs can be specific to targeted or global acetylation activity and affect processes that include replication, transcription, elongation and silencing.

At least five families of HAT proteins are defined based upon structural motifs: HAT1, Gcn5, GNAT, MYST, metazoan specific p300/CBP and fungal specific Regulator of Ty1 Transposition (Rtt109) (Lee & Workman 2007; Yuan & Marmorstein 2013). The catalytic mechanisms of these protein families are distinct. For example, the MYST HAT family uses conserved glutamate and cysteine residues to form an intermediate stage before finally acetylating the histone in what is called a ‘ping-pong’ kinetic catalytic mechanism (Yuan & Marmorstein 2013; Yan et al. 2002). Other types of HATs utilize acid base reactions with quick ‘hit and run’ transfers for catalysis (p300/CBP) or work in

conjunction with histone chaperones (i.e., Rtt109) (Liu et al. 2008; Lau et al. 2000; Albaugh et al. 2010; D'Arcy & Luger 2011). Rtt109 structurally resembles Gcn5 AND functions in a complex involved in oxidative stress-response with the SAGA complex (containing Gcn5 subunit) and NuB4 (Hat1 subunit) complexes (Kim et al. 2018; Lin & Yuan 2008).

The pattern of acetylation marks on histone tail lysine residues may hold a motif for interacting with Swi/Snf complexes. The recruitment of some HAT complexes follow the interaction of Swi/Snf remodeling complexes on histones and it is suggested that the Swi/Snf domains themselves may leave an epigenetic mark (Strahl & Allis 2000; Memedula & Belmont 2003). An experimental model to visualize this effect is described in Memedula & Belmont 2003, a domain (VP16 acidic activation domain) known for interacting with chromatin remodeling proteins was placed as bait (using a lac repressor fusion protein with fluorescence tagging) within condensed chromatin and recruitment timing of subunits of a HAT (mammalian Gcn5) and subunits of Swi/Snf complexes (mammalian BRM and BRG1) were measured. It was found that first the Swi/Snf complex is rapidly recruited and this occurs prior to the presence of HAT complexes and the acetylation of histones H3 and H4 (Memedula & Belmont 2003).

1.5.2 Histone deacetylase proteins

There are at least four functional classes of histone deacetylase (HDAC) proteins which remove acetyl groups from many types of proteins including histones (Seto & Yoshida 2014). HDAC proteins are categorized in four distinct classes based upon their function, oligomerization, localization and homology (Khochbin & Wolffe 1997; Gregoretti et al. 2004). An outline of the human and yeast proteins allocated to these classes can be seen in Fig. 1.10.

	H. sapiens	*S. cerevisiae*	*S. pombe*	*C. albicans*
Class 1	HDAC1, HDAC2, HDAC3	Rpd3, Hos1, Hos2	Clr6, Hos2	Rpd3, Hos1, Hos2
Class 2a	HDAC4, HDAC5, HDAC7, HDAC9	Hda1	Clr3	Hda1
Class 2b	HDAC6a, HDAC6b, HDAC10			
Unclassed	HDAC8	Hos3		Hos3
Class 3	SIRT1-SIRT7	Sir2, Hst1-Hst4	Sir2, Hst2, Hst4	
Class 4	HDAC11			

Figure 1.10 Classification of histone deacetylase proteins in humans and model yeasts
Chart of HDAC proteins by class in *H. sapiens*, *S. cerevisiae*, *S. pombe* and *C. albicans;* [Adapted from Figure 3 Srikantha et al. 2001 and Figures 2 and 4 Gregoretti et al. 2004 (Troejer et al. 2003; Grozinger et al. 1999; Wood et al. 2012; McDowall et al. 2015)]

Class 1 histone deacetylase protein group is based on the yeast Reduced Potassium Dependency 3 (Rpd3) protein (Srikantha et al. 2001). Yeast Rpd3 is 49 kDa while human HDAC1 is 55 kDa. A genome-wide study of *S. cerevisiae* histone deacetylase functions showed that Rpd3 works in cell-cycle progression (Bernstein et al. 2000; Srikantha et al. 2001; Skrzypek & Hirschman 2011; Skrzypek et al. 2017). It is also involved in chromatin remodeling, autophagy and silencing (Skrzypek & Hirschman 2011). Deletion of *S. cerevisiae RPD3* increases acetylation at H3 and H4 as well as silencing at telomeric loci and this effect is more pronounced than the deletion of Hda1 (Stephen E Rundlett et al. 1996).

The Class 2 histone deacetylase protein group is based on the yeast Hda1 protein (Srikantha et al. 2001). Yeast Hda1 is 80 kDa while human HDAC4 is 119 kDa (Skrzypek et al. 2017; Skrzypek & Hirschman 2011). A genome-wide study of *S. cerevisiae* histone deacetylase functions showed that Hda1 is involved in processing carbohydrates and carbon (Bernstein et al. 2000; Srikantha et al. 2001). It also has roles in azole resistance via Hsp90 and heat shock (Skrzypek & Hirschman 2011). Deletion of *S. cerevisiae* Hda1 increases acetylation at H3 and H4 as well as silencing at telomeric loci (Stephen E Rundlett et al. 1996). The yeast Hda1 protein does not have DNA binding domains (Skrzypek et al. 2017; Skrzypek & Hirschman 2011).

Most untargeted histone deacetylation is performed by two complexes, the Ume6 recruited Rpd3 HDAC complex (recruited through the Switch INdependent 3 (Sin3) subunit) and the Hda1 HDAC complex recruited by the Tup1 repressor (interacts with DNA binding proteins). However the majority of regions deacetylated by Hda1 are not

Tup1 dependent so there are likely alternative mechanisms for this protein's function (Lee et al. 2009). While H3 and H4 are the main substrates of yeast Hda1, it is known to specifically acetylate H3K9, H3K18 and H2BK16 in addition to other sites (Robyr et al. 2002; Jiansheng Wu, Suka, et al. 2001).

Class 3 proteins are also known as Silent mating type Information Regulators or sirtuins (Sir, Hst, SIRT); they are distinct from HDACs as they require coenzymes NAD+/FAD to modulate the acetylation of histones and have no sequence similarity to the other HDAC proteins (Imai et al. 2000). *S. cerevisiae* Sir2 (63 kDa) is involved in the biosynthesis of amino acids (Bernstein et al. 2000; Srikantha et al. 2001). It functions at telomeres, plays role in lifespan and contributes to the negative regulation of replication (Skrzypek & Hirschman 2011).

Class 4 histone deacetylase protein HDAC11 is placed into a separate class, which reflects its faster evolution than other human HDAC proteins (Gao et al. 2002). It is present in primates, mice, *Drosophila* and plants. The human protein is 39 kDa with a catalytic domain that has conserved residues from Class I and II HDACs (Gao et al. 2002; The UniProt Consortium 2017). It is expressed in distinct organ systems, namely the kidney, brain, heart, skeletal muscles and testis (Gao et al. 2002). The HDAC11 protein has a role in responsiveness in the immune system (Villagra et al. 2009). It may be present in complexes with HDAC6 (Gao et al. 2002).

There are also some uncategorized HDAC proteins. HDAC8 is not classed since it occurs only in vertebrates and has been diverging faster than other Class 1 HDACs, which implies that it has new functions. Additionally, HDAC8 proteins are not found in fungi but only in vertebrates. Hos3-like proteins also remain uncategorized having significant sequence divergence from mammalian HDACs (Gregoretti et al. 2004).

Class I, II and IV proteins require zinc for their catalytic function which hydrolyses the acetamide bond of acetylated lysine residues. Here, I would like to emphasize again the importance of the fact that the main classes of HDACs (which are named with a misnomer) originally occurred prior to the evolution of histones (Seto & Yoshida 2014). Many non-histone proteins with a variety of cellular functions are deacetylated by HDACs and the scale of this type of modification is on par with other major non-histone modifying proteins. Among these, it is notable that in *S. cerevisiae* DNA MethylTransferase 1 (DNMT1), a protein responsible for DNA methylation, is regulated by HDACs (Choudhary et al. 2009).

HDAC proteins themselves are regulated in many ways such as protein-protein interactions, PTMs (phosphorylation), alternative splicing as well as by more physical aspects like cellular localization or cofactor levels (Seto & Yoshida 2014). Incorporation of multiple HDAC proteins into complexes and self-associations are common (Gregoretti et al. 2004). Branching evolution is observed in the HDAC protein family which is possibly due to alternative splicing and many of these proteins are isoforms. Also, the catalytic region is well conserved and commonly duplicated (Seto & Yoshida 2014).

1.5.3 Drug therapies that target HATs and HDACs

Drugs targeting acetylation are a growing market for pharmaceutical companies treating cancer and other diseases since HATs and HDACs have many downstream targets and impact the expression of many genes (Zhang et al. 2009). Like other therapies for human disease, histone deacetylase inhibitor drugs that target human proteins have side effects which impact cohabiting fungal and bacterial colonies and may foster their drug resistance. Undesired reactions to HDAC inhibitors include cardiac toxicities, gastrointestinal effects and blood disorders (Afifi et al. 2015). In the case of fungal infections taking advantage of a compromised immune system, the dual effect on orthologous proteins of the human and indwelling fungal pathogens may be of benefit to the patient. However, given the complicated nature of this human/pathogen interface, it is important that the many aspects of this approach are carefully studied. Drugs targeting yeast can have secondary effects on the host and vice versa. In summary, given that the proteins of yeast and humans are considerably alike, it proves complicated to use this strategy to treat fungal infections without prohibitive side effects and understanding the specifics of targeting and elements of redundancy are key (Denning & Hope 2010).

1.5.3.1 Drug therapies that target HATs

HAT proteins have been associated with diseases ranging from neurological conditions to cancer. They have been shown to suppress and stimulate tumor growth, even within the same type of cancer cells. These proteins are thought to play a role in many aspects of normal development of embryonic, neuronal and skeletal systems (Wapenaar & Dekker 2016).

Drugs that target HATs (which include the common curcumin) need to target bi-substrate enzymes, since HATs themselves target Ac-CoA in conjunction with a lysine containing protein (Fig. 1.9) (Wapenaar & Dekker 2016).

Challenges of developing these drugs span from issues with substrate specificity (many HAT inhibitors have several mechanisms of action), molecular stability, low potency and complicated kinetics (Wapenaar & Dekker 2016). Research on HAT protein function and structure provides information for the development of drugs targeting these proteins. For example, translocations in HAT proteins have been connected to leukemia and lymphoma and it is suggested that inhibition of HAT proteins may be used to stop the proliferation of cancer cells (Sheikh et al. 2015).

Based on this research, new approaches to screening small molecules have been developed and inhibitors are identified (Falk et al. 2011). As a specific example, the HAT inhibitor, Garcinol, impacts DNA repair without affecting cell cycle checkpoint function and is designated for use as a radiosensitizer drug (Oike et al. 2012; Baell & Miao 2016). It has been shown to inhibit HAT dependent gene transcription specifically and it induces apoptosis in cancer cells (Balasubramanyam et al. 2004). This apoptosis is likely due to hypoacetylation and is shown experimentally as physical fragmentation of chromatin within the nuclei of HeLa cells. This fragmentation is comparable to the effects of treatment with the known apoptosis inducer hydrogen peroxide. This effect can be seen by Hoechst staining or by agarose gel electrophoresis of treated DNA samples (Balasubramanyam et al. 2004). The target of Garcinol is p300 and GCN5-like PCAF histone acetyl transferase proteins. In addition to histones, these HATs have non-histone targets that include transcriptional coactivators, transcription factors and HIV Tat proteins (Balasubramanyam et al. 2004; Kumar et al. 2001; Bonaldi et al. 2003; Balasubramanyam et al. 2003; Kaehlcke et al. 2003; Brès et al. 2002). Garcinol also affects PCAF HATs more strongly than p300. It was found that p300 dependent acetylation of histone H4 was completely inhibited but H3 inhibition was not, even with the application of 20x the normal dosage. Combination treatment with histone deacetylase inhibitors is more effective. For example a combination of Trichostatin A or sodium butyrate treatment combined with Garcinol inhibits acetylation in histones H4 and H2B however, Garcinol alone does not decrease acetylation levels (Balasubramanyam et al. 2004).

1.5.3.2 Drug therapies that target HDACs

HDAC proteins are involved in signaling pathways that impact heart development, as well as muscular and skeletal functions (Haberland et al. 2009). HDAC proteins are linked to a number of health-related issues including cancer, and central nervous system conditions such as Alzheimer’s disease (Volmar et al. 2017; Ropero & Esteller 2007; Kazantsev &

Thompson 2008). These proteins have roles in cellular development, proliferation, cell cycle regulation, promoter silencing and DNA translocations (as reviewed in Timmermann et al. 2001).

Additionally, there is growing use of HDAC inhibitor drugs as combination treatment for fungal infections in humans (Behera & Sinha 2015). As discussed in Section 1.2.9, growing resistance to the relatively small pool of available drugs for treating fungal infections is a challenge. To this end, it is shown that suberoylanilide hydroxamic acid (SAHA) and uracil based hydroxamates that inhibit HDAC enzymes can be used in conjunction with fluconazole to address issues of resistance (Mai et al. 2007).

The functional properties of histone deacetylase inhibitors have been defined based upon research on the common model organisms including yeast. Given their potential for development as medical treatments, it is important that this knowledge undergo focused development to understand the function of these proteins in pathogens. Future drug designs that successfully target fungal infections must minimize side effects while effectively targeting these pathogens within the human host's immune system environment. If standalone treatments are not enough to quell these infections, drugs may be used as combination treatments.

1.6 Chromatin modifiers in *C. albicans*: HATs and HDACs

C. albicans have many of the same histone modifications as other organisms, including methylation, acetylation, sumoylation and ubiquitination. Interestingly, the yeast and hyphal forms of *C. albicans* present different levels of methylation: hyphae have been shown to have lower levels of cytosine methylation (Russell et al. 1987). This section covers the proteins known to be involved in acetylation and deacetylation in this pathogenic yeast. These proteins have roles in morphological aspects that contribute to virulence and consequently they are of interest as drug targets.

1.6.1 *C. albicans* HAT proteins

Based upon sequence homology HAT proteins can be classified in three groups: Gcn5 family, the MYST family and others (Lee & Workman 2007). In *C. albicans* Gcn5 is the only protein known to fall under the first designation; it is essential for hyphal development and is induced by serum. This is perhaps due to its role in cell wall stress response (Chang et al. 2015).

The *C. albicans* Gcn5 protein changes its cellular localization in response to cellular growth state staying in the cytoplasm during growth and active cell division stages while moving to the nuclei during stationary phase (Chang et al. 2015). This HAT domain is very conserved (92 % identity) and the bromodomain of Gcn5 also has similarity (59 % identity) to the *S. cerevisiae* ortholog (Chang et al. 2015). The Gcn5 family of HAT proteins is responsible for acetylation that affects gene transcription and while targets in *C. albicans* have not been investigated, a good bit is known about *S. cerevisiae* Gcn5 which participates in the complexes SAGA, SILK and ADA and works with transcriptional activators (Grant et al. 1999; Utley et al. 1998; Pray-Grant et al. 2002; Chang et al. 2015; Strahl & Allis 2000). SAGA transcriptionally regulates ~10 % of the yeast genome through recruitment of RNA polymerase-II and other transcriptional machinery (Bonnet et al. 2014). The SAGA, SILK and ADA complexes all have somewhat overlapping and distinct functions and acetylation targets (Wittschieben et al. 2000; Pray-Grant et al. 2002). These complexes effect acetylation on free histones as well and target H2B (K11, K16), H3 (K9, K14, K18, K23, K27, K36) and H4 (K8, K16) (Cieniewicz et al. 2014; Suka et al. 2001; Zhang et al. 1998).

To engage hyphal elongation, *C. albicans* Gcn5 functions in conjunction with Esa1, a MYST family HAT. Esa1 is essential for filamentous growth, growth at high temperatures (37 °C) and hyphal initiation (Wang et al. 2013). The MYST domain of the *C. albicans* Esa1 protein is conserved (86 % identity) from *S. cerevisiae* with one additional insertion present. The chromodomain of Esa1 however, does not show much similarity. In contrast to Gcn5 the localization of Esa1 is consistently nuclear (Chang et al. 2015). Other *C. albicans* MYST family HATs include Something About Silencing proteins Sas2, and Sas3.

Other *C. albicans* HAT proteins include: Histone AcetylTransferase (Hat1), ELongator Protein 3 (Elp3), and Histone and other Protein Acetyltransferase 3 (Hpa3) whose orthologs in humans are grouped into the Gcn5 family (Sterner & Berger 2000; Nathan et al. 2006). *C. albicans* also has an ortholog of Rtt109 which acetylates histone H3 lysine 56 (Lopes da Rosa et al. 2010). The protein has four catalytic domains which are conserved relative to *S. cerevisiae* (Lopes da Rosa et al. 2010). *S. cerevisiae* Rtt109 also acetylates this site (H3K56) which has a role in localizing chromatin domains. It also targets other H3 sites (K14, K28, K27) and functions in complex with Vps75 and Asf1 to acetylate additional targets (H3K9, H3K23, H4K12 and H3K56 respectively) (Abshiru et al. 2013). *C. albicans* Rtt109 has roles in pathogenicity; Rtt109 homozygous mutant cells

are less pathogenic in mice and have increased susceptibility to killing by macrophage (Lopes da Rosa et al. 2010). Homozygous mutants in Rtt109 also show decreased white-opaque switching (Stevenson & Liu 2011).

1.6.2 *C. albicans* HDAC proteins

In total, eleven types of HDAC proteins are characterized in *C. albicans.*

Class I HDACs includes: Reduced Potassium Dependency Rpd31, Rpd32, Hos1 and Hos2. Rpd31 and Rpd32 (referred to as simply 'Rpd3' in early literature publications), which are both orthologs to *S. cerevisiae* Rpd3. Class I histone deacetylase Rpd31 works in complex with transcriptional corepressor Ssn6 to suppress hyphae and separately on its own to support filament development. Both of these proteins (Rpd31 and Ssn6) are necessary for the expression of Ume6 (Lee et al. 2015). The two histone deacetylase proteins Rpd3 and Rpd31 work together to affect the expression of the *WOR1* gene. In *C. albicans* (WO-1 strain; MTLα mating type), loss of either of these genes contributes opposing change in the white-opaque switch (see Fig.1.11). This functional difference is attributed to the unique C-terminal domain regions of Rpd3 and Rpd31. Also, it should be noted that interaction of these proteins with DNA has not been shown (Xie et al. 2016; Srikantha et al. 2001). The role of Hos1 is not understood (Garnaud et al. 2016). An *in vitro* enzymatic assay with purified *C. albicans* Hos2 protein showed that it functions to deacetylate tubulin but not histones (Karthikeyan et al. 2013; Srikantha et al. 2001; Garnaud et al. 2016).

Class II includes Hda1 and Hos3. Deletion of Hda1 does not affect the transcript levels of any Class I or Class II HDACs (Srikantha et al. 2001). While *C. albicans* Hda1 has been studied in some detail, the role of Hos3 is less defined (see Section 1.5.2).

Class III includes NAD+ dependent sirtuins Sir2, Hst1, Hst2 and Hst3. Sir2 deacetylates specific lysine residues of histones and is important for gene silencing at the repetitive nucleotide sequences at the end of chromosomes (telomeres) and this is dependent on environmental conditions (Srikantha et al. 2001; Freire-Benéitez et al. 2016a). In *S. cerevisiae* Hst1 functions in a complex with HDACs Hos2 and Set3 that impacts sporulation but in *C. albicans* it has a roles in white-opaque switching, filamentation and virulence (Pijnappel et al. 2001; Hnisz, Sehwarzmüller, et al. 2009; Hnisz et al. 2010). Hst3 modulates acetylation at H3K56 where it acts in interplay with HAT Rtt109 (Wurtele et al. 2010).

C. albicans Set3 is another histone deacetylase that is free standing from the Class designations. In *S. cerevisiae* Set3 is a fungal specific HDAC which forms a seven subunit complex made up of four core units and three histone deacetylase proteins (Hst1, Hos2 and Set3) which binds methylated H3K4 to recruit Set3C complex (Kim et al. 2012). The complex is conserved in *C. albicans* and it has roles in biofilm dispersal and antimicrobial drug resistance (Nobile et al. 2014; Hnisz et al. 2012). Set3 mutants show a hyper-filamentous phenotype (Hnisz et al. 2012)

1.7 Hda1 in *C. albicans*

The *C. albicans* Hda1 protein is known as a transcriptional regulator, an inducer of filamentation, regulator of white-opaque switching and it has greater expression in white cells. Deletion of *HDA1* is shown to decrease the occurrence of morphological switch from white-opaque and stunt hyphal development in *C. albicans* (Zacchi et al. 2010; Lu et al. 2011; Srikantha et al. 2001; Klar et al. 2001).

1.7.1 Hda1 role in white-opaque and opaque-white switching

HDA1 reportedly shows an even stronger morphological phenotype than *RPD31* when deleted. Its deletion dramatically increases the white-opaque switching frequency of *C. albicans* but it has no effect on opaque-white switching (Srikantha et al. 2001; Klar et al. 2001). This contrasts with the deletion of *RPD3* which increases switching in both directions. Expression of Hda1 or Rpd3 does not affect phase regulated expression of each other, Hos1, Hos2 or Hos3 (Srikantha et al. 2001). It has also been shown that deletion of *HDA1* considerably decreases expression of the Efg1 protein in white phase cells (Srikantha et al. 2001). This is important because Efg1 is essential for a portion of the phenotypic traits that distinguish white-phase cells and it is thought to be downstream of the gene responsible for the switch, *WOR1* (Srikantha et al. 2000). This implies a major role for Hda1 in suppressing white-opaque switching which is also supported by a study showing that cells which are homozygous mutants for Hda1 have a phenotype like trichostatin-A treated cells. Trichostatin-A is a histone deacetylase inhibitor. Treatment of *C. albicans* cells with trichostatin-A causes an increased white-opaque but not opaque-white switching (Klar et al. 2001).

Several other histone deacetylase genes are involved in white-opaque switching. *HOS1*, *HOS2* and *HOS3* are down regulated in opaque cells. Conversely, it has been shown that *HOS1* and *HOS2* have greater expression in white cells. These white and

opaque morphological states are all inherited by daughter cells (see Fig.1.11) (Srikantha et al. 2001).

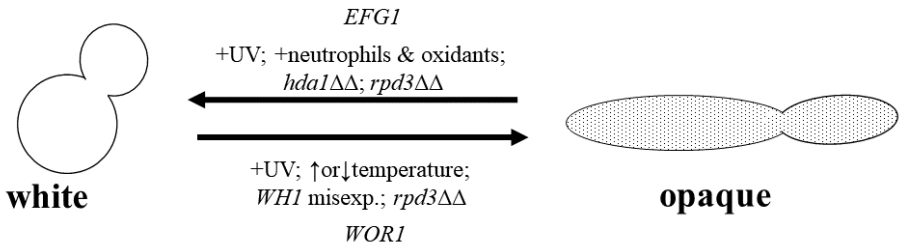

Figure 1.11 Effectors of white-opaque switching in *C. albicans*
Genes and environmental conditions that promote white-opaque and opaque-white switching in *C. albicans* [Adapted from Srikantha et al. 2001, Figure 9; Scaduto & Bennett 2015, Figure 1]

Interestingly, it has been noted that *SET3* is epistatic to *HDA1* and *RPD3*. deletion of the *SET3* gene suppresses the effect of deleting *HDA1* extinguishing its impact on white-opaque switching. The same effect is shown in *rpd3*ΔΔ mutants for which the increase of bi-direction switching is also suppressed by deletion of *HOS2* (Hnisz, Schwarzmüller, et al. 2009).

1.7.2 Hda1 role in *C. albicans* yeast-hyphae and hyphae-yeast transitions

Deleting *HDA1* has been shown to stunt development of hyphae when cells are grown on inducing solid medias at high temperature (M199 with pH 8, SLAD, Spider, and with 10 % serum; 37 °C) and embedded in solid media (23 °C) as well as in liquid medias (M199 with pH 8 and Spider; 3 hours 37 °C) (Lu et al. 2011; Zacchi et al. 2010). The fact that this phenotype is seen in liquid and solid conditions and with various inducers of filamentation confirms that Hda1 plays a role in hyphal development across many conditions (Fig. 1.12). Brg1 recruits Hda1 to hyphae-specific promoters yet Brg1 is not sufficient for the transition to hyphae (Lu et al. 2011).

Suggested mechanisms by which Hda1 may affect filamentation include exerting effects: (1) on positive and negative transcriptional regulators of hyphae development; (2) on filamentation regulators; (3) by deacetylation of non-histone proteins with direct and indirect effects on hyphae development (Zacchi et al. 2010; Glozak et al. 2005; Lu et al. 2011).

One mechanism for hyphae formation in *C. albicans* involves the recruitment of Hda1 by Brg1 and subsequent deacetylation of a subunit of the non-histone protein and

HAT, NuA4. A series of events take place which are triggered by environmental conditions. First, Nrg1 is inhibited through the cAMP-PKA pathway leading to histone disassembly at specific regions in hyphal gene promoters. This occurs at upstream activator regions that contain Nrg1 and Brg1 binding motifs. Brg1 has a homolog in *S. cerevisiae*, Gat2 which belongs to the GATA family of transcription factors, named for their ability to bind specific sequences in DNA (Lu et al. 2012). Initiation of hyphal development requires the disappearance of Nrg1 through activation of the cAMP-PKA pathway. This can be triggered by several environmental factors including increase of temperature to 37 °C, application of rapamycin or starvation (Lu et al. 2011). If conditions are conducive, this signal is maintained and suppresses the levels of Target of Rapamycin (Tor1) and this leads to the extinguishing of Nrg1 promoter access through recruitment of Hda1 (Fig.1.12).

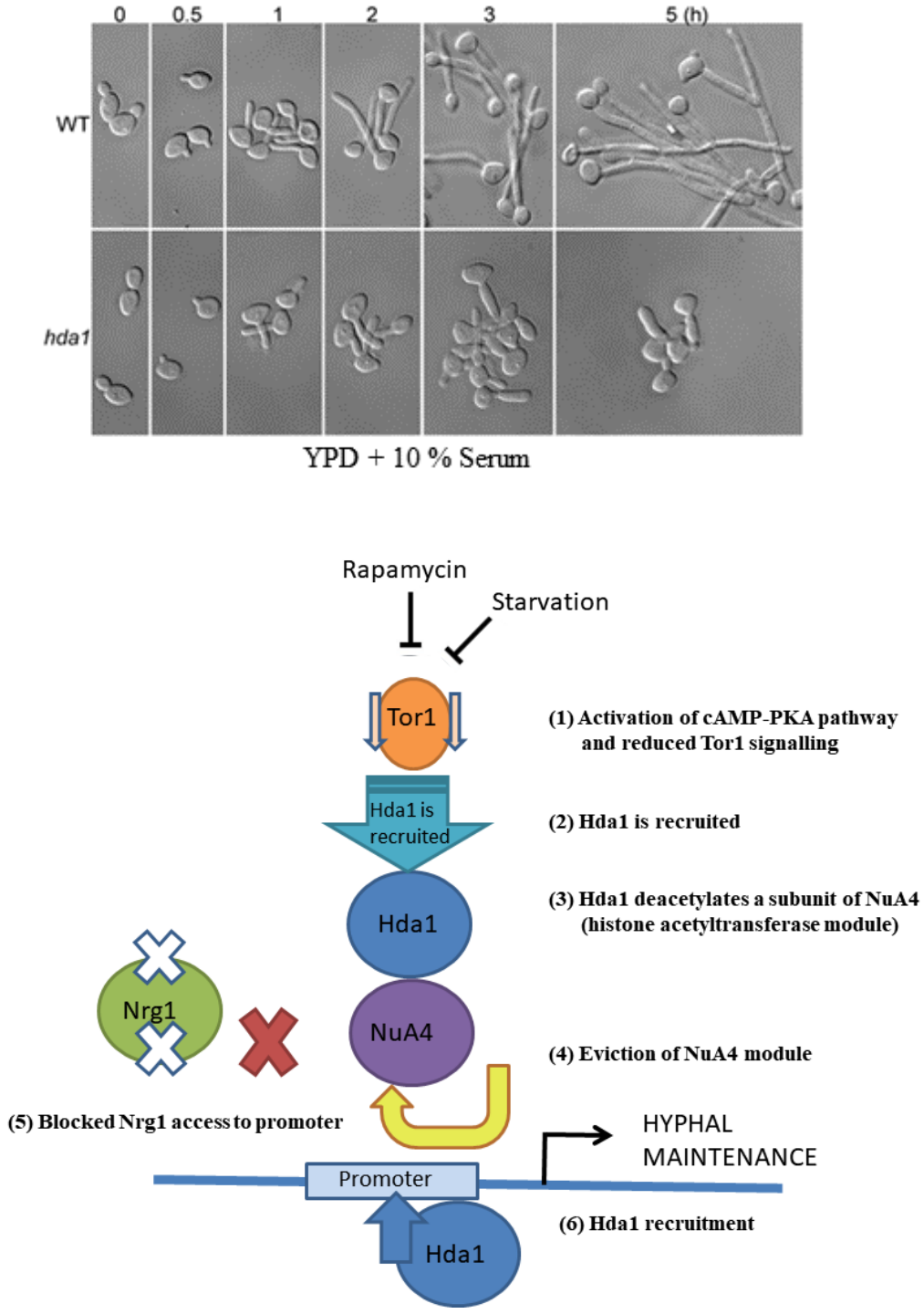

Figure 1.12 Phenotype of stunted hyphal development in *hda1*ΔΔ and model showing the molecular pathway for hyphal maintenance via Hda1 activity in *C. albicans*
(Top) Comparison of wildtype and *hda1*ΔΔ strains grown in filamentation inducing YPD + 10% serum at 37 °C; **[**Adapted from Figure 3 Lu et al. 2011]
(Bottom) Model showing the steps following activation of Tor1 pathway that support hyphal maintenance; [Adapted with extensive changes from Figure 9 in Lu et al. 2011]

Due to the environmental condition, the second step occurs which secures hyphal maintenance. Levels of Tor1 signaling become reduced (this can be simulated through Rapamycin exposure or other triggers which target Tor1) which allows for cell elongation through recruitment of Hda1 by transcription factor Brg1 and subsequent elongation of the yeast cell. Hda1 and Brg1 are required for the maintenance of hyphal development. Hda1 deacetylates a subunit of NuA4 acetyltransferase (Yng2). With this acetyltransferase gone, Nrg1 no longer has access to the region of DNA. This reinitiates the cycle of events. The repositioning of nucleosomes through chromatin rearrangement is fundamental to these events. The presence of Hda1 is also critical as it blocks the binding of Nrg1 (Lu et al. 2012). Figure 1.13 shows the occupancy of Hda1 and Nrg1 at the *HWP1* promoter during hyphal induction.

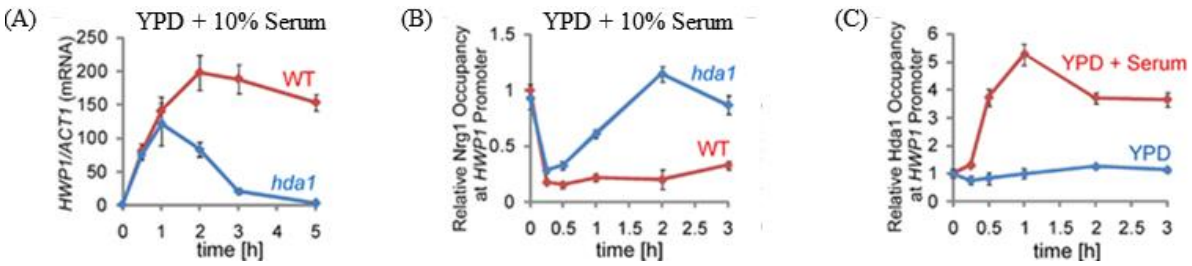

Figure 1.13 Evaluation of Hda1 and Nrg1 occupancy at the hypha-specific HWP1 promoter
(A) Expression of *HWP1* during hyphal induction is decreased in the *hda1*ΔΔ mutant strain (B) Nrg1 binds *HWP1* promoter in *hda1*ΔΔ during hyphal induction (C) Hda1 binding at *HWP1* promoter is serum dependent; [Adapted from Lu et al. 2011]

A downstream positive feedback loop governed by Brg1 targets Ume6 to perpetuate the effect (Lu et al. 2012; Lu et al. 2011). Brg1 also binds the hypha-specific expression and relatedness to G1 Cyclins (*HGC1*) protein during hyphal elongation. These proteins interact with Cdc28 to impart growth of yeast buds and participate in septin Cdc11 phosphorylation (Sinha et al. 2017; Zheng et al. 2004). Hgc1 is a hyphae specific G1 cyclin related protein which has roles in biofilm formation, it is necessary for hyphal growth and its deletion also impacts virulence (Zheng et al. 2004; Banerjee et al. 2013; Skrzypek et al. 2017). Cdc28 is a cyclin-dependent protein kinase that functions together with Hgc1 to phosphorylate Efg1 and this mark regulates cell separation (Wang et al. 2009; Skrzypek et al. 2017). It is involved in the regulation of many transcription factors that control morphology and have roles in polarized growth (Umeyama et al. 2006). Cdc11 is a septin protein which when deleted causes defects in bud growth and cytokinesis

and invasive growth. Mutants in this protein also form abnormal curved hyphae (Martin et al. 2005; Warenda et al. 2003; Frazier et al. 1998). While Ume6 is not necessary for Hda1 recruitment, a mutation of the gene decreases its overall promoter association. Constitutive expression of *UME6* (and not *BRG1*) can overcome the hyphal growth defect in a *hda1* homozygous mutant (Lu et al. 2012). *UME6* is a key regulator of hyphal development which functions through *HGC1* and other regulators (Banerjee et al. 2008). High expression of *UME6* causes increased tissue invasion by *C. albicans* cells *in vivo*. It also increases the development of hyphae related biofilm development *in vitro* (Banerjee et al. 2008).

1.7.3 Hda1 role in drug resistance

In *S. cerevisiae* Hda1 and Rpd3 cooperate to regulate Hsp90 deacetylation which controls drug resistance. Posttranslational modifications also likely modulate HSP90 (Robbins et al. 2012). It is notable that Li et al., 2014 showed that deletion of *RPD3* or *HDA1* in combination with low expression of efflux genes *CDR1, CDR2, MDR1* and FLUconazole resistance 1 (*FLU1*) (<50 % of the wildtype (WT) strain) caused sensitivity to azoles (Li et al. 2014). A more recent study from the same author (2017) on azole resistance in *C. albicans* showed that K30 and K271 are critical acetylation sites on Hsp90 in terms of the proteins ability to act as a chaperone. Strains mutated at these sites experience decreased virulence (these mutant strains mimic constitutive acetylation or deacetylation). The paper notes that many HDAC proteins interact with *HSP90* including: Hos2, Hda1, Rpd3, Rpd31 and that these proteins all mediate azole tolerance. An *erg3* homozygous mutant strain was used in this experiment, this mutant does not produce a toxic intermediate in response to azole exposure and its resistance is Hsp90 dependent. Deletion of *HOS2, HDA1, RPD3* or *RPD31* or all combinations of the genes did not reduce azole resistance but only when all four genes were deleted was the resistance lost. The paper concludes that the impact of HDACs on *HSP90* its through chaperone function and that additional lysine residues are likely involved in this effect. The complexity of this system of drug resistance presents important considerations that can inform approaches to pharmaceutical targeting of these mechanisms (Li et al. 2017).

1.7.4 Hda1 role in Tup1 specific repression

In *S. cerevisiae* the Tup1 protein interacts with Hda1 to regulate localized histone deacetylation. Consequently, many targets of Tup1 including *Exitus NAtru* (Latin, "exit sodium") 1 (Ena1) are also targets of Hda1. Also, Hda1 has specific activity at the

promoters of Tup1 regulated genes (Jiansheng Wu, Suka, et al. 2001). Deletion of Hda1 (or Tup1) results in hyperacetylation at the Ena1 promoter. Deacetylation happens by both Hda1 and Rpd3 on different histones at the *ENA1* promoter (H3/H2B and H4/H3 respectively) and the activity of both these proteins is required for full repression of the *ENA1* gene (Jiansheng Wu, Suka, et al. 2001). If this relationship exists in *C. albicans* is currently unknown.

A study that evaluated transcriptional profiling of *C. albicans* ortholog of Tup1 found that it is targeted to different sets of genes by two repressors, Mig1 and Nrg1 which have distinct roles in stress response, metabolism and morphogenesis (Murad et al. 2008). These findings support the hypothesis that *C. albicans* Tup1 has a similar role to its ortholog in *S. cerevisiae* which interacts with Ssn6 as a global repressor (Redd et al. 1997).

Several roles of Tup1 in *C. albicans* are known, homozygous mutants in the *TUP1* gene do not white-opaque switch but rather undergo distinctive filamentation switching sequence at the colony level which displays 'large fuzzy' (mostly hypha) colonies followed by small (pseudo hypha) and then smooth (budding yeast) colonies which finally revert to small fuzzy pseudo-hypha morphology. This sequence of phenotypes is also observed at the cellular level. *TUP1* upregulation causes the rapid switching of colonies to opaque phase and Tup1 may be necessary for the white-opaque transition (Zhao et al. 2002).

The Ena1/Ena2 protein is a sodium efflux pump which affects many different types of substrates (Skrzypek et al. 2017; Lamb & Mitchell 2003). In *S. cerevisiae* Rim101 indirectly activates Ena1 in conditions of alkaline pH or salt concentrations by repressing Nrg1 which encodes a Tup1-dependent transcriptional repressor of Ena1 (Lamb et al. 2001; Lamb & Mitchell 2003). The control of Ena1 is not conserved between *C. albicans* and *S. cerevisiae*. In *C. albicans* (wherein Ena1 is named Ena2) the protein is not regulated by Nrg1 (which is the case in *S. cerevisiae*). The role of the Rim101 pathway during alkaline pH in *C. albicans* is to adapt to iron deplete environments and this pathway is parallel and distinct from the Nrg1 pathway (Bensen et al. 2004).

1.8 Yeast Hda1 complex proteins: structures and interactions

As mentioned in Section 1.5.2, HDAC proteins often form complexes. While it has not been shown that *C. albicans* Hda1 participates in a complex, similar proteins in *S. cerevisiae* and *S. pombe* do. Comparisons made between yeast species such as *C. albicans*

and the common model yeasts such as *S. cerevisiae* need to be kept in perspective. It is key to keep in mind that they "last shared a common ancestor more than 900 million years ago; in terms of conserved coding sequences, the two species are approximately as divergent as fish and humans" (Herndayet al. 2010). This message is challenging to remember when one is digging for information from a relatively dry genome database of the newer model organism, *C. albicans*. This section discusses the existing structural information from orthologs for Hda1 in *S. pombe* (Clr3) as well as Hda1 and Histone DeAcetylase 3 (Hda3) in *S. cerevisiae* along with what is known about the Hda1, Histone DeAcetylase 2 (Hda2) and Hda3 proteins in *S. cerevisiae* and *C. albicans*. The *C. albicans* Hda2 and Hda3 proteins are of particular interest given that they are fungal specific and Hda2 is almost entirely uncharacterized (Finn et al. 2016).

1.8.1 The *S. cerevisiae* Hda1 complex

Information about *C. albicans* histone deacetylase protein structure may be derived by comparison to solved structures from similar proteins in the model yeast *S. cerevisiae*. Currently, the only actual structural information available is for the *S. cerevisiae* Hda1 Arb2 domain and Hda3 DNA binding domain. Three different proteins make up the *S. cerevisiae* Hda1 Complex: a dimer of Hda1 interacting with Hda2 and Hda3 proteins (Fig. 1.4) (Carmen et al. 1996). Given that all these proteins are named 'histone deacetylase', it is important to keep two points in mind: (1) that Hda1 participates in deacetylase activity on non-histone proteins and (2) Hda2 and Hda3 do not have catalytic deacetylase domains. The domains of all three proteins are discussed in detail in Chapter 3.

Interactions between the *S. cerevisiae* Hda1 complex proteins are necessary for its function *in vitro*, if any of the components are mutated, its deacetylase activity is disrupted (J Wu et al. 2001). As shown in Figure 1.14, stoichiometry of the complex is a hetero-dimer of Hda2 and Hda3 associating through C-terminal coiled-coil domains with a homo-dimer of Hda1 by the deacetylase domains (Lee et al. 2009; Jiansheng Wu, Carmen, et al. 2001). This was shown through a protein pull down experiment which showed interaction between all of these proteins (Hda1 with Hda2 or Hda3 and Hda2 with Hda3 in the absence of Hda1) (J Wu et al. 2001).

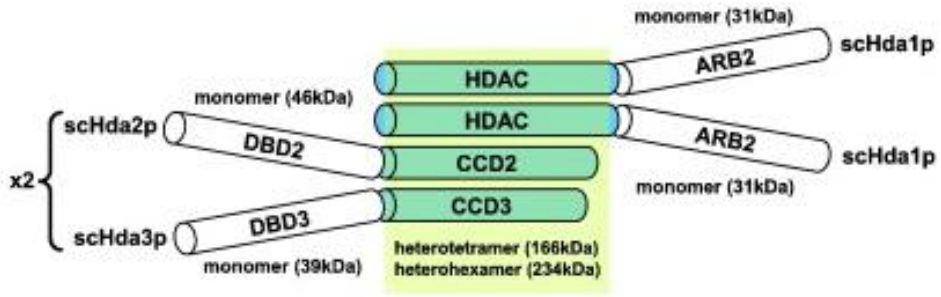

Figure 1.14 Interaction between Hda1 complex proteins in *S. cerevisiae*
Illustration of domains and stoichiometry observed for the Hda1, Hda2 and Hda3 [Adapted from Lee et al. 2009]

Three components of this complex are fungal specific, the Hda1 Arb2 domain, Hda2 and Hda3 (Finn et al. 2016; Gashaw et al. 2011; Lee et al. 2009; Geer et al. 2010). While *S. cerevisiae* Hda1 is shown to dimerize in the absence of Hda2 and/or Hda3, it is reported that the strongest interaction is between Hda1 and Hda3, 10x stronger than Hda1 and Hda2 interaction; Hda3 and Hda2 are shown to interact at a 60X greater level. This analysis led to the conclusion that *S. cerevisiae* Hda1 does not interact with Hda2 in the absence of Hda3 (Kanta et al. 2006). It has also been observed that the complex can take heterotetramer or heterohexamer form based on the availability of Hda2 and Hda3 (Lee et al. 2009).

It is proposed that in *S. cerevisiae* dimeric Hda1 allows for deacetylation of the duplicate histone proteins present in the nucleosome octamer, while Hda2 and Hda3 function to either structurally activate the dimer or recognize histones themselves. Whole-cell acetylation levels are greatly reduced upon deletion of any of these proteins and consequently the whole complex is thought to be necessary for Hda1 activity. It is known that these proteins are necessary for deacetylation at H3 and H2B sites at *ENA1* and *GAL10* (*TUP1* regulated) promoters. Also, a phosphopantetheine attachment site (residues 570-585) in Hda2 suggests an acetyl group carrier role for the protein (Jiansheng Wu, Carmen, et al. 2001).

1.8.2 *S. cerevisiae* Hda1 protein interactions and Arb2 domain structure

There is one documented transcriptional regulator of *S. cerevisiae* Hda1 during cellular response to heat: *TFC7* (Venters et al. 2011; Cipollina et al. 2008). *TFC7* is an RNA Pol III transcription initiation factor complex subunit which binds DNA at promotors of *tRNA* genes (Manaud et al. 1998). There are 28 proteins with evidence of physical interactions with Hda1 and 715 proteins have genetic interaction with Hda1 (total genetic interactions = 756; (additional genes have both physical and genetic interactions) (Skrzypek et al.

2017). Aside from Hda2 and Hda3, the physical interactions are from high-throughput experiments: two-hybrid, affinity capture- RNA, affinity capture- MS or biochemical activity (Pho85 and Tos3), experiments. Also, some physical interactors are identified through manually curated experiments: reconstituted complex, biochemical activity, two-hybrid or co-localization experiments. Most manually curated interactions were with histones but interactions with Sin3 and Tup1 are also reported. Pho85 is a cyclin-dependent kinase it has roles in regulating nutrient levels, environmental conditions, and cell cycle progression. Tos3 is a protein kinase that activates Snf1 which is another protein kinase that regulates *C. cerevisiae* filamentous growth. The genetic interactions are all from high-throughput experiments: synthetic rescue, phenotypic enhancement, synthetic growth defect, synthetic lethality, dosage lethality negative genetic, positive genetic experiments and manually curated: synthetic rescue, dosage lethality, synthetic growth defect, synthetic lethality, phenotypic suppression, phenotypic enhancement experiments.

13 phenotypes for HDA1 are published in *C. albicans* on the *Candida* Genome Database which are growth, white-opaque switching and filamentation related (Skrzypek et al. 2017). 17 phenotypes for HDA1 are published in *S. cerevisiae* on the *Saccharomyces* Genome Database these include decreased and increased responses to metals, chemical compounds and antifungals (Skrzypek & Hirschman 2011).

The Arb2 protein domain was originally characterized in the fission yeast *S. pombe* Arb2 protein (Buker et al. 2007). It is found in the Argonaute siRNA Chaperone (ARC) complex. This complex encompasses two other proteins (Arb1 and Aro1) and has roles in H3K9 methylation, heterochromatin assembly and generating siRNA. Arb2 is likely necessary for siRNA generation and RNAi-mediated heterochromatin assembly (Buker et al. 2007). Northern blot analysis with probes that hybridize to centromeric siRNAs show that ARC contains siRNAs since ~25 nucleotide species were seen in blots of purified Arb1, also no centromeric siRNA was observed in total RNA blots with *arb1*Δ and *arb2*Δ cells. In addition, immunofluorescence experiments show that Arb1 and Arb2 co-localize to centromeric heterochromatin and other foci in the nucleus and cytoplasm of cells (Buker et al. 2007).

As discussed, one of the issues with targeting HDACs by drug treatments is the conservation of these proteins and resulting side effects due to their homology. The ideal approach for targeting fungal infections with drugs is to identify domains which are unique to fungi to eliminate the potential side effects to the human host. The Arb2 domain is fungal specific and occurs in unique combination with a deacetylase catalytic domain.

This is why its drug-ability should be explored as a target for the development of new anti-fungal drugs (Gashaw et al. 2011). It is noteworthy that some similar domains do occur as a component of other types of proteins in humans which may complicate approaches to drug development (Li et al. 2010).

At the start of this project the structure of the Hda1 Arb2 was not characterized. It has since been defined in *S. cerevisiae* (Shen et al. 2016). In 2016 the structure of the Arb2 domain of *S. cerevisiae* Hda1 was characterized. Figure 1.15 shows overall current structural information for the Hda1 ARgonaute Binding Arb2 domain. This is the only solved structural portion of the *S. cerevisiae* Hda1 protein. The crystal structure of this protein and pull down assays show that a dimer of the domains has the ability to bind unmodified histones *in vitro* by dimerizing to form a functional "V" shaped groove (Shen et al. 2016).

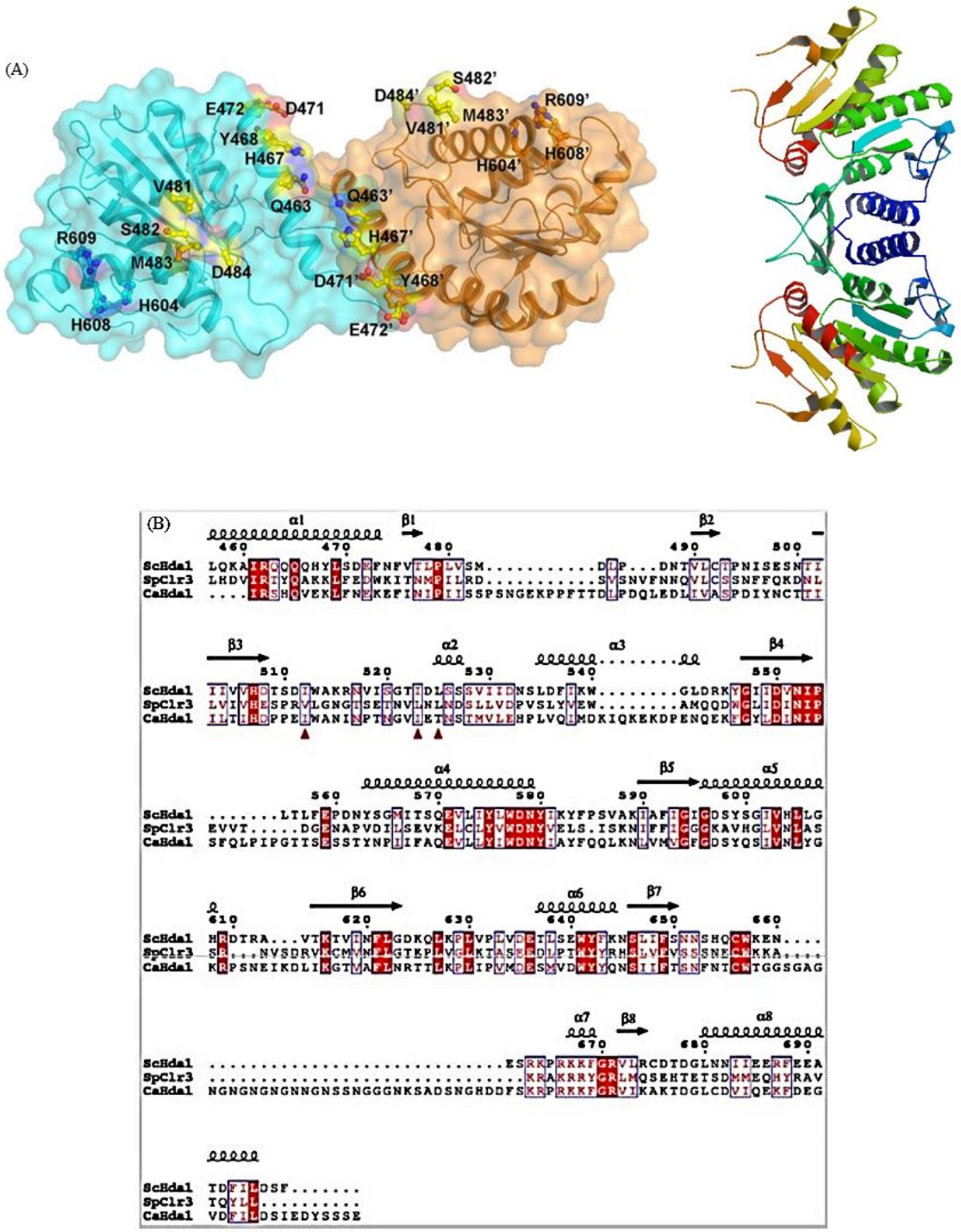

Figure 1.15 Combined Arb2 domain inverse "V" structured complexing, model of secondary structure and sequence comparison of Hda1 ortholog Arb2 domain of *S. cerevisiae*, *S. pombe* and *C. albicans*

(A) At left: Isothermal titration calorimetry image of the *ARB2* domain; red and blue lobes indicate two separate Arb2 domains which are joined and amino acids key to the interaction are labeled; At right: Hda1 Arb2 domain features α-helices and beta strands (PDB: 5J8J) (B) Alignment of Hda1 Arb2 domains from *S. cerevisiae*, *S. pombe* and *C. albicans*; [adapted from Shen, et al., 2016]

Shen et al. (2016) propose that Hda1 works with Hda2 and Hda3 to not only deacetylate histones but as a histone chaperone, affecting chromatin remodeling. They base this hypothesis on two points: (1) The protein orthologous to Hda1 in *S.* pombe, Clr3 complex recruits helicase Mannose Inositolphosphoceramide Transferase 1 (Mit1) and participates in both histone deacetylation and chromatin remodeling (Sugiyama et al. 2017) and (2) Hda2 and Hda3 have sequence similarities to helicase enzymes (Swi2/Snf2 of Rad54 family enzymes) (Shen et al. 2016; Lee et al. 2009).

Still, there are good reason for ongoing interest in solving the structure of the *C. albicans* Hda1 Arb2 domain; namely, that the protein is significantly distinct from its non-pathogenic *S. cerevisiae* homolog. The structure of *C. albicans* Hda1 Arb2 domain has not yet been solved (see Chapter 3).

1.8.3 *S. pombe* Clr3 complex structures

Information about *C. albicans* Hda1 protein structure may also be derived from existing data for similar proteins in the model yeast *S. pombe*, Clr3. The Clr3 complex is known as SHREC. It *S. pombe* consists of a Snf2 chromatin remodeler: Mit1, and a HDAC protein: Clr3. This is an evolutionarily conserved motif combination (Snf2 domain and HDAC domain) and their function may be cooperative, but their physical connection is not necessary. Mit1 contains a PHD binding domain, chromodomain and Clr3 is known to localize to centromeres and is involved in global transcription regulation. SHREC interacts with euchromatic DNA directly based on sequence-specific targeting (Job et al. 2016). Structural information is available for Clr3 yet no specific orthologs for *C. albicans* Hda2 or Hda3 exist in *S. pombe* and Clr3 interacts with proteins that are different. (see Section 1.8.2).

1.9 *C. albicans* and *S. cerevisiae* Hda2 interactions

It has been shown in *S. cerevisiae* that Hda2 responds quickly to hypoxia by re-localizing to the cytosol (Dastidar et al. 2012). Deletion of *S. cerevisiae* Hda2 has also been shown to make telomere length shorter (Askree et al. 2004). The only documented regulator of *S. cerevisiae* Hda2 is transcription factor ARS-Binding Factor 1 (*ABF1*) which was identified by computational analysis of sequence motifs that correspond to the DNA-binding specificity with proteins from chromatin immunoprecipitation experiments (MacIsaac et al. 2006; Skrzypek et al. 2017). *ABF1* is a DNA binding protein with roles in transcriptional activation, gene silencing, chromatin remodeling, DNA replication and

repair. There are 115 proteins with evidence of physical interactions with Hda2 and four of these proteins also interact genetically (total genetic interactions = 131) with the protein (Skrzypek et al. 2017). Aside from Hda1 and Hda3, the physical interactions were shown through high-throughput experiments: two-hybrid, affinity capture RNA, affinity capture MS or biochemical activity (phosphorylated residue: Ime2 and Yck2) experiments. The genetic interactions are also from high-throughput experiments: synthetic rescue, synthetic growth defect, synthetic lethality, dosage lethality, positive genetic and negative genetic assays while manually curated experiments included: synthetic rescue, synthetic growth defect, synthetic lethality, phenotypic suppression and phenotypic enhancement.

In *C. albicans,* there is no substantial information about the phenotypes of *HDA2*. A random transposon mutagenesis study shows that *HDA2* is not essential (Nobile et al. 2003). Homozygous mutants of *C. albicans HDA2* also show a phenotype of sensitivity to propolis, a natural compound which inhibits yeast-hyphal transitions (De Castro et al. 2013). 21 phenotypes for *HDA2* are published in *S. cerevisiae* on the *Saccharomyces* Genome Database these include decreased and increased responses to chemicals, chemical compounds and antifungals (Skrzypek & Hirschman 2011).

No portion of Hda2 structure has been solved in either *S. cerevisiae* or *C. albicans.*

1.10 *C. albicans* and *S. cerevisiae* Hda3 interactions and structure

It has been shown in *S. cerevisiae* that like Hda2, Hda3 responds quickly to hypoxia by re-localizing to the cytosol (Dastidar et al. 2012). There are five documented transcriptional regulators of Hda3: LEUcine biosynthesis 3 (*LEU3*), MEDiator complex 2 (*MED2*), *MED4*, Split Finger Protein 1(*SFP1*) and *Xho*I site-Binding Protein 1 (*XBP1*). These regulators act on Hda3 during cellular response to acute heat shock (*LEU3*, *MED2* and *MED4*) or following glucose pulse (*SFP1*) (Venters et al. 2011; Cipollina et al. 2008). *LEU3* is involved in the SAGA pathway where it regulates genes involved in amino acid biosynthesis and ammonia assimilation. *MED2* and *MED4* are subunits of the RNA polymerase II mediator complex and are essential for transcriptional regulation. *SFP1* regulates transcription of ribosomal protein and biogenesis genes, response to nutrients and stress and other cellular processes (Skrzypek & Hirschman 2011). Xbp1 is a transcriptional repressor that binds cyclin genes and is induced during stress response (Skrzypek et al. 2017). There are fifteen proteins with evidence of physical interactions with Hda3 and 395 have a genetic interaction (total genetic interactions = 410) with the

protein (Skrzypek et al. 2017). Most of these are found by a very recent high throughput study that identifies 408 interactions (Huang et al. 2017). Aside from Hda1 and Hda2, the physical interactions were shown by high-throughput experiments: two hybrid, affinity capture-RNA, affinity capture- MS of principle component analysis (PCA) experiments. The genetic interactions are also from high-throughput experiments: synthetic lethality, synthetic rescue, synthetic growth defect, negative genetic, positive genetic or phenotypic enhancement experiments; while manually curated are from: synthetic lethality, synthetic rescue, synthetic growth defect or phenotypic enhancement experiments.

No phenotypes for *HDA3* are published in *C. albicans* on the *Candida* Genome Database (Skrzypek et al. 2017). 18 phenotypes for *HDA3* are published in *S. cerevisiae* on the *Saccharomyces* Genome Database these include decreased and increased responses to chemicals, chemical compounds and antifungals (Skrzypek & Hirschman 2011).

The structure of *S. cerevisiae* Hda3 DBD has been characterized but the rest of the protein remains elusive. The solved crystallized structure of *S. cerevisiae* Hda3 DNA Binding Domain (DBD) reveals components that are reminiscent of Swi2/Snf2 ATPase Rad54 (Fig.1.17).

This domain of Hda3 contains only one helicase lobe (containing Rec-A like promoter) where these types of structures are generally bi-lobal and it has been suggested that given its sequence similarity, Hda2 may supply the complex with this additional lobe. Modeling of the crystal structure through DNA-binding area mutagenesis studies have shown that these two loops are essential for the helicase lobe to position itself into the DNA helix. Unlike most similar orthologous structures, this HDAC complex does not have ATPase activity. This bars it from acting as a translocase or participating in supercoiling of DNA. However, a fluorometric deacetylase assay with the complex core, lacking the Arb2 and DNA binding domains~~,~~ showed that this portion of the complex was sufficient for catalytic activity. Additionally, a N-terminal truncated complex of Hda2 or Hda3 were not able to interact with double stranded DNA (Lee et al. 2009).

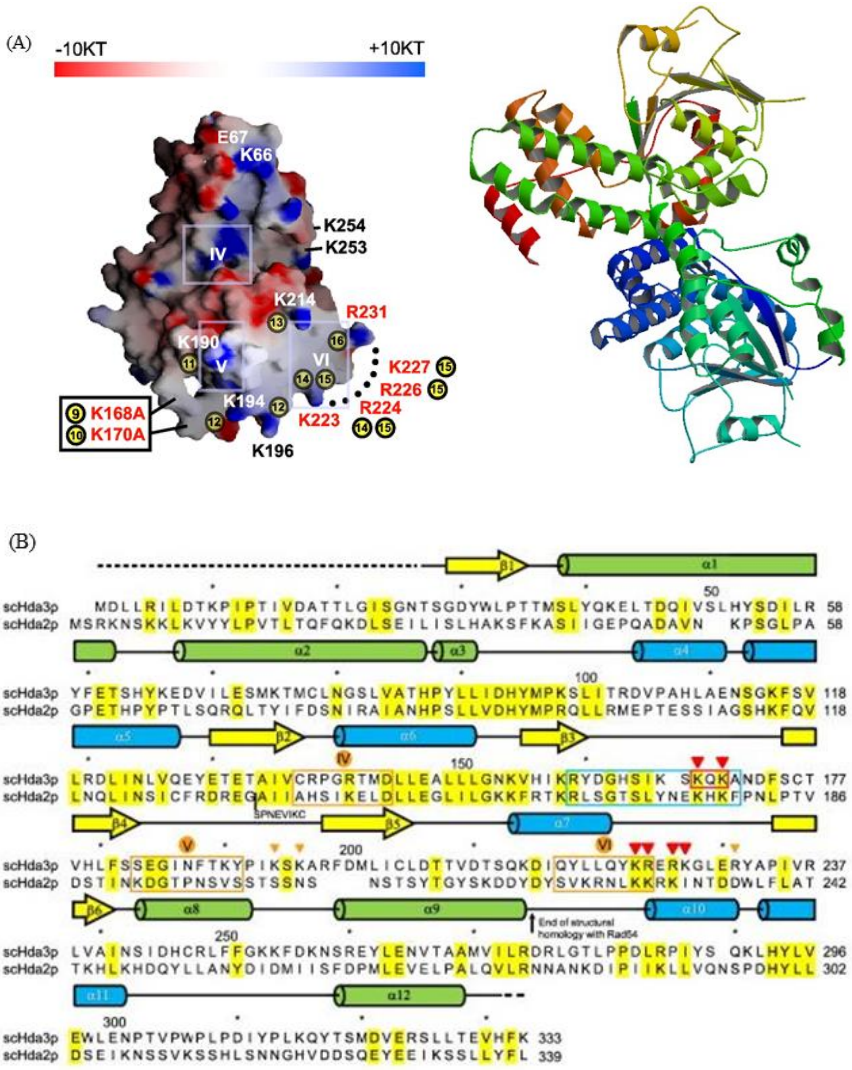

Figure 1.16 Hda3 DBD structural data and sequence comparison to Hda2 DBD
(A) At left: Electrostatic surface map with key residues in DNA recognition in red; KT: k= Boltzmann's constant (relates to average kinetic energy) T = Temperature; At right: Published structures of *S. cerevisiae* Hda3 DNA binding domain Hda3 DBD (PDB: 3HGT) (Lee et al. 2009) (B) Alignment of S. cerevisiae Hda2 and Hda3 DBDs; Swi2/Snf2-specific motif found in zebrafish drRad54 structure shown in blue box; Positively charged residues critical for DNA recognition are highlighted in red or orange (less effective); [Adapted from Lee et al., 2009 Figures 3 and 6]

The structural analysis of HDA3DBD showed two areas that were important for DNA recognition but did not have similarity to the Rad54 family of enzymes. These were the residues of the K168/K170 loop and motif VI (ex. K223, R224, R226) which, when mutated, extinguished DNA binding (Lee et al. 2009) (Fig.1.16).

1.11 Function of Hda2 and Hda3 in modulating Hda1

While proteins like yeast Hda1 exist in humans, the proteins that complex with it (Hda2 and Hda3), as shown in *S. cerevisiae*, are unique to yeast (Yang & Seto 2009). Homologs to *S. cerevisiae* Hda1, Hda2 and Hda3 have been shown to exist in a complex *C. albicans* but whether a complex of these proteins forms in *C. albicans* is unknown (Skrzypek et al. 2017). As was pointed out in Section 1.8.1, in *S. cerevisiae* whole-cell acetylation levels are greatly diminished upon deletion of any of the complex proteins (Jiansheng Wu, Carmen, et al. 2001). There are 21 other proteins with evidence of physical interactions with Hda1 and 7 also have genetic interactions (total genetic interactions = 427) with the protein (Skrzypek et al. 2017).

1.12 Hda1 and Hda3 role in Tup1 specific repression

As discussed in Section 1.7.4, *S. cerevisiae* Hda1 directly interacts with the protein Tup1 to facilitate directed deacetylation. This study also evaluated binding of the other Hda1 complex proteins, Hda2 and Hda3. It was found that Tup1 interacts with Hda1 and Hda3 only. The repression domain, N-terminal portion (aa73-386), of the Tup1 bound strongly to Hda1. The full-length Tup1 protein was required for binding with Hda3 (Jiansheng Wu, Suka, et al. 2001).

1.13 Applications for research on the *C. albicans* Hda1 complex

The yeast Hda1 complex has been biochemically evaluated at the protein level in *S. cerevisiae* and *S. pombe* (Clr3). Proteins analogous to *S. cerevisiae* Hda1, Hda2 and Hda3 are found in *C. albicans* (Skrzypek et al. 2017) but are uncharacterized.

Research on these proteins contributes to foundational studies on epigenetic control and systems evolution. Additionally, transitioning knowledge from conventional model organisms by relating it to pathogenic yeast species provides an opportunity for understanding inherent evolutionary aspects of these proteins.

Human HDAC proteins are currently a popular target for treatment of human diseases. Information derived from research on diverse histone deacetylase proteins may contribute toward development of these therapies and even adjustment of these treatments for applications to other organisms (for example, in wildlife or species conservation settings).

As a model or target, research upon histone modifying proteins within lesser studied yeasts such as *C. albicans* unveils information that can inform medical research and theoretical genetics. Above all, studies like the one covered in this thesis may contribute to the design of treatments for infections caused by yeast colonization.

This introduction frames one component of the complex network of histone and other protein modifications and their effects on the gene expression landscape in *C. albicans*. The following Chapters provide a detailed analysis of the work starting with the materials and the methods used (Chapter 2). The results from protein expression studies in *Escherichia coli* (henceforth: *E. coli*) (Chapter 3) and an evaluation of the Hda1 complex proteins, Hda2 and Hda3 in *C. albicans* (Chapter 4) include the following tasks focused on these goals:

Goal 1: Solve the structure of important protein domains of *C. albicans* Hda1 protein to evaluate its potential as a drug target.

- Evaluate Hda1 by structural alignment and domain analysis
- Express and purify recombinant Hda1
- Evaluate crystallization potential for purified Hda1 Arb2 domain

Goal 2: Solve the structure of *C. albicans* Hda2 and Hda3 proteins to evaluate their potentials as drug targets.

- Evaluate Hda2 and Hda3 by structural alignment and domain analysis
- Express recombinant Hda2 and Hda3

Goal 3: Understand the function of *C. albicans* Hda2 and Hda3 *in vivo* to evaluate their role in the virulence of this pathogen.

- Test the hypothesis that Hda1 complex forms
- Evaluate the roles of Hda2 and Hda3 by phenotype analysis, RNAseq and Chromatin Immunoprecipitation
- Evaluate the roles of Hda2 and Hda3 in hyphae inducing conditions by phenotype analysis and RNAseq
- Evaluate the virulence of *hda2*ΔΔ and *hda3*ΔΔ strains
- Compare *hda2*ΔΔ and *hda3*ΔΔ the strains phenotype, gene expression and protein levels in hyphae versus yeast inducing medias

Finally, Chapter 5 will offer a critical discussion of the results of this project as well as of areas for further study.

CHAPTER 2. Materials and Methods

2.1 General molecular biology techniques

This section outlines the general techniques used for the experiments.

Chemicals were purchased from various sources, including: Thermo Fisher Scientific (Waltham, Massachusetts, USA), Sigma-Aldrich Ltd. (Merck, St. Luis, Missouri, USA), VWR International (Radnor, Pennsylvania, USA), Becton Dickenson (BD) (Franklin Lakes, New Jersey, USA) and Melford Laboratories Inc. (Ipswich, Suffolk, UK).

All plasmids were sequenced with Sanger sequencing prior to expression testing by GATC Biotech DNA Sequencing (Eurofins, Konstanz, Germany) or Sigma-Aldrich.

Stationary incubation was done in a LEEC Classic Incubator (Colwick Industrial Estate Nottingham, UK).

Agitation and incubation of liquid cultures was done in large incubators. For smaller volumes, the following incubator was used: Infors HT Multitron Standard, (Novartis Pharmaceuticals UK Ltd, Horsham Research Centre, West Sussex, UK). To incubate trays or samples at unique temperatures a Stuart Scientific Orbital Incubator A150 (Staffordshire, UK) was used. For large batch *E. coli* growth (1 L-2 L volumes) an Innova44 (New Brunswick Scientific, VWR) shaking heated incubator was used.

If not stated otherwise all media, water and buffers were sterilized for 18 min at 121 °C and 1.05 Bar (15 psi) pressure in a bench top Prestige Medical autoclave (Coventry, UK). Temperature sensitive substances were filter sterilized (pore diameter 0.20 µm).

Media and stock solution were prepared using Ultra-pure deionized water (ddH2O) produced by Thermo Fisher Scientific Barnstead NanoPure Diamond system or autoclaved distilled water (dH_2O).

2.1.1 PCR and PCR product purification

All PCR reactions were performed in a BioRad PCR machine using Classic or High-Fidelity polymerase and provided buffers (PCR Biosystems, London, UK). dNTPs (VWR) and primers (Sigma-Aldrich) were ordered separately. The PCR reactions and temperature protocols utilized were as described in the manuals.

High Fidelity PCR reactions were used for PCRs with downstream applications such as cloning and integration to genome.

Once the PCR reaction was complete the product was subject to agarose gel electrophoresis (see Section 2.1.2) before imaging with UV by a SynGene Gel Doc Imaging System (BioRad).

DNA fragments resulting from a PCR reaction or from a restriction digest were purified (as necessary) using Omega E.Z.N.A. Cycle Pure Kit (VWR) according to the protocol provided with the kit.

Table 2.1 List of Oligos

ABo_#	Name	Sequence	Description	Section
ABo_145	PF1_*HDA1*	GTTCCAGCAGATGGCG AGTAC	Check *HDA3*-GFP or *HDA2*-GFP tagging	2.3.5
ABo_165	Pr1_chK_arg4	AGTGTGGAAAGAAGAG ATGC	Check presence of p80 cassette in *HDA2* or *HDA3* heterozygote	2.3.5
ABo_174	Act1_Fw2	CTACGTTTCCATTCA AGCTGTT	qRT-PCR for *ACT1*	2.3.7
ABo_176	Act1_Rev3	AAACTGTAACCACGT TCAGACA	qRT-PCR for *ACT1*	2.3.7
ABo_179	PR1_NAT	CTGTATCTATAAGCAG TATCATCC	Check presence of *HDA1-HA* integration cassette at native locus	2.3.5
ABo_229	HDA2D_Clox_ Fw1	TCTATTTTCAAGAAGTT AGACCCATTCTTGGAA TAATTATACTTGCAAG AGAAGGCATTGAAATT GCATTACGGCCAGTGA ATTGTAATA	Isolate deletion cassette from p80 or p83 with flanking integration sequences for *HDA2*; long oligo	2.3.5.1
ABo_230	HDA2D_Clox_ rev1	GCATGTATTTACAAATT TTTGGATAAGAAAAAG TAGCATATGGAAACAC AAAACCAAGAAAGAA ATCATGTCGGAATTAA CCCTCACTAA	Isolate deletion cassette from p80 or p83 with flanking integration sequences for *HDA2*; long oligo	2.3.5.1
ABo_231	HDA3D_Clox_ Fw1	GTTCTTAATATTTGTAA CTTTTCCAACTTAAAAT AATTATTGCATATTGCA CTAAAACTAAAACTAC TATAAATacggccagtgaattg taata	Isolate deletion cassette from p80 or p83 with flanking integration sequences for *HDA3*; long oligo	2.3.5.1
ABo_232	HDA3D_Clox_ Rev1	CAATCTTATCATTTACA TAATTAAAAAAACAAA AAACAAGCTAATCTTA TGTTTATGTGGGGGCC ACATTTTCTtcggaattaaccc tcactaa	Isolate deletion cassette from p80 or p83 with flanking integration sequences for *HDA3*; long oligo	2.3.5.1
ABo_247	Hda1_fw	CATGCTAAAGTATTCA CATCCT	Check *HDA1* integration	2.3.5
ABo_261	Pr4_hda2chk_r ev	GTAATATCTGATCAGA ACCTTT	Check *HDA2-GFP* tagging; Check presence of p80 cassette in *HDA2* heterozygote and *hda2*ΔΔ; check presence/absence of *HDA2* in *hda2*ΔΔ unresolved/resolved	2.3.5

ABo_262	Pr4_hda3chk_rev	TCGTTAATCAAAATTATACACTC	Check *HDA3-GFP* tagging; Check presence of p80 or p83 cassette in *HDA3* heterozygote or *hda3*ΔΔ	2.3.5
ABo_308	DAC_fw1	GCCCATATGCCACAATTATTTTATACCCCATTG	*HDA1* catalytic domain without hydrophobic region from p88 with *Nde*I	2.2.5
ABo_309	DAC_ fw2	GTACATATGGATTCTAATGGTATTGCCGACAATGATC	*HDA1* catalytic domain with hydrophobic region from p88 with *Nde*I	2.2.5
ABo_310	Arb2_fw	CACATATGAGCAAGAGTGCGTTGGCAGTA	*HDA1-Arb2-domain* from p88 with *Nde*I	2.2.5
ABo_311	HDA1_rev1	CAGCTCGAGATCTTCGGAAGAGGAGTA	*HDA1* from p88 with *Xho*I	2.2.5
ABo_312	HDA1__rev2	CAGCTCGAGCTAATCTTCGGAAGAGGAGTA	*HDA1* from p88 with *Xho*I and stop codon	2.2.5
ABo_350	Pf_sir2_adh1	CTCTATCACTGATAGGGAGTGG	Confirm reintegration of ABp_177 (*HDA3_pNIM*) cassette at *ADH1* locus	2.3.5.2
ABo_351	Pr_sir2_adh1	CGCACTCACGTAAACACTT	Check Hda1 in p17, p133; confirm reintegration of *HDA3_pNIM* cassette at *ADH1* locus	2.3.5.2
ABo_365	DAC_Clr3_fw	GCCCATATGGCTAAAGTATTCACATCCTATAGTGAATAC	*HDA1* catalytic domain from p88 with *Nde*I	2.2.5
ABo_366	DAC_pFam_fw	GCCCATATGGACCCACATCCAGAAGATCC	*HDA1* catalytic domain from p88 with *Nde*I	2.2.5
ABo_367	DAC _rev2	CAGCTCGAGCTAGCCGACCAATACTTTGGC	*HDA1* catalytic domain from p88 with *Xho*I and stop codon	2.2.5
ABo_408	HDA1_Xma_fw1	TAAGCACCCGGGatgtcgactggtcaagaagaa	Isolate synthetic *HDA1* from p88	2.2.5
ABo_409	HDA1_Xma_rev1	TAAGCACCCGGGatcttcggaagaggagtagtc	Isolate synthetic *HDA1* from p88	2.2.5
ABo_412	HDA1end_chkseq	GGAAATAGTTCGAACGGTGG	Check *HDA1* in p17; sequencing p133	2.3.11.2, 2.3.12
ABo_413	HDA2chk_internalfw	CAGCAGGTAGACTTGATG	Check presence/absence of *HDA2* in *hda2*ΔΔ unresolved/resolved	2.3.5.1
ABo_415	HDA3chk_internalfw	CAACAAGAAcTGTGGAACATG	Check presence/absence of *HDA3* in *hda3*ΔΔ unresolved/resolved	2.3.5.1
ABo_416	HDA3chk_internalrev	GGTGGTTCTATAAATCCCGG	Check presence/absence of *HDA3* in *hda3*ΔΔ unresolved/resolved; Confirm cloning of p177 (*HDA3-pNIM*)	2.3.5.1, 2.3.5.2
ABo_417	dwnstrmHDA1rev_check	CTCGATGCCTGATTTGGATG	Check presence of *HDA1-HA* integration cassette at native locus	2.3.5
ABo_423	HDA3_Natcloxchk	CCGGTGCTATGGTTAGATTG	Check presence of p83 cassette in *hda2*ΔΔ or *hda3*ΔΔ	2.3.5.1

ABo_424	HDA1_endchk	CAATACACGACCCACCAG	Check for presence of *HDA1-Arb2-domain* in p133	2.2.5
ABo_452	F1gaHDA1_Haintg	TCCGAAATTCATTATTAAGGAATTATATAGAAGCTACCATTTTCACATCTATTATCATTTTCCTTTTTAAGAatgtcgactggtcaagaagaaca	Isolate *HDA1-HA* integration cassette from p133; long oligo	2.3.12
ABo_453	R1gaHDA1_Haintg	CAGATCTATATCTATTCTCTTTCTTTCTTTTTTTTTGGTTTTTTGTTGTTGTTGTTGTTTCTACTCGAAgtaaaacgacggccagtgaattc	Isolate *HDA1-HA* integration cassette from p133; long oligo	2.3.12
ABo_456	F1HDA1_YFP	CAAGAAAAATTCGATGAAGGAGTAGATTTCATATTAGATTCAATTGAAGACTACTCCTCTTCCGAAGATGGTGGTGGTctaaaggtgaagaattatt	Tag *HDA1* with *GFP* at native locus	2.3.5.2
ABo_457	R2HDA1_YFP	GATCTATATCTATTCTCTTTCTTTCTTTTTTTTTGGTTTTTTGTTGTTGTTGTTGTTTCTACTCGAAgaattccggaatatttatgagaaac	Tag *HDA1* with *GFP* at native locus	2.3.5.2
ABo_458	F1HDA2_GFP	TGTTAGAAAACTCTGGCTCGGGTGCCAATAATAGACAAAATAATCGTATTAGTCGAGGTGCAACACCTCTTGGTGGTGGTtctaaaggtgaagaattatt	Isolate *GFP* tagging cassette from p11 with flanking integration sequences for *HDA2*; long oligo	2.3.5.2
ABo_459	R2HDA2_GFP	GCATGTATTTACAAATTTTTGGATAAGAAAAAGTAGCATATGGAAACACAAAACCAAGAAAGAAATCATGgaattccggaatatttatgagaaac	Isolate *GFP* tagging cassette from p11 with flanking integration sequences for *HDA2*; long oligo	2.3.5.2
ABo_460	F1HDA3_GFP	CAATGCTTTTACATTTTTAAATGATACTAAATATTTGAAAAAGAGGAAAAATCGAGGAATAACTCCTAAAGGTGGTGGTtctaaaggtgaagaattatt	Isolate *GFP* tagging cassette from p11 with flanking integration sequences for *HDA3*; long oligo	2.3.5.2
ABo_461	R2HDA3_GFP	CTTATCATTTACATAATTAAAAAAACAAAAAACAAGCTAATCTTATGTTTATGTGGGGGCCACATTTTCTgaattccggaatatttatgagaaac	Isolate *GFP* tagging cassette from p11 with flanking integration sequences for *HDA3*; long oligo	2.3.5.2
ABo_462	Pf_MTLa1_Chk	TTGAAGCGTGAGAGGCAGGAG	Check presence of MATa	2.3.5.4
ABo_463	Pr_MTLa1_Chk	GTTTGGGTTCCTTCTTTCTCATTC	Check presence of MATa	2.3.5.4
ABo_464	Pf_MTLalpha1_Chk	TTCGAGTACATTCTGGTCGCG	Check presence of MATα	2.3.5.4
ABo_465	Pr_MTLalpha1_Chk	TGTAAACATCCTCAATTGTACCCGA	Check presence of MATα	2.3.5.4
ABo_469	qALS3_Fw1	CCTATTCCAACAACTACAAT	qRT-PCR for *ALS3*	2.3.7

ABo_470	qALS3_Rev1	TATTGAGTCAGTTGG ATTAG	qRT-PCR for *ALS3*	2.3.7
ABo_471	qHWP1_Fw1	CCAGTTACTTCTGGA TCATC	qRT-PCR for *HWP1*	2.3.7
ABo_472	qHWP1_Rev1	TCGGTACAAACACTG TTAGA	qRT-PCR for *HWP1*	2.3.7
ABo_494	Arb_ rev1	AGCTCGAGGTTATCCC AAATATAAAGCAAAAC	Through *HDA1-Arb2-domain* from p88 with *Xho*I	2.2.8
ABo_495	Arb _rev2	CAGCTCGAGctaGTTAT CCCAAATATAAAGCAA AAC	Through *HDA1-Arb2-domain* from p88 with *Xho*I and stop codon	2.2.8
ABo_496	HDA1_fw1	gccCATATGTCGACTGG TCAAGAAGAAC	*HDA1* from p88 with *Nde*I	2.2.8
ABo_511	Pf_SAT1	GGTGGCGGAAACATTG GATG	Check presence of *SAT1*	2.3.5
ABo_512	Pr_SAT1	TCAATGCCGCCGAGAG TAAA	Check presence of *SAT1*	2.3.5
ABo_514	pNIM_Rev2	CCATCATAAAATGTCG AGCGTC	Sequencing of ABp_177 (*HDA3_pNIM*)	2.3.5
ABo_552	HDA1_fw2	CCGGAGCTCGAAAACC TGTATTTTCAGGGACAT ATGTCGACTGGTCAAG AAGAAC	*HDA1* from p88 with *Sac*I	2.2.8
LD_515	Pf_sir2_adh1	CTCTATCACTGATAGG GAGTGG	Confirm reintegration of ABp_177 (*HDA3_pNIM*) cassette at *ADH1* locus	2.3.5
ABo_577	HDA2_fw	GCCGgCGCGCCGAAAA CCTGTATTTTCAgaGGG	Isolate synthetic *HDA2* from p150 with *Asc*I	2.2.8
ABo_578	HDA2_rev	GGCCTTAAGTTAGGCG GCCGCAAGAGGTG	Isolate synthetic *HDA2* from p150 with *Afl*I	2.2.8
ABo_579	HDA3_fw	GCCCATATGCATCATC ACCATCACCATGG	*HDA3* from p152 with *Nde*I	2.2.8
ABo_580	HDA3_rev	GGCCTCGAGTTAGCAG CCGGATCTGGCGG	*HDA3* from p152 with *Ava*I	2.2.8
ABo_624	HDA3_XhoI_fw	taagcaCTCGAGATGgatttaa ggaaaattttg	Isolate *HDA3* from ABp152 with *XhoI* and *Bgl*II sites (for cloning into ABp111)	2.2.8
ABo_625	HDA3_stpBglII_rv	ttaacgAGATCTttaTTTAG GAGTTATTCCTCGAT	Isolate *HDA3* from ABp152 with *Xho*I and *Bgl*II sites (for cloning into ABp111: pNIM)	2.2.8
ABo_627	HDA3_nostrtAatII	TAAGCAGACGTCGATT TAAGGAAAATTTTG	Use to isolate *HDA3* prior to cloning with p140 *pTET* plasmid to make reintegration N terminal *GFP* tagged *HDA3* plasmid	2.3.5
ABo_628	HDA3_StuI_rev	TTAACGaggcctTTAGGC GGCCGCTTTAGGAGTT A	Use to isolate *HDA3* prior to cloning with p140 *pTET* plasmid to make reintegration N terminal *GFP* tagged *HDA3* plasmid	2.2.8
ABo_784	MDR1_fw1	AGCCAGTTGGAGATGG ACTT	qRT-PCR for *MDR1*	2.3.7
ABo_785	MDR1_rev1	GTCGTTACCGGTGATG GCTC	qRT-PCR for *MDR1*	2.3.7

2.1.2 Agarose gel electrophoresis of DNA and gel extraction purification

DNA fragments were separated by agarose gel electrophoresis in 1 % agarose gels in 1 x Tris/Borate/EDTA (TBE) buffer with the addition of EtBr (0.5 ug mL^{-1}) to a final concentration of 0.5 μg mL^{-1}. Each DNA sample containing ~33 % (v/v) DNA loading buffer was loaded into the wells next to a molecular marker ladder (1 kB Plus Invitrogen, Fisher Scientific) and electrophoresis was carried out at 120V. Gels were UV imaged by gel doc.

Isolation and purification of after gel electrophoresis (as needed) was carried out using an Omega E.Z.N.A. Gel Extraction Kit (VWR) according to the protocol provided with the kit. Briefly, the DNA band of interest was excised from an agarose gel using a sterilized scalpel blade UV light platform before column purification with kit buffers.

2.1.3 Plasmid isolation and restriction digest of DNA

An Omega Plasmid DNA Mini Kit I (VWR) was used for the isolation and purification of plasmid DNA. Briefly, the plasmid of interest was transformed into DH5α *E. coli* with appropriate antibiotic(s) to maintain the presence of the plasmid (see Sections 2.2.1). A 5 mL culture of transformed *E. coli* cells in LB with appropriate antibiotic(s) was grown in a shaking incubator for 18-22 hours at 37 °C. These cells were lysed by kit buffers before application to a column and purification with supplied buffers. Plasmids were stored at 4 °C or otherwise used for transformation, PCR or digestion.

Table 2.2 List of Plasmids

ABp_#	Plasmid	Description	Reference	Section
ABp_11	pGFP-His1	GFP tagging vector for integration at native locus, *Amp*^{R}	(Gerami-Nejad et al. 2001)	2.3.5.2
ABp_17	pHA_NAT	*HA* tagging vector, *Amp*^{R}	(Gerami-Nejad et al. 2012)	2.3.5.2
ABp_80	LAL (loxP-ARG4-loxP)	*Arg4* substitution products, , *Amp*^{R}	(Shahana et al. 2014)	2.3.5.1
ABp_83	NAT1-Clox (loxP-NAT1-MET3p-cre-loxP)	*Nat* substitution products, *Amp*^{R}	(Shahana et al. 2014)	2.3.5.1
ABp_88	*HDA1*_synth	*HDA1* synthetic in generic vector pYL2, *Kan*^{R}	GeneArt	2.3.5
ABp_90	pET21b	N-terminal *HiA6tag* fusion protein vector with T7 promoter, *Amp*^{R}	Novagen	2.3.5
ABp_92	*HDA1*-pET21b	Synthetic *HDA1* FL was digested cloned into *Nde*I & *Xho*I sites of pET21b, *Amp*^{R}	This study	2.3.5, 3.4, A2.2.1
ABp_109	6xHis-Arb2+C-pET28b	C-terminal *HiA6tag* fusion protein vector with T7 promoter, *Amp*^{R}	Novagen	2.3.5
AB_p111	pNIM	Vector for tetracycline inducible integration to *ADH1* locus, *Amp*^{R}	(Park et al. 2005)	2.3.5.3
ABp_119	Arb*Hda1*-Pet28b	PCR of p88 with ABo310&312 digested with *Nde*I and *Xho*I and cloned into p109; *Kan*^{R}	This study	2.2.5, A2.2.4, A2.5
ABp_133	*HDA1*synthetic_pHA_NAT	Source of *HDA1-HA* integration cassette, *Amp*^{R}	This study	2.3.11.2, 2.3.12
ABp_136	*SAT1* flipper + MTLαKO flanking regions	Deletion of *MAT*α , *Cm*^{R}	Anderson Lab, Ohio State University	2.3.5.4
ABp_140	pTET25-MNC	Plasmid for reintegration of GFP tagged gene at *ADH1* locus with potential for tetracycline induction, *Amp*^{R}	(Lai et al. 2011)	2.3.5.3, 2.3.13
ABp_143	*HDA1*-pET28b	Synthetic *HDA1* FL cloned into *Nde*I and *Xho*I sites of pET28b, *Kan*^{R}	This study	2.2.8
ABp_150	6XHis-AVI-*HDA2*	*Avi-HDA2* synthetic in pET151; 4x CUG->TCA; *Amp*^{R}	GeneArt	2.2.8, 3.4.2.1, A2.2.4
ABp_152	*HDA3*_synth	*HA-HDA3* synthetic in generic vector: 6x CUG- >TCA;*KanR*	GeneArt	2.2.8, 2.3.5
ABp_154	pETDuet-1	Vector designed for Co-expression of 2 target genes with T7 promoters, *Amp*^{R}	Novagen	2.2.8
ABp_156	pET41a	*GST* tagged protein vector with T7 promoter, *Kan*^{R}	Novagen	2.2.8
ABp_166	6xHis-DAC-Clr3-pET28b	*HDA1* deacetylase domain construct (based on Clr3 alignment) in pET28B, *Kan*^{R}	This study	2.2.8, 3.10, A2.3.5
ABp_167	6xHis-DAC-pFam-pET28b	*HDA1* deacetylase domain construct (based on pFam domain) in pET28B, *Kan*^{R}	This study	2.2.8
ABp_173	GST-6xHis-*HDA1*-pET41a	Synthetic *HDA1* FL cloned into *Sac*I & *Xho*I sites of pET41a, *Kan*^{R}	This study	2.2.8, 3.4, Fig. 3.6

ABp_177	*HDA3*-pNIM	Tetracycline inducible integration of *HDA3* to *ADH1* locus, Amp^R	This study	2.3.5.3
ABp_205	6xHis-AVI-*HDA2*/6xHis-HA-*HDA3*-pETDuet	Synthetic *HDA3* with *Nde*I & *Ava*I to *MCSII* and synthetic *HDA2* with *Asc*I & *Afl*I to *MCSI* of pETDuet; Amp^R	This study	2.2.8
ABp_213	*HDA3*-pTET	Plasmid for reintegration of *HDA3* to *ADH1* locus … with *GFP*, Amp^R	This study	2.2.8
ABp_220	*HDA3*noDBD-pTET	Synthetic *HDA3noDBD* aa Y499-Stop cloned into *Aat*II and *Stu*I sites of pTET, Amp^R	This study	2.2.8
ABp_234	6xHis-HA-*HDA3*-pET151	Synthetic *HDA3* cloned into pET151 with *Kpn*I and *Not*I. p151 was digested away from *HDA2* synthetic vector at same restriction sites., Amp^R	This study	2.2.8

Purified DNA (plasmid or PCR product) was digested using the relevant restriction enzymes (10 U μL^{-1}) and the optimal digestion buffer chosen according to guidelines provided by manual. The digest reactions were incubated overnight at the temperature required by the restriction enzyme (usually 37 °C) before being subjected to electrophoresis. For quick diagnostic tests, shorter incubation times (2+ hours) were used.

2.1.4 DNA optical density measurements

The optical density of cultures was measured using a BioDropDuo (BioDrop UK Ltd., Cambridge, UK). Absorbance readings were taken with microvolume samples of 1.5 µL at A260 with 0.5 mM pathlength in ng/µl units.

2.1.5 Ligation of DNA

Vector and insert were digested with the appropriate restriction enzymes and purified (see Section 2.1.3).

Ligations were made using Promega (Southhampton, UK) T4 DNA ligase and accompanying 10x ligase buffer. Ligation of DNA fragments into the vector was done at room temperature in a 5 µL reaction with added 0.5 µL ATP (25mM) and T4 DNA Ligase (1-3 U μL^{-1}) and 3:1 insert:vector ratio was used. Reactions were incubated at room temperature for 1-2 hours. A portion of this mixture (2.5 µl) was transformed to 50 µL of DH5α cells and plated to LB agar supplemented with appropriate antibiotics to select for growth of cells which had incorporated the plasmid (Table 2.4). The colonies were checked by digestion, PCR and/or sequencing.

2.1.6 Synthetic construct design, codon changes for *C. albicans HDA1, HDA2* and *HDA3* synthesis

Genes were synthesized by GeneArt (Invitrogen, Thermo Fisher Scientific). The sequence of *HDA1*, *HDA2* and *HDA3* was not codon optimized for optimal expression in *E. coli* the original sequence was used so that the synthesized gene could also be reintegrated into a *C. albicans* deletion mutant (see Section 2.3.5.3). CUG Clade accommodations were made for *HDA2* (4 codons) and *HDA3* (6 codons) constructs. All CTG codons were changed to TCA to allow coding for Serine in both *E. coli* and *C. albicans* expression systems. The codon TCA was chosen based on the expected number of occurrences 26.4 per 1000 in *C. albicans* and *E. coli* 7.8 per 1000 (Nakamura et al. 2000).

The *C. albicans HDA1* gene was synthesized by GeneArt into standard cloning vector pYL2/15 with flanking *Nde*I and *Xho*I cloning sites. This standard vector incorporates a kanamycin resistance gene.

The *HDA2* construct was synthesized with an Avi tag and directly into the pET151_D plasmid by the GeneArt Express Cloning Service. This vector incorporates an ampicillin resistance gene. The added Avi tag brings the opportunity for attachment of Biotin ligase BirA and biotinylation of the amino acids of the tagging sequence. This allows for isolation of the tag and attached proteins by streptavidin (a biotin binding protein (Fairhead & Howarth 2015). Additionally, the biotin can be fluorescently or radioactively labeled in order to detect the tagged protein (Kimple et al. 2013). The entire construct is flanked by *Kpn*I and *Not*1 restriction sites and the pET151 vector contributes a N-terminal Tobacco Etch Virus (TEV) protease cleavage site and cleavable 6xHis tag.

The *HDA3* gene was synthesized in frame with the sequence for a Human influenza hemagglutinin (HA) tag. Due to sequence complexity (repetitions and high AT content), HA tagged *HDA3* was synthesized into GeneArt Cloning Vector pMK (rather than directly to pET151_D). This standard vector also incorporates a kanamycin resistance gene. The construct is flanked by *Kpn*I and *Not*I restriction sites.

The *HDA2* and *HDA3* synthetic construct design incorporates a *Hind*III site so that the N-terminal Avi or HA tag can be cleaved as necessary, prior to cloning.

This design was executed in response to the observed low expression levels of Hda1. It offers the possibility of a downstream alternative to crystallization that requires much less protein: single molecule studies. Single molecule studies can be employed to look at interactions between these proteins and DNA, for example.

2.2 Microbiological techniques for *E. coli*

2.2.1 *E. coli* strains culturing, competent cells and genetic transformation

E. coli strains were from Novagen (Merck, Darmstadt, Germany), Sigma Aldrich or Thermo Fisher as indicated in Table 2.3, except for the BL21(DE3) Codonplus-RIL competent cells which were generously donated to the project by Agilent (at the request of Dr. Paul Wolber, Agilent, San Jose, CA, USA).

For long-term storage of transformed *E. coli*, frozen glycerol stocks were maintained at -80 °C (final concentration of 25 % glycerol (v/v).

Plate cultures of *E. coli* cells were streaked from a glycerol stock to plate from which single colony cultures were inoculated. Antibiotics were added when required. A list of these antibiotics can be found in Table 2.4. The agar plates were incubated overnight at 37 °C and enclosed by plastic bags during incubation.

Liquid cultures were inoculated with a single colony from an agar plate culture. The medium was supplemented with antibiotics as required. A list of these antibiotics can be found in Table 2.4. In general, *E. coli* aerobic cultures were grown on a platform shaker at ~ 180 rpm at 37 °C.

Competent *E. coli* cells were prepared as follows: an overnight starter culture derived from a single colony was inoculated into 20 mL fresh LB broth and grown to an OD_{600} = 0.3. The cells were cooled on ice for 10 min before isolation by centrifugation for 10 min at 3000 rpm (Eppendorf 5810 R). The pellets were gently resuspended in 20 mL of ice-cold 0.1 M $CaCl_2$. After incubation on ice for 20-60 min, the cells were collected by centrifugation and resuspended in 2 mL of ice cold 0.1 M $CaCl_2$ containing 15 % (v/v) glycerol. Aliquots of 100 μL were frozen rapidly and stored at -80 °C.

Transformation of *E. coli* was done according to the protocol detailed in the New England Biolabs BL21(DE3) manual. For maintenance of stocks and other routine transformations, the 5-min adaptation of the protocol was used.

Table 2.3 List of Bacterial strains

Strains	Genotype	Description	Reference
Escherichia coli			
BL21(DE3)	E. coli B F$^-$ *ompT hsdS*$_B$ (r_B^-, m_B^-) *gal dcm* (DE3)	General purpose expression host	Novagen
BL21(DE3)pLysS	E. coli B F$^-$ *ompT hsdS*$_B$ (r_B^-, m_B^-) *gal dcm* (DE3) pLysS (Cm^R)	High-stringency, expression host	Novagen
Rosetta (DE3)	E. coli B F$^-$ *omp*T *hsd*S$_B$ ($r_B^-m_B^-$) *gal dcm lacY1* (DE3) pRARE^6 (Cm^R)	Expression of rare codon tRNAs: Arg: AGA, AGG, Gly: GGA, Ile: AUA, Leu: CUA, and Pro: CCC	Novagen
Overexpress C43 (DE3)	BL21(DE3) + Proprietary mutations	Derived from BL21(DE3) with added mutations to prevent cell death associated with expression of recombinant toxic proteins	Sigma Aldrich
BL21 Codon Plus (DE3) RIL	E. coli B F– *omp*T hsdS(rB – mB –) *dcm*+ Tetr *gal* λ(DE3) *end*A *Hte* [argU *ile*Y *leu*W Cm^R]	Expression of rare codon tRNAs: Arg: AGA, AGG, IleY (AUA), Leu: (CUA)	Agilent
DH5α	F- φ80*lac*ZΔM15 Δ(*lac*ZYA-*arg*F) U169 *rec*A1 *end*A1 *hsd*R17 (rk-, mk+) *pho*A *sup*E44 λ- *thi*-1 *gyr*A96 *rel*A1	General purpose strain capable of being transformed efficiently with large plasmids	Thermo Fisher Scientific

*Genotypes and descriptions are taken from related manuals (Novagen 2003; Thermo Fisher Scientific 2004; Dumon-Seignovert et al. 2004; Agilent 2012b).

Table 2.4 Additives and Antibiotics for *E. coli* work

Solution	Stock concentration	Final concentration
Imidazole	5 M	10 mM-1 M
IPTG (Melford)	1 M in dH2O	0.4-1 mM
Zinc ($ZnCl_2$)	0.1 M	20 μM

Antibiotic	Stock concentration	Final concentration
Ampicillin (Melford)	100 mg mL^{-1}	100 μg mL^{-1}
Chloramphenicol (Sigma)	34 mg mL^{-1}	34 μg mL^{-1}
Kanamycin (Melford)	50 mg mL^{-1}	50 μg mL^{-1}

*All antibiotics were filter sterilized.

2.2.2 DNA from *E. coli* colonies for PCR

To perform PCR as a check of plasmids within *E. coli* colonies, cells from a single colony were placed directly into 5 ul of water; this served in the place of added DNA. The remaining PCR mix was added to reaction (less 5 ul water) and processed by the basic protocol (see Section 2.1.1).

2.2.3 Cloning with pET21b, pET28b, pET41a, pET151 and pETDuet-1 vectors

All pET vectors used in this study are listed in Table 2.2.

HDA1 synthetic and its domain constructs were cloned into *Nde*I and *Xho*I restriction enzyme sites of pET21b (ABp_90) and pET28b (ABp_109). The vector pET21b provides the gene product with a C-terminal 6xHis tag made up of six consecutive histidine residues. Vector pET28b can contribute N- and C-terminal tags but only N-terminal were used in this study.

HDA1 was synthesized with flanking *Nde*I and *Xho*I sites so that it could be digested and directly cloned to pET21b. Partial constructs were amplified by PCR from the synthetic *HDA1* vector (ABp_88) with primers that incorporated *Nde*I and *Xho*I. Following digestion, the PCR product was purified by gel extraction (see Section 2.1.2) and ligated (see Section 2.1.5) to either pET21b or pET28b.

A similar approach of PCR amplification (ABo496&311/312) was taken to clone full length *HDA1* (final plasmids ABp_92/143), the Arb2 (ABo310 & 311/312) domain (final plasmid ABp_119) and expressed catalytic domains (ABo365/366 & 367) into pET21/28b (final plasmids ABp_166/167) but it should be noted that in all cases of cloning to pET28b a stop codon was added by the amplification primer so that the C-terminal 6xHis tag was not incorporated during protein translation (final plasmids ABp_266/267).

Full length *HDA1* was amplified (ABo552&312) and cloned into pET41a (ABp_156) using *Sac*I and *Xho*I restriction sites (final plasmid ABp_173).

HDA2 was synthesized into the pET151 vector (ABp_150) and it was transformed with *E. coli* directly prior to expression.

For *HDA3*-pET151 cloning (ABp_234), both *HDA2* (ABp_150) and *HDA3* (ABp_152) GeneArt synthesized plasmids were digested with *Kpn*I and *Not*I with the goal of ligating *HDA3* into the pET151 backbone using the same restriction sites. In this case, the *Not*I site was prior to the stop codon in both vectors.

To clone *HDA2* and *HDA3* to pETDuet-1 (ABp_154) for dual expression, HA-*HDA3* was amplified (ABo579&580) by PCR from *HDA3*-pET151 (ABp_234). The purified PCR product was digested with *Nde*I and *Ava*I and cloned into same sites of pETDuet-1 *MCS2*. Next, Avi-*HDA2* was amplified by PCR (ABo577&578) from the His-Avi-*HDA2*-pET151 (ABp_150) plasmid and the purified, digested (*Asc*I and *Afl*II) product was ligated to HA-*HDA3*-pETDuet-1 in *MCS1* using the *Asc*I and *Afl*II restriction enzyme sites (final plasmid ABp_205).

In general, the genes of interest were digested at restriction sites from their original vector or amplified by PCR during which primers incorporated the appropriate restriction

sites (and stop codon if cloning to pET28b). If PCR amplification was used the product was purified by PCR clean-up (see Section 2.1.1) and digested overnight. After initial digestions, DNA was isolated by gel extraction and the vector and fragments were purified (see Section 2.1.2) before ligation (see Section 2.1.5). Competent DH5α *E. coli* cells were transformed with the ligation mixture and plated onto LB plates with appropriate antibiotic selection.

The presence of correctly integrated cloning was confirmed by single colonies PCR, restriction digest and sequencing.

2.2.4 Recombinant protein overproduction: culturing and harvest

To express recombinant proteins, the designated *E. coli* strain (Table 2.3) was transformed with a vector containing the gene of interest cloned in frame with the tag.

An example of the standard purification of 1 L culture is given here; smaller cultures were simply scaled down versions of this protocol: The recombinant strain was grown in 50 mL LB with the appropriate antibiotics for selecting the presence of plasmid(s) and glycerol (as indicated) in 37 °C incubator with shaking at 180 rpm overnight. The next day, 10 mL was reinoculated to a 1 L larger culture which was grown to OC_{600} = 0.6-0.8. Pre-induction samples were taken before induction with 400 mM – 1M IPTG (as indicated). If the cultures would be grown at cooler temperatures after induction, a cool down on ice for ~20 min allowed for temperature to shift prior to addition of IPTG. Induced cultures were grown at either 37 °C for 1-4 hours or at 16/20 °C for 20 - 24 hours (as indicated). At this point the cells were harvested at 5 K rpm for 15 min. The cells were weighed and resuspended with 10 mL lysis buffer per 1 g of cell pellet.

The cells were frozen to -80 °C. These cells were later defrosted for lysis by sonication or cell disruption (see Section 2.2.5). Cells were then spun down at 4 °C for 30 min at 15 K rpm (Beckman Coulter Avanti J-301 refrigerated ultra-centrifuge) to separate soluble and insoluble fractions.

Expression testing was optimized by adjusting temperature, expression times, IPTG levels, using additives, changing levels of buffer components with the specific conditions for each experiment as detailed in Chapter 3.

Addition of Zinc Chloride was evaluated, 20 μM of $ZnCl_2$ was added to the growth culture 30 min prior to induction with IPTG. In addition, for this purification, lysis buffers were altered to match the composition used for the protocol which was modelled after an expression study that crystalized the catalytic domain of human HDAC4. This protocol

was tested with Ni-NTA batch purification (see Section 2.2.7.1). The lysis buffer included added detergent and DTT and was followed by a wash buffer to lower levels of detergent and glycerol which was ½ lysis buffer and ½ dilution buffer. The protein was eluted using a similar buffer with much lower levels of detergent and glycerol as well as added 150 mM imidazole.

All high-speed harvest/washing of cultures was performed in Beckman Coulter Avanti J-301 refrigerated ultra-centrifuge. Lower speed 50 mL or smaller cultures were harvested/washed using a refrigerated centrifuge (Eppendorf 5810 R).

2.2.5 Lysis of *E. coli* cells

The lysis buffer for most experiments was composed of Tris-HCL at pH5 10 mM, NaCl 300 mM, 2-Mercaptoethanol (BME) 2 mM, imidazole 10 mM and glycerol 5 %. For His-HA-Hda3 the lysis buffer was composed of HEPES pH7 20 mM, NaCl 200 mM and glycerol 5 % (10x Hepes Running Buffer Stock: 47.66 g HEPES, 3.2 g EDTA, 9.5 g KOH; Make up to 1 L with ddH_2O; dilute to 1x in ddH_2O for use as running buffer).

Cell disruption lysis of *E. coli* by sonication was performed on ice using a Soniprep150 (MSE) ultrasonic disintegrator with the exponential microprobe at 3 x 30 sec spaced with 30 sec rests on ice with the maximum setting. The sonicated cells were centrifuged at 35,000 x *g* for 20 min at 4 °C to separate soluble and insoluble fractions.

Harvested cells from 1 L or 2 L cultures were broken by one passage through a cell disrupter (Stansted Fluid, Essex, UK) operating at 20 psi. Soluble and insoluble fractions were harvested on to ice by centrifugation at 35,000 x *g* for 20 min at 4 ºC.

2.2.6 Polyacrylamide gel electrophoresis: SDS-PAGE

Polyacrylamide gels were run at 90 V through the stacking layer and at 150 V through the resolving portion (7.5% or 10%) using an electrophoresis apparatus. Sample was denatured by addition of SDS sample buffer and boiling for 5 min. ~20 µL of denatured sample was loaded into each well and 7 µL of either Precision Plus Protein Standards All Blue (BioRad) or PageRuler Plus Prestained Protein Ladder (Thermo Fisher Scientific) molecular mass marker was run in parallel as a gauge of the protein size. However, for low abundance proteins it was necessary to load more of the sample (up to 150 µL) than allowed by the capacity of the well. This was done by applying power for ~5 min to move the sample from the well into the stacking layer. After electrophoresis was complete, the gel was stained and de-stained before imaging of the gel by a simple camera.

2.2.7 Protein purification procedures

All column purifications were done on an AKTA purifier (GE Life Sciences) at 4 °C.

Protein concentration was done by 10 kDa MW cut off Amicon Ultra 15ml and 0.5 mL centrifugal columns (Millipore). Purified protein was desalted using HiPrep 26/10 or PD-10 columns (Fisher Scientific).

The optical density of cultures was measured using a BioDropDuo. Protein concentrations were estimated by setting the molecular weight and extinction coefficient into the machine setup parameters.

During and following the purification, samples were taken to monitor the protein production and purity by Sodium Dodecyl Sulfate Polyacrylamide Gel Electrophoresis (SDS-PAGE) using Tris-Glycine gels (resolving: 7.5% or 10%) (see Section 2.2.6).

2.2.7.1 Immobilized metal (Nickel) ion affinity chromatography and Nickel-NTA batch purifications

Immobilised metal ion affinity columns take advantage of the natural affinity of the 6xHis tag amino acid sequence for transition metals. They selectively retain proteins by forming complexes with the exposed histidine residues. This complex can be broken by increasing concentrations of imidazole and the bound protein isolated (separate from other proteins) by this competitive elution.

Before purification by this column, the cells were sonicated or subjected to disruption. Following, the soluble and insoluble fractions were separated by centrifugation. The soluble fraction was loaded onto a HisTrap HC 5 mL prepacked column (GE Life Sciences) pre-equilibrated with buffer A (Tris-HCl pH7.5 10 mM, NaCl 300 mM, imidazole 10 mM, glycerol 5 % and BME 2 mM). The column was washed with 10 column volumes (CV) buffer A followed by a 20 CV linear gradient elution of the bound protein using 1 M imidazole. This step was performed at 4 °C. The eluted fractions were assessed on SDS polyacrylamide gel and the fractions containing the target protein were pooled and buffer exchanged into ion exchange buffer A (see Section 2.2.7.2).

A more time efficient alternative to metal ion affinity purification is nickel batch purification using Ni-NTA Agarose Resin (Qiagen, Manchester, UK) which is commonly employed with smaller volume samples. This method was used at the early assessment stage for several of the recombinant constructs to evaluate their potential for larger batch column purification. 0.5 mL (column volume) of Ni-NTA agarose resin was equilibrated with lysis buffer + imidazole before incubation in protein overnight at 4 °C with gentle

rotation. Washes and elution were performed either on a gravity flow column (PD-10 column) or by centrifugation at 1K rpm for 1 min at 4 °C. The beads were washed with 10 CV of Wash Buffer (W) followed by 2 CV Elution Buffer 1 (E1) and eluted by 4 CV Elution Buffer 2 (E2). Samples were taken at each stage and loaded to an SDS-PAGE gel for visualization of the purified protein. The wash buffer consisted of Tris-HCl pH7.5 20 mM, NaCl 200 mM, imidazole 20 mM and BME 4 mM and elution buffers utilized two increasing levels of imidazole with 50 mM and 1 M.

Nickel-NTA batch purification was also employed for final purification of the Arb2 domain after thrombin cleavage. In this case it was a secondary nickel batch purification following a first nickel ion affinity column purification, IEC column purification and SEC column purification. The secondary batch purification was done using the size exclusion column buffer (see Section 2.2.7.4) with added imidazole (10 mM for buffer A and 500 mM for buffer B). The protein was incubated with 500 µL of resin for 1 hour. After, the mixture was washed with 10 CV of Buffer A and eluted with 2 CV of Buffer B.

2.2.7.2 Ion Exchange Chromatography

Ion exchange chromatography (IEC) uses columns packed with charged resin. This allows for separation of proteins based on their net charge relative to their buffer. Using a buffer that is about 1 pH unit higher than that of the protein is ideal for an anion exchange column. This provides a negative charge to the protein and allows it to bind to the positively charged resin.

Ion exchange was performed using HiTrap GE-QHP anion exchange column and FPLC. The sample in IEC Buffer A (Tris-HCl pH7.5 10 mM, 100 mM NaCl, glycerol 5 % and BME 2 mM) was injected to the column and the flow through was collected as 4 mL fractions a gradient toward 100% of Buffer B with 1 M NaCl (1M was set over 50 min. Samples of all fractions were collected for visualization by SDS-PAGE gel electrophoresis (see Section 2.2.6).

After IEC column purification protein samples were concentrated to a maximum of 500 µL in preparation for size exclusion chromatography.

2.2.7.3 Gel filtration (Size Exclusion) chromatography

Gel Filtration (Size Exclusion) chromatography uses a column packed with size selection resin. The pores in the resin allow small proteins to pass through. Consequently, these

smaller proteins take longer to migrate through the column than larger proteins which do not make the size cut off and travel between the beads.

A Hiload 16/60 Superdex 75PG size exclusion column or Superdex 200 10/30 GL (GE Life Sciences) was pre-equilibrated with 1.2 column volumes of Buffer A (see section 2.2.7.4). Concentrated purified protein (0.5 mL) was loaded onto the column. The protein was eluted at a flow rate of 0.5-0.7 mL min^{-1} into 1 mL fractions with Buffer A. Fractions were analysed by SDS-PAGE and the fractions containing the protein were pooled (see Section 2.2.6). The column was recovered with 1 CV of Buffer B (Buffer A + 1 M imidazole) and stored in 20 % (v/v) ethanol.

2.2.7.4 6xHis tag cleavage and secondary nickel purification

The purified 6xHis tagged recombinant Arb2 protein was cleaved by incubation with 15 Units (U) of thrombin (1.5 U/µL) (Sigma-Aldrich) at 4 °C overnight in SEC buffer (Tris-HCl pH7.5 20 mM, NaCl 150 mM, glycerol 5 % and BME 2 mM) dilution.

The protein was buffer exchanged into SEC Buffer + 10 mM imidazole before it was purified by secondary Nickel batch purification with Ni-NTA Agarose Resin (Qiagen) to isolate the pure protein from the remaining tagged protein and cleaved tag (see Sections 3.3.2.5). To elute the protein, SEC Buffer + 500 mM imidazole was used.

2.2.8 Crystallization methods

2.2.8.1 Hanging drop vapor diffusion crystallization screens

Crystallization trials were performed by drop vapor diffusion technique in Granier 96 well polystyrene plates (SLS) at 20 °C or 4 °C using a mosquito liquid handling machine (TTP Labtech Limited, Melbourn, UK) maintaining a protein to crystallization solution ratio of 2:1. Commercial screens, namely Crystal Screen I and II (Hampton Research, Aliso Viejo, CA, USA), Pi-minimal screen (Jena Biosciences, Germany), Wizard Classic I, Midas, Morpheus (all Molecular Dimensions, Suffolk, UK) were employed. Plates were incubated in a crystal growth incubator (Molecular Dimensions) and observed periodically under a light microscope to check for the presence of crystals. For manual optimization of the hit conditions, 24 well SBS plates (Molecular Dimensions) were used, maintaining the same protein to crystallization solution ratio as used in the screening stage.

2.2.8.2 Crystal harvesting and X-ray analysis

The single Arb2 crystal was mounted on a CryoLoop (Hampton Research) and vitrified in liquid nitrogen for X-ray diffraction studies (Fig. 3.16). Prior to vitrification the crystals were cryo protected in the original growth condition supplemented with 25% (v/v)

glycerol. Crystal looping and X-ray diffraction study was performed at Diamond Light Source with beamline i03 (Didcot, UK) at 100 K by Dr. Abhimanyu K. Singh (Department of Biosciences, University of Kent).

2.2.9 Thermal shift assay

Differential Scanning Flourimetry (DSF) is a method that measures the thermal stability of a protein by assessing its melting temperature.

Fluorescent dye is used. A measure of change in fluorescence indicates unfolding of the protein over time in a qRT-PCR machine. This assay was performed at Argenta Laboratories (Canterbury, UK) using a 96 well plate with a screen of buffers made up to 150 µL per well which was combined with the protein 1 µL at 0.2 mg/mL and SYPRO Orange dye (Invitrogen). Plates were covered with stick film before calibration of qRT-PCR. This thermal shift assay qRT-PCR cycle program was run and managed by Steve Irving at Argenta.

The buffer screen was designed for this protein and screened combinations with various levels of pH, NaCl/KCl and adding glycerol (see Appendix 1.1.3).

2.2.10 InVision His-tag In-gel stain

The InVision His-tag In-gel stain (Thermo Fisher Scientific) was tested and used following the manual instructions. Briefly, the gel was fixed for 1 hour with fixing solution, washed with water and then stained with InVision for 1 hour. Finally, the gel was washed with 20 mM phosphate buffer pH 7.8 before visualization of fluorescent bands on a UV transilluminator at 560-590 nm.

2.2.11 MALDI-TOF mass spectrometry

Trypsin digestion and mass spec analysis were assisted by supervision of Dr. Kevin Howland (School of Biosciences, University of Kent) in the University of Kent Mass Spec Core Facility. Samples were cut with a clean scalpel from SDS-PAGE gel, further cut into ~1 x 1 mM pieces and moved to a treated 1.5 mL Eppendorf with 50 µL sterile ddH_2O. Eppendorfs were prepared by sterilizing, rinsing with methanol and air drying. Washes were applied to reduce and alkylate the samples.

The gel pieces were rehydrated for 30 min in 20 µL digestion buffer:10 mM NH_4HCO_3, 10 % (v/v) acetonitrile with added 10 ng μL^{-1} of trypsin at 4 °C (on ice). After removal of excess supernatant, 10 µL of the digestion buffer (without trypsin) was added (to keep gel pieces wet during enzyme cleavage) and samples were left to incubate at room temperature overnight. To extract the peptides, 5 µL of acetonitrile was added directly to

each digested sample. This mixture was sonicated for 15 min in an ultrasound bath. After collection of the supernatant, an additional incubation with 10ul 50% (v/v) acetonitrile with 5 % (v/v) formic acid) and 15 min sonication contributed further supernatant to the same collection. This was stored at -20 °C or (4 °C for same day analysis) until analysis by mass spectrometry.

The samples analysed by MALDI-TOF mass spectrometry were presented as dried droplets on an AnchorChip MALDI target plate. The calibration standard (Peptide Calibration Standard II Bruker Part #8222570) was vortexed and kept on ice while it was mixed with 125ul of TA30 (30% acetonitrile, 0.1% trifluoroacetic acid solution). The standard (0.5 µL) was applied to the center of four circular marks on the plate and left to dry (~5 min). The samples were then applied to the center of each of the four surrounding circles.

Once dried, a matrix solution of a-cyano-4 hydroxycinnamic acid (HCCA) in 85 % acetonitrile, 15 % water and 0.1 % trifluoroacetic acid with 1 mM ammonium dihydrogen phosphate was applied on top of the samples. This matrix will mix with the sample and form crystals.

Inside the vacuum chamber of the machine, adjustments are made so that the machine recognizes the exact location of each sample. The laser fired with a delay of 80 ns and the HCCA absorbed the laser energy which was transferred to the tryptic peptides causing them to ionize. An electric field was applied to these ions which encouraged them to move into an area without electric field so that the ions could move to sensors that documented their time of flight. Specifically, the sample plate sat below two charged grids and the difference in electric fields caused the particles to accelerate to a detector beyond grids. A measurement of this time of flight is used to calculate the mass-to-charge ratios of peptides present in the sample (Coombes et al. 2005). First the program performed mass spectrometry which gives information about the intact (digested) sample (the peptide mass fingerprint) and then mass spec/mass spec (mass fingerprint) which leads to fragmentation between amino acids providing peptide sequence data.

Mass spectrometry analysis was done on a Brukers ultrafleXtreme machine. Databases used for sample comparison were: KentProt 2015_06 (an in-house database consisting of SwissProt entries supplemented with protein sequences of interest to researchers at the University of Kent: 195282524 sequences; 195457817 residues); To identify GST-Hda1 and Hda1-His: SwissProt 2016_04 (550960 sequences; 196692942

residues) or Hda2: NCBInr 20160506 (86834168 sequences; 31854164354 residues). The Mascot Server Software was used for this analysis (Perkins et al. 1999).

The results of this assay are outlined throughout Chapter 3 and specific polypeptide matches are listed in Appendix 2.2.

2.2.12 Solubility tests

2.2.12.1 Solubility Screen Setup

Solubility Screen preparations tested pelleted cells from 1 mL samples with OD_{600} = 1 using (50 mM Tris pH 7.5, 50 mM NaCl, 5mM EDTA, 1mg/ml lysozyme) buffer with the addition of urea (0.5 M), salt (increased to 2 M NaCl), added detergent with decrease in Tris (20 mM Tris pH 7.5, 0.2 % NP 40) and altered pH (Tris pH to 7, 8 or 9, MES buffer pH 6 or Na Acetate pH 5) (Jeanne Perry Lab Protocol- Molecular Biology Institute, UCLA, Los Angeles, USA). Lysis was done by freeze thaw (see Section 2.2.12.2). Protein was isolated from supernatant by acetone treatment (see Section 2.2.12.3)

2.2.12.2 Freeze thaw of E. coli

Freeze thaw lysis was performed based on the protocol by Jeanne Perry (Molecular Biology Institute, University of California, Los Angeles). Cells resuspended in the designated screen buffer (see Section 2.2.12.1) were frozen quickly on dry ice for 3 min then thawed immediately at 42 °C. This cycle was repeated a total of 4 times. The sample was spun for 5 min at maximum speed in a microfuge before separation of supernatant and pellet.

2.2.12.3 Acetone precipitation of protein from soluble portion after lysis

Acetone was added in a 1:1 ratio to the supernatant. The mixture was frozen for 15 min before spinning for 5 min at maximum speed (microfuge). The acetone was pipetted from the mixture and the pellet dried at 37 °C.

2.2.13 Lysis and western blot for Hda3pET151

Information about cloning, transformation, cell growth and induction of Hda3 constructs can be found in Sections 2.2.4.

The 6xHis-HA-Hda3 frozen cells were resuspended in lysis buffer and sonicated (see Section 2.2.5). The lysed cells were centrifuged at 4 °C for 10 min at max speed. Supernatant (+10 µL loading buffer) and pellet (+10 µL loading buffer) were boiled for 5 min and loaded to gel (only ~8 µL pellet).

After blotting to NB Nitrocellulose paper (see Section 2.3.9), the blot with protein samples embedded was washed with ddH_2O and incubated with Tris Buffered Saline (with 0.1 %) Tween20 (TBST) on a plate shaker for 5 min. The membrane was blocked with 5 % (w/v) non-fat dry milk in TBST for 1 hour. Next, the blot was incubated overnight with 5 µL diluted anti-His antibody solution (1:1000 in TBST) in 5 ml TBST. The next day, the blot was rinsed twice with TBST with 5 min shaking. The TBST was removed and the blot developed with substrate solution (4-Chloronaphthol (VWR) 18 mg, Methanol 3 mL, TBS 47 mL and 12.5 mL H_2O_2 (30 % solution)). The chromophore developed during this time and became visible on the blot.

2.2.14 Controlled degradation of protein

To evaluate the potential for controlled degradation of protein, samples were incubated at 70 °C for 10 min, left at room temperature (25 °C) for 2.5 hrs., overnight at 4 °C and treated normally without the addition of BME in loading dye.

2.3 Microbiological techniques for *C. albicans* and *S. cerevisiae*

2.3.1 Yeast strain culturing

The yeast strains used for this project are listed in the following table (Table 2.5). Plasmid construction prior to genome integration was done following methods in Sections 2.1.3 and 2.1.5.

For storage of yeast, stocks were maintained made with either a scoop of yeast from a culture streaked on a plate and mixed directly in to 50 % glycerol or 1:1 50 % glycerol with saturated overnight liquid yeast culture (grown in YPD containing extra adenine (0.1 mg/mL) and uridine (0.08 mg/mL) or Synthetic Complete (SC) media).

Plate cultures of *C. albicans* and *S. cerevisiae* cells were streaked from a glycerol stock to an agar plate. Antibiotics were added when required. A list of antibiotics can be found in Table 2.6. The agar plates were incubated overnight at 30 °C and enclosed by either PARAFILM or plastic bags during incubation. Additives were included when required and are listed in Table 2.6.

Liquid cultures were inoculated with a small amount of streaked yeast from an agar plate culture. In general, aerobic cultures were grown on a platform shaker at ~ 180 rpm at 30 °C and antibiotics or additives were included as required (Table 2.6).

Table 2.5 Yeast strains

Strain Number	Description	Genotype	Figure	Source
C. albicans: ABy_# ; *S. cerevisiae*: CWG_#				
ABy_54	SN152	*MTL a/alpha ura3Δ-iro1Δ::imm434/URA3-IRO1 hiA1Δ/hiA1Δ arg4Δ/arg4Δ leu2Δ/leu2Δ*	4.4-8/10-11/26-31/22/35/37-38, A3.2.1-6	(Noble & Johnson 2005)
ABy_55	SC5314	*wildtype*	4.26-27	Gift from the Berman Lab Tel Aviv University
ABy_66	BWP17	*MTL a/alpha ura3Δ::Δimm434/ura3Δ::Δimm434 hiA1::hisG/hiA1::hisG arg4::hisG/arg4::hisG*	4.1-2/4/36, A3.1	(Wilson et al. 1999)
ABy_179	*hda1* Δ/Δ	*MTL a/a arg4Δ/arg4Δ hiA1Δ/hiA1Δ leu2Δ/leu2Δ URA3/ura3Δ::λimm434IRO1/iro1Δ::λimm434 hda1Δ::C.d.HIS1/hda1Δ::C.m.LEU2*	4.10-11/26-31/35-38, A3.2.2-5	(Hnisz, Sehwarzmüller, et al. 2009)
ABy_191	HDA3/Δ	*MTL a/alpha ura3Δ::Δimm434/ura3Δ::Δimm434 hiA1::hisG/hiA1::hisG arg4::hisG/arg4::hisG HDA3/hda3Δ::LAL*	4.36	This study
ABy_279	MRR1 gain of function P683S	*SC5314 MRR1P683S-FRT/MRR1P683S-FRT*	4.26-27	(Christoph et al. 2012)
ABy_331	BWP17 *hda3*Δ/Δ	*MTL a/alpha ura3Δ::Δimm434/ura3Δ::Δimm434 hiA1::hisG/hiA1::hisG arg4::hisG/arg4::hisG hda3Δ/hda3Δ*	4.4-35-36	This study
ABy_347	*hda2*Δ/Δ	*MTL a/alpha ura3Δ-iro1Δ::imm434/URA3-IRO1 hiA1Δ/hiA1Δ arg4Δ/arg4Δ leu2Δ/leu2Δ hda2Δ/hda2Δ*	4.4-8/10-11/26-31/35/38	This study
ABy_350	*hda2*Δ/Δ	*MTL a/alpha ura3Δ-iro1Δ::imm434/URA3-IRO1 his1Δ/his1Δ arg4Δ/arg4Δ leu2Δ/leu2Δ hda2Δ/hda2Δ*	4.35	This study
ABy_368	*HDA1:HDA1-GFP*	*MTL a/alpha ura3Δ::Δimm434/ura3Δ::Δimm434 hiA1::hisG/hiA1::hisG arg4::hisG/arg4::hisG HDA1::HIS/HDA1-GFP*	4.1	This study
ABy_372	*HDA2:HDA2-GFP*	*MTL a/alpha ura3Δ::Δimm434/ura3Δ::Δimm434 hiA1::hisG/hiA1::hisG arg4::hisG/arg4::hisG HDA2::HIS/HDA2-GFP*	4.1	This study
ABy_376	*HDA3:HDA3-GFP*	*MTL a/alpha ura3Δ::Δimm434/ura3Δ::Δimm434 hiA1::hisG/hiA1::hisG arg4::hisG/arg4::hisG HDA3::HIS/HDA3-GFP*	4.1/3/46	This study
ABy_393	BWP17 *MTLα*Δ	*MTLa/MTLalphaΔ ura3Δ::Δimm434/ura3Δ::Δimm434 hiA1::hisG/hiA1::hisG arg4::hisG/arg4::hisG*	4.22	This study

ABy_402	*hda1Δ/Δ::HDA1pre-Arb2only-*HA	*arg4Δ/arg4Δ hiA1Δ/hiA1Δ leu2Δ/leu2Δ URA3/ura3Δ::λimm434IRO1/iro1Δ::λimm434 hda1Δ::C.d.HIA1/hda1Δ::C.m.LEU2::HDA1pre-Arb2onnly-HA*	Section 4.3.3.6	This study
ABy_460	SN152 *hda3Δ/Δ*	*MTL a/alpha ura3Δ-iro1Δ::imm434/URA3-IRO1 hiA1Δ/hiA1Δ arg4Δ/arg4Δ leu2Δ/leu2Δ hda3Δ/hda3Δ*	4.4-8-10-11/26/31/37/38, A3.2.1-6	This study
ABy_472	*ADH1/ pNIM-HDA3:adh1Δ*	*MTL a/alpha ura3Δ::Δimm434/ura3Δ::Δimm434 hiA1::hisG/hiA1::hisG arg4::hisG/arg4::hisG hda3Δ/hda3Δ* pNIM-HDA3::adh1Δ/ADH1	4.36	This study
ABy_514	*SCMDR1E4A*	*SC5314 ADH1/adh1::PADH1-MDR1-caSAT1*	4.26-27	(Hiller et al. 2006)
ABy_516	*SCADH1G3A*	*SC5314 ADH1/adh1::GFP-caSAT1*	4.26-27	(Hiller et al. 2006)
ABy_525	*SN95 hda1Δ/Δ*	*arg4Δ/arg4Δ his1Δ/his1Δ URA3/ura3::λimm434 IRO1/iro1::λimm434 HIS1/his1::TAR-FRT hda1::FRT/hda1::FRT*	A3.2.4-5	(Li et al. 2017)
ABy_526	*SN95 Control for hda1Δ/Δ*	*arg4Δ/arg4Δ his1Δ/his1Δ URA3/ura3::λimm434 IRO1/iro1::λimm434 HIS1/his1::TAR-FRT*	A3.2.4-5	(Li et al. 2017)
ABy_529	*ADH1/ pTET-HDA3:adh1Δ*	*MTL a/alpha ura3Δ::Δimm434/ura3Δ::Δimm434 hiA1::hisG/hiA1::hisG arg4::hisG/arg4::hisG ADH1::adh1/pTETGFP-HDA3*	4.2	This study
ABy_532	*HDA2:HDA2-GFP*	*MTL a/alpha ura3Δ::Δimm434/ura3Δ::Δimm434 hiA1::hisG/hiA1::hisG arg4::hisG/arg4::hisG HDA2::HIS/HDA2-GFP*	4.3/46	This study
ABy_536	*HDA2:HDA2-GFP HDA1:HDA1-HA*	*MTL a/alpha ura3Δ::Δimm434/ura3Δ::Δimm434 hiA1::hisG/hiA1::hisG arg4::hisG/arg4::hisG HDA2::HIS/HDA2-GFP HDA1::NAT/HDA1-HA*	4.3	This study
ABy_539	*HDA3:HDA3-GFP HDA1:HDA1-HA*	*MTL a/alpha ura3Δ::Δimm434/ura3Δ::Δimm434 hiA1::hisG/hiA1::hisG arg4::hisG/arg4::hisG HDA3::HIS/HDA3-GFP HDA1::NAT/HDA1-HA*	4.3	This study
ABy_547	*hda2Δ/Δ MTLαΔ*	*MTL a/ MTLalphaΔ ura3Δ-iro1Δ::imm434/URA3-IRO1 hiA1Δ/hiA1Δ arg4Δ/arg4Δ leu2Δ/leu2Δ hda2Δ/hda2Δ*	4.22	This study
ABy_551	*hda3Δ/Δ MTLαΔ*	*MTL a/ MTLalphaΔ ura3Δ-iro1Δ::imm434/URA3-IRO1 hiA1Δ/hiA1Δ arg4Δ/arg4Δ leu2Δ/leu2Δ hda3Δ/hda3Δ*	4.22	This study
ABy_563	*HDA1:HDA1-HA*	*MTL a/alpha ura3Δ::Δimm434/ura3Δ::Δimm434 hiA1::hisG/hiA1::hisG arg4::hisG/arg4::hisG HDA1::NAT/HDA1-HA*	4.3/23/46	This study
ABy_597	*YNG2*-MYC	ura3::1 imm434/ura3::1 imm434 yng2::hisG/YNG2-13MYC-URA3	4.9	(Lu et al. 2011)

ABy_598	*yng2K175R-MYC*	ura3::1 imm434/ura3::1 imm434 yng2::hisG/YNG2K175R13MYC-URA3	4.9	(Lu et al. 2011)
ABy_599	*yng2K175Q-MYC*	ura3::1 imm434/ura3::1 imm434 yng2::hisG/YNG2K175Q13MYC-URA3	4.9	(Lu et al. 2011)
CWG_7698	BY4741	MATa hiA3Δ1 leu2Δ0 met15Δ0 ura3Δ0	3.2.2	Gift from the Gourlay Lab, University of Kent

To induce filamentation in *C. albicans*, cultures were grown at 37 °C while otherwise they were grown at 30 °C. Stationary incubation was done in a LEEC Classic Incubator (Colwick Industrial Estate Nottingham, UK). Growth conditions with CO_2 were done in an Infors HT minitron. Most additives were purchased from Sigma-Aldrich or Melford. Adenine was sourced from Duchefa Biochemical (Hamilton, New Zealand).

Table 2.6 Additives and Antibiotics for yeast work

Solution	Stock concentration	Final concentration
50X Adenine	1g/200 mL	1x
ATP	25 mM	2.5 mM
Caffeine	N/A	15 mM
Calcofluor White	5 mM	20 µM
Caspofungin	2ug/uL	365.8µM
Cerulenin	5 mg/ml	2 µM
Cobalt	1 M	1.5 mM
Copper ($CuSO_4$)	500 mM	5 & 7 mM
Cycloheximide	10 mg/mL	18 mM
Cysteine	250 mM	2.5 mM
EDTA	0.5 M	0.75 mM
EtOH	100 %	3 %
H_2O_2	9.79 M	4.5 mM
HU	11 M	25 mM
LiCl	1 M	300 mM
Methionine	250 M	2.5 mM
NaCl	10 M	2 M
Nicotinamide	N/A	120 mM
Phloxine	5 mg/mL	5 µg/mL
Rapamycin	2.5 mg/mL	7, 9 & 16 nM
SDS	10 %	0.01 %
Serum	100 %	10 %
SHAM	200 mM	1 mM
SNP	500 mM	1 mM
Sorbitol	5 M	1.5 M
100X Uridine	1.6g/200mL	1x
Zinc ($ZnCl_2$)	.05 M	3 mM

The filter-sterilized supplements were added medias prior to use. If stock concentration is not listed powder was mixed directly.

Antibiotic	Stock concentration	Final concentration
Nourseothricin (Nat)	200 mg mL^{-1}	200 µg/ml
Fluconazole	5 mg/mL	3.2 µM
Doxycycline	50 ug/uL	100 µg/mL- whole protein extraction 30-100 µg/mL- filamentation assays

All antibiotics were filter sterilized.

2.3.2 Yeast culture optical density measurements

The optical density of cultures was measured using an Eppendorf, kinetic BioSpectrometer or BioPhotometer plus using a polystyrene 1.6 mL cuvette (Sarstedt, Numbrecht, Germany). Absorbance readings were taken at a wavelength of 600 nM. The cell density approximation values used for calculations throughout this thesis are *C. albicans*- 1 OD_{600} = 3 x 10^7 cells/ ml.

2.3.3 Preparation of DNA from yeast colonies for PCR

To isolate DNA from yeast cells for PCR, small portion of colony was boiled at 100 °C in 40ul .02 M NaOH for 10 min and recovered on ice for another 10 min. Cell debris were pelleted at 2,000 xg for 5 min and 1-2 µL supernatant was taken as DNA for PCR reaction as detailed in Section 2.1.1.

2.3.4 Transformation of *C. albicans* cells

Transformation of *C. albicans* cells was done using either fresh or frozen competent cells. When many transformations are done with the same strain, storing competent cells saves time and materials. The protocol for using frozen competent cells can be easily scheduled around other lab work whereas fresh cell transformation must be done over a block of hours.

It must be noted that the impact of freezing cells prior to transformation has not been evaluated or documented in the model organism *C. albicans*. While it is common practice in *S. cerevisiae* labs, yeast does experience temperature change as a stress. Therefore, the protocol herein (see Sections 2.3.4.2) is somewhat novel and has the potential for being documented whereby the genomic implications could be explored in more detail.

2.3.4.1 Transformation by electroporation of fresh of *C. albicans* cells

To make fresh competent cells for immediate use, a culture of YPD was grown overnight at 30 °C in a shaking incubator. This culture was reinoculated and grown further before harvesting at an OD_{600} = 1.3. For fresh transformation 100mL of culture was harvested at 4K rpm for 2 min at 4 °C and washed with cold sterile ddH_2O. The cells were then pelleted and resuspended in 25 mL TELiDTT (stock: 10 mL 10x TE, 10 mL 1 M LiAc, 1 mL 1M DTT, 79 mL ddH_2O; filter sterile) and incubated for 1 hour with periodic inversion. After, the cells were centrifuged as before, and supernatant was discarded. The cells were washed, first with water and then with 1 M sorbitol (both ice-cold). Finally, the cells were resuspended into 100 µl 1 M sorbitol and kept on ice until transformation.

Transformation of fresh cells (see Section 2.3.4.1) was done by electroporation. DNA from concentrated miniprep or PCR product (~1-100 ng in 5 µL or more) was added to 40 µL competent cells and incubated on ice for 5 min. After transfer to an appropriate cuvette, which was prepared cold on ice, electroporation was performed at 1.5kV, 25 µFD and 200 ohms in electroporation chamber of the BioRad GenePulser XCell machine.

After transformation the cells were given time to recover in YPD before selection. The transformed cells were either plated (overnight to YPD) or grown liquid (~2 hours in YPD shaking) before final (replica) plating (~100 cells/plate) with necessary auxotrophic or antibiotic selection. After transformation, final plates were incubated at 30 °C for 3-5 days.

2.3.4.2 Lithium acetate transformation of frozen of *C. albicans* competent cells

Batches of freeze-stored competent cells were made and maintained at -80 °C for ongoing use. In this case, the cells were grown as detailed above, but all steps were done at room temperature to minimize temperature stress. 50 mL of culture was harvested and washed once with water and once with SORB (stock: 10 mM lithium acetate, 10 mM Tris-HCl pH 7.5, 1 mM EDTA/NaOH pH 7.5, 1 M Sorbitol; adjust with dilute acetic acid to pH 8; filter sterile; store at room temperature for several months). Resuspending in 360 ul SORB + 40 ul denatured carrier DNA (10 mg/ml salmon sperm DNA (Sigma-Aldrich), denatured at 100 °C for 10 min. and cooled on ice, stored at -20 °C) (0 °C). The cells were aliquoted in 50 µL portions and moved quickly to -80 °C for storage (Knop et al. 1999).

Transformation of freeze-stored competent cells was done by lithium acetate method. Cells were brought from storage at -80 °C directly to room temperature. ~5 uL of

DNA (~1-100 ng) from concentrated miniprep or PCR product which was added to cells with 300ul of PEG solution was added with thorough mixing (PEG stock: 100 mM lithium acetate, 10 mM Tris-HCl pH 7.5, 1 mM ETDA/NaOH pH7.5, PEG3500/4000 40 %; store at 4 °C for several months (Knop et al. 1999)). This mixture was incubated 21-24 hours at 30 °C with mixing at 12 hours and again 1 hour before end. After, the mixture was subject to heat shock at 44 °C for 15 min. The cells were pelleted at 2,000 rpm for 15 sec (x2), PEG was removed, and the cells were resuspended in YPD. This was followed by recovery (see Section 4.2.4.1) of the cells before plating to selective media.

2.3.5 Yeast strain construction

2.3.5.1 Homozygous deletion of *HDA2* and *HDA3*

Deletion of *HDA2* and *HDA3* were made using the *Clox* system for gene disruption as described in Shahana et al., 2014. The Clox deletion plasmids was a kind gift from Professor Alistair J P Brown, School of Medical Sciences, University of Aberdeen. This system allows for deletion of both alleles for a gene in diploid *C. albicans* with a recyclable cassette that can be resolved to remove the markers from the genome leaving the final strain cleanly absent of the target gene (Fig. 2.1). This is beneficial as markers themselves can confer phenotypes which can confuse attempts to characterize mutant strains.

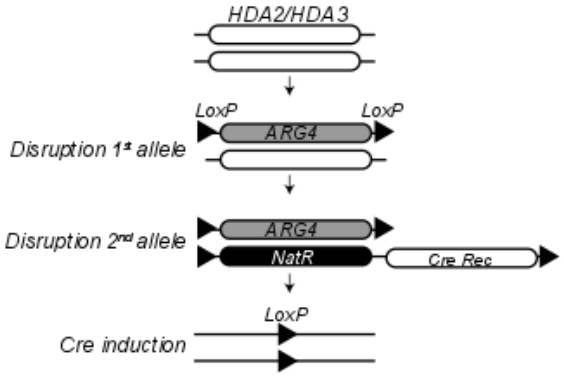

Figure 2.1 Schematic for Clox disruption of diploid gene and subsequent resolution of markers
Progression through installation of first and second markers in the place of *HDA2* or *HDA3* alleles followed by resolution at *LoxP* sites via induction of *Cre Recombinase*. The final mutant has both alleles deleted and no markers in place [Adapted from Shahana et al., 2014]

The *hda2*Δ/Δ and *hda3*Δ/Δ strains were constructed in SN152 and BWP17 background using the LAL (loxP-ARG4-loxP; ABp_80) and NAT1-Clox (loxP-NAT1-MET3p-cre-loxP; ABp_83) plasmids in succession. Prior to resolving markers, homozygous mutants were kept on YPD + 2.5mM methionine + 2.5 mM cysteine plates to prevent activity of Cre recombinase selection of non-resolvable transformants (as directed by lab communication with Professor Alistair J P Brown).

Markers were resolved by growing single colonies overnight ~18 hours at 30 °C in liquid synthetic complete media supplemented with 2.5mM methionine, 2.5 mM cysteine and 200 µg/ml Nat. These cultures were spun down (4K rpm for 3 min at 4 °C) and washed twice with ddH_2O before resuspension of cell pellets in 10 mL synthetic complete media (without additives). The cells were grown in the new media for 4 hours shaking at 30 °C after which ~100-500 cells were plated to synthetic complete agar. After growth, the colonies were replica plated to selective agar: SC, -arg dropout and with Nat. Positive colonies showed no growth on Nat or -arg dropout media (note additions to media of unresolved Clox deletions: Methionine 2.5 mM and Cysteine 2.5mM) at 30 °C. The replica of these colonies growing on the synthetic complete agar plates was further confirmed by PCR before storage in 50 % glycerol (see Sections 2.1.1).

2.3.5.2 *GFP* and *HA* tagging of *HDA1, HDA2* and *HDA3* at native locus

GFP tagging of *HDA1*, *HDA2* and *HDA3* respectively by adding the sequence at their native loci was done with the pGFP-His1 plasmid (ABp_11). The plasmid was subject to high fidelity PCR with long oligos that matched the plasmid and isolated a tagging cassette while contributing flanking nucleotides that matched *HDA1* (ABo_456&457), *HDA2* (ABo_458&459) or *HDA3* (ABo_460&460) up and downstream sequences. The PCR products were gel extracted and purified before they were transformed by electroporation into the native loci of the final [*HDA1*-GFP: BWP17 (ABy_66), *HDA2* and *HDA3*-GFP: SN152 (ABy_54)] yeast strain. Correct integration was confirmed by colony PCR (ABo_145 with ABo_417, ABo_261 or ABo_262 respectively). The final strains used for GFP localization microscopy check are: *HDA1-GFP*: ABy_376 (BWP17), *HDA2*-GFP: ABy_368 (SN152) and *HDA3*-GFP: ABy_372 (SN152). Similar strategies were used to further modify additional strains: ABy_376 (*HDA3*-GFP in BWP17) and ABy_532 (*HDA2*-GFP in BWP17), to make double tagged strains *HDA2*-GFP/*HDA1*-HA (ABy_536) and *HDA3*-GFP/*HDA1-HA* (ABy_539) used for immunoprecipitation and

whole protein assays. These have a C-terminal GFP tag and this integration is codon optimized for *C. albicans* (Gerami-Nejad et al. 2001). Tagging of Hda1 by HA was done with long oligo PCR using ABp_17 as a template.

Cells were grown in minimal media with added 2 % filter sterilized glucose (40 % stock) to an OD_{600} = 1.5 to achieve mid log phase before imaging (see Section 2.3.8.5).

2.3.5.3 Reintegration of HDA3 at ADH1 locus under doxycycline induction

To reintegrate *HDA3* with N terminal *GFP* tagging (with *GFP*: pTET; without *GFP*: pNIM) to the Alcohol Dehydrogenase 1 (ADH1) locus of both the *HDA3* homozygous mutant (ABy_331) and wildtype BWP17 (ABy_66) strains, *HDA3* PCR products were isolated from the synthesized *HDA3* plasmid (ABp_152) by high fidelity PCR with long oligos (full: pNIM: ABo_624& 625 or pTET ABo_627& 628), column purified, digested by *Xho*I/*Bgl*II and cloned to plasmids pNIM (ABp_111) or pTET (ABp_140) (Lai et al. 2011) (Weyler & Morschhäuser 2012). Digested PCR products were ligated into the gel extracted and purified pNIM plasmid which had been digested with *Xho*I/*Sal*I (compatible end cloning) and *Bgl*II or pTET with digestion at *Aat*II/*Stu*I. The ligations were plated to synthetic complete agar with ampicillin added for selection. Plasmids were confirmed by PCR, restriction digest and sequencing.

Cassettes were digested out of the cloned plasmids (pNIM/pTET: ABp177/213) at restriction sites (pNIM: *Sac*II & *Apa*I; pTET: *Kpn*I & *Sac*II). The cassettes were gel extracted and purified before transforming into *C. albicans* strain. Transformants were plated to YPD with Nat for pNIM or -ura dropout agar for pTET selection of positive colonies. Reintegration at the ADH1 locus was confirmed at the ADH1 gene locus by colony PCR before strains were frozen to the collection (pNIM/pTET: ABy_472/493 (in ABy_331-*hda3*ΔΔ) and ABy_471/529 (in ABy_66- BWP17). For doxycycline induction, the drug was added to the media at 30 µg/mL in 20 mL plates or at 100 µg/mL to overnight liquid cultures which were reinoculated and grown to log phase before imaging by microscope (see Section 2.3.8.5). Alternatively, strains were plated to this media as described in the colony filamentation assay (see Section 2.3.8.6).

2.3.5.4 Mating type knockout mutants: *HDA1*, *HDA2* and *HDA3*

Mating type Knockout Mutants of *hda1*Δ/Δ, *hda2*Δ/Δ and *hda3*Δ/Δ were constructed by the method described in Sasse and Morshhauser 2012. This strategy uses a *Candida* adapted flippase (FLP) gene under control of the *MAL2* promoter which can be integrated

and subsequently induced (by media made with maltose) allowing for removal of the cassette. The cassette features nourseothricin-resistance which allows for selection of successful transformants. The knockout was made in the WO-1 background.

The *SATI* flipping cassette plasmid (ABp_136) was generously provided by Dr. Matthew Anderson (Ohio State University, Ohio, USA). Here are the details of its construction: two regions that include 300-500 bp up and downstream of the target gene, in this case the alpha mating type locus, were amplified by PCR. The PCR products and plasmid were digested in 30 µL reactions; upstream PCR by *Apa*I and *Xho*I; downstream PCR by *Sac*I and *Sac*II; and plasmid sequentially by *Xho*I and *Sac*II (gives SAT1 flipper cassette) and again by *Apa*I and *Sac*I (gives vector backbone ~4 kb). These digests were made for 5 µg in a 50 µL reaction for three hours using 15 U of each restriction enzyme. Fragments were gel extracted, purified (see Section 2.1.2) and eluted into 10 µL ddH_2O. Ligation was performed overnight at 16 °C to a mixture of the vector, fragments and cassette in a 1:3:2 ratio using T4 ligase (1-3 U μL^{-1}) and this was transformed into competent DH5α *E. coli* cells which were plated to LB with 25 ug/mL Chloramphenicol for selection. The ligation was confirmed by PCR and sequencing.

The cassette was digested from the plasmid with *Apa*I and *Sac*I (fragment ~6 kb and vector). SAT1 digest product (50 µL) was separated by overnight gel electrophoresis in a 1 % agarose gel in 1x TAE buffer at 40 V and purified by gel extraction purification (see Section 2.1.3). The cassette was eluted into 6 µL ddH_2O and transformed into *hda2*ΔΔ and *hda3*ΔΔ homozygous mutants using electroporation. The transformed cells were selected by plating to YPD with 200 ug/ml Nat in two successive instances. Finally, colonies were analyzed for the presence of the mating type knockout cassette by PCR. Following this diagnostic, a colony positive for the cassette was inoculated for overnight growth in Yeast Extract-Peptone-Mannitol (YPM) media (30 °C) and plating to YPD with 20 ug/ml nourseothricin. Small colonies showing Nat sensitivity (having lost the cassette) were re-plated to YPD with 200 ug/ml Nat and observation of no growth confirmed the successfully resolved strain which was then further verified by PCR (ABo_511&512 (*SAT1*), ABo_462&463 (MTLa) and ABo_464&465 (MTLα)). These strains and a wildtype control were used to evaluate white-opaque switching as described in Sections 2.3.8.3 and 4.2.2.4.6.

2.3.6 Isolation of RNA, cDNA synthesis and real time qRT-PCR

2.3.6.1 RNA extractions, optical density measurement and electrophoresis

Overnight YPD culture (inoculated at OD_{600} = .00005; grown ~16.5 hours = 14 doublings) grown to OD_{600} = ~0.8. Cells were collected by spinning for 2 min at 1000 x g at 4 °C and washed once with ddH_2O. Cells were resuspended in 1ml final media (YPD or RPMI) and placed into 15 ml pre-warmed final media (30 °C or 37 °C respectively) then grown for 90 min. OD_{600} values were recorded (OD_{600} = ~1.5) followed by RNA extraction with Omega EZNA Yeast RNA Kit (VWR) following the kit protocol with two modifications: (1) 30 °C incubation in SE Buffer/2-mercaptoethanol/lyticase solution time was increased to 90 min, and (2) lysis was performed with bead mill at top speed for 30 min at 4 °C. DNase I digestion was included prior to final wash steps. RNA was eluted into 50 µL Diethyl pyrocarbonate (DEPC) water (RNase inactivated). Extracted RNA was assessed by nanodrop optical density reading and run on a formaldehyde gel to visualize denatured RNA. Final storage of RNA was at -80 °C.

Specifically, RNA was extracted from *hda1*ΔΔ, *hda2*ΔΔ and *hda3*ΔΔ homozygous mutants with matching wildtype SN152 in YPD and after growth for 90 min in RPMI or YPD as described above. This timepoint was chosen based on published results showing Hda1 enrichment at HWP1 promoter starting around 1.5 hours (see Fig. 1.13) (Lu et al. 2011). Extraction was done in 3 biological replicates, the two best quality (determined by optical density measurement and appearance of bands on gel) for each strain were sent for sequencing. RNA sequencing was done by GENECORE - EMBL Genomic Core Facilities. Before sending the RNA samples to sequence qRT-PCR was undertaken to confirm that hyphae development was evident at a transcriptional level (see Section 2.3.7 and Fig. 4.32).

Quantitation of extracted RNA was determined by spectrophotometer (BioDropDuo). Absorbance was measured at 260 nm. Since DEPC can lower absorbance values the samples were diluted 1:1 in TE for reading A260 and A280 (10x TE stock: 5 mL 1 M tris(hydroxymethyl)aminomethane (Tris) pH 7.5, 1 mL 0.5 M EDTA pH 8, 44 mL ddH_2O). Per RNA extraction kit guidelines, a ratio of 1.8-2.0 was considered 90-100 % pure.

Formaldehyde gel electrophoresis was employed to analyze the quality of extracted RNA. For each sample, 1 µg of RNA was diluted in water to a total of 5 µL and

3 volumes of loading buffer (15 uL) were added before denaturing samples for 10 min at 65 °C. Samples were cooled on ice 10 min before loading entirety to gel.

The formaldehyde gel was run at 80 volts for 40 min in 1 x HEPES running buffer in the fume hood (RNA Gel Composition: 1 g agarose, 73.8 mL ddH_2O, 10 mL 10x HEPES, 16.2 mL 37 % Formaldehyde; Gel rig (tray, comb, rubber ends) was washed with detergent and soaked in 0.1 M NaOH for 60 min in sterile fume hood prior to use; To construct gel, agarose was melted in water and cool before adding HEPES and cold formaldehyde, pour to 100 mL size cast in fume hood) . The RNA samples were diluted with three volumes of RNA loading buffer and loaded into the wells (RNA Loading Buffer: 200 µL 10x HEPES, 1 mL Deionised formamide, 120 µL Bromophenol (BrPh) blue*, 30 µL Ethidium Bromide, 320 µL 36.5-38 % Formaldehyde Solution, 33 µL ddH_2O; Make up to 2 mL with ddH_2O;*BrPh blue 0.25 % w/v in 50 % Glycerol). Electrophoresis was carried out 80 V for 30-40 min prior to imaging (Syngene G:Box with paired software). Two clear bands indicated presence of undegraded RNA (the 28S and 18S bands respectively).

2.3.6.2 cDNA synthesis

Synthesis of cDNA from RNA was done using the PCRBIOSYSTEMS qRT-PCRBIO cDNA Synthesis Kit following protocols designated by the manual. RNA was diluted on ice to 6.6 ng/µL and reaction was performed in PCR machine (BioRad). A no Reverse Transcriptase control was included for all reactions to confirm that there was no contamination with genomic DNA. Reactions were stored at -80 °C.

2.3.7 Real time qRT-PCR

All real time qRT-PCR reactions were performed in a BIORAD CFX Connect Real-Time System machine using BIORAD CFX software and 96 well plates. The basic real time qRT-PCR reactions and the cycles used followed directions in the manual. Each sample was run in duplicate and a no DNA control (ddH_2O) was run for each primer set. Enrichment was calculated relative to actin and experiments were done in biological replicate with three independent cultures for each strain.

2.3.8 Phenotyping methods

2.3.8.1 Serial dilution spotting assays

For spotting assays, starter cultures in YPD were grown overnight at 37 °C shaking. Overnight cultures were diluted to an OD_{600} = 1 and serially diluted by 1/5 in four permutations before spotting to appropriate experimental and control agar medias. The

additives tested are detailed in Chapter 4. Briefly, For analysis in stress conditions, YPD or SC agar media was supplemented with 7/9 nM rapamycin, 2 M sodium chloride, 1 mM SNP with 1 mM SHAM, 7 mM copper sulphate, 300 mM lithium chloride, 0.01 % sodium dodecyl sulfate (SDS), 15 mM caffeine, 1.5 M sorbitol, 18 mM cycloheximide, 1.5 mM cobalt, 25 mM hydroxyurea, 3 % ethanol, 20 µM Calcofluor White, 4.5 mM, hydrogen peroxide, 0.75 mM EDTA, 2 µM Cerulenin, 120 mM nicotinamide, 365.8 mM caspofungin, 3.2 µM fluconazole and 3 mM zinc chloride. RPMI media was supplemented with 25 nM rapamycin, 6 mM copper sulfate or 3.2 µM fluconazole (Oliver R. Homann et al. 2009). Cells were grown at 30 °C or 37 °C as indicated. Plates were imaged on an Epson scanner at 24-hour intervals for 3 or more days as needed to apparently reach full growth.

2.3.8.2 Biofilm Screen

To screen biofilm formation in the *hda3*ΔΔ mutant and matching wildtype strains employed a set up that used silicone rings (Silicone Swinnex 13 gaskets #SX0001301, Merck) attached to a silicone square base this formed a well to encase the biofilm as described in a recent paper and personal directions by Dr. Katherine Lagree (Mitchell Lab, Carnegie Mellon University, PA, USA) (Woolford et al. 2016). Setup was done in sterile conditions. In preparation, the silicone base was coated with 50 % heat-inactivated fetal calf serum (FCS) (Sigma-Aldrich) and incubated for 45 min at 30 °C. This was followed by two gentle washes with PBS. *C. albicans* cell culture OD_{600} = 1 was washed (4K rpm for 2 min) and resuspended in PBS and added to the prepared well. These cells were adhered by stationary incubation at 37 °C for 90 min. All washes during this setup were done to never let the biofilm go dry to avoid structural collapse. The cells were washed gently twice with PBS and the setup was grown covered in RPMI media for 48 hours stationary at 37 °C. A 24 well plate was used as a chamber for the silicone squares and the lid was sealed during this incubation by PARAFILM. Following, the biofilm was washed gently 2x with PBS and the setup was moved from the 24 well plate and glued (superglue) onto a glass microscope slide. The biofilms were next fixed (4 % formaldehyde & 1.5 % glutaraldehyde in 1x PBS) for 1 hour after which they were washed and stained with Concanavalin A AlexFlour 488 at 25 $\mu g ml^{-1}$ in PBS four 30 min with gentle orbital mixing at 37 °C. The samples were next dehydrated with 2 mL methanol with orbital mixing for 20 min. The methanol was removed and replaced with fresh methanol briefly before 50:50 methanol/methyl salicylate and finally 100 %

methyl salicylate. The top of the silicon ring well was glued to a glass microscope cover slide (excluding air pockets) and the samples were imaged with a confocal microscope using a dichromatic beam splitter fluorescent filter (#21473483648) with an excitation wavelength of 488 nm used at 2 % - 98 % and an emission/detection wavelength of 516 nm. The scan mode was laser line and Super resolution mode was used for the Airy scanning. Detector gain was set at 850 with 0 offset and a digital gain of 1. Pixel time was 2.05 µs; Line Time 0.80 µs; Frame Time 20.13 s. Photos were imaged and processed using Zeiss Zen software (ZEN Digital Imaging for Light Microscopy, RRID:SCR_013672).

2.3.8.3 White-opaque Screen

To screen for white-opaque phenotype, cells were freshly streaked from frozen stocks to isolate single colonies. These cells were resuspended in sterile water and plated to synthetic complete agar supplemented with 5 µg/ml Phloxine B (Sigma-Aldrich). Quantitative white-opaque phenotype evaluation was made after the cells had grown for 9 days unsealed at room temperature without light. The experiment was done in 3 biological replicates with 2 technical replicates for each strain. Formation of opaque, white and sectored colonies was scored. Statistical significance is assessed by two-tailed t-test. This protocol was modified from (Miller & Johnson 2002). Violin plots were made by Dr. Alessia Buscaino (Department of Biosciences, University of Kent) using the ggplot package in R studio.

2.3.8.4 UV sensitivity screen

To evaluate UV sensitivity, cells from an overnight culture were diluted to plate ~200 cells to YPD agar. The test plates were irradiated (UVitec, Cambridge) with 10 mJ/cm^2 (.0025 J for 5 sec) and incubated (with the untreated control plates) for 36 hours at 30 °C. Colonies were counted using the ImageJ Colony Counter Plugin (Vieira 2009; Schindelin et al. 2015). Colony Counter Plugin (https://imagej.nih.gov/ij/plugins/colony-counter.html ; settings: size 300-8000; area 0.75-1)

2.3.8.5 Liquid filamentation assay and microscopy

For filamentation in liquid, 5 mL cultures in YPD were grown overnight and throughout the day. From this stationary culture, 1 mL was spun down (2 K rpm for 2 min) and pellet was washed with ddH_2O before resuspending in 1 mL pre-warmed final RPMI or YPD + 10 % serum media. These cultures were grown at 37 °C for ~17 hours before imaging. All liquid filamentation assays were done in parallel with control culture grown with the same

preparation in YPD at 30 °C. Additives and antibiotics added to the liquid as stressors are detailed in Table 2.6.

Morphology of *C. albicans* in liquid cultures was evaluated from images produced by Olympus CellR imaging software. 3 µL of concentrated culture from vortexed (2 K for 2 min) sample on a slide (Thermo Fisher Scientific). Images were captured using an Olympus 1X81 inverted microscope with U-TV 1X-2 lens and an Andor Zyla sCMOS camera with light excitation from an Olympus MT20 illumination system with approximately the following typical settings: exposure time 50 milli. sec., bining 1x1 and brightness 197 -1850 using UPLSAPO 60x lens with 2085 µM Zdrive limit. GFP filter measuring emissions of 510-540 nm was applied for visualization of fluorescently tagged proteins via mercury arc lamp. Quantifications of morphology were made by measurement of the length of imaged yeast/hyphae cells by the following categories: $\leq$ 2.0 cm, 2.1-5.0 cm or $\geq$ 5.1 cm. Experiments were done on three separate days.

2.3.8.6 Colony filamentation assay

To assess filamentation in yeast colonies, cultures were grown overnight (~16 hours) in 5 mL liquid YPD at 30 °C. This starter culture was used to inoculate 10 mL of fresh liquid YPD media (Yeast extract, Peptone, Glucose with added Adenine 0.1 mg/mL and Uridine 0.08 mg/mL) which was grown for ~5 hours at 30 °C. Based on OD_{600} reading, 50 – 100 cells were plated to RPMI, Spider, Serum or SLAD Agar. The plates were grown for ~6 days at 37 °C with or without 5 % CO_2.

All colonies on plates were counted and phenotypes were noted as smooth, intermediate or filamented. Experiments were done on three separate days. Images representative of the phenotypes were obtained using a Leica MZFLIII microscope 1.25 or 2.5x magnification with ~30-70 ms exposure and 1x to 3.4x gain. Morphology was characterized upon visual assessment of filamentation around the edges of colonies.

2.3.8.7 Minimum Inhibitory Concentration (MIC) testing

Drug sensitivity testing was done in 96 well plates in a protocol modeled after the Clinical Laboratory Standards Institute guidelines (vol. 28 M27-A3; Wayne, PA, USA) Reference for Broth Dilution Antifungal Susceptibility Testing of Yeasts. Strains were streaked fresh to synthetic complete media the night before the assay. Drugs were aliquoted first to the 96 well plates in dilutions decreasing by ½ in each well of the horizontal rows 1-10 of the plate with the final two rows left for entirely cell culture (11) or media (12). The readied plate was stored at 4 °C while a dilution of all the cells was made such that (once added

to the wells with media + drug) the final concentration of the cells was $1x10^3$ cells/mL. The base media used was MOPS buffered RPMI 1640 pH 7.2. Drugs tested included concentrations of Fluconazole ranging from 0.15-100 µg/mL; Cerulenin, Diamide and Brefeldin A 0.195-100 µg/mL. The plates were sealed with PARAFILM and monitored by a Spectrostar Nano BMG labtech plate reader machine (VWR) with a two-part script with 8 min shaking followed by linear shake with readings at approximately every 12 min for 24-80 hours. Readings were taken throughout at OD_{595}, and the plates were also monitored with manual scoring. Manual scoring used a 0-4 ranking system with 0 = clear, 1 = slightly hazy, 2 = prominent decrease in visible growth (50 % decrease in turbidity), 3 = slight reduction in visible growth (turbidity), 4 = no reduction in visible growth. This was assessed at timepoints in 12-hour increments or at final endpoint. Plate reader results were analyzed at 24, 48, 72 and endpoint timepoints as available. However, guidelines indicate that 24 to 48 hours is an appropriate time to read results for *C. albicans* strains. There were no within plate replicates, but most drugs were trialed on more than one occasion. The strains included in these screens included: ABy_54, ABy_179, ABy_347 and ABy_460 (hda1 complex mutants and wildtype), *MDR1* drug resistant mutant (ABy_514) with control (ABy_516) and, *MRR1* drug resistant mutant (ABy_279) with control (ABy_55).

2.3.8.8 Macrophage screen

Macrophage cultures were taken from -80 °C, quickly thawed (<1 min) in a 37 °C water bath before isolation of the cells by centrifuge (200 g 5-10 min) and aseptically resuspension into Dulbecco's Modified Eagle Media (DMEM) (41966, Thermo Fisher Scientific) with high glucose and pyruvate and supplements. The media was supplemented with 10 % (v/v) FCS, 2 mM L-glutamine and 200 U/mL streptomycin/penicillin. This culture was incubated at 37 °C with CO_2 and subject to passage (maximum 20x) at 70-80 % confluence as required to keep populations at appropriate size. Mouse macrophages-J774A cell line, RAW 264.7 macrophage were used.

Assessment of *C. albicans* viability after microphage coincubation followed a previously described method (Johnnidis et al. 2008). The aim was 20 x 10^3 macrophage cells in 100 µL DMEM solution per well and these were grown in new media overnight.

For this test an overnight *C. albicans* cultures were diluted to OD_{600} = 15. 50 µL of this culture was mixed 1:1 with calcofluor white. This mixture was subject to centrifuge at 8.2 K rpm for 2 min and washed 3-4x with YPD to remove the stain. Density of the

cells was checked on a light microscope. 300 µL of macrophage cells were mixed with 3 µL of the *C. albicans* culture and grown together at 37 °C. As this was a test, the final ratio of macrophage to *C. albicans* was inconsistent and this should be more controlled (using cell counts) to improve accuracy of the result. Imaging was done at 0, 2 and 3 hours by Olympus 1X81 inverted microscope with white light and 100x amplification. Images were saved as stacked files that were visualized using the ImageJ interface (Schindelin et al. 2015). Macrophage counts were calculated as a ratio of captures/macrophages and relative saturation was noted.

2.3.8.9 Temperature sensitivity Screen

To evaluate temperature sensitivity, cells were grown to log phase. An overnight culture was reinoculated and grown to OD_{600} = 0.5. 1 mL of each culture was removed to a 1.5 mL Eppendorf incubated in a 50 °C water bath for a series of measured durations 0, 10, 20, 40 or 60 min. From each of these heat-treated samples 3 µL of a 1:10 dilution was plated to YPD. The plate was incubated at 30 °C and imaged at 12 hours. This protocol was developed from previously described assays (Zeuthen & Howard 1989; Harcus et al. 2004).

Spotting assays were also used to evaluate growth at 17 °C, 30 °C, 37 °C and 42 °C done by project student Alisha May (Imperial College, London) as described in Section 2.3.8.1.

2.3.9 Western blot

Western blot was used for several experiments in this thesis and the typical protocol is detailed in this section. The exception was to check expression of Hda3 protein, and the details of that protocol are detailed in Section 2.2.13.

Proteins separated by SDS-PAGE (see Section 2.2.6) were transferred onto polyvinylidene difluoride (PVDF) membrane (Immun-Blot, BIORAD). The following preparation was used: the PVDF membrane was activated by brief soaking in 100 % methanol before rinsing with distilled water and immersion in transfer buffer (1x Transfer Buffer: 50 mL 10x Transfer Buffer, 100 mL methanol, 350 mL H_2O; 10x Transfer Buffer stock: 58 g Tris Base, 29 g Glycine, 20 % SDS; Make up to 1 L with ddH_2O). The polyacrylamide gel, PVDF membrane, blotting paper and blotting filter papers (2.5 mm thickness, 7.5 cm x 8.4 cm, Invitrogen) were all soaked in transfer buffer (gel soaked for 15 min) before the blot was assembled. Once this blot was assembled, electrophoresis was done in an Invitrogen Semi-Dry Blotter (Novex) at 25 V for 45 min. Afterward, the PVDF

membrane was incubated with 5 % (w/v) non-fat dry milk in PBST for at least 30 min to block non-specific sites before probing with the primary antibody. Between the primary and secondary antibodies, the blot was thoroughly washed three times with PBST. Blots were washed with the same procedure afterward and moved to PBS before starting the developing process.

Proteins were detected in the dark room by imaging onto film (Amersham Hyperfilm ECL, GE Healthcare Life Sciences, Buckinghamshire, UK) after incubation of the membrane in Clarity Western ECL Substrates 1:1 mixture for 1 min before developing (Optimax 2010, Epsilon NDT, Bucharest, Romania). It should be noted that originally detection was done by Gel doc before a problem detecting the HA antibody led to successful imaging by film which was apparently more sensitive.

To probe for GFP tagged proteins, a dilution of 1:1000 1° anti-GFP antibody (Roche) was incubated overnight at 4 °C. Primary probing of HA tagged proteins was done with the same dilution and procedure using the 1° anti-HA antibody (Sigma-Aldrich). In both cases, the 2° anti-mouse antibody (Sigma-Aldrich) was diluted 1:25000 and incubated for 1 hour at room temperature.

To probe for Actin, a 1° anti-Actin (raised against *S. cerevisiae* actin) antibody was used. This antibody was a gift to Dr. Campbell Gourlay (Department of Biosciences, University of Kent) from the Cooper Lab (Washington University, St. Louis, Mo., USA). A dilution of 1:5000 was incubated overnight at 4 °C. The 2° anti-Sheep antibody (Sigma-Aldrich) was also diluted to 1:5000 and incubated for 1 hour at room temperature.

2.3.10 Whole protein extraction

Whole protein extraction was done in YPD and RPMI medias. The protocol used was derived from Tobias von der Haar's Yeast whole cell protein for SDS page method (von der Haar 2007).Cells were re-inoculated from an overnight culture and grown to OD_{600} = 0.8 – 1 before 10 O.D. were harvested at room temperature. For doxycycline induction GFP strains (constructed with pTet (ABp_140) 100 µg/ml doxycycline was added during growth in liquid media. The cells were resuspended in lysis buffer (lysis buffer: 0.1 M NaOH, 0.05 M EDTA, 2 % SDS, 2 % β-mercaptoethanol in ddH_2O) and heated for 10 min at 95 °C. After, 5 µL of 4 M Acetic acid was mixed in by vortex before incubation for 10 min at 90 °C. 50 µL of loading buffer was added and the extract was stored at -20 °C (Loading Buffer: 0.25 M Tris-HCl pH 6.8, 50 % Glycerol, 0.05 % Bromophenol Blue; in ddH_2O). Samples were heated at 96°C for 5 min and spun down (maximum speed 5

min) and otherwise kept on ice prior to use and the amount loaded varied based on abundance of protein (60 -150 µL) (von der Haar 2007).

2.3.11 Chromatin immunoprecipitation (ChIP)

ChIP was done using two separate experimental scenarios. The first utilized the histone H3K9 antibody and since wildtype, *hda1*Δ/Δ, *hda2*Δ/Δ and *hda3*Δ/Δ strains were being compared, it was possible to use a spike-in of *S. cerevisiae* to control for experimental variation (Orlando et al. 2014). The second experiment tested Hda1-HA with an anti-HA antibody. In this case, the spike-in was not used because it would require a tagged *S. cerevisiae* strain.

2.3.11.1 H3K9 ChIP with Spike-in

Cultures of 200 mL for *C. albicans* test strains and 50 mL BY4741 *S. cerevisiae* were inoculated at OD_{600} = 0.1 from overnight starter (YPD, 30 °C) and grown to OD_{600} = 0.4. For spike-in, the *Candida* test strains were combined with the BY4741 in a ratio of 2:1 OD units (10:5) in 50 mL and fixed with formaldehyde (37 % Formaldehyde solution, Sigma-Aldrich) to a final concentration of 1 % at room temperature for 15 min with gently mixing by hand every 5 min. Following the cross-linking, cells were spun down for 2 min at 4 K rpm at 4 °C (Eppendorf 5810 R). Cells pellets were washed twice with ice-cold PBS (mixed by turning tube) and transferred to round bottom screw top tubes (Simport Micrew Tube, Thermo Fisher Scientific). After a spin at 4 K rpm for 2 min and removal of the supernatant, pellets were stored at -80 °C.

Cell pellets were topped with 500 µL of small glass beads and 700 µL of ice-cold lysis buffer with PhenylMethylSulfonyl Fluoride (PMSF) added to 1 mM (lysis buffer: 50 mM HEPES-KOH pH 7.5, 140 mM NaCl, 1 mM EDTA, 1 % Triton X-100, 0.2 g sodium deoxycholate; add HEPES to 90 mL ddH_2O and pH to 7.5 with KOH, combine with other ingredients and add water to 200 mL). Cells lysis was performed using on a Biogenode Bioruptor Plus (ATG Scientific, Oxford, UK) for four 30 min-runs with 5 min on ice rests between each. Holes were punctured through the bottom of the tubes and disrupted samples were evacuated to ice cooled collection tubes by centrifugation (Eppendorf miniSpin) for 1min at 1K rpm. Sonication was carried out in a pre-cooled to 4 °C sonicator. Sonication was performed for 20 cycles of 30 sec on and 30 sec off. Afterward, the sonicated samples were centrifuged (Eppendorf refrigerated Centrifuge 5415 R) at 13K rpm for 10 min at 4 °C to remove debris. Meanwhile, 25 µL magnetic beads in protein G (Dynabeads, Invitrogen, Thermo Fisher Scientific) per sample were washed with 100

µL lysis buffer 2-4 times with spinning at 2K rpm for 2 min and using magnetic puller (MagnaRack, Thermo Fisher Scientific) to keep beads. The beads were finally resuspended in an equal volume of lysis buffer (25 µL/per). From the centrifuged, sonicated sample, 290 µL was taken to a new tube, and separately 10 µL as a calibration Input sample; To the sonicated sample for immunoprecipitation (290 µL), 2 µL of Histone H3K9ac (Active Motif, Aachen, Germany) 25 µL of washed beads were added. This slurry was mixed with slow rotation (rotator SB3, Stuart) at 4 °C overnight.

The next day beads were isolated using the magnetic puller during several wash steps as follows: The supernatant was removed prior to a wash with lysis buffer and brief inversion. This was followed by 10 min at 4 °C rotating washes first with lysis buffer with 0.5M NaCl (alter lysis buffer recipe: replace 140 mM NaCl with 500 mM NaCl) and second with wash buffer (wash buffer: 10 mM Tris-HCl pH 8, 0.25 M lithium chloride, 0.5 % NP-40, 1 mM EDTA, 0.5 % sodium deoxycholate; make 200 mL). As a final wash, 1x TE was applied and mixture was inverted until beads were resuspended. The supernatant was removed.

Fresh 10 % Chelex (BioRad) was prepared and 100 µL was added to each sample. Chelex was vortexed prior to each addition to insure even distribution. The mixtures were boiled for 12 min at 100 °C and then cooled to room temperature before the addition of 2.5 µL of 10 mg/ml Proteinase K (Melford) to each sample. After vertexing, the samples were incubated on a thermomixer at 55 °C with shaking at 1K rpm for 30 min. The samples were then boiled at 100 °C to inactivate the Proteinase K. The tubes were next centrifuged at 4K rpm for 3 min to clear the resin and beads. 60 µL of the supernatant was taken as a final sample to a clean Eppendorf and stored at -20 °C.

Inputs and IPs were diluted 1:10 in 1x TE and 2 µL were used for qRT-PCR with primers designed to amplify less than 350 bp. The primers used are specifically described in Table 2.1. The qRT-PCR is described in Section 2.3.7.

2.3.11.2 Hda1-HA tagging and ChIP

Tagging of Hda1-HA was done using long oligo PCR of plasmid ABp_17 as a template and the tag was transformed into ChIP, BWP17 (ABy_215). The Hda1-HA ChIP was done with the same protocol covered in Section 2.3.14.1 (above) with two exceptions: no spike-in was employed and the antibody was anti-HA (Sigma-Aldrich).

2.3.12 Co-Immunoprecipitation of Hda1 complex proteins

Co-IP is an experiment that looks at protein interactions by first using an antibody to pull down one tagged protein and second, checking for the presence of another potentially complexing protein (tagged) by western blot. The tagging of Hda2 and Hda3 with GFP for this experiment are detailed in Section 4.3.5.2. Tagging of Hda1 was done with long oligo PCR of ABp_133 as a template and transformed into Hda2-GFP (Aby_532) and Hda3-GFP (ABy_376).

Cultures were grown in 1 L YPD Media for 14 hours at 30 °C in a shaking incubator to an OD_{600} = 1 and harvested at 4K rpm at 4 °C for 10 min (Beckman Coulter Avanti J-301 and Eppendorf 5810 R). After washing the cells three times with cold water and resuspending in 1/5th volume (water/cells) the slurry was drop-frozen in liquid nitrogen before freezing these pellets to -80 °C. Subsequently, the pellets were ground in liquid nitrogen using a mortar and pestle for 30 (cells grown in YPD only) or 45 (RPMI treatment) min per sample. The powdered, lysed cells were stored at -80 °C.

Cell powders were later diluted into 10 ml of 4 °C cold lysis buffer and solubilized for 30 min in rotation at 4 °C (Lysis Buffer: 50 mM HEPES-NaOH pH7.5, 15 mM NaCl (5M stock), 5 mM EDTA (0.5 M), 0.1 % NP-40; Make 500 mL add fresh: 5 mM DTT, 1x protease inhibitor tablets- cOmplete, EDTA free (Roche, Shire Park, Welwyn Garden City, UK) and 0.2 mM PhanylMethane Sulfonyl Flouride (PMSF)). Once diluted lysed (frozen) cell powders were solubilized the supernatant was separated by centrifugation (Eppendorf 5810 R) with cooling to 4 °C at 4 K rpm and further separated by ultra-centrifuge (Beckman Coulter Avanti J-301) with cooling to 4 °C at 18 K rpm.

Concurrent to solubilizing cells, magnetic affinity beads (4ul per sample) were washed (3x PBS) and coupled in 0.5 ml PBS to 4 µL anti-HA antibody (Sigma-Aldrich) for 30 min in rotation 4 °C. The beads were then washed three times (2x PBS; 1x lysis buffer) and resuspended in 10 µL lysis buffer.

The solubilized cell powders were used for immunoprecipitation and evaluation of complexing interactions. First,100 µL input sample was taken (100 µL) and frozen (with 4x loading buffer at -20 °C). Next, 100 µL of coupled mini-beads were added to remaining supernatant. Third, the mixture was incubated for two hours with rotation at 4 °C.

Following, the adhered protein was harvested in 1 mL fractions using a magnetic rack (1.5 mL Eppendorf but 15 mL would be ideal). A final spin of collected cleared supernatant (2K rpm for 2 min- Eppendorf 5810 R) to isolate remaining beads. The beads

were thoroughly washed (4x with pipetting up/down ~10x) with lysis buffer and finally resuspended in 50 µL TE and 4x SDS loading buffer.

This mixture was frozen at -20 °C and later run by gel electrophoresis on SDS-PAGE before western blotting with anti-HA antibody (Sigma-Aldrich) for detection of Hda1-HA (~92.9 kDa + ~6 kDa HA tag: ~99 kDa) and confirmation of successful pull down. Gels were either stripped or a separate gel was run and blotted with anti-GFP antibody (Roche #1184460001) to detect presence of Hda2-GFP (~77 kDa + ~26.4 kDa GFP tag: ~103.4 kDa) or Hda3-GFP (~97.3 kDa + ~26.4 kDa GFP tag: ~123.7 kDa).

2.4 Bioinformatic methods and tools

2.4.1 RNA sequencing and analysis

RNA sequencing and library preparation was done by the European Molecular Biology Association (EMBO) core facility (Heidelberg, Germany). 1 µg of total RNA from each sample (in duplicate: wildtype, *hda1*ΔΔ, *hda2*ΔΔ and *hda3*ΔΔ strain extractions from RPMI and YPD) was used to generate strand-specific cDNA Illumina Barcoded Libraries which were sequenced by an Illumina iSeq200 platform.

The data was analyzed within the Galaxy platform. First, the raw sequencing reads were cleaned up; FASTQ Groomer was used to convert the data to a usable format (Andrews 2010). Trimmomatic was used to clip the adaptors off the single-ended reads and regulate the accuracy of alignment (we assigned a sliding window averaging across four bases keeping a minimum length of 50 reads). These steps were monitored by FastQC which provided feedback reports about the quality of the reads. Next, we put the data through HISAT2 which aligned the trimmed reads with the *C. albicans* reference genome (Assembly: ASM1829v3 A22_Chromosomes). The intron length was set from 20-5000 based on the relatively short (<500 nt) intron length observed in *C. albicans* (Mitrovich et al. 2007). To assemble the alignments into transcripts, StringTie was used. To eliminate artifacts in the form of precursors of processed transcripts a minimum isoform fraction setting of 0.15 was used. The special Stringtie transcript merge mode was employed to eliminate duplicate transcripts (Pertea et al. 2016). To quantify the transcripts the featureCounts (Subread) tool was used with minimum mapping quality set to 12 this resolved misplacement of reads based on the quality scores of matched and mismatched bases (Liao et al. 2014). Finally, the relative expression of genes was assigned using DESeq2 which is appropriate for the small number of replicates (2) in our sample and the

anticipated scope of differential changes we expect to see given deletion of a histone modifier and in RPMI media. This analysis uses a negative binomial distribution to account for number of gene fragments and sequencing depth of the samples which allows for compensation of factors including GC content (Love et al. 2014). The full output from this DESeq2 analysis can be found in the Supplementary Data online at ArrayExpress (accession number: E-MTAB-6920).

2.4.2 Analysis of DESeq2 data

Primary analysis was done using Excel 2016, by hand and using The Gene Ontology (GO) and GO Enrichment Analysis Tool (Ashburner et al. 2000; Mi et al. 2017). Reads from RNA-sequencing data were visualized on the genome using the Integrative Genomics Viewer (IGV) which allowed for scalable viewing of reads laid onto the genome (Robinson et al. 2011; Thorvaldsdóttir et al. 2013).

Images to visualize gene sets and patterns was performed with R Studio (https://www.rstudio.com/) (R Foundation for Statistical Computing 2008): Scatter Plot matrices, using Pearson correlation coefficients, were generated with the ggplot package. The box format output shows individual comparisons between the three mutant strains *hda1*ΔΔ, *hda2*ΔΔ or *hda3*ΔΔ listed diagonally from the top left to bottom right of the diagram. To the right of the diagonal strain list are plots showing with each gene according to its log2 fold change for each mutant strain with correlating values on the related x- and y-axis of the plot. The top left plot depicts log2 fold changes relating the genes from the *hda1*ΔΔ (y-axis) and *hda2*ΔΔ (x-axis) mutants; at top right *hda1*ΔΔ (y-axis) and *hda3*ΔΔ (x-axis) mutants; and at bottom right *hda2*ΔΔ (y-axis) and *hda3*ΔΔ (x-axis) mutants. The measure of the linear correlation of the x- and y- axis values is represented in the Pearson correlation coefficient (Pearson's r value) and significance scores (p value) depicted to the left of the diagonal strain list which are color coded according the scale in the legend (blue: r = -1, white: r = 0, or gold: r = 1). These relate to the diagonal strain list as follows, top left: *hda1*ΔΔ versus *hda2*ΔΔ; bottom left: *hda1*ΔΔ versus *hda3*ΔΔ; bottom right: *hda2*ΔΔ versus *hda3*ΔΔ. Heatmaps were generated with the pheatmap package and Pearson correlation for clustering. Heatmaps show the log2 fold changes of differentially expressed genes in *hda1*ΔΔ, *hda2*ΔΔ or *hda3*ΔΔ compared to wild-type expression. Venn diagrams were generated using the FunRich programme (Pathan et al. 2017). These visualizations were constructed by Dr. Alessia Buscaino.

Pathway information was discovered by the Broad Institute's Gene Set Enrichment Analysis (GSEA) (Subramanian et al. 2005; Mootha et al. 2003) using the PreRanked tool to compare the DESeq2 ranked gene sets with defined gene sets (Sellam et al. 2010) and (*Sellam et al*, lab communication). The weighted enrichment statistics given in the form of Normalized Enrichment Score (NES) were calculated on 10512 gene sets each containing 5-1000 genes, and the false discovery rate (FDR) was calculated from 1000 permutations. Gene set source: Hao et al. 2009. Selected results graphs are shown. Since enrichment profiles can exhibit correlations with hundreds of overlapping gene sets, Cytoscape 3.6 (http://www.cytoscape.org) (Shannon et al. 2003) and the Enrichment Map Pipeline Collection plug-ins (http://apps.cytoscape.org/apps/enrichmentmappipelinecollection) were used to further organize and visualize the GSEA. Enrichment maps were calculated using default parameters (Merico et al. 2010).

2.4.3 Bioinformatic resources: databases, design, viewing, modeling and alignments

Unless otherwise noted, the following programs with default settings were used for all analyses:

- Protein sequences were compared to existing structural models using Basic Local Alignment Search Tool (BLAST- NCBI) or Phyre2 intensive mode (Altschul et al. 1990; Altschul et al. 1997; Kelley et al. 2015).
- Secondary structure was estimated using ESPript (http://espript.ibcp.fr,) (Robert & Gouet 2014).
- Models of protein structure were constructed using Pymol visualizing software (DeLano 2002; DeLano 2009).
- Protein alignments were done using the following programs: Clustal Omega, Emboss Needle and BLAST (NCBI) (Altschul et al. 1990; Altschul et al. 1997; Sievers et al. 2011; Sievers & Higgins 2014; Rice et al. 2000).
- Percent Identity and Similarity were calculated by EMBOSS Needle or Stretcher pairwise protein sequence alignment tool (Rice et al. 2000).
- Protein domain modelling was done by a Simple Modular Architecture Research Tool SMART database search (Letunic et al. 2015; Schultz et al. 1998).
- Information about *C. albicans* genomes, genes, GO analysis and proteins was obtained via the *Candida* Genome Database (Skrzypek et al. 2017).

- Information about *S. Cerevisiae* genes, GO analysis and proteins was obtained via the *Cerevisiae* Genome Database (Ashburner et al. 2000; Consortium 2017).
- Visualization of DNA and protein sequences, primers and features were performed using SnapGene (Viewer) software (from GSL Biotech; available at snapgene.com).
- Manipulation of DNA sequences to construct images of recombinant plasmids to feed into SnapGene (Viewer) were done using A plasmid Editor (ApE) software (Davis 2010).
- Nucleotide to Amino Acid Translation Estimates were done using ExPASy Bioinformatics Resource Portal and protein molecular weight estimations by ExPASy Compute pI/MW Tool and ProtParam Tool (Bjellqvist et al. 1993; Bjellqvist et al. 1994; Gasteiger et al. 2005; Gasteiger et al. 2003).

CHAPTER 3. Toward solving the structure of *C. albicans* Hda1, Hda2 and Hda3 proteins using an *E. coli* expression system

3.1 Introduction

The goal of this thesis is to better understand the Hda1, Hda2 and Hda3 proteins of *C. albicans.* There is a rapidly developing market for drugs that target HDAC proteins in the treatment of various diseases (Tang et al. 2013). Targeting of these enzymes can be used in the treatment of fungal diseases (Kmetzsch 2015). The catalytic component of Hda1 is known to play a key role in the development of fully formed hyphae in the pathogenic yeast *C. albicans*, and therefore molecular structural data could contribute to drug development in addition to a better understanding of HDAC protein evolution. However, surprisingly little is known about the structure and function of the yeast counterparts of these enzymes. The Hda1 enzyme exists as a protein complex in *S. cerevisiae* but there is little information about the proteins that complex with it, Hda2 and Hda3 which are unique to yeast and could therefore be potential therapeutic targets (see Section 1.8.1). In this chapter, I will describe studies aimed at the biochemical characterization of these protein complexes.

3.2 Contributions to this study

Supervision for experiments throughout this entire project including yeast and most protein work was provided by Dr. Alessia Buscaino and members of the Buscaino Lab as detailed throughout this thesis (School of Biosciences, University of Kent). Primary supervision of protein work was provided by Dr. Abhimanyu K. Singh in the laboratory of Professor David Brown (School of Biosciences, University of Kent). Trypsin digestion and mass spec analysis were assisted by supervision of Dr. Kevin Howland (School of Biosciences, University of Kent). Supervision for crystal tray preparation, microscope observations, thermal shift assay and other aspects of protein work was provided by Dr. Susanne Schroeder (School of Biosciences, University of Kent), Colin Robinson, Richard Bazin and Stephen Irving at Argenta/Charles River Laboratories (Canterbury, UK). Supervision of microscopy by Microscope Facilities Manager Ian Brown (Department of Biosciences, University of Kent). Generation of codon adaptation graphs was done by Dr. Tobias von der Haar (School of Biosciences, University of Kent).

3.3 Goal 1: Solve the structure of important domains of *C. albicans* Hda1 protein to evaluate its potential as a drug target.

3.3.1 Evaluate Hda1 by structural alignment and domain analysis

Currently structural information about Hda1 is lacking, we sought to optimize a purification and crystallization protocol to provide structural information, gather information about the folding of this protein and to inform strategies for the development of inhibitors as potential therapeutics. In order to begin characterizing the predicted domain structure of *C. albicans* Hda1 we used the Simple Modular Architecture Research Tool (SMART) to learn more about the potential structure and domain architecture of this protein (Letunic et al. 2015; Schultz et al. 1998). SMART analyses showed that *C. albicans* Hda1 protein is likely composed of two domains: (1) catalytic core domain and (2) an Arb2 domain (Fig. 3.2). A closer analysis of the data showed that the catalytic domain was highly conserved while the Arb2 domain had less conservation and may be species specific (Fig. 3.1).

Further computational analysis using BLAST also demonstrated that the catalytic domain is conserved. We observed conservation from *Candida* to HDAC sequences in humans (Fig. 3.1). The closest human homolog of Hda1 was the HDAC6 Isoform 2 (42 % identity; 61 % similarity; E-value: 2e-93) which was followed by HDAC10 (31 % identity; 50 % similarity; E-value: 3e-64) and HDAC4 (34 % identity; 48 % similarity; E-value: 2e-79) (see Section 1.5.2).

BLAST analysis also showed that this conservation does not extend to the Arb2 domain which was matched only with low significance to the *Homo sapiens* protein cadherin-13 isoforms (21 % identity; 28 % similarity; E-value = 0.093) which is a very different protein that has no histone deacetylase activity (Geer et al. 2010).

Another notable component of the Hda1 protein is the N-terminal sequence region which is absent in the yeast proteins relative to their human counterparts. Analysis of *C. albicans* Hda1 sequence with human sequences clearly delineates the differences in conservation between the domains (Fig. 3.1; strict identity is noted as white letters on red background). Identity is observed throughout the catalytic domain while it is absent in the Arb2 region.

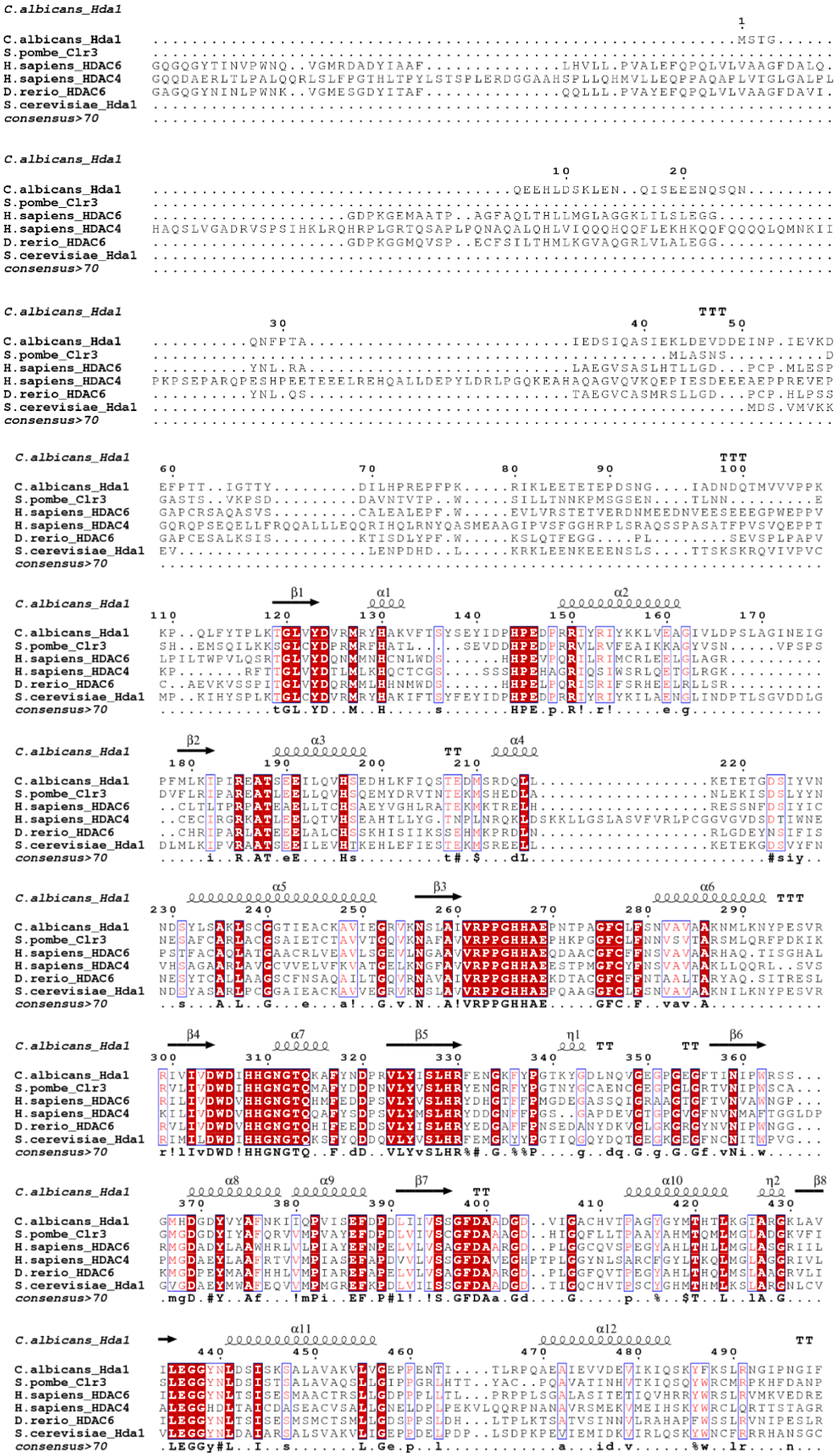
C.albicans_Hda1
C.albicans_Hda1
S.pombe_Clr3
H.sapiens_HDAC6
H.sapiens_HDAC4
D.rerio_HDAC6
S.cerevisiae_Hda1
consensus>70

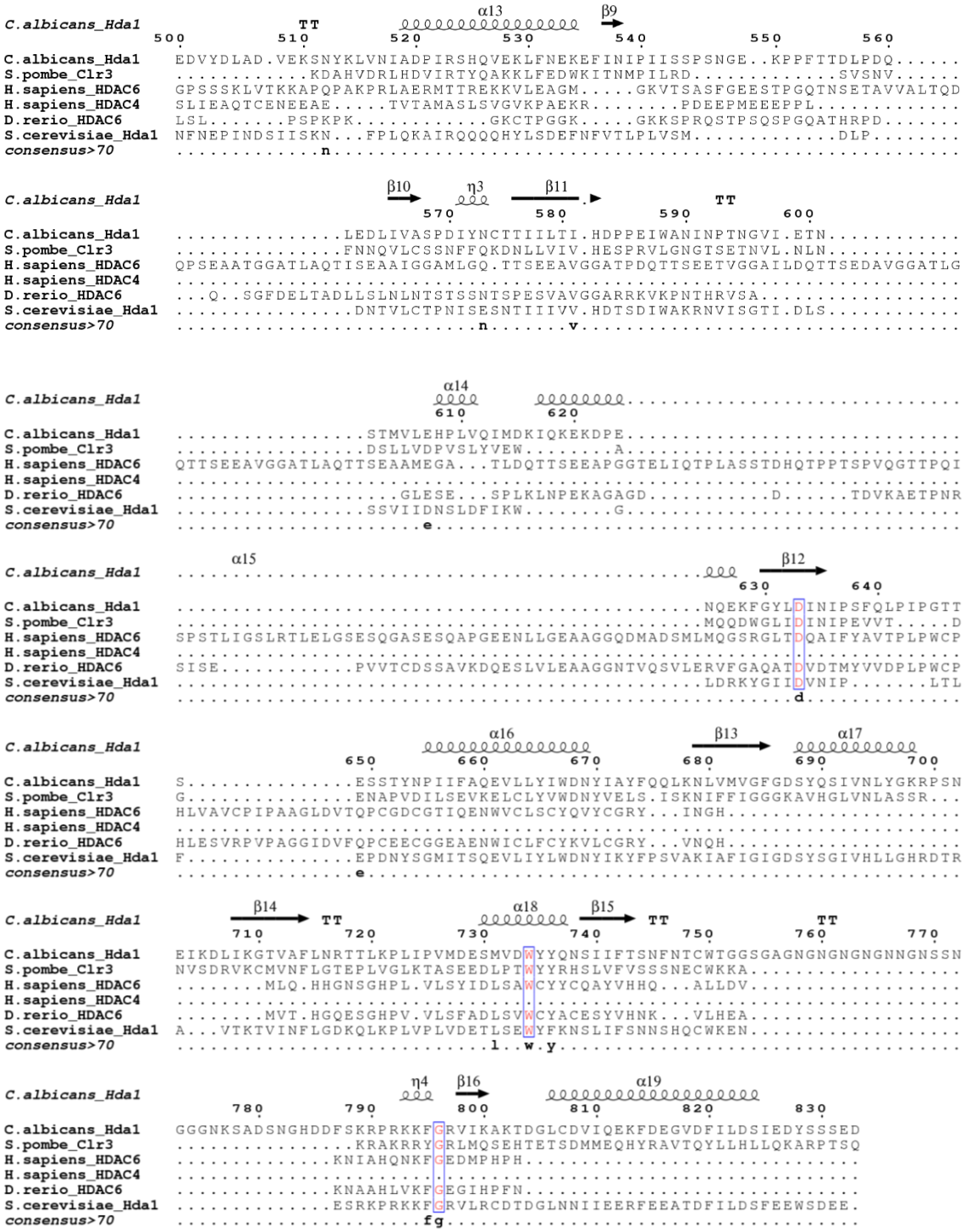

Figure 3.1 Alignment of *C. albicans* Hda1 with similar human and yeast protein sequences and overlay of secondary structures

Secondary structure identified by Phyre2; Consensus sequence displayed by ESPript 3.0 with a global score threshold setting of 0.7; strict identity is noted as white letters on red background and highly similar residues are colored in red with blue frame

SMART analysis predicts that the Hda1 protein (833 amino acids) includes the following Pfam domains: Histone deacetylase (aa 130-456), Arb2 (aa 467-669). Outlier homolog SMART searches identified the HDAC4 zinc binding domain having similarity (aa 119-491) to *Candida* Hda1 in the catalytic core further confirming the conservation of this region. HDAC4 has an additional stretch of amino acids in this region. The SMART analysis also notes three regions of low complexity (aa 14-28, 537-547 and 752-783) one within the Arb2 domain and the others located near each of the protein's termini. Low complexity regions are also identified in *S. cerevisiae* (aa 21-39) and *S. pombe* (aa 640-648) suggesting that these may be yeast specific regions.

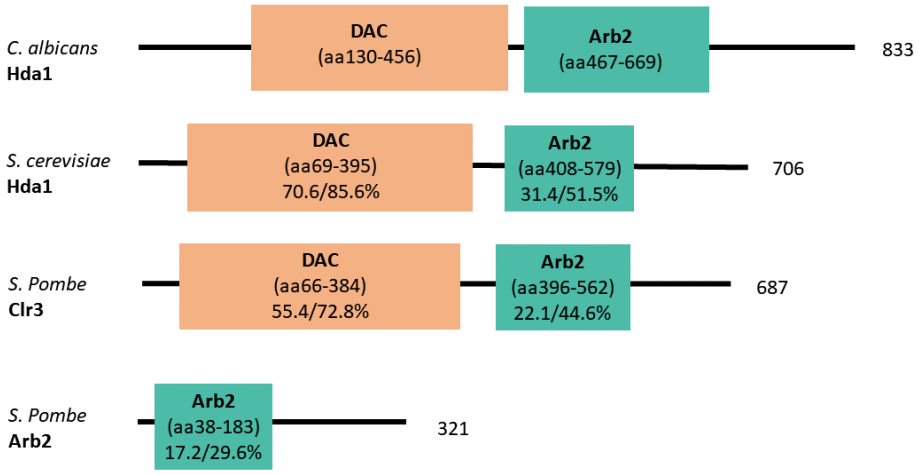

Figure 3.2 Homology between major *C. albicans* Hda1 domains and those of similar yeast proteins
Values show comparison with *C. albicans* Hda1 (% identity/% similarity); comparisons made using EMBOSS Stretcher and SMART [Adapted from portion of Figure 1B from Yang Seto 2009 (Schultz et al. 1998; Letunic et al. 2015; Yang & Seto 2009; Rice et al. 2000)]

SMART analysis depends on prior structure determination of related proteins. Over 500 domain families have been annotated in the SMART database (Schultz et al. 1998; Letunic et al. 2015). The structures of several histone deacetylase domains are present in the database. The closest functional homolog of Hda1 in the database is the *S. pombe* histone deacetylase Clr3. The modeling of Hda1 based on solved structure provides a realistic estimation of the structure (Fig. 3.3).

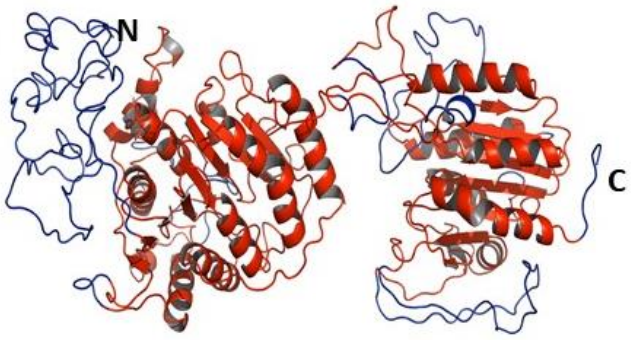

Figure 3.3 Model showing prediction of *C. albicans* Hda1 protein structure
Colored by Phyre2 model confidence: Red > 97%; Blue, 0%; Hda1: 71% of residues at > 90% confidence based upon S. pombe Clr3 (Protein Data Base DOI: 5IKK)(Kelley et al. 2015; DeLano 2002; DeLano 2009)

Taken together the in silico analysis suggests that structurally there is significant conservation between Clr3 and *C. albicans* Hda1. The conserved residues lie in the region of amino acids L117 to E826 and other regions of Hda1 have no predicted structure or model identified. This matched region of 593 aligned residues shows 43 % identity with 100 % confidence and 11 insertions (sized 1-35 nucleotides) (see FASTA pairwise alignment Appendix 1.1.1).

3.3.2 Express and purify recombinant Hda1

Having computationally identified the putative domains of Hda1 I approached analyzing this protein structurally. The initial goal of the experiment was to express soluble *C. albicans* Hda1 protein in an *E. coli* expression system from a synthetic construct of the *HDA1* gene. Since not much is known about the actual structure of the full-length yeast *C. albicans* Hda1 protein, expression of this protein is the first step toward gathering important information about the proteins' folding and functions. Of specific interest are the domains of this protein which are unique to yeast since they have the potential to be exploited as drug targets to combat infections by this pathogen.

3.3.2.1 His tagged Hda1

Protein expression in *E. coli* is a tried and tested method to obtain large amounts of a protein for further analysis. I decided to express a tagged version of Hda1 which would therefore be amenable to purification. I constructed a plasmid with Hda1 in the vector pET21 (ABp_92) and this recombinant construct was then transformed into BL21(DE3) pLysS cells. This *E. coli* expression strain expresses low levels of T7 lysozyme which functions as an inhibitor of T7 RNA polymerase and reduces basal leaky transcription of

recombinant proteins while inducing of expression of the recombinant protein simply involves the addition of IPTG. Furthermore, glucose (0.2 %) was added to the media to decrease leaky expression of target proteins within the pET vector expression system (Novagen 2003). Additionally, this strain (and all BL21) is deficient in proteases known to degrade proteins (*Ion* and *ompT*).

Cultures were grown at 37 °C to an OD_{600} of 0.6-0.8 and induced with 1 M IPTG. Following induction growth was allowed for 1-3 hours at 37 °C or 20 hours at 20 °C before harvesting. Harvested cells were lysed by sonication (see Section 2.2.5) and the cell debris (insoluble fraction) removed by centrifugation before protein levels assessed by SDS-PAGE gel electrophoresis. This analysis showed that Hda1 could be expressed using *E. coli*. Full length Hda1 containing a C-terminal 6xHis tag is estimated to be 94 kDa and two bands were observed in the post-induction samples with sizes around 120 kDa and 85 kDa (Fig. 3.4; Arrows). This dual banding pattern may be due to degradation.

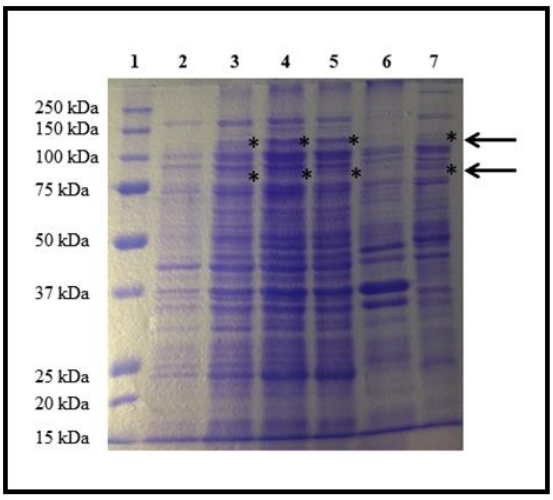

Figure 3.4 Hda1-6xHis expression and solubility tests show potential low level soluble expression
Tests show low level soluble expression: Expression test at 37 °C at 1, 2 and 3 hours and Solubility test at 20 °C overnight. Lane 1: Marker; Lane 2: Pre-induction; Lane 3: 37 °C 1 hour; Lane 4: 37 °C 2 hour; Lane 5: 37 °C 3 hour; Lane 6: 20 °C insoluble fraction; Lane 7: 20 °C soluble fraction. The arrow points to the two bands at ~120 kDa and ~85 kDa that were thought to be soluble tagged (*) Hda1 (~93.98 kDa) protein.

Closer inspection of the SDS PAGE gel showed that while we could see expression of this protein, the levels of expression were not significant. We therefore decided to

optimize conditions for high level expression to generate enough protein for further biochemical and structural studies.

Our analysis of the expression was premised on the presence of bands of approximately the correct size. We decided to confirm the identity of the protein using mass spectrometry.

Expression of *HDA1*-6xHis was induced and the in-gel trypsin digestion and MALDI-TOF peptide mass fingerprinting were performed (see Section 2.2.11). While this could perhaps have been tested more easily by western blot, a quick evaluation by InVision His tag stain showed many background bands which led to a decision to test the various bands by mass spectrometry. A list of peptide mass values from an enzymatic digest of 6xHis- Hda1 were queried against the SwissProt database. The analysis showed that the band above 100kD had the highest MS total score: 192, $p < .05$/ MSMS peptide recognition score: 49, $p < .05$ and this band matched the sequence of *C. albicans* Hda1. This unambiguously demonstrated that the protein was being expressed and was the band with an apparent molecular weight of ~120 kDa. In addition to this band analysis also confirmed that the protein band near 75 kDa matched *C. albicans* Hda1 (highest MS total score: 239, $p < .05$) /MSMS peptide recognition score: 38; significant if > 39) (see Appendix 2.2.1 for full list of peptides found). While other lower bands (present in post- but not pre-induction samples) were analysed (~70 kDa and ~50 kDa), they did not match Hda1 protein. The results clearly showed that the ~75 kDa band was a truncated fragment of Hda1. Given the molecular weight of this band and the C-terminal tagging of the construct, which was analysed by Mass-spec, it is likely that the degradation occurred near the N-terminus. The estimated molecular weight for the amino acids from K108 through the end of the His tag is 84.9 kDa suggesting a specific cleavage at or near this lysine. These data suggest that the protein was either unstable in *E. coli* cells or degraded during protein purification.

To confirm that the presence of pLysS plasmid was not affecting protein levels through over-regulation, BL21(DE3) cells were also used in the expression analysis but this did not change the outcome (Novagen 2003). In addition to low expression levels, partial insolubility was also observed as a band of the same size was also observed in the insoluble fraction (Fig.3.4, Lane 6). Unfortunately reducing ambient temperature during the nickel batch purification did not improve solubility.

One of the reasons why specific proteins are not expressed in high level in *E. coli* is due to differences in codon frequencies. To try and understand why we were seeing

such low expression levels, we computationally analyzed the synthetic *C. albicans* Hda1 sequence in the context of codon usage by *E. coli*. This evaluation was performed to check the suitability of this synthetic *C. albicans* based Hda1 sequence for translation in *E. coli* given the organismal differences in tRNA populations (Marín et al. 2017) (Fig. 3.5).

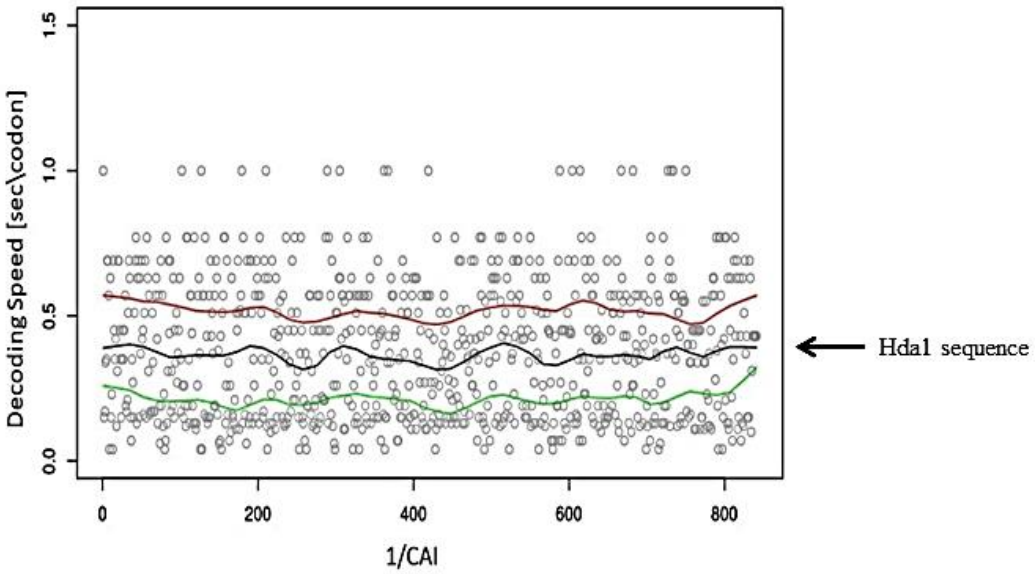

Figure 3.5 Codon adaptation of synthesized *HDA1* sequence for expression in both *E. coli* and *S. cerevisiae* is not ideal for *E. coli* specific expression
CAI -codon adaptation index (1/CAI: 0 good 1 bad; green = best possible sequence and red = worst; black = synthetic Hda1 sequence- this study. The traces are averaged over a window of 50 codons. The circles are the adaptation values of the individual codons. Note: Figure made based upon *HDA1* synthetic sequence by Dr. Tobias von der Haar (Chu & von der Haar 2012)

The evaluation shows many badly adapted codons which could suppress expression in *E. coli*. As can be seen in Figure 3.5, while the sequence (black) is not the worst possible (red) it is also not ideal (green). To address this issue, we expressed *HDA1* in an *E. coli* strain Rosetta (DE3) that incorporates additional copies of tRNAs: AUA, AGG, AGA, CUA, CCC and GGA (with their native promoters). Additionally, the Rosetta strain is mutant in the *lac* permease membrane transport protein which provides for regulated protein expression by level of applied IPTG (Novagen 2003). To check whether varying IPTG levels might enhance the expression we performed a test with expression of the vector Rosetta and BL21 (DE3) with incremental increase of IPTG added (400 mM to 1 M). However, no significant increase in expression was observed (Fig 3.6).

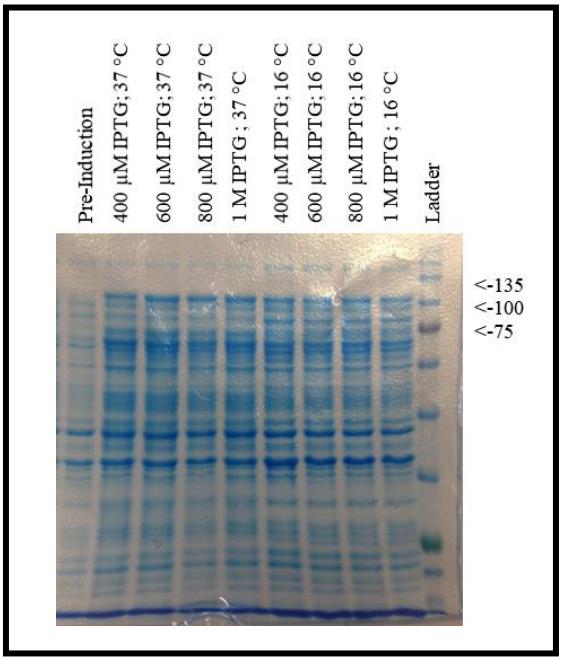

Figure 3.6 Trial of Hda1-6xHis with various IPTG levels shows no apparent effect on protein expression level

I next hypothesized that the low levels of expression could be a result of the tag at the C-terminus of the protein. I therefore cloned Hda1 into pET28b to provide a thrombin protease cleavable N-terminal 6xHis tag.

The resulting plasmid was transformed and cultured at 37 °C and protein expression was induced for three hours with 500 mM IPTG. However, increased expression was not observed (Data not shown).

Further optimization experiments were performed. Based upon the presence of the zinc binding site in homologs of this protein (see Section 3.3.1) and results from *homo sapiens* HDAC4, (Bottomley et al. 2008) the culture was supplemented with 20µM $ZnCl_2$ 30 min prior to induction. Following modifications published protocol, this analysis was performed with both *HDA1*-6xHis and 6xHis-*HDA1* (Lysis Buffer: HEPES pH7.5 25 mM, KCl 200 mM, Glycerol 30%, NP-40 0.5 %, DTT 1 mM; Wash Buffer: Dilution Buffer: Lysis Buffer excluding NP-40 detergent and glycerol mixed 1:1 with lysis buffer; Elution Buffer: HEPES pH7.5 25 mM, KCl 200 mM, Glycerol 10%, NP-40 0.1 %, DTT 1 mM, imidazole 150 mM) (Bottomley et al. 2008). However, no significant improvement in protein expression was obtained (Data not shown).

Additional adjustments were made in attempt to increase protein expression and solubility, including lowering the temperature to 16 °C (grown overnight) as well as addition of PMSF or protease inhibitors to reduce degradation. However, none of these

manipulations led to a substantial increase in protein expression. Consequently, we hypothesized that the reason for the low expression was inherent instability of the tagged protein.

3.3.2.2 GST tagged Hda1

As shown in the previous Section, the level of expression of Hda1 with 6xHis tagging was too low to use for structural studies. Protein expression is often reduced due to suboptimal sequences in the N-termini of recombinant proteins. Several tags are used to remedy expression problems including the Maltose Binding Protein (MBP) and Small Ubiquitin-like Modifier (SUMO) protein. We chose to try the a large highly-soluble Glutathione S-transferase (GST) tag in the N-terminus has been shown to allow for higher expression of recombinant protein (Novagen 2003).

The recombinant plasmid: Hda1 full-length tagged at its N terminus with GST and 6xHis, was transformed into Rosetta (DE3) and the culture was grown at 37 °C to OD_{600} = 0.6-0.8 before induction with 400 mM IPTG. It was then grown another 20 hours at 16 °C. Harvested cells were lysed by sonication (for batch purification) or cell disruption (1 L culture) and the cell debris (insoluble fraction) were removed by centrifugation.

Making use of the 6xHis tag the resulting supernatant was passed over Ni-NTA resin for batch purification (see Section 2.2.7.1) and eluted with 400 mM imidazole. Presence of GST-6xHis-Hda1 in the elution was confirmed by SDS-PAGE analysis. GST-6xHis-Hda1 full length construct has a predicted size of 133.72 kDa and the isolated protein ran to a molecular mass seen around 150 kDa (data not shown; representative gel in Fig. 3.7A).

The identity of GST-Hda1 was confirmed by gel excision and mass spectrometry. A list of peptide mass values from an enzymatic digest of GST tagged Hda1 were queried against the SwissProt database (see Section 2.2.11) and matched *C. albicans* Hda1. This analysis confirmed the presence of Hda1 peptides in the digested samples of excised bands from just below 150 kDa marker line (MS total score: 145, $p < .05$/ MSMS peptide recognition score: 45, $p < .05$) (see Appendix 2.2.2 for a full list of peptides found). Most importantly, preliminary analysis using Ni-column batch purification showed that GST tagging improved yields (Fig. 3.7A).

This system was taken for larger quantity purification. *E. coli* cultures were grown in 1 L of LB media. After harvesting and lysis, the protein was purified from the soluble fraction.

The supernatant was applied to the nickel affinity column and eluted with an increasing gradient reaching 1 M imidazole (Fig. 3.7B).

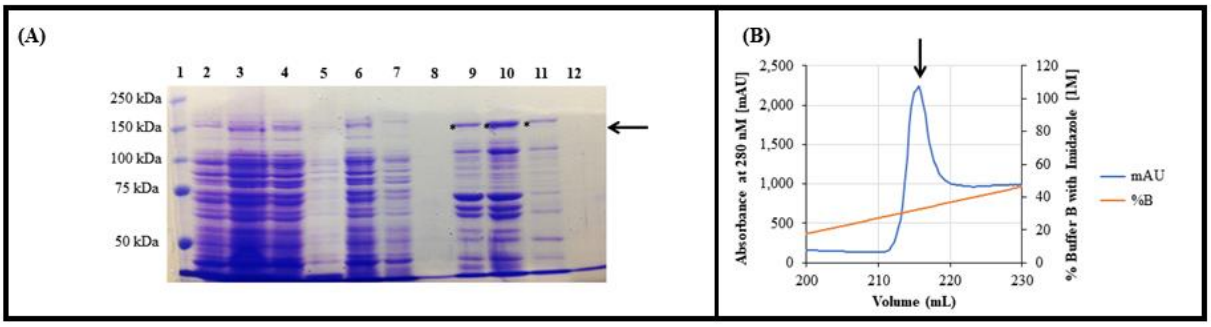

Figure 3.7 Purification of GST-6xHis-Hda1 by FPLC: Nickel affinity chromatography
(A) 10 % (w/v) SDS-PAGE Gel- Lane 1: molecular mass marker; Lane 2: Pre-induction; Lane 3: Post-induction; Lane 4: crude lysate; Lane 5: insoluble fraction; Lane 6: flow through from crude lysate; Lane 7: 10 mM imidazole wash; Lane 8 – 12: fractions from increasing levels (%) of 1 M imidazole Wash Buffer B (Tris-HCl pH7.5 20 mM, NaCl 200 mM, imidazole 20 mM and BME 4 mM with added imidazole). GST and 6xHis tagged Hda1 (*) (B) FPLC chromatogram of tagged full length Hda1. The arrow points to tagged Hda1.

SDS-Page analysis after nickel affinity column purification showed a purified protein of the predicted size (~133.72 kDa; Arrow). Additional bands in this fraction are either degradation or minor protein contaminants. The eluted protein was pooled, and buffer exchanged into IEC Buffer A (see Section 2.2.7.2).

To further purify the protein, ion exchange chromatography was performed using a 5 mL HiTrapQ HP anion exchange column (GE Life Sciences) (Fig. 3.8B). The PI of GST-Hda1 is 4.76 and the buffer pH = 7.5 left the protein with an overall negative charge so that it would bind to the positively charged resin in the column.

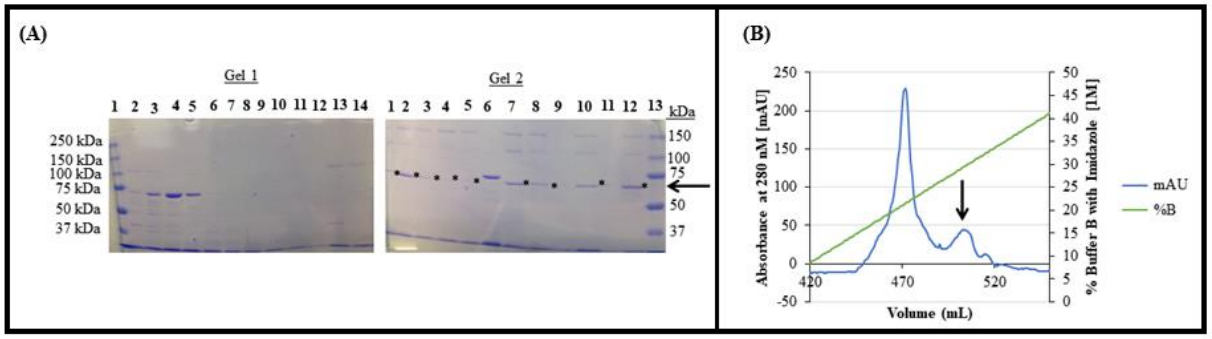

Figure 3.8 Purification of GST-6xHis-Hda1 by FPLC: Ion exchange chromatography

(A) 7.5 % (w/v) SDS-PAGE: Gel 1- Lane 1: molecular mass marker; Lane 2 - 14: fractions from increasing levels (%) of 1 M NaCl wash. Gel 2- Lane 13: molecular mass marker; Lanes 9 and 11: spacer Lane- no sample; Lane 2 – 8, 10 and 12: fractions from increasing levels (%) of 1 M NaCl wash- ~133.72 kD GST and 6xHis tagged Hda1 (*) is observed in Lanes 1-5, 7-8, 10 and 12 (B) FPLC chromatogram of tagged Hda1. The arrow points to GST-Hda1.

After IEC samples were assessed by SDS-PAGE, as can be seen in Figure 3.8A and the protein had a retention volume of 496-524 mL and was eluted at 27.5-34.5 % NaCl is observed (Lanes 9 – 11 of Fig. 3.8A). This reduced but did not eliminate the background banding patterns and further purification was needed. The approximated size of the GST tag is 26 kDa and could account for only the very smallest of the background bands.

These samples were pooled and further purified by size exclusion chromatography (Fig. 3.9). Purification by size exclusion chromatography is described in Section 2.2.7.3. The SDS-PAGE gel visualizes the fractions eluted from this sizing column (Fig. 3.9A).

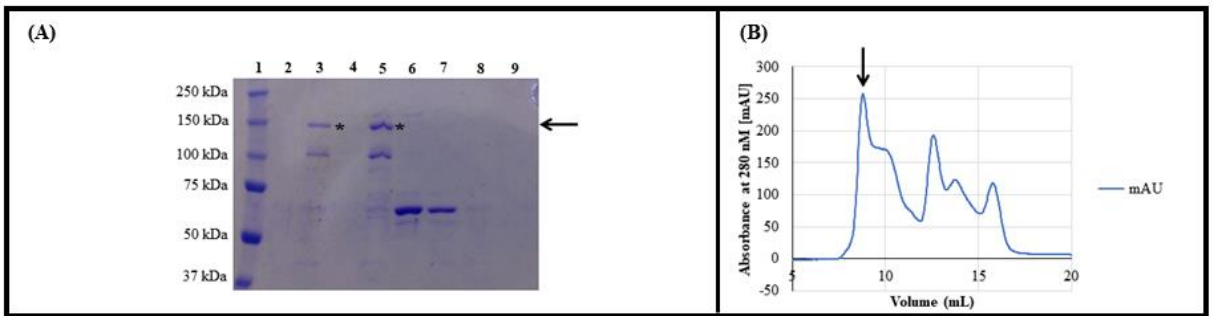

Figure 3.9 Purification of GST- 6xHis-Hda1 by FPLC: Size exclusion chromatography
(A) 7.5 % (w/v) SDS-PAGE- Lane 1: molecular mass marker; Lane 2: Concentration column flow through; Lane 4: spacer Lane- no sample; Lane 3, 5 – 9: fractions from wash- ~133.72 kD GST and 6xHis tagged Hda1 (*) is observed in Lanes 3 and 5 (B) FPLC chromatogram (Superdex 200 10/30 GL) of protein sample. The arrow points to tagged Hda1.

Full length tagged Hda1 protein had a retention volume of ~7.5-12 mL. The final samples containing the protein were pooled, and final protein concentration was 82.28 µg/ml.

Since lower bands were observed (Fig. 3.9A rows 6&7) and degradation was likely given prior mass spectrometry results (see Section 3.3.2.1), a defrost experiment was carried out to see if the full-length protein could be degraded in a controlled manner. While crystal nucleation is reluctant to occur in a heterogeneous sample, a homogenous degraded state can increase the possibility of nucleation. The strategy was trialed to see if controlled degradation could move the mixture of full-length and smaller protein isolates to the stable degraded size observed in the lower bands with the goal of harvesting enough protein with this existing protocol for crystallization studies. This trial for degradation was performed on protein samples by four approaches (see Section 2.2.14 and Fig. 3.10). However, when assessed by SDS-Page gel, no further degradation had taken place and banding held the same pattern as the post-SEC gel.

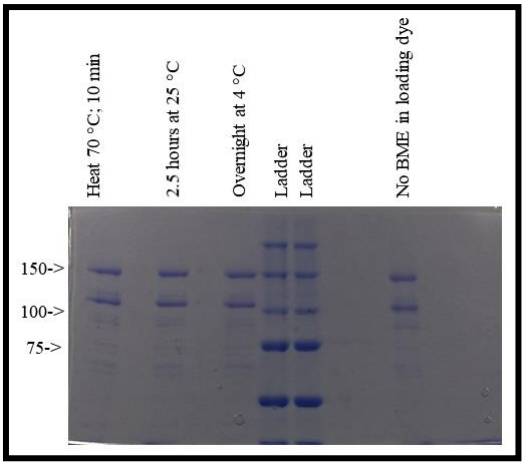

Figure 3.10 Trials with stressors to GST-Hda1 protein show no further degredation
Degradation trials: (1) heat at 70 °C for 10 min, (2) incubate at room temperature for 2.5 hours, (3) store overnight at 4 °C, (4) As normally processed but with BME excluded from loading dye.

These data show that GST-tagged Hda1 can be obtained at higher levels compared to His tagged Hda1. One concern that could be addressed in future experiments is whether removal of the tag is necessary. This could be important because the tags themselves could affect complex interactions. While the final amount of purified GST-Hda1 from one liter of culture was not sufficient for crystallization trials which usually require protein concentrated to 2-50 mg/mL with 1-2 µL per well for 24 well or 0.2-0.3 µL per well for 96 well mosquito trays by hanging-drop diffusion method (Dessau & Modis 2011). The protein could be used for other studies such as single molecule biophysics analysis (Hughes et al. 2014). However, these steps were not taken, as before progressing with this work, it became important that we proceed with trails at expression of the other complex proteins, Hda2 and Hda3.

3.3.2.3 Expression testing of Hda1 domains

Expressing full length Hda1 is challenging and will require additional optimization before sufficient amounts of the protein can be isolated for crystallization studies to be easily performed. While we are currently unable to gain structural information on the intact protein, we decided try expression of the individual domains. The mass spectrometry data confirmed degradation of Hda1 to at least one species (~75 kDa). This partially stable degradation product suggested the presence of a stable folded domain of the protein. We designed constructs around the likely degradation sites and at nearby SMART predicted domain transition points with the aim of obtaining stable and better expressed protein domains that could be analyzed structurally.

Many constructs (Fig. 3.11) were designed based on modeling of Hda1 domains: namely the catalytic domain and Arb domain alone or through the end of the gene with various start sites (see Section 3.3.1). These fragments of the gene were amplified by PCR (Fig. 3.11) and cloned in frame with a C-terminal 6xHis and/or N-terminal 6x His for expression testing (see Section 2.2.3).

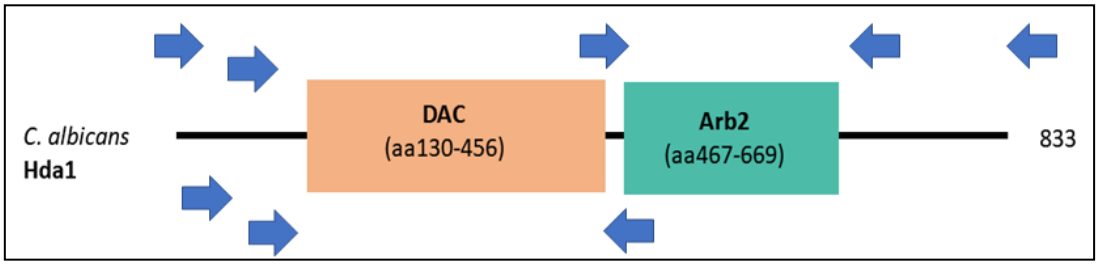

Construct Description	primers (ABo_)	Amino acids	Cloned plasmid (ABp_)	pET plasmid
catalytic with hydrophobic domain	309 & 311/312	91D-833D	112/116	21b/28b
catalytic w/o hydrophobic domain	308 & 311/312	P110-833D	114/118	21b/28b
catalytic w/o hydrophobic domain through Arb2 domain only	494/495 & 308	P110-N669	164/146	21b/28b
catalytic with hydrophobic domain through Arb2 domain only	494/495 & 309	91D-N669	159/168	21b/28b
Arb2 domain only	494/495 & 310	A445-N669	162/147	21b/28b
alternate catalytic domain start with hydrophobic region through Arb2 domain only	494/495 & 365	A131-N669	160/169	21b/28b
alternate catalytic domain start without hydrophobic region through Arb2 domain only	494/495 & 366	D142-N669	161/163	21b/28b

Figure 3.11 Schematic showing Hda1 construct boundaries and table with details of constructs trialed
(Top) Construct start and end points are indicated by blue arrows; these are oligo anneal sites for amplification of portions of Hda1 protein prior to cloning into expression vector. (Bottom) Table listing details of non-expressing constructs.
*All constructs were cloned into the *Nde*I and *Xho*I restriction sites of the vector plasmid. (Letunic et al. 2015; Schultz et al. 1998).

All but three of these constructs did not express well. These three were further characterized. Only the plasmid with the Arb2 domain through the end of the gene had

enough soluble expression to be further purified (see Section 3.3.2.5). As described in the next section, the two catalytic domain only constructs expressed well but were insoluble.

3.3.2.4 Cloning and expression of *C. albicans* Hda1 deacetylase domain

While several start and end site versions of constructs to express the deacetylase domain of *C. albicans* Hda1 were evaluated, two showed significant expression levels.

The first of these domain constructs was designed based upon the Clr3 catalytic start site (*S. pombe* Clr3: D75) as it aligned *C. albicans* Hda1 sequence (DAC-Clr3). The second was a similar Pfam Histone deacetylase domain informed construct (DAC-Pfam). Both constructs carry an N-terminal 6xHis tag. These constructs end just after the catalytic domain (G457) and vary in start site based upon the catalytic domains defined by Clr3 (A131) and Pfam (D142) designations.

For protein over production the *E. coli* strain BL21(DE3) was transformed with 6xHis-DAC-Clr3 or 6xHis-DAC-Pfam. The resulting strain was grown at 37 °C in LB and protein expression induced with 1 M IPTG for 20 hours at 16 °C. Multiple batches were done in parallel in attempt to solubilize these proteins and adjustments included addition of $ZnSO_4$ (100 mM) to the growth media 30 min prior to induction, addition of protease inhibitor tablets before sonication and growth in 2YT media (LB media with 2x yeast extract and tryptone). After lysis by sonication the cell debris (insoluble fraction) were isolated by centrifugation. Expression was visualized by SDS-PAGE gel electrophoresis. The two proteins gave virtually equivalent band density at their theoretical molecular weights of 6xHis-DAC-Clr3 = 38 kDa and 6xHis-DAC-Pfam = 37 kDa, both ran to a location just above the 37 kDa molecular marker line with the latter taking a slightly lower position (Fig. 3.12A).

Making use of the N-terminal 6xHis tag the resulting supernatant was incubated with Ni-NTA resin for batch purification and eluted 1 M imidazole. Presence of 6xHis-DAC-Clr3 or 6xHis-DAC-Pfam (Arrow) in the elution visualized by SDS-PAGE analysis (Fig. 3.12B).

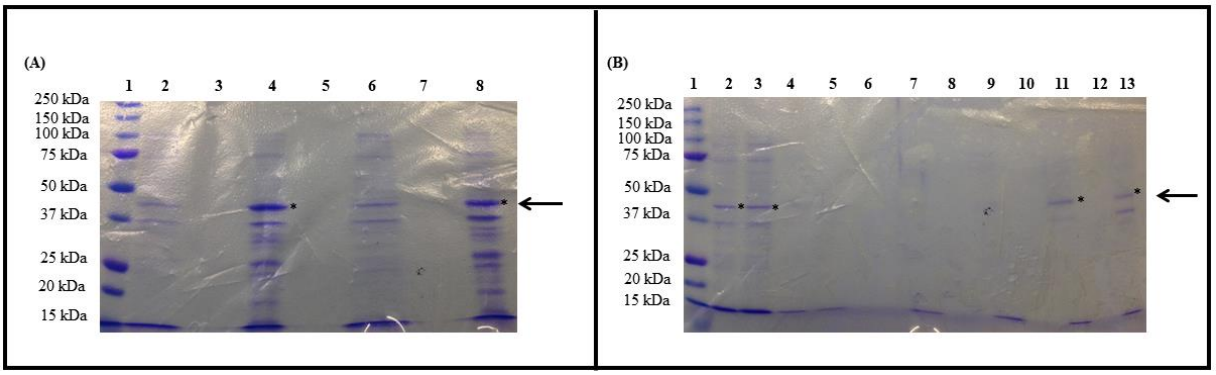

Figure 3.12 Expression and solubility tests of 6xHis-DAC-Clr3 and 6xHis-DAC-Pfam show insoluble expression
(A) Expression Test 10 % (w/v) SDS-PAGE, Lane 1: molecular mass marker; Lane 2: Pre-induction; Lane 3: Skip; Lane 4: Post-induction; Lane 5: Skip; Lane 6: Pre-induction; Lane 7: Skip; Lane 8: Post-induction (B) Solubility Test, Lane 1: molecular mass marker; Lane 2: Flow through 6xHis-DAC-Clr3; Lane 3: Flow through 6xHis-DAC-Pfam; Lane 4: Wash; Lane 5: Wash; Lane 6: Skip; Lane 7: Elution 6xHis-DAC-Clr3; Lane 8: skip; Lane9: Elution 6xHis-DAC-Pfam; Lane 10: skip; Lane 11: insoluble fraction 6xHis-DAC-Clr3; Lane 12: skip; Lane 13: insoluble fraction 6xHis-DAC-Pfam. (*) indicates location of potential protein bands and arrow designates molecular weight location.

Solubility tests showed bands in the insoluble fractions (Fig. 3.12B, Lanes 11 and 13). In conclusion, the two catalytic only domain constructs expressed insoluble protein.

3.3.2.5 Cloning, expression and purification of *C. albicans* Hda1 Arb2 domain

The construct that expressed best was the Arb2 through the end of the C-terminus (Arb2+C) construct. The cloned plasmids allowed the protein to be translated with a C-terminal or N-terminal 6xHis tag (respectively).

For protein over production the *E. coli* strain BL21(DE3) was transformed with 6xHis-Arb2+C or Arb2+C-6xHis. The resulting strains were grown at 37 °C and expression of 6xHis-Arb2+C or Arb2+C-6xHis was induced with 400 mM IPTG for 20 hours at 16 °C. Harvested cells were lysed by sonication (see Section 2.2.5) and the cell debris (insoluble fraction) were removed by centrifugation.

Making use of the 6xHis tag the resulting supernatants were passed over Ni-NTA resin for batch purification and was eluted with 600 mM imidazole. Presence of the protein in the elution was confirmed by SDS-PAGE analysis. The two plasmids gave protein with virtually equivalent band density with the estimated molecular weight of 43 kDa protein running to a location just above the 50 kDa molecular weight marker line (data not shown; representative gel in Fig. 3.13A). While expression was somewhat low, it was potentially

enough for further purification. The N-terminal tagged (6xHis-Arb2+C) version was used for further expression tests (ABp_119).

Additional trials tested transformation with *E.coli* expression strains (BL21(DE3)pLysS, Overexpress C43(DE3) and Rosetta(DE3)). The Overexpress C43(DE3) strain is a derivative of the BL21(DE3) strain which has been studied for its ability to increase plasmid stability in the case of toxic recombinant protein expression (Dumon-Seignovert et al. 2004). None of these strains significantly improved the expression levels of this protein (data not shown).

For final cultures, the 6xHis-Arb2+C plasmid was transformed into BL21 (DE3) cells which were grown in 1 litre LB media using the same protocol (detailed above). The harvest gave ~20 grams of cells which were lysed by cell disruption and from the supernatant, protein was purified as detailed below (see Section 2.2.5).

The supernatant was applied to the nickel affinity column and eluted with an increasing gradient toward 1 M imidazole (Fig. 3.13).

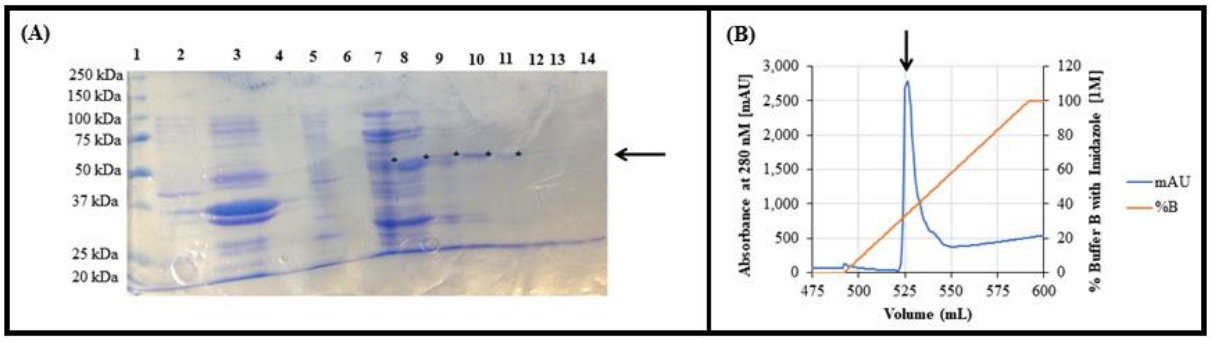

Figure 3.13 Purification of 6xHis-Arb2+C by FPLC: Nickel affinity chromatography
(A) 10 % (w/v) SDS-PAGE, Lane 1: molecular mass marker; Lane 2: crude lysate; Lane 3: insoluble fraction; Lane 4: flow through from crude lysate; Lane 5: 10 mM imidazole wash; Lanes 6-13: fractions from gradually increasing levels of 1 M imidazole; 6xHis-Arb2+C construct (estimated: 47.7 kDa) of Hda1 (*) is observed in Lanes 7-11 (B) FPLC chromatogram by of tagged Arb2+C. The arrow points to tagged 6xHis-Arb2+C construct.

The retention volume was 525-541 mL and the protein eluted at 33-49 % imidazole. As seen in Figure 3.13A, after nickel affinity column purification the sample showed some additional bands of either contamination or degradation in addition to a protein of the correct size. The samples with eluted protein can be seen in Lanes 7-11 below the 50 kDa molecular marker line which is appropriate given the estimated weight of the tagged construct which is 47.7 kDa. These samples were pooled, and buffer exchanged into IEC Buffer A (see Section 2.2.7.2).

To try to increase the protein yield, we increased the lysis buffer imidazole level (to 20 mM) since imidazole levels can decrease non-specific binding of host proteins to nickel by interfering with the binding of untagged proteins to the column (Qiagen 2003). However, this adjustment to the lysis buffer showed no significant elimination of the additional bands (data not shown).

Protein samples from Nickel His Trap column were kept overnight at 4 °C. The next day this sample was subject to buffer exchange into IEC buffer A by a PD-10 or HiPrep26/10 desalting column (see Section 2.2.7.2). Ion exchange was performed by anion exchange column on 6xHis-Arb2+C protein as described in Section 2.2.7.2. The isoelectric point (pI) of this tagged protein is 4.68 and buffer pH = 7.5 which left the protein with an overall negative charge so that it would bind to the positively charged resin in the column. The purified protein is observed in the SDS-PAGE gel (Fig. 3.14A)

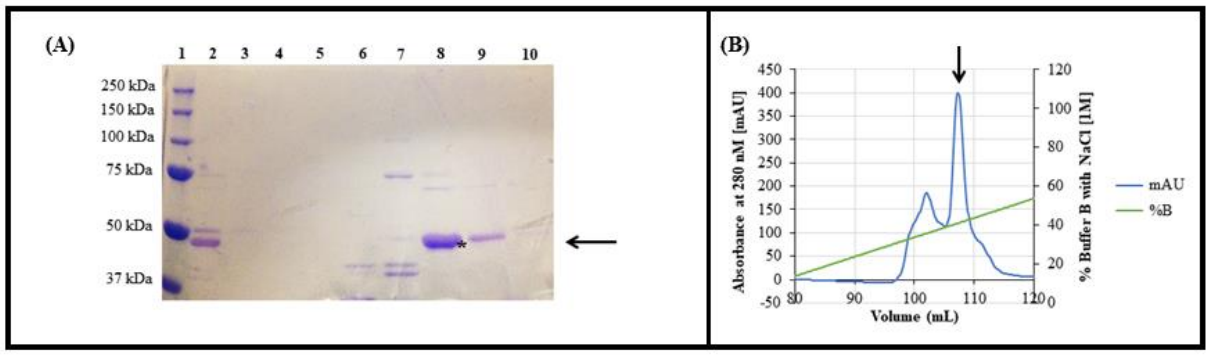

Figure 3.14 Purification of 6xHis-Arb2+C by FPLC: Ion exchange chromatography
(A) 10 % (w/v) SDS-PAGE, Lane 1: molecular mass marker; Lane 2: Pooled samples from nickel affinity column; Lane 3: flow through; Lane 4: wash with 100 mM NaCl; Lanes 5-10: fractions from increasing levels (%) of 1 M NaCl wash- estimated: 47.7 kD 6xHis-Arb2+C construct of Hda1 (*) is observed in Lane 8 (B) FPLC chromatogram of tagged 6xHis-Arb2+C. The arrow points to 6xHis-Arb2+C protein.

The protein (Arrow) had a retention volume of 107-11 mL and eluted from the column at 40- 44 % 1M NaCl. The samples were pooled, and SEC purification was performed using a Hiload 16/60 Superdex 75PG size exclusion column (Fig. 3.15B) (see Section 2.2.7.3).

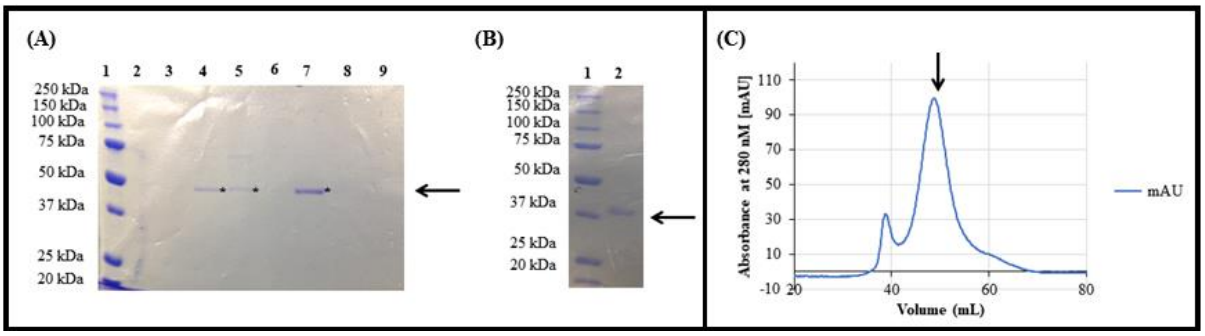

Figure 3.15 Purification of 6xHis-Arb2+C by FPLC: Size exclusion chromatography (A) 10 % (w/v) SDS-PAGE, Lane 1: molecular mass marker; Lane 2: Concentration column flow through; Lanes 6 & 8: spacer Lane- no sample; Lane 3 – 5, 7, 9: fractions from size exclusion column wash- ~47.7 kD 6xHis-Arb2+C construct of Hda1. (*) is observed in Lanes 4, 5 and 7 (~37-53 mL) (B) Secondary Nickel Batch Purification of thrombin cleaved Arb2+C construct: 10 % (w/v) SDS-PAGE, Lane 1: molecular mass marker; Lane 2: Flow through from secondary nickel containing Cleaved Arb2+C domain (C) FPLC chromatogram of 6xHis-Arb2+C. The arrow points to tagged 6xHis-Arb2+C.

The SDS-PAGE gel visualizes the fractions eluted from this sizing column and the protein in Lanes 4, 5 and 7 with a retention volume of ~37-53 mL (Fig. 3.15A). The purified 6xHis-Arb2+C construct yielded ~15 mL of protein at 0.089 µg/µL which concentrated to ~30 µL at 9 µg/µL (Fig. 3.15B).

This purified protein was allocated to crystallization studies done with small volume mosquito screening: Wizard and Hampton-HT. These and several other screens (for full list see Section 2.2.8.1) yielded no crystals. Some protein (30 µg) was allocated for a thrombin cleavage test and the resulting cleaved protein was used for crystallization screens. The goal of the thrombin cleavage test was to see if cleavage of the tag might yield protein which was more inclined to form crystals. Rather than cleave the entire isolate, this initial test was undertaken based on the fact that thrombin cleavage can vary in its specificity and proteins can undergo degradation (Cantwell & Cerca 2006).

The protein was diluted in SEC buffer and thrombin was added for overnight incubation at 4 °C (see Section 2.2.7.4). The cleavage mixture (protein components: cleaved Arb2+C, uncleaved 6xHis-Arb2+C, thrombin and 6xHis tag) was purified by secondary Nickel batch purification (see Section 2.2.7.1) with Ni-NTA Agarose Resin to isolate the pure protein from the remaining tagged protein and cleaved tag. The cleaved protein sample was observed in the flow through. A portion of the protein was unaffected by the thrombin. This uncleaved fraction was observed in the elution done with Buffer B: SEC Buffer + 500 mM imidazole (Fig. 3.15B, Lane 2) at .06 µg/µL in 15 mL and once

concentrated to 0.9 ug was brought forward to a mosquito crystallization screen (see Section 3.3.2.6). This sample concentration includes the added thrombin which runs in very close size (~37 kDa) to the Arb2+C (~45.6 kDa) protein. There is an apparent shift in size with loss of the thrombin site and 6xHis tag of ~2.27 kDa as was apparent on running the samples through SDS-PAGE gel (Fig. 3.15B).

3.3.2.6 Crystal Screens, analysis and Thermal Shift assay with Hda1 Arb2 domain protein

Before setting up crystal tray the 6xHis-Arb2+C protein was concentrated, and buffer exchanged to an appropriate crystallization buffer (Tris-HCl pH 7.5 20 mM, NaCl 50 mM, glycerol 5 % and BME 2 mM).

The purified 6xHis-Arb2+C protein was screened by hanging drop crystallization using a mosquito LCP machine with Wizard and Hampton HT screens at 4 °C (Wizard and Hampton HT) and 20 °C (Hampton HT) and by thermal melt assay to evaluate protein folding.

The crystal tray for Arb2+C (thrombin cleaved- without 6xHis) was prepared by mosquito LCP using a Hampton HT screen at 20 °C. Early monitoring of the tray saw no crystal nucleation.

After six weeks, one crystal was harvested from well. The crystal was removed via a CryoLoop (Fig. 3.16). It was stored in its original growth buffer with added glycerol and frozen in liquid nitrogen until synchrotron analysis (Diamond Light Source, Didcot by Dr. Abhimanyu K. Singh (Department of Biosciences, University of Kent)) (see Section 2.2.8.2) This imaging did not give diffraction which can be due to the cryo-conditions used (H10 buffer + 25 % glycerol), deterioration or other causes.

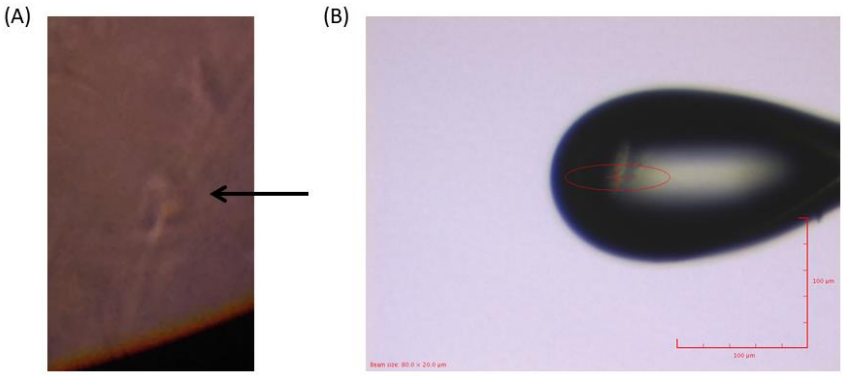

Figure 3.16 Image of 6xHis-Arb2+C in growth conditions and non-diffracting crystal on loop in synchrotron
(A) As found in Hampton screen of 6xHis-Arb2+C domain construct: H10 (20 % Polyethlene Glycol monoethyl ether 550) (B) Crystal on loop before X-ray diffraction with beam line 80 x 20 µm. [Crystal harvesting and synchrotron analysis was done by Dr. Abhimanyu K. Singh]

Since crystallization screens had initially not been producing crystals, we proceeded to evaluate the folding of the purified 6xHis-Arb2+C by thermal shift assay. The 6xHis-Arb2+C screen was designed based upon observations of the crystallization trays and expression protocols (for detailed screen layout see Appendix 1.1.3). This screen showed no apparent melt, but it still offered to contribute some information about the preferred conditions. Among those tested, the conditions with an observed slight change in fluorescence included those with the base buffers: HEPES, Tris or MES, pH 6.5-8, addition of Glycerol 0.25 % and 150-200 mM NaCl or KCl. The best condition observed was simply Tris pH = 7.5. This is only informative at the most minimal level though since assay did not show a normal melt curve.

3.4 Goal 2: Solve the structure of *C. albicans* Hda2 and Hda3 proteins to evaluate their potentials as drug targets.

Since *C. albicans* Hda2 and Hda3 proteins are thought to have DNA binding domains that likely play a role in their function, information about their structure is important in understanding their precise role. While this section shows that attempts at solubilizing these proteins did not prove enough (thwarting further steps toward structural analysis), it nonetheless, outlines their successful expression and contributes toward protocols and directions for future work on these proteins.

3.4.1 Evaluate Hda2 and Hda3 by structural alignment and domain analysis

Currently no structural information exists about *C. albicans* Hda2 and Hda3 proteins. We sought to optimize a purification protocol to provide protein for downstream studies that would unveil structural or functional aspects of these proteins.

To evaluate the predicted domain structure of *C. albicans* Hda2 and Hda3 I used SMART analysis which predict that Hda2 (699 amino acids) and Hda3 (835 amino acids) each have one Hda2-3 Pfam domain (aa 68-340 and 24-410 respectively) (Fig. 3.17).

The Hda2-3 Pfam domain is specifically found in Class II histone deacetylase complex members 2 and 3 in fungi (this includes Ccq1 of pombe) (Finn et al. 2016). However, despite the existence of a group of proteins that contains the Hda2-3 Pfam domain, the only structural information about this region is derived from *S. cerevisiae* Hda3DBD (Finn et al. 2016; Lee et al. 2009).

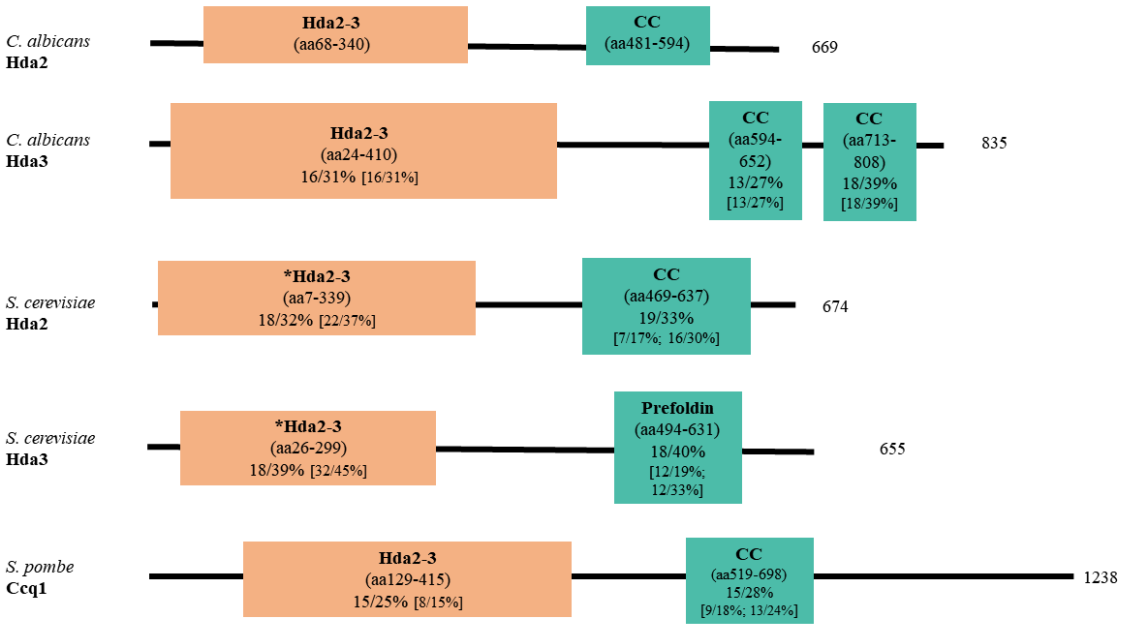

Figure 3.17 Comparisons of major domains of *C. albicans* Hda2 and Hda3 and similar yeast proteins shows homology

Emboss Stretcher and SMART analysis comparison with *C. albicans* Hda2 (% identity/% similarity) and within brackets [ ] designate comparison with *C. albicans* Hda3 domain (s) *DBD domains evaluated in Lee paper were larger than the SMART designated Hda2-3 domain of S. cerevisiae: Hda2 N5-K415 and Hda3 I6-K333. Not shown in Figure: Amino acids 6-75 of C. albicans Hda2 domain is homologous to a hydrolase domain of rhamnogalacturonase a from Aspergillus aculeatus SCOPe entry d1rmga_; low complexity domains. (Schultz et al. 1998; Letunic et al. 2015; Yang & Seto 2009; Rice et al. 2000; Fox et al. 2014). [Adapted from portion of Figure 1B, Yang and Seto 2009]

Hda2 has one predicted C-terminal coiled-coil domain (aa 481-594) and two low complexity regions (aa 21-39 and 611-626); in addition, there is a third low complexity region overlapping (aa 40-73) the Hda2-3 domain (Fig. 3.15).

Model predictions for the *C.albicans* Hda3 C-terminal coiled-coil domain show that there are two adjacent regions (aa 594-652 and 713-808) with this motif separated by a low complexity region (aa 670-687) (Fig. 3.17) (Schultz et al. 1998; Letunic et al. 2015).

Interspacing the features of Hda3 are additional low complexity region nearer the Pfam domain (aa 6-20, 431-455 and two others that overlap the Hda2-3 domain (at aa 176-221 & 282-298). The protein also matches two outlier homolog regions (aa 24-172 and 348-484) with significant similarity to the characterized structure of *S. cerevisiae* Hda3 DBD (Fig. 3.17) and some conservation is observed with the related Rad54 functional motifs (Letunic et al. 2015; Schultz et al. 1998).

It is notable that the *C. albicans* Hda2 Pfam Hda2-3 domain and coiled-coil domains have in fact more similarity with *S. cerevisiae* Hda3 than Hda2 (Fig. 3.17). This is reflected in the entire Hda3 proteins which share 26.0 % amino acid identity and 41.5 % similarity. Whereas, the *C. albicans* and *S. cerevisiae* Hda2 proteins have 20.2 % identity and 36.2 % similarity (EMBOSS Needle pairwise alignment) (Rice et al. 2000).

While *S. pombe* Ccq1 pombe carries a Pfam Hda2-3 domain and is somewhat comparable to Hda2 (identity 15 %/similarity 31 %) and Hda3 (identity 15 %/similarity 29 %) it also has a characterized coiled-coil domain (aa 519-698) and low complexity region (aa 484-490 there are also three predicted overlapping low complexity regions: aa 118-132, 363-381 & 567-586). This protein works in cooperation with the SHREC complex which contains proteins that function in the capacity of *SNF2* (Mit1) HDAC (Clr3) (see Section 1.8.2).

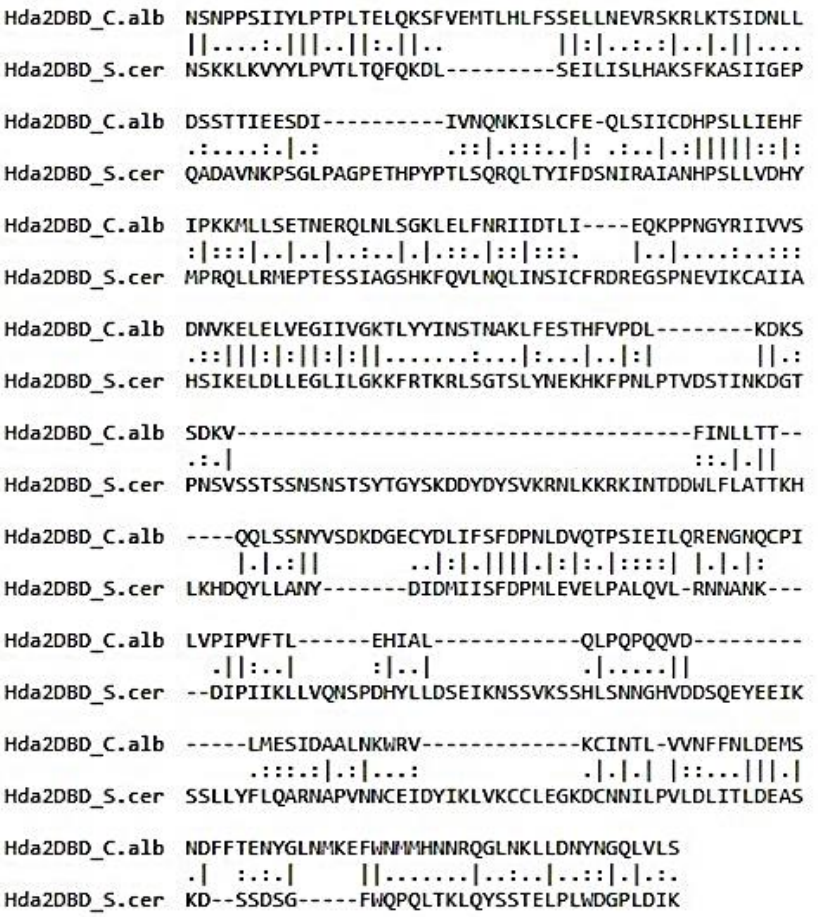

Figure 3.18 Conservation between *S. cerevisiae* Hda2DBD and *C. albicans* Hda2DBD
Alignment of *S. cerevisiae* Hda2DBD (N5-K415) to (aa N66-A393; ~22.3 % identity/ 38.9 % similarity) *C. albicans* Hda2DBD protein (Lee et al. 2009; Rice et al. 2000). Symbols : (colon) indicates strong similarity and . (period) weak similarity of the compared amino acids; EMBOSS Needle.

Alignment with *S. cerevisiae* DNA binding domains by the Huber lab (that contributed the structure of Hda3DBD) estimated that the *C. albicans* Hda2 and Hda3 DNA binding domains span and overreach the SMART modeled Hda2-3 Pfam domains (Figs 3.17, 3.18 and 3.19) (Lee et al. 2009).

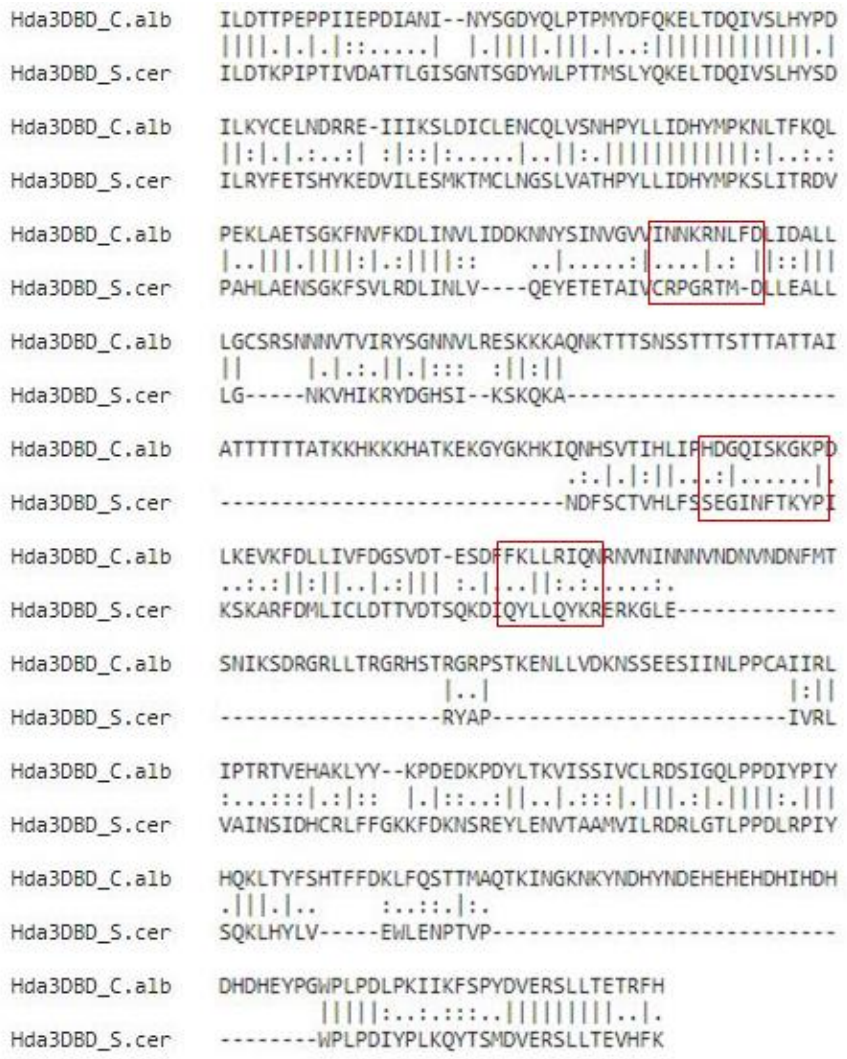

Figure 3.19 Conservation between *S. cerevisiae* Hda3DBD with *C. albicans* Hda3DBD includes functional motifs
S. cerevisiae Hda3DBD (I6-K333) with area matched by EMBOSS Needle pairwise alignment tool to (aa I6-H485; 30.2 % identity/ 43.4 % similarity) *C. albicans* Hda3DBD protein. Functional motifs as identified in *S. cerevisiae* are not well conserved, these are marked by red boxes (Lee et al. 2009; Rice et al. 2000). Symbol : (colon) indicates strong similarity and (period) weak similarity of the compared amino acids.

The Hda3 DBD of *C.albicans* shares 30.2 % identity/ 43.4 % similarity with *S. cerevisiae* Hda3 DBD which has been crystalized (Lee et al. 2009). However, the DBD of two yeasts Hda2 proteins are less similar sharing 22.3 % identity and 38.9 % similarity (EMBOSS Needle pairwise alignment) (Rice et al. 2000). In comparison of the two, the DBD of *S. cerevisiae* Hda2 and Hda3 share 20.3 % identity/ 32.3 % similarity while the same comparison in *C. albicans* gives 15.7 % identity and 29.8 % similarity.

This analysis shows that overall, the Hda3 DBD, Pfam and coiled-coil/prefoldin domains are more conserved between *S. cerevisiae* and *C. albicans* than the comparable domains of Hda2. This pattern of conservation is also observed in the relative larger bodies of these proteins.

Overall very little is known about the structure *C. albicans* Hda2 and Hda3 proteins. Consequently, if information is to be derived by comparisons, existing structural data-based estimations are a good starting point. As such, this section offers a discussion of the existing proteins whose structural data are used as templates for models of *C. albicans* Hda2 and Hda3. These are insights that may guide further studies about these proteins.

Structure-wise, the most is known about Hda2 which finds templates in several existing structures from the Protein Database (PDB). Phyre2 models 97 % of residues at > 90 % confidence (Fig. 3.18). Percent identity for the proteins used to model Hda2 ranges from ~29-54 % with the closest similarity to *S. cerevisiae* (Fox et al. 2014; Kelley et al. 2015).

Figure 3.20 Model showing highly confident prediction of *C. albicans* Hda2 structure
Colored by Phyre2 model confidence: Red > 97 %; Blue, 0 %; Hda2: 97 % of residues at > 90 % confidence based upon C. albicans: Hda3; S. cerevisiae: CHD1; a S. pnemoniae: PcsB (secreted protein), A. gambiae protein binding region, D. discoideum dynein motor domain, and H. sapiens STAT1 (PDB: 3MWY, 3HGT, 5O9G, 4CGK, 3OJA, 3VKG, 1YVL) (Kelley et al. 2015; DeLano 2002; DeLano 2009).

The model in Figure 3.20 estimates the structure of *C. albicans* Hda2. It depicts a two-lobed protein rotated such that the C-terminal coiled-coil domain extends backward and into the page at the bottom right of the image. Seven templates were chosen by Phyre2 to model Hda2 based on the need to cover all regions and their identity to the submitted Hda2 sequence. While no part of the Hda2 crystal structure has been solved in *S. cerevisiae*, its similarity with the Hda3DBD solved structure (PDB: 3HGT) is the first noted hit on the

Phyre2 search. This protein forms a dimer and the templated region (3HGT: aa 23-305) aligns with most of the N-terminal half of Hda2 (aa 70-373; 45 % coverage). Information about other templates for this model can be found in Appendix 1.1.2. The aligned residues lie in the region of amino acids K9 to P668 with only one small unmodeled region and small areas of the N- and C-terminals of the protein have no predicted structure or model identified.

Taken together the in silico analysis of Hda2 structure suggests that the first part of the protein has considerable similarity to *S. cerevisiae* Hda3 and Chd chromatin remodeler complexes. The rest of the protein is modeled based on divergent organisms, but the sequence does not overall suggest unknown motifs.

Phyre2 modeling of Hda3 contributes a less defined model as about half of the structure lacks a modeling template (Fig. 3.21). The structure model shows a very different form from that of Hda2 with considerably more asymmetry, and the coiled-coil domain extends as a long protrusion.

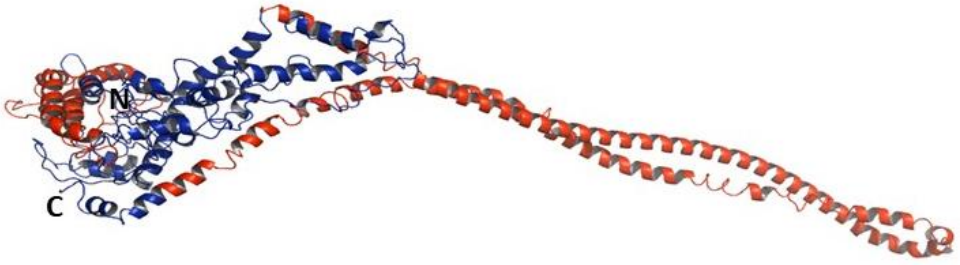

Figure 3.21 Model showing prediction of *C. albicans* Hda3 protein structure with regions of high confidence and also large areas with structure uninformed
Colored by Phyre2 model confidence: Red ≥ 97 %; Blue, 0 % ; Hda3: 51 % of residues at > 90 % confidence based on *S. cerevisiae* HDA3, *S. pneumoniae* PcsB, *S. scrofa* Tropomyosin, and *P. yayanosii* SMC (PDB: 3HGT, 4CGK, 5XG2, 1C1G) (Kelley et al. 2015; DeLano 2002; DeLano 2009).

Hda3 modeling also found a template in *S. cerevisiae* HDA3 (PDB: 3HGT) and *S. pneumoniae* PcsB (PDB: 4CGK). These contributed to the model by aligning with regions at the first part of the Hda2-3 domain and through most of the coiled-coil domain respectively (3HGT: aa 22-158 with Hda3: aa 25-170; 4CGK aa 46-252/17 % coverage with Hda3: aa 582-788/ 24 % coverage). Information about these and other templates for this model can be found in Appendix 1.1.2. The conserved residues lie in the region of Hda3 amino acids Y25 to N170 and L535-D820 with a large unmodelled region in between

and smaller areas of the N- and C-terminals of the protein have no predicted structure or model identified.

Taken together the in silico analysis of Hda3 suggests that the first part of the protein has considerable similarity to *S. cerevisiae* Hda3. The rest of the protein can only partially be modeled based on proteins from more divergent organisms and so the sequence does suggest the presence of unknown motifs.

3.4.2 Express recombinant Hda2 and Hda3

The overall goal of the experiments in this section was to solve the structure of *C. albicans* Hda2 and Hda3. To express the Hda2 and Hda3 *C. albicans* proteins, synthetic versions of the sequences were designed to maintain the native sequence with only one adjustment, the change of CTG codons for TCA to accommodate for CUG clade differences (see Section 1.2.6). These codons occurred four times in *HDA2* and six times in *HDA3*. Synthetic *HDA2* was synthesized into pET151 (see Section 2.1.6) with Avi and 6xHis tagging. The first aim of these experiments was to express soluble Hda2 and Hda3 proteins.

3.4.2.1 Expression and Solubility Tests of *C. albicans* Hda2

The synthesized plasmid was designed to allow the Hda2 protein to be translated with a TEV protease cleavage site and N-terminal 6xHis and Avi tags (6xHis-Avi-Hda2) (see Sections 2.1.7 and 2.2.1).

The *E. coli* strain Rosetta (DE3) was directly transformed with the synthetic 6xHis-Avi-*HDA2* plasmid (ABp_150). The resulting strain was grown at 37 °C the protein was induced with 500 mM IPTG for 20 hours at 20 °C. Harvested cells were lysed by sonication (see Section 2.2.5) and the cell debris (insoluble fraction) were removed by centrifugation. Expression was visualized by SDS-PAGE gel electrophoresis (Fig. 3.22).

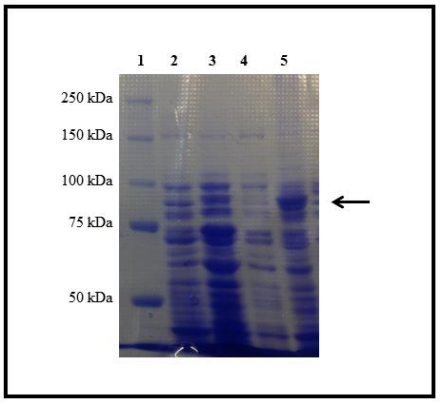

Figure 3.22 Expression and insolubility of 6xHis-Avi-Hda2
Lane 1: molecular mass marker; Lane 2: Pre-induction; Lane 3: Post-induction; Lane 4: soluble fraction; Lane 5: insoluble fraction. The arrow points to insoluble tagged Hda2 (~86.9 kDa).

A band around the estimated molecular weight of ~86.9 kDa was present in the insoluble fraction (Fig. 3.20). Addition of 1 % glucose and lowering growth temperature to 16 °C may have affected a slight increase expression level but the protein remained insoluble (data not shown).

To address the issue with solubility, freeze thaw lysis was tested with sets of different lysis buffers designed to survey a range of conditions known to encourage solubility of protein (see Section 2.2.12). This assay showed that solubility was not improved by addition of detergent, urea, decrease in salt or change in pH for this 6xHis-Avi-Hda2 construct (Fig. 3.23 and 3.24).

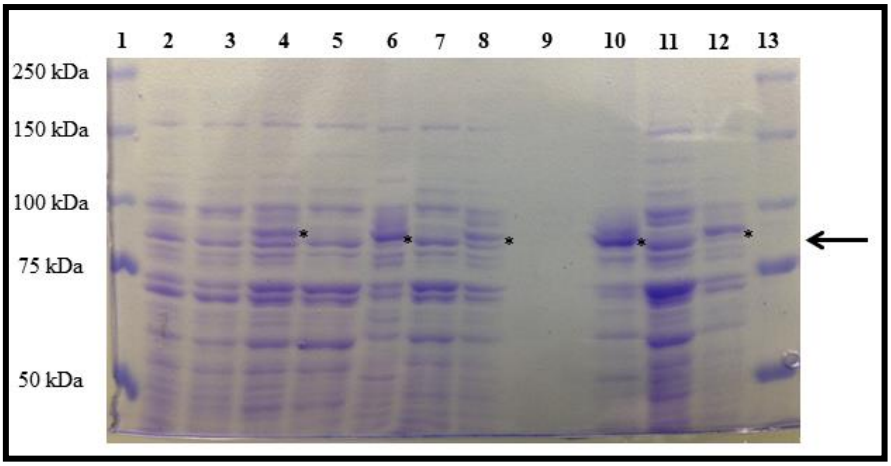

Figure 3.23 Hda2 Solubility Testing: Wide screen shows no substantial change of insolubility
Solubility screen on Hda2pET151. Primary Widescreen Solubility Test 10 % (w/v) SDS-PAGE: Lane 1: molecular mass marker; Lane 2: Pre-induction; Lane 3: Pre-induction; Lane 4: Post-induction ; Lane 5: Supernatant pH Screen; Lane 6: Pellet pH Screen; Lane 7: Supernatant Salt Screen; Lane 8: Pellet Salt Screen; Lane 9: Supernatant Urea Screen; Lane 10: Pellet Urea Screen; Lane 11: Supernatant Detergent Screen; Lane 12: Pellet Detergent Screen; Lane 13: molecular mass marker Hda2 (*) is observed in the pellet portion (lanes 4, 6, 8, 10, and 12). The arrow points to expected molecular weight (~87kDkD).

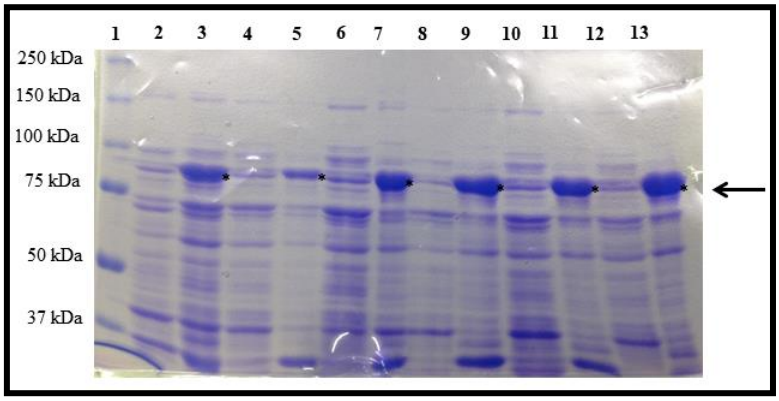

Figure 3.24 Hda2 Solubility Testing: pH screen shows no change of insolubility
Solubility screen on Hda2pET151. Extensive pH Solubility Test 10 % (w/v) SDS-PAGE: Lane 1: molecular mass marker; Lane 2: Pre-induction; Lane 3: Post-induction; Lane 4: Supernatant pH 5; Lane 5: Pellet pH 5; Lane 6: Supernatant pH 6; Lane 7: Pellet pH 6; Lane 8: Supernatant pH 7; Lane 9: Pellet pH 7; Lane 10: Supernatant pH 8; Lane 11: Pellet pH 8; Lane 12: Supernatant pH 9; Lane 13: Pellet pH 9

Separately, other trials were made: salt was lowered to 200 mM for an expression test and different IPTG levels (400 mM, 600 mM, 800 mM) or *E. coli* expression strains (BL21(DE3)) were trialed; yet these did not significantly improve expression or solubility levels (data not shown).

Like Hda1, codon adaptation evaluation shows many badly adapted codons which are likely a problem for expression in *E. coli* (Fig. 3.25).

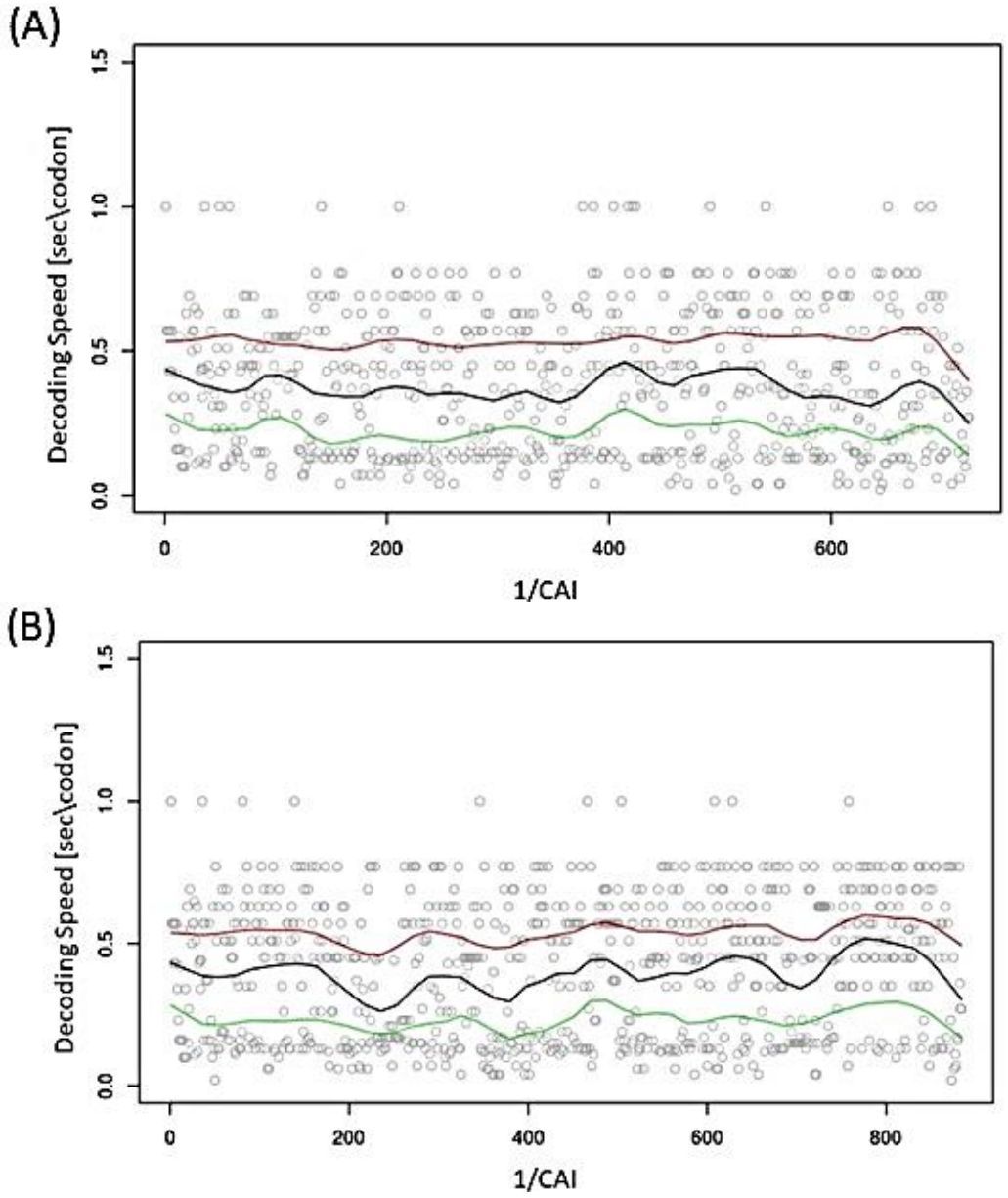

Figure 3.25 Codon adaptation of synthesized *HDA2* and *HDA3* sequence for expression in both *E. coli* and *S. cerevisiae* is not ideal for *E. coli* specific expression
(A) *HDA2* and (B) *HDA3* CAI -codon adaptation index (1/CAI: 0 good 1 bad; green = best possible sequence and red = worst; black = synthetic HDA sequence) The traces are averaged over a window of 50 codons. The circles are the adaptation values of the individual codons (Chu & von der Haar 2012). Note: Figures made based upon *HDA2* and *HDA3* synthetic sequences by Dr. Tobias von der Haar (School of Biosciences, University of Kent).

To confirm that the insoluble band was in fact 6xHis-Avi-Hda2, gel excision and mass spectrometry were used. A list of peptide mass values from an enzymatic digest of

Hda2 was queried against the NCBI database (see Section 2.2.11) and several hits for *C. albicans* Hda2 protein had significant protein scores (score = 417, $p < .05$) for these matches (see Appendix 2.1.1 for full list of peptides found).

3.4.2.2 Expression and solubility tests of Hda3

The tagged full-length synthetic HA-Hda3 gene sequence was cloned in frame with a N-terminal 6xHis tag sequence (see Section 2.2.3).

Recombinant protein expression was conducted in the *E. coli* strain BL21 (DE3) Codon Plus RIL upon induction with 500 mM IPTG for 20 hours at 16 °C. The RIL strain was chosen based on the difficulties in expressing Hda1 and Hda2 because this strain of *E. coli* is constructed for expression of genes that come from organisms with AT rich genomes and it was used in the *S. cerevisiae* Hda3DBD structural analysis study (Lee et al. 2009). It incorporates genes for tRNAs recognize the arginine codons AGA and AGG, the isoleucine codon AUA, and the leucine codon CUA (Agilent 2012b). In fact, it is even more sensible to use this strain for expressing *C. albicans* proteins in *E. coli* since its genome is even more AT rich than *S. cerevisiae* (GC content at synonymous codon position median value is 26 % for *C. albicans* and 36 % in *S.* cerevisiae) (Lynch et al. 2010).

Expression was visualized by SDS-PAGE gel electrophoresis and western blot (Fig. 3.26).

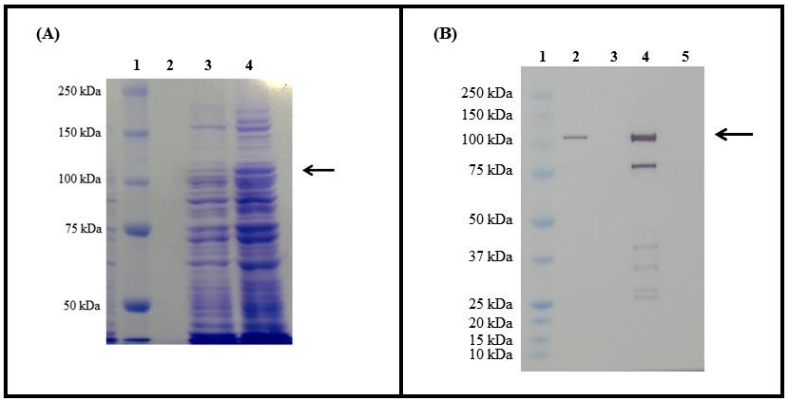

Figure 3.26 Expression and insolubility of 6xHis-HA-Hda3 and confirmation by Western blot
(A) Expression of 6xHis-HA-Hda3: Lane 1: molecular mass marker; Lane 2: skip; Lane 3: pre-induction; Lane 4: post-induction **(B) Western blot of 6xHis-HA-Hda3**: Lane 1: molecular mass marker; Lane 2: Post-induction; Lane 3: Pre-induction; Lane 4: insoluble fraction; Lane 5: soluble fraction. The arrow points to insoluble tagged Hda3 (~104.9 kDa). [Cloning, expression, solubility test and western blot of Hda3 protein were done by placement student Theo Hewitt (University of York)]

A band in the post- but not pre-expression sample was seen just above the 100 kDa marker line to match the estimated molecular weight of 104.9 kDa (Fig. 3.26; Arrow).

Harvested cells were lysed by sonication and the cell debris (insoluble fraction) were removed by centrifugation. These samples were taken for SDS-PAGE and western blot with an anti-His antibody specifically recognizing the 6xHis tag (Fig.3.26; see Sections 2.2.19 and 2.3.12). These assays show that the Hda3 protein was expressed. However, lysis by sonication of the protein found it to be insoluble.

Some lower bands are seen in the insoluble fraction sample (Fig. 3.26B, Lane 4). These bands likely show degradation of the protein which can be due to several factors including the absence of its normal complex binding partners or this could simply be due to non-specific binding of the 6xHis antibody (see Section 3.3.2.1). Ultimately, the protein was expressed insolubly. Both its solubility and stability might be improved by expression with other complex partners.

3.4.2.3 Cloning and Expression of Hda2 and Hda3 together

Since it had been documented that, when expressed together, Hda2 and Hda3 became soluble in *S. cerevisiae* (Lee et al. 2009), the intuitive next step was to try co-expression of the two proteins. Both genes were cloned into the pETDuet-1 (see Section 2.2.3) expression vector which allows for co-expression of two different genes under the control of two different promoters (Novagen 2011).

The *E. coli* strain BL21 (DE3) Rosetta was transformed with 6xHis-Avi-*HDA2*-6xHis-HA-*HDA3*-pETDuet-1 (see Section 2.2.3). The resulting strain was grown at 37 °C and protein expression was induced with 500 mM IPTG for 20 hours at 18 °C.

Expression of whole cell extract was visualized by SDS-PAGE gel electrophoresis. The expected molecular weight of His-Avi-Hda2 is 86.9 kDa His-HA-Hda3 is 104.9 kDa (Fig. 3.27).

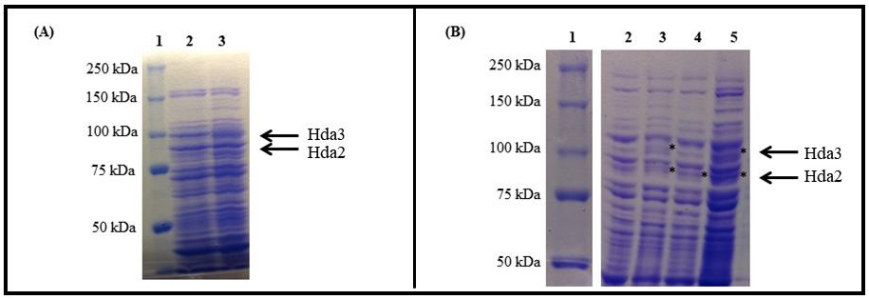

Figure 3.27 Expression and potential partial solubility of co-expressed 6xHis-Avi-Hda2 and insolubility of 6xHis-HA-Hda3
(A) Coexpression: Lane 1: molecular mass marker; Lane 2: Pre-induction; Lane 3: Post-induction (B) Solubility: Lane 1: molecular mass marker; Lane 2: Pre-induction; Lane 3: Post-induction; Lane 4: Supernatant; Lane 5: insoluble fraction. The arrow points to bands (*) at estimated molecular weight of tagged Hda2 (86.9 kDa) or tagged Hda3 (104.9 kDa).

A band in the post- but not pre-expression sample was seen at both the estimated molecular weights (Arrows). Expression was much lower than observed in individual expression tests. Consequently, only a single simple assessment of solubility was made (Fig. 3.27B).

The solubility test showed potential bands for Hda3 in the insoluble fraction (Fig. 3.27B5) while Hda2 had bands in both the soluble (B4) and insoluble fractions (B5). These would need further identified by western blot or mass spectrometry before these results can be taken as conclusive. However, expression levels were low, so this was not pursued.

In attempt to improve the protein expression levels, temperature was lowered, IPTG levels were changed and expression was trialed in Rosetta (DE3), but none of these adjustments made a significant difference in the levels of their expression (data not shown). While solubility of Hda2 showed possible improvement by co-expression, this was possibly at the expense of quantity of protein expressed.

3.5 Discussion

In this chapter an exploration into the expression of *C. albicans* Hda1, Hda2 and Hda3 proteins has been presented. This has led to the understanding that *E. coli* may not be the optimal system for expression of these proteins. The overall conclusions of this Chapter are: (1) Full length Hda1 protein can be solubly expressed at low levels and purified with N-terminal 6xHis and GST tagging, (2) The Hda1 Arb2 domain can be solubly expressed at low levels and purified with 6xHis tagging and potential crystallization conditions for the Arb2 domain been shown, (3) Dual expression of Hda2 and Hda3 may improve the solubility of Hda2 which requires further assessment.

As with Hda1, evaluation of Hda2 and Hda3 sequences show many badly adapted codons which are likely a problem for expression in *E. coli*. Hda2 and Hda3 both expressed but were not soluble. Expression of the proteins together may have improved the solubility of Hda2, but levels of expression were low (Fig. 3.2.7). Ultimately, additional troubleshooting is needed to diagnose whether significant amounts of soluble Hda2 and Hda3 could be obtained via this expression system. Despite trying many approaches to optimize expression by changing *E. coli* strain there are still other strains which might bring improvement, for example ArcticExpress competent cells (Agilent), etc. A western blot needs to be done to verify the presence of soluble Hda2. Following this assurance, manipulations to the *E. coli* strain and expression media may allow for the increased production of small amounts of this soluble protein. Separately, other tagging approaches and expression of the entire complex (or even with Hda1 catalytic domain constructs) can be trialed to see if expression levels of all three proteins and solubility of Hda2 and Hda3 might be improved.

Additionally, specific domain expression trials of Hda2 and Hda3 can also be pursued particularly given that the *S. cerevisiae* Hda3DBD was crystalized and its structure has been solved.

3.5.1 Design of synthetic Hda1, Hda2 and Hda3

During this work, analyses showed the unsuitability of the codons in the synthesized constructs of *HDA1*, *HDA2* and *HDA3* for expression in *E. coli*. Changing to *E. coli* expression strains (Rosetta, RIL) to introduce codons in an approach to overcoming this problem did again not bring any radical improvement in the expression of these proteins. This issue may have many causes including issues at the synthesis stage due to codon optimization or translation related issues that could be avoided through expression in a more similar organism such as *S. cerevisiae*. The sequences synthesized for these trials largely maintained their native *C. albicans* coding sequences and were not codon optimized for expression in *E. coli* based upon goals for experimental design that included expressing the synthetic constructs *in vivo*. Adjustments of the CTG codons could have affected the proteins abilities to fold (Miranda et al. 2013). The translation systems in bacteria and yeast are considerably diverged (Dever et al. 2016). It is notable that in *C. albicans*, it is usually but not always the case that CTG codons are met with serine tRNA synthetases (Miranda et al. 2013). In hindsight, as the extent of the project was met with challenges on the protein expression front, it should be noted that optimization of the

synthetic sequences for expression in *E. coli* may have resulted in a better protein expression outcome. Otherwise, using higher organism or yeast expression systems may overcome this codon issue.

3.5.2 Alignments, modelling and mapping of *C. albicans* Hda1 proteins

From our evaluation we note that sequence and structural features are somewhat conserved between *C. albicans* Hda1 complex proteins (Hda1, Hda2 and Hda3) and other yeasts (Figs. 3.1 – 3.3 and 3.7 – 3.21). Additionally, some features share resemblance with other more distant organisms.

It is interesting that Arb2 is not well conserved relative to the catalytic domain and that the only match among human protein (albeit with low significance) was to the *Homo sapiens* protein cadherin-13 isoforms (see Section 3.3.1). According to NCBI, cadherin-13 is involved in the regulation of axon growth in neurons and is hypermethylated in several types of cancer (Geer et al. 2010). While cadherins are not histone deacetylase proteins (very) divergent connections can be drawn between axon growth in neurons and hypha development. The protein contributes to adhesion (Ranscht & Dours-Zimmermann 1991). Although it is doubtful if conclusions could be drawn from such distant systems, discussions comparing disparate biological paradigms have the potential of leading to creative hypotheses (Simon 1983).

Low complexity regions were identified in the domain analyses of Hda2 and Hda3 *C. albicans* Hda1. Low complexity regions in *homo sapiens* protein populations have been studied for their tendency to expand and contract due to issues with nucleotide alignment during replication also these regions contribute to the emergence of novel phenotypes, protein functions and even functional genes (Toll-Riera et al. 2012; Ellegren 2004; Kashi & King 2006). These low complexity regions may give similar characteristics to *C. albicans* Hda2 and Hda3 proteins.

3.5.3 Expression of *C. albicans* Hda1 and Arb2 domain

While GST tagging did confer a better yield of the Hda1 protein, the harvest was low and would require very large batch purification for crystallization trails (Figs. 3.9). This protein was stored at -80 °C and full extraction quantities are appropriate for future single-molecule analysis. Single-molecule analysis can evaluate the interaction of this protein with DNA or perhaps histones. Future experiments would also consider cleavage of the GST tag as it could interrupt the natural processes of this protein. This cleavage would

entail protein loss so increasing the batch size for further use of this purification protocol would be advised.

Expression and purification of the Arb2+C domain did yield a good amount of protein. This expression construct and the purification approach are enough for use in further research. The crystal observed in trials with the 6xHis-Arb2+C construct suggests suitable conditions for this protein that deserve further investigation. While the crystal itself took a long time to appear (and may have just formed from salt or some other component of the buffer) it may provide a starting point for understanding the crystallization conditions that suit this protein. The conditions (20 % Polyethlene Glycol monoethyl ether 550) of the well (H10) that generated this crystal should be included in future evaluations of this protein construct.

3.5.4 Alignments, modelling and mapping of *C. albicans* Hda2 and Hda3 proteins

Architecturally speaking, the Hda2-Hda3 pfam domain (PF11496) is found in combination with other functional domains in various fungal proteins, including: (1) minichromosome maintenance complex (*MCM*)- a DNA helicase domain used in replication, (2) flavin-containing monooxygenase like (*FMO*) protein- responsible for oxidation of substrates, (3) transcriptional regulation protein SNF-2 N-terminal domain, (4) tRNA-synthase, and (5) Glutathione-dependent formaldehyde-activating enzyme (GFA) domains and currently the only structure of this domain type is from *S. cerevisiae* Hda3 (Finn et al. 2016).

3.5.5 Expression of *C. albicans* Hda2 and Hda3

Based on the low expression levels seen with the Hda1 construct, the *HDA2* and *HDA3* plasmids were designed for this project were designed with tags to allow for the potential of future tagging for single-molecule evaluation, an alternative to the original pursuit of crystalizing the proteins. Single molecule work requires much less protein than crystallization (see Section 3.3.2.2). It allows direct visualization of protein-protein and protein-DNA interactions and assessment of the biophysics of proteins in four dimensions (Hughes et al. 2014). This approach fits well with the low levels of soluble Hda2 protein expression which may have been observed (Fig. 3.27). However, it is possible that these tags interfere with soluble complexed or even individual expression of these proteins and future studies might trial expression without these additions. The *HDA2* and *HDA3* designs allow for a construct that takes advantage of the designed *Hind*III restriction site

which can exclude the Avi tag. For example, the *Not*I site at the end of the gene (in combination with *Hind*III) can allow easy digest-based cloning to the *MCS1* of pETDuet1. This is a quick option to checking expression without this tag and should be considered for future trials.

The study in *S.* cerevisiae which yielded the crystal structure of Hda3DBD used a different combination of proteins in the pETDuet vector (Hda1 and Hda2 on one vector and Hda3 on a lower level expression vector) to overcome similar issues with insolubility for individual expression of these proteins (Lee et al. 2009). Here, we may have expressed soluble *C. albicans* Hda2 in combination with insoluble Hda3. Verification that these proteins are in fact expressed and follow up by larger expression cultures with further purification steps are a clear next step toward the end goal of using tagged Hda2 in combination with the stored GST-Hda1 for single molecule work (see Section 3.3.2.2). Other arrangements of the Hda1 complex proteins and other co-expression strategies should be explored in future attempts at soluble expression of these proteins.

3.5.6 Conclusions and future directions

This study provides information about how to express soluble *C. albicans* GST-6xHis-Hda1 in small quantities. We also now know how to purify the Arb2+C domain of Hda1 and have a condition that may work for crystallization of this protein. This research has also shown that *C. albicans* Hda2 and Hda3 were insoluble when expressed alone which is a feature observed in *S. cerevisiae* (Lee et al. 2009). However, it is notable that in *C. albicans,* Hda2 but not Hda3 may have become soluble on dual expression.

The RIL strain showed good expression levels for *HDA3*-pET151 but was not trialled in earlier expression studies or for Hda2 and Hda3 co-expression. This strain was a kind donation from Agilent (San Jose, California) which was obtained quite late into this study and could prove fruitful for future work in this and other *C. albicans* protein expression projects. Here we have introduced a foundation for more experimental exploration of these proteins including resources and protocols.

The work in Chapter 3 was developed in parallel to the genetics approach outlined in Chapter 4 thatcomplements the work here by providing insight into the roles of these proteins from genetic, phenotypic, interaction and population standpoints.

Overall, expressing these proteins in *E. coli* is difficult. Due to time and resource constraints, yeast or higher expression system were not tried in this study but should be considered for future research.

In conclusion, this study of the Hda1 complex proteins contributes to future approaches for research about expression of these proteins. Solving these proteins structures and identifying their interaction domains can contribute to the existing knowledge about the histone deacetylase proteins in general as players in the epigenetic systems of pathogenic and non-pathogenic organisms. This may lead to the advancement of medical treatments or simply add to a holistic understanding of the evolution and current functions of histone deacetylase proteins Hda2 and Hda3.

CHAPTER 4. The function of *C. albicans* Hda2 and Hda3 *in vivo*

4.1 Introduction

This chapter explores the roles of *C. albicans* Hda2 and Hda3 in yeast and hyphae inducing conditions. The objective of this study is to evaluate the roles of these proteins under different conditions to understand their function.

Several strategies are used to replicate conditions (usually found in a host) that are conducive to the development of hyphae. Along with increasing temperature to 37 °C, different medias are used that manipulate the availability of nutrients. While one basic adjustment is simply adding serum to YPD, more honed media recipes include: spider, SLAD and RPMI (Weerasekera et al. 2016). These medias take unique approaches to induce filamentation: (a) Spider media provides mannitol as a carbon source with added ammonium salts and beef extracts (Daniels et al. 2013); (b) SLAD media has low levels of ammonium; and (c) Roswell Park Memorial Institute Medium (RPMI) contributes nutrients developed for the culturing of human cells, it is also very pH sensitive (Kucharíková et al. 2011; Moore et al. 1967). The levels of ambient CO_2 and pH of the media and other factors also contribute to the maintenance of a hyphae phenotype (Setiadi et al. 2006; Buffo et al. 1984).

Screens for phenotypes are assessed by measured growth on media aimed at unveiling the role of nutrients in biochemical pathways. Likewise, additives such as drugs or toxic agents can unveil weaknesses or bypass mechanisms within targeted pathways. Protocols that evaluate a specific broad range of these medias have been developed for use with mutant yeast strains to investigate phenotypes associated with genes (Oliver R Homann et al. 2009).

Another technique used to understand the impact of gene deletions is RNAseq. This is one of several next generation sequencing strategies which uses extracted RNA to evaluate the gene transcripts in a sample (Nagalakshmi et al. 2008).

In this chapter we aim to understand more about the *C.* albicans non-catalytic Hda1 complex proteins, Hda2 and Hda3. These proteins are known to have nuclear localization in other yeasts. For example, *S. pombe* Clr3 has been is found in the nucleolus where it functions as a deacetylase H3K14 (Bjerling et al. 2002) and nuclear localization patterns showing distinct punctae are observed by microscopy of fluorescence tagged Clr3. These

localization patterns have also been noted in studies of human HDAC proteins (Downes et al. 2000).

Histone deacetylase proteins often complex with other proteins. Moreover, it has been shown that in *S. cerevisiae*, Hda1, Hda2 and Hda3 proteins complex and function together (see Section 1.8.1). If Hda1 functions alone or in complex with Hda2 and Hda3 in *C. albicans* has not been established.

In *C. albicans* Hda1 is involved in molecular signaling that affects hyphal maintenance (Lu et al. 2011). During hypha initiation Hda1 deacetylates the Yng2 subunit of the NuA4 histone acetyltransferase complex causing its eviction and the clearance of Nrg1 from hyphae specific loci by activation of the cAMP-PKA pathway (Lu et al. 2011). Next Hda1 is recruited to the promoters of these loci which requires reduced Tor1 (Target of rapamycin) signaling (see Section 1.7.2, Fig. 1.12 and Lu et al. 2011).Whether Hda2 and/or Hda3 are involved in some or all of these activities is unknown.

Relating molecular pathways to emergent phenotypes using genetically modified or mutant yeast strains is one approach that can be taken to study these questions. When this type of investigation is applied to fungal pathogens, it is vital to question the impact on an organism's capability to infect. There are several ways that the virulence and pathways of pathogenic strains of yeast are tested in a lab setting. For example, *in vitro* macrophage systems are used to simulate a host immune response or *in vivo* systems of multicellular organisms are used to evaluate infection, such as *Caenorhabditis elegans* (henceforth: *C. elegans*) and even mammalian (murine) models (Pukkila-Worley et al. 2009b; Bain et al. 2012; MacCallum & Odds 2005; Balish et al. 1999). Deletion of Hda1 has been tested previously in a murine model and the strain did not show compromised virulence (Lu et al. 2013). The virulence of the mutant strain contrasts with the observed stunted filamentation phenotype and this may be explained by the finding that *UME6*, a downstream target of the Hda1 pathway necessary for virulence, is known to have another parallel regulatory pathway that can influence its stability (the oxygen sensing Ofd1 pathway) (Banerjee et al. 2008; Kadosh & Lopez-Ribot 2013).

There is limited information in the scientific literature about the *C. albicans* proteins Hda1, Hda2 and Hda3. This chapter explores the roles of these proteins *in vivo* using specially constructed deletion strains and strains with tags incorporated onto these proteins. This study tests the hypothesis that proteins complex to function in a similar way to their *S. cerevisiae* orthologs. Through experiments in yeast and hyphae inducing

medias, the specific roles of these proteins are explored through phenotype analysis, RNA sequencing and Chromatin ImmunoPrecipiatation (ChIP).

4.2 Goal 3: Understand the function of C. albicans Hda2 and Hda3 *in vivo* to evaluate their role in the virulence of this pathogen.

This results section includes evaluations of *C. albicans* Hda1 complex proteins and their gene expression. Tagged proteins and homozygous mutant strains were assessed in many conditions and on various levels: histone modification, mRNA transcript, protein, as single cells grown in liquid media or by colony population analysis on agar plates. Most of these assays were done with and without hyphae induction and additional stressors were also evaluated.

4.2.1 *C. albicans* Hda1 forms a complex with Hda2 and Hda3

This section outlines tests toward the hypothesis that Hda1 forms a complex with Hda2 and Hda3 in *C. albicans.* Several strains were constructed with tagged Hda1, Hda2 and Hda3 proteins by attaching Green Fluorescent Protein (GFP). Integration of the tag was confirmed by fluorescence microscopy (Figs. 4.1 and 4.2). Results from a coimmunoprecipitation experiment show interactions between the proteins (Fig. 4.3).

4.2.1.1 GFP tagging of *C. albicans* Hda1, Hda2 and Hda3 proteins

The proteins (Hda1, Hda2 and Hda3) were tagged with a C-terminal GFP at their native loci. Once these strains were built (see Section 2.3.5.2) their ability to fluoresce was checked as a way of confirming the presence of a GFP tag. Fluorescence microscopy was used to visualize the green fluorescent tag on the natively tagged protein within each strain. This was trialed on two occasions using two different microscopes (see Section 2.3.8.5). As can be seen in the Hda3-GFP strain in Figure 4.1 at the top, the results were, unfortunately, dim. There was background fluorescence, and this was observed in all the tagged strains (Hda1-GFP, Hda2-GFP and Hda3-GFP) as well as in the wildtype.

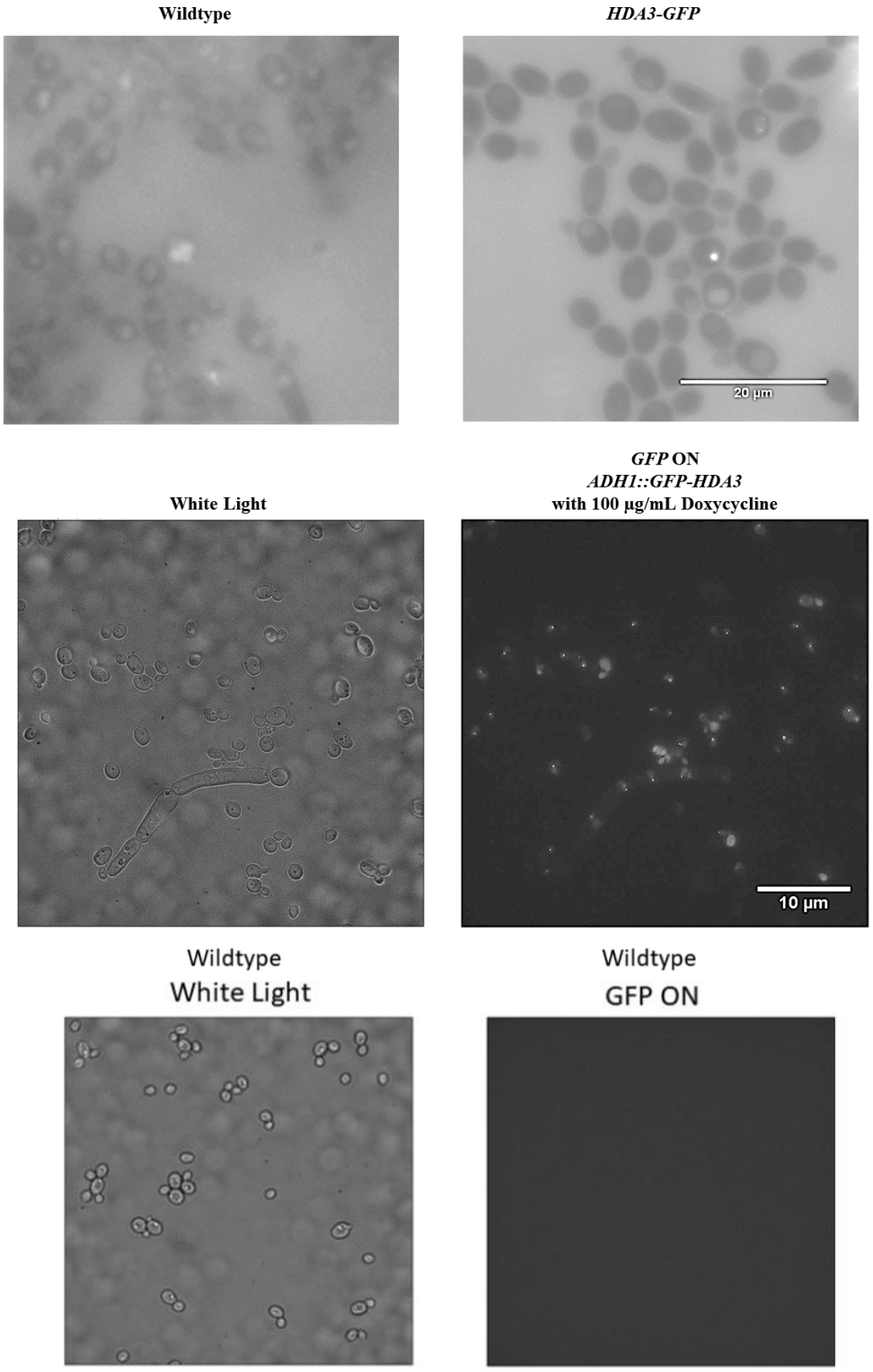

Figure 4.1 Fluorescence microscopy with native tagging of Hda3 shows faint background signal which is improved with change of tag location and controlled expression by inducible promoter at *ADH1* locus.
(Top) C-terminal GFP tagged Hda3 at native locus strain and wildtype strain without tag with GFP filter on;
(Middle) N-terminal GFP tagged Hda3 reintegrated at ADH1 with modulated expression under control of Tet-ON system (doxycycline); scale bars in white are 20 µM and 10 µM respectively; (Bottom) wildtype parental (strain shown as control).

The results indicate that either the experiment is not optimal (tag or location of tag is problematic, background fluorescence is obstructive, filter range is not adequate, etc.) or that the proteins have low levels of expression. As these were preliminary assays, further evaluation of these strains is needed to draw any definitive conclusion about the ability of these strains to fluoresce. These might include simple growth curves for comparison to the parent wildtype strain and/or phenotyping assessment as described later in this chapter to evaluate loss of protein function (filamentation, white-opaque, spotting assay with zinc, etc.). However, it was found by later experimentation that these tagged strains were usable as they are seen by antibody analysis in western blot (see Section 4.2.1.2)

Given the suboptimal outcome of native tagging screens we took the following approach: we cloned a plasmid to facilitate integration of a tagged *GFP-HDA3* (N-terminal) cassette at the *ADH1* locus under a Tet-ON system using doxycycline regulation (see Section 2.3.5.3). This allowed for some control over the level of expression by the amount of antibiotic added.

To evaluate the fluorescence of Hda3 integrated with N-terminal GFP tagging at the *ADH1* promoter, expression was induced with 100 µg/mL of doxycycline during cell growth and the cells were again visualized by fluorescence microscopy (see Section 2.3.8.5). As can be seen at the middle of Figure 4.1, the tagged protein was observed in these cells. Like the natively tagged strains, further evaluation of the impact of this reintegration and GFP tagging should include growth curve comparison to wildtype and phenotype evaluation. Assessment of the tagged Hda3 protein integrated to the *ADH1* site and induced by doxycycline was made by reintegration in the *hda3*ΔΔ mutant and also filamentation assay which is discussed later in this chapter (see Section 4.2.3.2.2-4). It is important to note that induction by doxycycline could result in non-natural levels or localizations of the protein and the integration itself could be causing the phenotype. Other controls could provide more definitive elimination of these possibilities, including tests of a strain with reintegration at the native loci or integration of GFP alone at *ADH1*.

This trial with high levels of doxycycline showed a significant amount of pinpointed fluorescence as can be seen in Figure 4.1 (middle). This hypothesis is consistent with reports in the literature for similar proteins (see Section 4.1) Based on a comparison of this image to the diagram in Figure 1.4, it can be suggested that the pinpointed bright spots located at the septum of the hyphae and periphery of yeast cells may indicate localization to a portion of the actin cortical patch. In a small portion of the

yeast cells the fluorescence is more diffuse which contrasts with pinpointed spots observed in the majority of cells and these distinct localization patterns of fluorescence may represent stage specific association with actin structures, patches or cables (in cell cycle, mitosis, budding, hypha emergence, etc.) (Anderson & Soll 1986; Moseley & Goode 2006). This is supported by the fact that many proteins which interact with the *S. cerevisiae* orthologs of Hda1, Hda2 and Hda3 have actin related functions (for further analysis see Chapter 5 Discussion of Goal 3). As these were preliminary results, additional studies that incorporate evaluation of colocalizations are required to assess this hypothesis. In the yeast cells large portions of some cells are fluorescent which may indicate localization of these proteins to the nucleus of these cells. This could be evaluated by larger images and further clarified by 4′,6-diamidino-2-phenylindole 4′,6-diamidino-2-phenylindole (DAPI) staining of DNA.

The conclusions drawn from this analysis of live cultures under fluorescence are: (1) the natural protein levels are low and (2) artificial induction of high levels of Hda3 and/or N-terminal tagging improve the visibility of the fluorescence. While localization studies were not done extensively, these images contributed to method development strategies for subsequent western Blot analyses as are shown in the next section.

4.2.1.2 Co-Immunoprecipitation of *C. albicans* Hda1 and Hda2 or Hda1 and Hda3

To investigate interactions between Hda1, Hda2 and Hda3 it was necessary to double tagged strains. After, both native and *ADH1* locus reintegration versions of GFP tagging were evaluated in trials by western blot. It was found that, despite the faint display by microscopy (Fig. 4.1), the native GFP tagged strains were visible by western blot antibody analysis. Double tagged strains were constructed by adding a C-terminal HA tag to Hda1 (in natively tagged Hda2 and Hda3 GFP strains) (see Section 2.3.5.2). These strains were used for co-immunoprecipitation assays with pull down by anti-HA antibody (Fig. 4.2). The goal of this assay was to pull down Hda1 with its HA tag and check if GFP tagged Hda2 or Hda3 were brought along. This assessed whether the proteins interact to discern whether they may form a complex.

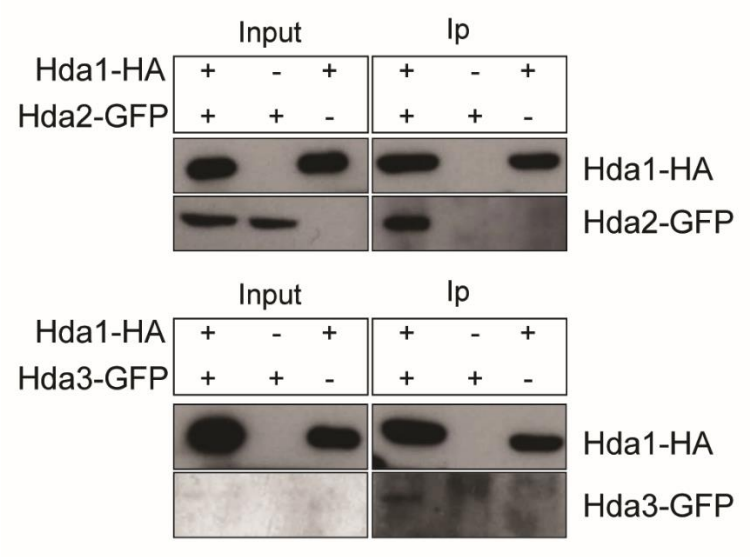

Figure 4.2 Interaction between *C. albicans* Hda1 and Hda2, Hda1 and Hda3 proteins
Western blots of single and double tagged Hda1-HA and Hda2/3-GFP by anti-HA and anti-GFP antibodies following Co-Immunoprecipitation of Hda1 using anti-HA antibody pull down. [image was composed by Dr. Alessia Buscaino for the article in Appendix 4]

In the double tagged strains, pull down of Hda1 by HA also brought along Hda2 or Hda3. In the end, expression level did turn out to be a problem with the Hda3-GFP strain as can be seen by the observed faint band (Fig. 4.2, bottom right panel), but interactions were present between Hda1 and Hda2 as well as between Hda1 and Hda3. We conclude that these interactions support the hypothesis that the Hda1 complex forms in *C. albicans*.

4.2.2 *C. albicans* Hda2 and Hda3: phenotype analysis, RNAseq and Chromatin Immunoprecipitation

To evaluate the roles of Hda2 and Hda3 in *C. albicans*, deletion strains were constructed to create homozygous mutant strains. This section covers a study of these strains. Rich nutrient media (YPD or synthetic complete) was used to analyze the basic growth of *hda2*ΔΔ and *hda3*ΔΔ. Stresses in the form of additions to and manipulations of the media were used to identify growth differences in the strains. Assessments of the cell wall and survival of the strains under temperature and ultraviolet radiation stress are also presented. Isolation and sequencing of RNA from these strains is outlined along with information about their gene expression profiles.

4.2.2.1 Construction of *hda2*ΔΔ and *hda3*ΔΔ mutants

Homozygous mutants were made by the Clox Gene disruption method and the markers were resolved from the strains for each *hda2*ΔΔ and *hda3*ΔΔ mutants (see Section 2.3.5.1 and Shahana et al. 2014).

The mutant strains of *hda2*ΔΔ and *hda3*ΔΔ were first evaluated for growth rate (Fig. 4.3).

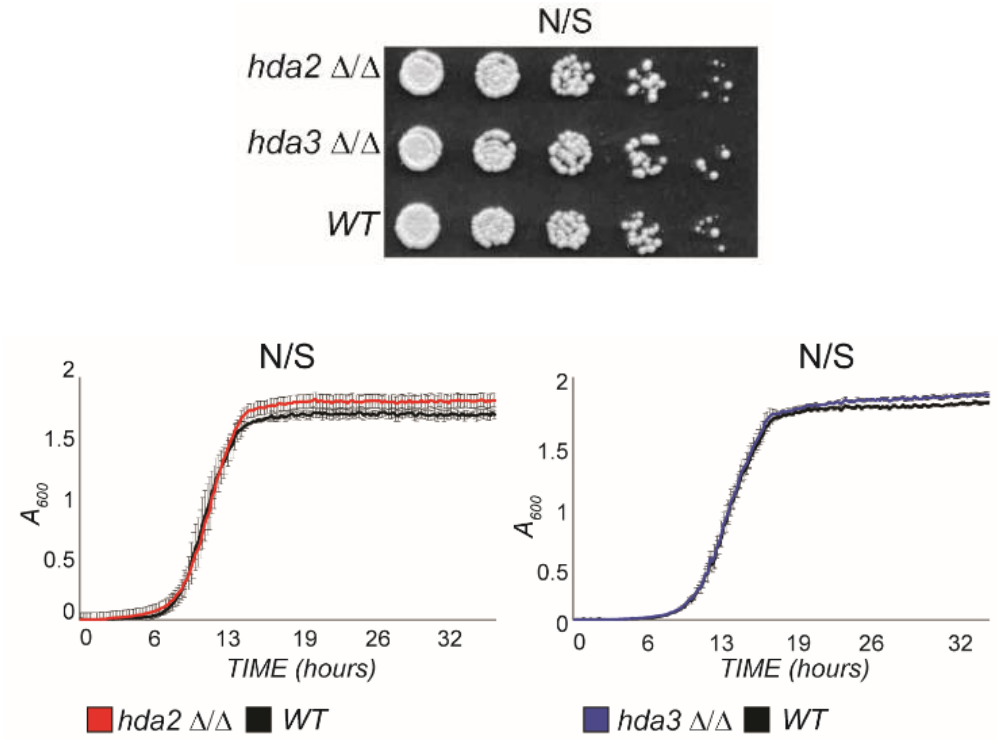

Figure 4.3 Homozygous mutants *hda2*ΔΔ and *hda3*ΔΔ growth on non-selective solid and in liquid media is comparable to wildtype
(Top) Serial dilution on YPD agar; (Bottom) Optical density over time in liquid YPD. [These growth assays and figures were made by Sarah Gourlay (Department of Biosciences, University of Kent)]

Serial dilution and spotting of these strains to solid media showed growth consistent with the wildtype as did growth in liquid YPD. Following this diagnostic, the deletion strains were evaluated with phenotype assays.

4.2.2.2 Phenotype screen of *hda2*ΔΔ and *hda3*ΔΔ

To investigate the phenotypes of *hda2*ΔΔ and *hda3*ΔΔ strains, serial dilutions of the strains were spotted onto a screen of medias to evaluate the relative sensitivity of the mutants to different stressors (see Section 2.3.8.1). While these diagnostics are often designed with the objective of stressing certain molecular pathways, our aim was to look at a variety of additives and alterations to the media as a way of gathering some information about these mutants.

4.2.2.2.1 Phenotype screen in yeast media

Phenotyping medias were assessed to identify growth inhibition or chemical resistance phenotypes for the *hda2*ΔΔ and *hda3*ΔΔ homozygous mutants.

Note about Hda1:

A *hda1*ΔΔ mutant was tested along with the *hda2*ΔΔ and *hda3*ΔΔ mutants and was used for the RNAseq experiments discussed later in this chapter (*hda1*ΔΔ mutant was shared by the Kuchler lab- Department of Medical Biochemistry, University of Vienna). This strain was constructed by replacing the the *HDA1* genes with *LEU2* and *HIS1* cassettes in the SN152 background. In some cases, the phenotype was the same but for others, the *hda1*ΔΔ mutant showed a strongly different phenotype to the *hda2*ΔΔ and *hda3*ΔΔ mutants.

These results are mostly not included in the phenotyping data since it is difficult to ascertain whether this was due to the markers in the strain (LEU2 and HIS1) and further confirmation of this fact is required. Phenotypes due to markers have been reported in other studies (Pronk 2002; Leng & Song 2016). This was surprising and these results evolved late in the course of this project. The request for an alternative marker free strain was made at this time since it was important to confirm whether these phenotypes might be due to the presence of markers. The phenotypes observed for *hda1*ΔΔ (ABy_179) but not included as results in this thesis were sensitivity to cycloheximide, calcofluor white and ethanol. Resistance in *hda1*ΔΔ (ABy_179) was observed in hydroxyurea, sodium dodecyl sulfate (SDS), sorbitol and cobalt. In media with other additives there was no growth difference (LiCl, caffeine, H2O2, EDTA, pH2.6 and pH10.5). Also notable was some filamentation in the *hda1*ΔΔ mutant only on media with pH10.5.

For some phenotypes I did additional spotting assays to address the issue of markers and an alternative *hda1*ΔΔ mutant (ABy_525) was evaluated for some of the screens. These results are discussed or shown in this chapter. This strain is made in the SN95 background without any deletion markers present and was provided by the Cowen Lab (Department of Molecular Genetics, University of Toronto). The medias tested included: nicotinamide, caffeine, cobalt, copper, fluconazole and SDS. The phenotypes seen in ABy_179 were not observed in ABy_525, which may confirm that the phenotype was due to the presence of markers but there were other differences including the strain backgrounds (SN152 and SN95 respectively). [End note about Hda1]

Most of the serial dilution assays did not show a difference in growth between the mutants and the wildtype (Fig. 4.4).

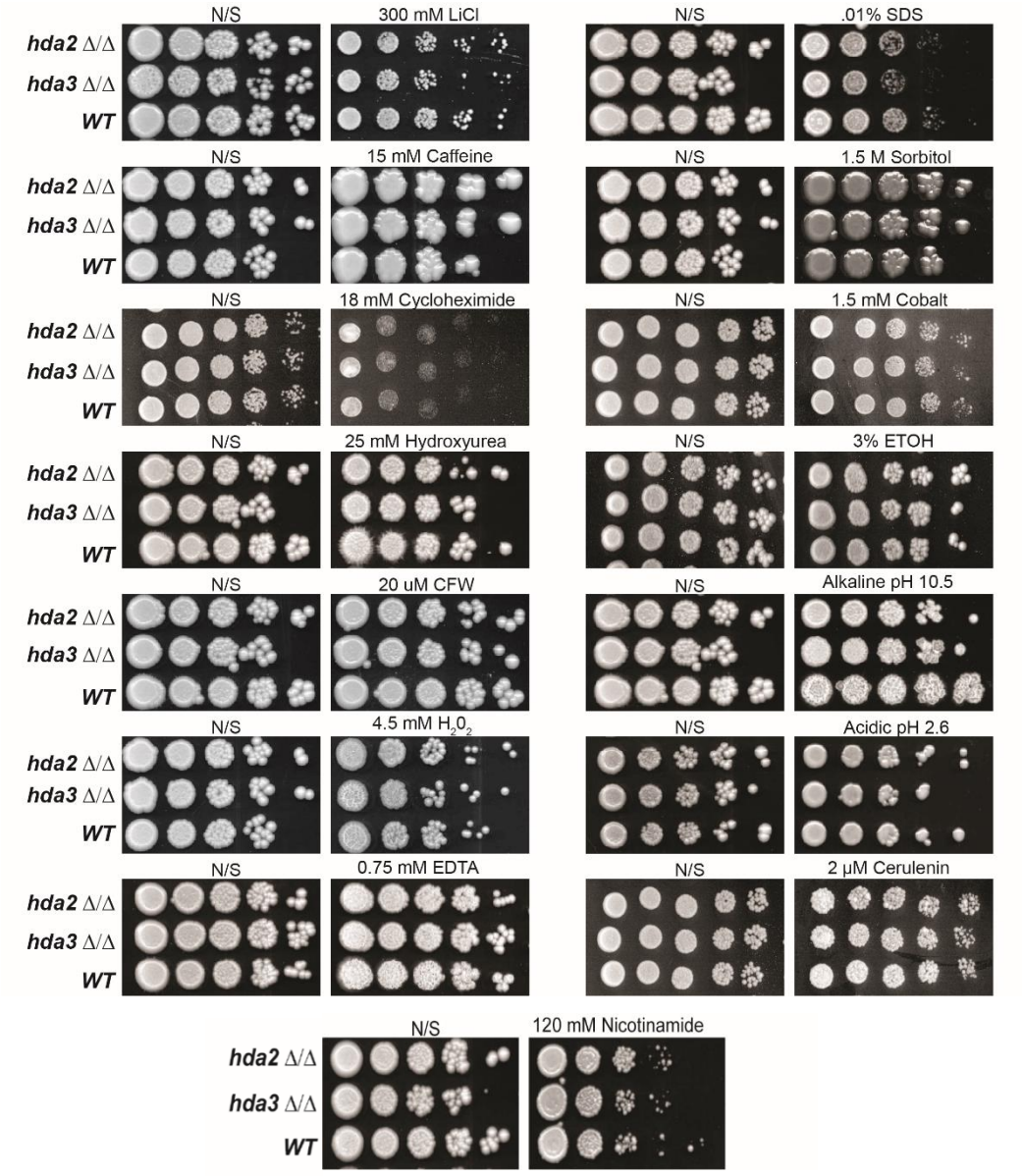

Figure 4.4 Serial dilution assays with medias where no growth differences were observed

N/S indicates non-selective media. Background media was either synthetic complete or YPD.

Mutants were evaluated for sensitivity to temperature. The assays were done in two ways (see Section 2.3.8.9), in solid and/or liquid medias but no difference was observed (Fig. 4.5; liquid media results are not shown).

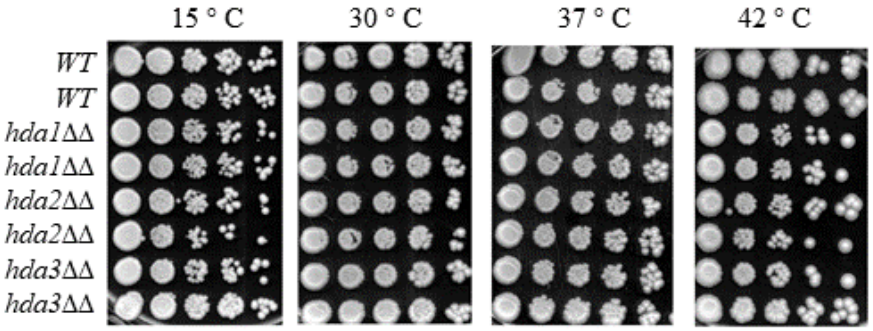

Figure 4.5 Serial dilution assays at high and low temperatures where no growth differences were observed
[these spotting assays were performed by Alisha May (Imperial College, London)]

Some medias did induce a unique pattern of growth for the mutants relative to the wildtype (Fig. 4.6).

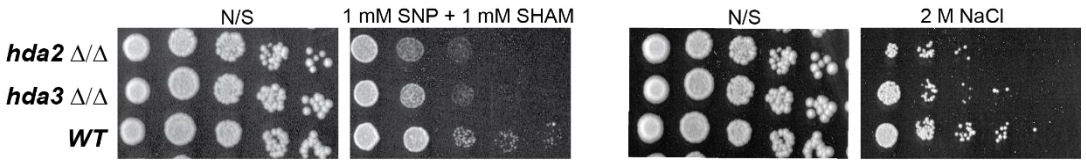

Figure 4.6 The *hda2*ΔΔ and *hda3*ΔΔ mutant strains are sensitive to SNP and SHAM or NaCl
N/S indicates non-selective media. Spotting assays show results for growth at 30 °C.

Sensitivity was apparent with oxidative stressors SNP and SHAM or by osmotic stress through added NaCl (see Section 4.2.2.4.3). Again, these phenotypes were only partially consistent in the *hda1*ΔΔ strain which could be due to the presence of markers. The *hda1*ΔΔ strain did not show sensitivity when grown on media with SNP and SHAM. Sensitivity was observed to sodium chloride.

Unique phenotypes also emerged for the mutants. The hda2 mutant presented resistance to caspofungin (Fig. 4.7). As mentioned in Chapter 1, caspofungin is an echinocandin antifungal drug (see Section 1.2.9). Caspofungin inhibits the synthesis of the cell wall protein β-(1,3)-D-glucan which makes it susceptible to osmotic disruption (McCormack & Perry 2005). Its essential target in *C. albicans* is the *FKS1* gene (Douglas et al. 1997).

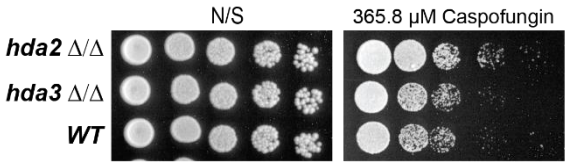

Figure 4.7 The *hda2*ΔΔ mutant strain is resistant to caspofungin
N/S indicates non-selective media. Spotting assays show results for growth at 30 °C.

The *hda1*ΔΔ mutant (ABy_179) showed sensitivity when grown on solid YPD media with caspofungin and this may be due to the presence of markers. To address the issue of markers, the alternative *hda1*ΔΔ (ABy_525) mutant was evaluated for caspofungin. This alternative *hda1*ΔΔ mutant did not show sensitivity (data not shown). This indicates that the phenotype observed in ABy_179 may be due to markers or background strain difference.

Likewise, *hda3*Δ/Δ has a sensitive phenotype when grown on zinc (Fig. 4.8).

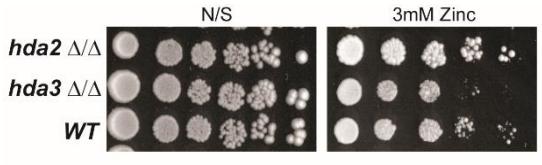

Figure 4.8 The *hda3*ΔΔ mutant strain is sensitive to zinc
N/S indicates non-selective media. Spotting assays show results for growth at 30 °C.

The observed sensitivity of *hda3*ΔΔ to zinc was not present in *hda2*ΔΔ. The *hda1*ΔΔ strain is even more sensitive than *hda3*ΔΔ. The alternative *hda1*ΔΔ mutant (ABy_525) has not yet been evaluated on media with zinc.

In conclusion, these strains show both similar and dissimilar phenotypes depending on the stressor present. The *hda2*ΔΔ and *hda3*ΔΔ mutants both show sensitivity to media with added SNP and SHAM or NaCl. The *hda2*ΔΔ strain shows resistance to caspofungin while the *hda3*ΔΔ strain shows sensitivity to zinc. Further verification of these phenotypes in different scenarios including hyphae induction and in liquid will yield a greater understanding about the pervasiveness of these effects.

4.2.2.2.2 Phenotype screen with rapamycin, copper and fluconazole in yeast versus hyphae inducing medias

After noticing phenotypes in YPD, spotting assays for rapamycin, copper and fluconazole were also performed on hyphae inducing medias with these additives (Fig. 4.9).

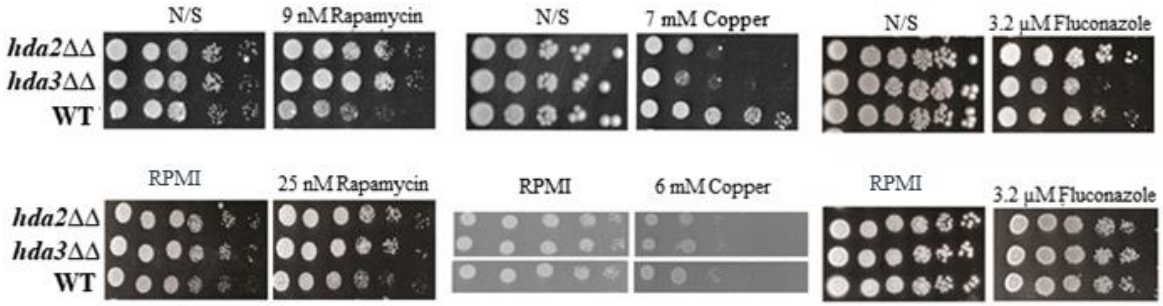

Figure 4.9 Growth phenotype of hda2ΔΔ and hda3ΔΔ mutants change across yeast and hyphae inducing medias with added: rapamycin, copper and fluconazole
Top: Spotting assays in yeast inducing medias (YPD or SC) growth at 30 °C. N/S indicates non-selective media. Bottom: Spotting assays in hyphae inducing media (RPMI) grown at 37 °C.

In YPD resistance of *hda2*ΔΔ and *hda3*ΔΔ was shown to rapamycin while sensitivity was apparent for growth on copper. These phenotypes were only partially consistent in the *hda1*ΔΔ strain which could be due to the presence of markers. The *hda1*ΔΔ (ABy_179) strain did not show sensitivity when grown on YPD media with copper but this may be due to markers (Fig. 4.11). On YPD agar media supplemented with copper, ABy_525 showed sensitivity (Fig. 4.11). Otherwise, this ABy_179 mutant showed the same phenotype as the other strains (resistance with rapamycin (Fig. 4.9). When tested with RPMI and copper, the *hda2*ΔΔ and *hda3*ΔΔ mutants are sensitive, paralleling their phenotype on YPD (Fig. 4.9). Preliminary assessments of *hda2*ΔΔ and *hda3*ΔΔ phenotypes in liquid media supported the growth patterns observed on solid agar (Fig. 4.10).

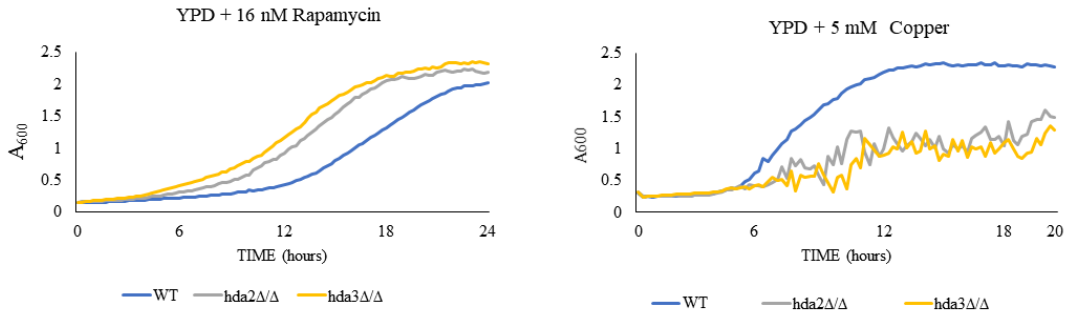

Figure 4.10. Preliminary phenotype evaluations of *hda2*ΔΔ and *hda3*ΔΔ in liquid media
Graphs show results from a single experiment for growth in YPD with added rapamycin or copper at 30 °C.

The hda2 mutant presented resistance to fluconazole in YPD while no difference was observed with the same level of fluconazole in RPMI (Fig. 4.9). On solid YPD, SC

or RPMI agar with fluconazole *hda1*ΔΔ (ABy_179) is sensitive relative to wildtype ABy_54 (SN152) while the alternative *hda1*ΔΔ (ABy_525) shows no difference (Fig. 4.11). A preliminary liquid assay indicated that the alternate *hda1*ΔΔ mutant (ABy_525) grows the same as matching wildtype in SC media with fluconazole (data not shown).

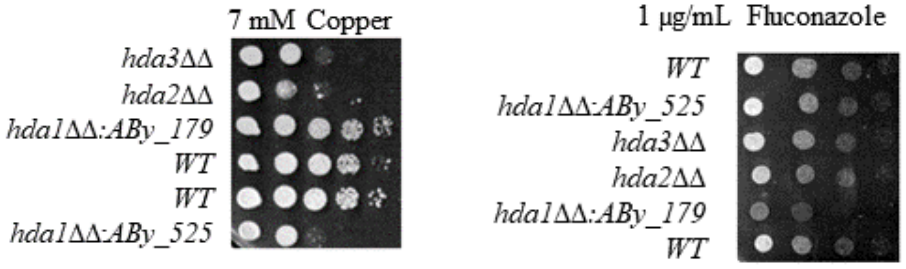

Figure 4.11 Evaluation of two *hda1*ΔΔ mutants shows potential effect of markers on phenotype
Spotting assays show results for growth on YPD with added copper or fluconazole at 30 °C.

Spotting the mutants to RPMI with rapamycin showed a less dramatic but similar phenotype to YPD. In this case, the relative sensitivity of the wildtype strain resolved itself in later days (2-3) of growth (Fig. 4.9). Side-by-side assessment of the *S. cerevisiae* resistant and sensitive mutants shows the effect of rapamycin treatment in RPMI to be normal.

To summarize, the *hda1*ΔΔ phenotype for these was the same as *hda2*ΔΔ and *hda3*ΔΔ for rapamycin on both YPD and RPMI mediums. On YPD with copper, resistance was observed in ABy_179 but when the alternative *hda1*ΔΔ strain (ABy_525) was tested, it was sensitive like *hda2*ΔΔ and *hda3*ΔΔ. With fluconazole *hda2* resistance in YPD was the only phenotype observed.

The alternative *hda1*ΔΔ strain (ABy_525) strain has not yet been assessed by spotting assay on RPMI with copper. On YPD with fluconazole, sensitivity was observed in ABy_179 but not ABy_525, growth with fluconazole has not been tested on RPMI. Overall, these two *hda1*ΔΔ strains do not show the same phenotypes and whether this is due to the presence or absence of markers or the genetic background of these strains. Further explorations of his effect is a topic for a different project which can evaluate these hypotheses through reintegration of Hda1 into ABy_179 or creation of a new marker-free deletion strain in the SN152 background. If the potential differences in background are ignored ABy_525 can be taken as giving the true phenotype and these assays should be

further verified by repetition. This issue also complicates interpretation of the RNAseq analysis which was done for strain ABy_179 (see Section 4.2.2.3).

Next, given that there is some information known about roles of Hda1 within the Tor1 pathway (see Section 1.7.2), a comparison was made with published strains that have contributed to the research on this pathway. These strains (kindly provided by the Liu Lab at University of California in Irvine) include a fully functional Myc tagged Yng2 (*YNG2/YNG2-Myc13*ΔΔ), as well as the following two point-mutants: K175R (*YNG2/yng2-K175R-Myc13*ΔΔ) which blocks acetylation on Yng2 and K175Q (*YNG2/yng2-K175Q-Myc13*ΔΔ) which mimics constitutive acetylation (see Section 1.7.2 and Lu et al. 2011). These mutants are made in the background Red 3/6 (a derivative of WO-1).

A single assessment of growth of the YNG2 mutant strains was done on YPD and RPMI medias with added rapamycin, copper and fluconazole as seen in Figure 4.12.

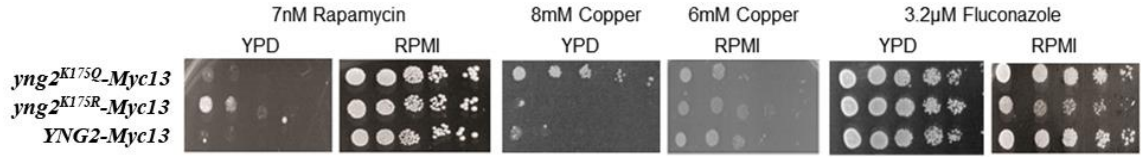

Figure 4.12 Spotting assays of YNG2 strains in yeast and hyphae inducing medias with added: rapamycin, copper and fluconazole
Spotting assays on yeast and hyphae inducing medias. Spotting assays show results for growth at 30 °C on YPD or 37 °C on RPMI.

On rapamycin and copper phenotypes were only seen on YPD media. In the YNG2 strains, resistance to rapamycin was observed in the K175R strain relative to its matching wildtype (Fig. 4.12). This pattern reflects the resistance shown by Hda2 and Hda3 (also Hda1) relative to wildtype (Fig. 4.9). While resistance to fluconazole was observed in the *hda2*ΔΔ mutant, in YPD none of the *YNG2* strains showed any difference in growth.

The rapamycin phenotype for *YNG2/yng2-K175R* (blocks acetylation) was resistant like *hda2*ΔΔ and *hda3*ΔΔ. On copper supplemented YPD, sensitivity may be seen in this mutant but lower dosage analysis would be needed to confirm (this was not seen on copper supplemented RPMI). On fluconazole supplemented RPMI, *hda2*ΔΔ and *hda3*ΔΔ strains showed no growth difference which contrasts with the *YNG2* strains (Fig. 4.9). A potential sensitivity or difference in growth appearance was observed in the *K175R*

mutant. It is notable that this is different from the growth pattern in YPD where no difference in growth is observed (Fig. 4.12)..

In conclusion, phenotypes of *hda1*ΔΔ, *hda2*ΔΔ and *hda3*ΔΔ are not always consistent with each other nor are they necessarily conserved in hyphae inducing conditions. Ideally further studies of these phenotypes would include untagged strains (without Myc).

4.2.2.3 RNA extraction from *hda2*ΔΔ and *hda3*ΔΔ in YPD

Evaluating the roles of Hda2 and Hda3 by phenotype alone contributed some information about the strains and the intuitive next step was to evaluate their roles at a transcriptional profile. With the final goal of evaluating homozygous mutants of these proteins using RNAseq, RNA was extracted from the *hda1*ΔΔ (ABy_179), *hda2*ΔΔ, *hda3*ΔΔ homozygous mutants and a matching wildtype strain. To evaluate the quality of extracted RNA the samples were visualized in a denaturing formaldehyde gel (see Section 2.3.6.1 and Fig. 4.13).

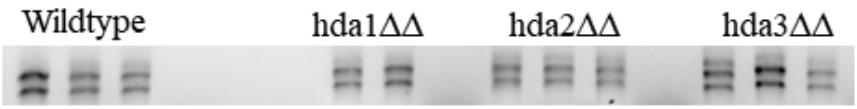

Figure 4.13 Formaldehyde gel with entact RNA samples from yeast cultures grown in yeast inducing conditions
Cultures were grown in triplicate in YPD at 30 °C before RNA was extracted.

Two clear bands indicated isolated rRNA and degradation was not observed. Based on optical density readings and appearance on the gel, the best two samples from each strain were sent for sequencing at the Genomics Core Facility at EMBL (Heidelberg, Germany).

The final RNAseq data was evaluated by DeSeq2 analysis and final log2 expression change values were obtained (see Section 2.4.2). RNAseq results analysis and further GSEA analysis was supervised by Dr. R. Jordan Price. This and two additional separate extractions of RNA were used to synthesize cDNA which was tested by qRT-PCR (Fig. 4.14). Primers were designed to evaluate the expression of genes with high log2 values and also were decided based on Fragments Per Kilobase of transcript per Million mapped reads (FPKM) values from an earlier analysis of the RNAseq data by CuffDiff (Trapnell et al. 2012).

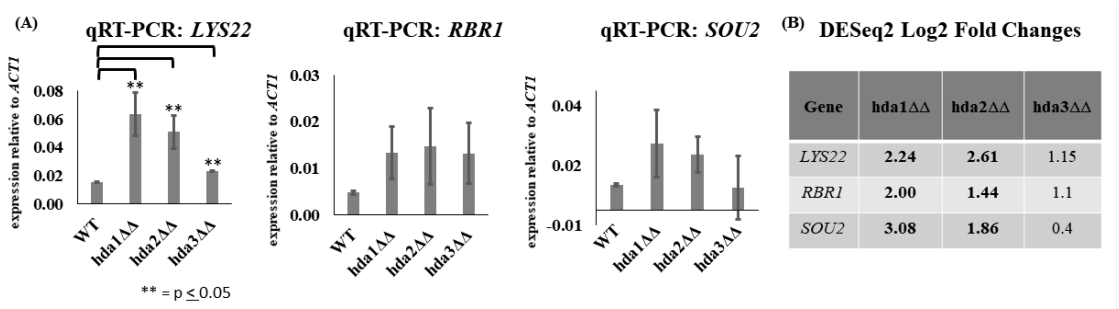

Gene	hda1ΔΔ	hda2ΔΔ	hda3ΔΔ
LYS22	**2.24**	**2.61**	1.15
RBR1	**2.00**	**1.44**	1.1
SOU2	**3.08**	**1.86**	0.4

Figure 4.14 qRT-PCR verifies YPD DESeq2 Log2 values at three genetic loci
(A) qRT-PCR results; transcript levels are visualized relative to *ACT1*; Error bars in each panel: standard deviation of three replicates; All data is adjusted to exclude >1 standard deviation from mean (B) DESeq2 log2 values, DESeq2 log2 values; Bold = significant q $\leq$ 0.05

Trends were consistent with the DESeq2 log2 results for *LYS22*, *RBR1* and *SOU2*. Greater expression was shown in the mutants relative to the wildtype, but the degree of expression difference is much lower than predicted by the DESeq2 log2 values. Still, some statistically significant differences were observed. A two tailed independent samples t-test was conducted to compare expression of *LYS22*, *RBR1* and *SOU2* relative to *ACT1*. Only the *LYS22* primers showed significant differences ($p \leq 0.05$) between the scores of *hda1*ΔΔ, *hda2*ΔΔ and *hda3*ΔΔ mutants relative to the wildtype. A table with these results can be found in Appendix 3.1.1. It should be noted that *ACT1* log2 values showed some expression changes in the *hda1*ΔΔ and *hda3*ΔΔ mutants in these extractions from YPD only (*hda1*ΔΔ, log2 *ACT1* = -1.06; *hda3*ΔΔ, log2 *ACT1* = -0.67) and while use of other housekeeping genes was trialed for qRT-PCR, these did not contribute a clear difference to the results (data not shown). More replicates of these experiments would strengthen these results, but based on these and additional, similar, assessments (data not shown), the qRT-PCR data was taken to confirm the DESeq2 RNAseq2 log2 values.

Next an evaluation was made of the overall expression patterns of the DESeq2 log2 values.

4.2.2.4 RNAseq and phenotype analysis of *hda2*Δ/Δ and *hda3*Δ/Δ in YPD

RNA sequencing data are deposited into ArrayExpress (accession number: E-MTAB-6920). To look at the trends in the DESeq2 RNASeq data, several plots were constructed to assist with visualization (Fig. 4.15).

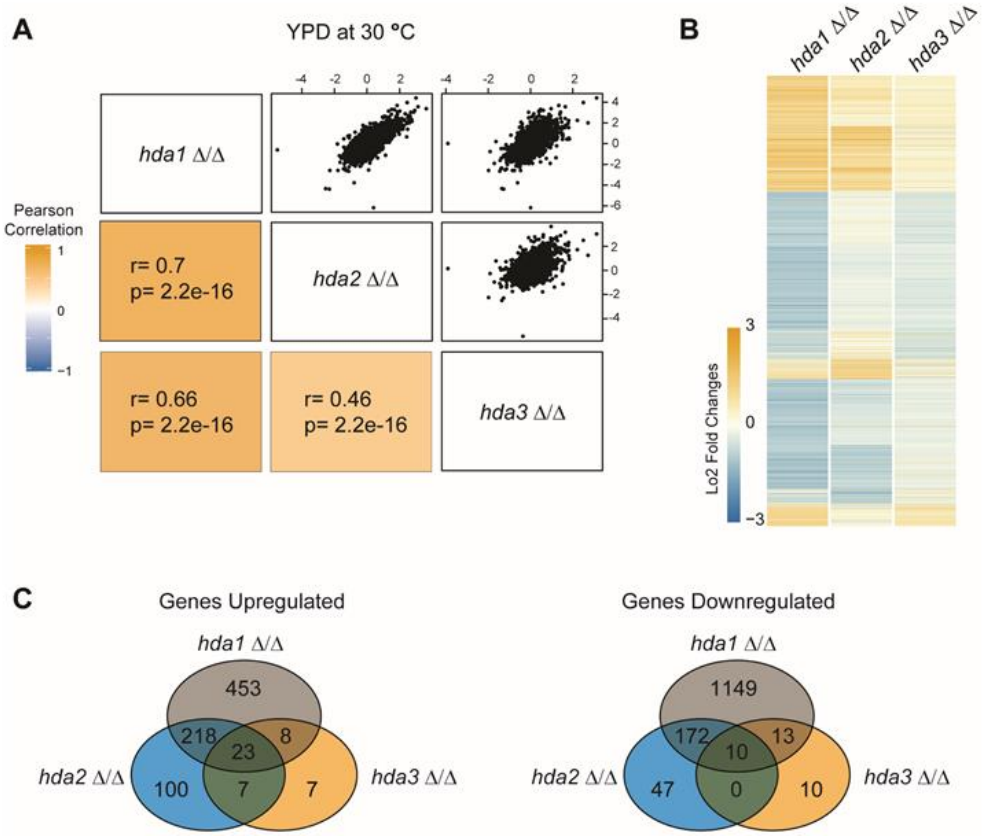

Figure 4.15 Global gene expression changes in the absence of Hda1, Hda2 and Hda3 include significantly up or down regulated genes that are consistent across the three mutants

(A) Pearson correlation matrix of gene expression changes observed in *hda1*ΔΔ, *hda2*ΔΔ and *hda3*ΔΔ grown in YPD at 30 °C; r = Pearson correlation coefficient, p = p-value (B) Heat Map of DESeq2 log2 showing log2 fold changes (C) Venn diagrams of up and downregulated gene sets from each mutant. [these figures were made by Dr. Alessia Buscaino for the article in Appendix 4]

Pearson correlations plot the linear correlation between two variables (see Section 2.4.2). The results in Figure 4.15A show Pearson correlations of the DeSeq2 log2 data for the homozygous mutant strains. These show strongly positive linear correlations between the *hda1*ΔΔ with *hda2*ΔΔ (r = 0.7) and *hda1*ΔΔ with *hda3*ΔΔ (0.66) comparisons of gene expression changes (log2 values) measured in the mutants relative to the wildtype. This analysis showed a moderately positive correlation in the comparison of *hda2*ΔΔ with *hda3*ΔΔ (r = 0.46). Therefore, the changes of expression observed for most genes in each of the mutants are consistent with the other mutants. The heatmap of all the expression changes shows that most of the genes with significantly different expression relative to wildtype have similar pattern of difference (positive or negative log2) in each of the mutants in YPD.

The *hda1*ΔΔ has many more significantly downregulated genes than the other mutants (6x *hda2*ΔΔ and 40x *hda3*ΔΔ). This is also the case for the upregulated gene set (2x *hda2*ΔΔ and 15x *hda3*ΔΔ). In both upregulated and downregulated sets, the majority of the *hda2*ΔΔ and *hda3*ΔΔ genes with changed regulation are shared with *hda1*ΔΔ. A subset of genes is shared between *hda2*ΔΔ and *hda3*ΔΔ in the upregulated set, but not in the downregulated. However, both *hda2*ΔΔ and *hda3*ΔΔ have fewer total genes in the downregulated set. RNA sequencing data are deposited into ArrayExpress (accession number: E-MTAB-6920).

4.2.2.4.1 *RFX2*: UV

It was notable that the *RFX2* gene showed elevated log2 values in all mutants (Fig. 4.16A). *RFX2* is UV-induced and Nrg1 regulated gene (Skrzypek et al. 2017).

(A) **Yeast inducing media: YPD**

Gene	hda1ΔΔ	hda2ΔΔ	hda3ΔΔ
CEK1	**2.02**	**1.16**	0.88
DDR48	0.52	**0.87**	0.75
HWP1	**1.14**	0.66	-0.33
RFX1	**0.96**	0.79	**0.96**
RFX2	**1.07**	**1.38**	**1.07**
RNR3	**-0.98**	-0.66	**-0.98**

(B)

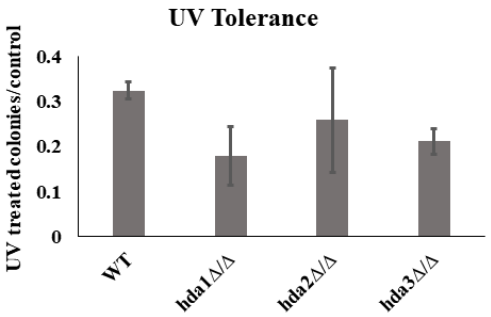

Figure 4.16 Table with significant expression changes for UV related genes and graph showing no significant difference between the UV tolerance of mutants and wildtype strains
(A) DESeq2 log2 values for genes related to UV response (B) Results graph for UV tolerance screen showing no significant difference between mutants and wildtype strains; Error bars: standard deviation of experiments on two separate days in biological triplicate; Values are given as number of colonies on UV treated plates normalized to the number of colonies on untreated control plates.

Genes related to UV response pathways showed some differences in expression although only *RFX2* showed a consistent difference across all the mutants (for a full list of genes and values see Appendix 3.2.13).

Homozygous deletion mutants in *C. albicans RFX2* are reported to have decreased resistance to UV, but *RFX2* was overexpressed in these mutant strains. *C. albicans* Rfx2 is the ortholog of *S. cerevisiae* Rfx1. Homozygous mutants in *S. cerevisiae* Rfx1 show an increased resistance to UV and when this deletion is complemented by *C. albicans* Rfx2 sequence the phenotype of sensitivity to UV in the *S. cerevisiae* strain is restored (Hao et al. 2009). No published studies have yet explored the impact of overexpression of Rfx2

on response to UV. A preliminary assay was used to investigate whether a difference in UV tolerance might be observed in the wildtype relative to the mutants.

Some sensitivity to UV was observed in the *hda1*ΔΔ, *hda2*ΔΔ and *hda3*ΔΔ mutant strains (Fig. 4.16B). The untreated control plates had 2-7x as many colonies as the UV treated plates. The differences between treated wildtype and mutant strains were not significant when assessed by two-tailed independent samples t-test (data not shown).

To conclude, this assay shows no significant evidence of a UV related phenotype for the *hda1*, *hda2*, and *hda3* deletion mutants.

4.2.2.4.2 General patterns of gene expression changes

To evaluate patterns of gene enrichment in the mutants relative to the wildtype strains. Gene Set Enrichment (GSEA) analysis was used. This analysis allows for comparison of experimental gene sets with many existing published gene sets. Preliminary GSEA analysis was done by Dr. R. Jordan Price (Department of Biosciences, University of Kent). Gene sets are named with suffix notation that indicates their contents; for example, _BIND indicates a list of genes that interact with the designated protein. These results take the form of enrichment maps were further imaged on another mapping software, Cytoscape. Cytoscape provides plots that network the gene sets (Shannon et al. 2003). This provides a spatial distribution of the GSEA results so that they can be represented more easily. Each individual node in the map represents a gene set with color and size relative to the regulation of genes in the sample and given gene set. Color indicates upregulation (peach) or downregulation (blue) and the node diameter relates to the number of transcripts in each set. Gene sets related to RNA and Ribosome biogenesis and transporters were downregulated as visualized in the Cytoscape map below (Fig. 4.14).

This map shows that many gene sets related to RNA and ribosome biogenesis gene sets were downregulated. The opposite was observed for data sets related to transporters which are upregulated. These results are discussed in more detail in Section 4.2.4.

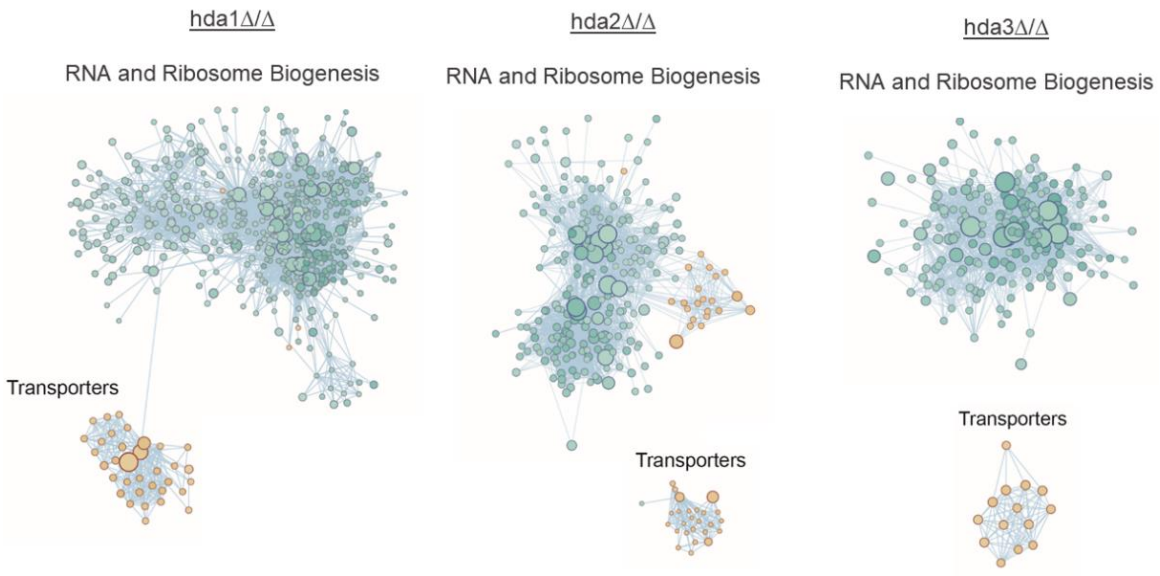

Figure 4.17 Cytoscape map: GSEA Analysis of DESeq2 log2 data showing significant changes in the regulation of RNA and Ribosome Biogenesis and Transporters gene set networks

The Cytoscape network map represents the network of functional groups of genes regulated by Hda1, Hda2 and Hda3 constructed by GSEA and Enrichment Map. Blue circles represent downregulated while peach circles depict upregulated gene sets which are linked in the network by grey lines. The diameter of the circles varies based upon the number of transcripts within each set. [these maps were made by Dr. R. Jordan Price]

Enrichment plots provide the data captured in a single 'node' of the Cytoscape network map (Fig. 4.18).

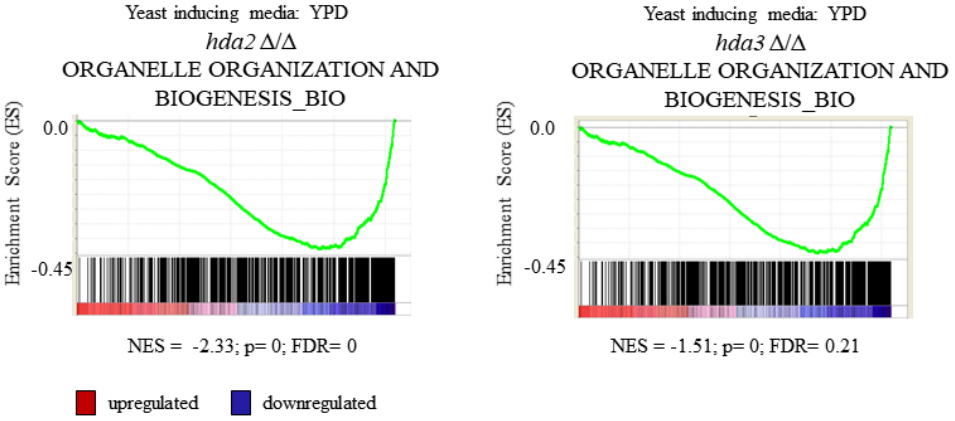

Figure 4.18 GSEA Enrichment Plots show overall downregulation in DESeq2 log2 data for genes in the Organelle Organization and Biogenesis gene set

Negative regulation of ORGANELLE ORGANIZATION AND BIOGENESIS gene set; The x-axis shows genes ranked according to their expression in the mutants from up-regulated (left) to down-regulated (right) genes. Black vertical lines mark individual genes. The cumulative value of the enrichment score (y-axis) is represented by the green line. A positive normalized enrichment score (NES) indicates enrichment in the up-regulated group of genes in the *hda2*ΔΔ or *hda3*ΔΔ mutant strains relative to wildtype.

The ORGANELLE ORGANIZATION AND BIOGENESIS_BIO gene set is negatively regulated in all mutants. The Normalized Enrichment Score (NES) value indicates the pattern of regulation and is provided as a result of the GSEA analysis along with several significance rankings including p-value and FDR. For details about interpreting gene expression maps see Figure 4.18 legend. The definition of the GO term (GO:0006996) related to this gene set cites that it includes cellular processes that result in the assembly or disassembly of organelles excluding the plasma membrane (Consortium 2017; Ashburner et al. 2000). The *hda1*ΔΔ mutant follows the same pattern for ORGANELLE ORG AND BIOGENESIS with negative correlation (NES = -2.27, p-value = 0.00, FDR = 0.00). These gene regulation observations are discussed in more detail later in this chapter (see Section 4.2.4.1).

4.2.2.4.3 SNP &SHAM and NaCl phenotype: Gene expression change analysis

In *hda2*ΔΔ and *hda3*ΔΔ sensitivity to the combination of stressors SNP with SHAM was observed. SNP is a nitric oxide donor that inhibits the mitochondrial complex IV: cytochrome C oxidase which is the final haem-copper oxidase in the main respiratory chain pathway (Joseph-Horne et al. 2001). Salicylhydroxamic acid (SHAM) is an alternative oxidase (AOX) respiratory chain pathway inhibitor in fungi (Joseph-Horne et al. 2001). While GSEA analysis of the DESeq2 log2 data for these mutants did not show pathways related to respiration with significant dysregulation, several mitochondrial related pathways were significantly altered (Fig. 4.19A). Addition of NaCl to growth media causes osmotic stress to yeast and dysregulation of pathways related to osmolarity were also observed in the GSEA results (Fig. 4.19B) (Posas et al. 2000).

(A) Yeast inducing media: YPD

Gene Set (# genes)	*hda1*ΔΔ	*hda2*ΔΔ	*hda3*ΔΔ
MITOCHONDRIAL RIBOSOME_CEL (64)	(-1.32)	-1.65	**-1.87**

(B) Yeast inducing media: YPD

Gene Set (# genes)	*hda1*ΔΔ	*hda2*ΔΔ	*hda3*ΔΔ
OS(HOG1)_UP (78)	**2.90**	**2.21**	**2.09**
OS_DN (219)	**-2.53**	**-3.31**	**-2.28**

Figure 4.19 Downregulation is observed in *hda1*ΔΔ, *hda2*ΔΔ and *hda3*ΔΔ mutants for gene sets related to the mitochondrial ribosome and significant changes in regulation are observed for the mutants for gene sets relating to osmolarity
GSEA expression changes in (A) YPD and (B) RPMI, for *hda1*ΔΔ, *hda2*ΔΔ and *hda3*ΔΔ; Gene set analysis NES score results; Values are $p \leq 0.05$; ( ) indicate not significant (p-value ≥ 0.05); FDR < 0.05 value is highly significant and bolded.

*Note: This format for GSEA analysis which captures the essential data from the enrichment plot graph (# genes and Normalized Enrichment Score (NES) scores) will be used for the remainder of the thesis (see Fig. 4.18).

The largest and most significantly dysregulated pathway that came out of the GSEA analysis of mitochondrial related pathways was MITOCHONDRIAL RIBOSOME_CELL, this gene set includes over sixty genes related to the gene ontology grouping (GO: 0005761) of mitochondrial ribosome proteins (Ashburner et al. 2000; Consortium 2017). The mitochondrial ribosome is responsible for the synthesis of hydrophobic proteins and dysregulation this synthesis can lead to mitochondrial inner-membrane stress and issues with assembly of oxidative phosphorylation complexes (Richter et al. 2015; De Silva et al. 2015).

Gene sets with osmolarity related themes were significantly dysregulated in YPD. The gene set OS(HOG1)_UP consists of genes upregulated during osmotic shock in a *HOG1* mutant (Enjalbert et al. 2006). According to the *Candida* Genome Database, *HOG1* is a Mitogen-Activated Protein (MAP) kinase involved in osmotic, heavy metal and core-stress response (Skrzypek et al. 2017). It should be noted that *HOG1* itself did not have changed regulation in the DESeq2 log2 data of any of the mutants (see Appendix 3.2.1). The OS_DN gene set is comprised of genes downregulated in response to osmotic shock by NaCl (Enjalbert et al. 2003).

To conclude, gene expression was evaluated based upon the observed sensitivity of the *hda2*ΔΔ and *hda3*ΔΔ mutants to media with added SNP and SHAM or NaCl. Downregulation of genes related to the mitochondrial ribosome was measured in these

mutants which may relate to the SNP and SHAM sensitivity as this media targets respiration. However, other respiration related gene sets did not have significantly changed regulation. The analysis of osmolarity related gene sets showed changed regulation of two sets related to osmotic shock which is the effect caused by addition of high NaCl levels to growth media. These observations show potential molecular pathways that may underly these phenotypes.

4.2.2.4.4 Caspofungin phenotype: gene expression change analysis

Given that a phenotype of resistance was seen for the *hda2*ΔΔ mutant in the spotting assays, it was notable that significant changes in the *YAK1* gene set emerged in the GSEA analysis; *YAK1* is induced in core caspofungin response and significant downregulation was shown in the *hda2*ΔΔ GSEA results (Fig. 4.21).

Yeast inducing media: YPD

Gene Set (# genes)	*hda1*ΔΔ	*hda2*ΔΔ	*hda3*ΔΔ
YAK1_Y_UP (96)	**-1.76**	-1.64	(1.28)

Figure 4.20 Downregulation is observed in *hda1*ΔΔ and *hda2*ΔΔ mutants for a caspofungin related gene set
GSEA expression changes in (A) YPD and (B) RPMI for *hda1*ΔΔ, *hda2*ΔΔ and *hda3*ΔΔ; Gene set analysis NES score results; Values are $p \leq 0.05$; ( ) indicate not significant (p-value ≥ 0.05); FDR < 0.05 value is highly significant and bolded.

The YAK1_Y_UP gene set includes genes upregulated in a microarray experiment with a *C. albicans YAK1* knockout mutant (Goyard et al. 2008). These results are representative of several other *YAK1* related gene sets which also had significantly downregulated expression in the *hda2*ΔΔ GSEA results but this was not the case for *hda3*ΔΔ.

In conclusion, an evaluation of the GSEA results showed that genes upregulated in a *yak1* homozygous deletion mutant are downregulated in the *hda2*ΔΔ mutant which suggests a molecular pathway that may be related to the observed resistance of this mutant to caspofungin in spotting assays (Fig. 4.7).

4.2.2.4.5 Zinc phenotype: gene expression change analysis

In relation to sensitivity that had been observed in the *hda3*ΔΔ spotting experiments with zinc, an evaluation was done for genes related to zinc processing (Fig. 4.8, 4.22 and for a full list of genes evaluated see Appendix 3.2.8).

Zinc related genes- Yeast inducing media: YPD

Gene	hda1ΔΔ	hda2ΔΔ	hda3ΔΔ
CSH1	**2.20**	**2.02**	0.72
IFD6	**3.38**	**3.63**	0.97

Figure 4.21 Significant upregulation is observed in *hda1*ΔΔ and *hda2*ΔΔ DESeq2 log2 data for zinc related genes
DeSeq2 log2 values from RNAseq analysis; Bolded values are $p \leq 0.05$.

The genes *CSH1* and *IFD6* show significantly increased log2 values relative to wildtype on a considerably stronger level than *hda3*ΔΔ. *CSH1* and *IFD6* code for aldo keto reductase proteins which have roles in biofilm formation (Skrzypek et al. 2017). *CSH1* and *IFD6* are under control of zinc response factor Zap1 which binds their promoters (Nobile et al. 2009). However, no phenotypes in relation to zinc are recorded in the databases for any of these proteins in *C. albicans* or *S. cerevisiae* (Skrzypek et al. 2017; Skrzypek & Hirschman 2011).

Evaluation of the log2 values of genes related to zinc processing *CSH1* AND *IFD6* indicate a change of regulation in zinc processing for the mutant strains. Evaluation of the zinc regulator Zap1 related gene set is also discussed in Section 4.2.4.2.2.

4.2.2.4.6 White-Opaque switching: gene expression changes and phenotype analysis

As discussed in Section 1.2.2 and 1.2.10.1 White Opaque phenotype switching has been linked to mating and virulence in *C. albicans* and deletion of Hda1 has been shown to increase the frequency of this switch (Srikantha et al. 2001). The RNAseq analysis showed a significant increase in genes related to this pathway in all mutants (Fig. 4.22).

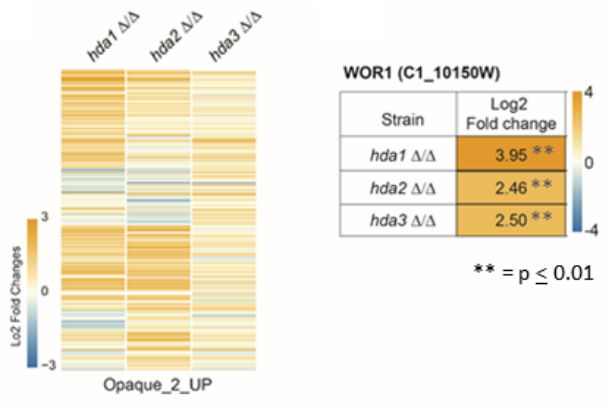

Figure 4.22 Opaque related gene set and *WOR1* expression are overall upregulated RNAseq data for *hda1*ΔΔ, *hda2*ΔΔ and *hda3*ΔΔ mutant strains
(Left) Heat map depicting the log2 fold change in *hda1*ΔΔ, *hda2*ΔΔ and *hda3*ΔΔ isolates compared to WT for the OPAQUE_UP gene set; and (Right) Deseq2 log2 fold change values show significant upregulation of *WOR1* expression in *hda1*ΔΔ, *hda2*ΔΔ and *hda3*ΔΔ compared to WT. [This image adapted from one made by Dr. Alessia Buscaino for the article in Appendix 4]

The heat map shows an overall trend of increased expression in genes related to white-opaque switching and log2 values of the master regulator *WOR1* confirm this trend (see Section 1.2.10.1)

GSEA analysis further illustrates this gene expression difference in the mutants relative to wildtype (Fig. 4.23).

Yeast inducing media: YPD

Gene Set (# genes)	hda1ΔΔ	hda2ΔΔ	hda3ΔΔ
OPAQUE_UP (181)	**2.86**	**2.59**	**2.84**
OPAQUE_2_UP (287)	**3.31**	**2.92**	**3.42**
WHITE_UP (104)	1.43	(1.31)	-1.62

Figure 4.23 Significant upregulation is observed in *hda1*ΔΔ, *hda2*ΔΔ and *hda3*ΔΔ mutants for sets of genes upregulated in opaque cells. Mixed non-significant changes are observed for sets of genes upregulated in white cells
GSEA expression changes in (A) YPD and (B) RPMI for *hda1*ΔΔ, *hda2*ΔΔ and *hda3*ΔΔ; Gene set analysis NES score results; Values are $p \leq 0.05$; ( ) indicate not significant (p-value ≥ 0.05); FDR < 0.05 value is highly significant and bolded.

A positive expression change is seen for many genes in the OPAQUE2_UP gene set which contains genes upregulated in opaque *C. albicans* cells (Tuch et al. 2010). Sets of genes upregulated in opaque cells (OPAQUE_UP and OPAQUE_2_UP) were positively regulated in YPD in the *hda1*ΔΔ, *hda2*ΔΔ and *hda3*ΔΔ mutants relative to the

wildtype strain. Assessment of genes upregulated in white cells (WHITE_UP) did not show consistently changed regulation.

Based on these results we hypothesized that Hda2 and Hda3 also have roles in white opaque switching, an assay was done to measure the actual rate of white-opaque switching in the *hda1*ΔΔ, *hda2*ΔΔ and *hda3*ΔΔ mutants. Mating type knockout strains of Hda2 and Hda3 were constructed for this assay (see Section 2.3.5.4). A special media with added Phloxine B dye was used to quantify this switching rate (see Section 2.3.8.3). This media causes opaque colonies (or sectors of colonies) to turn pink (Fig. 4.24).

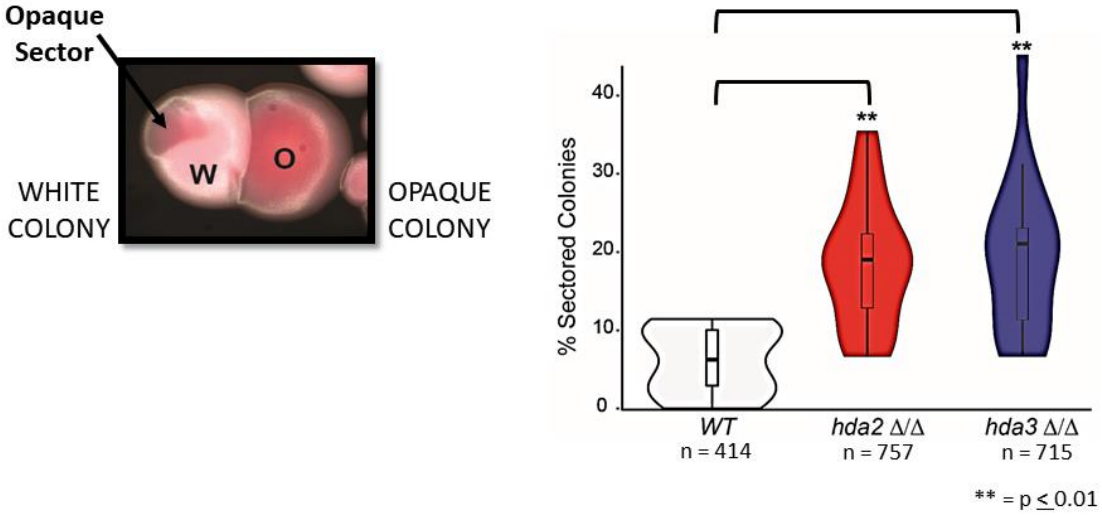

Figure 4.24 Increased white opaque switching in *hda2*ΔΔ and *hda3*ΔΔ mutant strains (Left) Representative image of cells grown on Phloxine B agar. O = opaque; W = white; (Right) Percentage of sector colonies in WT, *hda2*ΔΔ and *hda3*ΔΔ isolates ** = p-value < 0.01. [violin plot was made by Dr. Alessia Buscaino for the article in Appendix 4]

Increased switching was observed for *hda1*ΔΔ, *hda2*ΔΔ and *hda3*ΔΔ mutants (Fig. 4.24). This was considerably more pronounced in the hda1 mutant which exhibits switching on the level of an opaque control strain. *hda1*ΔΔ is not depicted in the graph as it was out of the range with considerably higher (~4-fold: 55 - 95 %) white-opaque switching than *hda2*ΔΔ and *hda3*ΔΔ. Also, the phenotype of increased white-opaque switching in *hda1*ΔΔ has already been published (Srikantha et al. 2001).

These gene transcription changes and phenotype observations support the hypothesis that in addition to Hda1, Hda2 and Hda3 have roles in white opaque switching.

To see if the relationship between deletion of Hda1 and the increased expression of *WOR1* was due to direct or indirect interaction of the protein with the gene promoter, a

ChIP experiment was used. *WOR1* and *HWP1* primer sets were employed for this assessment (Fig. 4.25). It has been previously shown by ChIP that Hda1-Myc interacts with the *HWP1* promoter in a serum dependent manner and the protein exerts positive control over *HWP1* during hyphal induction (Fig. 1.13 and Lu et al. 2011).

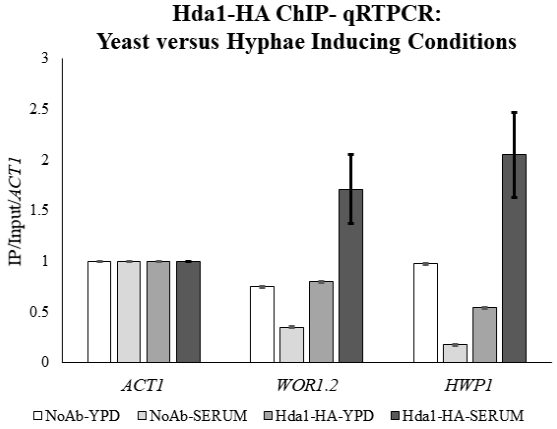

Figure 4.25 Analysis by qRT-PCR of Hda1-HA ChIP samples does not show significant enrichment at *WOR1* but show a trend of enrichment in hyphae induction conditions that may be confirmed with further experiments
Normalization is against the housekeeping *ACT1* gene. Results are from an experiment done in triplicate.

Cultures were grown in YPD at 30 °C or in hyphae inducing conditions, YPD with 10 % serum at 37 °C.

The data looked excellent for this experiment in terms of standard error ($p \leq 0.05$) for all the samples unadjusted, except for the Hda1-HA serum group. Here the standard deviations were very high, and this variance was most pronounced in *HWP1* while lesser in *WOR1.2* and *ACT1*. This can likely be accounted for by variations in the cultures themselves, due to media related factors including flocculation, circulation and pH changes among others. However, a potential trend of enrichment that should be evaluated with additional replicates is observed when the data is adjusted to exclude outliers (> 1 SD from mean) The differences between *ACT1* and *HWP1* or *WOR1.2* values are not however significant by t-test assessment. Once adjusted there was no significance difference in scores for *WOR1* primers for samples of the Hda1-HA strain processed with antibody (M = 0.45, SD = 0.34) and without antibody (M = 0.004, SD = 0.0003); $t(2) = 1.8608$, $p = 0.2038$. Likewise, no significant difference was observed for the *HWP1* primers for samples of the Hda1-HA strain processed with antibody (M = 0.54, SD = 0.42)

and without antibody (M = 0.002, SD = 0.0001); t(2) = 1.8024, p = 0.2133. This is likely due to the existence of one outlier in each the antibody and no-antibody data sets which were done in triplicate. Additional replicates might bring significance to this statistical trend.

These are preliminary results and additional tests are needed to validate them more strongly. Ultimately a request for Hda1-Myc was fulfilled and may be used for future experiments since it is known to function well in ChIP experiment settings (Lu et al. 2011).

These results suggest that Hda1 directly regulates *WOR1* in hyphae but not yeast inducing conditions. The white opaque screen shows that *hda2*ΔΔ and *hda3*ΔΔ mutants have increased white opaque switching relative to wildtype strains though to a lesser extent than *hda1*ΔΔ. In conclusion, these assays show that Hda2 and Hda3 play a role in white opaque switching.

4.2.2.4.7 Response to drugs and sensitivity testing

Other findings from the GSEA analysis were related to drug response. As mentioned *GCN4* is found to have changed regulation with drug pump *MDR1* overexpression (see Section 1.2.9).

Genes in the gene set GCN4P_TFMOTIF (Fig. 4.26) were significantly upregulated in the DESEQ2 log2 gene sets from all of the mutants. This gene set includes genes with a promoter motif recognized by the Gcn4 transcription factor (Arndt & Fink 1986).

Another drug response pathway with significantly upregulated gene expression was ketoconazole (Fig. 4.26). The Ketoconazole_up gene set includes genes upregulated in a microarray experiment with wildtype SC5314 *C. albicans* cells grown in the presence of 0.04 µg/mL ketoconazole for 3.5 hours (Synnott, Guida, Mulhern-Haughey, et al. 2010). The *hda1*ΔΔ mutant has the same positive pattern (NES = 2.76, p-value = 0.00, FDR = 0.00).

(A) Yeast inducing media: YPD

Gene Set (# genes)	*hda1*ΔΔ	*hda2*ΔΔ	*hda3*ΔΔ
GCN4_TFMOTIF (864)	**1.83**	**1.80**	1.69
KETOCONAZOLE_UP (195)	**2.76**	**2.55**	**3.11**

(B) Hyphae inducing media: RPMI

Gene Set (# genes)	*hda1*ΔΔ	*hda2*ΔΔ	*hda3*ΔΔ
GCN4_TFMOTIF (864)	-1.28	**(-1.05)**	**(-1.18)**
KETACONAZOLE_UP (195)	**(-1.24)**	1.38	**(-1.19)**

Figure 4.26 Upregulation is observed in *hda1*ΔΔ, *hda2*ΔΔ and *hda3*ΔΔ mutant strains grown in yeast inducing media but not hyphae inducing media for *GCN4* and ketoconazole related gene sets
GSEA expression changes in (A) YPD and (B) RPMI, for *hda1*ΔΔ, *hda2*ΔΔ and *hda3*ΔΔ; Gene set analysis NES score results; Values are $p \leq 0.05$; FDR < 0.05 value is highly significant and bolded

Several genes related to *MDR1* and *MRR1* had altered regulation in the *hda1*ΔΔ, *hda2*ΔΔ and *hda3*ΔΔ strains relative to wildtype (for descriptions of the genes in Figure 4.24 see section 1.2.9. Many *MDR1* related genes were significantly upregulated in the *hda1*ΔΔ and *hda2*ΔΔ mutants (Fig. 4.27). It should be noted that the RNAseq log2 values for *MRR1* for the mutants were not as relatively inflated (for a full list of analyzed genes see Appendix 3.2).

(A)

Gene	hda1ΔΔ	hda2ΔΔ	hda3ΔΔ
CDR2	**0.82**	0.72	0.42
HAP43/CAP2	**-0.69**	-0.07	-0.17

(B)

Gene	hda1ΔΔ	hda2ΔΔ	hda3ΔΔ
MDR1	**3.21**	**2.92**	0.61
GRP2	**1.35**	**1.52**	0.56
CR_09100C	**2.67**	**2.63**	0.96
GCN4	**1.16**	**1.16**	0.27
CAP1	**1.56**	**0.89**	0.02
IFD6	**3.38**	**3.63**	0.97

Figure 4.27 Drug resistance related genes *MRR1* and *MDR1* that are significant up or downregulated in the *hda1*ΔΔ mutant grown in yeast inducing conditions and significantly upregulated in the *hda1*ΔΔ and *hda2*ΔΔ mutants grown in hyphae inducing conditions
DeSeq2 log2 values from RNAseq analysis: (A) values for *MRR1* and related genes (B) Values for *MDR1* and related genes; Bold log2 value indicates significance $q \leq 0.05$; (for a full list of analyzed genes see Appendix 3.2).

The next step was to evaluate drug response phenotypes in the *hda1*ΔΔ, *hda2*ΔΔ and *hda3*ΔΔ mutants. Based upon the high DESeq2 log2 values for multi-drug efflux pump gene *MDR1* (see Section 1.2.9), it was important that the strains be further evaluated for drug resistance phenotypes (Fig. 4.28 and 4.30). A Minimum Inhibitory Concentration (MIC) assay was used as an approach which monitored relative sensitivity of the yeast

strains to several drugs (see Section 2.3.8.7). For points of comparison some known resistant strains that over expressed *MDR1* or another resistance related gene *MRR1*, were included in these assays (see Section 1.2.9).

As discussed in Section 1.2.9, specific gain of function mutation (P683S) in *MRR1* is known to manifest resistance of *C. albicans* strains to fluconazole. This strain (ABy_279) was found to be very resistant, growing at levels of 16 µg/mL fluconazole and greater. It served as a strongly resistant control in these MIC tests (Christoph et al. 2012).

Similarly, a gain of function mutation in the *MDR1* gene has been shown to manifest resistance to cerulenin and brefeldin A. This strain was four times more resistant to these drugs than the wildtype control. Fluconazole resistance was also observed for this mutant but it was strain dependent (CAI4 not SC5314) (Hiller et al. 2006).

The *hda1*ΔΔ (ABy_179), *hda2*ΔΔ (ABy_347), and *hda3*ΔΔ (ABy_460) mutants with their matching wildtype (ABy_54) were tested in all assays.

A MIC assay of fluconazole was performed prior to cerulenin and brefeldin A (see Section 4.2.2.4.7). Both *MDR1* and *MRR1* overexpression mutants were tested beside the mutants and relative control strains. Initially, tests were done using MOPS buffered RPMI which is a prescribed growth media for MIC testing. After trials showedresults were variable and resistance was not evident, the media was switched to synthetic complete. Synthetic complete which closely resembles the YPD media used for RNA extractions. It offers an increased clarity that reduces background for optical density plate readings. This media change resulted from an evaluation of the RNAseq log2 values for *MDR1* and RPMI media. Values in RPMI were much lower than those grown in YPD (*hda1*ΔΔ log2 = 0.45, *hda2*ΔΔ log2 = -0.06 and *hda3*ΔΔ log2 = -0.33). Consequently, subsequent evaluations were done in synthetic complete media only.

The Clinical Laboratory Standards Institute guidelines Reference for Broth Dilution Antifungal Susceptibility Testing of Yeasts notes that for azoles the results of minimum inhibitory concentration tests show great variability and it is suggested that an endpoint score of 2 indicating a prominent decrease in visible growth be used (50 % decrease in turbidity) for reading results (Guidelines Reference: vol28 M27-A3; Wayne, PA, USA). In accordance with the guidelines, our tests did show this variability. Consistent with the findings published in literature the *MRR1* overexpression mutant showed resistance to fluconazole (see Section 1.2.9 and Fig. 4.28).

(A)

Fluconazole in synthetic complete (SC) media at 72 hours

ABy_#	strain	100 µg/mL	50 µg/mL	25 µg/mL	12.5 µg/mL	62.5 µg/mL	3.13 µg/mL	1.56 µg/mL	0.78 µg/mL	0.39 µg/mL	0.20 µg/mL
55	WT	1	1	1	1	1	1	2	2	3	4
279	*MRR1* overexp.	Some E; 1	1	1	1	3	3	3	3	4	4
54	WT	Some E; 1	1	1	1	1	1	1	2	3	4
179	*hda1*ΔΔ	1	1	1	1	1	1	1	1	2	4
347	*hda2*ΔΔ	1	1	1	1	1	2	2	2	3	4
460	*hda3*ΔΔ	1	1	1	1	1	1	3	3	3	4
514	*MDR1* overexp.	2	1	1	1	1	2	2	3	4	4
516	Control	E	Some E; 2	Some E; 1	Some E; 1	Some E; 1	1	2	3	3	4

E = Evaporation

(B)

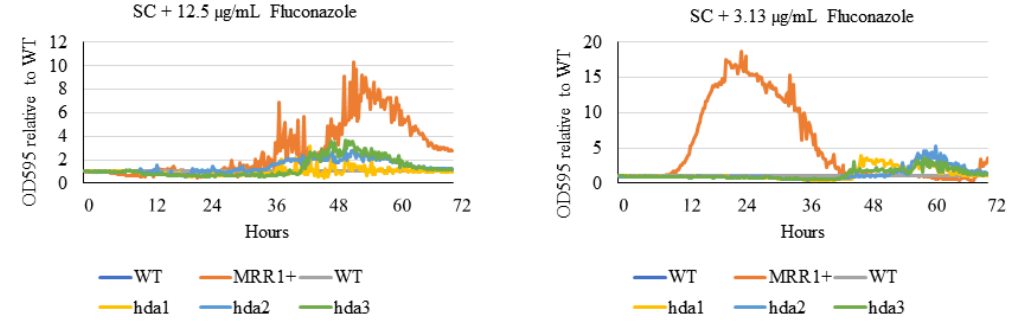

Figure 4.28 Resistance to fluconazole is not apparent for *hda1*ΔΔ, *hda2*ΔΔ and *hda3*ΔΔ mutant strains when grown in liquid with added fluconazole.
Minimum Inhibitory Concentration Assay: (A) Scoring by eye at 72 hours. Key: 0 = clear, 1 = slightly hazy, 2 = prominent decrease in visible growth (50 % decrease in turbidity), 3 = slight reduction in visible growth (turbidity), 4 = no reduction in visible growth, E = Evaporation (B) Optical density readings (relative to matching wildtype) over time with two levels of fluconazole.; Results are from growth at 30 °C.

The resistance of *MRR1* was apparent (through 62.5 µg/mL) on MIC testing with fluconazole and this was more evident in the scoring by eye than by the plate reader data. Somewhat more sensitivity was visible in *hda1*ΔΔ (at 0.39 µg/mL) than *hda2*ΔΔ (at 0.78 µg/mL) and *hda3*ΔΔ (at 3.13 µg/mL).

While *MDR1* resistance was not apparent in the fluconazole screen it was pronounced in the screen with cerulenin (Fig. 4.29). The absence of error bars in these data indicates that this experiment was only trialed once, and further analysis is needed for any conclusion to be drawn about the MIC of these strains in the presence of fluconazole or cerulenin (Figs. 4.28 and 4.29).

(A)

Cerulenin in synthetic complete (SC) media at 72 hours

ABy_#	strain	100 µg/mL	50 µg/mL	25 µg/mL	12.5 µg/mL	62.5 µg/mL	3.13 µg/mL	1.56 µg/mL	0.78 µg/mL	0.39 µg/mL	0.20 µg/mL
54	WT	0	0	0	0	3	3	3	3	3	4
179	*hda1*ΔΔ	0	0	0	0	0	1	2	3	3	4
347	*hda2*ΔΔ	0	0	0	0	0	1	3	3	3	4
460	*hda3*ΔΔ	0	0	0	0	0	1	3	3	3	4
514	*MDR1* overexp.	0	3	4	4	4	4	4	4	4	4
516	Control	0	1	1	1	1	1	3	3	3	4

(B)

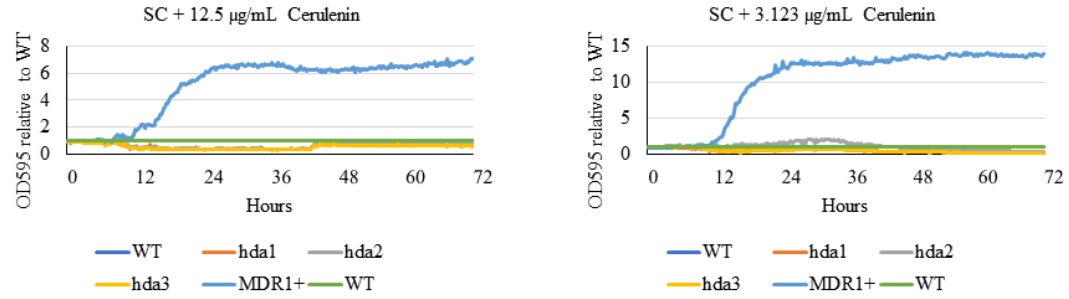

Figure 4.29 Resistance to cerulenin is not apparent in liquid for *hda1*ΔΔ, *hda2*ΔΔ and *hda3*ΔΔ mutant strains

Minimum Inhibitory Concentration Assay: (A) Scoring by eye at 72 hours. Key: 0 = clear, 1 = slightly hazy, 2 = prominent decrease in visible growth (50 % decrease in turbidity), 3 = slight reduction in visible growth (turbidity), 4 = no reduction in visible growth, E = Evaporation (B) Optical density readings (relative to matching wildtype) over time with two levels of Cerulenin; Results are from growth at 30 °C.

The resistance of *MDR1* was apparent (through 50 µg/mL) on MIC testing with cerulenin as can be seen more clearly in the scoring by eye than by the plate reader data. Somewhat more sensitivity was visible in *hda1*ΔΔ (at 1.56 µg/mL) than *hda2*ΔΔ (at 3.13 µg/mL) and *hda3*ΔΔ (at 3.13 µg/mL).

The resistance of the *MDR1* overexpression strain was apparent in both the scoring by eye and plate reader data. The mutants showed some sensitivity relative to the wildtype in the scoring by eye and plate reader data.

Like cerulenin, single assessment of brefeldin A and diamide showed no resistance among the Hda1, Hda2 and Hda3 mutants (data not shown; see Section 2.3.8.7). As is a common effect, these assays were accompanied by clumping, trailing effects and evaporation, and as was mentioned earlier the normal RPMI media could not be used (Marr et al. 1999). Consequently, these assays were not pursued further, and as stated, the data presented are from single assays without repetition.

In conclusion, evaluation of transcriptional changes in the *hda1*ΔΔ, *hda2*ΔΔ and *hda3*ΔΔ mutants show gene sets related to *MDR1* (*GCN4*) and ketoconazole resistance upregulated in the DESeq2 log2 data and these results are supported by the individual gene analyses particularly for *hda1*ΔΔ and *hda2*ΔΔ mutants (as the *hda3*ΔΔ had somewhat lower values). MIC assays showed some sensitivity of the mutants to fluconazole and cerulenin but not to brefeldin or diamide. These experiments were not replicated and so these results would need further confirmation for conclusions to be drawn from these liquid drug tolerance assays.

4.2.2.5 Chromatin Immunoprecipitation of Hda2 and Hda3 with H3K9

To evaluate whether loci identified by RNAseq analysis (log2 value) had significantly altered patterns of histone acetylation in the complex mutants, quantitative Chromatin ImmunoPrecipitation (qChiP) was performed using the histone H3 lysine 9 acetylation (H3K9ac) antibody (see Section 2.3.11.1). This antibody was chosen since the H3K9 site has increased acetylation upon the deletion of Hda1 in *S. cerevisiae* (Guillemette et al. 2011). This experiment aimed to evaluate whether the RNAseq effects observed were due to direct or indirect activity of these proteins. For normalization, spike-in of *S. cerevisiae* was used which allowed for stable measurement of gene expression. This normalization was done based on the enrichment at *S. cerevisiae ACT1* locus by which each value from the test strain was divided. The calculated addition of *S. cerevisiae* and assessment of the expression of its unique housekeeping gene *ACT1*, allows for reduction of variation in the data that is due to growth conditions or other factors.

qRT-PCR provided analysis of enrichment for DNA sequences of interest within the precipitated sample. The *MDR1* locus, but not the *ACT1* control locus, showed enrichment for H3K9 acetylation in hyphae induction conditions (Fig. 4.30).

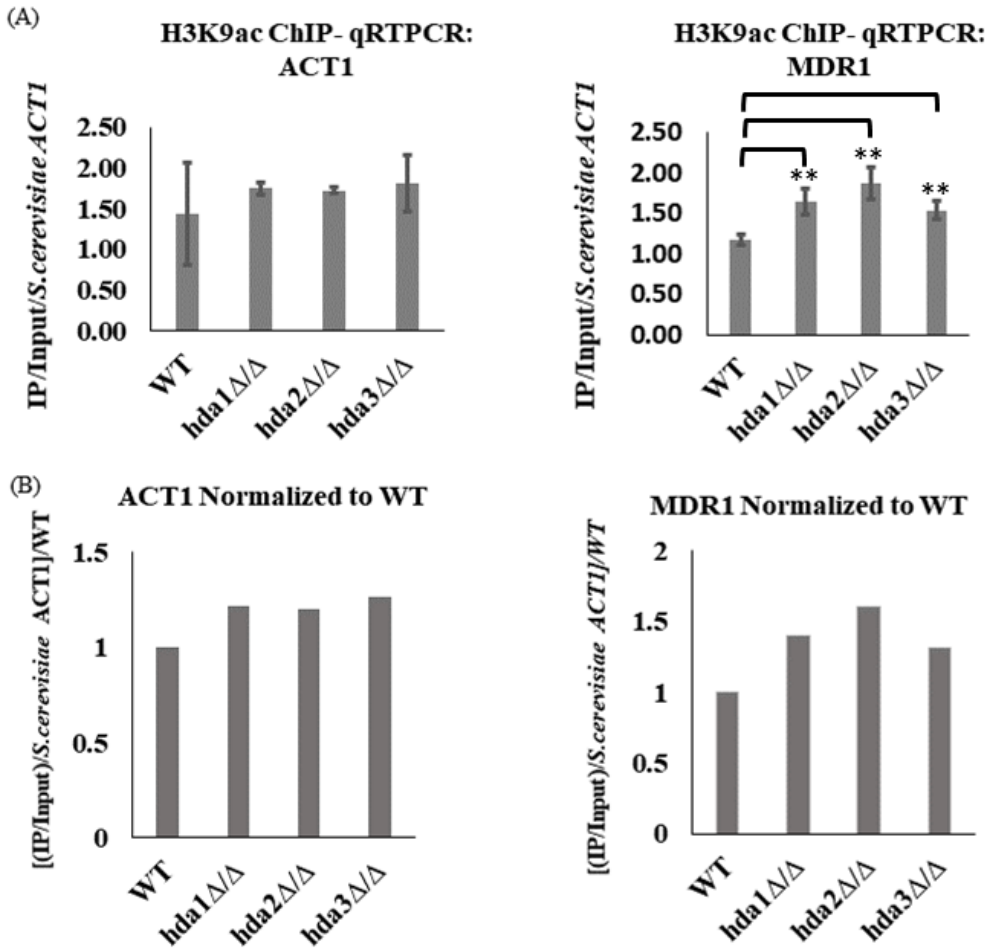

Figure 4.30 Enrichment of histone H3 lysine 9 acetylation at *MDR1* sequence in *hda1*ΔΔ, *hda2*ΔΔ and *hda3*ΔΔ mutant strains
(A) IP/Input values for enrichment at *ACT1* in mutants and wildtype relative to *S. cerevisiae ACT1* (B) Normalization of mutant enrichment level to wildtype level.

ACT1 control shows no significant difference with any mutant. This data is averaged from three technical replicates (separate experiments done on different days). A one-way between-subjects ANOVA test was conducted to compare wildtype versus each *hda1*Δ/Δ, *hda2*Δ/Δ and *hda3*Δ/Δ mutants. Using the values from the qRT-PCR with *ACT1* primers, no significant effect was observed for any of these mutants [$F(3,8) = 0.663$, $p = 0.597$].

The same test was conducted using the values from the qRT-PCR with *MDR1* primers. There was a significant effect of amplification by this primer set at the $p < 0.05$ level for these mutants [$F(3,8) = 12.23$, $p = 0.0023$, $R^2 = 0.821$]. However, to the Brown-Forsyth test showed that these groups did not have significantly different standard deviations [$F(3,8) = 0.351$, $p = 0.790$]. Group differences were further analyzed by

Welch's unpaired t-test and a statistically significant difference ($p < 0.05$) was only found for the wildtype group in relation to each of the mutants. No statistical difference was found in variance between the mutant groups. Finally, Dunnett's multiple comparison test was used to compare the means of the mutants to the wildtype. Each showed significance: wildtype was compared to each mutant: *hda1*Δ/Δ (MD(8) = -0.469, $p < 0.05$, 95% CL:-0.809, -0.129), *hda2*Δ/Δ (MD(8) = -0.7020, $p < .001$, 95% CL:-1.042, -0.3617), and *hda3*Δ/Δ (MD(8) = -0.3650, $p < .05$, 95 % CL:-0.7054, -0.025). Taken together, these results suggest that histone H3 lysine 9 acetylation is more prevalent at *MDR1* sites in *hda1*Δ/Δ, *hda2*Δ/Δ and *hda3*Δ/Δ strains. When these results are normalized to wildtype as seen in Figure 4.30B, the actual difference is quite small (< 2x). Additional tests are needed to create stronger validation of these results.

4.2.3 *C. albicans* Hda2 and Hda3: phenotype analysis and RNAseq in hyphae inducing conditions

To evaluate the roles of Hda2 and Hda3 in hyphae inducing media, the *hda2*ΔΔ and *hda3*ΔΔ strains were grown in RPMI and subject to RNAseq analysis and phenotype screens to evaluate hyphae and biofilm development and virulence.

4.2.3.1 RNA extraction from *hda2*Δ/Δ and *hda3*Δ/Δ in RPMI

RNA was extracted from *hda1*, *hda2* and *hda3* homozygous mutant strains along with a matching wildtype after growing for 90 minutes in RPMI at 37 °C (Fig. 4.31). This was done in parallel with the YPD extractions and all samples were treated identically (see Sections 2.3.6.1). Degradation was not observed on visualization of the samples by formaldehyde gel (Fig. 4.31)

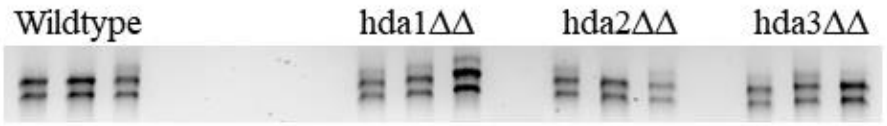

Figure 4.31 Formaldehyde gel with entact RNA samples from yeast cultures grown in hyphae inducing conditions
Cultures were grown in triplicate in RPMI at 37 °C before RNA was extracted.

Before sending the samples for sequencing it was important to validate that at the molecular level, gene expression had changed in a way that was consistent with the induction of hyphae. *HWP1* and *ALS3* are two genes which encode signature proteins of hyphae induction (see Section 1.2.2)

qRT-PCR was used to evaluate the expression of these genes (*HWP1* and *ALS3*) using cDNA made from RNA extractions from cultures grown in yeast and hyphae inducing media. to ensure that gene signatures of hypha pathways were observed in the conditions used for the RNA extraction (Fig. 4.32).

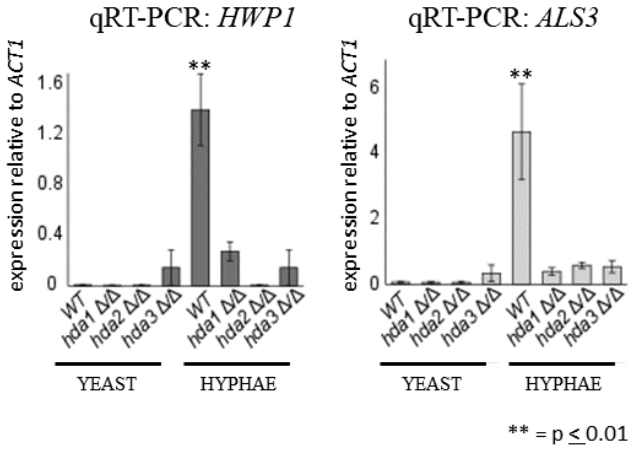

Figure 4.32 Amplification of hyphae related genes in wildtype in hyphae inducing conditions, but not *hda1*ΔΔ, *hda2*ΔΔ and *hda3*ΔΔ strains
Quantitative reverse transcriptase PCR (qRT-PCR) analyses to measure *HWP1* and *ALS3* transcript levels in WT, *hda1*ΔΔ, *hda2*ΔΔ and *hda3*ΔΔ isolates grown in yeast (YPD at 30 °C) or hyphae (RPMI at 37 °C) inducing conditions. Transcripts levels are visualized relative to *ACT1* transcript levels. Error bars in each panel: standard deviation of three biological replicates. [image was made by Dr. Alessia Buscaino for the article in Appendix 4]

This qRT-PCR analysis confirmed that the wildtype *C. albicans* strain had increased expression of hyphae related genes when grown in hyphae induction media (RPMI). Expression of hyphae related genes in yeast inducing media (YPD) was very low. The levels of expression for the *hda1*ΔΔ, *hda2*ΔΔ and *hda3*ΔΔ mutants in RPMI were very low in comparison to the wildtype.

Next, based on results of the final RNAseq analysis by DESeq2, the log2 values of specific genes from the RNAseq was confirmed by qRT-PCR trials on cDNA made from extracted RNA (see Section 2.4.2 and Fig. 4.33).

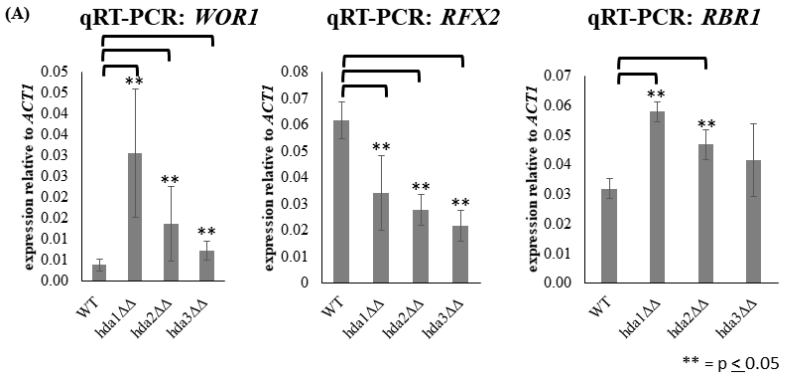

(B) DESeq2 Log2 Fold Changes

Gene	hda1ΔΔ	hda2ΔΔ	hda3ΔΔ
WOR1	**3.86**	**1.92**	**1.88**
RFX2	**-0.74**	-0.27	**-0.77**
RBR1	**0.7**	**1.15**	**0.9**

Figure 4.33 qRT-PCR verifies RPMI DESeq2 log2 values at three genetic loci
(A) qRT-PCR results; transcript levels are visualized relative to *ACT1*; Error bars in each panel: standard deviation of three biological replicates; isolates grown in hyphae (RPMI at 37 °C) inducing conditions (B) DESeq2 log2 values; Bold = significant q-value < 0.05.

Genes from the DESeq2 log2 analysis of results from this RPMI extraction were confirmed by qRT-PCR. These included *WOR1*, *RBR1*, and *RFX2* (Fig. 4.29). The degree of expression difference reported by RNAseq analysis was greater in many cases than that observed by qRT-PCR (as in section 4.2.2.3). This is not an uncommon outcome of qRTPCR with cDNA made from RNA extractions and this may be do to minor degredation which are subject to PCR, primer biases and human error among other issues (Rajkumar et al. 2015; Fang & Cui 2011; Williams et al. 2014). A two tailed independent samples t-test was conducted to compare expression of *WOR1*, *RFX2*, and *RBR1* relative to *ACT1*. There were significant differences in the scores of all mutants relative to the wildtype $p \leq 0.05$ for all the primer sets except for the *hda3*ΔΔ mutant relative to the wildtype with the *RBR1* primers. A table with these results can be found in Appendix 3.1.2.

In summary, RNA was extracted from *C. albicans* cultures grown in hyphae induction media (RPMI). To verify the engagement of molecular pathways involved in the switch the expression of two hyphae-expressed genes were evaluated by qRT-PCR and it was shown that these genes were elevated in the wildtype sample. The increased expression of these genes was not observed in this mutant and this is consistent with the published finding that deletion of Hda1 has been shown to stunt hyphal development. The fact that *hda2*ΔΔ and *hda3*ΔΔ showed the same result was consistent with the hypotheses that the three proteins act together in a complex. Confirmation of the sequencing was made by the observation that the DESEq2 log2 data was consistent with the qRT-PCR results. RNA was successfully extracted, and gene expression levels were collected from wildtype, *hda1*ΔΔ, *hda2*ΔΔ and *hda3*ΔΔ strains in hyphae inducing conditions.

4.2.3.2 RNASeq and phenotype analysis of *hda2*ΔΔ and *hda3*ΔΔ in RPMI

After confirming the DESeq2 results by qRT-PCR they were plotted in several ways to visualize the overall expression patterns of the DESeq2 log2 values (see Section 2.4.2 and Fig. 4.34). RNA sequencing data are deposited into ArrayExpress (accession number: E-MTAB-6920).

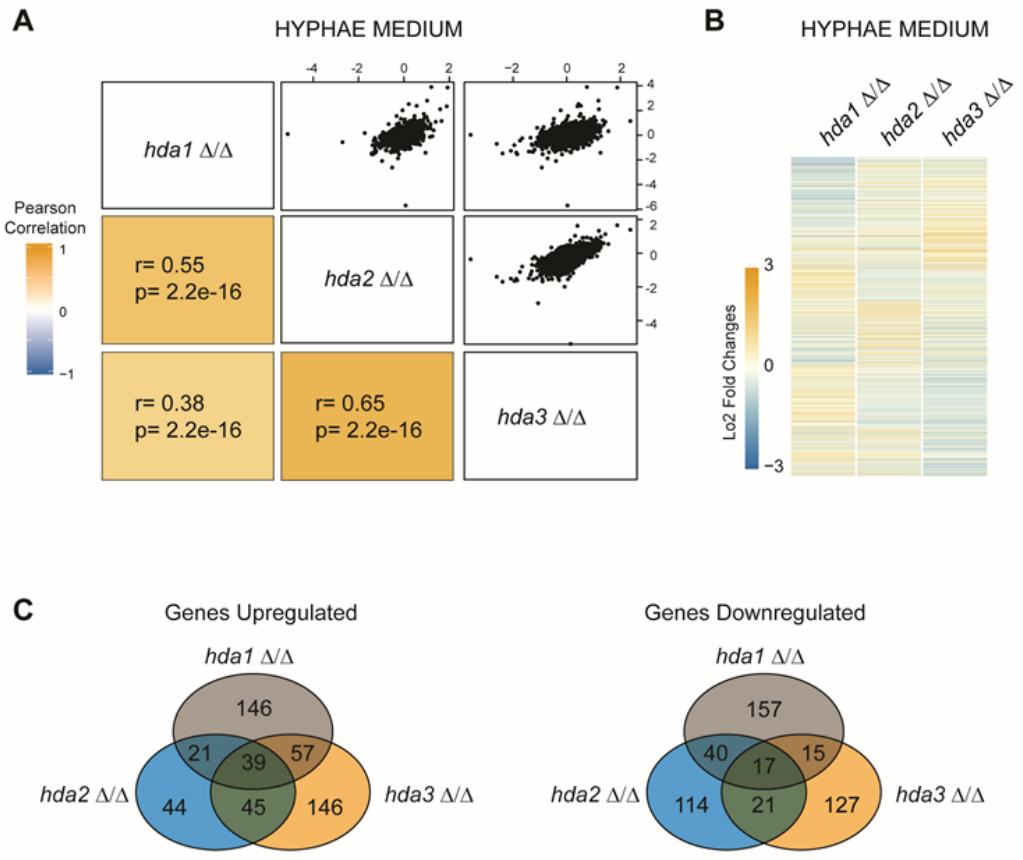

Figure 4.34 Global gene expression changes in hyphae inducing conditions do not show consistent up or down regulation across *hda1*ΔΔ, *hda2*ΔΔ and *hda3*ΔΔ mutants (A) Pearson correlation matrix of significant gene expression changes observed in *hda1*ΔΔ, *hda2*ΔΔ and *hda3*ΔΔ grown in in hyphae growth media (RPMI) at 37 °C; r = Pearson correlation coefficient; p = value (B) Heat Map of DESeq2 log2 showing log2 fold changes > 1 or < -1 in at least one mutant (C) Venn diagrams of significantly up and downregulated gene sets from each mutant. [these plots were made by Dr. Alessia Buscaino for the article in Appendix 4]

The Pearson correlations plots strongly positive linear correlations between the log2 data of the *hda2*ΔΔ with *hda3*ΔΔ (r = 0.65) mutants, moderately positive correlation in the comparison of *hda1*ΔΔ with *hda2*ΔΔ (r = 0.55) and a weak correlation exists

between *hda1*ΔΔ and *hda3*ΔΔ (0.38) (see Section 2.4.2). The gene expression changes of *hda1*ΔΔ and *hda3*ΔΔ are overall less similar than the other compared mutants. This is also reflected in the heatmap showing the significant expression changes of the genes with log2 change > 1 or < - 1 in at least one of the mutants.

The Venn diagrams depict the number of genes upregulated or downregulated in each of the mutants. Both upregulated and downregulated gene sets for the *hda1*ΔΔ, *hda2*ΔΔ and *hda3*ΔΔ mutants were close in size (149-263 genes).

In summary, analysis of the RNASeq data from extractions in hyphae inducing conditions shows a range of correlated gene expressions from a weak correlation between *hda1*ΔΔ and *hda3*ΔΔ to a strong correlation between *hda2*ΔΔ and *hda3*ΔΔ with *hda1*ΔΔ and *hda2*ΔΔ lying in the middle with moderate correlation. This finding is confirmed by the heat map analysis and Venn diagram representation shows an equal distribution of upregulated and downregulated genes with the exception of *hda2*ΔΔ which has relatively less upregulated genes. In conclusion, the gene expression changes observed in RPMI are not consistent with these proteins functioning together in a complex.

4.2.3.2.1 Gene expression change analysis: yeast and hyphae morphogenesis

The DESeq2 log2 data analysis of genes related to: (1) hyphal growth, (2) biofilms and (3) those with changed expression in the wildtype across the two medias (YPD and RPMI) showed many genes related to yeast-hypha and hypha-yeast switching with altered expression in *hda1*ΔΔ, *hda2*ΔΔ and *hda3*ΔΔ mutant strains relative to wildtype (Fig. 4.35).

(A) Positive regulation of hyphae- Hyphae inducing media: RPMI

Gene	hda1ΔΔ	hda2ΔΔ	hda3ΔΔ
DCK1	-0.31	**-0.65**	-0.38
FGR23	**1.56**	-0.32	0.05
TEC1	**-0.85**	-0.13	-0.12
UME6	**-1.54**	**-1.35**	**-1.84**

(B) Negative regulation of hyphae- Hyphae inducing media: RPMI

Gene	hda1ΔΔ	hda2ΔΔ	hda3ΔΔ
BRG1	**0.74**	0.15	**0.65**
NRG1	-0.09	0.42	**0.84**
SFL1	0.38	**0.66**	0.11

(C) Hyphae-yeast transition- Hyphae inducing media: RPMI

Gene	hda1ΔΔ	hda2ΔΔ	hda3ΔΔ
PES1	**0.76**	**0.59**	**1.13**

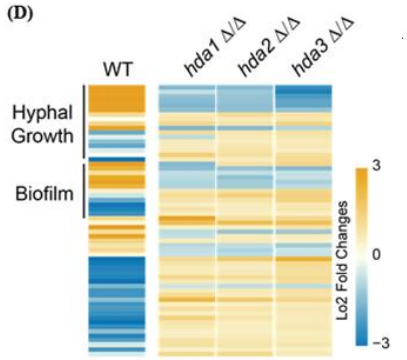

(E)

Gene Set (# genes)	*hda1*ΔΔ	*hda2*ΔΔ	*hda3*ΔΔ
HYPHAE_FBS_37_UP (51)	**-2.26**	**-2.21**	-1.62

Figure 4.35 Expression changes for yeast-hyphae related genes show some consistancy across the *hda1*ΔΔ, *hda2*ΔΔ and *hda3*ΔΔ mutant strains in hyphae inducing conditions
(A) RPMI DeSeq2 log2 values for genes related to positive regulation of hyphae in C. albicans **(**B) RPMI DeSeq2 log2 values for genes related to negative regulation of hyphae in C. albicans **(**A) RPMI DeSeq2 log2 values for genes related to hyphae-yeast transition in C. albicans (D) Heat map depicting the log2 fold change in WT cells grown in hyphae-inducing conditions (RPMI at 37 °C) versus WT cells grown in yeast-inducing conditions (YPD at 30 °C) and the same genes in the *hda1*ΔΔ, *hda2*ΔΔ and *hda3*ΔΔ mutants. Genes known to be involved in hyphae formation or biofilm formation are indicated (E) Gene set analysis NES score result; values are $p \leq 0.05$; FDR < 0.05 highly significant and bolded. [this heatmap was made by Dr. Alessia Buscaino for the article in Appendix 4]

Most of the genes individually assessed that are involved in the yeast-hyphae/hyphae-yeast transition were altered in at least one of the mutants in RPMI, in many cases the expression change was observed in all mutants (see Fig. 4.35A-C and Section 1.2.10.2; for full list of log2 values assessed see Appendix 3.2.3). The exceptions were genes related to hyphal elongation (*ESA1* and *GCN5*) which did not have a significant DESeq2 log2 change of expression relative to wildtype. In the genes related to positive regulation of hyphae, it was notable that there was significant downregulation in the DESeq2 log2 values of *UME6* in all mutants. Genes related to negative regulation of hyphae showed significant upregulation in either *hda2*ΔΔ or *hda3*ΔΔ but not both strains (Fig. 4.35B). Genes related to hyphae-yeast transition show upregulation in all mutants (for full list see Appendix 3.2.3). The hypothesis that *hda2*ΔΔ and *hda3*ΔΔ have a similar role to *hda1*ΔΔ in development of hyphae is supported by this data.

The heatmap (Fig. 4.35D) shows that the direction of the relative up or down regulation of expression of hyphae related genes was generally the same across the three

mutants and opposite to the change up or downregulation of the wildtype gene expression in hyphae inducing conditions compared to yeast inducing conditions. It is important to note that the strong expression changes in were observed to be the same in all the mutants for this set of hypha related genes which is different from the overall gene expression trend (Fig. 4.34 and Fig. 4.35).

In the GSEA analysis, the hyphae gene set HYPHAE_FBS_37_UP had significant negative regulation in all three homozygous mutants relative to the wildtype (Fig. 4.35E). This gene set is comprised of genes downregulated after growth for six hours in YPD with 10 % serum at 37 °C (Nantel et al. 2002). These results are representative of several other hyphae related gene sets with changed regulation found by analysis of the DESeq2 log2 values of the *hda1*ΔΔ, *hda2*ΔΔ and *hda3*ΔΔ mutants by GSEA analysis.

This overview of gene expression changes shows that many genes normally upregulated during hyphal induction are downregulated in the mutants including *UME6*. The heat map also shows that genes downregulated in the wildtype during hyphal induction are upregulated in the mutants. Based on the deletion of the deacetylase protein, the mutants are expected to have increased acetylation at the sites normally targeted by Hda1. The effect of histone acetylation is known to overall facilitate the transcription of genes (Fib. 1.7). Down regulation of genes related to hypha development may implicated these proteins as influencing this phenotype by non-histone acetylation targets like the yng2 domain of NuA4 (see Fig. 1.12).

4.2.3.2.2 Colony filamentation screens

The results of the RNAseq analysis which showed that *hda1*ΔΔ, *hda2*ΔΔ and *hda3*ΔΔ mutant strains have consistently altered expression relative to the wildtype strain indicated that these proteins may all have a role in filamentation. This made for a strong case given for functional relatedness that it is known that the deletion of *HDA1* stunts filamentation in *C. albicans* (Lu et al. 2011). Next, we evaluated the filamentation phenotype of the mutants. To do this, the wildtype, *hda1*ΔΔ, *hda2*ΔΔ and *hda3*ΔΔ deletion strains were plated to Spider or RPMI agar plates and incubated at 37 °C (Fig. 4.36).

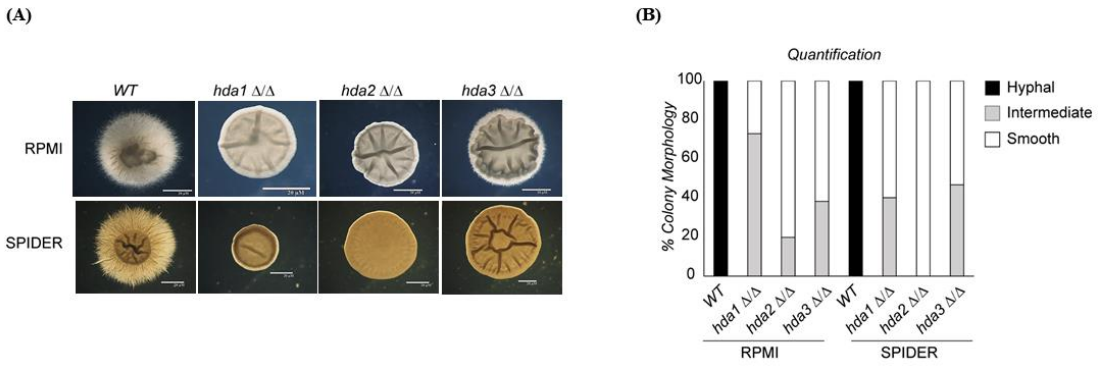

Figure 4.36 Colony filamentation is stunted in the *hda1*ΔΔ, *hda2*ΔΔ and *hda3*ΔΔ mutant strains grown on solid hyphae inducing media
(A) Representative images of colony morphology of WT, *hda1*ΔΔ, *hda2*ΔΔ and *hda3*ΔΔ grown on hypha inducing Spider and RPMI agar at 37 °C; scale bars in white are 20 µM (B) Quantification of colony morphologies for WT and mutants on hypha induction medias. [A portion of the solid media filamentation screens were performed by Sarah Gourlay (Department of Biosciences, University of Kent)]

Filamentation was observed to a much greater degree in the wildtype strain which (100 % hyphal colony morphology). The mutants showed intermediate and smooth colony morphology in both hyphae induction medias (RPMI and Spider).

4.2.3.2.3 Liquid filamentation screens

Since phenotypes can vary in the differing environments of solid and liquid media, it was important to see if the same phenotype occurred in liquid RPMI (Fig. 4.37) (Azadmanesh et al. 2017). To evaluate the phenotype in liquid media, strains were grown in RPMI at 37 °C with and without CO_2, which can induce filamentation (Fig. 4.37).

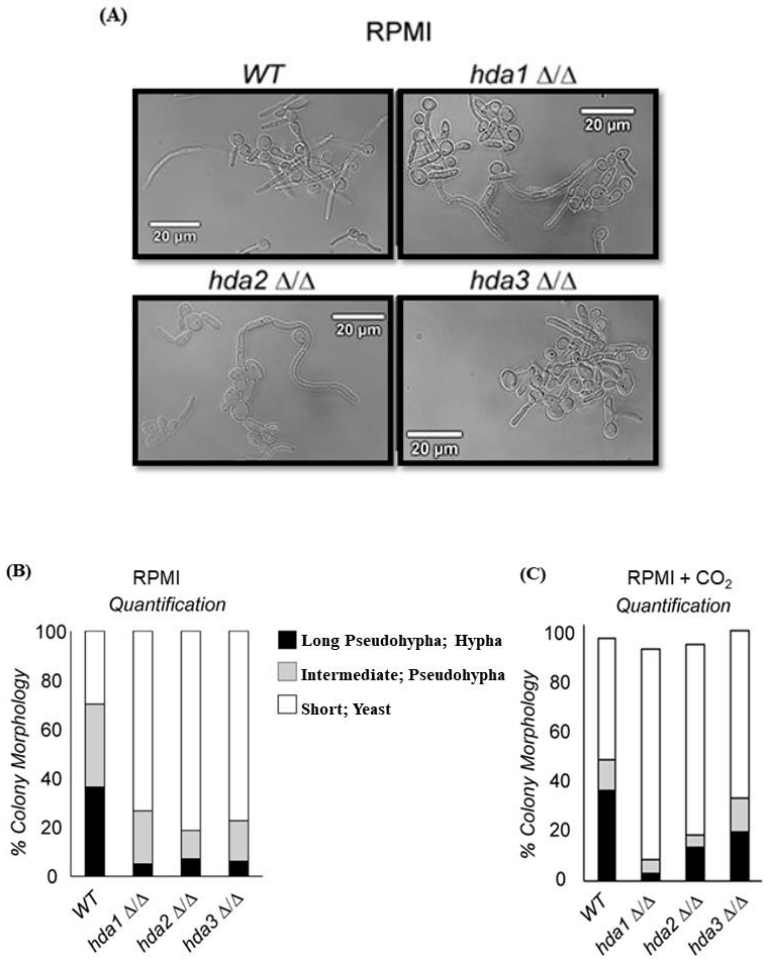

Figure 4.37 Filamentation is stunted in the *hda1*ΔΔ, *hda2*ΔΔ and *hda3*ΔΔ mutant strains in hyphae inducing liquid growth conditions with and without 5 % CO_2
Growth in liquid RPMI media at 37 °C: (A) cellular morphologies of WT, *hda1*ΔΔ, *hda2*ΔΔ and *hda3*ΔΔ; scale bars in white are 20 µm (B) Quantification of colony morphologies without CO_2 (C) Quantification of colony morphologies with CO_2.

The results of the growth in liquid media confirmed those from the solid media and development of hyphae was much less pronounced in the mutants than the wildtype. Growth in liquid with 5 % ambient CO_2 showed less difference between the *hda3*ΔΔ mutant and wildtype. Also, less overall intermediate length cell growth was observed with CO_2.

4.2.3.2.4 Reintegration and phenotype recovery: Hda3

To ensure that the phenotype was due to the absence of these proteins rather than the effect of the deletion process, the *HDA3* gene was reintegrated to the homozygous mutant at the *ADH1* promoter under doxycycline induction control (see Section 2.3.5.3 and Fig. 4.38).

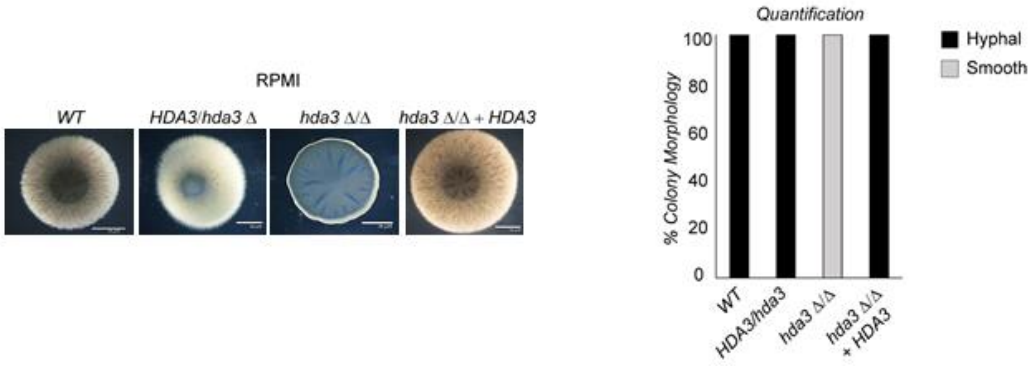

Figure 4.38 *HDA3* reintegration restores the filamentation phenotype on solid hyphae inducing media
Colony filamentation screen on RPMI media with *HDA3* reintegration strain: (A) Rescue experiment of colony morphology upon genomic integration of the *HDA3* gene in the *hda3*ΔΔ mutant background (*hda3*ΔΔ + *HDA3*). WT, heterozygous (*HDA3*/*hda3*Δ) and homozygous *hda3*ΔΔ isolates were included as a control; scale bars (white) are 20 μM (B) Quantification of colony morphologies

Reintegration of *HDA3* brought full recovery of filamentation phenotype and 100 % of colonies were hyphal in the strain with reintegration of Hda3 while the homozygous mutant showed a completely smooth colony phenotype.

To conclude, morphology screens at both the colony and individual cell levels show that deletion of Hda2 or Hda3 stunts the development of hyphae in *C. albicans.* Reintegration of Hda3 shows recovery of the phenotype. While this has not yet been confirmed for Hda1 or Hda2 these strains are currently being built for later assessment.

4.2.3.2.5 Biofilm imaging phenotype screen

With the loss of filamentation observed in the *hda2*ΔΔ and *hda3*ΔΔ mutants it was interesting to see if the degree of their biofilm development was altered relative to the wildtype. A protocol was developed to evaluate the depth of these biofilms by confocal microscopy (see Section 2.3.8.2 and Fig. 4.39).

Initial confocal microscopy images show wildtype and *hda3*ΔΔ biofilms that have very different compositions in terms of yeast and hyphae makeup with more yeast cells observed in the *hda3*ΔΔ strain (Fig. 4.39, top).

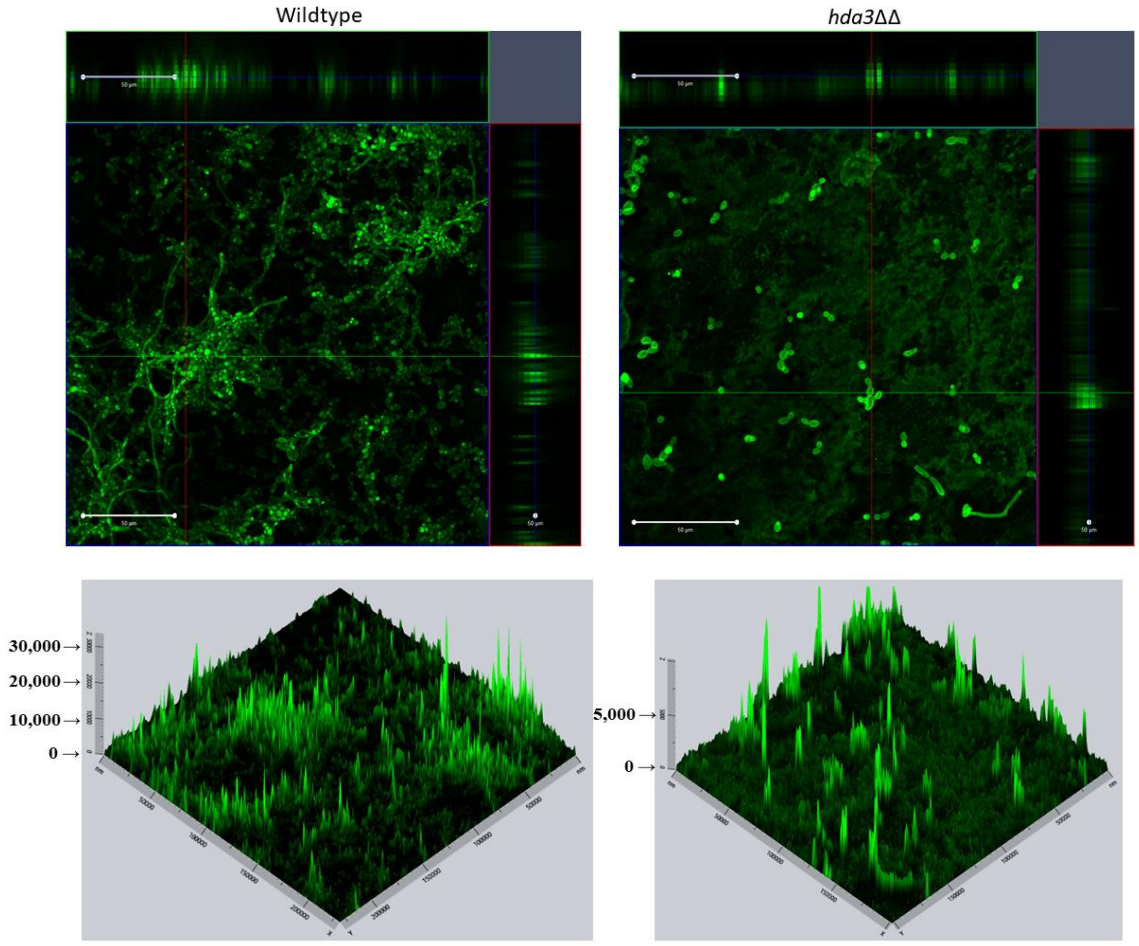

Figure 4.39 Images showing unique biofilm structures of wildtype and *hda3*Δ/Δ strains
Images show in 2D (top) and 2.5D (bottom) the biofilm of wildtype and *hda3*ΔΔ strains; (scale bars (white) are 50 µm). The 2.5D image is a simulation of a 3D image which based upon the 2D image and allow for another spatial perspective of the image data. These images were generated by Zeiss Zen software (see Section 2.3.8.2). [Confocal scanning was supervised and performed by Microscope Facilities Manager Ian Brown (Department of Biosciences, University of Kent)]

Measurements from this single experiment with three biological replicates did not show any significant difference in depth (wildtype: 126 µm, 49 µm, 43 µm; *hda3*ΔΔ: 46 µm, 34 µm, 92 µm). The side bars show the depth by side views of the images. Our results visualize depths in the 40-100 µM range (for reference this is about approximately 30x the diameter of a mature hyphae (Gow & Gooday 1982)). The experiment shown here was done once with samples in triplicate however further replicates and experimental design development and are necessary for any conclusion to be drawn about biofilm development in these strains. In summary, while no consistent difference in depth was observed between the biofilms of the *wildtype* and *hda3*ΔΔ strains a difference in morphology was

seen with more yeast apparent in the biofilm of the mutant. However, given that this was a single experiment further confirmation of these findings is necessary.

4.2.3.2.6 Gene expression change analysis: Biofilm

Many of the genes related to biofilm development had altered expression in the mutant relative to wildtype in YPD (see Appendix 3.2.4) but this trend did not persist with growth in RPMI. The single exception was, cell wall and biofilm related *XOG1* which had elevated log2 values in DESeq2 data from extractions in both YPD (*hda1*ΔΔ: 0.96, *hda2*ΔΔ: 0.88, *hda3*ΔΔ: 1.26) and RPMI (*hda1*ΔΔ: 1.09, *hda2*ΔΔ: 1.40, *hda3*ΔΔ: 1.44) (see Section 1.2.3 and Fig. 1.2).

In the GSEA analysis, the zinc processing and biofilm related ZAP1_TF gene set was significantly negatively regulated in *hda2*ΔΔ relative to wildtype (it has negative regulation in the other mutants as well) (see Section 1.2.8 and Fig. 4.46). This gene set is comprised of Zap1 target genes identified by a ChIP-chip experiment (Nobile et al. 2009). These expression changes are discussed further later in this chapter (see Section 4.2.4.2.2).

4.2.3.2.7 *C. albicans* hda2ΔΔ and hda3ΔΔ strains: virulence

At the core of this project is the question about whether Hda2 and Hda3 proteins are involved in the virulence of *C. albicans*.

4.2.3.2.8 Macrophage engulfment assessment

Cells from the *hda1*ΔΔ, *hda2*ΔΔ and *hda3*ΔΔ homozygous mutant strains were introduced into culture with macrophages (see Section 2.3.8.8). These strains did not show compromised virulence in this setting (Fig. 4.40). Protocols, maintenance of macrophage stocks and supervision for this entire macrophage assay were provided by Sarah Gourlay (Department of Biosciences, University of Kent).

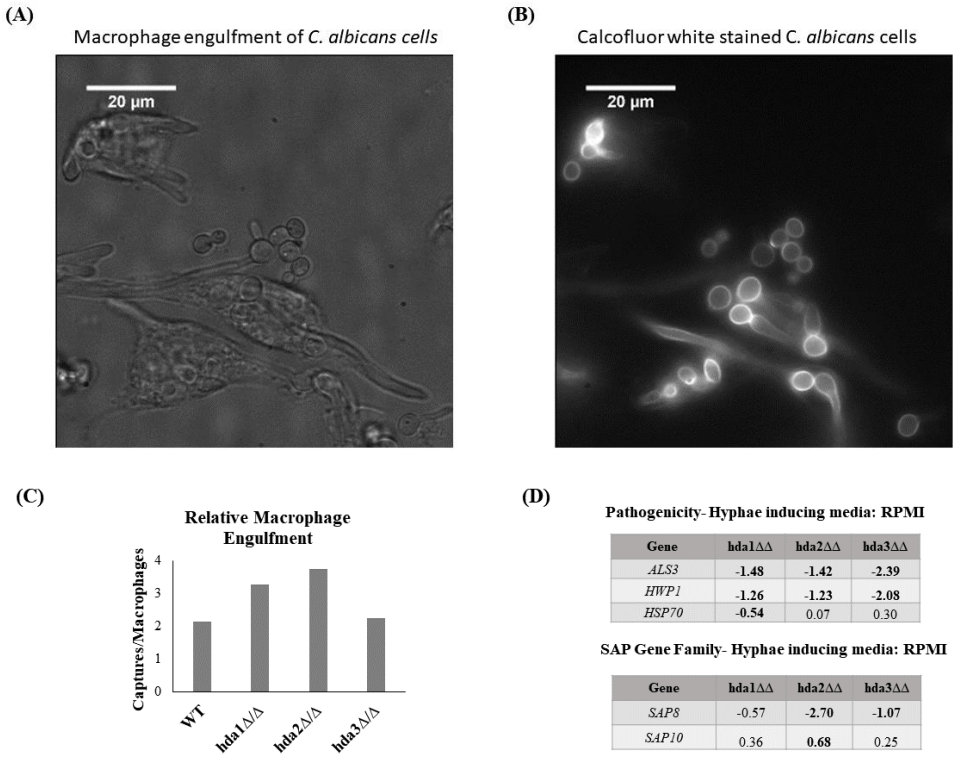

Figure 4.40 Preliminary assessment of macrophage engulfment of *hda1*ΔΔ, *hda2*ΔΔ and *hda3*ΔΔ *C. albicans* cells show somewhat greater levels of engulfment in *hda1* and *hda2* mutants and some virulence related genes show down regulation
(A) Image of engulfment of wildtype (SN152) *C. albicans* cells by macrophages (J774A cell line, RAW 264.7) (B) Visualization calcofluor white staining of same cells (C) Graph showing quantification of engulfment of *C. albicans* wildtype and mutant strains by macrophages. Experiment done as a single trial with n > 14 macrophages counted per strain. (D) Significant gene expression changes from DEseq2 log2 analysis of genes related to pathogenicity analysis of RNA extraction from RPMI media.; values are $p \leq 0.05$; FDR < 0.05 valued is highly significant and bolded.

The level of captures was not shown to be significantly different from the wildtype in this preliminary test which observed the engulfment of *C. albicans* by macrophages (Fig. 4.40), we wondered if this could be due to the required growth of macrophages in conditions with CO_2 since we had seen a somewhat less pronounced hyphal growth effect in the liquid filamentation assay condition with CO_2 (Fig. 4.37C).

The cells for this experiment had been induced for filamentation (YPD + 10 % serum + 37 °C). RPMI log2 values are shown in Figure 4.40 (for full list of log2 values assessed see Appendix 3.2.5 and description of genes see Section 1.2.2). Overall most of the significantly altered virulence related genes were downregulated in the RPMI sample Deseq2 log2 data, except for *SAP10* which was upregulated in *hda2*ΔΔ. *SAP10* is induced in low iron and functions specifically at the cell membrane with roles in adhesion and

virulence (Skrzypek et al. 2017). *ALS3* and *HWP1* are downregulated in all mutants. As discussed throughout the introduction, these genes also have a role in surface invasion, hyphal development and adhesion. *HSP70* is significantly downregulated in *hda1*ΔΔ only. This cell surface localized chaperone is heat-shock, ketoconazole and spider biofilm induced (Skrzypek et al. 2017). Many other genes related to virulence did not have changed regulation (for full list see Appendix 3.2.5). The individual *LIP* family genes assessed had little or no change in regulation. Likewise, many other genes in the *SAP* family were unaffected by deletion of *hda1*ΔΔ, *hda2*ΔΔ or *hda3*ΔΔ.

Gene sets for these families were represented in the GSEA analysis but significantly changed regulation was mostly observed in YPD conditions (Fig. 4.41).

(A) Yeast inducing media: YPD

Gene Set (# genes)	*hda1*ΔΔ	*hda2*ΔΔ	*hda3*ΔΔ
SAP30_BIND (133)	**-1.83**	-1.64	-1.45
LIP2_SGA (102)	-1.48	(-0.93)	-1.42
LIP5_BIND (92)	-1.63	(-0.98)	-1.42

(B) Hyphae inducing media: RPMI

Gene Set (# genes)	*hda1*ΔΔ	*hda2*ΔΔ	*hda3*ΔΔ
SAP30_BIND (133)	(-1.10)	(-1.18)	(0.76)
LIP2_SGA (102)	(1.05)	(-0.87)	(-0.92)
LIP5_BIND (92)	1.51	(1.19)	(1.23)

Figure 4.41 Downregulation is observed in *hda1*ΔΔ, *hda2*ΔΔ and *hda3*ΔΔ mutant strains grown in yeast inducing media but not hyphae inducing media for pathogenicity related gene sets
GSEA expression changes in (A) YPD and (B) RPMI for *hda1*ΔΔ, *hda2*ΔΔ and *hda3*ΔΔ; Gene set analysis NES score results; Values are $p \leq 0.05$; ( ) indicate not significant (p-value $\geq$0.05); FDR < 0.05 value is highly significant and bolded.

The LIP2_SGA includes a set of genes identified by synthetic gene array to interact with *LIP2* (Baryshnikova et al. 2010; Skrzypek et al. 2017). *LIP2* is a secreted lipase which is part of the differentially expressed lipase family (Skrzypek et al. 2017; Hube et al. 2000).The LIP5_BIND and SAP30_BIND gene sets are comprised of genes which have been shown to interact with *LIP5* and *SAP30* (Skrzypek & Hirschman 2011). *LIP5* is a cold activated lipase that has a role in filamentation and is secreted at all stages of systemic infection by *C. albicans* (Skrzypek et al. 2017). *SAP30* is an aspartic-type endopeptidase that is involved in degradation of the alpha pheromone (Skrzypek et al. 2017).

To conclude, genes that relate to pathogenicity are mostly unaffected or downregulated in the *hda2*ΔΔ or *hda3*ΔΔ mutants. This preliminary assay shows increased engulfment by macrophages of *hda1*ΔΔ, *hda2*ΔΔ cells relative to wildtype *C. albicans*

cells and little difference for *hda3*ΔΔ cells but as this was tested in a single trial further replicating experiments would be necessary to confirm this effect.

We next moved to test the strains in a *Caenorhabditis elegans.* This work was done by Dr. R. Jordan Price (Department of Biosciences, University of Kent) and is discussed within the attached article (see Appendix 4). Again, no deficiency was seen in the virulence of these strains which invaded the *C. elegans* on a similar level to the wildtype strain (see Appendix 4 Fig. 6.D). This and the macrophage assay introduced the *C. albicans* pathogen to realistic and dynamic host environmental scenarios which are quite different from hyphae inducing agar (RPMI, Spider, etc.). In this assay, the *hda1*ΔΔ, *hda2*ΔΔ and *hda3*ΔΔ mutant strains all formed filamentous cells which is likely due the activation of parallel pathways for filamentation that do not require Hda1 (see Section 4.1 para.8).

4.2.4 Gene expression and protein levels: yeast versus hyphae induced

To compare *hda2*ΔΔ and *hda3*ΔΔ activity in yeast and hyphae inducing media, DESeq2 log2 data analysis and protein expression were utilized. Dramatic differences were observed in gene expression and phenotypes between the YPD and RPMI medias. This section aims to directly compare gene expression of *hda1*ΔΔ, *hda2*ΔΔ and *hda3*ΔΔ and to evaluate the protein expression level of Hda1, Hda2 and Hda3 in order to develop a model for the function of these proteins.

4.2.4.1 Gene expression analysis: Trends

When the GSEA analysis results were analyzed using a high significance cut off (FWER p-value $\leq$ 0.05), few gene sets were found to be positively regulated in the YPD data relative to the RPMI (YPD: *hda1*ΔΔ: 33, *hda2*ΔΔ: 47 and *hda3*ΔΔ: 11 significant gene sets; RPMI: *hda1*ΔΔ: 201, *hda2*ΔΔ: 104 and *hda3*ΔΔ: 264 significant gene sets). The opposite was the case for the negatively regulated gene sets (YPD: *hda1*ΔΔ: 217, *hda2*ΔΔ: 251 and *hda3*ΔΔ: 108 significant gene sets; RPMI: *hda1*ΔΔ: 7 *hda2*ΔΔ: 2 and *hda3*ΔΔ: 0 significant gene sets).

Consistent with this observation, many gene sets had opposite patterns of downregulation in YPD and upregulation in RPMI when compared by GSEA analysis in and we will discuss three of these gene sets (Fig. 4.42).

(A) Yeast inducing media: YPD

Gene Set (# genes)	hda1ΔΔ	hda2ΔΔ	hda3ΔΔ
ORGANELLE ORGANIZATION & BIOGENESIS (576)	**-2.28**	**-2.33**	-1.51
RPL4A_BIND (61)	**-2.21**	**-2.45**	**-1.86**
TRANSLATION_BIO (245)	**-3.12**	**-2.58**	**-3.02**

(B) Hyphae inducing media: RPMI

Gene Set (# genes)	hda1ΔΔ	hda2ΔΔ	hda3ΔΔ
ORGANELLE ORGANIZATION & BIOGENESIS (576)	1.40	(1.01)	**2.17**
RPL4A_BIND (61)	**2.27**	**1.90**	**2.64**
TRANSLATION_BIO (245)	**2.68**	**2.39**	**2.58**

Figure 4.42 Examples of opposite pattern of gene set expression changes for *hda1*ΔΔ, *hda2*ΔΔ and *hda3*ΔΔ mutant strains grown in yeast versus hyphae inducing media
GSEA expression changes in (A) YPD and (B) RPMI for *hda1*ΔΔ, *hda2*ΔΔ and *hda3*ΔΔ; Gene set analysis NES score results; Values are $p \leq 0.05$; ( ) indicate not significant (p-value $\geq$0.05); FDR < 0.05 value is highly significant and bolded.

The first gene set, ORGANELLE ORGANIZATION & BIOGENESIS is a very large gene set with over 500 genes represented. It is discussed in detail in Section 4.2.2.4.2 (Fig. 4.19). The ORGANELLE ORGANIZATION AND BIOGENESIS_BIO gene set was negatively regulated in the YPD log2 results, the RPMI data analysis showed positive regulation of this gene set.

In Section 4.2.2.4.2 we also saw gene sets related to RNA and ribosome biogenesis were downregulated in the mutants in YPD (Fig. 4.17). RPL4A_BIND was chosen as a specific set to represent this trend. This is the second example of a gene set which finds contrasting upregulated log2 values in RPMI (Fig. 4.42).

Ribosomal protein RPL4A is repressed on phagocytosis by macrophage and by Spider biofilm (Skrzypek et al. 2017). The RPL4A_BIND gene list is a list of genes from the *Saccharomyces* Genome Database that bind *S. cerevisiae* RPL4A (Skrzypek & Hirschman 2011).

Thirdly, the TRANSLATION_BIO gene set also had the same pattern of downregulation in YPD and upregulation in RPMI datasets (Fig. 4.42). This gene set is based on a gene ontology categorization (GO: 0006412) which includes genes from metabolic processes relating to translation (Consortium 2017; Ashburner et al. 2000). While these are only some examples among many gene sets observed to have this trend, other expression patterns were likewise notable including genes that were upregulated consistently across the two conditions (Fig. 4.43). Given that acetylation is characteristic of open, active chromatin states, perhaps in the future more of these genes should be evaluated by ChIP for possible enrichment of Hda1 related acetylation.

Some gene sets had consistent up or down regulation in all the mutants in both YPD and RPMI (Fig. 4.43).

(A) Yeast inducing media: YPD

Gene Set (# genes)	hda1ΔΔ	hda2ΔΔ	hda3ΔΔ
TRANSPORTER ACTIVITY (331)	**1.92**	**1.88**	1.58

(B) Hyphae inducing media: RPMI

Gene Set (# genes)	hda1ΔΔ	hda2ΔΔ	hda3ΔΔ
TRANSPORTER ACTIVITY (331)	1.41	1.23	-1.45

(C) Yeast inducing media: YPD

Gene Set (# genes)	*hda1*ΔΔ	*hda2*ΔΔ	*hda3*ΔΔ
BMDM_PHAGOCYTOSIS _DN (530)	**2.59**	**2.64**	**2.41**

(D) Hyphae inducing media: RPMI

Gene Set (# genes)	*hda1*ΔΔ	*hda2*ΔΔ	*hda3*ΔΔ
BMDM_PHAGOCYTOSIS _DN (530)	**2.46**	1.58	**2.42**

Figure 4.43 Examples of overall upregulated pattern of gene set expression changes for *hda1*ΔΔ, *hda2*ΔΔ and *hda3*ΔΔ mutant strains grown in yeast and hyphae inducing media

GSEA expression changes in (A/C) YPD and (B/D) RPMI for *hda1*ΔΔ, *hda2*ΔΔ and *hda3*ΔΔ; Gene set analysis NES score results; Values are $p \leq 0.05$; FDR < 0.05 value is highly significant and bolded.

In Section 4.2.2.4.2 we saw that gene sets related to transporters were upregulated in the YPD log2 values of *hda1*ΔΔ, *hda2*ΔΔ and *hda3*ΔΔ (Fig. 4.1). The TRANSPORTER ACTIVITY_MOL gene set was chosen to represent this trend (Fig. 4.43A/B). This gene set was found to be positively correlated in the RPMI analysis but only for *hda1*ΔΔ, *hda2*ΔΔ. This gene set is comprised of genes involved with the movement of molecules in and out of cells (GO:0005215) (Consortium 2017) gene on (Ashburner et al. 2000).

A similar pattern was seen for gene sets relating to phagocytosis (Fig. 4.43C/D). BMDM_PHAGOCYTOSIS_DN is a set of genes which are downregulated following engulfment by primary Bone Marrow Derived Macrophages (Marcil et al. 2008). However, the genes in this set are positively correlated with the log2 values of *hda1*ΔΔ, *hda2*ΔΔ and *hda3*ΔΔ across both conditions.

4.2.4.2 Gene expression analysis: Tor1 and rapamycin, metals and copper, drug resistance and fluconazole

To continue looking more closely at the phenotypes observed in the spotting assays (see Section 4.2.2.2). This section performs a comparative analysis of genes and gene sets associated with rapamycin, copper and fluconazole since the resistance and sensitivity were observed with these stressors occurred mostly in YPD and not RPMI. This section explores potential molecular contributors to these stress media dependent phenotypes.

4.2.4.2.1 Gene expression analysis: Rapamycin

Rapamycin gives its name to the gene Tor1, which is known to play a role in the resistance and sensitivity of *C. albicans* to this drug (see Section 1.7.2). This section holds an investigation into Tor1 related genes and rapamycin resistance related genes and gene sets to look at their expression in the *hda1*ΔΔ, *hda2*ΔΔ and *hda3*ΔΔ mutants.

As discussed in Section 1.7.2, Hda1 plays an important role in Tor1 signaling pathways (Lu et al. 2011). Among the list genes evaluated that were related to rapamycin, only two had changed expression for all mutants in YPD that was not present in RPMI (Fig. 4.44; for full list see Appendix 3.2.6).

(A) Yeast inducing media: YPD

Gene	hda1ΔΔ	hda2ΔΔ	hda3ΔΔ
NRG1	**-0.91**	**-0.75**	-0.62
BCR1	**1.15**	0.65	0.72

(B) Hyphae inducing media: RPMI

Gene	hda1ΔΔ	hda2ΔΔ	hda3ΔΔ
NRG1	-0.09	0.42	**0.84**
BCR1	-0.28	0.21	0.14

(C) Yeast inducing media: YPD

Gene Set (# genes)	*hda1*ΔΔ	*hda2*ΔΔ	*hda3*ΔΔ
Genes Repressed By Rapamycin (324)	**-2.59**	**-2.06**	**-3.08**

(D) Hyphae inducing media: RPMI

Gene Set (# genes)	*hda1*ΔΔ	*hda2*ΔΔ	*hda3*ΔΔ
Genes Repressed By Rapamycin (324)	**2.24**	**1.26**	**2.07**

(E) Yeast inducing media: YPD

Gene Set (# genes)	*hda1*ΔΔ	*hda2*ΔΔ	*hda3*ΔΔ
NRG1_TF (157)	**-1.92**	**-1.92**	(0.85)

(F) Hyphae inducing media: RPMI

Gene Set (# genes)	*hda1*ΔΔ	*hda2*ΔΔ	*hda3*ΔΔ
NRG1_TF (157)	**(1.27)**	**(-1.13)**	1.58

Figure 4.44 Varied expression changes for Tor1 related genes and opposite pattern for rapamycin related gene set for *hda1*ΔΔ, *hda2*ΔΔ and *hda3*ΔΔ mutant strains grown in yeast and hyphae inducing media
Expression changes and gene set correlations in (A/C/E) YPD and (B/D/F) RPMI for *hda1*ΔΔ, *hda2*ΔΔ and *hda3*ΔΔ; Individual gene values are $p \leq 0.05$; FDR < 0.05 valued is highly significant and bolded. Gene set analysis NES score results; Values are $p \leq 0.05$; FDR < 0.05 value is highly significant and bolded.

While many genes in this analysis did not have significantly changed regulation there was a downregulation of Nrg1 and upregulation of Bcr1 across all the mutants in YPD. The Tor1 pathway involving Nrg1 and other proteins is detailed in Figure 1.12. Tor1 regulates cell adhesions by targeting Bcr1 (Bastidas et al. 2009). It is also notable that this change of expression was not observed in RPMI but an increased expression of Nrg1 was observed in the *hda3*ΔΔ mutant alone (Fig. 4.44B/F).

Therefore, this supports a hypothesis that these proteins function together in the Tor1 pathway in yeast but not in hyphae induction conditions.

GSEA analysis showed the gene set GENES REPRESSED BY RAPAMYCIN is negatively correlated with the YPD log2 results and positively correlated with the RPMI log2 results for all the mutants. This gene set consists of genes repressed by rapamycin treatment of wildtype cells (SC5314) during growth in YPD at 30 °C (Fig. 4.44C/D).

The specific Tor1 related GSEA gene sets (TOR1_BIND, _SGA or Tor2_BIND, _DAMP_SGA, etc.) were not significantly changed in the log2 values of the mutants, Nrg1 and other related gene sets were significantly altered in mainly the YPD GSEA data (Fig. 4.44E/F). Consistent with the individual gene expression change result, the GSEA gene set Nrg1_TF had a negative expression when correlated with the log2 data for *hda1*ΔΔ and *hda2*ΔΔ. Also, a significant positive correlation was observed for genes in this set with the log2 results of *hda3*ΔΔ in RPMI. The NRG1_TF gene set is made up of genes targeted by Nrg1. It is compiled from unpublished ChIP-chip data from the Nantel lab (Biotechnology Research Institute, Quebec, Canada). *NRG1* is a transcription factor involved in Tup1 dependent and independent responses (see Section 1.7.2/4).

In conclusion, individual gene expression change data provides evidence that supports Hda1, Hda2 and Hda3 functioning together in Tor signaling pathways in YPD media. Also, gene set analysis shows opposite, regulation for genes repressed by rapamycin in YPD (downregulated) versus in RPMI (upregulated) medias which suggests that these proteins are involved in molecular pathways associated with Rapamycin.

4.2.4.2.2 Gene expression analysis: Copper

Next, based on the sensitivity of *hda2*ΔΔ and *hda3*ΔΔ mutant strains observed in the spotting assay with added copper in YPD only (Fig.4.9) an evaluation of the genes related to copper processing was made (see Appendix 3.2.7). The Deseq2 log2 values for copper sensitivity genes show mixed changes of upregulation and downregulation in both YPD and RPMI. The list includes not only copper processing genes but also Superoxide Dismutase (SOD) proteins which are engaged by *C. albicans* as a response mechanism to host copper levels (Schwartz et al. 2013; Li et al. 2015). Looking more widely at other metal assimilation genes it was apparent that metal pathways other than those related to copper were affected in the mutants (see Appendix 3.2.8). However, many genes in this set are elevated but not significant.

Many related genes have significantly changed log2 in *hda1*ΔΔ only. For example, *FRE2* is significantly upregulated in all mutants in RPMI only while *FRE10* has opposite upregulation in *hda3*ΔΔ in YPD relative to downregulation in the other mutants. In RPMI

*hda1*ΔΔ and *hda3*ΔΔ have upregulated log2 for *FRE10* while *hda2*ΔΔ does not (for full analysis see Appendix 3.2.8).

Some gene sets related to metal processing did show clear patterns in the GSEA analyses of the YPD log2 data (Fig. 4.46).

(A) Yeast inducing media: YPD

Gene	hda1ΔΔ	hda2ΔΔ	hda3ΔΔ
CUP2_TFMOTIF (85)	**2.15**	**2.18**	**1.97**
ZAP1_TF (61)	**2.11**	1.71	1.66

(B) Hyphae inducing media: RPMI

Gene	hda1ΔΔ	hda2ΔΔ	hda3ΔΔ
CUP2_TFMOTIF (85)	(1.29)	(1.32)	**-1.66**
ZAP1_TF (61)	-1.97	**-2.13**	(-1.25)

Figure 4.45 Upregulation of copper and zinc related gene sets for *hda1*ΔΔ, *hda2*ΔΔ and *hda3*ΔΔ mutant strains grown in yeast but not hyphae inducing media
GSEA expression changes in (A) YPD and (B) RPMI; Gene set analysis NES score results; Values are $p \leq 0.05$; ( ) indicate not significant (p-value ≥ 0.05); FDR < 0.05 value is highly significant and bolded.

The CUP2_TFMOTIF gene set is upregulated in the mutants in YPD. *CUP2* is a copper binding transcription factor which regulates the transcription of metallothionein genes that are required for normal resistance to copper (Skrzypek et al. 2017; Buchman et al. 1989). This gene set is compiled of genes that have a transcription factor motif (the *CUP1* upstream activator sequence (UASc)) which is bound by Cup2 (Buchman et al. 1990). This gene set did not have significantly changed expression in the GSEA RPMI results for *hda1*ΔΔ or *hda2*ΔΔ but it was downregulated in *hda3*ΔΔ.

The ZAP1_TF gene set also showed upregulation in YPD and downregulation in RPMI. This gene set is a compilation of the targets of Zap1 which were identified through ChIP-chip analysis (Nobile et al. 2009). Zap1 is the controller of zinc homeostasis has roles in hyphae formation and biofilm development (see Section 1.2.8).

To summarize, analysis of metal assimilation related gene sets showed upregulation of Cup2 and Zap1 related genes in YPD.

4.2.4.2.3 Gene expression analysis: Fluconazole and drug resistance

Fluconazole pathways have been discussed in detail in the introduction (see Section 1.2.9) and in relation to the minimum inhibitory concentration assays (see Section 4.2.2.4.7). The *hda2*ΔΔ strain showed resistance in spotting assays on fluconazole with YPD but not RPMI (Fig. 4.9).

Many genes related to drug resistance had significantly altered DESeq2 log2 values in the mutants compared to the wildtype strain (Fig. 4.46).

(A) Yeast inducing media: YPD

Gene	hda1ΔΔ	hda2ΔΔ	hda3ΔΔ
CAP1	**1.56**	**0.89**	0.02
GCN4	**1.16**	**1.16**	0.27
GRP2	**1.35**	**1.52**	0.56
HSP90	**0.61**	0.66	-0.33
IFD6	**3.38**	**3.63**	0.97
MDR1	**3.21**	**2.92**	0.61

(B) Hyphae inducing media: RPMI

Gene	hda1ΔΔ	hda2ΔΔ	hda3ΔΔ
CAP1	-0.09	0.26	0.14
GCN4	0.01	0.07	-0.19
GRP2	0.21	0.10	0.10
HSP90	0.21	0.14	-0.22
IFD6	0.23	-0.27	0.32
MDR1	0.45	-0.06	-0.33

(C) Yeast inducing media: YPD

Gene Set (# genes)	*hda1*ΔΔ	*hda2*ΔΔ	*hda3*ΔΔ
UPC2_DN (260)	**-3.18**	**-3.73**	**-2.36**

(D) Hyphae inducing media: RPMI

Gene Set (# genes)	*hda1*ΔΔ	*hda2*ΔΔ	*hda3*ΔΔ
UPC2_DN (260)	**3.17**	**2.39**	**3.49**

(E) Yeast inducing media: YPD

Gene Set (# genes)	*hda1*ΔΔ	*hda2*ΔΔ	*hda3*ΔΔ
KETOCONAZOLE_DN (149)	**-2.74**	**-2.31**	**-2.72**

(F) Hyphae inducing media: RPMI

Gene Set (# genes)	*hda1*ΔΔ	*hda2*ΔΔ	*hda3*ΔΔ
KETOCONAZOLE_DN (149)	**2.28**	1.45	**2.64**

Figure 4.46 Opposite regulation of drug resistance related gene sets and genes for *hda1*ΔΔ, *hda2*ΔΔ and/or *hda3*ΔΔ mutant strains grown in yeast versus hyphae inducing media

(A/C/E) in YPD (B/D/F) in RPMI; Gene set analysis NES score results; Individual gene values are $p \leq 0.05$; FDR < 0.05; Values are $p \leq 0.05$; ( ) indicate not significant (p-value $\geq$0.05); FDR < 0.05 value is highly significant and bolded.

While several genes related to drug resistance are upregulated in the mutant strains relative to wildtype in YPD it is apparent that none of these genes have significantly altered expression in the *hda3*ΔΔ mutant and that these expression differences do not persist in RPMI (for full list see Appendix 3.2.9).

GSEA analysis of the DESeq2 log2 values show gene sets related to drug resistance with significantly correlated regulation pattern (Fig. 4.46).

Several *UPC2* gene sets were significantly altered however UPC2_DN showed negative expression changes in the log2 results of all mutants in YPD but positive in RPMI. The UPC2 genes set are based on genes upregulated and downregulated in a *upc2* knockout strain (Synnott, Guida, Mulhern-haughey, et al. 2010). *UPC2* is a regulator of ergosterol genes that is induced by azole antifungal treatment (Skrzypek et al. 2017).

This same pattern is observed for the ketoconazole related gene set. The Ketoconazole_DN is a set of genes upregulated in *C. albicans* cells grown in the presence of ketoconazole (Synnott, Guida, Mulhern-haughey, et al. 2010).

In conclusion, while individual log2 analysis of genes related to drug resistance showed upregulation in *hda1*ΔΔ and *hda2*ΔΔ. Gene set analysis revealed the downregulation of gene sets normally downregulated in response to UPC2 deletion or

ketoconazole exposure in YPD. While these gene sets were upregulated in RPMI, the individual genes assessed showed no significant change in regulation in RPMI. This discrepancy is likely due to the measurement of different drug resistance pathways and further evaluation of this data can provide clearer insight to this observation.

4.2.4.3 Gene expression analysis: *S. cerevisiae* Hda1, Hda2 and Hda3

In *S. cerevisiae* only one regulator is known for each Hda1 (Tfc7) and Hda2 (Abf1) but several are identified for Hda3 (Leu3, Med4, Med2, Sfp1, Xbp1). The DeSeq2 log2 values for the *C. albicans* orthologs of these Hda1 and Hda3 regulating proteins with significant changes in expression are listed in Figure 4.47A/B. The regulator of Hda2, Abf1, does not have a clear ortholog nor does Med2.

SFP1 was downregulated in the mutants in YPD only. Only the *hda2*ΔΔ mutant showed increased regulation of *XBP1* which is known to regulate Hda3 in *S. cerevisiae.* Other genes did not have significant change in expression (*LEU3* and *MED4*) and the read value for *TFC7* was not calculated by DESeq2 (see Section 1.9 and 1.10) (for a full list see Appendix 3.2.11).

Gene sets comprised of the interactors with the *S. cerevisiae* orthologs are HDA1_BIND, HDA2_BIND and HDA3_BIND (Skrzypek & Hirschman 2011). These sets were significantly downregulated in the log2 data of the *hda1*ΔΔ, *hda2*ΔΔ and *hda3*ΔΔ mutants in some cases (Fig. 4.47C/D).

(A) Yeast inducing media: YPD

Gene	hda1ΔΔ	hda2ΔΔ	hda3ΔΔ
SFP1	**-0.84**	**-0.93**	-0.71
XBP1/C2_05860C	0.47	**1.08**	-0.48

(B) Hyphae inducing media: RPMI

Gene	hda1ΔΔ	hda2ΔΔ	hda3ΔΔ
SFP1	0.18	0.17	0.26
XBP1/C2_05860C	-0.25	-0.12	0.21

(C) Yeast inducing media: YPD

Gene Set (# genes)	*hda1*ΔΔ	*hda2*ΔΔ	*hda3*ΔΔ
HDA1_BIND (104)	-1.79	-1.51	-1.47
HDA2_BIND (45)	-1.79	(-1.38)	(-1.41)
HDA3_BIND (71)	-1.93	-1.79	(-1.28)

(D) Hyphae inducing media: RPMI

Gene Set (# genes)	*hda1*ΔΔ	*hda2*ΔΔ	*hda3*ΔΔ
HDA1_BIND (104)	(-1.16)	(-1.21)	(-1.77)
HDA2_BIND (45)	(1.57)	(-0.5)	(-1.41)
HDA3_BIND (71)	(-1.21)	(-1.13)	1.36

Figure 4.47 Unique changes for individual genes and overall downregulation of genes sets related to *S. cerevisiae* orthologs for *hda1*ΔΔ, *hda2*ΔΔ and/or *hda3*ΔΔ mutant strains grown in yeast inducing conditions are not the same as in hyphae inducing media

GSEA gene set gene expression changes in (A/C) YPD and (B/D) RPMI for *hda1*ΔΔ, *hda2*ΔΔ and *hda3*ΔΔ; Values are $p \leq 0.05$; FDR < 0.05 valued is highly significant and bolded. Gene set analysis NES score results; Values are $p \leq 0.05$; ( ) indicate not significant (p-value >0.05).

These gene sets showed downregulation in YPD for all the mutants, however, only some of these scores were significant. Most of the gene sets showed a similar pattern in the RPMI extraction data (except *hda1*ΔΔ: HDA2_BIND which was positive) though not significantly. The HDA3_BIND gene set stood out as the one significantly positively correlated set among this group.

The only documented regulator of *S. cerevisiae* Hda1 is transcription factor *TFC7* that functions during cellular response to heat. Venters et al. 2011 have proposed that cross-talk may happen with PolII given that Hda1 occupancy was increased at tRNA genes and heat shock proteins.

To conclude, gene sets related to interactions of *S. cerevisiae* Hda1, Hda2 and Hda3 were overall downregulated in the mutants. The regulators of these genes were not broadly affected in the *C. albicans hda1*ΔΔ, *hda2*ΔΔ and *hda3*ΔΔ mutant strains.

4.2.4.4 Whole protein extraction in yeast versus hyphae induction

Since relative expression of these proteins could contribute to the population of complexed versus free *C. albicans* Hda1, Hda2 and Hda3, whole protein extraction was used to evaluate protein levels (Fig. 4.48).

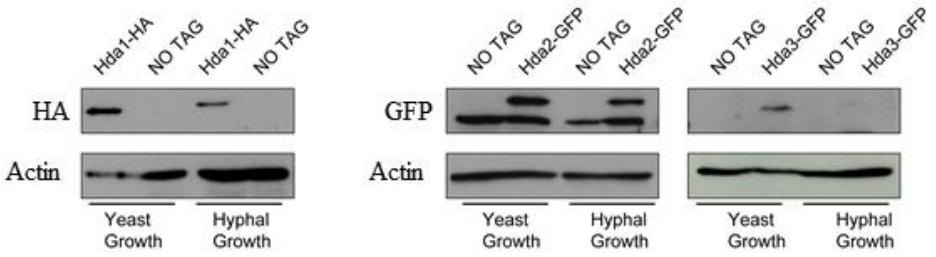

Figure 4.48 Whole Protein Extracts indicate reduced levels of Hda1 and possibly Hda3 in hyphae inducing conditions
HA or GFP Western blots of whole protein extract from strains: Hda1-HA, Hda2-GFP and Hda3-GFP. Actin is shown as a loading control. [image made by Dr. Alessia Buscaino (Appendix 4)]

The whole protein extractions from Hda1-HA, Hda2-GFP and Hda3-GFP tagged strains showed higher levels of Hda1-HA and possibly Hda3-GFP proteins in YPD media versus RPMI. Actin is shown as a control to ensure that expression of other proteins was stable. The observed levels of Hda3 were consistently low regardless of the growth media.

We conclude that yeast and hyphae inducing medias confer very different gene transcription, phenotype and possibly protein level profiles for Hda2 and Hda3.

4.2.4.5 Model for protein level control based on in yeast versus hyphae induction

The model in Figure 4. illustrates downregulation of the Hda1 complex component proteins: Hda1, Hda2 and Hda3 in hyphae induction conditions. It also illustrates other potential functional arrangements and interactions of these proteins. In addition, the proteins may be found in varying stochiometric rations. This model is informed by results by the co-immunoprecipitation of Hda1 and Hda2, and also Hda1 Hda3 (Figure 4.2). Although it must be noted that specific interaction between the three proteins or Hda2 and Hda3 has not been shown and these should be evaluated by future experiments which can include serial co-immunoprecipitation and/or employ uniquely tagged Hda2 or Hda3 (this is indicated by the dashed line in the figure). More information about sub-complexing or other interaction partners can, in the future,, be evaluated by size fractioning and molecular weight quantifications or mass spec evaluation.

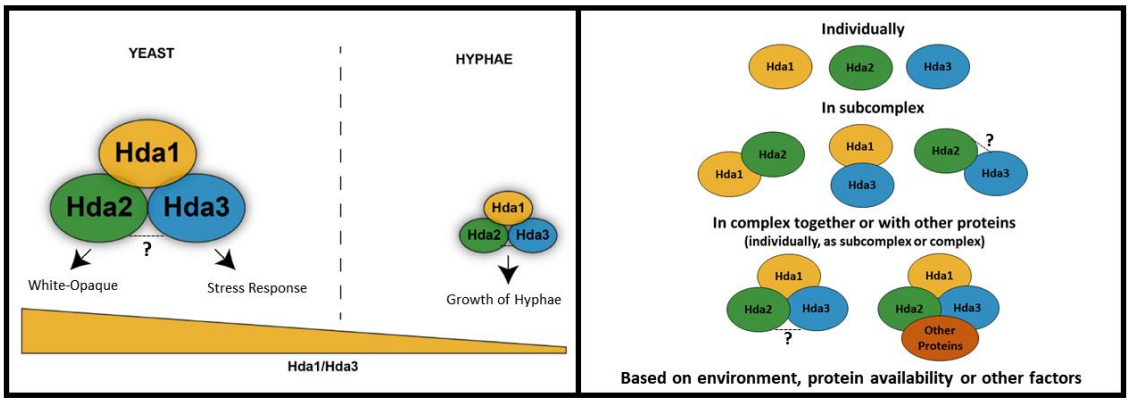

Figure 4.49 Speculative model of dynamic Hda1 protein complex functional regulation in different environments and other potential arrangements for the Hda1, Hda2 and Hda3 proteins.
(Left) Model showing that Hda1 complex proteins are involved in various physiological processes in yeast induction conditions while its function is focused on growth of hyphae in inducing conditions. Dashed line and question mark annotate that the interaction between Hda2 and Hda3 has not been tested in *C. albicans*. [Base figure was constructed by Dr. Alessia Buscaino for the article in progress. Hda2—Hda3 interaction note and additional figure at right were added for this thesis]
(Right) Individual, subcomplex and extra-complex arrangements that may explain unique phenotypes and gene expression results observed for *hda2*ΔΔ and *hda3*ΔΔ mutants.

We have discussed significant changes to phenotypes and gene expression of mutant strains in these proteins and observed their interactions. The results provide evidence of individual and common phenotypes and gene regulation trends that suggests the function of these proteins in roles outside of the full complex, individually or with

other binding partners. It is also not necessarily the case that the complex itself is less common just because protein levels are lower. Likewise, it is also important to note the intertwined nature of white-opaque switching and that opaque cell types are induced by different environmental cues into filamentation (Ene et al. 2016). This must be taken into consideration when interpreting the results from the strains mutant in these proteins that have increased rates of white-opaque switching (Fig. 4.25). Overall this study provides a limited view of the potentially very dynamic adjustment of the function of the Hda1, Hda2 and Hda3 proteins within the pathogen *C. albicans* as it responds to different environmental situations.

4.3 Discussion

In this chapter, an investigation into the roles of *C. albicans* Hda2 and Hda3 proteins was been presented. This has led to the understanding that these proteins form complexes with Hda1 and that they likely function both together and independently in different molecular pathways. The overall conclusions of this Chapter are: Hda1 interacts with Hda2 and Hda1 interacts with Hda3 (Fig. 4.2). Phenotypes of *hda2*ΔΔ and *hda3*ΔΔ homozygous mutants include sensitivity to respiratory pathway inhibitors SNP and SHAM and osmotic stress by NaCl (Fig. 4.6). A phenotype of increased resistance to caspofungin is observed in the *hda2*ΔΔ mutant and sensitivity to zinc is observed in the *hda3*ΔΔ homozygous mutant (Figs. 4.7 and 4.8). A phenotype of resistance to rapamycin is observed in both *hda2*ΔΔ and *hda3*ΔΔ deletion mutants in YPD but these phenotypes are not observed in RPMI (Fig. 4.9). Likewise, *hda2*ΔΔ shows resistance to fluconazole in YPD media only. Sensitivity to copper is observed in these mutants in both YPD and RPMI medias. Spotting assays with these three (rapamycin, copper and fluconazole) phenotypes medias and a Yng2 mutant strain that mimics deletion of Hda1 show phenotypes consistent with the *hda2* and *hda3* mutants when grown on YPD and RPMI with added rapamycin. In copper, the sensitivity is shown in YPD but in RPMI the other Yng2 mutant which blocks acetylation showed a sensitive phenotype (Fig. 4.12). While levels of fluconazole were not high enough to evaluate resistance, sensitivity was observed in the Yng2 mutant in RPMI and this was not seen in *hda2*ΔΔ or *hda3*ΔΔ.

4.3.1 Similarities of *C. albicans HDA1, HDA2* and *HDA3* to *S. cerevisiae* orthologs

The results presented in Section 4.2.2 strongly suggest that Hda2 and Hda3 proteins complex with Hda1. This observation shows these proteins interact like the orthologous *S. cerevisiae* proteins which are shown to form the Hda1 Complex (Lee et al. 2009). This is also supported by the strong Pearson correlations of the DESeq2 RNAseq log2 data for the homozygous mutants of *hda1*ΔΔ, *hda2*ΔΔ and *hda3*ΔΔ, particularly in the yeast inducing conditions.

Generally, individual genes that are reported to regulate Hda1, Hda2 and Hda3 in *S. cerevisiae* did not have significantly changed regulation in the DESeq2 log2 data from *C. albicans hda1*ΔΔ, *hda2*ΔΔ and *hda3*ΔΔ mutants. There were a couple of significantly changed regulators in the YPD data only although these were observed in a different mutant than that of their recorded regulation in *S. cerevisiae.* For example, *XBP1* was upregulated in yeast inducing conditions for *hda2*ΔΔ when it is a regulator of *S. cerevisiae* Hda3 protein. Among the genes known to interact with *S. cerevisiae* Hda1, Hda2 and Hda3 proteins overall negative regulation was seen in the yeast inducing (YPD) conditions only. The results imply that the interaction partners and systems of regulation are evolutionarily diverged in *S. cerevisiae*. Together this suggests that the downstream aspects of Hda1 complex related activity may be more conserved than upstream regulation. One outstanding finding in the GSEA analysis was that genes in the HDA3_BIND set were positively regulated in the *hda3*ΔΔ mutant in hyphae inducing conditions (RPMI) only (Fig. 4.47) which deserves further exploration and may point at roles of this protein during the maintenance of hyphae.

4.3.2 Overall gene expression analysis of RNAseq data

The Pearson Correlations were stronger in the analysis of DESeq2 RNAseq log2 results from the YPD samples (Fig. 4.12) and only weak correlation was observed between *hda1*ΔΔ and *hda3*ΔΔ in RPMI (Fig. 4.34). The heatmaps reflect these differences. The relationships between gene expression patterns in yeast inducing conditions (YPD) support the hypothesis that the proteins function together in a complex. However, the results in hyphae inducing conditions (RPMI) are not as strong and suggest that Hda1, Hda2 and Hda3 may not work together so tightly in those conditions as in YPD. Although to qualify this statement it must be pointed out that a strong correlation is seen between the *hda1*ΔΔ, *hda2*ΔΔ and *hda3*ΔΔ mutants in their expression of hyphae and biofilm

related genes (Fig. 4.35). This supports the model with Hda1 complex function directed toward hyphal growth in hyphae inducing conditions (Fig. 4.49).

The Venn diagrams show that RPMI analysis differed from the YPD analysis in several ways. The number of genes with significantly changed regulation in *hda1*ΔΔ and *hda2*ΔΔ gene sets are much smaller in RPMI (~3-6x;) than in the YPD extraction and the *hda3*ΔΔ are much larger (~5-6x) (Figs. 4.15 and 4.35). There are about double the *hda2*ΔΔ upregulated genes in YPD but the number of downregulated remained about the same in both medias. The percentage overlap of gene sets in downregulated genes for *hda1*ΔΔ and *hda2*ΔΔ in YPD was much smaller than in RPMI. The opposite was observed for the percentage overlap of downregulated genes in *hda2*ΔΔ and *hda3*ΔΔ. A noticeable difference for upregulated genes in RPMI was an increased percentage of overlapping gene sets for *hda3*ΔΔ relative to YPD. It would be interesting to account for the number of genes with consistently changed regulation in these mutants across conditions.

4.3.3 Phenotypes and related gene expression in homozygous mutants of *C. albicans HDA1, HDA2* and *HDA3*.

In analyzing the phenotypes of the *hda1*ΔΔ, *hda2*ΔΔ and *hda3*ΔΔ mutants, several observable similarities as well as unique differences are observed.

Strong patterns of downregulation in YPD and contrasting upregulation in RPMI were observed for RNA and Ribosome Biogenesis and for Organelle Organization and Biogenesis gene sets (Figs. 4.18, 4.19 and 4.43). Transporters were generally upregulated in all conditions apart from the *hda3*ΔΔ mutants in RPMI.

Evaluation of gene sets associated with the white or opaque phenotypes of *C. albicans* showed strong changes in regulation (Fig. 4.23). In opaque gene sets, the mutants showed clear positive regulation in YPD. The same was the case for gene sets that are upregulated in white cells except for the *hda3*ΔΔ mutant which showed negative correlation. The phenotype analysis clearly showed that the *hda2*ΔΔ and *hda3*ΔΔ mutants have increased white-opaque switching (Fig. 4.24). This fits with a published phenotype for *hda1*ΔΔ which we also observed. The observed level of increased *hda2*ΔΔ and *hda3*ΔΔ switching was much lower than that of *hda1*ΔΔ. Assessing a double mutant in these proteins for white opaque switching phenotype would check for potential functional redundancy in these proteins and is a good idea for future exploration of this effect.

The filamentation phenotype was clearly stunted in *hda1*ΔΔ, *hda2*ΔΔ and *hda3*ΔΔ mutants (Figs. 4.37 and 4.38). It is worth noting that assessment of filamentation in liquid

is done by grading based upon simple measurement of the length of the cells and does not properly qualify cells as hypha. Yet, the objective of this survey was to evaluate whether their development is stunted so this crude assessment was an efficient way to quantify this phenotype. Reintegration of Hda3 showed restoration of the filamentation phenotype and while Hda1 and Hda2 reintegration strains have been built, evaluation of their phenotype was beyond the time scope of this thesis project (Fig. 4.38). Likewise, there are plans to reintegrate the DNA binding domain, Arb2 and Catalytic domain to homozygous deletion strains in the future.

The biofilm assay was not ideal and was not done in repetition, but differences were observed between the *hda3*ΔΔ strain and wildtype. Publications report depths of about 350-450 µm which led us to think that analysis could be made with stronger lens magnification (Nobile & Mitchell 2005). Another experimental reason for our lower depth values may have been disruption of the biofilm during preparation steps including fixing, dehydration and staining, although every effort was made to avoid their disruption. Different approaches have since been developed in our lab that employ racks that suspend the silicon squares allowing them to dip into plates which have provided much better results and would be used for future investigations. Likewise, the macrophage studies would require more investigation to be definitive but given the *C. elegans* data, this is unlikely to be worthwhile (see Appendix 4, Fig. 6D). Changes in expression of biofilm related genes and gene sets (GSEA) including upregulation of *XOG1* and downregulation of Zap1 related genes may indicate that further biofilm analysis is worthwhile. Strains which are homozygous mutants in *XOG1* show decreased biofilm formation but perhaps more relevant is the phenotype of homozygous Zap1 mutants which display abnormal biofilm development characterized by the increased presence of yeast cells (see Section 1.2.3) (Taff et al. 2012; Ganguly et al. 2011). The expression changes of genes related to hypha development and other aspects of this switch were generally consistent across all the mutants (Fig. 4.35)

A spotting assay showed resistance to rapamycin in the *hda2*ΔΔ and *hda3*ΔΔ mutants in YPD only. Individual analysis of the log2 values of genes related to rapamycin identified Nrg1 and Bcr1 which had changed regulation in YPD only. Nrg1 was downregulated and Bcr1 was upregulated. It is proposed that Bcr1 and Tup1 regulate Nrg1 through separate pathways and that Nrg1 represses filamentation (Guan et al. 2013). It seems that the downregulation of Nrg1 is due to regulation other than from Tup1 since this pathway did not show altered regulation in the GSEA results.

Gene sets with genes repressed by rapamycin were negatively regulated in these mutant's data sets from YPD growth but positively regulated in RPMI sets. Other sets related to Nrg1, Yng1 and Rim101 showed mixed regulation across medias in the mutants. Evaluation of Tor1 related pathways showed most changes of expression occurring in the *hda1*ΔΔ mutant. While several related genes were downregulated in RPMI (*ALS3, HWP1,* and *ECE1*), they were all also related to the development of hypha. *PHO84* was however upregulated in all mutants in RPMI. This protein is required for normal TORC1 function and virulence, and also has a role in metal transport (Liu et al. 2018).

Spotting assays with copper showed sensitivity in the *hda2*ΔΔ and *hda3*ΔΔ mutants in YPD and in RPMI. While in *S. cerevisiae*, copper is known as an oxidative stressor, and it has been shown that *C. albicans* adapts to this type of stress by expressing superoxide dismutase (SOD) proteins (Shanmuganathan et al. 2003; Li et al. 2015). In *hda2*ΔΔ only, the expression of SOD*1* was downregulated and *SOD3* was upregulated in YPD (see Appendix 3.2.7). While differing and divergent expression patterns were observed for *FRE10* in the mutants in YPD and RPMI these do not account for the sensitive phenotype observed (YPD: significantly upregulated in *hda3*ΔΔ and downregulated in *hda1*ΔΔ and *hda2*ΔΔ; RPMI: significantly upregulated in *hda1*ΔΔ and *hda3*ΔΔ only, expression unchanged in *hda2*ΔΔ).

Another spotting assay with added zinc showed sensitivity in the *hda3*ΔΔ mutant only. Zinc is an essential nutrient for yeast that becomes toxic at high doses, creates reactive oxygen species and causes problems with protein folding, iron and sulfur metabolism (Pagani et al. 2007). The *hda3*ΔΔ mutant shows opposite regulation to the other mutants which may play a role in its sensitivity. This phenotype has not yet been checked in RPMI. Homozygous deletion strains of the *S. cerevisiae* ortholog (*FRE2*) show strong sensitivity to copper although no experiments are recorded for zinc (Skrzypek & Hirschman 2011). Gene set analysis for *CUP2* and *ZAP1* related gene sets show upregulation in YPD while all significant values were downregulated in RPMI.

In relation to the response of these strains to drugs, trends in the GSEA analysis showed increased expression in all mutants to genes upregulated in response to ketoconazole and GCN4_TFMotif gene set, whereas Yak1_Y_UP gene set was upregulated in *hda2*ΔΔ and *hda3*ΔΔ but downregulated in *hda1*ΔΔ. Resistance was shown in the *hda2*ΔΔ mutant when grown by spotting assay on YPD media supplemented with caspofungin (Fig. 4.7). Caspofungin is an echinocandin drug (one of the main classes of drugs used for medical treatment of *C. albicans* infection, see Section 1.2.9) which targets

C. albicans cell wall synthesis pathways (Clancy et al. 2006). Although there were no significant changes in expression of *FKS1* which the main target of caspofungin in C. albicans is, *YAK1* which is induced in the core caspofungin response did show downregulation in the *hda1*ΔΔ and *hda2*ΔΔ mutants.

Analysis of *MDR1* and *MRR1* related genes showed genes upregulated in *hda1*ΔΔ and *hda2*ΔΔ mutants for genes related to *MDR1*. Few changes were observed in the regulation of genes related to *MRR1* and those altered were in the *hda1*ΔΔ mutant. Likewise, log2 assessment of genes related to drug resistance showed several genes with significant upregulation in *hda1*ΔΔ and *hda2*ΔΔ in YPD (*CAP1*, *GCN4*, *GRP2*, *HSP90*, *IFD6*, *MDR1*) which was not the case in RPMI. Several of these genes and *ZAP1* (which was upregulated in all mutants in YPD) are related to *MDR1* overexpression (see Sections 1.2.9). MIC assays showed some sensitivity of the mutants to synthetic complete liquid supplemented with fluconazole or cerulenin. No resistance was observed in the MIC assay with brefeldin A or diamide. Although these MIC assays were not done with replicates, cerulenin resistance was also not observed in an evaluation of the mutants by spotting assay (Fig. 4.4). Attention should be drawn to the fact that the *MDR1* log2 values were distinctly upregulated in YPD but not RPMI. In the ChIP experimental results some enrichment may have been observed in the mutants at the *MDR1* sites but result needs further confirmation (see Section 4.2.2.5). On solid agar resistance was observed in *hda2*ΔΔ on YPD media (only) supplemented with fluconazole, this is perhaps explained by the individual gene expression change analysis which finds most upregulation occurring in the *hda1*ΔΔ and *hda2*ΔΔ mutants but not the *hda3*ΔΔ (Fig. 4.46A).

Other phenotypes included sensitivity of *hda2*ΔΔ and in *hda3*ΔΔ on agar with additions of SNP & SHAM or NaCl (Fig. 4.6). As stressors, SNP is a nitric oxide donator which induces oxidative stress in yeast and SHAM inhibits alternative oxidases (Lushchak & Lushchak 2008; Joseph-Horne et al. 2001). The GSEA results showed a mitochondrial ribosome related gene set with downregulation in *hda2*ΔΔ and *hda3*ΔΔ (Fig. 4.19). In RPMI this gene set was upregulated, fitting with the typical pattern of opposite regulation for YPD and RPMI datasets. In terms of the NaCl sensitivity phenotype, several osmolarity gene sets had significantly changed expression in the YPD results and in RPMI significant opposite (positive) expression change was observed. While one of these gene sets was constructed from a *hog1* mutant, dysregulation of this gene was not observed in the DESeq2 log2 data of the *hda1*ΔΔ, *hda2*ΔΔ or *hda3*ΔΔ mutant relative to wildtype.

While pathways relating to respiration and osmolarity were not investigated in much detail here, these are viable pursuits for future analysis of these proteins.

While for many medias and treatments no difference was observed in the growth of these mutants, additional assessment with other conditions or alterations to the exposure regime may prove that sensitivity or resistance occur based on flexible adaptation to a slightly different environmental setting.

4.3.4 Tor1 and chromatin remodeling pathway assessments of *C. albicans* *hda2*ΔΔ and *hda3*ΔΔ

Given that Hda1 is known to deacetylate the Yng2 subunit of NuA4 and to have a role in Tor1 signaling (see Section 1.7.2), it was intuitive to see if *hda2*ΔΔ and *hda3*ΔΔ mutants would show the same phenotype as the Yng2 mutants that blocked acetylation or mimicked constitutive acetylation. Although each was done as a single assay, results are presented from spotting assays of these strains on both yeast (YPD) and hyphae (RPMI) inducing medias with three additions: rapamycin, fluconazole and copper (Fig. 4.9). Phenotypes for the *yng2K175R* mutant strain were mostly consistent with hda2 and hda3 with perhaps the exception of RPMI with fluconazole on which the *K175R* grows with sensitive appearance. Ironically, the only strain that also showed sensitivity in this screen was *hda1*ΔΔ ABy_179. Although, sensitivity to the fluconazole has been previously reported in a Hda1 homozygous mutant strain (Li et al. 2014). This indicated that the proteins may be functioning in different pathways during fluconazole resistance.

Further studies of gene expression in the mutants showed that the genes Nrg1 and Bcr1 had significant expression changes (Fig. 4.44). Curiously, there was no change in expression for these gene sets in RPMI except for Nrg1 which was upregulated in *hda3*ΔΔ. This was reinforced when the same pattern was observed in the GSEA analysis with the gene set Nrg1_TF which includes 157 genes.

This evidence supports the model (Fig. 4.49) that the complex functions differently based on environmental conditions and may even suggest an addition to the model, that the proteins work together in some conditions and have individual roles in others. The participation of histone deacetylase proteins in multiple protein complexes with and without other histone proteins or lone function without a complex has been observed in human systems (Seto & Yoshida 2014).

4.3.5 Study limitations, important considerations and perspectives

Fluorescence studies of GFP tagged strains showed potentially low levels of native expression of the Hda1, Hda2 and Hda3 proteins (Fig. 4.1). Additional experiments are needed to draw conclusions about localization of these proteins as this was a brief investigation targeted toward information gathering to see if: (1) tagging had worked and (2) relative expression level and visibility of such strains for localization studies could be pursued. Controlled expression at the *ADH1* promoter seemed to improve these levels with the downside of potential artificial localization of these proteins as a repercussion of their under or overexpression level dictated by doxycycline induction. Improved fluorescence with *ADH1* locus-based expression may be due to induction of a higher level of the protein or increased visibility of the fluorescence by moving tag to N-terminal of protein. This can be tested by tagging the protein at the native locus with an N-terminal tag and comparing the visible fluorescence to the C-terminally tagged strain.

The co-immunoprecipitation showed interactions between Hda1 and Hda2 or Hda1 and Hda3 suggesting that the Hda1 complex forms in *C. albicans*. However, interactions between Hda2 and Hda3 were not assessed nor were stoichiometry or other important aspects to evaluate of the dynamics of this potential complex. Many of these facets have been evaluated in *S. cerevisiae* and drawing further conclusions regarding the similarity of these complexes should be suspended until more information is gathered. Further pulldown experiments could be employed to evaluate the complexing of these proteins. For example, there exists a conclusion in the literature that Hda1 does not interact with Hda2 in the absence of Hda3 (Kanta et al. 2006) (see Section 1.8.1). This could be tested by tagging the Hda1 and Hda2 proteins in the *hda3*ΔΔ strain. Alternatively, fusing Hda2 or Hda3 with a unique tag would provide the opportunity to see if these two proteins interact. Additionally, a serial co-immunoprecipitation experiment can evaluate whether the three proteins are interacting.

Low Hda3 protein levels were an issue that made it a challenge to obtain a clear result for the Hda1-Hda3 interaction. In retrospect, it may have been worth trying silver staining for detection of the low level Hda3 protein in both co-immunoprecipitation and the whole protein experiments since it is known for detecting low levels of protein (Fig. 4.2 and Laemmli 1970). Seperately, the low levels of Hda3 could be due to the tag affecting expression of the protein, a simple growth curve to compare single, double and tripple tagged strains with wildtype should be performed and alternative options for tagging can be trialed. Future evaluation should consider quantification of these proteins

by use of dilution series, near-infared (NIR) fluorophores coupled with infared imaging (LI-COR, etc.) or other methods. Finally, since irregular strain growth (clumping) and other experimental difficulties were faced on attempt to test co-immunoprecipitation with RPMI, further experiments could explore the media additives which showed different growth phenotypes in the spotting assays of the *hda2*ΔΔ and *hda3*ΔΔ mutants such as caspofungin, zinc or fluconazole to see if the observed interactions between Hda1 and Hda2 or Hda1 and Hda3 occur in these growth medias.

The chromatin immunoprecipitation using H3K9 did show a slightly significant difference in the acetylation at MDR1 but neither the statistics nor the level of enrichment were convincing (Fig. 4.30). Further experiments are needed to justify this result. The primers used in this experiment were within the middle of the sequence for *MDR1*. Future experiments can test primers in the promoter region of *MDR1* which would consider the known recruitment of Hda1 to promoter regions (Lu et al. 2012). Likewise, the Hda1-HA ChIP may have experienced experimental difficulties. This was not necessarily related to the strains since the HA antibody had not been tested with ChIP in our lab (Fig. 4.25). Considerable variation was observed in the Ct values for one of the samples grown in serum. The control primers for *HWP1* had been previously used in an experiment to show that Hda1-Myc interacts with the *HWP1* promoter in a serum dependent manner which was consistent with our results that only showed enrichment in the serum condition and not the YPD (Lu et al. 2011 and Fig. 1.13). However, given that increased log2 expression of *WOR1* was evident in both YPD and RPMI analysis this result is surprising and requires further evaluation (Fig. 4.25). A Hda1-Myc strain will be trialed for future experiments.

One issue that may compound this and the other qRT-PCR results was that *ACT1* expression is downregulated in *hda1*ΔΔ and *hda3*ΔΔ in YPD (see Section 4.2.2.3).

Throughout this study there have been questions about whether the *hda1*ΔΔ strain phenotypes are due to the presence of its marker genes. Comparisons with an alternative strain contributed different phenotypes seeming to confirm that some of the phenotypes could be due to a difference other than the deletion of *HDA1* (e.g. copper, fluconazole). To get completely around this confusion, a strain without markers would be needed, and ideally, several different strain backgrounds would be assessed. While we looked at one strain without markers (ABy_525) it did not have the same background as the *hda2*ΔΔ and *hda3*ΔΔ mutant strains. Another approach would be to reintegrate of Hda1 to the deletion strain/ Without these diagnostics it is difficult to assign much meaning to any of

these results (or even the RNAseq data for *hda1*ΔΔ) in terms of the *hda1*ΔΔ ABy_179 strain. Fortunately, the *hda2*ΔΔ and *hda3*ΔΔ strains had no markers in place.

4.3.6 Conclusion

Overall, this chapter evaluated the roles of Hda2 and Hda3 in yeast and hyphae inducing conditions. These experiments show that these proteins complex with Hda1 and have both common and distinct phenotypes. Their deletion causes stunted hyphal development and increased white opaque switching.

Relationships observed in the overarching analysis of gene expression show distinct trends of expression for these mutants. For example, in *hda3*ΔΔ many more genes were significantly upregulated and downregulated in RPMI which could point to additional roles for this protein in hypha inducing conditions. In the GSEA analysis of YPD samples many more pathways (5-10x) were downregulated than upregulated whereas in RPMI hardly any pathways were downregulated relative to the GSEA sets in the *hda1*ΔΔ, *hda2*ΔΔ *and hda3*ΔΔ mutants. It is notable that sensitivity to zinc is observed in the *hda3*ΔΔ mutant which is also the case in *S. cerevisiae* although sensitivity was also observed in the *S. cerevisiae hda2*ΔΔ mutant which was not seen in our assays (Skrzypek & Hirschman 2011; North et al. 2012). These numbers point to a shifting of roles for these proteins that happens with the changing medias these likely reflect changing pathways that developed through evolution and other intriguing aspects that contribute to the difficult nature of deciphering the *in vivo* functions of proteins in *C. albicans.*

CHAPTER 5. Discussion

This thesis encompasses a multifaceted study of two important proteins thought to be involved in the epigenetic regulation of the pathogenic yeast *C. albicans.* It addresses several aims which result in the functional characterization of the Histone Deacetylase 2 and Histone Deacetylase 3 proteins. Specifically:

Goal 1: Solve the structure of important protein domains of *C. albicans* Hda1 protein to evaluate its potential as a drug target.

Through structural alignment it was shown that the *C. albicans* Hda1 catalytic and Arb2 domains share some sequence similarity with its *S. cerevisiae* ortholog and its theoretical structure can be mostly modelled based on existing structures of *S. pombe* Clr3.

A successful strategy is presented for the expression and purification of full length *HDA1*. Optimization found that N-terminal GST tagging improved expression levels of this protein. Levels of protein expression were low, and this aspect will need to be considered when designing downstream applications of this protocol.

Chapter 3 describes a design for expression and purification of the important protein domain, Arb2 of *C. albicans* Hda1. It was found to be necessary that the design for the Arb2 expression construct include the C-terminus of the protein. Levels of protein expression were enough for downstream applications including some crystallization trials. During this project an article was published that contained the solved structure of the *S. cerevisiae* Arb2 domain (see Section 1.8.2). The structure of the domain is like alpha and beta fold hydrolases and has a protrusion that contributes half of the inverse "V" shape, fully composed on dimerization. The key residues involved in dimerization and within this groove are Ile^{512}, Ile^{523} and Leu^{525}. It is apparent in the alignment (Fig. 1.15B) that the Leu^{525} residue is not conserved in *C. albicans*. This motif and several residues are required for histone binding including His^{604}, His^{608} and Arb^{609}. Only the last of these residues is conserved in *S. pombe* and *C. albicans* (Shen et al. 2016). This alignment shows that there are significant differences between the *S. cerevisiae* and *C. albicans* Hda1 Arb2 domains.

Overall, the best option for expression of these proteins may not be done in *E. coli* and a better approach may be developed in yeast or another expression system such as insect or mammalian cells. Insect cells might be considered since they are known to help solubilize proteins and for their high protein expression levels. However, the most success may be found in using a yeast expression system which, despite taking a bit more time for

culture growth, would supply more appropriate translational codon matches and post-translational modifications (Gomes et al. 2016; Nascimento & Leite 2012).

Crystallization potential for the Arb2 domain was evaluated in several broad screens of conditions. A non-diffracting crystal was harvested which identifies a condition that may be suitable for growing this protein crystal.

Goal 2: Solve the structure of *C. albicans* Hda2 and Hda3 to evaluate their potentials as drug targets.

Through domain analysis it was shown that Hda2 and Hda3 have DNA binding domains and coiled-coil domains. These domains have some amino acid sequence conservation relative to each other as well as to orthologous proteins in other model yeasts. Theoretical models could be generated for these proteins as well with less accuracy for Hda3. Hda2 is mostly modeled on the structure of *S. cerevisiae HDA3DBD* and *CHD3*. Hda3 is also partially modelled on the structure of *S. cerevisiae HDA3DBD* but structures from more distantly related proteins also contribute. A good portion of the protein cannot be modelled with confidence. Through structural alignment it was found that functional motifs identified by the crystallization of *S. cerevisiae HDA3DBD* are only somewhat conserved in *C. albicans* Hda3 (Fig. 3.19).

Expression of low levels of soluble Hda2 protein may have been obtained through co-expression of the protein with Hda3. This trial finds a similar effect of solubility with co-expression as those seen for the *S. cerevisiae* proteins. *S. cerevisiae* finding that these proteins to overcome the issue of insolubility through co-expression (Lee et al. 2009). This contributes information about likely dependence of these proteins on binding partners (eachother) for their stability. Solubility tests did not unveil additional mechanisms for solubilizing Hda2 protein. The expression of insoluble Hda2 and Hda3 was confirmed by mass spectrometry or western blot.

Goal 3: Understand the function of *C. albicans* Hda2 and Hda3 *in vivo* to evaluate their role in the virulence of this pathogen.

The fluorescence imaging of the GFP-Hda3 strain showed some intriguing pinpoints which may indicate localization of the protein to actin cortical patches. In fact, close to 40 interacting proteins of *S. cerevisiae* Hda1 are actin related, this includes actin itself. This is also the case for *S. cerevisiae* Hda2 and Hda3 with over 20 proteins and Act1 (Skrzypek & Hirschman 2011). This hypothesis is something which can be explored in future cell

biology experiments by colocalization studies with tagged actin proteins, by using a stain for the septa of hypha. Large areas were fluorescent in some cells and staining can also be done to evaluate colocalization of this protein with DNA in the nucleus. Alternatively, additional analysis of the RNAseq data with GO or GSEA may support localization to these regions.

The co-immunoprecipitation results show that Hda1 is found in complex with Hda2 and separately with Hda3. This supports the hypothesis that the Hda1 complex forms in *C. albicans*.

Phenotyping assays of the *hda2*ΔΔ and *hda3*ΔΔ showed that the proteins likely function in distinct and unique pathways since different patterns of growth in these strains relative to the wildtype and each other were observed on certain stress medias.

Sensitivity of *hda2*ΔΔ and *hda3*ΔΔ to NaCl as well as SNP and SHAM were observed on YPD agar media. RNAseq analysis unveiled an upregulation of *SOU2* which can be followed up as a potential genetic mechanisms for the NaCl phenotype based on existing data in *S. cerevisiae* (Skrzypek & Hirschman 2011). DESeq2 log2 analysis showed changed regulation in some genes linked to important molecular processes including UV (*RFX2*) and cell wall modification (*MNN4-4*).

Larger scale gene expression analysis using sets of genes from existing published data showed that many gene sets related to RNA and ribosome biogenesis were downregulated in contrast to those related to transporters which were upregulated. This fits with findings from a study of the *C. albicans* acetylome that shows the regulatory roles of acetylation on ribosome related proteins (Zhou et al. 2016). Individual gene set analysis showed that genes related to organelle organization and biogenesis were negatively regulated while those relating to white-opaque switching phenotype and drug response were upregulated.

The first major phenotype which was found to be associated with the deletion of these genes is white-opaque switching which was significantly increased in these mutants. This finding fits with the published data for Hda1 (see Section 1.7.1, Zacchi et al. 2010 and Lu et al. 2011). Given that white colonies have an overall filamenting phenotype it seems logical that strains exhibiting an overall increase in white-opaque switching may also experience an effect to their filamentation (see Section 1.2.10.1 and Fig 1.3).

Coherently, the second major phenotype found associated with *hda2*ΔΔ and *hda3*ΔΔ during growth in hypha inducting media was the stunting of hypha development. This finding fits with the published data for Hda1 (see Section 1.7.1, Lu et al. 2011 and

Zacchi et al. 2010). The RNAseq analysis unveiled strongly changed expression in genes related to hyphal growth in these mutants relative to the wildtype as well as effects to specific genes that may be involved including downregulation of *UME6* (which regulates filamentous growth downstream of Tup1 pathways) and upregulation of *PES1* (hyphae-yeast switch regulator) (see Fig. 4.31, Shen et al. 2008 and Banerjee et al. 2008). Gene set analysis found these molecular mechanisms reinforced by a downregulation of genes normally upregulated in hyphae induction by fetal bovine serum (FBS) and 37 °C conditions (Fig. 4.31 and Nantel et al. 2002). Despite this phenotype and viable differences in biofilm development, virulence assays show no impact of these gene deletions on pathogenicity in macrophage or *C. elegans* models (see Figs. 4.36 and 4.37, and Fig. 6D of Appendix 4). This finding fits with the published data for Hda1 (see Section 1.7.1 and Lu et al. 2013). In fact, the DEseq2 log2 values show some possible support of this result with downregulation in genes that have roles related to pathogenicity: surface invasion regulator *ALS3,* hypha associated *HWP1* and biofilm related *SAP8*. However, virulence may not be viewed as the only end goal when targeting these proteins for treatment of *C. albicans* infection, since it should be noted, that deletion of these proteins has also been shown to decrease in the adaptability of strains to azole drugs (resistance) and MIC assays of strains with *hda1*ΔΔ have been shown to have a large decrease in their trailing growth phenotype in the context of three different azole drugs (Kmetzsch 2015; Li et al. 2014).

Chromatin immunoprecipitation experiments showed some increase of H3K9 acetylation at the *MDR1* locus. Although one of the samples of the experiment (done in triplicate) had an outlier result, interaction of Hda1 with the *WOR1* promoter was potentially shown these samples derived from growth of cultures with serum. This enrichment was consistent with *HWP1* enrichment which has previously been shown in the literature (Fig. 1.13). For further evaluation of the complex future experiments can evaluate enrichment of tagged Hda2 and Hda3 at *WOR1* by ChIP. Alternatively, enrichment at *WOR1* can be assessed in strains made using the *HDA1-HA* parental background that are homozygous mutant for one or both of the co-complexing proteins (*hda2*ΔΔ and *hda3*ΔΔ). The predicted outcome may be based on the complexing of these proteins in *S. cerevisiae* and the hypothesis that the DNA binding domains of Hda2 and Hda3 bring Hda1 to the DNA it is hypothesized that in the absence of one or both proteins, the enrichment of Hda1 at *WOR1* would be lost.

Gene sets often have opposite regulation of their gene expression changes in *hda2*ΔΔ and *hda3*ΔΔ in hyphae compared to yeast inducing conditions. However, there are examples of consistently increased or decreased expression that is consistent across the medias. Significantly different regulation is also seen for some genes in the mutants within a single media condition. These are perhaps the most interesting, since they indicate potentially distinct roles away from the complex.

A comparison of the phenotypes and genetic mechanisms observed in the yeast and hyphae inducing conditions focused on three phenotypes of *hda2*ΔΔ and/or *hda3*ΔΔ shown with the following additives only in YPD: resistance to rapamycin, sensitivity to copper and resistance of *hda2*ΔΔ to fluconazole. The role of *Hda1* in Tor1 signaling through the deacetylation of the Yng2 subunit of NuA4 is studied in relation to these additives (see Sections 1.7.2 and 4.2.2.2.2). The side-by-side evaluation of Yng2 mutant strains with the *hda2*ΔΔ and *hda3*ΔΔ mutants by spotting assay showed the same phenotype for the K175R except for rapamycin and copper. The mutant had a phenotype like Hda3 on YPD with fluconazole and it was uniquely sensitive on RPMI with fluconazole. The *hda1*ΔΔ mutant also showed sensitivity in this condition and these results, in combination with the growth of the *hda2*ΔΔ and *hda3*ΔΔ mutants, imply that the proteins may function differently in pathways when a cell is responding to fluconazole. Gene set analysis showed a downregulation of genes repressed by rapamycin in YPD and upregulation in RPMI in the mutants relative to wildtype. The individual gene log2 analysis showed a significant downregulation of the iron related gene *RBT5* in these mutants which was present in the yeast but not hypha inducing media. This gene is repressed by Tup1. Upregulation was seen in the gene set analysis of Cup2 and Zap1 related genes, but these changes do not account for the observed sensitivity of the mutants to copper.

The log2 values for many drug resistance related genes were upregulated in the *hda2*ΔΔ in YPD but not in RPMI, although the Hda2 or Hda3 expression levels were not significantly downregulated in any case (Figs. 4.8 and 4.47). No changed regulation was observed in RPMI. While several significant expression correlations with gene sets were found by GSEA analysis, significant differences of regulation between *hda2*ΔΔ and *hda3*ΔΔ strains were only noted in the YPD results including the *YAK1* related gene set.

Evaluation of gene sets that interact with *S. cerevisiae* Hda1, Hda2 and Hda3 show downregulation in most cases with the interesting exception of the *hda3*ΔΔ mutant in RPMI. Two regulators of *S. cerevisiae* Hda3 have significantly changed regulation in YPD

only, *SFP1* is downregulated in all the mutants (though not significantly in Hda3) and *XBP1* is upregulated in *hda2*ΔΔ. This suggests that these regulators may be networked with these proteins in *C. albicans* but the fact that their transcription is affected only in YPD suggests that their normal role may not exist in hypha inducing conditions. In the introduction we discussed the physical biochemical interactors of Hda1 (Tos3 and Pho85) (see Sections 1.8.2 and 1.9). Most of these genes have known orthologs in *C. albicans* (except *TOS3*). None of these genes showed changed regulation in either the YPD or RPMI results.

Finally, a *TBF1* related gene set was negatively correlated with the expression of genes in the *hda2*ΔΔ and *hda3*ΔΔ mutant in YPD and positively correlated in RPMI. As discussed in Section 1.8.2. the Tbf1 protein is involved in telomeric silencing. An evaluation of the log2 values of genes related to chromatin remodeling and silencing showed most significant changes to genes of this type in the *hda1*ΔΔ mutant in YPD only (see Appendix 3.2.10).

The differences that were seen in the comparison of phenotype and gene expression may be best accounted for by the observation that the expression levels of these proteins are reduced in hyphae inducing media (Fig. 4.48). Consequently, we have presented a model based on the activity and expressions observed in these different environmental conditions (Fig. 4.49).

In summary, this study has been designed to evaluate the potential of *E. coli* as an expression system for *C. albicans* Hda1, Hda2 and Hda3 proteins and to contribute to the understanding of the role of these proteins *in vivo*. The methods for expression and purification of these proteins and the data from RNA sequencing analysis can be used for further explorations toward understanding these proteins which complex, at least individually, with Hda1 in *C. albicans*. The following sections outline how this information fits into the existing fields of research on related topics.

5.1 Contributions of research on *C. albicans* Hda2 and Hda3

While yeast has been used as a model organism for a very long time, research on the pathogenic model yeast *C.* albicans, is relatively new. Its genome was first sequenced in 2004, eight years after the genome of *S. cerevisiae* (Jones et al. 2004; Mewes et al. 1997). This pathogenic organism offers a fast adapting system for responsive changes to gene expression, which is compelling from an epigenetic standpoint. Given the repeating

patterns of nature and conservative nature of evolution, it is certain that shadows of the mechanisms utilized in the *C. albicans* system are found in even distantly related organisms. The quickly adaptive nature of this yeast may provide mechanistic insights into histone deacetylase proteins which may be apparent on shorter observation of *C. albicans* than other experimental models. Consequently, similar molecular mechanisms in other, less reactive organisms may not be as readily observed. It is likely that at least some aspects of these gene expression systems are conserved and so the fruits of such research impact can be wide reaching.

In *S. cerevisiae*, all three components of the Hda1 complex must be present for Hda1 to have its deacetylase activity (see Section 1.8.1 and J Wu et al. 2001). It was also shown that Hda1 and Hda3 interact with Tup1 during deacetylation activity at Tup1 regulated promoters (see Section 1.12 and Jiansheng Wu et al. 2001). There are two possible explanations for this: either Hda2 is present for this interaction but not interfacing specifically with Tup1, or Tup1 is stabilizing the Hda1/Hda3 complex allowing it to function and/or the complex is functioning without Hda2 despite the absence of Hda2. In Chapter 4, we evaluated the Tup1 pathway related changes in the RNAseq gene expression data using GSEA analysis but did not see consistent differences in this pathway that are unique to any specific mutant or common to all three.

In analysis of the gene sets related to orthologs and regulators in *S. cerevisiae* (Fig. 4.47 and Appendix 3.2.11), gene sets for proteins that bind Hda1, Hda2 and Hda3 are downregulated in most of the mutants, which suggests that the proteins have conserved functions. In RPMI however, the *hda3*ΔΔ has a positive correlation with the gene group of *S. cerevisiae* binding partners. It is possible that in this environmental condition, there a redundant pathway allows for these gene sets to continue expression as though Hda3 were present.

The fact that histone deacetylase proteins have been conserved and even elaborated upon across evolution (see Section 1.5.2 and Gregoretti et al. 2004) emphasizes the importance of establishing an understanding of the function of these proteins. Compounding these qualities is the development of medicines that target these and other related proteins as treatments for various human diseases (see Section 1.5.3). The reality of using drugs that target conserved proteins is that multiple organisms are potentially susceptible. In a time where discussions about the human microbiome are developing, this is an important consideration particularly when concomitant infections contribute life

threatening symptoms in systemically compromised individuals (Hallen-Adams & Suhr 2017).

5.2 Limitations of this study

One important piece of this study is the reinforcement of the previous finding that deletion of Hda1 does not clearly reduce virulence. Given the adaptive nature of this organism, it is impossible to say that this is true across the board. The numerous microenvironments that *C. albicans* encounters in a host are difficult to replicate in an experimental setting.

In the sense that this study applies to the nature of *C. albicans* as a human health risk, it is important to note that in some situations, rates of *C. albicans* being the main culprit in infection are decreasing. Likewise, infections by some other species (for example *C. parapsilosis*) are on the rise (Pfaller & Diekema 2007). Targeting one organism in a population can change population dynamics and understanding drug resistance when many cohabiting and potentially invasive species are present in an individual is very complicated. The infection systems may not represent a realistic model for all human infection which can be distinct depending on the physiological niche affected. The *SAP8* gene, for example, which was downregulated in the mutants in hyphal growth conditions, typically has lower expression levels in oral infections (Naglik et al. 2003).

To evaluate the druggability of proteins like Hda2 and Hda3 it is ideal to solve the molecular structure. While *E. coli* is often a fast and effective system for expressing recombinant protein, it turned out to be complicated to use, which might be due to the adjustments that were made as attempts to compensate for the CUG clade attributes of Hda1, Hda2 and Hda3 proteins. Ideally, rather than skipping codon optimization for expression in *E. coli*, we might have created separate constructs for protein expression and reintegration into yeast. Additional issues around the sequence complexity of Hda3 may have also contributed at some unknown level. It should be kept in mind that GeneArt refused to synthesize Hda3 directly into the expression vector. This may indicate specific reliance on *C. albicans'* unique translation system.

Low levels of Hda3 were observed in the strain with natively tagged protein (Figs. 4.1 and 4.2). While the overall protein expression level was normalized by measurement of *ACT1* expression, it should be noted that the low levels of the protein could be due to the disruptive presence of the tag.

5.3 Future studies based on this research

This study has shown several new phenotypes related to *C. albicans* Hda2 and Hda3. It provides insights about expression, purification and crystallization of an Hda1 domain as well as the full-length protein. As this thesis contains some of the first studies of their type of Hda2 and Hda3 proteins in this fungal pathogen, this research provides a foundation for new explorations into these topics.

Establishing protocols for expression and purification of these proteins is the first step to structurally characterize these proteins. Additional studies can use protein harvested and purified by the protocols in Chapter 3 for single molecule work. This technique can assess, for example, the interactions between DNA binding domains and DNA or between the Arb2 domain and histones. The protein could also be used for crystallization studies as levels permitted. Beyond that, additional biochemical analysis can be done to look at functional acetylation of histones, complexing stoichiometry and binding kinetics. Possibilities for improvements to the existing protocols may be unveiled by experiments that test changes to the co-expression cloning set up, for example, by different use of pETDuet vectors (including co-expression of all three proteins) or experiments that adjustment expression or crystallization conditions. Further attempts to solubilize Hda1 catalytic domain constructs, Hda2 and Hda3 can be made, for example, protocols that solubilize and refold *E. coli* inclusion body aggregates can be trialed (Singh & Panda 2005). Constructs of the domains of Hda2 and Hda3 should be trialed, namely the DNA binding domain which has already been crystalized successfully in *S. cerevisiae* but also the coiled-coil domain. Coiled-coil domains are features of some human HDACs which allow for interaction with other proteins and self-association (Gregoretti et al. 2004). Understanding these domains may contribute to understanding the evolution of these proteins. Dimerization, self-association and association with other HDACs has been suggested as a strategy that allows for the flexible activity of to these proteins (Gregoretti et al. 2004).

Given the flexible nature of epigenetic modifications and *C. albicans* in general, the proposal that Hda2 and Hda3 would only interact with Hda1 seems unlikely. To further unveil other binding partners of these proteins, pull-down combined with mass spec analysis can be used. Outside partners would provide the proteins with functions that are unique. Another possibility is that the complex itself forms in different ways and different

combinations of Hda1, Hda2 and Hda3 proteins may have different roles in the cell. In this case, one of the proteins may be excluded or different stochiometric proportions may adjust functional interaction dynamics. Finally, the proteins may, in some capacities, work alone.

Further evaluation of the RNAseq data may point toward pathways that unveil their function in these capacities. Further experiments to evaluate phenotypes associated with orthologous proteins also have the potential to contribute an understanding of whether these proteins work only together in a set complex. For example, orthologous complex proteins in *S. cerevisiae* (Hda1) and *S. pombe* (Clr3) have roles in gene silencing. Strains are currently in the process of being built for testing the potential role of *C. albicans* Hda1, Hda2 and Hda3 in silencing (S. E. Rundlett et al. 1996; Hansen et al. 2005). Separately, experiments culminating in ChIPseq analysis can provide information about the proteins and their interaction with specific genetic loci (Wei et al. 2012).

Based on the existence of the Swi/Snf-like domain in *S. cerevisiae* Hda3 (Maskos, & Huber, 2009), I would like to propose that that the *C. albicans* Hda1 complexcontributes to what I call 'epigenetic transcriptional learning' through multitasked roles: deacetylating with Hda1 while using the Hda3 Swi/Snf domain to leave a mark. This impact from the interaction of Hda1 complex with chromatin would educate the proteins that later encounter the region. This takes form as a bookkeeping by documenting prior rounds of deacetylation. The mark might not specifically be implemented through histone modification but would perhaps be for example, a nucleosome borne area of openness or repression given the Swi/Snf domain's capacity for displacement of acetylated nucleosomes (Chandy et al. 2006). This mechanism would allow for a dynamic response (a flexible 'educated vs. uneducated' response), which can be employed within the *C. albicans* in response to 'educated vs. uneducated' host immune system. It would allow for better survival in future environmental niches (Tyc et al. 2016).

It has been shown that a lack of ATPase activity (observed within HDAC Swi/Snf) does not necessarily abolish chromatin remodeling (Lee et al. 2009; Bultman et al. 2005) The absence of this ATPase activity in *C. albicans* HDAC1 could support this proposed role of the Swi/Snf domain in documenting or 'writing' of epigenetic experience through may contribute relatively low levels of nucleosome remodeling (Lee et al. 2009; Bultman et al. 2005). While this is purely a hypothesis, future experiments can be designed to measure the level of histone deacetylation. Strains with point mutations can be tested with assays that monitor chromatin remodeling, for example: chromatin structure mapping by

DNase I or MNase. Also, transcriptional changes can be monitored by qRT-PCR or RNAseq and/or acetylation levels using ChIPseq or mass spectrometry (Wang & Simpson 2001; Baum et al. 2006; Kuo & Andrews 2013). In support of this hypothesis, it has been shown in the *S. pombe* Clr3 related SHREC complex, higher order chromatin structures are observed which result from the cooperation action of the HDAC and Mit1 (a SNF2 family ATPase) (Sugiyama et al. 2017).

The idea of "epigenetic memory" was suggested in the literature almost twenty years ago and an example was given based upon the HO endonuclease promoter of *S. cerevisiae* (Cosma et al. 1999). Like many acetylation regulated proteins, this gene is subject to complicated orchestrated direction by Swi proteins and the Swi/Snf complex. The timing of these players involves an interplay manipulated by cell cycle, protein levels, phosphorylation state, transient promoter complexing, nucleosome structure alterations and transcription factor regulated transcriptional programs. This activity ultimately results in a sustained switch to an active promoter state which has been shown to persist for several days within the G1 cell cycle despite absence of persistent triggering factors (Cosma et al. 1999; Krebs et al. 1999). The self-sustaining feedback loops of white-opaque switching that persist in cell lines in *C. albicans* are implicated as a form of transgenerational inheritance of epigenetic state that occurs separately from histone modification (Lim & Brunet 2013; Zordan et al. 2006). These are exciting developments that provide a foundation to shaping the future science of epigenetics. The fungal specific proteins Hda2 and Hda3 and their roles in complex with histone modifier Hda1 and potentially other *C. albicans* proteins can contribute to the landscape of this field.

5.4 Conclusion

This work relates to medical issues touching many people's lives today. Better understanding the evolution of systems of histone and protein modifications can contribute to the development of medical treatments. Histone deacetylase inhibitor drugs are a growing class in pharmaceutical industry with common applications in treatments of diseases including cancer (Eckschlager et al. 2017). We live in a world saturated by fungal pathogens and it is important to have information about how fast adapting pathogens respond to different environmental scenarios by evading host defenses and drug treatments. The scope of histone deacetylase inhibitor drugs includes treatment of fungal infection (Kmetzsch 2015). Beyond practical applications, the implications of a thorough

understanding of these ‘histone deacetylase proteins’ contribute to a model of evolutionary genetics and acetylation system dynamics. Studying these proteins through evolution, molecular anatomy and functional attributes is an important step toward developing a clear understanding of post translational regulation that occurs across the kingdoms of life.

Bibliography

Abshiru, N. et al., 2013. Chaperone-mediated acetylation of histones by Rtt109 identified by quantitative proteomics. Journal of proteomics, 81, pp.80–90.

Agilent, 2012. BL21-CodonPlus Competent Cells Instruction Manual, (Revision C.0), p.3.

Al-Fattani, M.A. & Douglas, L.J., 2006. Biofilm matrix of Candida albicans and Candida tropicalis: chemical composition and role in drug resistance. Journal of medical microbiology, 55(Pt 8), pp.999–1008.

Albaugh, B.N., Kolonko, E.M. & Denu, J.M., 2010. Kinetic mechanism of histone acetyltransferase and chaperone complex, Rtt109-Vps75. Biochemistry, 49(30), pp.6375–6385.

Alberts B, Johnson A, L.J., 2002. Molecular Biology of the Cell: Chromosomal DNA and Its Packaging in the Chromatin Fiber 4th ed., New York: Garland Science. Chapter 4 by browsing on NCBI [Accessed: 08/02/2019]

Almeida, R.S. et al., 2008. The Hyphal-Associated Adhesin and Invasin Als3 of Candida albicans Mediates Iron Acquisition from Host Ferritin A. P. Mitchell, ed. PLoS Pathogens, 4(11), e1000217.

Almeida, R.S., Wilson, D. & Hube, B., 2009. Candida albicans iron acquisition within the host. FEMS yeast research, 9(7), pp.1000–1012.

Altschul, S.F. et al., 1990. Basic local alignment search tool. Journal of molecular biology, 215(3), pp.403–410.

Altschul, S.F. et al., 1997. Gapped BLAST and PSI-BLAST: a new generation of protein database search programs. Nucleic acids research, 25(17), pp.3389–3402.

Alves, C.T. et al., 2014. Candida albicans promotes invasion and colonisation of Candida glabrata in a reconstituted human vaginal epithelium. The Journal of infection, 69(4), pp.396–407.

Anderson, J.M. & Soll, D.R., 1987. Unique phenotype of opaque cells in the white-opaque transition of Candida albicans. Journal of bacteriology, 169(12), pp.5579–5588.

Anderson, J.M. & Soll, D.R., 1987. Unique phenotype of opaque cells in the white-opaque transition of Candida albicans. Journal of bacteriology, 169(12), pp.5579–5588.

Anderson, M.Z. et al., 2014. Silencing Is Noisy: Population and Cell Level Noise in Telomere-Adjacent Genes Is Dependent on Telomere Position and Sir2 G. P. Copenhaver, ed. PLoS Genetics, 10(7), e1004436.

Andes, D. et al., 2004. Development and Characterization of an In Vivo Central Venous Catheter Candida albicans Biofilm Model . Infection and Immunity, 72(10), pp.6023–6031.

Andrews, S., 2010. FastQC: a quality control tool for high throughput sequence data. Available online at: http://www.bioinformatics.babraham.ac.uk/projects/ fastqc

Arndt, K. & Fink, G.R., 1986. GCN4 protein, a positive transcription factor in yeast, binds general control promoters at all 5 TGACTC 3 sequences. Proceedings of the National Academy of Sciences, 83(22), pp.8516–8520.

Ashburner, M. et al., 2000. Gene ontology: tool for the unification of biology. The Gene Ontology Consortium. Nature genetics, 25(1), pp.25–29.

Askree, S.H. et al., 2004. A genome-wide screen for Saccharomyces cerevisiae deletion mutants that affect telomere length. Proceedings of the National Academy of Sciences, 101(23), pp.8658–8663.

Azadmanesh, J. et al., 2017. Filamentation Involves Two Overlapping, but Distinct, Programs of Filamentation in the Pathogenic Fungus Candida albicans. G3: Genes|Genomes|Genetics, 7(11), pp.3797–3808.

Baell, J.B. & Miao, W., 2016. Histone acetyltransferase inhibitors: where art thou? Future Medicinal Chemistry, 8(13), pp.1525–1528.

Bain, J.M. et al., 2012. Non-lytic expulsion/exocytosis of Candida albicans from macrophages. Fungal Genetics and Biology, 49(9), pp.677–678.

Balasubramanyam, K. et al., 2004. Polyisoprenylated benzophenone, garcinol, a natural histone acetyltransferase inhibitor, represses chromatin transcription and alters global gene expression. The Journal of biological chemistry, 279(32), pp.33716–33726.

Balasubramanyam, K. et al., 2003. Small molecule modulators of histone acetyltransferase p300. The Journal of biological chemistry, 278(21), pp.19134–19140.

Balish, E. et al., 1999. Mucosal and systemic candidiasis in IL-8Rh−/− BALB/c mice. Journal of Leukocyte Biology, 66(1), pp.144–150.

Banerjee, M. et al., 2013. Expression of UME6, a Key Regulator of Candida albicans Hyphal Development, Enhances Biofilm Formation via Hgc1- and Sun41-Dependent Mechanisms. Eukaryotic Cell, 12(2), pp.224–232.

Banerjee, M. et al., 2008. UME6, a novel filament-specific regulator of Candida albicans hyphal extension and virulence. Molecular biology of the cell, 19(4), pp.1354–1365.

Bannister, A.J. & Kouzarides, T., 2011. Regulation of chromatin by histone modifications. Cell Res, 21(3), pp.381-395.
Baryshnikova, A. et al., 2010. Chapter 7 - Synthetic Genetic Array (SGA) Analysis in Saccharomyces cerevisiae and Schizosaccharomyces pombe. In Guide to Yeast Genetics: Functional Genomics, Proteomics, and Other Systems Analysis. Academic Press, pp. 145–179.
Bastidas, R.J., Heitman, J. & Cardenas, M.E., 2009. The Protein Kinase Tor1 Regulates Adhesin Gene Expression in Candida albicans S. G. Filler, ed. PLoS Pathogens, 5(2), p.e1000294.
Bauer, J. & Wendland, J., 2007. Candida albicans Sfl1 Suppresses Flocculation and Filamentation . Eukaryotic Cell, 6(10), pp.1736–1744.
Baum, M. et al., 2006. Formation of functional centromeric chromatin is specified epigenetically in Candida albicans. Proceedings of the National Academy of Sciences of the United States of America, 103(40), pp.14877–14882.
Beck, H.C. et al., 2006. Quantitative proteomic analysis of post-translational modifications of human histones. Molecular & cellular proteomics : MCP, 5(7), pp.1314–1325.
Begley, U. et al., 2007. Trm9 Catalyzed tRNA Modifications Link Translation to the DNA Damage Response. Molecular cell, 28(5), pp.860–870.
Behera, J. & Sinha, V.J. and B.N., 2015. Histone Deacetylase Inhibitors: A Review on Class-I Specific Inhibition. Mini-Reviews in Medicinal Chemistry, 15(9), pp.731–750.
Bennett, R.J. & Johnson, A.D., 2005. Mating in Candida albicans and the Search for a Sexual Cycle. Annu. Rev. Microbiol, 59, pp.233–55.
Bensen, E.S. et al., 2004. Transcriptional profiling in Candida albicans reveals new adaptive responses to extracellular pH and functions for Rim101p. Molecular microbiology, 54(5), pp.1335–1351.
Bernstein, B.E., Tong, J.K. & Schreiber, S.L., 2000. Genomewide studies of histone deacetylase function in yeast. Proceedings of the National Academy of Sciences of the United States of America, 97(25), pp.13708–13713.
Bezerra, A.R. et al., 2013. Reversion of a fungal genetic code alteration links proteome instability with genomic and phenotypic diversification. Proceedings of the National Academy of Sciences, 110(27), pp.11079–11084.
Biswas, K. & Morschhäuser, J., 2005. The Mep2p ammonium permease controls nitrogen starvation-induced filamentous growth in Candida albicans. Molecular Microbiology, 56(3), pp.649–669.
Biswas, S., Dijck, P. Van & Datta, A., 2007. Environmental Sensing and Signal Transduction Pathways Regulating Morphopathogenic Determinants of Candida albicans. Microbiology and Molecular Biology Reviews, 71(2), pp.348–376.
Biswas, S., Van Dijck, P. & Datta, A., 2007. Environmental Sensing and Signal Transduction Pathways Regulating Morphopathogenic Determinants of Candida albicans. Microbiology and Molecular Biology Reviews, 71(2), pp.348–376.
Biswas, S., Roy, M. & Datta, A., 2003. N-acetylglucosamine-inducible CaGAP1 encodes a general amino acid permease which co-ordinates external nitrogen source response and morphogenesis in Candida albicans. Microbiology (Reading, England), 149(Pt 9), pp.2597–2608.
Bjellqvist, B. et al., 1994. Reference points for comparisons of two-dimensional maps of proteins from different human cell types defined in a pH scale where isoelectric points correlate with polypeptide compositions. Electrophoresis, 15(3–4), pp.529–539.
Bjellqvist, B. et al., 1993. The focusing positions of polypeptides in immobilized pH gradients can be predicted from their amino acid sequences. Electrophoresis, 14(10), pp.1023–1031.
Bjerling, P. et al., 2002. Functional Divergence between Histone Deacetylases in Fission Yeast by Distinct Cellular Localization and In Vivo Specificity. MOLECULAR AND CELLULAR BIOLOGY, 22(7), pp.2170–2181.
Bommanavar, S.B., Gugwad, S. & Malik, N., 2017. Phenotypic switch: The enigmatic white-gray-opaque transition system of Candida albicans. Journal of oral and maxillofacial pathology : JOMFP, 21(1), pp.82–86.
Bonaldi, T. et al., 2003. Monocytic cells hyperacetylate chromatin protein HMGB1 to redirect it towards secretion. The EMBO Journal, 22(20), p.5551-5560.
Bongomin, F. et al., 2017. Global and Multi-National Prevalence of Fungal Diseases—Estimate Precision. Journal of Fungi, 3(4), p.57.
Bonnet, J. et al., 2014. The SAGA coactivator complex acts on the whole transcribed genome and is required for RNA polymerase II transcription. Genes & Development, 28(18), pp.1999–2012.
Bottomley, M.J. et al., 2008. Structural and Functional Analysis of the Human HDAC4 Catalytic Domain Reveals a Regulatory Structural Zinc-binding Domain. The Journal of Biological Chemistry, 283(39), pp.26694–26704.

Boyce, K.J. & Andrianopoulos, A., 2015. Fungal dimorphism: the switch from hyphae to yeast is a specialized morphogenetic adaptation allowing colonization of a host. FEMS Microbiology Reviews, 39(6), pp.797–811.
Brand, A., 2012. Hyphal growth in human fungal pathogens and its role in virulence. International Journal of Microbiology, p.11.
Braun, B.R. & Johnson, A.D., 2000. TUP1, CPH1 and EFG1 make independent contributions to filamentation in Candida albicans. Genetics, 155(1), pp. 57-67.
Brega, E., Zufferey, R. & Mamoun, C. Ben, 2004. Candida albicans Csy1p Is a Nutrient Sensor Important for Activation of Amino Acid Uptake and Hyphal Morphogenesis. Eukaryotic Cell, 3(1), pp.135–143.
Brès, V. et al., 2002. Differential acetylation of Tat coordinates its interaction with the co-activators cyclin T1 and PCAF. The EMBO Journal, 21(24), p.6811-6819.
Brown, A.J.P. & Gow, N.A.R., 1999. Regulatory networks controlling Candida albicans morphogenesis. Trends in Microbiology, 7(8), pp.333–338.
Brown, D.H. et al., 1999. Filamentous growth of Candida albicans in response to physical environmental cues and its regulation by the unique CZF1 gene. Nov 34(4), pp.651-662.
Brown, G.D. et al., 2012. Hidden killers: Human fungal infections. Science Translational Medicine, 4(165), pp.165rv13.
Buchman, C. et al., 1990. A single amino acid change in CUP2 alters its mode of DNA binding. Molecular and cellular biology, 10(9), pp.4778–4787.
Buchman, C. et al., 1989. The CUP2 gene product, regulator of yeast metallothionein expression, is a copper-activated DNA-binding protein. Molecular and cellular biology, 9(9), pp.4091–4095.
Buffo, J., Herman, M.A. & Soll, D.R., 1984. A characterization of pH-regulated dimorphism in Candida albicans. Mycopathologia, 85(1–2), pp.21–30.
Buker, S.M. et al., 2007. Two different Argonaute complexes are required for siRNA generation and heterochromatin assembly in fission yeast. Nature Structural and Molecular Biology, 14(3), pp.200–207.
Bultman, S.J., Gebuhr, T.C. & Magnuson, T., 2005. A Brg1 mutation that uncouples ATPase activity from chromatin remodeling reveals an essential role for SWI/SNF-related complexes in β-globin expression and erythroid development. Genes & Development, 19(23), pp.2849–2861.
van Burik, J.-A.H. & Magee, P.T., 2001. Aspects of Fungal Pathogenesis in Humans. Annual Review of Microbiology, 55(1), pp.743–772.
Butler, G. et al., 2009. Evolution of pathogenicity and sexual reproduction in eight Candida genomes. Nature, 459, p.657.
Cantwell, A.M. & Cerca, E.D., 2006. Determinants of Thrombin Specificity. Annals of the New York Academy of Sciences, 936(1), pp.133–146.
Cao, F. et al., 2006. The Flo8 Transcription Factor Is Essential for Hyphal Development and Virulence in Candida albicans T. Stearns, ed. Molecular Biology of the Cell, 17(1), pp.295–307.
Cao, J. & Yan, Q., 2012. Histone Ubiquitination and Deubiquitination in Transcription, DNA Damage Response, and Cancer. Frontiers in Oncology, 2, p.26.
Carlson, E., 1982. Synergistic effect of Candida albicans and Staphylococcus aureus on mouse mortality. Infection and immunity, 38(3), pp.921–924.
Carmen, A.A., Rundlett, S.E. & Grunstein, M., 1996. HDA1 and HDA3 are components of a yeast histone deacetylase (HDA) complex. The Journal of biological chemistry, 271(26), pp.15837–15844.
Caron, C., Boyault, C. & Khochbin, S., 2005. Regulatory cross-talk between lysine acetylation and ubiquitination: role in the control of protein stability. BioEssays, 27(4), pp.408–415.
De Castro, P.A. et al., 2013. Identification of the cell targets important for propolis-induced cell death in Candida albicans. Fungal Genetics and Biology, Nov; 60, pp.74-86.
Centers for Disease Control and Prevention, 2017. CDC Other Fungal Diseases Talaromycosis. September 26, 2017. Available at: https://www.cdc.gov/fungal/diseases/other/talaromycosis.html [Accessed January 24, 2019].
Centers for Disease Control and Prevention, 2018. Types of Fungal Diseases. Centers for Disease Control and Prevention, (Last Update 01.05.2018). Available at: https://www.cdc.gov/fungal/diseases/index.html [Accessed September 23, 2018].
Chakalova, L. & Fraser, P., 2010. Organization of Transcription. Cold Spring Harbor Perspectives in Biology, 2(9), a000729.
Chan, C.T.Y. et al., 2012. Reprogramming of tRNA modifications controls the oxidative stress response by codon-biased translation of proteins. Nature communications, 3, p.937.
Chandy, M. et al., 2006. SWI/SNF Displaces SAGA-Acetylated Nucleosomes. Eukaryotic Cell, 5(10), pp.1738–1747.
Chang, P., Fan, X. & Chen, J., 2015. Function and subcellular localization of Gcn5, a histone acetyltransferase in Candida albicans. Fungal Genetics and Biology, 81, pp.132–141.

Chen, H. et al., 2004. Tyrosol is a quorum-sensing molecule in Candida albicans. Proceedings of the National Academy of Sciences of the United States of America, 101(14), pp.5048–5052.
Cheung, P., Allis, C.D. & Sassone-Corsi, P., 2000. Signaling to Chromatin through Histone Modifications. Cell, 103(2), pp.263–271.
Choudhary, C. et al., 2009. Lysine Acetylation Targets Protein Complexes and Co-Regulates Major Cellular Functions. Science, 325(5942), p.834-840.
Christoph, S. et al., 2012. The stepwise acquisition of fluconazole resistance mutations causes a gradual loss of fitness in Candida albicans. Molecular Microbiology, 86(3), pp.539–55. Molecular Microbiology, 86(3), pp.539–556.
Chu, D. & von der Haar, T., 2012. The architecture of eukaryotic translation. Nucleic Acids Research, 40(20), pp.10098–10106.
Cieniewicz, A.M. et al., 2014. The Bromodomain of Gcn5 Regulates Site Specificity of Lysine Acetylation on Histone H3. Molecular & Cellular Proteomics : MCP, 13(11), pp.2896–2910.
Ciesielski, F. et al., 2016. Recognition of Membrane Sterols by Polyene Antifungals Amphotericin B and Natamycin, A (13)C MAS NMR Study. Frontiers in Cell and Developmental Biology, 4, p.57.
Cipollina, C. et al., 2008. Saccharomyces cerevisiaeSFP1: at the crossroads of central metabolism and ribosome biogenesis. Microbiology, 154(6), pp.1686–1699.
Citiulo, F. et al., 2012. Candida albicans Scavenges Host Zinc via Pra1 during Endothelial Invasion A. P. Mitchell, ed. PLoS Pathogens, 8(6), e1002777.
Clancy, C.J. et al., 2006. Characterizing the Effects of Caspofungin on Candida albicans, Candida parapsilosis, and Candida glabrata Isolates by Simultaneous Time-Kill and Postantifungal-Effect Experiments. Antimicrobial Agents and Chemotherapy, 50(7), pp.2569–2572.
Clark-Adams, C. et al., 1988. Changes in Histone dosage alter transcription in yeast. Genes and Development, 2, pp.150–159.
Cole, M.F. et al., 1995. Avirulence of Candida albicans auxotrophic mutants in a rat model of oropharyngeal candidiasis. FEMS microbiology letters, 126(2), pp.177–180.
Consortium, T.G.O., 2017. Expansion of the Gene Ontology knowledgebase and resources. Nucleic acids research, 45(D1), pp.D331–D338.
Coombes, K.R. et al., 2005. Understanding the characteristics of mass spectrometry data through the use of simulation. Cancer Informatics, 1(1), pp.41–52.
Cosma, M.P., Tanaka, T. & Nasmyth, K., 1999. Ordered Recruitment of Transcription and Chromatin Remodeling Factors to a Cell Cycle and Developmentally Regulated Promoter. Cell, 97(3), pp.299–311.
Cowen, L.E. et al., 2009. Harnessing Hsp90 function as a powerful, broadly effective therapeutic strategy for fungal infectious disease. Proceedings of the National Academy of Sciences of the United States of America, 106(8), pp.2818–2823.
Cowen, L.E., 2009. Hsp90 Orchestrates Stress Response Signaling Governing Fungal Drug Resistance H. D. Madhani, ed. PLoS Pathogens, 5(8), e1000471.
Cowen, L.E. et al., 2002. Population genomics of drug resistance in Candida albicans Proceedings of the National Academy of Sciences, 99(14), p.9284-9289.
Csank, C. et al., 1998. Roles of the Candida albicans Mitogen-Activated Protein Kinase Homolog, Cek1p, in Hyphal Development and Systemic Candidiasis. Infection and Immunity, 66(6), pp.2713–2721.
D'Arcy, S. & Luger, K., 2011. Understanding Histone Acetyltransferase Rtt109 Structure and Function: how many chaperones does it take? Current opinion in structural biology, 21(6), pp.728–734.
Dalle, F. et al., 2010. Cellular interactions of Candida albicans with human oral epithelial cells and enterocytes. Cellular Microbiology, 12(2), pp.248–271.
Damery, S. et al., 2013. Assessing the predictive value of HIV indicator conditions in general practice: A case-control study using the THIN database. British Journal of General Practice, 63(611), pp.370–377.
Daniels, K.J. et al., 2013. Impact of Environmental Conditions on the Form and Function of Candida albicans Biofilms. Eukaryotic Cell, 12(10), pp.1389–1402.
Daniels, K.J. et al., 2006. Opaque cells signal white cells to form biofilms in Candida albicans. The EMBO journal, 25(10), pp.2240–2252.
Daniluk, T. et al., 2006. Occurrence rate of oral Candida albicans in denture wearer patients. Advances in medical sciences, 51 Suppl 1, pp.77–80.
Dastidar, R.G. et al., 2012. The nuclear localization of SWI/SNF proteins is subjected to oxygen regulation. Cell and Bioscience, 2(1), pp.1–13.
Davis, D., Wilson, R.B. & Mitchell, A.P., 2000. RIM101-dependent and-independent pathways govern pH responses in Candida albicans. Molecular and cellular biology, 20(3), pp.971–978.
Davis, W., 2010. A plasmid Editor (ApE), p.v.1.17. Available at: http://jorgensen.biology.utah.edu/wayned/ape/

Dehennaut, V., Leprince, D. & Lefebvre, T., 2014. O-GlcNAcylation, an Epigenetic Mark. Focus on the Histone Code, TET Family Proteins, and Polycomb Group Proteins. Frontiers in Endocrinology, 5, p.155.
DeLano, W.L., 2009. PyMOL: An open-source molecular graphics tool. CCP4 Newsletter on protein crystallography, 40, pp.82–92.
DeLano, W.L., 2002. PyMOL. DeLano Scientific, San Carlos, CA, p.700. Available at: https://pymol.org/2/
Denning, D.W., 2015. The ambitious "95-95 by 2025" roadmap for the diagnosis and management of fungal diseases. Thorax, 70(7), pp.613–614.
Denning, D.W. & Hope, W.W., 2010. Therapy for fungal diseases: Opportunities and priorities. Trends in Microbiology, 18(5), pp.195–204.
Desai, J. V, Mitchell, A.P. & Andes, D.R., 2014. Fungal Biofilms, Drug Resistance, and Recurrent Infection. Cold Spring Harbor Perspectives in Medicine, 4(10), a019729.
Dessau, M.A. & Modis, Y., 2011. Protein Crystallization for X-ray Crystallography. Journal of Visualized Experiments : JoVE, (47), p.2285.
Dever, T.E., Kinzy, T.G. & Pavitt, G.D., 2016. Mechanism and Regulation of Protein Synthesis in Saccharomyces cerevisiae. Genetics, 203(1), pp.65–107.
Dhalluin, C. et al., 1999. Structure and ligand of a histone acetyltransferase bromodomain. Nature, 399, p.491.
Diez-Orejas, R. et al., 1997. Reduced virulence of Candida albicans MKC1 mutants: a role for mitogen-activated protein kinase in pathogenesis. Infection and Immunity, 65(2), p.833-837.
Diwischek, F., Morschhäuser, J. & Holzgrabe, U., 2009. Cerulenin Analogues as Inhibitors of Efflux Pumps in Drug-resistant Candida albicans. Archiv der Pharmazie, 342(3), pp.150–164.
Donlan, R.M. & Costerton, J.W., 2002. Biofilms: Survival Mechanisms of Clinically Relevant Microorganisms. Clinical Microbiology Reviews, 15(2), pp.167–193.
Douglas, C.M., 2001. Fungal beta(1,3)-D-glucan synthesis. Medical mycology, 39 Suppl 1, pp.55–66.
Douglas, C.M. et al., 1997. Identification of the FKS1 gene of Candida albicans as the essential target of 1,3-beta-D-glucan synthase inhibitors. Antimicrobial agents and chemotherapy, 41(11), pp.2471–2479.
Downes, M. et al., 2000. Identification of a nuclear domain with deacetylase activity. Proceedings of the National Academy of Sciences of the United States of America, 97(19), pp.10330–10335.
Dühring, S. et al., 2015. Host-pathogen interactions between the human innate immune system and Candida albicans—understanding and modeling defense and evasion strategies. Frontiers in Microbiology, 6, p.625.
Dumon-Seignovert, L., Cariot, G. & Vuillard, L., 2004. The toxicity of recombinant proteins in Escherichia coli: a comparison of overexpression in BL21(DE3), C41(DE3), and C43(DE3). Protein expression and purification, 37(1), pp.203–206.
Duncan, E.M. et al., 2008. Cathepsin L Proteolytically Processes Histone H3 During Mouse Embryonic Stem Cell Differentiation. Cell, 135(2), pp.284–294.
Eberharter, A. & Becker, P.B., 2002. Histone acetylation: a switch between repressive and permissive chromatin. Second in review series on chromatin dynamics. EMBO reports, 3(3), pp.224–229.
Eckschlager, T. et al., 2017. Histone Deacetylase Inhibitors as Anticancer Drugs. International Journal of Molecular Sciences, 18(7), p.1414.
Eisman, B. et al., 2006. The Cek1 and Hog1 mitogen-activated protein kinases play complementary roles in cell wall biogenesis and chlamydospore formation in the fungal pathogen Candida albicans. Eukaryotic cell, 5(2), pp.347–358.
Ellegren, H., 2004. Microsatellites: simple sequences with complex evolution. Nature Reviews Genetics, 5, p.435.
Ene, I. V et al., 2016. Phenotypic Profiling Reveals that Candida albicans Opaque Cells Represent a Metabolically Specialized Cell State Compared to Default White Cells M. B. Whiteway Judith, ed. mBio, 7(6), e01269-16.
Ene, I. V et al., 2018. Global analysis of mutations driving microevolution of a heterozygous diploid fungal pathogen. Proceedings of the National Academy of Sciences, 115(37), pp.E8688--E8697.
Enjalbert, B. et al., 2006. Role of the Hog1 stress-activated protein kinase in the global transcriptional response to stress in the fungal pathogen Candida albicans. Molecular biology of the cell, 17(2), pp.1018–1032.
Enjalbert, B., Nantel, A. & Whiteway, M., 2003. Stress-induced gene expression in Candida albicans: absence of a general stress response. Molecular biology of the cell, 14(4), pp.1460–7.
Erdel, F. & Rippe, K., 2018. Formation of Chromatin Subcompartments by Phase Separation. Biophysical Journal, 114(10), pp.2262–2270.
Espinel-Ingroff, A. et al., 2014. Multilaboratory Study of Epidemiological Cutoff Values for Detection of Resistance in Eight Candida Species to Fluconazole, Posaconazole, and Voriconazole. Antimicrobial Agents and Chemotherapy, 58(4), pp.2006–2012.

Fahrenkrog, B., 2015. Histone modifications as regulators of life and death in Saccharomyces cerevisiae. Microbial Cell, 3(1), pp.1–13.
Fairhead, M. & Howarth, M., 2015. Site-specific biotinylation of purified proteins using BirA. Methods in molecular biology (Clifton, N.J.), 1266, pp.171–184.
Falk, H. et al., 2011. An efficient high-throughput screening method for MYST family acetyltransferases, a new class of epigenetic drug targets. Journal of biomolecular screening, 16(10), pp.1196–1205.
Fang, Z. & Cui, X., 2011. Design and validation issues in RNA-seq experiments. Briefings in Bioinformatics, 12(3), pp.280–287.
Feng, Q. et al., 1999. Ras Signaling Is Required for Serum-Induced Hyphal Differentiation in Candida albicans. Journal of Bacteriology, 181(20), p.6339-6346.
Finkel, J.S. & Mitchell, A.P., 2011. GENETIC CONTROL OF CANDIDA ALBICANS BIOFILM DEVELOPMENT. Nature reviews. Microbiology, 9(2), pp.109–118.
Finn, R.D. et al., 2016. The Pfam protein families database: towards a more sustainable future. Nucleic Acids Research, 44(D1), pp.D279–D285.
Fischle, W., Wang, Y. & Allis, C.D., 2003. Histone and chromatin cross-talk. Current Opinion in Cell Biology, 15(2), pp.172–183.
Fonzi, W.A. & Irwin, M.Y., 1993. Isogenic Strain Construction and Gene Mapping in Candida Albicans. Genetics, 134(3), pp.717–728.
Fox, E.P. & Nobile, C.J., 2012. A sticky situation: Untangling the transcriptional network controlling biofilm development in Candida albicans. Transcription, 3(6), pp.315–322.
Fox, N.K., Brenner, S.E. & Chandonia, J.-M., 2014. SCOPe: Structural Classification of Proteins—extended, integrating SCOP and ASTRAL data and classification of new structures. Nucleic Acids Research, 42(D1), pp.D304–D309.
Frazier, J.A. et al., 1998. Polymerization of Purified Yeast Septins: Evidence That Organized Filament Arrays May Not Be Required for Septin Function . The Journal of Cell Biology, 143(3), pp.737–749.
Freire-Benéitez, V. et al., 2016a. Candida albicans repetitive elements display epigenetic diversity and plasticity. Scientific Reports, 6, p.22989.
Ganguly, S. et al., 2011. Zap1 Control of Cell-Cell Signaling in Candida albicans Biofilms. Eukaryotic Cell, 10(11), p.1448-1454.
Gao, L. et al., 2002. Cloning and functional characterization of HDAC11, a novel member of the human histone deacetylase family. The Journal of biological chemistry, 277(28), pp.25748–25755.
García-Sánchez, S. et al., 2004. Candida albicans Biofilms: a Developmental State Associated With Specific and Stable Gene Expression Patterns. Eukaryotic Cell, 3(2), pp.536–545.
Garcia, B.A. et al., 2007. Organismal differences in post-translational modifications in histones H3 and H4. The Journal of biological chemistry, 282(10), pp.7641–7655.
Garcia, M.G. et al., 2001. Isolation of a Candida albicans gene, tightly linked to URA3, coding for a putative transcription factor that suppresses a Saccharomyces cerevisiae aft1 mutation. Yeast (Chichester, England), 18(4), pp.301–311.
Garey, K.W. et al., 2006. Time to Initiation of Fluconazole Therapy Impacts Mortality in Patients with Candidemia: A Multi-Institutional Study. Clinical Infectious Diseases, 43(1), pp.25–31.
Garnaud, C. et al., 2016. Histone Deacetylases and Their Inhibition in Candida Species. Frontiers in Microbiology, 7, p.1238.
Gashaw, I. et al., 2011. What makes a good drug target? Drug Discovery Today, 16(23–24), pp.1037–1043.
Gasteiger, E. et al., 2003. ExPASy: the proteomics server for in-depth protein knowledge and analysis. Nucleic Acids Research, 31(13), pp.3784–3788.
Gasteiger, E. et al., 2005. Protein Identification and Analysis Tools on the ExPASy Server. In The Proteomics Protocols Handbook. pp. 571–607.
Geer, L.Y. et al., 2010. The NCBI BioSystems database. Nucleic Acids Research, 38(suppl_1), pp.D492–D496.
Gerami-Nejad, M., Berman, J. & Gale, C.A., 2001. Cassettes for PCR-mediated construction of green, yellow, and cyan fluorescent protein fusions in Candida albicans. Yeast, 18(9), pp.859–864.
Gerwien, F. et al., 2018. Metals in fungal virulence. FEMS Microbiology Reviews, 42(1), fux050.
Ghannoum, M.A. & Rice, L.B., 1999. Antifungal Agents: Mode of Action, Mechanisms of Resistance, and Correlation of These Mechanisms with Bacterial Resistance. Clinical Microbiology Reviews, 12(4), pp.501–517.
Giusani, A.D., Vinces, M. & Kumamoto, C.A., 2002. Invasive Filamentous Growth of Candida albicans Is Promoted by Czf1p-Dependent Relief of Efg1p-Mediated Repression. Genetics, 160(4), pp.1749–1753.
Glozak, M.A. et al., 2005. Acetylation and deacetylation of non-histone proteins. Gene, 363(1–2), pp.15–23.

Gomes, A.C. et al., 2007. A genetic code alteration generates a proteome of high diversity in the human pathogen Candida albicans. Genome Biology, 8(10), p.R206.
Gomes, A.R. et al., 2016. An Overview of Heterologous Expression Host Systems for the Production of Recombinant Proteins. Advances in Animal and Veterinary Sciences, 4(7), pp.346–356.
Govind, C.K. et al., 2007. Gcn5 promotes acetylation, eviction, and methylation of nucleosomes in transcribed coding regions. Molecular cell, 25(1), pp.31–42.
Gow, N.A. & Gooday, G.W., 1982. Growth kinetics and morphology of colonies of the filamentous form of Candida albicans. Journal of general microbiology, 128(9), pp.2187–2194.
Gow, N.A.R., Brown, A.J.P. & Odds, F.C., 2002. Fungal morphogenesis and host invasion. Current opinion in microbiology, 5(4), pp.366–371.
Gow, N.A.R. & Netea, M.G., 2016. Medical mycology and fungal immunology: new research perspectives addressing a major world health challenge. Philosophical Transactions of the Royal Society B: Biological Sciences, 371(1709), 20150462.
Goyard, S. et al., 2008. The Yak1 Kinase Is Involved in the Initiation and Maintenance of Hyphal Growth in Candida albicans D. Lew, ed. Molecular Biology of the Cell, 19(5), pp.2251–2266.
Grant, P.A. et al., 1999. Expanded lysine acetylation specificity of Gcn5 in native complexes. The Journal of biological chemistry, 274(9), pp.5895–5900.
Gregoretti, I., Lee, Y.-M. & Goodson, H. V, 2004. Molecular Evolution of the Histone Deacetylase Family: Functional Implications of Phylogenetic Analysis. Journal of Molecular Biology, 338(1), pp.17–31.
Grewal, S.I.S. & Elgin, S.C.R., 2002. Heterochromatin: New possibilities for the inheritance of structure. Current Opinion in Genetics and Development, 12(2), pp.178–187.
Gropp, K. et al., 2009. The yeast Candida albicans evades human complement attack by secretion of aspartic proteases. Molecular immunology, 47(2–3), pp.465–475.
Grozinger, C.M., Hassig, C.A. & Schreiber, S.L., 1999. Three proteins define a class of human histone deacetylases related to yeast Hda1p. Biochemistry, 96, pp.4868–4873.
Guan, G. et al., 2013. Bcr1 plays a central role in the regulation of opaque cell filamentation in Candida albicans. Molecular microbiology, 89(4), pp.732–750.
Gudlaugsson, O. et al., 2003. Attributable Mortality of Nosocomial Candidemia, Revisited. Clinical Infectious Diseases, 37(9), pp.1172–1177.
Guelen, L. et al., 2008. Domain organization of human chromosomes revealed by mapping of nuclear lamina interactions. Nature, 453, p.948.
Guillemette, B. et al., 2011. H3 Lysine 4 Is Acetylated at Active Gene Promoters and Is Regulated by H3 Lysine 4 Methylation. PLOS Genetics, 7(3), e1001354.
Guinea, J., 2014. Global trends in the distribution of Candida species causing candidemia. Clinical Microbiology and Infection, 20(6), pp.5–10.
Guinea, J., 2014. Global trends in the distribution of Candida species causing candidemia. Clinical Microbiology and Infection, 20(s6), pp.5–10.
Gulati, M. & Nobile, C.J., 2016. Candida albicans biofilms: development, regulation, and molecular mechanisms. Microbes and Infection, 18(5), pp.310–321.
Gutiérrez, J.L. et al., 2007. Activation domains drive nucleosome eviction by SWI/SNF. The EMBO Journal, 26(3), pp.730–740.
von der Haar, T., 2007. Optimized protein extraction for quantitative proteomics of yeasts. PLoS ONE, 2(10), e1078.
Haberland, M., Montgomery, R.L. & Olson, E.N., 2009. The many roles of histone deacetylases in development and physiology: implications for disease and therapy. Nat Rev Genet, 10(1), pp.32–42.
Hall, R.A. et al., 2011. The Quorum-Sensing Molecules Farnesol/Homoserine Lactone and Dodecanol Operate via Distinct Modes of Action in Candida albicans. Eukaryotic Cell, 10(8), pp.1034–1042.
Hall, R.A. & Gow, N.A.R., 2013. Mannosylation in Candida albicans: role in cell wall function and immune recognition. Molecular Microbiology, 90(6), pp.1147–1161.
Hallen-Adams, H.E. & Suhr, M.J., 2017. Fungi in the healthy human gastrointestinal tract. Virulence, 8(3), pp.352–358.
Hansen, K.R. et al., 2005. Global Effects on Gene Expression in Fission Yeast by Silencing and RNA Interference Machineries . Molecular and Cellular Biology, 25(2), pp.590–601.
Hao, B. et al., 2009. Candida albicans RFX2 Encodes a DNA Binding Protein Involved in DNA Damage Responses, Morphogenesis, and Virulence . Eukaryotic Cell, 8(4), pp.627–639.
Harcus, D. et al., 2004. Transcription Profiling of Cyclic AMP Signaling in Candida albicans K. Yamamoto, ed. Molecular Biology of the Cell, 15(10), pp.4490–4499.
Hawksworth, D.L. & Lucking, R., 2017. Fungal Diversity Revisited: 2.2 to 3.8 Million Species. Microbiology spectrum, 5(4).

Henikoff, B.M. & Turner, S., 2006. Is it a Code: The Debate. The Scientist, (May 1). Available at: https://www.the-scientist.com/uncategorized/is-it-a-code-the-debate-47600. [Accessed: February 8, 2019]
Hernday, A.D. et al., 2010. Genetics and molecular biology in Candida albicans. Methods in Enzymology. vol. 470, pp.737-758.
Heymann, P. et al., 2002. The siderophore iron transporter of Candida albicans (Sit1p/Arn1p) mediates uptake of ferrichrome-type siderophores and is required for epithelial invasion. Infection and immunity, 70(9), pp.5246–5255.
Hickman, M.A. et al., 2013. The 'obligate diploid' Candida albicans forms mating-competent haploids. Nature, 494(7435), pp.55–59.
Hiller, D., Sanglard, D. & Morschhauser, J., 2006. Overexpression of the MDR1 gene is sufficient to confer increased resistance to toxic compounds in Candida albicans. Antimicrobial agents and chemotherapy, 50(4), pp.1365–1371.
Hnisz, D. et al., 2012. A histone deacetylase adjusts transcription kinetics at coding sequences during Candida albicans morphogenesis. PLoS genetics, 8(12), e1003118.
Hnisz, D. et al., 2010. The Set3/Hos2 Histone Deacetylase Complex Attenuates cAMP/PKA Signaling to Regulate Morphogenesis and Virulence of Candida albicans. PLOS Pathogens, 6(5), p.e1000889. Available at: https://doi.org/10.1371/journal.ppat.1000889.
Hnisz, D., Schwarzmüller, T. & Kuchler, K., 2009. Transcriptional loops meet chromatin: a dual-layer network controls white–opaque switching in Candida albicans. Molecular Microbiology, 74(1), pp.1–15.
Hnisz, D., Sehwarzmüller, T. & Kuchler, K., 2009. Transcriptional loops meet chromatin: A dual-layer network controls white-opaque switching in Candida albicans. Molecular Microbiology, 74(1), pp.1–15.
Hoberg, K.A., Cihlar, R.L. & Calderone, R.A., 1983. Inhibitory effect of cerulenin and sodium butyrate on germination of Candida albicans. Antimicrobial Agents and Chemotherapy, 24(3), pp.401–408.
Hobson, R.P. et al., 2004. Loss of cell wall mannosylphosphate in Candida albicans does not influence macrophage recognition. The Journal of biological chemistry, 279(38), pp.39628–39635.
Homann, O.R. et al., 2009. A Phenotypic Profile of the Candida albicans Regulatory Network. PLOS Genetics, 5(12), e1000783.
van het Hoog, M. et al., 2007. Assembly of the Candida albicans genome into sixteen supercontigs aligned on the eight chromosomes. Genome Biology, 8(4), p.R52.
Hope, H. et al., 2008. Activation of Rac1 by the Guanine Nucleotide Exchange Factor Dck1 Is Required for Invasive Filamentous Growth in the Pathogen Candida albicans P. J. Brennwald, ed. Molecular Biology of the Cell, 19(9), pp.3638–3651.
Hope, W.W., 2010. Flucytosine (5-fluorocytosine; 5FC). In Kucers' The Use of Antibiotics (ed. M. Lindsay Grayson, 2012 CRC Press). pp. 2919–2926.
Hornby, J.M. et al., 2001. Quorum Sensing in the Dimorphic Fungus Candida albicans Is Mediated by Farnesol. Applied and Environmental Microbiology, 67(7), pp.2982–2992.
Hoyer, L.L., 2001. The ALS gene family of Candida albicans. Trends in Microbiology, 9(4), pp.176–180.
Huang, G. et al., 2006. Bistable expression of WOR1, a master regulator of white-opaque switching in Candida albicans. Proceedings of the National Academy of Sciences, 103(34), pp.12813–12818.
Huang, H. et al., 2017. Landscape of the regulatory elements for lysine 2-hydroxyisobutyrylation pathway. Cell Research, 28, p.111.
Hube, B. et al., 2000. Secreted lipases of Candida albicans: cloning, characterisation and expression analysis of a new gene family with at least ten members. Archives of Microbiology, 174(5), pp.362–374..
Hughes, C.D. et al., 2014. Single molecule techniques in DNA repair: A primer. DNA repair, 20, pp.2–13.
Hull, C.M. & Johnson, A.D., 1999. Identification of a mating type-like locus in the asexual pathogenic yeast Candida albicans. Science (New York, N.Y.), 285(5431), pp.1271–1275.
Hull, C.M., Raisner, R.M. & Johnson, A.D., 2000. Evidence for Mating of the "Asexual" Yeast Candida albicans in a Mammalian Host. Science, 289(5477), p.307-310.
Iglesias, N. & Moazed, D., 2017. Silencing repetitive DNA. eLife, 6, e29503.
Imai, S. et al., 2000. Transcriptional silencing and longevity protein Sir2 is an NAD- dependent histone deacetylase. Nature, 403(6771), pp.795–800.
Ishii, N. et al., 1997. Biochemical and genetic characterization of Rbf1p, a putative transcription factor of Candida albicans. Microbiology (Reading, England), 143 (Pt 2), pp.429–435.
Jacobsen, I.D. et al., 2012. Candida albicans dimorphism as a therapeutic target. Expert review of anti-infective therapy, 10(1), pp.85–93.
Jeon, J., Kwon, S. & Lee, Y.H., 2014. Histone acetylation in fungal pathogens of plants. Plant Pathology Journal, 30(1), pp.1–9.
Job, G. et al., 2016. SHREC Silences Heterochromatin via Distinct Remodeling and Deacetylation Modules. Molecular Cell, 62(2), pp.207–221.

Johnnidis, J.B. et al., 2008. Regulation of progenitor cell proliferation and granulocyte function by microRNA-223. Nature, 451(7182), pp.1125–1129.
Johnsson, A. et al., 2009. HAT–HDAC interplay modulates global histone H3K14 acetylation in gene-coding regions during stress. EMBO Reports, 10(9), pp.1009–1014.
Jones, K.E. et al., 2008. Global trends in emerging infectious diseases HHS Public Access. Nature, 451(7181), pp.990–993.
Jones, T. et al., 2004. The diploid genome sequence of Candida albicans. Proceedings of the National Academy of Sciences of the United States of America, 101(19), pp.7329–7334.
Joseph-Horne, T., Hollomon, D.W. & Wood, P.M., 2001. Fungal respiration: a fusion of standard and alternative components. Biochimica et Biophysica Acta (BBA) - Bioenergetics, 1504(2), pp.179–195.
Josling, G.A. et al., 2012. The Role of Bromodomain Proteins in Regulating Gene Expression. Genes, 3(2), pp.320–343.
Kadauke, S. & Blobel, G.A., 2009. Chromatin loops in gene regulation. Biochimica et biophysica acta, 1789(1), pp.17–25.
Kadosh, D. & Lopez-Ribot, J.L., 2013. Candida albicans: Adapting to Succeed. Cell Host and Microbe, 14(5), pp.483–485.
Kaehlcke, K. et al., 2003. Acetylation of Tat Defines a CyclinT1-Independent Step in HIV Transactivation. Molecular Cell, 12(1), pp.167–176.
Kan, P.-Y. et al., 2007. The H3 tail domain participates in multiple interactions during folding and self-association of nucleosome arrays. Molecular and cellular biology, 27(6), pp.2084–2091.
Kanta, H. et al., 2006. Suppressor Analysis of a Histone Defect Identifies a New Function for the Hda1 Complex in Chromosome Segregation. Genetics, 173(1), pp.435–450.
Karababa, M. et al., 2004. Comparison of gene expression profiles of Candida albicans azole-resistant clinical isolates and laboratory strains exposed to drugs inducing multidrug transporters. Antimicrobial agents and chemotherapy, 48(8), pp.3064–3079.
Karthikeyan, G. et al., 2013. Functional characterization of Candida albicans Hos2 histone deacetylase. F1000Research, 2, p.238.
Kashi, Y. & King, D.G., 2006. Simple sequence repeats as advantageous mutators in evolution. Trends in Genetics, 22(5), pp.253–259.
Kazantsev, A.G. & Thompson, L.M., 2008. Therapeutic application of histone deacetylase inhibitors for central nervous system disorders. Nature Reviews Drug Discovery, 7(10), pp.854–868.
Kelley, L.A. et al., 2015. The Phyre2 web portal for protein modeling, prediction and analysis. Nat. Protocols, 10(6), pp.845–858.
Khochbin, S. & Wolffe, A.P., 1997. The origin and utility of histone deacetylases. FEBS Letters, 419(2–3), pp.157–160.
Kim, G.-W. et al., 2010. Dietary, metabolic, and potentially environmental modulation of the lysine acetylation machinery. International journal of cell biology, 2010, p.632739.
Kim, J., Park, S. & Lee, J.S., 2018. Epigenetic control of oxidative stresses by histone acetyltransferases in Candida albicans. Journal of Microbiology and Biotechnology, 28(2), pp.181–189.
Kim, T. et al., 2012. Set3 HDAC mediates effects of overlapping non-coding transcription on gene induction kinetics. Cell, 150(6), pp.1158–1169.
Kimple, M.E., Brill, A.L. & Pasker, R.L., 2013. Overview of Affinity Tags for Protein Purification. Current protocols in protein science / editorial board, John E. Coligan et al, 73, Unit-9.9.
Kirkpatrick, W.R. et al., 2000. Growth competition between Candida dubliniensis and Candida albicans under broth and biofilm growing conditions. Journal of clinical microbiology, 38(2), pp.902–904.
Klar, A.J., Srikantha, T. & Soll, D.R., 2001. A histone deacetylation inhibitor and mutant promote colony-type switching of the human pathogen Candida albicans. Genetics, 158(2), pp.919–924.
Klosin, A. & Hyman, A.A., 2017. A liquid reservoir for silent chromatin. Nature, 547, p.168.
Kmetzsch, L., 2015. Histone deacetylases: Targets for antifungal drug development. Virulence, 6(6), pp.535–536.
Knop, M. et al., 1999. Epitope tagging of yeast genes using a PCR-based strategy: more tags and improved practical routines. Yeast, 15(10B), pp.963–972.
Kohler, J.R., Casadevall, A. & Perfect, J., 2014. The spectrum of fungi that infects humans. Cold Spring Harbor perspectives in medicine, 5(1), a019273.
Köhler, J.R. & Fink, G.R., 1996. Candida albicans strains heterozygous and homozygous for mutations in mitogen-activated protein kinase signaling components have defects in hyphal development. Proceedings of the National Academy of Sciences of the United States of America, 93(23), pp.13223–13228.
Kojic, E.M. & Darouiche, R.O., 2004. Candida Infections of Medical Devices. Clinical Microbiology Reviews, 17(2), pp.255–267.

Kouzarides, T., 2000. Acetylation: a regulatory modification to rival phosphorylation? The EMBO Journal, 19(6), p.1176 LP-1179.
Kouzarides, T., 2007. Chromatin Modifications and Their Function. Cell, 128(4), pp.693–705.
Krebs, J.E. et al., 1999. Cell cycle-regulated histone acetylation required for expression of the yeast HO gene. Genes & Development, 13(11), pp.1412–1421.
Kruppa, M., 2008. Quorum sensing and Candida albicans. Mycoses, 52(1), pp.1–10.
Krysan, D.J., Sutterwala, F.S. & Wellington, M., 2014. Catching fire: Candida albicans, macrophages, and pyroptosis. PLoS pathogens, 10(6), e1004139.
Kucharíková, S. et al., 2011. Detailed comparison of Candida albicans and Candida glabrata biofilms under different conditions and their susceptibility to caspofungin and anidulafungin. Journal of Medical Microbiology, 60(9), pp.1261–1269.
Kumar, B.R. et al., 2001. p300-mediated acetylation of human transcriptional coactivator PC4 is inhibited by phosphorylation. The Journal of biological chemistry, 276(20), pp.16804–16809.
Kuo, Y.-M. & Andrews, A.J., 2013. Quantitating the Specificity and Selectivity of Gcn5-Mediated Acetylation of Histone H3 A. Pastore, ed. PLoS ONE, 8(2), e54896.
Kusch, H. et al., 2004. A proteomic approach to understanding the development of multidrug-resistant Candida albicans strains. Molecular Genetics and Genomics, 271(5), pp.554–565.
LA, W., AD, S. & DG, A., 1991. Comparative efficacies of soft contact lens disinfectant solutions against microbial films in lens cases. Archives of Ophthalmology, 109(8), pp.1155–1157.
Lai, W.C. et al., 2011. Construction of Candida albicans Tet-on tagging vectors with a Ura-blaster cassette. Yeast. 28(3), pp.253-263.
Lamb, T.M. et al., 2001. Alkaline response genes of Saccharomyces cerevisiae and their relationship to the RIM101 pathway. The Journal of biological chemistry, 276(3), pp.1850–6.
Lamb, T.M. & Mitchell, A.P., 2003. The Transcription Factor Rim101p Governs Ion Tolerance and Cell Differentiation by Direct Repression of the Regulatory Genes NRG1 and SMP1 in Saccharomyces cerevisiae. Molecular and Cellular Biology, 23(2), pp.677–686.
Lamoth, F. et al., 2018. Changes in the epidemiological landscape of invasive candidiasis. Journal of Antimicrobial Chemotherapy, 73(May), pp.i4–i13.
Lamoth, F. et al., 2014. Identification of a key lysine residue in heat shock protein 90 required for azole and echinocandin resistance in Aspergillus fumigatus. Antimicrobial agents and chemotherapy, 58(4), pp.1889–1896.
Lane, S. et al., 2001. DNA array studies demonstrate convergent regulation of virulence factors by Cph1, Cph2, and Efg1 in Candida albicans. The Journal of biological chemistry, 276(52), pp.48988–48996.
Langford, M.L. et al., 2013. Candida albicans Czf1 and Efg1 Coordinate the Response to Farnesol during Quorum Sensing, White-Opaque Thermal Dimorphism, and Cell Death. Eukaryotic Cell, 12(9), pp.1281–1292.
Larson, A.G. et al., 2017. Liquid droplet formation by HP1α suggests a role for phase separation in heterochromatin. Nature, 547, p.236. Available at: http://dx.doi.org/10.1038/nature22822.
Lau, O.D. et al., 2000. HATs off. Molecular Cell, 5(3), pp.589–595.
Law, D. et al., 1994. High prevalence of antifungal resistance in Candida spp. from patients with AIDS. Journal of Antimicrobial Chemotherapy, 34(5), pp.659–668.
Le, T.B.K. & Laub, M.T., 2016. Transcription rate and transcript length drive formation of chromosomal interaction domain boundaries. The EMBO Journal, 35(14), pp.1582–1595.
Leach, M.D., 2012. Modelling the Regulation of Thermal Adaptation in Candida albicans, a Major Fungal Pathogen of Humans, 7(3), e32467.
Lee, J.-E. et al., 2015. Ssn6 has dual roles in Candida albicans filament development through the interaction with Rpd31. FEBS Letters, 589(4), pp.513–520.
Lee, J.-H., Maskos, K. & Huber, R., 2009. Structural and Functional Studies of the Yeast Class II Hda1 Histone Deacetylase Complex. Journal of Molecular Biology, 391(4), pp.744–757.
Lee, J.-S., Smith, E. & Shilatifard, A., 2010. The Language of Histone Crosstalk. Cell, 142(5), pp.682–685.
Lee, J.A. et al., 2016. Functional Genomic Analysis of Candida albicans Adherence Reveals a Key Role for the Arp2/3 Complex in Cell Wall Remodelling and Biofilm Formation C. Nobile, ed. PLoS Genetics, 12(11), e1006452.
Lee, K.K. & Workman, J.L., 2007. Histone acetyltransferase complexes: One size doesn't fit all. Nature Reviews Molecular Cell Biology, 8(4), pp.284–295.
Lemos, L.B., Baliga, M. & Guo, M., 2001. Acute respiratory distress syndrome and blastomycosis: Presentation of nine cases and review of the literature. Annals of Diagnostic Pathology, 5(1), pp.1–9.
Leng, G. & Song, K., 2016. Watch out for your TRP1 marker: the effect of TRP1 gene on the growth at high and low temperatures in budding yeast. FEMS Microbiology Letters, 363(10), fnw093-fnw093.

Letunic, I., Doerks, T. & Bork, P., 2015. SMART: recent updates, new developments and status in 2015. Nucleic Acids Research, 43(Database issue), pp.D257–D260.
Li, C.X. et al., 2015. Candida albicans adapts to host copper during infection by swapping metal cofactors for superoxide dismutase. Proceedings of the National Academy of Sciences, 112(38), p.E5336-E5342.
Li, F. et al., 2008. Lid2, a JmjC domain-Containing Histone Demethylase, is Required for Coordinating H3K4 and H3K9 Methylation of Heterochromatin and Euchromatin. Cell, 135(2), pp.272–283.
Li, G. & Reinberg, D., 2011. Chromatin higher-order structures and gene regulation. Current opinion in genetics & development, 21(2), pp.175–186.
Li, H.-M. et al., 2016. White-opaque Switching in Different Mating Type-like Locus Gene Types of Clinical Candida albicans Isolates. Chinese Medical Journal, 129(22), pp.2725–2732.
Li, L. et al., 2010. Identification of the novel protein FAM172A, and its up-regulation by high glucose in human aortic smooth muscle cells. International Journal of Molecular Medicine, 26(4), pp.483–490.
Li, X. et al., 2017. Extensive Functional Redundancy in the Regulation of Candida albicans Drug Resistance and Morphogenesis by Lysine Deacetylases Hos2, Hda1, Rpd3, and Rpd31. Molecular microbiology, 103(4), pp.635–656.
Li, X. et al., 2014. The Rpd3/Hda1 family of histone deacetylases regulates azole resistance in Candida albicans. Journal of Antimicrobial Chemotherapy. 70(7), pp.1993-2003.
Liao, Y., Smyth, G.K. & Shi, W., 2014. featureCounts: an efficient general purpose program for assigning sequence reads to genomic features. Bioinformatics (Oxford, England), 30(7), pp.923–930.
Lim, J.P. & Brunet, A., 2013. Bridging the transgenerational gap with epigenetic memory. Trends in genetics : TIG, 29(3), pp.176–186. Available at: http://www.ncbi.nlm.nih.gov/pmc/articles/PMC3595609/.
Lin, C. & Yuan, Y.A., 2008. Structural insights into histone H3 lysine 56 acetylation by Rtt109. Structure (London, England : 1993), 16(10), pp.1503–1510.
Lindsay, A.K. et al., 2012. Farnesol and Cyclic AMP Signaling Effects on the Hypha-to-Yeast Transition in Candida albicans. Eukaryotic Cell, 11(10), pp.1219–1225.
Liu, N.-N. et al., 2018. Intersection of phosphate transport, oxidative stress and TOR signalling in Candida albicans virulence. PLOS Pathogens, 14(7), e1007076.
Liu, X. et al., 2008. The structural basis of protein acetylation by the p300/CBP transcriptional coactivator. Nature, 451, p.846.
Liu, Y. & Filler, S.G., 2011. Candida albicans Als3, a Multifunctional Adhesin and Invasin . Eukaryotic Cell, 10(2), pp.168–173.
Lo, H.J. et al., 1997. Nonfilamentous C. albicans mutants are avirulent. Cell, 90(5), pp.939–949.
Lockhart, S.R. et al., 2002. In Candida albicans, white-opaque switchers are homozygous for mating type. Genetics, 162(2), pp.737–745.
Lohse, M.B. & Johnson, A.D., 2009. White-opaque switching in Candida albicans. Current Opinion in Microbiology. 12(6), pp.650-654.
Lopes da Rosa, J. et al., 2010. Histone acetyltransferase Rtt109 is required for Candida albicans pathogenesis. Proceedings of the National Academy of Sciences of the United States of America, 107(4), pp.1594–1599.
Lopes da Rosa, J. & Kaufman, P.D., 2012. Chromatin-Mediated Candida albicans Virulence. Biochimica et Biophysica Acta, 1819(3–4), pp.349–355.
Lorenz, M.C., Bender, J.A. & Fink, G.R., 2004. Transcriptional Response of Candida albicans upon Internalization by Macrophages. Eukaryotic Cell, 3(5), pp.1076–1087.
Love, M.I., Huber, W. & Anders, S., 2014. Moderated estimation of fold change and dispersion for RNA-seq data with DESeq2. Genome Biology, 15(12), p.550.
Lu, Y. et al., 2011. Hyphal development in Candida albicans requires two temporally linked changes in promoter chromatin for initiation and maintenance. PLoS Biology 9(7), pp.1-17: e1001105.
Lu, Y. et al., 2013. Synergistic regulation of hyphal elongation by hypoxia, CO2, and nutrient conditions controls the virulence of Candida albicans. Cell Host and Microbe, 14(5), pp.499–509.
Lu, Y., Su, C. & Liu, H., 2012. A GATA Transcription Factor Recruits Hda1 in Response to Reduced Tor1 Signaling to Establish a Hyphal Chromatin State in Candida albicans. PLOS Pathogens, 8(4): e1002663.
Luger, K. et al., 1997. Crystal structure of the nucleosome core particle at 2.8 Å resolution. Nature, 389, p.251.
Lushchak, O. V & Lushchak, V.I., 2008. Sodium nitroprusside induces mild oxidative stress in Saccharomyces cerevisiae. Redox report : communications in free radical research, 13(4), pp.144–152.
Lynch, D.B. et al., 2010. Chromosomal G + C Content Evolution in Yeasts: Systematic Interspecies Differences, and GC-Poor Troughs at Centromeres. Genome Biology and Evolution, 2, pp.572–583.
MacCallum, D.M. & Odds, F.C., 2005. Temporal events in the intravenous challenge model for experimental Candida albicans infections in female mice. Mycoses, 48(3), pp.151–161.

MacIsaac, K.D. et al., 2006. An improved map of conserved regulatory sites for Saccharomyces cerevisiae. BMC Bioinformatics, 7(1), p.113.
Magee, B.B., 2000. Induction of Mating in Candida albicans by Construction of MTLa and MTLalpha Strains-annotated. Science, 289, pp.310–313.
Magee, B.B. et al., 1993. The genes encoding the secreted aspartyl proteinases of Candida albicans constitute a family with at least three members. Infection and immunity, 61(8), pp.3240–3243.
Mai, A. et al., 2007. Discovery of uracil-based histone deacetylase inhibitors able to reduce acquired antifungal resistance and trailing growth in Candida albicans. Bioorganic & Medicinal Chemistry Letters, 17(5), pp.1221–1225.
Maidan, M.M. et al., 2005. The G Protein-coupled Receptor Gpr1 and the Gα Protein Gpa2 Act through the cAMP-Protein Kinase A Pathway to Induce Morphogenesis in Candida albicans H. Riezman, ed. Molecular Biology of the Cell, 16(4), pp.1971–1986.
Manaud, N. et al., 1998. A Chimeric Subunit of Yeast Transcription Factor IIIC Forms a Subcomplex with τ95. Molecular and Cellular Biology, 18(6), pp.3191–3200.
Mao, X. et al., 2006. The Swi/Snf chromatin remodeling complex is essential for hyphal development in Candida albicans. FEBS Letters, 580(11), pp.2615–2622.
Marcil, A. et al., 2008. Analysis of PRA1 and its relationship to Candida albicans-macrophage interactions. Infection and Immunity, 76(9), pp.4345–4358.
Marcil, A. et al., 2002. Candida albicans Killing by RAW 264.7 Mouse Macrophage Cells: Effects of Candida Genotype, Infection Ratios, and Gamma Interferon Treatment. Infection and Immunity, 70(11), p.6319-6329.
Marín, M., Fernández-Calero, T. & Ehrlich, R., 2017. Protein folding and tRNA biology. Biophysical Reviews, 9(5), pp.573–588.
Marmorstein, R. & Zhou, M.-M., 2014. Writers and Readers of Histone Acetylation: Structure, Mechanism, and Inhibition. Cold Spring Harbor Perspectives in Biology, 6(7): a018762.
Marr, K.A. et al., 1999. The Trailing End Point Phenotype in Antifungal Susceptibility Testing Is pH Dependent. Antimicrobial Agents and Chemotherapy, 43(6), pp.1383–1386.
Martin, S.W., Douglas, L.M. & Konopka, J.B., 2005. Cell cycle dynamics and quorum sensing in Candida albicans chlamydospores are distinct from budding and hyphal growth. Eukaryotic cell, 4(7), pp.1191–1202.
Martins, C.H.G. et al., 2016. Candida/Candida biofilms. First description of dual-species Candida albicans/C. rugosa biofilm. Fungal biology, 120(4), pp.530–537.
Martins, N. et al., 2014. Candidiasis: Predisposing Factors, Prevention, Diagnosis and Alternative Treatment. Mycopathologia, 177(5), pp.223–240.
Mayer, F.L., Wilson, D. & Hube, B., 2013. Candida albicans pathogenicity mechanisms. Virulence, 4(2), pp.119–128.
McAlester, G., O'Gara, F. & Morrissey, J.P., 2008. Signal-mediated interactions between Pseudomonas aeruginosa and Candida albicans. Journal of medical microbiology, 57(Pt 5), pp.563–569.
McCormack, P.L. & Perry, C.M., 2005. Caspofungin: a review of its use in the treatment of fungal infections. Drugs, 65(14), pp.2049–2068.
McKenzie, C.G.J. et al., 2010. Contribution of Candida albicans Cell Wall Components to Recognition by and Escape from Murine Macrophages. Infection and Immunity, 78(4), p.1650 -1658.
Memedula, S. & Belmont, A.S., 2003. Sequential Recruitment of HAT and SWI/SNF Components to Condensed Chromatin by VP16. Current Biology, 13(3), pp.241–246.
Merico, D. et al., 2010. Enrichment Map: A Network-Based Method for Gene-Set Enrichment Visualization and Interpretation T. Ravasi, ed. PLoS ONE, 5(11): e13984.
Messner, S. & Hottiger, M.O., 2011. Histone ADP-ribosylation in DNA repair, replication and transcription. Trends in Cell Biology, 21(9), pp.534–542.
Mewes, H.W. et al., 1997. Overview of the yeast genome. Nature, 387, pp.7–8.
Mi, H. et al., 2017. PANTHER version 11: expanded annotation data from Gene Ontology and Reactome pathways, and data analysis tool enhancements. Nucleic Acids Research, 45(D1), pp.D183–D189.
Miller, M.G. & Johnson, A.D., 2002. White-opaque switching in Candida albicans is controlled by mating-type locus homeodomain proteins and allows efficient mating. Cell, 110(3), pp.293–302.
Miranda, I. et al., 2013. Candida albicans CUG Mistranslation Is a Mechanism To Create Cell Surface Variation. mBio, 4(4): e00285-13.
Mitchell, A.P., 1998. Dimorphism and virulence in Candida albicans. Current Opinion in Microbiology, 1(6), pp.687–692.
Mitrovich, Q.M. et al., 2007. Computational and experimental approaches double the number of known introns in the pathogenic yeast Candida albicans. *Genome research*, 17(4), pp.492–502.
Monge, R.A. et al., 2006. The MAP kinase signal transduction network in Candida albicans. Microbiology (Reading, England), 152(Pt 4), pp.905–912.

Montravers, P. et al., 2011. A multicentre study of antifungal strategies and outcome of Candida spp. peritonitis in intensive-care units. Clinical Microbiology and Infection, 17(7), pp.1061–1067.
Moore, G.E., Gerner, R.E. & Franklin, H.A., 1967. Culture of normal human leukocytes. JAMA, 199(8), pp.519–524.
Moosa, M.-Y.S. et al., 2004. Fungicidal Activity of Fluconazole against Candida albicans in a Synthetic Vagina-Simulative Medium. Antimicrobial Agents and Chemotherapy, 48(1), pp.161–167.
Mootha, V.K. et al., 2003. PGC-1alpha-responsive genes involved in oxidative phosphorylation are coordinately downregulated in human diabetes. Nature genetics, 34(3), pp.267–273.
Mora-Montes, H.M. et al., 2010. A multifunctional mannosyltransferase family in Candida albicans determines cell wall mannan structure and host-fungus interactions. The Journal of biological chemistry, 285(16), pp.12087–12095.
Mora-Montes, H.M. et al., 2007. Endoplasmic reticulum alpha-glycosidases of Candida albicans are required for N glycosylation, cell wall integrity, and normal host-fungus interaction. Eukaryotic cell, 6(12), pp.2184–2193.
Moseley, J.B. & Goode, B.L., 2006. The Yeast Actin Cytoskeleton: from Cellular Function to Biochemical Mechanism. Microbiology and Molecular Biology Reviews, 70(3), p.605-645.
Murad, A.M. et al., 2001. NRG1 represses yeast-hypha morphogenesis and hypha-specific gene expression in Candida albicans. The EMBO journal, 20(17), pp.4742–4752.
Murad, A.M.A. et al., 2008. Transcript profiling in Candida albicans reveals new cellular functions for the transcriptional repressors CaTup1, CaMig1 and CaNrg1. Molecular Microbiology, 42(4), pp.981–993.
Nagalakshmi, U. et al., 2008. The Transcriptional Landscape of the Yeast Genome Defined by RNA Sequencing. Science (New York, N.Y.), 320(5881), pp.1344–1349.
Naglik, J.R. et al., 2003. Differential expression of Candida albicans secreted aspartyl proteinase and phospholipase B genes in humans correlates with active oral and vaginal infections. The Journal of infectious diseases, 188(3), pp.469–479.
Nakamura, Y., Gojobori, T. & Ikemura, T., 2000. Codon usage tabulated from international DNA sequence databases: status for the year 2000. Nucleic acids research, 28(1), p.292.
Nantel, A. et al., 2002. Transcription profiling of Candida albicans cells undergoing the yeast-to-hyphal transition. Molecular biology of the cell, 13(10), pp.3452–3465.
Nascimento, I.P. & Leite, L.C.C., 2012. Recombinant vaccines and the development of new vaccine strategies. Brazilian Journal of Medical and Biological Research, 45(12), pp.1102–1111.
Natarajan, S. & Subramanian, P., 2014. Allergic bronchopulmonary aspergillosis: A clinical review of 24 patients: Are we right in frequent serologic monitoring? Annals of Thoracic Medicine, 9(4), pp.216–220.
Nathan, D. et al., 2006. Histone sumoylation is a negative regulator in Sccharomyces cervisiae and shows dynamic interplay with positive-acting histone modifications. Genes and Development, 20, pp.966–976.
Nathan, D., Sterner, D.E. & Berger, S.L., 2003. Histone modifications: Now summoning sumoylation. Proceedings of the National Academy of Sciences of the United States of America, 100(23), pp.13118–13120.
Nett, J.E. et al., 2010. Development and Validation of an In Vivo Candida albicans Biofilm Denture Model. Infection and Immunity, 78(9), p.3650-3659.
Nie, X. et al., 2010. Deletion of EFG1 promotes Candida albicans opaque formation responding to pH via Rim101. Acta biochimica et biophysica Sinica, 42(10), pp.735–744.
Nobile, C.J. et al., 2014. A histone deacetylase complex mediates biofilm dispersal and drug resistance in Candida albicans. mBio, 5(3), e01201-14.
Nobile, C.J. et al., 2012. A Recently Evolved Transcriptional Network Controls Biofilm Development in Candida albicans. Cell, 148(1–2), pp.126–138.
Nobile, C.J. et al., 2009. Biofilm Matrix Regulation by Candida albicans Zap1. PLOS Biology, 7(6), pp.1–15.
Nobile, C.J. et al., 2008. Complementary Adhesin Function in C. albicans Biofilm Formation. Current Biology, 18(14), pp.1017–1024.
Nobile, C.J. et al., 2003. Genetic control of chlamydospore formation in Candida albicans. Microbiology, 149, pp.3629-3637.
Nobile, C.J. & Johnson, A.D., 2015. Candida albicans Biofilms and Human Disease. Annual review of microbiology, 69, pp.71–92.
Nobile, C.J. & Mitchell, A.P., 2005. Regulation of cell-surface genes and biofilm formation by the C. albicans transcription factor Bcr1p. Current biology : CB, 15(12), pp.1150–1155.
Noble, S.M. et al., 2010. Systematic screens of a Candida albicans homozygous deletion library decouple morphogenetic switching and pathogenicity. Nature genetics, 42(7), pp.590–8.
North, M. et al., 2012. Genome-Wide Functional Profiling Identifies Genes and Processes Important for Zinc-Limited Growth of Saccharomyces cerevisiae C. C. Philpott, ed. PLoS Genetics, 8(6): e1002699.

Novagen, 2011. Duet Vector Manual. TB340(E0305).
Novagen, 2003. pET System Manual. Available at: http://lifeserv.bgu.ac.il/wp/zarivach/wp-content/uploads/2017/11/Novagen-pET-system-manual-1.pdf [Accessed July 5, 2018].
Nucci, M. & Anaissie, E., 2007. Fusarium infections in immunocompromised patients. Clinical microbiology reviews, 20(4), pp.695–704.
Odani, T. et al., 1996. Cloning and analysis of the MNN4 geneOdani, T. et al., 1996. Cloning and analysis of the MNN4 gene required for phosphorylation of N-linked oligosaccharides in Saccharomyces cerevisiae. Glycobiology, 6(8), pp.805–810. required for phosphorylation of N-lin. Glycobiology, 6(8), pp.805–810.
Oike, T. et al., 2012. Garcinol, a Histone Acetyltransferase Inhibitor, Radiosensitizes Cancer Cells by Inhibiting Non-Homologous End Joining. International Journal of Radiation Oncology Biology Physics, 84(3), pp.815–821.
Olaiya, A.F. & Sogin, S.J., 1979. Ploidy determination of Canadida albicans. Journal of Bacteriology, 140(3), pp.1043–1049.
Orlando, D.A. et al., 2014. Quantitative ChIP-Seq Normalization Reveals Global Modulation of the Epigenome Resource Quantitative ChIP-Seq Normalization Reveals Global Modulation of the Epigenome. CellReports, 9(3), pp.1163–1170.
Pagani, M.A. et al., 2007. Disruption of iron homeostasis in Saccharomyces cerevisiae by high zinc levels: a genome-wide study. Molecular Microbiology, 65(2), pp.521–537.
Pande, K., Chen, C. & Noble, S.M., 2013. Passage through the mammalian gut triggers a phenotypic switch that promotes Candida albicans commensalism. Nature genetics, 45(9), pp.1088–1091.
Pasini, D. et al., 2010. Characterization of an antagonistic switch between histone H3 lysine 27 methylation and acetylation in the transcriptional regulation of Polycomb group target genes. Nucleic Acids Research, 38(15), pp.4958–4969.
Pathan, M. et al., 2017. A novel community driven software for functional enrichment analysis of extracellular vesicles data. Journal of Extracellular Vesicles, 6(1): 1321455.
Pendrak, M.L. & Roberts, D.D., 2015. Hbr1 Activates and Represses Hyphal Growth in Candida albicans and Regulates Fungal Morphogenesis under Embedded Conditions S. G. Filler, ed. PLoS ONE, 10(6): e0126919.
Pendrak, M.L., Yan, S.S. & Roberts, D.D., 2004. Hemoglobin Regulates Expression of an Activator of Mating-Type Locus α Genes in Candida albicans. Eukaryotic Cell, 3(3), pp.764-775.
Perfect, J.R., 2017. The antifungal pipeline: a reality check. Nature reviews. Drug discovery, 16(9), pp.603–616.
Perkins, D.N. et al., 1999. Probability-based protein identification by searching sequence databases using mass spectrometry data. Electrophoresis, 20(18), pp.3551–3567.
Pertea, M. et al., 2016. Transcript-level expression analysis of RNA-seq experiments with HISAT, StringTie, and Ballgown. Nature protocols, 11(9), pp.1650–1667.
Pfaller, M.A. & Diekema, D.J., 2007. Epidemiology of Invasive Candidiasis: a Persistent Public Health Problem. Clinical Microbiology Reviews, 20(1), pp.133–163.
Pfaller, M.A. & Diekema, D.J., 2010. Epidemiology of invasive mycoses in North America. Critical reviews in microbiology, 36(1), pp.1–53.
Phan, Q.T. et al., 2007. Als3 Is a Candida albicans Invasin That Binds to Cadherins and Induces Endocytosis by Host Cells J. Heitman, ed. PLoS Biology, 5(3), e64.
Phan, Q.T., Belanger, P.H. & Filler, S.G., 2000. Role of Hyphal Formation in Interactions of Candida albicans with Endothelial Cells T. R. Kozel, ed. Infection and Immunity, 68(6), pp.3485–3490.
Pijnappel, W.W. et al., 2001. The S. cerevisiae SET3 complex includes two histone deacetylases, Hos2 and Hst1, and is a meiotic-specific repressor of the sporulation gene program. Genes & development, 15(22), pp.2991–3004.
Posas, F. et al., 2000. The transcriptional response of yeast to saline stress. The Journal of biological chemistry, 275(23), pp.17249–17255.
Pray-Grant, M.G. et al., 2002. The Novel SLIK Histone Acetyltransferase Complex Functions in the Yeast Retrograde Response Pathway. MOLECULAR AND CELLULAR BIOLOGY, 22(24), pp.8774–8786.
Pronk, J.T., 2002. Auxotrophic Yeast Strains in Fundamental and Applied Research. Applied and Environmental Microbiology, 68(5), pp.2095-2100.
Pugliese, A. et. al., 2000. Candida albicans and HIV infection. Cell Biochemistry and Function, 18, pp.235-241.
Pukkila-Worley, R. et al., 2009a. Candida albicans hyphal formation and virulence assessed using a Caenorhabditis elegans infection model. Eukaryotic cell, 8(11), pp.1750–8.
Pukkila-Worley, R. et al., 2009b. Candida albicans Hyphal Formation and Virulence Assessed Using a Caenorhabditis elegans Infection Model. Eukaryotic Cell, 8(11), pp.1750-1758.

Qiagen, 2003. The QIAexpressionist., (5th Edition), pp.1–128. Available at: https://www.qiagen.com/it/resources/resourcedetail?id=79ca2f7d-42fe-4d62-8676-4cfa948c9435&lang=en [Accessed: February 9, 2019]
Quan, C. & Spellberg, B., 2010. Mucormycosis, Pseudallescheriasis, and Other Uncommon Mold Infections. Proceedings of the American Thoracic Society, 7(3), pp.210–215.
Quax, T.E.F. et al., 2015. Codon Bias as a Means to Fine-Tune Gene Expression. Molecular cell, 59(2), pp.149–161.
R Foundation for Statistical Computing, 2008. R: A language and environment for statistical computing. Vienna, Austria. Accessable at: https://www.r-project.org [Accessed: February 9, 2019]
Rajkumar, A.P. et al., 2015. Experimental validation of methods for differential gene expression analysis and sample pooling in RNA-seq. BMC Genomics, 16(1), p.548.
Ramage, G. et al., 2004. Denture stomatitis: a role for Candida biofilms. Oral Surgery, Oral Medicine, Oral Pathology, Oral Radiology, and Endodontology, 98(1), pp.53–59.
Ramage, G., Martínez, J.P. & López-Ribot, J.L., 2006. Candida biofilms on implanted biomaterials: a clinically significant problem. FEMS Yeast Research, 6(7), pp.979–986.
Ramírez-Zavala, B. et al., 2013. Activation of the Cph1-Dependent MAP Kinase Signaling Pathway Induces White-Opaque Switching in Candida albicans. PLOS Pathogens, 9(10), e1003696.
Rando, O.J. & Winston, F., 2012. Chromatin and Transcription in Yeast. Genetics, 190(2), pp.351–387.
Ranscht, B. & Dours-Zimmermann, M.T., 1991. T-cadherin, a novel cadherin cell adhesion molecule in the nervous system lacks the conserved cytoplasmic region. Neuron, 7(3), pp.391–402.
Redd, M.J., Arnaud, M.B. & Johnson, A.D., 1997. A complex composed of tup1 and ssn6 represses transcription in vitro. The Journal of biological chemistry, 272(17), p.11193-11197.
Rees, J.R. et al., 1998. The epidemiological features of invasive mycotic infections in the San Francisco Bay area, 1992-1993: results of population-based laboratory active surveillance. Clinical infectious diseases : an official publication of the Infectious Diseases Society of America, 27(5), pp.1138–1147.
de Repentigny, L., Lewandowski, D. & Jolicoeur, P., 2004. Immunopathogenesis of Oropharyngeal Candidiasis in Human Immunodeficiency Virus Infection. Clinical Microbiology Reviews, 17(4), pp.729–759.
Revankar, S.G., 2017. MSD Manual: Overview of Fungal Infections, Available at: https://www.msdmanuals.com/en-gb/professional/infectious-diseases/fungi/overview-of-fungal-infections. [Accessed: February 9, 2019]
Rex, J.H. et al., 1994. A randomized trial comparing fluconazole with amphotericin B for the treatment of candidemia in patients without neutropenia. Candidemia Study Group and the National Institute. The New England journal of medicine, 331(20), pp.1325–1330.
Rice, P., Longden, I. & Bleasby, A., 2000. Emboss: The European Molecular Biology Open Software Suite. Trends in Genetics, 6(16), pp.276–277.
Richard, M.L. et al., 2005. Candida albicans Biofilm-Defective Mutants. EUKARYOTIC CELL, 4(8), pp.1493–1502.
Richmond, R.K. et al., 1997. Crystal structure of the nucleosome resolution core particle at 2 . 8 A. Nature, 389, pp.251–260.
Richter, U. et al., 2015. Quality control of mitochondrial protein synthesis is required for membrane integrity and cell fitness. The Journal of Cell Biology, 211(2), pp.373–389.
Riggsby, W.S. et al., 1982. DNA content, kinetic complexity, and the ploidy question in Candida albicans. Molecular and cellular biology, 2(7), pp.853–862.
Robbins, N. et al., 2011. Hsp90 governs dispersion and drug resistance of fungal biofilms. PLoS pathogens, 7(9), e1002257.
Robbins, N., Leach, M.D. & Cowen, L.E., 2012. Lysine Deacetylases Hda1 and Rpd3 Regulate Hsp90 Function thereby Governing Fungal Drug Resistance. Cell Reports, 2(4), pp.878–888.
Robert, X. & Gouet, P., 2014. Deciphering key features in protein structures with the new ENDscript server. Nucleic Acids Research, 42(W1), pp.W320–W324.
Robinson, J.T. et al., 2011. Integrative genomics viewer. Nature Biotechnology, 29, p.24.
Robinson, P.J.J. et al., 2006. EM measurements define the dimensions of the “30-nm” chromatin fiber: Evidence for a compact, interdigitated structure. Proceedings of the National Academy of Sciences of the United States of America, 103(17), pp.6506–6511.
Robyr, D. et al., 2002. Microarray Deacetylation Maps Determine Genome-Wide Functions for Yeast Histone Deacetylases. Cell, 109(4), pp.437–446.
Rocha, C.R.C. et al., 2001. Signaling through Adenylyl Cyclase Is Essential for Hyphal Growth and Virulence in the Pathogenic Fungus Candida albicans P. N. Devreotes, ed. Molecular Biology of the Cell, 12(11), pp.3631–3643.

Rogers, P.D. & Barker, K.S., 2003. Genome-wide expression profile analysis reveals coordinately regulated genes associated with stepwise acquisition of azole resistance in Candida albicans clinical isolates. Antimicrobial agents and chemotherapy, 47(4), pp.1220–1227.
Ropero, S. & Esteller, M., 2007. The role of histone deacetylases (HDACs) in human cancer. Molecular Oncology, 1(1), pp.19–25.
Rossetto, D., Avvakumov, N. & Côté, J., 2012. Histone phosphorylation: A chromatin modification involved in diverse nuclear events. Epigenetics, 7(10), pp.1098–1108.
Roth, S.Y., Denu, J.M. & Allis, C.D., 2001. Histone acetyltransferases. Annual review of biochemistry, 70, pp.81–120.
Rundlett, S.E. et al., 1996. HDA1 and RPD3 are members of distinct yeast histone deacetylase complexes that regulate silencing and transcription. Proceedings of the National Academy of Sciences of the United States of America, 93(25), pp.14503–14508.
Rundlett, S.E. et al., 1996. HDA1 and RPD3 are members of distinct yeast histone deacetylase complexes that regulate silencing and transcription. Proceedings of the National Academy of Sciences, 93(25), pp.14503–14508. Available at: http://www.pnas.org/cgi/doi/10.1073/pnas.93.25.14503.
Russell, P.J. et al., 1987. Different levels of DNA methylation in yeast and mycelial forms of Candida albicans. Journal of bacteriology, 169(9), pp.4393–4395.
Saccente, M. & Woods, G.L., 2010. Clinical and Laboratory Update on Blastomycosis. Clinical Microbiology Reviews, 23(2), pp.367–381.
Saksouk, N., Simboeck, E. & Déjardin, J., 2015. Constitutive heterochromatin formation and transcription in mammals. Epigenetics {&} Chromatin, 8(1), p.3.
Sanchez, R. & Zhou, M.-M., 2009. The role of human bromodomains in chromatin biology and gene transcription. Current opinion in drug discovery & development, 12(5), pp.659–665.
Sasse, C. et al., 2013. White-opaque switching of Candida albicans allows immune evasion in an environment-dependent fashion. Eukaryotic Cell, 12(1), pp.50–58.
Sato, T. et al., 2004. Farnesol, a morphogenetic autoregulatory substance in the dimorphic fungus Candida albicans, inhibits hyphae growth through suppression of a mitogen-activated protein kinase cascade. Biological & pharmaceutical bulletin, 27(5), pp.751–752.
Saville, S.P. et al., 2003. Engineered control of cell morphology in vivo reveals distinct roles for yeast and filamentous forms of Candida albicans during infection. Eukaryotic cell, 2(5), pp.1053–1060.
Scaduto, C.M. & Bennett, R.J., 2015. Candida albicans the chameleon: Transitions and interactions between multiple phenotypic states confer phenotypic plasticity. Current Opinion in Microbiology, 26, pp.102-108.
Schalch, T. et al., 2005. X-ray structure of a tetranucleosome and its implications for the chromatin fibre. Nature, 436, p.138.
Schindelin, J. et al., 2015. The ImageJ ecosystem: An open platform for biomedical image analysis. Molecular reproduction and development, 82(7–8), pp.518–529.
Schultz, J. et al., 1998. SMART, a simple modular architecture research tool: Identification of signaling domains. Proceedings of the National Academy of Sciences of the United States of America, 95(11), pp.5857–5864.
Schwartz, J.A. et al., 2013. Regulation of Copper Toxicity by Candida albicans GPA2. Eukaryotic Cell, 12(7), pp.954–961.
Sellam, A. et al., 2010. Experimental annotation of the human pathogen Candida albicans coding and noncoding transcribed regions using high-resolution tiling arrays. Genome biology, 11(7), R71.
Selmecki, A., Forche, A. & Berman, J., 2010. Genomic plasticity of the human fungal pathogen Candida albicans. Eukaryotic Cell, 9(7), pp.991-1008
Setiadi, E.R. et al., 2006. Transcriptional Response of Candida albicans to Hypoxia: Linkage of Oxygen Sensing and Efg1p-regulatory Networks. Journal of Molecular Biology, 361(3), pp.399–411.
Seto, E. & Yoshida, M., 2014. Erasers of histone acetylation: The histone deacetylase enzymes. Cold Spring Harbor Perspectives in Biology, 6(4), pp.1–26.
Shahana, S. et al., 2014. New Clox systems for rapid and efficient gene disruption in Candida albicans. PLoS ONE, 9(6):e100390.
Shanmuganathan, A. et al., 2003. Copper-induced oxidative stress in Saccharomyces cerevisiae targets enzymes of the glycolytic pathway. FEBS Letters, 556(1–3), pp.253–259.
Shannon, P. et al., 2003. Cytoscape: a software environment for integrated models of biomolecular interaction networks. Genome research, 13(11), pp.2498–2504.
Sharakhov, I. V. & Sharakhova, M. V., 2015. Heterochromatin, histone modifications, and nuclear architecture in disease vectors. , August 1(10), pp.110–117.
Sharkey, L.L. et al., 1999. HWP1 Functions in the Morphological Development of Candida albicans Downstream ofEFG1, TUP1, and RBF1. Journal of Bacteriology, 181(17), pp.5273–5279.

Sheikh, B.N. et al., 2015. MOZ regulates B-cell progenitors and, consequently, Moz haploinsufficiency dramatically retards MYC-induced lymphoma development. Blood, 125(12), pp.1910–1921.
Shen, H. et al., 2016a. Structural and histone binding ability characterization of the ARB2 domain of a histone deacetylase Hda1 from Saccharomyces cerevisiae. Scientific Reports, 6.
Shen, H. et al., 2016b. Structural and histone binding ability characterization of the ARB2 domain of a histone deacetylase Hda1 from Saccharomyces cerevisiae. Scientific Reports, 6, p.33905.
Shen, J. et al., 2008. The Candida albicans pescadillo homolog is required for normal hypha-to-yeast morphogenesis and yeast proliferation. Proceedings of the National Academy of Sciences of the United States of America, 105(52), pp.20918–20923.
Shiio, Y. & Eisenman, R.N., 2003. Histone sumoylation is associated with transcriptional repression. Proceedings of the National Academy of Sciences, 100(23), p.13225-13230.
Si, H. et al., 2013. Candida albicans White and Opaque Cells Undergo Distinct Programs of Filamentous Growth A. P. Mitchell, ed. PLoS Pathogens, 9(3), e1003210.
Sievers, F. et al., 2011. Fast, scalable generation of high-quality protein multiple sequence alignments using Clustal Omega. Molecular Systems Biology, 7, p.539.
Sievers, F. & Higgins, D., 2014. Clustal Omega. Current Protocols in BioInformatics, 48(1), p.3.13.1-3.13.16.
De Silva, D. et al., 2015. Mitochondrial ribosome assembly in health and disease. Cell Cycle, 14(14), pp.2226–2250.
da Silva Dantas, A. et al., 2016. Cell biology of Candida albicans–host interactions. Current Opinion in Microbiology, 34, pp.111–118.
Simões, J. et al., 2016. The Fungus Candida albicans Tolerates Ambiguity at Multiple Codons. Frontiers in Microbiology, 7, p.401.
Simon, H.A., 1983. Discovery, invention, and development: human creative thinking. Proceedings of the National Academy of Sciences of the United States of America, 80(14), pp.4569–4571.
Singh, A. et al., 2014. Oral candidiasis: An overview. Journal of Oral and Maxillofacial Pathology : JOMFP, 18(Suppl 1), pp.S81-5.
Singh, S.M. & Panda, A.K., 2005. Solubilization and refolding of bacterial inclusion body proteins. Journal of Bioscience and Bioengineering, 99(4), pp.303–310.
Sinha, I. et al., 2017. Cyclin-Dependent Kinases Control Septin Phosphorylation in Candida albicans Hyphal Development. Developmental Cell, 13(3), pp.421–432.
Skrzypek, M. et al., 2017. The Candida Genome Database (CGD): incorporation of Assembly 22, systematic identifiers and visualization of high throughput sequencing data. Nucleic Acids Res, 45(D1), pp.D592-596.
Skrzypek, M.S. & Hirschman, J., 2011. Using the Saccharomyces Genome Database (SGD) for analysis of genomic information. Current protocols in bioinformatics / editoral board, Andreas D. Baxevanis ... [et al.], CHAPTER, Unit1.20.
Slutsky, B. et al., 1987. White-opaque transition a second high-frequency switching system in Candida albicans. Journal of bacteriology, 169(1), pp.189–97.
Sohn, K. et al., 2003. EFG1 is a major regulator of cell wall dynamics in Candida albicans as revealed by DNA microarrays. Molecular microbiology, 47(1), pp.89–102.
Soll, D.R. & Daniels, K.J., 2016. Plasticity of Candida albicans Biofilms. Microbiology and Molecular Biology Reviews, 80(3), p.595.
Southern, P. et al., 2008. C. albicans Colonization of Human Mucosal Surfaces D. Beier, ed. PLoS ONE, 3(4), e2067.
Srikantha, T. et al., 2000. EFG1 Null Mutants of Candida albicans Switch but Cannot Express the Complete Phenotype of White-Phase Budding Cells. Journal of Bacteriology, 182(6), pp.1580–1591.
Srikantha, T. et al., 2001. The histone deacetylase genes HDA1 and RPD3 play distinct roles in regulation of high-frequency phenotypic switching in Candida albicans. Journal of Bacteriology, 183(15), pp.4614–4625.
van Steensel, B., 2005. Mapping of genetic and epigenetic regulatory networks using microarrays. Nature genetics, 37 Suppl, pp.S18-24.
Sterner, D.E. & Berger, S.L., 2000. Acetylation of Histones and Transcription-Related Factors. Microbiology and Molecular Biology Reviews, 64(2), pp.435–459.
Stevenson, J.S. & Liu, H., 2011. Regulation of white and opaque cell type formation in Candida albicans by Rtt109 and Hst3. Molecular microbiology, 81(4), pp.1078–1091.
Stichternoth, C. & Ernst, J.F., 2009. Hypoxic Adaptation by Efg1 Regulates Biofilm Formation by Candida albicans. Applied and Environmental Microbiology, 75(11), pp.3663-3672.
Stoldt, V.R. et al., 1997. Efg1p, an essential regulator of morphogenesis of the human pathogen Candida albicans, is a member of a conserved class of bHLH proteins regulating morphogenetic processes in fungi. The EMBO Journal, 16(8), pp.1982–1991.

Strahl, B.D. & Allis, C.D., 2000. The language of covalent histone modifications. Nature, 403(6765), pp.41–45.
Strati, F. et al., 2016. Age and Gender Affect the Composition of Fungal Population of the Human Gastrointestinal Tract. Frontiers in Microbiology, 7, p.1227.
Strollo, S. et al., 2016. Epidemiology of Hospitalizations Associated with Invasive Candidiasis, United States, 2002–20121. Emerging Infectious Diseases, 23(1), pp.7–13.
Strom, A.R. et al., 2017. Phase separation drives heterochromatin domain formation. Nature, 547, p.241.
Su, C. et al., 2009. Mss11, a Transcriptional Activator, Is Required for Hyphal Development in Candida albicans . Eukaryotic Cell, 8(11), pp.1780–1791.
Subramanian, A. et al., 2005. Gene set enrichment analysis: a knowledge-based approach for interpreting genome-wide expression profiles. Proceedings of the National Academy of Sciences of the United States of America, 102(43), pp.15545–15550.
Sudbery, P., Gow, N. & Berman, J., 2004. The distinct morphogenic states of Candida albicans. Trends in Microbiology, 12(7), pp.317–324.
Sudbery, P.E., 2011. Growth of Candida albicans hyphae. Nature Reviews Microbiology, 9(10), pp.737-748.
Suganuma, T. & Workman, J.L., 2008. Crosstalk among Histone Modifications. Cell, 135(4), pp.604–607.
Sugiyama, T. et al., 2017. SHREC, an Effector Complex for Heterochromatic Transcriptional Silencing. Cell, 128(3), pp.491–504.
Suka, N. et al., 2001. Highly Specific Antibodies Determine Histone Acetylation Site Usage in Yeast Heterochromatin and Euchromatin. Molecular Cell, 8(2), pp.473–479.
Sun, J.N. et al., 2010. Host Cell Invasion and Virulence Mediated by Candida albicans Ssa1. PLOS Pathogens, 6(11), e1001181.
Suzuki, T., Ueda, T. & Watanabe, K., 1997. The “polysemous” codon--a codon with multiple amino acid assignment caused by dual specificity of tRNA identity. The EMBO Journal, 16(5), pp.1122–1134.
Synnott, J.M., Guida, A., Mulhern-Haughey, S., et al., 2010. Regulation of the Hypoxic Response in Candida albicans. Eukaryotic Cell, 9(11), pp.1734–1746.
Synnott, J.M., Guida, A., Mulhern-haughey, S., et al., 2010. Regulation of the Hypoxic Response in Candida albicans □ †. , 9(11), pp.1734–1746.
Taff, H.T. et al., 2012. A Candida Biofilm-Induced Pathway for Matrix Glucan Delivery: Implications for Drug Resistance. PLOS Pathogens, 8(8), e1002848.
Taff, H.T. et al., 2013. Mechanisms of Candidabiofilm drug resistance Access. , 8(10), pp.1–19.
Tang, J., Yan, H. & Zhuang, S., 2013. Histone deacetylases as targets for treatment of multiple diseases. Clinical science (London, England : 1979), 124(11), pp.651–662.
Tao, L. et al., 2014. Discovery of a “White-Gray-Opaque” Tristable Phenotypic Switching System in Candida albicans: Roles of Non-genetic Diversity in Host Adaptation. PLOS Biology, 12(4), e1001830.
Taylor, L.H., Latham, S.M. & Woolhouse, M.E., 2001. Risk factors for human disease emergence. Philosophical transactions of the Royal Society of London. Series B, Biological sciences, 356(1411), pp.983–989.
The UniProt Consortium, 2017. UniProt: the universal protein knowledgebase. Nucleic Acids Research, 45(D1), pp.D158–D169.
Thomson, D.D. et al., 2015. Contact-induced apical asymmetry drives the thigmotropic responses of Candida albicans hyphae. Cellular Microbiology, 17(3), pp.342–354.
Thorvaldsdóttir, H., Robinson, J.T. & Mesirov, J.P., 2013. Integrative Genomics Viewer (IGV): high-performance genomics data visualization and exploration. Briefings in Bioinformatics, 14(2), pp.178–192.
Timmermann, S. et al., 2001. Histone acetylation and disease. Cellular and Molecular Life Sciences CMLS, 58(5), pp.728–736.
Toll-Riera, M. et al., 2012. Role of Low-Complexity Sequences in the Formation of Novel Protein Coding Sequences. Molecular Biology and Evolution, 29(3), pp.883–886.
Torres, H.A. et al., 2003. Aspergillosis caused by non-fumigatus Aspergillus species: risk factors and in vitro susceptibility compared with Aspergillus fumigatus. Diagnostic microbiology and infectious disease, 46(1), pp.25–28.
Trapnell, C. et al., 2012. Differential gene and transcript expression analysis of RNA-seq experiments with TopHat and Cufflinks. Nature Protocols, 7(3), pp.562–578.
Tremethick, D.J., 2007. Higher-Order Structures of Chromatin: The Elusive 30 nm Fiber. Cell, 128(4), pp.651–654.
Troejer, P. et al., 2003. Histone deacetylases in fungi: Novel members, new facts. Nucleic Acids Research, 31(14), pp.3971–3981.
Trojer, P. & Reinberg, D., 2007. Facultative Heterochromatin: Is There a Distinctive Molecular Signature? Molecular Cell, 28(1), pp.1–13.

Tuch, B.B. et al., 2008. The Evolution of Combinatorial Gene Regulation in Fungi L. D. Hurst, ed. PLoS Biology, 6(2), e38.
Tuch, B.B. et al., 2010. The Transcriptomes of Two Heritable Cell Types Illuminate the Circuit Governing Their Differentiation G. P. Copenhaver, ed. PLoS Genetics, 6(8), e1001070.
Tyc, K.M. et al., 2016. The game theory of Candida albicans colonization dynamics reveals host status-responsive gene expression. BMC Systems Biology, 10(1), p.20.
Umeyama, T. et al., 2006. Repression of CDC28 reduces the expression of the morphology-related transcription factors, Efg1p, Nrg1p, Rbf1p, Rim101p, Fkh2p and Tec1p and induces cell elongation in Candida albicans. Yeast, 23(7), pp.537–552.\
Underhill, D.M. & Pearlman, E., 2015. Immune Interactions with Pathogenic and Commensal Fungi: A Two-Way Street. Immunity, 43(5), pp.845–858.
Uppuluri, P. et al., 2010. Dispersion as an important step in the Candida albicans biofilm developmental cycle. PLoS pathogens, 6(3), e1000828.
Uppuluri, P., Mekala, S. & Chaffin, W.L., 2007. Farnesol-mediated inhibition of Candida albicans yeast growth and rescue by a diacylglycerol analogue. Yeast, 24(8), pp.681–693.
Utley, R.T. et al., 1998. Transcriptional activators direct histone acetyltransferase complexes to nucleosomes. Nature, 394, pp.498-502.
van de Veerdonk, F.L., Joosten, L.A.B. & Netea, M.G., 2015. The interplay between inflammasome activation and antifungal host defense. Immunological reviews, 265(1), pp.172–180.
Venters, B.J. et al., 2011. A comprehensive genomic binding map of gene and chromatin regulatory proteins in Saccharomyces. Molecular cell, 41(4), pp.480–492.
Verdone, L. et al., 2006. Histone acetylation in gene regulation. Briefings in Functional Genomics, 5(3), pp.209–221.
Veses, V. & Gow, N.A.R., 2009. Pseudohypha budding patterns of Candida albicans. Medical mycology, 47(3), pp.268–275.
Vieira, B., 2009. Colony Counter Plugin. Available at: https://imagej.nih.gov/ij/plugins/colony-counter.html [Accessed: February 9, 2019]
Villagra, A. et al., 2009. The histone deacetylase HDAC11 regulates the expression of interleukin 10 and immune tolerance. Nature immunology, 10(1), pp.92–100.
Volmar, C.-H. et al., 2017. M344 promotes nonamyloidogenic amyloid precursor protein processing while normalizing Alzheimer's disease genes and improving memory. Proceedings of the National Academy of Sciences, 114(43), pp.E9135–E9144.
Vylkova, S. & Lorenz, M.C., 2014. Modulation of Phagosomal pH by Candida albicans Promotes Hyphal Morphogenesis and Requires Stp2p, a Regulator of Amino Acid Transport. PLOS Pathogens, 10(3), pp.1–13.
Walsh, T. & Dixon, D., 1996. Medical Microbiology, 4th edition: Spectrum of Mycoses, Chapter 75.
Walter, W. et al., 2008. 14-3-3 Interaction with Histone H3 Involves a Dual Modification Pattern of Phosphoacetylation . Molecular and Cellular Biology, 28(8), pp.2840–2849.
Wang, A. et al., 2009. Hyphal Chain Formation in Candida albicans: Cdc28-Hgc1 Phosphorylation of Efg1 Represses Cell Separation Genes . Molecular and Cellular Biology, 29(16), pp.4406–4416.
Wang, X. et al., 2013. Distinct and Redundant Roles of the Two MYST Histone Acetyltransferases Esa1 and Sas2 in Cell Growth and Morphogenesis of Candida albicans. Eukaryotic Cell, 12(3), pp.438–449
Wang, X. & Simpson, R.T., 2001. Chromatin structure mapping in Saccharomyces cerevisiae in vivo with DNase I. Nucleic Acids Research, 29(9), pp.1943–1950. Available at: http://www.ncbi.nlm.nih.gov/pmc/articles/PMC37252/.
Wapenaar, H. & Dekker, F.J., 2016. Histone acetyltransferases: challenges in targeting bi-substrate enzymes. Clinical Epigenetics, 8(1), p.59.
Warenda, A.J. et al., 2003. Candida albicans septin mutants are defective for invasive growth and virulence. Infection and immunity, 71(7), pp.4045–4051.
Weerasekera, M.M. et al., 2016. Culture media profoundly affect Candida albicans and Candida tropicalis growth, adhesion and biofilm development. Memórias do Instituto Oswaldo Cruz, 111(11), pp.697–702.
Wei, G. et al., 2012. Chapter Thirteen - Genome-Wide Mapping of Nucleosome Occupancy, Histone Modifications, and Gene Expression Using Next-Generation Sequencing Technology. In C. Wu & C. D. B. T.-M. in E. Allis, eds. Nucleosomes, Histones & Chromatin Part B. Academic Press, pp. 297–313.
Weissman, Z. et al., 2000. The high copper tolerance of Candida albicans is mediated by a P-type ATPase. Proceedings of the National Academy of Sciences, 97(7), p.3520-3525.
Weissman, Z. & Kornitzer, D., 2004. A family of Candida cell surface haem-binding proteins involved in haemin and haemoglobin-iron utilization. Molecular Microbiology, 53(4), pp.1209–1220.
Weyler, M. & Morschhäuser, J., 2012. Tetracycline-inducible gene expression in Candida albicans. Methods in Molecular Biology, 845, pp.201-210.

Whaley, S.G. et al., 2016. Azole Antifungal Resistance in Candida albicans and Emerging Non-albicans Candida Species. Frontiers in Microbiology, 7, p.2173.
Williams, A.G. et al., 2014. RNA-seq Data: Challenges in and Recommendations for Experimental Design and Analysis. Current protocols in human genetics / editorial board, Jonathan L. Haines ... [et al.], 83, pp.11.13.1-11.13.20.
Williams, S.P. et al., 1986. Chromatin fibers are left-handed double helices with diameter and mass per unit length that depend on linker length. Biophysical Journal, 49(1), pp.233–248.
Wirsching, S. et al., 2001. MDR1-mediated drug resistance in Candida dubliniensis. Antimicrobial agents and chemotherapy, 45(12), pp.3416–3421.
Wisplinghoff, H. et al., 2006. Inflammatory response and clinical course of adult patients with nosocomial bloodstream infections caused by Candida spp. Clinical Microbiology and Infection, 12(2), pp.170–177.
Wisplinghoff, H. et al., 2004. Nosocomial bloodstream infections in US hospitals: analysis of 24,179 cases from a prospective nationwide surveillance study. Clinical infectious diseases : an official publication of the Infectious Diseases Society of America, 39(3), pp.309–317.
Wittschieben, B.Ø. et al., 2000. Overlapping roles for the histone acetyltransferase activities of SAGA and Elongator in vivo. The EMBO Journal, 19(12), pp.3060–3068.
Won, H. et al., 2006. Iron Regulation of the Major Virulence Factors in the AIDS-Associated Pathogen Cryptococcus neoformans., 4(12): e410.
Woolford, C.A. et al., 2016. Bypass of Candida albicans Filamentation/Biofilm Regulators through Diminished Expression of Protein Kinase Cak1 J. Heitman, ed. PLoS Genetics, 12(12), e1006487.
Wu, J. et al., 2001. HDA2 and HDA3 are related proteins that interact with and are essential for the activity of the yeast histone deacetylase HDA1. Proceedings of the National Academy of Sciences of the United States of America, 98(8), pp.4391–6.
Wu, J., Carmen, A.A., et al., 2001. HDA2 and HDA3 are related proteins that interact with and are essential for the activity of the yeast histone deacetylase HDA1. Proceedings of the National Academy of Sciences of the United States of America, 98(8), pp.4391–4396.
Wu, J., Suka, N., et al., 2001. TUP1 Utilizes Histone H3/H2B Specific HDA1 Deacetylase to Repress Gene Activity in Yeast. Molecular Cell, 7(1), pp.117–126. Available at: http://dx.doi.org/10.1016/S1097-2765(01)00160-5.
Wurtele, H. et al., 2010. Modulation of histone H3 lysine 56 acetylation as an antifungal therapeutic strategy. Nature medicine, 16(7), pp.774–780. Available at: http://www.ncbi.nlm.nih.gov/pmc/articles/PMC4108442/.
Xie, J. et al., 2016. The Paralogous Histone Deacetylases Rpd3 and Rpd31 Play Opposing Roles in Regulating the White-Opaque Switch in the Fungal Pathogen Candida albicans. mBio, 7(6), e01807-16.
Xie, J. et al., 2013. White-opaque switching in natural MTLa/alpha isolates of Candida albicans: evolutionary implications for roles in host adaptation, pathogenesis, and sex. PLoS biology, 11(3), e1001525.
Xiong, L. et al., 2010. Mapping of Lysine Methylation and Acetylation in Core Histones of Neurospora crassa. Biochemistry, 49(25), pp.5236–5243.
Xue-Franzén, Y. et al., 2013. Distinct roles of the Gcn5 histone acetyltransferase revealed during transient stress-induced reprogramming of the genome. BMC Genomics, 14, p.479.
Yan, Y. et al., 2002. The catalytic mechanism of the ESA1 histone acetyltransferase involves a self-acetylated intermediate. Nature Structural Biology, 9, p.862.
Yang, W. et al., 2014. Fungal invasion of epithelial cells. Microbiological Research, 169(11), pp.803–810.
Yang, X.-J. & Seto, E., 2009. The Rpd3/Hda1 family of lysine deacetylases: from bacteria and Yeast To Mice and Men. Molecular Cell, 9(3), pp.206–218.
Yi, S. et al., 2011. Alternative Mating Type Configurations (a/α versus a/a or α/α) of Candida albicans Result in Alternative Biofilms Regulated by Different Pathways. PLOS Biology, 9(8), pp.1–17.
Yuan, H. & Marmorstein, R., 2013. Histone Acetyltransferases: Rising Ancient Counterparts to Protein Kinases. Biopolymers, 99(2), pp.98–111.
Yuan, J. et al., 2009. Histone H3-K56 acetylation is important for genomic stability in mammals. Cell cycle (Georgetown, Tex.), 8(11), pp.1747–1753.
Zacchi, L.F., Schulz, W.L. & Davis, D.A., 2010. HOS2 and HDA1 encode histone deacetylases with opposing roles in Candida albicans Morphogenesis. PLoS ONE, 5(8), e12171.
Zeuthen, M.L. & Howard, D.H., 1989. Thermotolerance and the heat-shock response in Candida albicans. Journal of general microbiology, 135(9), pp.2509–2518.
Zhang, L., Fang, H. & Xu, W., 2009. Strategies in Developing Promising Histone Deacetylase Inhibitors, 30(4), pp.585-602.

Zhang, S. et al., 2011. Modification of Histones by Sugar β-N-Acetylglucosamine (GlcNAc) Occurs on Multiple Residues, Including Histone H3 Serine 10, and Is Cell Cycle-regulated. The Journal of Biological Chemistry, 286(43), pp.37483–37495.
Zhang, W. et al., 1998. Essential and redundant functions of histone acetylation revealed by mutation of target lysines and loss of the Gcn5p acetyltransferase. The EMBO Journal, 17(11), pp.3155–3167.
Zhang, Y. & Reinberg, D., 2001. Transcription regulation by histone methylation: interplay between different covalent modifications of the core histone tails. Genes & development, 15(18), pp.2343–2360.
Zhao, R. et al., 2002. Roles of TUP1 in Switching, Phase Maintenance, and Phase-Specific Gene Expression in Candida albicans. Eukaryotic Cell, 1(3), p.353-365.
Zheng, X., Wang, Y. & Wang, Y., 2004. Hgc1, a novel hypha-specific G1 cyclin-related protein regulates Candida albicans hyphal morphogenesis. The EMBO Journal, 23(8), p.1845-1856.
Zhou, X. et al., 2016. Systematic Analysis of the Lysine Acetylome in Candida albicans. Journal of Proteome Research, 15(8), pp.2525–2536.
Zordan, R.E., Galgoczy, D.J. & Johnson, A.D., 2006. Epigenetic properties of white-opaque switching in Candida albicans are based on a self-sustaining transcriptional feedback loop. Proceedings of the National Academy of Sciences of the United States of America, 103(34), pp.12807–12.

APPENDIX 1. *E. coli* related data

1.1: Alignments and Modeling

1.1.1 FASTA pairwise alignment of *C. albicans* Hda1 with Clr3 shows insertions are present relative to the *S. pombe* Clr3 sequence

>Hda1_*C. albicans*
MSTGQEEHLDSKLENQISEEENQSQNQNFPTAIEDSIQASIEKLDEVDDEINPIEVKDEFPTTIGTTY
DILHPREPFPKRIKLEETETEPDSNGIADNDQTMVVVPPKKPQLFYTPLKTGLVYDVRMRYHAKV
FTSYSEYIDPHPEDPRRIYRIYKKLVEAGIVLDPSLAGINEIGPFMLKIPIREATSEEILQVHSEDHLK
FIQSTEDMSRDQLLKETETGDSIYVNNDSYLSAKLSCGGTIEACKAVIEGRVKNSLAIVRPPGHHA
EPNTPAGFCLFSNVAVAAKNMLKNYPESVRRIVIVDWDIHHGNGTQKAFYNDPRVLYISLHRFEN
GKFYPGTKYGDLNQVGEGPGEGFTINIPWRSSGMHDGDYVYAFNKIIQPVISEFDPDLIIVSSGFDA
ADGDVIGACHVTPAGYGYMTHTLKGIARGKLAVILEGGYNLDSISKSALAVAKVLVGEPPENTIT
LRPQAEAIEVVDEVIKIQSKYFKSLRNGIPNGIFEDVYDLADVEKSNYKLVNIADPIRSHQVEKLFN
EKEFINIPIISSPSNGEKPPFTTDLPDQLEDLIVASPDIYNCTTIILTIHDPPEIWANINPTNGVIETNST
MVLEHPLVQIMDKIQKEKDPENQEKFGYLDINIPSFQLPIPGTTSESSTYNPIIFAQEVLLYIWDNYI
AYFQQLKNLVMVGFGDSYQSIVNLYGKRPSNEIKDLIKGTVAFLNRTTLKPLIPVMDESMVDWY
YQNSIIFTSNFNTCWTGGSGAGNGNGNGNNGNSSNGGGNKSADSNGHDDFSKRPRKKFGRVI
KAKTDGLCDVIQEKFDEGVDFILDSIEDYSSSED

>c5ikkA_Clr3_*S. pombe*

KKSGLCYDPRMRFHATLSE--------HPEDPRRVLRVFEAIKKAGYVSNV-----
PSPSDVFLRIPAREATLEELLQVHSQEMYDKMSHEDLANLEKISD------
SLYYNNESAFCARLACGSAIETCTAVVTGQVKNAFAVVRPPGHH---------
ALFNNVSVTARSMLQRFPDKIKRVLIVDWDIHHGNGTQMAFYDDPNVLYVSLHRYENGRFYPGT
NYGCAENCGEGPGLGRTVNIPWSCAGMGDGDYIYAFQRVVMPVAYEFDPDLVIVSCGFDAAAG
DHIGQFLLTPAAYAHMTQMLMGLADGKVFISLEGGYNLDSISTSALAVAQSLLGIPPGRLHTTYA
CPQAVATINHVTKIQSQYWRCMRPKH------
-----FDANPKDAHVDRLHDVIRTYQAKKLFEDWKITNMPIL----------
RDNNQVLCSSNFFQKDNLLVIVHESPRVLGNGTSETNVLNLNDSL--------
LVDPVSLYVEWAMQQDWGLIDINIPEV----------
DILSEVKELCLYVWDNYVELSISKNIFFIGGGKAVHGLVNLASSR---
NVSDRVKCMVNFLGTEPLVGLKTASEEDLPTWYYRHSLVFVSSSNECW----------
---KKAKRAKRRYGRLMQSEHTETSDMMEQHYRAVTQYLLHLLQ-------

1.1.2 Information about templates for Hda2 and Hda3 protein models

<u>Hda2</u>

While no part of this crystal structure has been solved in *S. cerevisiae*, its similarity with the Hda3DBD solved structure (PDB: 3HGT) is the first noted hit on the Phyre2 search. This protein forms a dimer and the templated region (3HGT: aa 23-305 aligns with most of the N-terminal half of Hda2 (aa 70-373; 45 % coverage).

Otherwise, the closest N-terminal region modeling template for this protein rests upon two known structures of the yeast CHD1 protein (PDB: 5O9G, 3MWY). The templated mid-protein region of CHD1 (aa 519-1023) aligns with the N-terminal half of

Hda2 and contributes information closer to the start of the protein (aa 9-342; 49 % coverage) compared to the 3HGT template.

The other templates for this model are proteins from organisms outside the fungal kingdom. *S. pnemoniae* PcsB (PDB: 4CGK) is an essential virulence related cell-cycle protein involved in bacterial cell division. The templated region (aa 43-281) aligns over the coiled-coil domain of Hda2 (aa 440-668; 32 % coverage) (Bartual et al. 2014).

The *A. gambiae* protein binding region, heterodimer protein complex (PDB: 3OJA) of Leucine-Rich Immune Molecule 1 (LRIM1) and *Anopheles Plasmodium*-responsive Leucine-rich repeat protein 1 (APL1). These two leucine-rich proteins control the function of thioester-containing protein 1 (TEP1) which is an immune response protein that marks invading organisms for degradation (Baxter et al. 2010). The templating region used to construct the Hda2 model is in the C-terminal portion of APL1 (aa 400-580) which contributes structure for the coiled-coil domain region of Hda2 (aa 450-593; 21 % coverage).

The amoeba or slime mold, *D. discoideum* dynein motor domain (PDB: 3VKG), is part of a complex that works based upon microtubules and it contributes to cellular transport and cell division. (Kon et al. 2012) The templated mid-protein region (aa 1896-2103) aligns over the coiled-coil domain of Hda2 (aa 418-618; 29 % coverage).

The final template used to model the structure of *C. albicans* Hda2 is unphosphorylated *H. sapiens* Signal Transducers and Activators of Transcription (STAT1). This human protein serves as a template aligning with Hda2 from the region after the Hda2-3 domain through the coiled-coil domain (aa 376-594; 32 % coverage). When phosphorylated, these proteins move from their regular location in the cytoplasm into the nucleus. Their phosphorylation is cytokine and growth factor dependent. Phosphorylation of STAT1 protein also triggers their dimerization, DNA binding and subsequent activation of transcription. The templated region (PDB: 1YVL) covers most of the coiled-coil domain (CCD) of this protein. The dimer forms through the coiled-coil domain of one monomer and the DNA binding domain (DBD) of the other with an uncommon hydrophilic interaction but the key residues of this interaction are not conserved or are outside of the aligned region (aa 80-312) (Mao et al. 2005).

Hda3

Hda3 modeling also found a template in *S. cerevisiae* Hda3 (PDB: 3HGT) and *S.pneumoniae* PcsB (PDB: 4CGK). These contributed to the model by aligning with

regions at the first part of the Hda2-3 domain and through most of the coiled-coil domain respectively (3HGT: aa 22-158 with Hda3: aa 25-170; 4CGK aa 46-252/17 % coverage with Hda3: aa 582-788/ 24 % coverage).

Almost the entire sequence for *S. scrofa* (wild boar) tropomycin (PDB: 1C1G) also contributes a template (aa 1-238) for the C-terminal region (aa 535-820/34% coverage). This tropomycin protein is structurally a coiled-coil. It forms a polymerized filament that works in complex with troponin to form a calcium sensitive switch and changes the ability of actin to interact with myosin in muscle and non-muscle cells (Whitby & Phillips 2000).

The hydrothermal vent dwelling archaeon, Pyrococcus yayanosii is noted as having a high GC content (Jun et al. 2011). This may be why a similarity is found between the SMC protein of this organism (PDB: 5XG2) and *C. albicans* Hda3 (aa 581-813/27 % coverage) although the GC content of this region is 21 %. Almost the entire characterized portion (aa 2-245) of this proteins structure is used as a template for this model of the region covering the two Hda3CCD (Diebold-Durand et al. 2017).

Paradoxically, a more realistic estimation can be constructed for the structure of *C. albicans* Hda2 protein and yet a portion of the Hda3 DNA binding domain from *S. cerevisiae* is the main solved structure that provides experimental data about both *C. albicans* Hda2 and Hda3.

1.1.3 Thermal shift Assay

Buffer layout

	2	3	4	5	6	7	8	9	10	11
Row C	Tris pH7 0 NaCl 0 Glycerol	Tris pH7.5 0 NaCl 0 Glycerol	Tris pH8 0 NaCl 0 Glycerol	Tris pH9.8 0 NaCl 0 Glycerol	MES pH5.5 0 NaCl 0 Glycerol	MES pH6 0 NaCl 0 Glycerol	MES pH6.5 0 NaCl 0 Glycerol	HEPES pH6.5 0 NaCl 0 Glycerol	HEPES pH 7 0 NaCl 0 Glycerol	HEPES pH7.5 0 NaCl 0 Glycerol
Row D	Tris pH7 100mM NaCl	Tris pH7.5 100mM NaCl	Tris pH8 100mM NaCl	Tris pH9 100mM NaCl	MES pH5.5 100mM NaCl	MES pH6 100mM NaCl	MES pH6.5 100mM NaCl	HEPES pH6.5 100mM NaCl	HEPES pH 7 100mM NaCl	HEPES pH7.5 100mM NaCl
Row E	Tris pH7 200mM NaCl	Tris pH7.5 200mM NaCl	Tris pH8 200mM NaCl	Tris pH9 200mM NaCl	MES pH5.5 200mM NaCl	MES pH6 200mM NaCl	MES pH6.5 200mM NaCl	HEPES pH6.5 200mM NaCl	HEPES pH 7 200mM NaCl	HEPES pH7.5 200mM NaCl
Row F	Tris pH7.5 100mM KCl	Tris pH9 100mM KCl	Tris pH7 200mM KCl	Tris pH8 200mM KCl	Tris pH8 0.5% Glycerol 15mM KCl	Tris pH8 150mM KCl 3mM MgCl 0.25% Glycerol	MES pH5.5 100mM KCl	MES pH6.5 200mM KCl	HEPES pH6.5 100mM KCl	HEPES pH7.5 200mM KCl
Row G (There was not enough protein to run this row)	Tris pH7 100mM NaCl 5% Glycerol	Tris pH7.5 0 NaCl 5% Glycerol	Tris pH8 75mM KCl 10% Glycerol MES 5.5	Tris pH9 200mM NaCl 5% Glycerol	MES pH5.5 0 NaCl 5% Glycerol	MES pH6 100mM NaCl 5% Glycerol	MES pH6.5 200mM KCl 5% Glycerol	HEPES pH6.5 200mM NaCl 5% Glycerol	HEPES pH 7 0 NaCl 5% Glycerol	HEPES pH7.5 150mM KCl 10% Glycerol

APPENDIX 2. *C. albicans* related data

2.1: Constructs and sequences

2.1.1 Sequences of *C. albicans* Hda1 complex proteins with detail of domain and expression designations

green = deacetylase domain (Hda1)/ Pfam Hda2-3 domain (Hda2 or Hda3)
yellow = Arb2 domain (Hda1)/ Coiled-coil domain (Hda2 or Hda3)
fuchsia = construct start sites
blue = construct end sites

>Hda1
MSTGQEEHLDSKLENQISEEENQSQNQNFPTAIEDSIQASIEKLDEVDDEINPIEVKDEFPTTIG
TTYDILHPREPFPKRIKLEETETEPDSNGIADNDQTMVVVPPKKPQLFYTPLKTGLVYDVRMR
YHAKVFTSYSEYIDPHPEDPRRIYRIYKKLVEAGIVLDPSLAGINEIGPFMLKIPIREATSEEILQ
VHSEDHLKFIQSTEDMSRDQLLKETETGDSIYVNNDSYLSAKLSCGGTIEACKAVIEGRVKNS
LAIVRPPGHHAEPNTPAGFCLFSNVAVAAKNMLKNYPEVRRIVIVDWDIHHGNGTQKAFYN
DPRVLYISLHRFENGKFYPGTKYGDLNQVGEGPGEGFTINIPWRSSGMHDGDYVYAFNKIIQ
PVISEFDPDLIIVSSGFDAADGDVIGACHVTPAGYGYMTHTLKGIARGKLAVILEGGYNLDSI
SKSALAVAKVLVGEPPENTITLRPQAEAIEVVDEVIKIQSKYFKSLRNGIPNGIFEDVYDLADV
EKSNYKLVNIADPIRSHQVEKLFNEKEFINIPIISSPSNGEKPPFTTDLPDQLEDLIVASPDIYNC
TTIILTIHDPPEIWANINPTNGVIETNSTMVLEHPLVQIMDKIQKEKDPENQEKFGYLDINIPSF
QLPIPGTTSESSTYNPIIFAQEVLLYIWDNYIAYFQQLKNLVMVGFGDSYQSIVNLYGKRPSNE
IKDLIKGTVAFLNRTTLKPLIPVMDESMVDWYYQNSIIFTSNFNTCWTGGSGAGNGNGNGN
GNNGNSSNGGGNKSADSNGHDDFSKRPRKKFGRVIKAKTDGLCDVIQEKFDEGVDFILDSIE
DYSSSED*

>Hda2
MNLIDMLSKDPPSSLYNPELEENIQNNEISNGISISESQDNIILDNNSNGNINNNNNNDINININ
NSNPPSIIYLPTPLTELQKSFVEMTLHLFSSELLNEVRSKRLKTSIDNLLDSSTTIEESDIIVNQN
KISLCFEQLSIICDHPSLLIEHFIPKKMLLSETNERQLNLSGKLELFNRIIDTLIEQKPPNGYRIIV
VSDNVKELELVEGIIVGKTLYYINSTNAKLFESTHFVPDLKDKSSDKVFINLLTTQQLSSNYV
SDKDGECYDLIFSFDPNLDVQTPSIEILQRENGNQCPILVPIPVFTLEHIALQLPQPQQVDLMES
IDAALNKWRVKCINTLVVNFFNLDEMSNDFFTENYGLNMKEFWNMMHNNRQGLNKLLDN
YNGQLVLSFSEEKLIKKLNSFYNRGGNGGFDQVRDANCQLFKSKLAEAVYQKFMDLDEGV
DEIELNLNGKREYETARELQYDDDEDYIANNYKKFRRLNDDANMSERKLARVDTDLLKQK
QKLVFLKNKLEHLVDIADKEITDAEATSQTQSSKTLQQEVENLKKEFNRINVECEGTREKYQ
SSSSVALQLSHRLTQLKQQNEKI ERKLFGPGMAQLPELIKKDALLSYELKLKHLEKKNEFMQ
Q FFSSKIEMTYQERQQLLENSGSGANNRQNNRISRGATPL*

>Hda3
MDLRKILDTTPEPPIIEPDIANINYSGDYQ LPTPMYDFQKELTDQIVSLHYPDILKYCELNDRR
EIIIKSLDICLENCQLVSNHPYLLIDHYMPKNLTFKQLPEKLAETSGKFNVFKDLINVLIDDKN
NYSINVGVVINNKRNLFDLIDALLLGCSRSNNNVTVIRYSGN NVLRESKKKAQNKTTTSNSS
TTTSTTTATTAIATTTTTTA TKKHKKKHATKEKGYGKHKIQNHSVTIHLI PHDGQISKGKPD
LKEVKFDLLIVFDGSVDT ESDFFKLLRIQNRNVNINNNVNDNVNDNFMTSNIKSDRGR LLT
RGRHSTRGRPSTKENLLVDKNSSEESIINLPPCAIIRLIPTRTVEHAKLYYKPDEDKPDYLTKVI
SSIVCLRDSIGQLPPDIYPIYHQKLTYFSHTFFDKLFQSTTMAQTKINGKNKYNDHYNDEHEH
EHDHIHDHDHDHEYPGWPLPDLPKIIKFSPYDVERSLLTETRFHYTPYDFNPNHLNNENSSKD
YKNQLKSTYYESKRLQSEYITNPLKNSYDVLTGIYRTTNNDAKILTHKLILQLNEAFMKRDR
LNKELETYNKFHNNDWQINKIGRRDHILKSTKKSIEDDINQCQIRINNVNKSIDEKTQELESIK
LEIKQLQLQLENFKSKNPNSSSSSSSSTSKTKATTSENENNSKRKRSDDDDDNDDDSLAPDTT
TTTINTKNQQFIDEQFKIWELQEQINDYIHKIELKNNEKQFAFKEYE NCLKSIDDSNKQIENLI

DQYNNNKRKFDELIEKNPLNNNN NNNNQFEIEKQKLITKIKDQEIINESLKFKLNNAFTFLND
TKYLKKRKNRGITPK*

2.2: Sequences with mass spectroscopy identified peptides

highly significant score as detailed in Figure legend (p<.05) = bold and underlined
matched peptides = bold

2.2.1 Mass spectrometry detail: Hda1 C-terminal tagging

MSTGQEEHLDSKLENQISEE ENQSQNQNFPTAIEDSIQASIEKLDEVDDEINPIEV**KDEFPTTI**
GTTYDILHPREPFPKRIKLEETETEPDSNGIADNDQTMVVVPPKKPQLFYTPLKTG**LVYDVR**
MRYHAKVFTSYSEYIDPHPEDPRRIYRIYKKLVEAGIVLDPSLAGINEIGPFMLKIPIREATSE
EILQVHSEDHLKFIQSTEDMSRDQLLKETETGDSIYVNNDSYLSAKLSCGGTIEACKAVIEGR
VKNSLAIVRPPGHHAEPNTPAGFCLFSNVAVAA**KNMLKNYPESV**RRIVIVDWDIHHGNGTQ
KA**FYNDP**RVLYISLHRFENGKFYPGTKYGDLNQVGEGPGEGFTINI PWRS**SGMHDGDYVY**
AFNKIIQPVISEFDPDLIIVSSGFDAADGDVIGACHVTPAGYGYMTHTLKGIARG**KLAVILEG**
GYNLDSISKSALAVA**KVLVGEPPENTITLRPQAEAIEVVDEVIKI**QSKYFKSLRNGIPNGIF
EDVYDLADVEK SNYKLVNIADPIRSHQVEKLFNEKEFINIPIISSPSNGEKPPFTTDLPDQLED
LIVASPDIYNCTTIILTIHDPPEIWANINPTNGVIETNSTMVLEHPLVQIMDKIQKEKDPENQEK
FGYLDINPSFQLPIPGTTSESSTYNPIIFAQEVLLYIWDNYIAYFQQL**KNLVMVGFGDSYQSIV**
NLYGKRPSNEIKDLIKGTVAFLNRTTLKPLIPVMDESMVDWYYQNSIIFTSNFNTCWTGGS
GAGNGNGNGNGNNGNSSNGGGNKSADSNGHDDFSKRPRKKFGRVIKAKTDGLCDVIQEKF
DEGVDFILDSIEDYSSSED*

Key: **Bold:** matched peptide regions from 6x His tagged Hda1pET21b MSMS with scores; in fuchsia are the portions also recognized in the ~75kD band. The **bold and underlined**: was recognized in MSMS of the full length and ~75 kDa samples with scores of 43 and 61 respectively, two other peptides were also recognized with high significance among within the fuchia marked peptide sequences (RIVIVDWDIHHGNGTQKA and RNGIPNGIFEDVYDLADVEKS; scores 45 and 50 respectively).

2.2.2 Mass spectrometry detail: Hda1 N-terminal tagging

MSTGQEEHLDSKLENQISEEENQSQNQNFPTAIEDSIQASIEKLDEVDDEINPIEV**KDEFPTTI**
GTTYDILHPREPFPKRIKLEETETEPDSNGIADNDQTMVVVPPKKPQLFYTPLKT**GLVYDVR**
MRYHA**KVFTSYSEYIDPHPEDPRR**IYRIYKKLVEAGIVLDPSLAGINEIGPFMLKIP**IREATS**
EEILQVHSEDHLKFIQSTEDMSRDQLLKETETGDSIYVNNDSYLSAKLSCGGTIEACKAVIE
GRVKNSLAIVRPPGHHAEPNTPAGFCLFSNVAVAAKNML**KNYPESVRRIVIVDWDIHHGN**
GTQKAFYNDPRVLYISLHRFENGKFYPGT**KYGDLNQVGEGPGEGFTINIPWRSSGMHDG**
DYVYAFNKIIQPVISEFDPDLIIVSSGFDAADGDVIGACHVTPAGYGYMTHTLKGIARG**KLA**
VILEGGYNLDSISKSALAVA**KVLVGEPPENTITLRPQAEAIEVVDEVIKI**QSKYFKSL**RNGI**
PNGIFEDVYDLADVEKSNY**KLVNIADPIRS**HQVEKLFNEKEFINIPIISSPSNGEKPPFTTDLP
DQLEDLIVASPDIYNCTTIILTIHDPPEIWANINPTNGVIETNSTMVLEHPLVQIMDKIQKEKDP
ENQEKFGYLDINIPSFQLPIPGTTSESSTYNPIIFAQEVLLYIWDNYIAYFQQL**KNLVMVGFGD**
SYQSIVNLYGKRPSNEIKDLIKGTVAFLNRTTLKPLIPVMDESMVDWYYQNSIIFTSNFNTC
WTGGSGAGNGNGNGNGNNGNSSNGGGNKSADSNGHDDFSKRPRKKFGRVIKAKTDGLCD
VIQEKFDEGVDFILDSIEDYSSSED*

Key: Protein Sequence with highlighted **bold** matched peptide regions from GST-Hda1 MSMS with scores. The **bold and underlined** peptide was recognized in MSMS with a scores of 45.

2.2.3 Mass spectrometry detail: 6xHis-Arb2-C

MSTGQEEHLDSKLENQISEEENQSQNQNFPTAIEDSIQASIEKLDEVDDEINPIEVKDEFPTTIG
TTYDILHPREPFPKRIKLEETETEPDSNGIADNDQTMVVVPPKKPQLFYTPLKTGLVYDVRMR

YHAKVFTSYSEY IDPHPEDPRRIYRIYKKLVEAGIVLDPSLAGINEIGPFMLKIPIREATSEEIL
QVHSEDHLKFIQSTEDMSRDQLLKETETGDSIYVNNDSYLSAKLSCG GTIEACKAVIEGRVK
NSLAIVRPPGHHAEPNTPAGFCLFS NVAVAAKNMLKNYPESVRRIVIVDWDIHHGNGTQKA
FYNDPRVLYISLHRFENGKFYPGTKYGDLNQVGEGPGEGFTINIPWRSSGMHDGDYVYAFN
KIIQPVISEFDPDLIIVSSGFDAADGDVIGACHVTPAGYGYMTHTLKGIARGKLAVILEGGYNL
DSISKSALAVA**KVLVGEPPENTITLRPQAEAIEVVDEVIKI**QSKYFKSLRNGIPNGIFE DVY
DLADVEKSNYKLVNIADPIRS**HQVEKL**FNEKEFINIPIISSPSNGEKPPFTTDLPDQLEDLIVAS
PDIYNCTTIILTIHDPPEIWAN INPTNGVIETNSTMVLEHPLVQIMDKIQKEKDPENQEKFGYL
DINIPSFQLPIPGTTSESSTYNPIIFAQEVLLYIWDNYIAYFQQL**KNLVMVGFGDSYQSIVNLY
G**KRPSNEIKDLIKG**TVAFLNRT**TLKPLIPVMDESMVDWYYQNSIIFTSNFNTCWTGGSGAGN
GNGNGNGNNGNSSNGGGN**KSADSNGHDDFSKRPRK**KFGRVIKAKTDGLCDVIQEKFDEG
VDFILDSIEDYSSSED*

Key: Protein Sequence with **bold**: matched peptide regions from 6xHis tagged Arb2 domain through end of Hda1. The **bold and underlined**: peptide was recognized in MSMS with a scores of 70, 64 and 51 respectively.

2.2.4 Mass spectrometry detail: Hda2

MNLIDMLSKDPPSSLYNPELEENIQNNEISNGISISESQD NIILDNNSNGNINNNNNNDINININ
NSNPPSIIYLPTPLTELQ**KSFVEMTLHLFSSELLNEVRS**KRLKTSIDNLLDSSTTIEESDIIVNQ
NKISLCFEQLSIICDHPSLLIEHFIPKKMLLSETNE**RQLN LSGKLELFNRIIDTLIEQKPPNGY
RI**IVVSDNVKELELVE GIIVGKTLYY INSTNAKLFESTHFVPDLKDKSSDKVFINLLTTQQLSS
NYVSDKDGECYDLIFSFDPNLDVQTPSIEILQRENGNQCPILVPIPVFTLEHIALQLPQPQQVDL
MESIDAALNKWRVKCINTLVVNFFNLDEMSNDFFTENYGLNM**KEFWNMMHNNRQ**GLN**K
LLDNYNGQLVLSFSEEKL**IKKLNSFYNRGGNGGFDQVRDANCQLFKSKLAEAVYQKFMDL
DEGVDEIELNLNGKREYETARELQYDDDEDYIANNYKKFRRLNDDANMSERKLARVDTDL
LKQKQKLVFLKNKLEHLVDIADKEITDAEATSQTQSSKTLQQEVENLKKEFNRINVECEGTR
E**KYQSSSSVALQLSHRL**TQLKQQNEKIERKLFGPGMAQLPELIKKDALLSYELKLKHLEKK
NEFMQQFFSSKIEMTYQERQQLLENSGSGANNRQNNRISRGATPL*

Key: Sequence with Bold: matched peptides regions from MSMS with scores ≥25 in **bold**; score = 70 ($p < .05$) designated in **bold and underline**.

APPENDIX 3. Gene expression related data

3.1 Statistical analyses

3.1.1 T-test results for verification of YPD DESeq2 results by qRT-PCR

(A) **LYS22**

t(2) = 4.52 ; p = **0.046**

Strain	Mean	Standard Deviation	DESeq2 log2
WT	0.016	0.00	
*hda1*ΔΔ	0.064	0.015	2.25

t(2) = 4.38 ; p = **0.048**

Strain	Mean	Standard Deviation	DESeq2 log2
WT	0.020	0.01	
*hda2*ΔΔ	0.045	0.01	2.61

t(2) = 27.83 ; p = **0.001**

Strain	Mean	Standard Deviation	DESeq2 log2
WT	0.016	0.00	
*hda3*ΔΔ	0.023	0.00	1.15

(B) **SOU2**

t(2) = 1.73 ; p = 0.23

Strain	Mean	Standard Deviation	DESeq2 log2
WT	0.009	0.00	
*hda1*ΔΔ	0.022	0.01	3.08

t(2) = 2.39 ; p = 0.14

Strain	Mean	Standard Deviation	DESeq2 log2
WT	0.009	0.11	
*hda2*ΔΔ	0.019	0.01	1.86

t(2) = 0.13 ; p = 0.9

Strain	Mean	Standard Deviation	DESeq2 log2
WT	0.009	0.000	
*hda3*ΔΔ	0.008	0.011	0.40

(C) **RBR1**

t(2) = 2.17 ; p = 0.16

Strain	Mean	Standard Deviation	DESeq2 log2
WT	0.005	0.00	
*hda1*ΔΔ	0.013	0.01	2.00

t(2) = 1.72 ; p = 0.23

Strain	Mean	Standard Deviation	DESeq2 log2
WT	0.005	0.00	
*hda2*ΔΔ	0.147	0.01	1.44

t(2) = 1.85 ; p = 0.21

Strain	Mean	Standard Deviation	DESeq2 log2
WT	0.005	0.00	
*hda3*ΔΔ	0.013	0.01	1.11

3.1.2 T-test results for verification of RPMI DESeq2 results by qRT-PCR

(A) **WOR1**

t(6) = 5.21 ; p = **0.002**

Strain	Mean	Standard Deviation	DESeq2 log2
WT	0.004	0.001	
*hda1*ΔΔ	0.023	0.007	**3.86**

t(5) = 2.95 ; p = **0.03**

Strain	Mean	Standard Deviation	DESeq2 log2
WT	.004	0.001	
*hda2*ΔΔ	.006	0.00	**1.92**

t(6) = 2.72 ; p = **0.035**

Strain	Mean	Standard Deviation	DESeq2 log2
WT	.0044	0.00	
*hda3*ΔΔ	.0077	0.00	**1.88**

(B) **RFX2**

t(4) = 3.10 ; p = **0.04**

Strain	Mean	Standard Deviation	DESeq2 log2
WT	0.062	0.01	
*hda1*ΔΔ	0.034	0.01	**-0.74**

t(4) = 6.40 ; p = **0.003**

Strain	Mean	Standard Deviation	DESeq2 log2
WT	0.062	0.01	
*hda2*ΔΔ	0.028	0.01	-0.27

t(4) = 7.84 ; p = **0.001**

Strain	Mean	Standard Deviation	DESeq2 log2
WT	0.062	0.01	
*hda3*ΔΔ	0.022	0.01	**-0.77**

(C) **RBR1**

t(4) = 9.31 ; p = **0.001**

Strain	Mean	Standard Deviation	DESeq2 log2
WT	0.032	0.00	
*hda1*ΔΔ	0.058	0.00	**0.70**

t(4) = 4.35 ; p = **0.01**

Strain	Mean	Standard Deviation	DESeq2 log2
WT	0.032	0.00	
*hda2*ΔΔ	0.047	0.00	**1.15**

t(4) = 1.32 ; p = 0.26

Strain	Mean	Standard Deviation	DESeq2 log2
WT	0.032	0.00	
*hda3*ΔΔ	0.042	0.01	**0.90**

3.2 DEseq2 Log2 values for some genes of interest

3.2.1 Osmolarity and NaCl related

(A)

Yeast inducing media: YPD

Gene	hda1ΔΔ	hda2ΔΔ	hda3ΔΔ
ENA2	0.84	0.30	-0.03
HOG1	-0.50	0.20	-0.30

(B)

Hyphae inducing media: RPMI

Gene	hda1ΔΔ	hda2ΔΔ	hda3ΔΔ
ENA2	-0.35	0.47	**0.64**
HOG1	-0.03	-0.01	-0.01

3.2.2 *MDR1* and *MRR1* related

(A)

Gene	hda1ΔΔ	hda2ΔΔ	hda3ΔΔ
CDR1	0.59	0.27	0.17
CDR2	**0.82**	0.72	0.42
ERG11	-0.28	-0.3	-0.1
HAP43 (CAP2)	**-0.69**	-0.07	-0.17
MRR1	0.54	0.39	0.06
TAC1	0.48	0.61	0.064
UPC2	-0.1	0.26	-0.61

(B)

Gene	hda1ΔΔ	hda2ΔΔ	hda3ΔΔ
CAP1	**1.56**	**0.89**	0.02
CR_09100C	**2.67**	**2.63**	0.96
GCN4	**1.16**	**1.16**	0.27
GRP2	**1.35**	**1.52**	0.56
IFD6	**3.38**	**3.63**	0.97
MDR1	**3.21**	**2.92**	0.61
SNZ1	-0.05	0.22	0.19

3.2.3 Filamentation related genes

(A)

Positive regulation of hyphae- Yeast inducing media: YPD

Gene	hda1ΔΔ	hda2ΔΔ	hda3ΔΔ
BCR1	**1.15**	0.65	0.72
CDC11	**-0.82**	-0.27	-0.26
CDC28	-0.29	-0.19	-0.37
CPH2	-0.00	-0.64	0.07
CPP1	0.25	0.40	0.66
CZF1	0.35	0.27	0.56
DCK1	**-1.04**	**-0.79**	-0.22
FGR23	**1.95**	0.43	0.34
FGR47	**0.94**	0.67	0.94
FGR6-1	-0.52	-0.75	0.18
FGR6-10	-0.40	-0.39	0.07
HOS2	0.76	0.32	-0.03
HST3	-0.41	-0.51	-0.15
MSS1/C2_00820W_A	-0.33	-0.20	-0.20
RAC1	-0.42	-0.23	-0.12
TEC1	-0.43	-0.12	0.16
UME6	0.46	0.58	1.05
YNG2/NBN1	-0.39	-0.23	-0.26

(B)

Positive regulation of hyphae- Hyphae inducing media: RPMI

Gene	hda1ΔΔ	hda2ΔΔ	hda3ΔΔ
BCR1	-0.28	0.21	0.14
CDC11	-0.56	-0.43	-0.16
CDC28	-0.41	-0.37	-0.22
CPH2	-0.21	-0.12	0.29
CPP1	0.32	0.22	0.09
CZF1	-0.50	0.29	0.34
DCK1	-0.31	**-0.65**	-0.38
FGR23	**1.56**	-0.32	0.05
FGR47	0.17	0.11	0.04
FGR6-1	-0.10	0.13	0.30
FGR6-10	-0.22	-0.02	0.34
HOS2	0.11	0.01	-0.14
HST3	0.14	0.03	-0.05
MSS1/C2_00820W_A	0.26	0.00	-0.32
RAC1	-0.34	-0.18	-0.17
TEC1	**-0.85**	-0.13	-0.12
UME6	**-1.54**	**-1.35**	**-1.84**
YNG2/NBN1	0.08	0.21	0.26

(C) Elongation of hyphae- Yeast inducing media: YPD

Gene	hda1ΔΔ	hda2ΔΔ	hda3ΔΔ
ESA1	-0.31	0.10	-0.20
GCN5	-0.12	-0.06	0.07

(D) Elongation of hyphae- Hyphae inducing media: RPMI

Gene	hda1ΔΔ	hda2ΔΔ	hda3ΔΔ
ESA1	-0.21	-0.03	0.18
GCN5	0.20	0.25	0.43

(E) Bidirectional regulation- Yeast inducing media: YPD

Gene	hda1ΔΔ	hda2ΔΔ	hda3ΔΔ
EFG1	-0.33	-0.16	-0.38
FLO8	0.39	-0.39	-0.38
HBR1	**-1.14**	-0.57	-0.37

(F) Bidirectional regulation- Hyphae inducing media: RPMI

Gene	hda1ΔΔ	hda2ΔΔ	hda3ΔΔ
EFG1	-0.36	0.12	0.02
FLO8	-0.07	0.05	0.25
HBR1	0.12	0.10	0.31

(G) Negative regulation of hyphae- Yeast inducing media: YPD

Gene	hda1ΔΔ	hda2ΔΔ	hda3ΔΔ
BRG1	0.51	-0.09	0.33
NRG1	**-0.91**	**-0.75**	-0.62
RBF1	-0.13	0.01	-0.32
RFG1	-0.65	-0.49	-0.12
RPD31	**-0.79**	-0.25	-0.04
SET3	**-0.73**	-0.75	-0.18
SFL1	**0.83**	**0.71**	0.03
SSN6	-0.04	-0.03	0.01
TUP1	**-0.85**	-0.16	-0.35
YAK1	0.27	0.03	0.35

(H) Negative regulation of hyphae- Hyphae inducing media: RPMI

Gene	hda1ΔΔ	hda2ΔΔ	hda3ΔΔ
BRG1	**0.74**	0.15	**0.65**
NRG1	-0.09	0.42	**0.84**
RBF1	0.37	0.31	0.28
RFG1	-0.82	-0.21	-0.25
RPD31	0.02	-0.11	-0.13
SET3	-0.14	-0.08	0.31
SFL1	0.38	**0.66**	0.11
SSN6	-0.16	0.12	0.32
TUP1	0.13	0.18	0.31
YAK1	-0.47	-0.11	0.30

(I) Hyphae-yeast transition- Yeast inducing media: YPD

Gene	hda1ΔΔ	hda2ΔΔ	hda3ΔΔ
PES1	**-1.31**	**-1.20**	-0.26

(J) Hyphae-yeast transition- Hyphae inducing media: RPMI

Gene	hda1ΔΔ	hda2ΔΔ	hda3ΔΔ
PES1	**0.76**	**0.59**	**1.13**

3.2.4 Biofilm related genes

(A) Biofilm formation- Yeast inducing media: YPD

Gene	hda1ΔΔ	hda2ΔΔ	hda3ΔΔ
BCR1	**1.15**	**0.65**	0.72
NDT80	-0.40	-0.25	0.19
ROB1	**-0.80**	-0.45	-0.11

(B) Biofilm formation- Hyphae inducing media: RPMI

Gene	hda1ΔΔ	hda2ΔΔ	hda3ΔΔ
BCR1	-0.28	0.21	0.14
NDT80	0.17	0.33	0.47
ROB1	-0.21	-0.23	0.28

(C) Adherence of biofilm- Yeast inducing media: YPD

Gene	hda1ΔΔ	hda2ΔΔ	hda3ΔΔ
ACE2	-0.43	-0.34	0.03
ARG81	0.48	-0.15	0.22
RLM1	0.38	0.16	0.01
SNF5	-0.30	0.06	-0.03

(D) Adherence of biofilm- Hyphae inducing media: RPMI

Gene	hda1ΔΔ	hda2ΔΔ	hda3ΔΔ
ACE2	-0.23	-0.21	-0.13
ARG81	-0.03	0.11	0.07
RLM1	-0.28	0.22	0.11
SNF5	0.05	0.10	0.08

(E) Cell wall and biofilm- Yeast inducing media: YPD

Gene	hda1ΔΔ	hda2ΔΔ	hda3ΔΔ
BGL2	**-0.85**	-0.12	-0.27
GSC1	-0.19	-0.37	0.36
GSL1	-0.67	-0.24	0.18
PHR1	**1.58**	**1.51**	0.40
XOG1	**0.96**	**0.88**	**1.26**

(F) Cell wall and biofilm- Hyphae inducing media: RPMI

Gene	hda1ΔΔ	hda2ΔΔ	hda3ΔΔ
BGL2	-0.29	-0.12	0.01
GSC1	-0.16	-0.01	0.23
GSL1	-0.17	-0.18	-0.43
PHR1	-0.49	-0.21	-0.15
XOG1	**1.09**	**1.40**	**1.44**

(G) Cell dispersal and biofilm- Yeast inducing media: YPD

Gene	hda1ΔΔ	hda2ΔΔ	hda3ΔΔ
HSP90	**0.61**	0.66	-0.33
RBT5	**-4.38**	**-2.32**	**-1.27**
YWP1	-0.26	-0.50	-0.46

(H) Cell dispersal and biofilm- Hyphae inducing media: RPMI

Gene	hda1ΔΔ	hda2ΔΔ	hda3ΔΔ
HSP90	0.18	0.14	-0.22
RBT5	0.39	0.15	0.48
YWP1	0.26	0.18	0.75

3.2.5 Pathogenicity and host interaction related genes

(A)

Pathogenicity- Yeast inducing media: YPD

Gene	hda1ΔΔ	hda2ΔΔ	hda3ΔΔ
ALS3	**0.44**	0.28	0.12
ALS4	**-2.45**	**-1.42**	-1.14
ALS9	-0.77	0.01	**-1.02**
HWP1	**1.14**	0.66	-0.33
HSP70	**1.19**	**0.86**	0.48
HSP90	**0.61**	0.66	-0.33
SSA2	0.75	0.34	-0.09

(B)

Pathogenicity- Hyphae inducing media: RPMI

Gene	hda1ΔΔ	hda2ΔΔ	hda3ΔΔ
ALS3	**-1.48**	**-1.42**	**-2.39**
ALS4	-0.42	0.18	0.31
ALS9	0.22	0.22	0.10
HWP1	**-1.26**	**-1.23**	**-2.08**
HSP70	**-0.54**	0.07	0.30
HSP90	0.21	0.14	-0.22
SSA2	0.23	-0.02	-0.58

(C)

Pathogenicity- Yeast inducing media: YPD

Gene	hda1ΔΔ	hda2ΔΔ	hda3ΔΔ
LIP1	1.37	1.37	0.04
LIP2	**1.24**	0.67	0.23
LIP3	**2.24**	**1.82**	0.22
LIP4	1.07	0.07	0.68
LIP5	**0.91**	-0.10	0.32
LIP6	-0.52	-0.40	-0.76
LIP7	0.27	0.21	-0.03
LIP8	0.48	-0.24	0.11
LIP9	1.06	0.70	0.27
LIP10	1.40	0.13	1.40

(D)

Pathogenicity- Hyphae inducing media: RPMI

Gene	hda1ΔΔ	hda2ΔΔ	hda3ΔΔ
LIP1	0.15	0.11	-0.09
LIP2	-0.09	-0.09	-0.28
LIP3	-0.18	-0.27	0.24
LIP4	0.35	0.11	0.20
LIP5	-0.20	-0.33	-0.30
LIP6	-0.06	-0.14	-0.01
LIP7	-0.38	-0.44	-0.45
LIP8	-0.19	-0.32	-0.27
LIP9	0.12	0.04	0.04
LIP10	0.15	0.03	0.21

(E)

Gene	hda1ΔΔ	hda2ΔΔ	hda3ΔΔ
SAP1	**1.12**	**1.41**	0.18
SAP2	0.56	-0.43	-0.37
SAP3	0.78	0.68	0.51
SAP4	0.68	0.72	0.64
SAP5	0.74	0.66	0.18
SAP6	0.82	-0.48	-0.26
SAP7	0.56	-0.48	-0.31
SAP8	-0.35	-1.43	-0.49
SAP9	0.55	-0.00	-0.01
SAP10	**0.90**	**1.15**	0.63

(F)

Gene	hda1ΔΔ	hda2ΔΔ	hda3ΔΔ
SAP1	0.48	0.36	0.15
SAP2	-0.11	0.06	-0.06
SAP3	-0.03	0.04	0.08
SAP4	-0.03	0.00	0.08
SAP5	-0.25	0.00	-0.23
SAP6	-0.24	-0.21	-0.70
SAP7	-0.31	-0.26	-0.28
SAP8	-0.57	**-2.70**	**-1.07**
SAP9	-0.04	0.49	0.28
SAP10	0.36	**0.68**	0.25

3.2.6 Rapamycin related

(A)

Yeast inducing media: YPD

Gene	hda1ΔΔ	hda2ΔΔ	hda3ΔΔ
ALS1	-0.81	0.37	-0.17
ALS3	0.44	0.28	0.12
BCR1	**1.15**	0.65	0.72
ECE1	**0.66**	0.24	-0.42
HWP1	**1.15**	0.66	-0.33
MDS3	**-0.95**	-0.43	-0.28
NRG1	**-0.91**	**-0.75**	-0.62
PHO84	**0.84**	**1.06**	0.09
TOR1	-0.71	-0.16	-0.24
TUP1	**-0.85**	-0.16	-0.35

(B)

Hyphae inducing media: RPMI

Gene	hda1ΔΔ	hda2ΔΔ	hda3ΔΔ
ALS1	-0.52	0.32	-0.24
ALS3	**-1.48**	**-1.42**	**-2.39**
BCR1	-0.28	0.21	0.14
ECE1	**-1.41**	**-1.25**	**-1.88**
HWP1	**-1.26**	**-1.23**	**-2.08**
MDS3	-0.11	-0.12	0.08
NRG1	-0.09	0.42	**0.84**
PHO84	**1.07**	**0.81**	**0.89**
TOR1	0.18	0.32	0.2
TUP1	0.13	0.18	0.31

3.2.7 Copper related genes

(A) Yeast inducing media: YPD

Gene	hda1ΔΔ	hda2ΔΔ	hda3ΔΔ
CRD2	0.77	-1.07	0.13
CRP1	-0.13	-0.15	-0.89
CTR1	**2.02**	**1.39**	0.33
CUP1	0.24	0.46	-0.14
FRE10	**-1.9**	-0.88	**0.93**
FRE7	0.85	0.25	-0.34
GPA2	**-0.68**	-0.24	0.06
MAC1	0.55	0.35	0.15
SOD1	-0.07	**-1.07**	0.05
SOD3	**0.65**	**1.69**	-0.22

(B) Hyphae inducing media: RPMI

Gene	hda1ΔΔ	hda2ΔΔ	hda3ΔΔ
CRD2	0.2	-0.27	-0.07
CRP1	**0.86**	-0.32	-0.16
CTR1	-0.33	0.36	0.18
CUP1	-0.03	0.39	0.38
FRE10	**1.23**	0.4	**1.03**
FRE7	-0.81	0.19	-0.2
GPA2	**-0.58**	-0.46	-0.23
MAC1	-0.39	0.14	-0.1
SOD1	0.33	0.02	0.02
SOD3	**-0.98**	0.27	0.62

3.2.8 Metal assimilation

(A) Iron related genes- Yeast inducing media: YPD

Gene	hda1ΔΔ	hda2ΔΔ	hda3ΔΔ
CCC2	-0.58	-0.65	0.23
FET3	0.18	0.43	0.04
FET99	0.20	0.27	0.13
FRE1/CFL1	-0.32	-0.16	-0.01
FRE2/CFL2	-0.13	0.93	0.92
FRE3/FRE11/C1_11020W	1.11	0.61	0.56
FRE4/CFL5	0.58	0.36	0.38
FRE5/CFL4	1.18	0.96	0.45
FRE6/CR_07300W	-0.20	-0.01	-0.46
FRE7	0.85	0.25	-0.34
FRE8/CFL11	0.35	0.41	0.01
FRE9	**1.45**	**1.31**	0.21
FRE10	**-1.90**	**-0.88**	**0.93**
FRP1	**-1.63**	**-0.96**	-0.50
FRP2	**-1.14**	0.11	-0.51
FTH1	**-1.46**	-0.42	-0.28
FTH2	0.30	0.60	0.51
FTR1	**-2.58**	**-1.29**	-0.47
HMX1	0.61	0.34	0.15
SIT1	**1.20**	**1.36**	0.79
RBT5	**-4.38**	**-2.32**	**-1.27**

(B) Iron related genes- Hyphae inducing media: RPMI

Gene	hda1ΔΔ	hda2ΔΔ	hda3ΔΔ
CCC2	0.02	-0.11	-0.22
FET3	0.31	0.29	0.14
FET99	0.39	-0.40	-0.18
FRE1/CFL1	0.13	-0.18	-0.12
FRE2/CFL2	**1.20**	**0.84**	**1.35**
FRE3/FRE11/C1_11020W	0.38	0.35	0.13
FRE4/CFL5	0.32	0.25	0.08
FRE5/CFL4	**1.55**	0.47	0.48
FRE6/CR_07300W	-0.06	0.07	-0.07
FRE7	-0.81	0.19	-0.20
FRE8/CFL11	-0.21	**-1.00**	**-1.35**
FRE9	0.35	0.73	0.00
FRE10	**1.24**	0.4	**1.03**
FRP1	**0.84**	0.29	0.44
FRP2	0.34	0.08	-0.37
FTH1	0.03	0.26	-0.14
FTH2	**-1.06**	-0.26	-0.43
FTR1	0.63	-0.28	0.43
HMX1	0.31	0.01	-0.10
SIT1	0.66	0.77	0.54
RBT5	0.39	0.15	0.48

(C) pH related genes- Yeast inducing media: YPD

Gene	hda1ΔΔ	hda2ΔΔ	hda3ΔΔ
DFG16	-0.69	0.18	-0.15
RIM101	**-0.75**	**-0.65**	-0.28

(D) pH related genes- Hyphae inducing media: RPMI

Gene	hda1ΔΔ	hda2ΔΔ	hda3ΔΔ
DFG16	-0.17	0.15	0.13
RIM101	-0.38	0.37	0.54

(E) Zinc related genes- Yeast inducing media: YPD

Gene	hda1ΔΔ	hda2ΔΔ	hda3ΔΔ
ADH5	-0.64	0.18	-0.05
CSH1	**2.20**	**2.02**	0.72
CSR1/ZAP1	-0.18	-0.05	-0.19
DPP1	-0.06	0.04	-0.50
HSP30	0.38	-0.11	0.10
IFD6	**3.38**	**3.63**	0.97
LAP3	**-1.16**	0.47	-0.82
PRA1	-0.18	0.24	-0.59
STE23	**0.66**	0.08	0.15
ZRT1	0.24	-0.04	-0.37
ZRT2	0.37	0.35	-0.63
ZRT3/C2_02180W	-0.22	-0.22	-0.04

(F) Zinc related genes- Hyphae inducing media: RPMI

Gene	hda1ΔΔ	hda2ΔΔ	hda3ΔΔ
ADH5	0.10	-0.21	0.24
CSH1	-0.33	**-0.59**	-0.15
CSR1/ZAP1	-0.42	-0.5	-0.12
DPP1	-0.14	-0.49	-0.58
HSP30	-0.20	0.03	0.59
IFD6	0.23	-0.27	0.32
LAP3	-0.42	**-0.78**	-0.24
PRA1	-0.14	-0.58	-0.45
STE23	-0.02	**-0.59**	-0.51
ZRT1	-0.22	-0.47	**-0.53**
ZRT2	0.08	-0.25	0.04
ZRT3/C2_02180W	**-0.72**	-0.39	-0.43

3.2.9 Drug resistance related genes

(A) Yeast inducing media: YPD

Gene	hda1ΔΔ	hda2ΔΔ	hda3ΔΔ
CAP1	**1.56**	**0.89**	0.02
CDR1	0.59	0.27	0.17
CDR2	**0.823**	0.72	0.42
CR_09100C	**2.67**	**2.63**	0.96
ERG11	-0.28	-0.3	-0.1
FLU1	**1.47**	0.83	0.67
GCN4	**1.16**	**1.16**	0.27
GRP2	**1.35**	**1.52**	0.56
HAP43 (CAP2)	**-0.69**	-0.07	-0.17
HSP90	**0.61**	0.66	-0.33
IFD6	**3.38**	**3.63**	0.97
MDR1	**3.21**	**2.92**	0.61
MRR1	0.54	0.39	0.06
RPD3	**0.79**	0.60	0.32
RPD31	**-0.78**	-0.25	-0.04
TAC1	0.48	0.61	0.064
UPC2	-0.1	0.26	-0.61

(B) Hyphae inducing media: RPMI

Gene	hda1ΔΔ	hda2ΔΔ	hda3ΔΔ
CAP1	-0.09	0.26	0.14
CDR1	0.25	0.19	0.17
CDR2	-0.03	0.13	-0.34
CR_09100C	0.49	-0.24	0.16
ERG11	-0.24	**-0.71**	-0.20
FLU1	0.25	0.35	0.41
GCN4	0.01	0.07	-0.19
GRP2	0.21	0.10	0.10
HAP43 (CAP2)	0.13	0.24	0.03
HSP90	0.21	0.14	-0.22
IFD6	0.23	-0.27	0.32
MDR1	0.45	-0.06	-0.33
MRR1	-0.12	-0.33	-0.22
RPD3	0.06	0.22	0.13
RPD31	0.02	-0.11	-0.13
TAC1	-0.03	0.11	-0.07
UPC2	0.28	-0.29	-0.06

3.2.10 Chromatin remodeling and silencing related genes

(A) Yeast inducing media: YPD

Gene	hda1ΔΔ	hda2ΔΔ	hda3ΔΔ
APC1	**-0.75**	-0.42	-0.42
CBF1	-0.01	0.21	-0.23
CDC20	-0.11	-0.14	-0.25
CYP1/CPR1	**-1.11**	-0.02	-0.47
HMT1	**-1.63**	**-0.90**	-0.47
HOS2	0.76	0.32	-0.03
HOS4/C1_08770W	**-1.05**	-0.34	-0.60
HST1	0.52	0.03	0.44
MAD2	-0.23	0.24	0.04
SET1	-0.03	0.05	0.26
SET3	**-0.73**	0.75	-0.18
SIF2/C6_01220C_A	0.22	0.31	0.29
SNF2	0.31	0.14	0.21
SNT1	0.48	0.20	0.42
SWI1	-0.16	0.04	-0.14
TBF1	-0.18	-0.41	0.20

(B) Hyphae inducing media: RPMI

Gene	hda1ΔΔ	hda2ΔΔ	hda3ΔΔ
APC1	-0.26	-0.17	-0.07
CBF1	0.18	0.31	0.55
CDC20	-0.36	-0.48	-0.33
CYP1/CPR1	0.16	-0.15	-0.20
HMT1	0.59	0.31	**0.68**
HOS2	0.11	0.01	-0.14
HOS4/C1_08770W	-0.43	0.01	-0.52
HST1	-0.09	0.02	0.16
MAD2	0.02	0.10	0.09
SET1	-0.01	0.21	0.05
SET3	-0.14	-0.08	0.31
SIF2/C6_01220C_A	0.10	-0.12	-0.05
SNF2	-0.06	0.03	0.01
SNT1	-0.20	0.04	0.16
SWI1	0.14	0.07	0.07
TBF1	0.30	0.21	0.52

3.2.11 Regulators of *S. cerevisiae* orthologs

(A) Yeast inducing media: YPD

Gene	hda1ΔΔ	hda2ΔΔ	hda3ΔΔ
TFC7/C7_01650W	NA	NA	NA
LEU3	-0.12	-0.30	-0.35
MED4	-0.63	-0.13	-0.09
SFP1	**-0.84**	**-0.93**	-0.71
XBP1/C2_05860C	0.47	**1.08**	-0.48

(B) Hyphae inducing media: RPMI

Gene	hda1ΔΔ	hda2ΔΔ	hda3ΔΔ
TFC7/C7_01650W	NA	NA	NA
LEU3	0.65	0.16	0.22
MED4	-0.06	0.02	-0.16
SFP1	0.18	0.17	0.26
XBP1/C2_05860C	-0.25	-0.12	0.21

No known ortholog in *C. albicans* of *S. cerevisiae MED2*. See Section 1.10.

3.2.12 UV/*RFX2* related genes

(A) Yeast inducing media: YPD

Gene	hda1ΔΔ	hda2ΔΔ	hda3ΔΔ
ALS3	0.44	0.28	0.12
CEK1	**2.02**	**1.16**	0.88
DDR48	0.52	**0.87**	0.75
ECE1	0.66	0.24	-0.42
HWP1	**1.14**	0.66	-0.33
HYR1	0.47	0.52	0.47
MEC1	-0.24	-0.44	-0.24
RAD53	0.08	-0.17	0.08
RAD6	-0.56	-0.27	-0.56
RFX1	**0.96**	0.79	**0.96**
RFX2	**1.07**	**1.38**	**1.07**
RNR3	**-0.98**	-0.66	**-0.98**

(B) Hyphae inducing media: RPMI

Gene	hda1ΔΔ	hda2ΔΔ	hda3ΔΔ
ALS3	**-1.47**	**-1.42**	**-2.39**
CEK1	-0.43	-0.39	-0.52
DDR48	-0.32	0.17	0.19
ECE1	**-1.41**	**-1.25**	**-1.88**
HWP1	**-1.26**	**-1.23**	**-2.08**
HYR1	**-1.35**	-0.42	**-1.29**
MEC1	-0.07	-0.36	-0.23
RAD53	-0.04	-0.03	0.06
RAD6	-0.31	-0.24	-0.06
RFX1	0.20	0.44	-0.37
RFX2	**-0.74**	-0.27	**-0.77**
RNR3	0.67	0.22	0.14

APPENDIX 4. Article: preprint available at bioRxiv

Title: The fungal-specific Hda2 and Hda3 proteins regulate morphological switches in the human fungal pathogen *C. albicans*.
Running title: Hda2 and Hda3 control *C. albicans* morphogenesis

Misty R. Peterson[a], Robert Jordan Price[a], Sarah Gourlay[a], Alisha May[a]*, Jennifer Tullet[a] and Alessia Buscaino[a#]
a: Kent Fungal Group, School of Biosciences, University of Kent, Canterbury, United Kingdom
#Address correspondence to Alessia Buscaino, A.Buscaino@kent.ac.uk
* : Present address: Department of Life Sciences, Imperial College London, South Kensington Campus, London, SW7 2AZ

ABSTRACT
The human fungal pathogen *C. albicans* is responsible for millions of infections annually. Due to the few available anti-fungal drugs and the increasing incidence of drug resistance, the number of *C. albicans* infections is dramatically increasing. Morphological switches, such as the white-opaque switch and the yeast-hyphae switch, are key for the development of *C. albicans* pathogenic traits. Lysine deacetylases are emerging as important regulators of morphological switches. Yet, targeting lysine deacetylases for drug development is problematic due to the high homology between the fungal and human proteins that could result in toxicity. Here we provide evidence that the fungal specific proteins Hda2 and Hda3 interact with the lysine deacetylase Hda1. By combining phenotypic analyses with genome-wide transcriptome analyses, we demonstrate that Hda2 and Hda3 control *C. albicans* morphological switches. Under nutrient-rich conditions, deletion of *HDA2* or *HDA3* leads to moderate overexpression of the master regulator of white-opaque switching *WOR1* and increase switching frequency. Under hyphae inducing conditions, deletion of *HDA2* and *HDA3* block hyphae development. However, deletion of *HDA2* and *HDA3* does not affect hyphae-formation and virulence in vivo. We propose that Hda2 and Hda3 are good targets for the development of anti-fungal drugs to be used in combination therapy.

INTRODUCTION
Fungal pathogens are a leading cause of human mortality causing over 1.5 million deaths per year (1). C. albicans is a commensal organism that colonises the mouth, gastrointestinal and reproductive tract of healthy individuals without causing any harm. Still, *C. albicans* is also the most common human fungal pathogen and the principal causal agent of mycotic death (2). This is because, in immune- compromised patients, *C. albicans* can invade vital organs and cause serious, life- threating systemic infections associated with a mortality rate up to 70 % (2). The ability to transition between different morphological forms in response to changing environments is a key virulence trait in *C. albicans*.
For example, *C. albicans* cells can reversibly switch between white and opaque Forms (3). White and opaque cells are genetically identical, yet they differ in cellular morphology, colony shape, gene expression profile and mating behaviour (4). In addition, white cells are more virulent in a murine model of systemic infection (5, 6) whereas opaque cells preferentially colonise the skin (7). White-opaque switching is under the control of the master regulator Wor1, a transcription factor whose expression is necessary and sufficient for opaque cell formation (8–11). Stochastic increases in Wor1 levels drives the transition from the white to the opaque phase.
Furthermore, Wor1 expression produces a direct positive feedback loop by binding its own promoter and turning on its own expression (8, 9, 11). Switching is also regulated by the mating type locus as opaque formation occurs predominantly in a or α cells (12).
C. albicans virulence also depends on its ability to convert between yeast and hyphal morphology: yeast cells are critical for colonisation, early infection and dissemination, while hyphal growth is responsible for tissue invasion and chronic infections (13). Hyphal morphogenesis is coupled with virulence, as several of the genes, that are specifically expressed in hyphae, encode virulence factors (14–17).
Hyphal morphogenesis is a complex and highly orchestrated process, and *C. albicans* uses multiple redundant pathways to integrate host signals and promote hyphae development. Indeed, *C. albicans* filamentation can be induced by many environmental cues such mammalian serum, body temperature, hypoxia and CO_2 concentration which reflects the variety of signals sensed by the fungus in the different microenvironments encountered in the host. In yeast cells, hyphae morphogenesis is inhibited by the DNA-binding repressor Nrg1 that, together with Tup1, blocks expression of a subset of filament-specific genes (18). Upon hyphal induction, filamentous growth is promoted by Efg1 and Flo8, two transcription regulators essential for hyphal development and virulence [14–16]. During the initiation phase of hyphae morphogenesis, Nrg1-mediated repression is cleared via *NRG1* transcriptional repression and Nrg1 protein

degradation. During hyphae maintenance, chromatin remodelling of hyphae promoters prevents Nrg1 binding despite its increased protein levels (19).
Due to the close evolutionary relationship between fungi and the human host, effective treatment for *C. albicans* infections is hindered by the limited number of sufficiently divergent potential drug targets. There are only three classes of antifungal drugs effective for the treatment of systemic fungal infections and their clinical utility is limited by the rapid emergence of drug resistance (1, 20). Hence, there is an immediate and urgent need to develop alternative treatments. A potential strategy is to target *C. albicans* morphological plasticity.
Lysine deacetylases (KDACs, also known as HDACs) act as global regulators of gene expression by catalysing the removal of acetyl functional groups from the lysine residues of histones and non-histone proteins (21). KDACs can favour transcriptional repression by deacetylating lysine residues on histone tails allowing chromatin compaction and/or preventing binding of bromodomain-containing transcriptional activators (21). KDACs can also activate transcription by deacetylation of non-histone proteins (22). As a consequence, deletion or inhibition of KDACs often results in the upregulation and downregulation of an approximately equivalent number of genes (23). KDACs are highly conserved across eukaryotes and can be phylogenetically divided into three main classes: the Rpd3 and Hos2-like (class I) enzymes, the Hda1-like (class II) enzymes and the Sir2-like (class III) enzymes. The class I and class II enzymes are related, sharing a conserved central enzymatic domain. The class III enzymes are nicotinamide adenine dinucleotide (NAD) dependent. KDACs lack intrinsic DNA-binding activity and are recruited to target genes via incorporation into large multiprotein complexes or direct association with transcriptional activators and repressors (24).
In *C. albicans*, the lysine deacetylase Hda1 (class II) is an important regulator of morphological switches. Hda1 controls white-opaque switching as deletion of the *HDA1* gene increases switching rates from white to opaque (25, 26). In response to serum, N-acetylglucosamine or nutrient limitation, Hda1 also controls the yeast to hyphae switch by deacetylating Yng2, a component of the histone acetyltransferase NuA4 complex, blocking maintenance of hyphal growth (19). However, the Hda1 pathway is not required for hyphae elongation in hypoxia or in the presence of elevated CO_2 because of the presence of redundant pathways (27, 28). As a result, the Hda1-mediated hyphae maintenance pathway contributes, but it is not absolutely required, for virulence in vivo (27). These results suggest that Hda1 is a good target for antifungal drugs development to be used in combination therapies.

KDACs are promising druggable targets: one KDAC inhibitor is currently used for cancer treatment and several other KDAC inhibitors are in clinical trials (29, 30). However effective targeting of Hda1 for anti-fungal drug development is impaired by the high sequence similarities between Hda1 and its human orthologs and consequently a likeliness for high toxicity.
In Saccharomyces cerevisiae, Hda1 assembles with two non-catalytic subunits, Hda2 and Hda3, essential for Hda1 deacetylation activity both in vivo and in vitro (31). Interestingly, no metazoan homologous of Hda2 and Hda3 have been identified. Hda2 and Hda3 are similar in sequence and share a similar protein organisation with an N-terminal DNA binding domain (DBD) and a C-terminal coil-coil domain (CCD). The DBD domain, similar in structure to the helicase domain of the SWI-SNF chromatin remodellers, is sufficient to bind DNA in vitro. The CCD domains act as a scaffold for the assembly of the Hda1 complex (32).
Here for the first time, we analyse the role of *C. albicans* Hda2 and Hda3. We demonstrate that the Hda1 complex is conserved in *C. albicans* as Hda2 and Hda3 interact with Hda1 in vivo. Our analyses demonstrated that, in yeast-inducing conditions, deletion of HDA2 and HDA3 leads to transcriptional upregulation of
WOR1 and that Hda2 and Hda3 inhibit white and opaque switching. In contrast, under hyphae-inducing conditions, Hda2 and Hda3 regulate the yeast to hyphae switch. This functional rewiring is linked to a reduced expression of components of the Hda1 complex. Our study demonstrates that Hda2 and Hda3 control key morphological switches in *C. albicans*. Therefore, we propose that Hda2 and Hda3 are attractive targets for the development of novel antifungal drugs.

RESULTS

The Hda1 complex is conserved in *C. albicans*

S. cerevisiae Hda2 and Hda3 are critical components of the Hda1 complex as they are required for the Hda1-mediated histone deacetylation activity (31). BLAST analyses reveal that the *C. albicans* genome contains two genes encoding proteins with homology to *S. cerevisiae* Hda2 (C3_03670W) and Hda3 (CR_09490W_A).
Structural alignments predict that Hda2 and Hda3 have a similar protein organization with an N-terminal DNA binding domain (DBD) and a C-terminal coil-coil domain (CCD) (Fig.1A and 1B). To explore the potential functional relationship between *C. albicans* Hda2, Hda3 and Hda1, we assessed whether we

could detect a physical interaction between these proteins. To this end, we generated strains expressing at the endogenous locus an epitope-tagged Hda1 protein (Hda1-HA) together with either Hda2-GFP or Hda3-GFP. Western analyses show that the Hda1-HA and Hda2-GFP tagged proteins are expressed at high levels while we could not detect Hda3-GFP in whole cell extract indicating that the protein is expressed at low levels (Fig.1C). Immuno-precipitation (Ip) of Hda1-HA with a highly specific anti-HA antibody demonstrates that Hda2 strongly interacts with Hda1. We could also detect an interaction between Hda1 and Hda3, despite the low level of expression of Hda3 (Fig.1C). Thus, Hda2 and Hda3 physically interact with Hda1. To delineate the function of C. albicans Hda2 and Hda3, we generated homozygous deletions mutants for *HDA2* (*hda2*ΔΔ) and *HDA3* (*hda3*ΔΔ) genes using a recyclable Clox system (Fig.1D) (33). The Clox system allows for the generation of a homozygous deletion mutant lacking any marker genes and therefore genetically identical to the parental strain except for the deleted gene. This allows for the direct comparison of phenotypes between mutant and parental strains. Growth analyses reveal that Hda2 and Hda3 are not required for survival and fitness as the *hda2*ΔΔ and *hda3*ΔΔ strains grow similarly to the wild-type (WT) control both on solid and in liquid media (Fig.1E and 1F). Therefore, *C. albicans* Hda2 and Hda3 are bonafide components of the Hda1 complex that are not required for cell fitness and survival under optimal growth conditions.

Global gene expression changes in the absence of Hda2 and Hda3

To gain insights about the function of Hda2 and Hda3 in conditions stimulating yeast growth, we analysed changes in gene expression by strand-specific RNA-sequencing (RNA-seq) upon deletion of the *HDA2* and *HDA3* genes. As a comparison, we also performed RNA-seq on strains with the *HDA1* gene deleted. Deletion of *HDA2* results in 577 genes significantly differentially regulated (348 upregulated and 229 downregulated, $q < 0.05$; Dataset S1). These gene expression changes are highly similar to the ones observed in *hda1*ΔΔ (Pearson correlation coefficient $r = 0.7$, Dataset S1) (Fig.2A). Deletion of the *HDA3* gene has a less profound effect on gene expression as only 78 genes are significantly differentially expressed (45 upregulated and 33 downregulated, $q < 0.05$; Dataset S1). Despite this difference, changes in *hda3*ΔΔ cells correlate with *hda1*ΔΔ and *hda2*ΔΔ gene expression changes (Pearson correlation coefficient $r = 0.66$ and 0.46, respectively) (Fig.2A).

To reveal the cellular pathways regulated by Hda2 and Hda3 in C. albicans, we performed Gene Set Enrichment Analysis (GSEA) of the RNA-seq datasets (34). To this end, transcript profiles of *hda2*ΔΔ or *hda3*ΔΔ isolates were ranked according to their differential expression and this list was compared to gene sets identified in other experimental analyses (35) and (Sellam et al, personal communications). This allows the identification of statistically significant gene sets enriched in the top (up-regulated) or the bottom (down-regulated genes) of the ranked list (34). The network of similar gene sets was visualized using Cytoscape where nodes represent gene sets, and lines connect nodes sharing a significant number of genes (36). GSEA detected enrichment for rRNA and ribosome biogenesis genes and genes involved in transport (Fig.2B). Enrichment was also found in gene sets important for virulence-promoting function in *C. albicans*. This includes genes differentially expressed during C. albicans-host interactions with mouse macrophages and in response to drugs (Fig.2C).

Modulation of several gene sets enriched in hda2 ΔΔ and/or hda3 ΔΔ mutants, for example, down-regulation of genes required for protein synthesis, are part of stress response in C. albicans (37). Accordingly, we subjected the *hda2*ΔΔ and *hda3*ΔΔ mutants to a phenotypic analysis by applying a set of different stress conditions (38).

For most conditions, we did not observe any difference between the WT and the mutant strains. However, lack of Hda2 or Hda3 leads to sensitivity to copper, sodium chloride and sodium nitroprusside (SNP) with salicylhydroxamic acid (SHAM). Strains mutant in these proteins also show resistance to rapamycin (Fig.3) indicating a role for Hda2 and Hda3 in specific stress responses.

Hda2 and Hda3 inhibit white-opaque switching

The GSEA analysis identifies white-opaque switching as a process potentially regulated by Hda2 and Hda3 as genes upregulated in the opaque state are also upregulated upon deletion of *HDA2* and *HDA3* (Fig.4A and 4B). Wor1 is the master regulator of white-opaque phenotypic switching and a stochastic increase in Wor1 levels drives the transition from the white to the opaque phase (8, 9, 11). Therefore, we asked whether *WOR1* expression levels were increased in *hda2*ΔΔ and *hda3*ΔΔ isolates compared to WT cells.

The RNA sequencing analysis demonstrates that deletion of *HDA2* or *HDA3* leads to transcriptional upregulation of *WOR1* (Fig.4C). This result suggests that, in WT cells, Hda2 and Hda3 repress *WOR1* transcription and inhibit white-opaque switching. To test this hypothesis, we generated *MTL* a/a homozygous *hda2*ΔΔ and *hda3*ΔΔ mutants and measured the frequency of white to opaque conversion using quantitative switching assays. Briefly, cells were plated on Phloxine B plates and the frequency of opaque colonies or colonies containing at least one opaque sector was scored. This analysis demonstrates that deletion of both *HDA2* and *HDA3* increases the frequency of white-opaque switching (Fig.4D). Thus,

Hda2 and Hda3 control white-opaque switching, a process that is linked to *WOR1* overexpression. Hda2 and Hda3 contribute to filamentous growth but not virulence

To investigate the role of Hda2 and Hda3 under hyphae-inducing conditions, we performed RNA-seq analyses of WT, *hda2*ΔΔ and *hda3*ΔΔ strains grown in RPMI, a medium which mimics human physiological conditions and therefore strongly induces hyphal growth. As a control, RNA-seq analyses were also performed in *hda1*ΔΔ strain. GSEA analysis of the gene expression changes of WT cells grown in yeast-inducing conditions (YPD) and hyphae-inducing conditions (RPMI) confirmed the validity of our experimental approach as genes reported to be upregulated in hyphae compared to yeast are less expressed in YPD compared to RPMI while genes with a yeast-specific expression are expressed at higher levels in YPD than RPMI (Fig.5A).

In hyphae-inducing conditions, deletions of *HDA2* and *HDA3* genes result in 350 and 484 significantly differentially expressed genes, respectively ($q < 0.05$; Dataset S1). Gene expression changes in *hda2*ΔΔ and *hda3*ΔΔ correlate with gene expression changes observed in *hda1*ΔΔ although less profoundly than in yeast-inducing conditions (Pearson correlation coefficient, $r = 0.55$ and 0.38, respectively; Fig.5B).

The RNA-seq analysis reveals that filamentation is the major pathway misexpressed in the deletion mutants as hyphae-responsive genes are differentially expressed in *hda2*ΔΔ and *hda3*ΔΔ isolates compared to WT cells (Fig.5C). qRT-PCR analyses of two hyphal growth markers, *HWP1* and *ALS3*, confirmed the RNA-seq results as, in hyphae inducing conditions, expression of *HWP1* and *ALS3* is downregulated in *hda2*ΔΔ and *hda3*ΔΔ but not in WT cells (Fig.5D).

Collectively, our results suggest that Hda2 and Hda3 are important for hyphal growth. To test this hypothesis, we assessed the morphology of WT, *hda2*ΔΔ and *hda3*ΔΔ strains upon growth in two different hyphae-inducing media (RPMI and Spider). While WT cells form hyphae efficiently, hyphal growth is defective in *hda2*ΔΔ and *hda3*ΔΔ cells on both solid and in liquid media (Fig.6A and B). This phenotype was rescued by reintroduction of the *HDA3* gene (Fig.6C). Therefore, Hda2 and Hda3 are important regulators of the yeast to hyphae switch. To test whether the hyphae-defective phenotype observed in *hda2*ΔΔ and *hda3*ΔΔ isolates is sufficient to impair hyphal growth in vivo, we performed killing assays using the nematode Caenorhabditis elegans as an infection system (39, 40). These analyses revealed no differences in hyphae formation or percentage of killing between WT, *hda2*ΔΔ and *hda3*ΔΔ strains (Fig.6D). Therefore, although Hda2 and Hda3 are critical for hyphae-formation in specific media, additional redundant pathways can compensate for the lack of Hda2 and Hda3 in a more complex *in vivo* situation.

Stability of Hda1 protein is regulated by environmental changes.

Comparison of the gene expression profiles in yeast-promoting conditions (YPD 30 °C) and hyphae-promoting conditions (RPMI 37 °C) reveals that deletion of *HDA1* leads to different transcriptional changes in different environments (Fig.7A). In yeast inducing conditions, 2046 genes are significantly differentially expressed upon deletion of Hda1 compared to WT cells, suggesting that Hda1 acts as a global regulator of gene expression (Fig.7A and Dataset S1). In contrast, in hyphae inducing conditions, 507 genes are significantly differentially expressed with hyphal growth being one of the major pathways that is altered (Fig.7B and Dataset S1). These results suggest that Hda1 function is rewired during the yeast to hyphae switch. We hypothesise that this change in function could be due to a differential gene expression profile of *HDA1* in yeast compared to hyphae. While analysis of the RNA-seq dataset reveals that *HDA1*, *HDA2* and *HDA3* transcription levels are similar across these two conditions, Western analyses clearly demonstrate that levels of Hda1 and Hda3 proteins, but not Hda2, are lower in hyphal cells compared to yeast cells (Fig.7C). Therefore, the functional rewiring of the Hda1 complex upon an environmental change is linked to a reduced expression of this subunit.

DISCUSSION

The role of the Hda1 complex in regulating morphological switches in *C. albicans*

Results presented in this study show that the fungal-specific proteins Hda2 and Hda3 are important regulators of morphological switches in *C. albicans*. We propose that this regulation is mediated via the Hda1 complex. This hypothesis is supported by our observation that Hda1, Hda2 and Hda3 physically interact and by the published results demonstrating that Hda1 controls both the white-opaque and the yeast-hyphae morphological switches (19, 25, 26). Based on the data presented here, it is possible that Hda2 and Hda3 control the activity of the Hda1 complex by different non-mutually exclusive mechanisms. First, Hda2 and Hda3 could mediate Hda1 recruitment to target sites regulating their chromatin acetylation state and their transcriptional activity. Indeed, in *S. cerevisiae*, Hda2 and Hda3 DNA-binding domains are sufficient to bind DNA in vitro (32). The structural alignment presented in this study demonstrates that, similar to *S. cerevisiae*, *C. albicans* Hda2 and Hda3 contain a DNA binding domains with structure resembling the helicase fold found in the SWI2/SNF2-type chromatin-remodeling ATPase (32). We hypothesise that Hda2 and Hda3 could target Hda1 to key genomic locations leading to

transcriptional downregulation of associated genes. In support of this hypothesis, we have found that *WOR1*, the master regulator of white-opaque switching, is moderately upregulated in cells deleted for *HDA2* and *HDA3* genes. A similar upregulation is observed in *hda1*ΔΔ isolates. We propose that this upregulation is sufficient to activate the Wor1 positive feedback loop promoting white-opaque switching. Indeed, *hda2*ΔΔ and *hda3*ΔΔ cells undergo white-opaque switching more frequently than WT cells. Alternatively, interactions between Hda1, Hda2 and Hda3 may induce a conformational change promoting Hda1 deacetylase activity. In support of this hypothesis, it has been established that the in vitro catalytic activity of S. cerevisiae Hda1 depends on Hda2 and Hda3 (31). This regulation could be critical for controlling deacetylation of non-histone substrates. For example, *C. albicans* Hda1 controls the yeast to hyphae switch by deacetylating a non-histone substrate, the NuA4 component Yng2 (19). We hypothesise that interaction between Hda1, Hda2 and Hda3 causes a conformational change in Hda1 allowing deacetylation of Yng2. Chromatin modifiers are ideal sensors of changing environments as they can respond to external stimuli by rapidly and reversibly changing the transcriptional state of many genes simultaneously. Our results indicate that the activity of the Hda1 complex is rewired in different environmental conditions. While in yeast cells, Hda1 acts as a globular regulator of gene expression, in hyphae-inducing conditions Hda1 function is dedicated to the yeast-hyphae switch. This functional rewiring is accompanied by changes in the protein levels of Hda1 and Hda3. These findings suggest a model through which hyphae-specific function is achieved by diminishing the concentration of key proteins of the Hda1 complex. We did not observe any changes in the RNA levels of *HDA1* and *HDA3* and therefore we hypothesise that translation efficiency and/or stability of these two proteins is differentially regulated in different environments.

Chromatin modifiers are often embedded in multiprotein complexes associated with several non-catalytic subunits that regulate their targeting to substrates or their catalytic activity (24). Our results highlight how Hda2 and Hda3, the non-catalytic subunits of the Hda1 complex, play important roles in regulating morphological switches in response to environmental changes.

Hda2 and Hda3 as potential targets for anti-fungal therapy

The yeast to hyphae switch is central to C. albicans virulence and pathogenesis. Our results signify that while Hda2 and Hda3 promote hyphae formation under specific growth conditions (RPMI and Spider media at 37 °C), they are dispensable for hyphae formation and virulence in the C. elegans infection system. We hypothesise that this is due to the presence of redundant pathways that stimulate hyphae formation. Indeed, it has been shown that hyphae induction is a highly orchestrated process integrating several different environmental signals (13). The finding that, in vivo, lack of Hda2 and Hda3 does not impair hyphae formation is in agreement with the observation that strains mutant for the *YNG2* gene, the target of Hda1, also do not impair hyphae growth in vivo while they are defective for hyphae formation in vitro (27).

There is an urgent need to develop new anti-fungal drugs due to emergence of fungal strains resistant to currently available drugs. We propose that Hda2 and Hda3 could be targets for novel antifungal drugs to be used in combination therapy. Combination therapy offers several advantages compared to single-drug therapy. This is because it allows for widening of the spectrum and potency of drug activity and it can also lead to reduction in the dosage of individual agents preventing emergence of antifungal resistance (41). Several features make Hda2 and Hda3 attractive targets for antifungal drug development. First and most importantly, the proteins are present in fungi but absent in humans minimising potential toxicity. Secondly, drugs targeting Hda2 and Hda3 could have a broad spectrum of activity against a variety of human fungal pathogens as Hda2 and Hda3 orthologs are present in other human fungal pathogens, such as *C. glabrata* (CAGL0H01331g and CAGL0G09867g) and *A. fumigatus* (Hda2: Afu5g03390). KDACs are emerging as promising candidates for drug development and several small molecules inhibiting KDAC activity are currently in clinical trials as potential anti-cancer therapeutics. We propose that inhibition of Hda2 and Hda3 will impair C. albicans Hda1 activity but not human KDACs reducing the risk of toxicity.

MATERIAL AND METHODS

Growth conditions

Strains are listed in Table 1. Yeast cells were cultured in rich medium (YPD) containing extra adenine (0.1 mg/ml) and extra uridine (0.08 mg/ml), complete SC medium (Formedium) or RPMI medium (Sigma-Aldrich). When indicated, media were supplemented with 30 µg/ml doxycycline. For analysis in stress conditions, YPD agar media was supplemented with 9 nM rapamycin, 2 M sodium chloride, 1 mM SNP with 1 mM SHAM, 7 mM copper sulphate, 300 mM lithium chloride, .01 % sodium dodecyl sulfate (SDS), 15mM caffeine, 1.5 M sorbitol, 18 mM cycloheximide, 1.5 mM cobalt, 25 mM hydroxyurea, 3 % ethanol, 20 µM Calcofluor White, 4.5 mM hydrogen peroxide, 0.75 mM EDTA and 2 µM Cerulenin (42). Cells were grown at 30 °C or 37 °C as indicated.

Plasmid construction

Oligos and plasmids used in this study are listed in Table 2 and 3. Plasmid ABp133 contains the C. albicans *HDA1* gene cloned in frame to a C-terminal HA tag. To generate this plasmid, the full length *HDA1* gene was amplified from plasmid ABp88 (synthesised by GeneArt) with oligos Abo408 and Abo409, containing recognition sites for *Xma*I. The digested PCR product was cloned into plasmid pHA-NAT (ABp17)(43) digested with *Xma*I. Cloning was confirmed by PCR and Sanger sequencing. HDA3 was cloned in the pNIM plasmid (ABp111) (44) to generate plasmid ABp177. For this purpose, the full length *HDA3* gene was amplified from plasmid ABp152 (synthesised by GeneArt) with oligos ABo624 and ABo625, containing *Xho*I and *Bgl*II restriction sites. ABo625 also supplied a stop codon upstream the restriction site. This PCR fragment was cloned in pNIM digested with *Sal*I and *Bgl*II. Cloning was confirmed by PCR and Sanger sequencing.

Construction of *C. albicans* mutants

Deletions of *HDA2* and *HDA3* were generated in the SN152 or BWP17 background using the Clox system for gene disruption (33) using long-oligos PCR, the LAL (loxP- ARG4-loxP) and NAT1-Clox (loxP-NAT1-MET3p-cre-loxP) plasmids as templates. During all selections for Clox transformants media was supplemented with 2.5 mM methionine and 2.5 mM cysteine to repress the MET3 promoter and minimize Cre- loxP mediated recombination. Nourseothricin resistant (NouR) transformants were selected using 200 µg/ml nourseothricin (Melford). *HDA2* and *HDA3* gene deletions were confirmed by PCR and markers were resolved by allowing Cre expression in medium lacking methionine and cysteine as previously described (33). C-terminal GFP tagging of *HDA2* and *HDA3* genes at the endogenous loci was performed by long oligos PCR using plasmid pGFP-His1 (ABp11) as a template (45). C-terminal HA tagging of Hda1 was performed by long oligos PCR using plasmid ABp133 as a template and transformation into BWP17 (ABy215), *HDA2*-GFP (ABy532) and *HDA3*-GFP (ABy376).

For rescue experiments, *HDA3* re-integrated at the *ADH1* locus by digesting ABp177 with *Kpn*I and *Sac*II and transforming the product into the *hda3*ΔΔ (ABy331) deletion strain. Correct integration was confirmed by colony PCR. Transformations of *C. albicans* strains were performed by electroporation using the protocol described in (46) or by lithium acetate transformation (47) of competent cells (48) with a *S. cerevisiae* method adapted to *C. albicans* (49).

Hyphal growth induction and quantification

Cultures were grown overnight (~16 hours) in 5 ml liquid YPD at 30 °C. Overnight cultures were diluted 1:100 in YPD media and grown ~5 hours at 30 °C. 50 – 100 cells were plated to RPMI or Spider agar and incubated for ~6 days at 37 °C. For doxycycline induction, the drug was added to the media at 30 µg/ml in 20 ml plates. Phenotypes were documented by imaging with a Leica MZFLIII microscope at 10x t 16x magnification A minimum of 150 colonies were counted for each strain. For liquid filamentation assays, overnight cultures were grown throughout the day and from this stationary culture, 1 mL was harvested and washed with distilled water before resuspending in 10 mL pre-warmed final media (YPD (control) or RPMI). These cultures were grown at 37 °C (control at 30 °C) for 15-17 hours before imaging on an Olympus IX81 inverted microscope at 60x magnification. Samples were evaluated on four separate days and a minimum of 400 cells were counted per sample.

White-opaque switching essay

Quantitative switching assays were performed as previously described (12) with modifications. Briefly, strains were streaked from frozen stocks on YPD plates and grown at 30 °C for 2 days. Single colonies were picked, resuspended in sterile water and spread onto synthetic complete agar containing 5 µg/ml Phloxine B (Sigma- Aldrich). Formation of opaque colonies or sectors was scored after 9 days. Experiments were done in biological duplicate or triplicate on at least three separate days. A minimum of 400 total colonies were counted for each strain. The ggplot package in R studio was used to construct violin plots. Unpaired t-tests were performed to test for significant differences between wild-type and mutant strains.

Structural modelling

The model of Hda3 DBD and CCS domain was produced using Phyre2 in intensive mode (50) and visualised using PyMol (The PyMOL Molecular Graphics System, Version 1.8 Schrödinger, LLC.)

Whole cell extracts

Preparation of whole cell extracts was performed as described (51). Briefly, overnight YPD cultures were diluted in YPD or RPMI and grown to OD600 = ~0.8 at 30 °C. Cells were harvested, resuspended in 200 µl lysis buffer (0.1 M NaOH, 0.05 M EDTA, 2 % SDS, 2% β-mercaptoethanol) and heated for 10 minutes at 95 °C before adding 5 µl of 4 M Acetic acid and incubating for further 10 minutes at 90 °C. Extracts were mixed with 50 µl loading buffer (0.25 M Tris-HCl pH 6.8, 50 % Glycerol, 0.05 % Bromophenol

Blue), incubated at 96 °C for 5 minutes and centrifuged at 13000 rpm for 5 minutes. Supernatants were collected and analysed by SDS-PAGE and Western blot analyses.

Immunoprecipitation

Immunoprecipitation was performed as described (52) with modifications. 1 L YPD cultures (OD600 = 1) were harvested at 4000 rpm. Cell were washed 3 times in cold water and resuspended in 1/5th volume (water/cells). Cell pellets were ground in liquid nitrogen using a mortar and pestle for 30 minutes and resuspended in 10 ml of cold lysis buffer (50 mM HEPES-NaOH pH 7.5, 150 mM NaCl, 5 mM EDTA, 0.1 % NP-40, 5 mM DTT, 1x Roche EDTA-free protease inhibitor cocktail and 0.2 mM PMSF added fresh before use). The cells were solubilized for 30 minutes with rotation at 4 °C. Following centrifugation, supernatant samples were incubated with 4 µl of magnetic beads pre-coupled with anti-HA antibody (Sigma-Aldrich) for 2 hours with rotation at 4 °C. Beads were washed four times in lysis buffer and analysed by SDS-PAGE and Western blot.

Antibodies information

The following antibodies were used for Western analyses. Anti-HA antibody (#11666606001, Sigma-Aldrich) diluted at 1:1000, anti-GFP antibody (Roche #1184460001) diluted at 1:5000, anti-actin (Cooper Lab, Washington University, St. Louis, Mo., USA) diluted at 1:5000.

RNA extraction

Overnight YPD cultures were diluted in YPD and grown to OD600 = ~0.8. Cells were pelleted, washed once with sterile water and resuspended in pre-warmed YPD (30 ºC) or RPMI (37 ºC) for 90 minutes. RNA extraction was performed using a yeast RNA extraction kit (E.Z.N.A. Isolation Kit RNA Yeast, Omega Bio-Tek) following the manufacturer's instructions with the following modifications: (1) 30 °C incubation in SE Buffer/2-mercaptoethanol/lyticase solution time was increased to 90 minutes; (2) lysis was performed with bead mill at top speed for 30 minutes at 4 °C. RNA was treated with DNAse I and RNA quality was checked by electrophoresis under denaturing conditions in 1% agarose, 1× HEPES, 6% Formaldehyde (Sigma-Aldrich). RNA concentration was measured using a NanoDrop ND-1000 Spectrophotometer. cDNA synthesis was performed using qPCRBIO cDNA Synthesis Kit (PCR Biosystems) following manufacturer's instructions.

High-throughput RNA sequencing

Strand-specific cDNA Illumina Barcoded Libraries were generated from 1 µg of total RNA extracted from WT, *hda1*ΔΔ, *hda2*ΔΔ and hda3ΔΔ and sequenced with an Illumina iSeq2000 platform. Illumina library preparation and deep- sequencing was performed by the Genomics Core Facility at EMBL (Heidelberg, Germany). RNA sequencing was performed in duplicates. Raw reads were analysed following the RNA deep sequencing analysis pipeline using the Galaxy platform (https://usegalaxy.org/). Downstream analysis of differential expressed genes was performed with R Studio (https://www.rstudio.com/). Scatter Plot matrices, using Pearson correlation coefficients, were generated with the ggplot package. Heatmaps were generated with the pheatmap package and Pearson correlation for clustering. Heatmaps show the log2 fold changes of differentially expressed genes in *hda1*ΔΔ, *hda2*ΔΔ or *hda3*ΔΔ compared to wild-type expression. Venn diagrams were generated using the FunRich programme(53). RNA sequencing data are deposited into ArrayExpress (accession number: E-MTAB-6920).

qRT-PCR

qRT-PCR was performed in the presence of SYBR Green (Bio-Rad) on a Bio-Rad CFXConnect Real-Time System. Data was analysed with Bio-Rad CFX Manager 3.1 software and Microsoft Excel. Enrichment was calculated over actin. Histograms represent data from three biological replicates. Error bars: standard deviation of three biological replicates generated from 3 independent cultures of the same strain.

Functional analysis and modelling of transcriptional profiles

Gene set enrichment analysis (GSEA) (34, 54) was performed using the GSEA PreRanked tool to determine whether a ranked gene list exhibited statistically significant bias in their distribution within defined gene sets (55) and (Sellam et al, personal communication). The weighted enrichment statistics were calculated on 10512 gene sets each containing 5-1000 genes, and the false discovery rate (FDR) was calculated from 1000 permutations. Selected results graphs are shown. Since enrichment profiles can exhibit correlations with hundreds of overlapping gene sets, Cytoscape 3.6 (http://www.cytoscape.org) (56) and the Enrichment Map Pipeline Collection plug-ins (http://apps.cytoscape.org/apps/enrichmentmappipelinecollection) were used to further organise and visualise the GSEA. Enrichment maps were calculated using default parameters.

C. albicans-C. elegans pathogenesis assay

The *C. elegans* glp-4/sek-1 strain was used as described previously (39, 57). Briefly, *C. elegans* were propagated on nematode growth medium (NGM) on lawns of *E. coli* OP50. The *C. albicans*-*C. elegans* pathogenesis assay was performed as previously described (40). Briefly, 100 µl of *C. albicans* cells from an overnight culture were spread into a square lawn on a 10 cm plate containing brain-heart infusion (BHI) agar and kanamycin (45 µg/ml). These were incubated for approximately 20 hours at 30 °C. Synchronized adult *C. elegans* glp-4/sek-1 nematodes grown at 25°C were carefully washed from NGM plates using sterile M9 buffer. Approximately 100 to 200 washed animals were then added to the centre of the *C. albicans* lawns and the plates were incubated at 25°C for 4 hours. Worms were then carefully washed into a 15 ml tube using 10 ml of sterile M9, taking care to minimize the transfer of yeast. Worms were washed four or five times with sterile M9. 30-40 worms were then transferred into three wells of a six-well tissue culture plate (Corning, Inc.) containing 2 ml of liquid medium (80% M9, 20% BHI) and kanamycin (45 µg/ml). Worms were scored daily into one of three categories: alive, dead with hyphae piercing the cuticle, and dead without hyphae piercing the cuticle. Worms were considered to be dead if they did not move in response to mechanical stimulation with a pick. Dead worms were removed from the assay. *C. elegans* survival was examined by using the Kaplan-Meier method and differences were determined by using the log-rank test using OASIS 2 tool (58). Differences in the number of worms with *C. albicans* hyphal formation were determined by using a one-way ANOVA with Dunnett's test for multiple comparisons. The *C. elegans* pathogenesis assay presented here is an average of three independent biologic replicates. A p-value of <0.05 was considered statistically significant.

FUNDING INFORMATION
A.B and R.J.P: Medical Research Council [MR/M019713/1]; S.G: [BB/L008041/1]. Funding for open access charge: University of Kent.

ACKNOWLEDGMENTS
We thank GeneCore at EMBL for performing Illumina library preparation and sequencing. We thank Dr Sellam (Biotechnology Research Institute, National Research Council of Canada) and Dr Traven (Monash University) for help with the GSEA analysis. We are grateful to Dr Anderson (The Ohio State University) for the plasmid allowing deletion of mating type cassette and Prod Alistair Brown (University of Aberdeen) for the Clox system. We thank members of the Kent Fungal Group for useful discussions and critical reading of the manuscript.

REFERENCES
1. Brown GD, Denning DW, Gow NAR, Levitz SM, Netea MG, White TC. 2012. Hidden Killers: Human Fungal Infections. Sci Transl Med 4:165rv13-165rv13.
2. Pfaller MA, Diekema DJ. 2010. Epidemiology of invasive mycoses in North America. Crit Rev Microbiol 36:1–53.
3. Slutsky B, Staebell M, Anderson J, Risen L, Pfaller M, Soll DR. 1987. & White-opaque transition & a second high-frequency switching system in C. albicans. J Bacteriol 169:189–97.
4. Bennett RJ, Johnson a D. 2005. Mating in C. albicans and the search for a sexual cycle. Annu Rev Microbiol 59:233–55.
5. Kvaal C, Lachke SA, Srikantha T, Daniels K, McCoy J, Soll DR. 1999. Misexpression of the opaque-phase-specific gene PEP1 (SAP1) in the white phase of C. albicans confers increased virulence in a mouse model of cutaneous infection. Infect Immun 67:6652–62.
6. Kvaal CA, Srikantha T, Soll DR. 1997. Misexpression of the white-phase- specific gene WH11 in the opaque phase of C. albicans affects switching and virulence. Infect Immun 65:4468–75.
7. Lachke SA, Lockhart SR, Daniels KJ, Soll DR. 2003. Skin facilitates Candida albicans mating. Infect Immun 71:4970–6.
8. Huang G, Wang H, Chou S, Nie X, Chen J, Liu H. 2006. Bistable expression of *WOR1*, a master regulator of white-opaque switching in C. albicans. Proc Natl Acad Sci 103:12813–12818.
9. Srikantha T, Borneman AR, Daniels KJ, Pujol C, Wu W, Seringhaus MR, Gerstein M, Yi S, Snyder M, Soll DR. 2006. TOS9 Regulates White-Opaque Switching in C. albicans. Eukaryot Cell 5:1674–1687.
10. Zordan RE, Miller MG, Galgoczy DJ, Tuch BB, Johnson AD. 2007. Interlocking Transcriptional Feedback Loops Control White-Opaque Switching in Candida albicans. PLoS Biol 5:e256.
11. Zordan RE, Galgoczy DJ, Johnson AD. 2006. Epigenetic properties of white opaque switching in C. albicans are based on a self-sustaining transcriptional feedback loop. Proc Natl Acad Sci U S A 103:12807–12.
12. Miller MG, Johnson AD. 2002. White-opaque switching in C. albicans is controlled by mating-type locus homeodomain proteins and allows efficient mating. Cell 110:293–302.

13. Noble SM, Gianetti BA, Witchley JN. 2017. C. albicans cell-type switching and functional plasticity in the mammalian host. Nat Rev Microbiol 15:96–108.
14. Staab JF, Bradway SD, Fidel PL, Sundstrom P. 1999. Adhesive and mammalian transglutaminase substrate properties of C. albicans Hwp1. Science 283:1535–8.
15. Almeida RS, Brunke S, Albrecht A, Thewes S, Laue M, Edwards JE, Filler SG, Hube B. 2008. The Hyphal-Associated Adhesin and Invasin Als3 of Candida albicans Mediates Iron Acquisition from Host Ferritin. PLoS Pathog 4:e1000217.
16. Phan QT, Myers CL, Fu Y, Sheppard DC, Yeaman MR, Welch WH, Ibrahim AS, Edwards JE, Filler SG. 2007. Als3 Is a C. albicans Invasin That Binds to Cadherins and Induces Endocytosis by Host Cells. PLoS Biol 5:e64.
17. Weissman Z, Kornitzer D. 2004. A family of Candida cell surface haem-binding proteins involved in haemin and haemoglobin-iron utilization. Mol Microbiol 53:1209–1220.
18. Braun BR, Kadosh D, Johnson AD. 2001. NRG1, a repressor of filamentous growth in C.albicans, is down-regulated during filament induction. EMBO J 20:4753–4761.
19. Lu Y, Su C, Wang A, Liu H. 2011. Hyphal Development in C. albicans Requires Two Temporally Linked Changes in Promoter Chromatin for Initiation and Maintenance. PLoS Biol 9:e1001105.
20. Denning DW, Hope WW. 2010. Therapy for fungal diseases: opportunities and priorities. Trends Microbiol 18:195–204.
21. Kurdistani SK, Grunstein M. 2003. Histone acetylation and deacetylation in yeast. Nat Rev Mol Cell Biol 4:276–284.
22. Glozak MA, Sengupta N, Zhang X, Seto E. 2005. Acetylation and deacetylation of non-histone proteins. Gene 363:15–23.
23. Haberland M, Montgomery RL, Olson EN. 2009. The many roles of histone deacetylases in development and physiology: Implications for disease and therapy. Nat Rev Genet 10:32–42.
24. Falkenberg KJ, Johnstone RW. 2014. Histone deacetylases and their inhibitors in cancer, neurological diseases and immune disorders. Nat Rev Drug Discov 13:673–691.
25. Srikantha T, Tsai L, Daniels K, Klar AJS, Soll DR. 2001. The Histone Deacetylase Genes HDA1 and RPD3 Play Distinct Roles in Regulation of High-Frequency Phenotypic Switching in C. albicans. Society 183:4614– 4625.
26. Hnisz D, Schwarzmüller T, Kuchler K. 2009. Transcriptional loops meet chromatin: a dual-layer network controls white-opaque switching in Candida albicans. Mol Microbiol 74:1–15.
27. Lu Y, Su C, Solis N V., Filler SG, Liu H. 2013. Synergistic regulation of hyphal elongation by hypoxia, CO2, and nutrient conditions controls the virulence of C. albicans. Cell Host Microbe 14:499–509.
28. Kadosh D, Lopez-Ribot JL. 2013. C. albicans: Adapting to Succeed. Cell Host Microbe 14:483-485.
29. Tzogani K, van Hennik P, Walsh I, De Graeff P, Folin A, Sjöberg J, Salmonson T, Bergh J, Laane E, Ludwig H, Gisselbrecht C, Pignatti F. 2018. EMA Review of Panobinostat (Farydak) for the Treatment of Adult Patients with Relapsed and/or Refractory Multiple Myeloma. Oncologist 23:631–636.
30. Simó-Riudalbas L, Esteller M. 2015. Targeting the histone orthography of cancer: drugs for writers, erasers and readers. Br J Pharmacol 172:2716–2732.
31. Wu J, Carmen a a, Kobayashi R, Suka N, Grunstein M. 2001. HDA2 and *HDA3* are related proteins that interact with and are essential for the activity of the yeast histone deacetylase *HDA1*. Proc Natl Acad Sci U S A 98:4391–6.
32. Lee JH, Maskos K, Huber R. 2009. Structural and Functional Studies of the Yeast Class II Hda1 Histone Deacetylase Complex. J Mol Biol 391:744–757.
33. Shahana S, Childers DS, Ballou ER, Bohovych I, Odds FC, Gow N a R, Brown AJP. 2014. New Clox Systems for rapid and efficient gene disruption in *C. albicans*. PLoS One 9:e100390.
34. Subramanian A, Tamayo P, Mootha VK, Mukherjee S, Ebert BL, Gillette MA, Paulovich A, Pomeroy SL, Golub TR, Lander ES, Mesirov JP. 2005. Gene set enrichment analysis: a knowledge-based approach for interpreting genome- wide expression profiles. Proc Natl Acad Sci U S A 102:15545–50.
35. Sellam A, van het Hoog M, Tebbji F, Beaurepaire C, Whiteway M, Nantel A. 2014. Modeling the transcriptional regulatory network that controls the early hypoxic response in C. albicans. Eukaryot Cell 13:675–90.
36. Merico D, Isserlin R, Stueker O, Emili A, Bader GD. 2010. Enrichment Map: A Network-Based Method for Gene-Set Enrichment Visualization and Interpretation. PLoS One 5:e13984.
37. Enjalbert B, Nantel A, Whiteway M. 2003. Stress-induced gene expression in C. albicans: absence of a general stress response. Mol Biol Cell 14:1460–7.

38. Tuch BB, Mitrovich QM, Homann OR, Hernday AD, Monighetti CK, De La Vega FM, Johnson AD. 2010. The transcriptomes of two heritable cell types illuminate the circuit governing their differentiation. PLoS Genet 6:e1001070.
39. Breger J, Fuchs BB, Aperis G, Moy TI, Ausubel FM, Mylonakis E. 2007. Antifungal Chemical Compounds Identified Using a C. elegans Pathogenicity Assay. PLoS Pathog 3:e18.
40. Pukkila-Worley R, Peleg AY, Tampakakis E, Mylonakis E. 2009. Candida albicans hyphal formation and virulence assessed using a *Caenorhabditis elegans* infection model. Eukaryot Cell 8:1750–8.
41. Lewis RE, Kontoyiannis DP. 2001. Rationale for combination antifungal therapy. Pharmacotherapy 21:149S–164S.
42. Homann OR, Dea J, Noble SM, Johnson AD. 2009. A phenotypic profile of the *C. albicans* regulatory network. PLoS Genet 5.
43. Gerami-nejad M, Forche A, Mcclellan M, Berman J. 2012. Analysis of protein function in clinical C . albicans isolates 5314.
44. Park Y, Park Y, Morschhauser J, Morschhauser J. 2005. Tetracycline- Inducible Gene Expression and Gene Deletion in *C. albicans*. Microbiology 4:1328–1342.
45 Gerami-Nejad M, Berman J, Gale CA. 2001. Cassettes for PCR-mediated construction of green, yellow, and cyan fluorescent protein fusions in *Candida albicans*. Yeast 18:859–864.
46. De Backer MD, Maes D, Vandoninck S, Logghe M, Contreras R, Luyten WHML. 1999. Transformation of *C. albicans* by Electroporation. Yeast 15:1609–1618.
47. Schiestl RH, Gietz RD. 1989. High efficiency transformation of intact yeast cells using single stranded nucleic acids as a carrier. Curr Genet 16:339–346.
48. Knop M, Siegers K, Pereira G, Zachariae W, Winsor B, Nasmyth K, Schiebel E. 1999. Epitope tagging of yeast genes using a PCR-based strategy: more tags and improved practical routines. Yeast 15:963–972.
49. Walther A, Wendland J. 2003. An improved transformation protocol for the human fungal pathogen C. albicans. Curr Genet 42:339–343.
50. Kelley LA, Mezulis S, Yates CM, Wass MN, Sternberg MJE. 2015. The Phyre2 web portal for protein modeling, prediction and analysis. Nat Protoc 10:845–58
51. von der Haar T. 2007. Optimized protein extraction for quantitative proteomics of yeasts. PLoS One 2:e1078.
52. Buscaino A, White SA, Houston DR, Lejeune E, Simmer F, de Lima Alves F, Diyora PT, Urano T, Bayne EH, Rappsilber J, Allshire RC. 2012. Raf1 Is a DCAF for the Rik1 DDB1-Like Protein and Has Separable Roles in siRNA Generation and Chromatin Modification. PLoS Genet 8:e1002499.
53. Pathan M, Keerthikumar S, Chisanga D, Alessandro R, Ang C-S, Askenase P, Batagov AO, Benito-Martin A, Camussi G, Clayton A, Collino F, Di Vizio D, Falcon-Perez JM, Fonseca P, Fonseka P, Fontana S, Gho YS, Hendrix A, Hoen EN-'t, Iraci N, Kastaniegaard K, Kislinger T, Kowal J, Kurochkin I V., Leonardi T, Liang Y, Llorente A, Lunavat TR, Maji S, Monteleone F, Øverbye A, Panaretakis T, Patel T, Peinado H, Pluchino S, Principe S, Ronquist G, Royo F, Sahoo S, Spinelli C, Stensballe A, Théry C, van Herwijnen MJC, Wauben M, Welton JL, Zhao K, Mathivanan S. 2017. A novel community, driven software for functional enrichment analysis of extracellular vesicles data. J Extracell Vesicles 6:1321455.
54. Mootha VK, Lindgren CM, Eriksson K-F, Subramanian A, Sihag S, Lehar J, Puigserver P, Carlsson E, Ridderstråle M, Laurila E, Houstis N, Daly MJ, Patterson N, Mesirov JP, Golub TR, Tamayo P, Spiegelman B, Lander ES, Hirschhorn JN, Altshuler D, Groop LC. 2003. PGC-1alpha-responsive genes involved in oxidative phosphorylation are coordinately downregulated in human diabetes. Nat Genet 34:267–73.
55. Sellam A, Hogues H, Askew C, Tebbji F, van Het Hoog M, Lavoie H, Kumamoto C a, Whiteway M, Nantel A. 2010. Experimental annotation of the human pathogen C. albicans coding and noncoding transcribed regions using high-resolution tiling arrays. Genome Biol 11:R71.
56. Shannon P, Markiel A, Ozier O, Baliga NS, Wang JT, Ramage D, Amin N, Schwikowski B, Ideker T. 2003. Cytoscape: A Software Environment for Integrated Models of Biomolecular Interaction Networks. Genome Res13:2498–2504.
57. Moy TI, Ball AR, Anklesaria Z, Casadei G, Lewis K, Ausubel FM. 2006. Identification of novel antimicrobials using a live-animal infection model. Proc Natl Acad Sci U S A 103:10414–10419.
58. Han SK, Lee D, Lee H, Kim D, Son HG, Yang J-S, Lee S-J V., Kim S. 2016. OASIS 2: online application for survival analysis 2 with features for the analysis of maximal lifespan and healthspan in aging research. Oncotarget 7:56147–56152.
59. Synnott JM, Guida A, Mulhern-Haughey S, Higgins DG, Butler G. 2010. Regulation of the Hypoxic Response in C. albicans. Eukaryot Cell 9:1734–1746.

60. Marcil A, Gadoury C, Ash J, Zhang J, Nantel A, Whiteway M. 2008. Analysis of PRA1 and its relationship to C. albicans-macrophage interactions. Infect Immun 76:4345–4358.
61. Noble SM, Johnson AD. 2005. Strains and Strategies for Large-Scale Gene Deletion Studies of the Diploid Human Fungal Pathogen C. albicans Eukaryot Cell 4: 298-309.
62. Wilson RB, Davis D, Mitchell AP. 1999. Rapid Hypothesis Testing with C. albicans through Gene Disruption with Short Homology Regions Journal of bacteriology 181: 1868-74.

FIGURE LEGENDS

Figure 1. The Hda1 complex is conserved in C. albicans
(A) Domain organisation of C. albicans Hda2 and Hda3 proteins (B) Left: Structural alignment of C. albicans DBD3 domain (red) with S. cerevisiae DBD3 domain (yellow); Right: Structural modelling of C. albicans CCD3 (C) Co-Immunoprecipitation of Hda1 with Hda2 and Hda3. Hda1-HA Immunoprecipitation (Ip) analysed with anti-HA or with anti-GFP to detect Hda2 and Hda3. (D) Schematic of Clox gene disruption strategy used to construct *hda2*Δ/Δ and *hda3*Δ/Δ mutants. (E) Serial dilution assay of WT, *hda2*Δ/Δ and *hda3*Δ/Δ mutants on solid YPD media at 30 °C. (F) Growth curves of WT, *hda2*Δ/Δ and *hda3*Δ/Δ isolates in YPD liquid media at 30 °C.

Figure 2. Global gene expression changes in the absence of Hda2 and Hda3
(A) Pearson correlation matrix of gene expression changes observed in *hda1*Δ/Δ, *hda2*Δ/Δ and *hda3*Δ/Δ grown in YPD at 30 °C. r = Pearson correlation coefficient. p = p-value. (B) The network of functional groups of genes regulated by Hda2 and Hda3 constructed by GSEA and Enrichment Map. Blue circles represent down regulated while orange circles depict upregulated gene sets which are linked in the network by grey lines. The diameter of the circles varies based upon the number of transcripts within each set. (C) Example enrichment plots for selected genes sets differentially expressed in *hda2*Δ/Δ (left) and *hda3*Δ/Δ (right). Ketoconazole_up: set of genes upregulated in C. albicans cells grown in the presence of ketoconazole (59); Phagocytosis_up: gene set upregulated following engulfment by primary Bone Marrow Derived Macrophages (60). The x-axis shows genes ranked according to their expression in the mutants from up-regulated (left) to down-regulated (right) genes. Black vertical lines mark individual genes. The cumulative value of the enrichment score (y-axis) is represented by the green line. A positive normalized enrichment score (NES) indicates enrichment in the up-regulated group of genes in *hda2*Δ/Δ and *hda3*Δ/Δ.

Figure 3. Phenotyping of *hda2*Δ/Δ and *hda3*Δ/Δ strains
Serial dilution assay showing growth of *hda2*Δ/Δ and *hda3*Δ/Δ mutants on solid YPD media with additives as indicated and incubation at 30 °C for 2 - 4 days. (A) Additives affecting *hda2*Δ/Δ and *hda3*Δ/Δ growth relative to wildtype strain. Mutants are resistant to rapamycin and sensitive to SNP and SHAM, sodium chloride and copper sulphate. (B) Conditions eliciting normal growth of mutant strains relative to matching wildtype.

Figure 4. Hda2 and Hda3 inhibit white-opaque switching
(A) Enrichment plots for genes differentially expressed in *hda1*Δ/Δ, *hda2*Δ/Δ and *hda3*Δ/Δ in comparison to genes upregulated in opaque cells (38). The x-axis shows genes ranked according to their expression in the mutants from up-regulated (left) to down-regulated (right) genes. Black vertical lines mark individual genes. The cumulative value of the enrichment score (y-axis) is represented by the green line. A positive normalised enrichment score (NES) indicates enrichment in the up-regulated group of genes in *hda1*Δ/Δ, *hda2*Δ/Δ and *hda3*Δ/Δ. (B) Heat map depicting the log2 fold change in *hda1*Δ/Δ, *hda2*Δ/Δ and *hda3*Δ/Δ isolates compared to WT for the Opaque_up gene set. (C) Log2 fold change values and significance for *WOR1* gene expression in *hda1*Δ/Δ, *hda2*Δ/Δ and *hda3*Δ/Δ compared to WT. (D) Left: Percentage of sector colonies in WT, *hda2*Δ/Δ and *hda3*Δ/Δ isolates. ** = p value < .01. Right: Representative image of cells grown on Phloxine B agar. O = opaque; W = white.

Figure 5. Gene expression profiling in hyphae-inducing conditions in WT, *hda1*Δ/Δ, *hda2*Δ/Δ and *hda3*Δ/Δ isolates
(A) The network representing changes in gene expression in WT cells grown in yeast-inducing conditions (YPD) versus hyphae-inducing conditions (RPMI) constructed by GSEA and Enrichment Map. Blue circles represent down regulated gene sets, while orange depicts upregulated gene sets which are linked in the network by grey lines that indicate function. The diameter of the circles varies based upon the number of transcripts within each set. (B) Pearson correlation matrix of gene expression changes observed in *hda1*Δ/Δ, *hda2*Δ/Δ and *hda3*Δ/Δ grown in hyphae growth media (RPMI) at 37 °C. r = Pearson correlation coefficient. p = p-value. (C) Left: Heat map depicting the log2 fold change in WT cells grown in hyphae-inducing conditions (RPMI at 37 °C) versus WT cells grown in yeast-inducing conditions (YPD at 30 °C).

Gene known to be involved in hyphae formation or biofilm formation are indicated. Right: Log2 fold changes of hyphae-induced and repressed-genes in *hda1*Δ/Δ, *hda2*Δ/Δ and *hda3*Δ/Δ isolates. Cell were grown in RPMI at 37 °C. (D) Quantitative reverse transcriptase PCR (qRT-PCR) analyses to measure *HWP1* and *ALS3* transcript levels in WT, *hda1*Δ/Δ, *hda2*Δ/Δ and *hda3*Δ/Δ isolates grown in yeast (YPD at 30 °C) or hyphae (RPMI at 37 °C) inducing conditions. Transcripts levels are visualized relative to *ACT1* transcript levels. Error bars in each panel: standard deviation of three biological replicates.

Figure 6. Hda2 and Hda3 contribute to filamentation growth but not virulence
(A) Left: Representative images of colony morphology of WT, *hda1*Δ/Δ, *hda2*Δ/Δ and *hda3*Δ/Δ grown on hyphal inducing Spider and RPMI agar at 37 °C. Right: Quantification of colony morphologies. (B) Quantification of cellular morphologies of WT, *hda1*Δ/Δ, *hda2*Δ/Δ and *hda3*Δ/Δ grown in liquid RPMI media at 37 °C. (C) Rescue experiment of colony morphology upon genomic integration of the *HDA3* gene in the *hda3*Δ/Δ mutant background (*hda3*Δ/Δ+ *HDA3*). WT, heterozygous (*HDA3*/ *hda3*Δ) and homozygous *hda3*Δ/Δ isolates were included as a control. Cell were grown on hyphal inducing RPMI agar at 37 °C. (D) Left: Representative images of dead C. elegans with and without hyphae-mediated killing. Middle: Survival curve of worms incubated with WT, *hda2*Δ/Δ and *hda3*Δ/Δ strains over a 72 hour period. Right: The percentage of total worms dead (black bars) and worms killed by hyphae piercing the cuticle (grey bars) after the 72 hour incubation period. Error bars represent the standard deviation of three independent biological replicates.

Figure 7. Stability of the Hda1 protein is regulated by environmental changes
(A) Venn diagram of genes differentially expressed in hda1Δ/Δ relative to WT in yeast and hyphal growth conditions. (B) Enrichment plots for genes differentially expressed in hda1 Δ/Δ relative to genes downregulated (Hyphae_Lee_DN) or upregulated (Hyphae_Lee_up) in hyphae-growth condition in Lee's media. The x-axis shows genes ranking according to their expression in hda1Δ/Δ from up- regulated (left) to down-regulated (right) genes. Black vertical lines mark individual genes. The cumulative value of the enrichment score (y-axis) is represented by the green line. A positive normalised enrichment score (NES) indicates enrichment in the up-regulated group of genes while a negative NES indicates prevalence of the genes in the down-regulated group. (C) HA and GFP Western blots of whole protein extract from strains: Hda1-HA, Hda2-GFP and Hda3-GFP. Actin is shown as a loading control. Cells were grown in yeast (YPD 30 °C) or hyphae-inducing (RPMI 37 °C) conditions. (D) Model showing how decreased Hda1 and Hda3 protein levels leading to the functional rewiring of the Hda1 complex in C. albicans in different environments. Under yeast growth condition, the Hda1 complex functions as a global regulator of gene expression due to the high level of Hda1 and Hda3. Under hyphae growth conditions, decreased levels of Hda1 and Hda3 leads to specialisation of the Hda1 complex controlling only filamentous growth.

Table 1. *C.albicans* strains used in this study.

Strain	Description	Genotype	Figure	Source
ABy_54	SN152	*MTL a/alpha ura3*Δ- *iro1*Δ*::imm434/URA3-IRO1 his1*Δ*/his1*Δ *arg4*Δ*/arg4*Δ *leu2*Δ*/leu2*Δ	1E-F,2A-C,3A-B,4A-C,5A-D,6A- B,6D, 7A-B	(61)
ABy_66	BWP17	*MTL a/alpha ura3Δ::Δimm434/ura3Δ::Δi mm434 his1::hisG/his1::hisG arg4::hisG/arg4::hisG*	1F, 6B-C	(62)
ABy_179	*hda1* Δ/Δ	*MTL a/a arg4Δ/arg4Δ his1Δ/his1Δ leu2Δ/leu2Δ URA3/ura3Δ::λimm434IRO1/iro1Δ::λimm434 hda1Δ::C.d.HIS1/hda1Δ::C. m.LEU2*	2A-C, 3A-B, 4A-C,5A-D, 6A-B, 6D, 7A-B	(26)
ABy_191	HDA3/Δ	MTL a/alpha ura3Δ::Δimm434/ura3Δ::Δimm434 his1::hisG/his1::hisG arg4::hisG/arg4::hisG HDA3/hda3Δ::LAL	6C	This study

ABy_331	BWP17 *hda3*Δ/Δ	MTL a/alpha ura3Δ::Δimm434/ura3Δ::Δimm434 his1::hisG/his1::hisG arg4::hisG/arg4::hisG hda3Δ/hda3Δ	1F, 6B-C	This study
ABy_347	*hda2*Δ/Δ	MTL a/alpha ura3Δ-iro1Δ::imm434/URA3-IRO1his1Δ/his1Δ arg4Δ/arg4Δ leu2Δ/leu2Δ hda2Δ/hda2Δ	1E-F, 2A-C, 3A-B, 4A-D, 5A-C, 6B,6D, 6A	This study
ABy_376	*HDA3:HDA3-GFP*	MTL a/alpha ura3Δ::Δimm434/ura3Δ::Δimm434 his1::hisG/his1::hisG arg4::hisG/arg4::hisG HDA3::HIS/HDA3-GFP	1C, 7C	This study
ABy_393	BWP17 *MTLα*Δ	MTLa/MTLalphaΔ ura3Δ::Δimm434/ura3Δ::Δimm434 his1::hisG/his1::hisG arg4::hisG/arg4::hisG	4D	This study
ABy_460	SN152 *hda3*Δ/Δ	MTL a/alpha ura3Δ- iro1Δ::imm434/URA3-IRO1 his1Δ/his1Δ arg4Δ/arg4Δ leu2Δ/leu2Δ hda3Δ/hda3Δ	1E, 2A-C, 3A-B, 4A-C, 5A-D, 6A-B, 6D	This study
ABy_472	*ADH1/ pNIM-HDA3:adh1Δ*	MTL a/alpha ura3Δ::Δimm434/ura3Δ::Δimm434 his1::hisG/his1::hisG arg4::hisG/arg4::hisG hda3Δ/hda3Δ pNIM- HDA3::adh1Δ/ADH1	6C	This study
ABy_532	*HDA2:HDA2-GFP*	MTL a/alpha ura3Δ::Δimm434/ura3Δ::Δimm434 his1::hisG/his1::hisG arg4::hisG/arg4::hisG HDA2::HIS/HDA2-GFP	1C, 7C	This study
ABy_536	*HDA2:HDA2-GFP HDA1:HDA1-HA*	MTL a/alpha ura3Δ::Δimm434/ura3Δ::Δimm434 his1::hisG/his1::hisG arg4::hisG/arg4::hisG HDA2::HIS/HDA2-GFP HDA1::NAT/HDA1 HA	1C	This study
ABy_539	*HDA3:HDA3-GFP HDA1:HDA1-HA*	MTL a/alpha ura3Δ::Δimm434/ura3Δ::Δimm434 his1::hisG/his1::hisG arg4::hisG/arg4::hisG HDA3::HIS/HDA3-GFP HDA1::NAT/HDA1-HA	1C	This study
ABy_547	*hda2*Δ/Δ *MTLα*Δ	MTL a/ MTLalphaΔ ura3Δ-iro1Δ::imm434/URA3-IRO1 his1Δ/his1Δ arg4Δ/arg4Δ leu2Δ/leu2Δ hda2Δ/hda2Δ	4D	This study
ABy_551	*hda3*Δ/Δ *MTLα*Δ	MTL a/ MTLalphaΔ ura3Δ-iro1Δ::imm434/URA3-IRO1 his1Δ/his1Δ arg4Δ/arg4Δ leu2Δ/leu2Δ hda3Δ/hda3Δ	4D	This study
ABy_563	*HDA1:HDA1-HA*	MTL a/alpha ura3Δ::Δimm434/ura3Δ::Δimm434 his1::hisG/his1::hisG arg4::hisG/arg4::hisG HDA1::NAT/HDA1-HA	1C, 7C	This study

Table 2. Oligos used in this study.

Number	Primer	Sequence	Figure	Description
ABo_408	HDA1_Xma_fw1	TAAGCACCCGGGatgtcgactggtcaagaagaa	1C, 7C-D	Isolate synthetic Hda1 from p88
ABo_409	HDA1_Xma_rev1	TAAGCACCCGGGatcttcggaagaggagtagtc	1C, 7C-D	Isolate synthetic Hda1

ABo_351	Pr_sir2_adh1	CGCACTCACGTAAAC ACTT	1C, 6C, 7C-D	Check Hda1 in p17; confirm reintegration of Hda3_pNIM cassette at ADH1 locus
ABo_412	HDA1end_chkseq	GGAAATAGTTCGAACGGTGG	1C, 7C-D	Check Hda1 in p17; sequencing p133
ABo_452	F1gaHDA1_Haintg	TCCGAAATTCATTATTAAGGA ATTATATAGAAGCTACCATT TTCACATCTATTATCATTTTC CTTTTTAAGAatgtcgact ggtcaagaagaaca	1C, 7C-D	Isolate Hda1-HA integration cassette from p133; long oligo
ABo_453	R1gaHDA1_Haintg	CAGATCTATATCTATTCTCTT TCTTTCTTTTTTTTTGGTTTTT TGTTGTTGTTGTTGTTGTTTC TACTCGAAgtaaaacgacggccagtg aattc	1C, 7C-D	Isolate Hda1-HA integration cassette from p133; long oligo
ABo_179	PR1_NAT	CTGTATCTATAAGCA GTATCATCC	1C, 7C-D	Check presence of Hda1-HA integration cassette at native locus
ABo_417	dwnstrmHDA1rev_ check	CTCGATGCCTGATTT GGATG	1C, 7C-D	Check presence of Hda1-HA integration cassette at native locus
ABo_458	F1HDA2_GFP	TGTTAGAAAACTCTGGCTCG GGTGCCAATAATAGACAAAA TAATCGTATTAGTCGAGGTG CAACACCTCTTGGTGGTGGTt ctaaaggtgaagaattatt	1C, 7C-D	Isolate GFP tagging cassette from p11 with flanking integration sequences for Hda2; long oligo
ABo_459	R2HDA2_GFP	GCATGTATTTACAAATTTTT GGATAAGAAAAAGTAGCATA TGGAAACACAAAACCAAGAA AGAAATCATGgaattccggaatatttat gagaaac	1C, 7C-D	Isolate GFP tagging cassette from p11 with flanking integration sequences for Hda2; long oligo
ABo_460	F1HDA3_GFP	CAATGCTTTTACATTTTTAAA TGATACTAAATATTTGAAAA AGAGGAAAAATCGAGGAAT AACTCCTAAAGGTGGTG GTtctaaaggtgaagaattatt	1C, 7C-D	Isolate GFP tagging cassette from p11 with flanking integration sequences for Hda3; long oligo
ABo_461	R2HDA3_GFP	CTTATCATTTACATAATTAA AAAAACAAAAA ACAAGCTAATCTTAT GTTTATGTGGGGGCCACATT TTCTgaattccgg aatatttatgagaaac	1C, 7C-D	Isolate GFP tagging cassette from p11 with flanking integration sequences for Hda3; long oligo
ABo_145	PF1_his1	GTTCCAGCAGATGGCGAGTA C	1C, 7C-D	Check Hda3-GFP or Hda2-GFP tagging
ABo_261	Pr4_hda2chk_rev	GTAATATCTGATCAG AACCTTT	1C, 7C-D	Check Hda2-GFP tagging
ABo_262	Pr4_hda3chk_rev	TCGTTAATCAAAATTATACA CTC	1C, 7C-D	Check Hda3-GFP tagging
ABo_229	HDA2D_Clox_Fw1	TCTATTTTCAAGAAGTTAGA CCCATTCTTGGAATAATTAT ACTTGCAAGAGAAGGCATTG AAATTGCATTACGGCCAGTG AATTGTAATA	1D	Isolate deletion cassette from p80 or p83 with flanking integration sequences for Hda2; long oligo

ABo_230	HDA2D_Clox_rev1	GCATGTATTTACAAATTTTTGGATAAGAAAAAGTAGCATATGGAAACACAAAACCAAGAAAGAAATCATGTCGGAATTAACCCTCACTAA	1D	Isolate deletion cassette from p80 or p83 with flanking integration sequences for Hda2; long oligo
ABo_165	Pr1_chck_arg4	AGTGTGGAAAGAAGAGATGC	1D	Check presence of p80 cassette in Hda2 or Hda3 heterozygote
ABo_423	HDA3_Natcloxchk	CCGGTGCTATGGTTAGATTG	1D	Check presence of p83 cassette in hda2ΔΔ or hda3ΔΔ
ABo_261	Pr4_hda2chk_rev	GTAATATCTGATCAGAACCTTT	1D	Check presence of p80 cassette in Hda2 heterozygote and hda2ΔΔ
ABo_413	HDA2chk_internalf w	CAGCAGGTAGACTTGATG	1D	Check presence/absence of Hda2 in hda2ΔΔ unresolved/resolved
ABo_261	Pr4_hda2chk_rev	GTAATATCTGATCAGAACCTTT	1D	Check presence/absence of Hda2 in hda2ΔΔ unresolved/resolved
ABo_231	HDA3D_Clox_Fw1	GTTCTTAATATTTGTAACTTTTCCAACTTAAAATAATTATTGCATATTGCACTAAAACTAAAACTACTATAAATacggccagtgaattgtaata	1D	Isolate deletion cassette from p80 or p83 with flanking integration sequences for Hda3; long oligo
ABo_232	HDA3D_Clox_Rev 1	CAATCTTATCATTTACATAATTAAAAAAACAAAAAACAAGCTAATCTTATGTTTATGTGGGGGCCACATTTTCTtcggaattaacctcactaa	1D	Isolate deletion cassette from p80 or p83 with flanking integration sequences for Hda3; long oligo
ABo_262	Pr4_hda3chk_rev	TCGTTAATCAAAATTATACACTC	1D	Check presence of p80 or p83 cassette in Hda3 heterozygote or hda3ΔΔ
ABo_415	HDA3chk_internalfw	CAACAAGAAcTGTGGAACATG	1D	Check presence/absence of Hda3 in hda3ΔΔ
ABo_416	HDA3chk_internalrev	GGTGGTTCTATAAATCCCGG	1D	Check presence/absence of Hda3 in hda3ΔΔ unresolved/resolved
ABo_462	Pf_MTLa1_Chk	TTGAAGCGTGAGAGGCAGGAG	4D	Check presence of MATa
ABo_463	Pr_MTLa1_Chk	GTTTGGGTTCCTTCTTTCTCATTC	4D	Check presence of MATa
ABo_464	Pf_MTLalpha1_Ch k	TTCGAGTACATTCTGGTCGCG	4D	Check presence of MATα
ABo_465	Pr_MTLalpha1_Chk	TGTAAACATCCTCAATTGTACCCGA	4D	Check presence of MATα
ABo_511	Pf_SAT1	GGTGGCGGAAACATTGGATG	4D	Check presence of Sat1
ABo_512	Pr_SAT1	TCAATGCCGCCGAGAGTAAA	4D	Check presence of Sat1

ABo_624	HDA3_XhoI_fw	TAAGCACTCGAGATGgatttaag gaaaattttg	6C	Isolate Hda3 from ABp152 with XhoI and BglII sites (for cloning into ABp111)
ABo_625	HDA3_stpBglII_rv	TTAACGAGATCTttattta ggagttattcctcgat	6C	Isolate Hda3 from ABp152 with XhoI and BglII sites (for cloning into ABp111: pNIM)
ABo_416	HDA3chk_internalr ev	GGTGGTTCTATAAATCCCGG	6C	Confirm cloning of p177 (Hda3_pNIM)
ABo_514	pNIM_Rev2	CAGTTTGGTTCAGCA CCTTG	6C	Confirm cloning of ABp_177 (Hda3_pNIM)
LD_515		CCATCATAAAATGTC GAGCGTC	6C	Sequencing of ABp_177 (Hda3_pNIM)
ABo_350	Pf_sir2_adh1	ctctatcactgatagggagtgg	6C	Confirm reintegration of ABp_177 (Hda3_pNIM) cassette at ADH1 locus
ABo_174	Act1_Fw2	CTACGTTTCCATTCAAGCTG TT	5D	qRT-PCR for ACT1
ABo_176	Act1_Rev3	AAACTGTAACCACGTTCAGA CA	5D	qRT-PCR for ACT1
ABo_469	qALS3_Fw1	CCTATTCCAACAACTACAAT	5D	qRT-PCR for ALS3
ABo_470	qALS3_Rev1	TATTGAGTCAGTTGGATTAG	5D	qRT-PCR for ALS3
ABo_471	qHWP1_Fw1	CCAGTTACTTCTGGATCATC	5D	qRT-PCR for HWP1
ABo_472	qHWP1_Rev1	TCGGTACAAACACTGTTAGA	5D	qRT-PCR for HWP1

Table 3. Plasmids used in this study.

ABp_Number	Plasmid	Figure	Description/Source	Source
ABp_11	pGFP-His1	1C	GFP tagging vector	(45)
ABp_17	pHA_*NAT1*	1C	HA tagging vector	(43)
ABp_80	LAL (loxP- ARG4-loxP)	1D	*Arg4* substitution products	(33)
ABp_83	NAT1-Clox (loxP-NAT1-MET3p-cre- loxP)	1D	*Nat* substitution products	(33)
ABp_88	HDA1_synthetic	1C	Hda1 synthetic	GeneArt
ABp_111	pNIM	6C	Tetracycline inducible integration to ADH1 locus	(44)
ABp_133	HDA1synthetic_pHA_NAT	1C	Source of Hda1- HA integration cassette	This study
ABp_136	Sat1 flipper with MTLαKO flanking regions	4D	Deletion of MATα	Anderson Lab, Ohio State University
ABp_152	HDA3 synthetic	6C	HA-HDA3 synthetic: 6x CUG->TCA	GeneArt
ABp_177	HDA3-pNIM	6C	Tetracycline inducible integration of Hda3 to ADH1 locus	This study

Peterson et al_Fig1

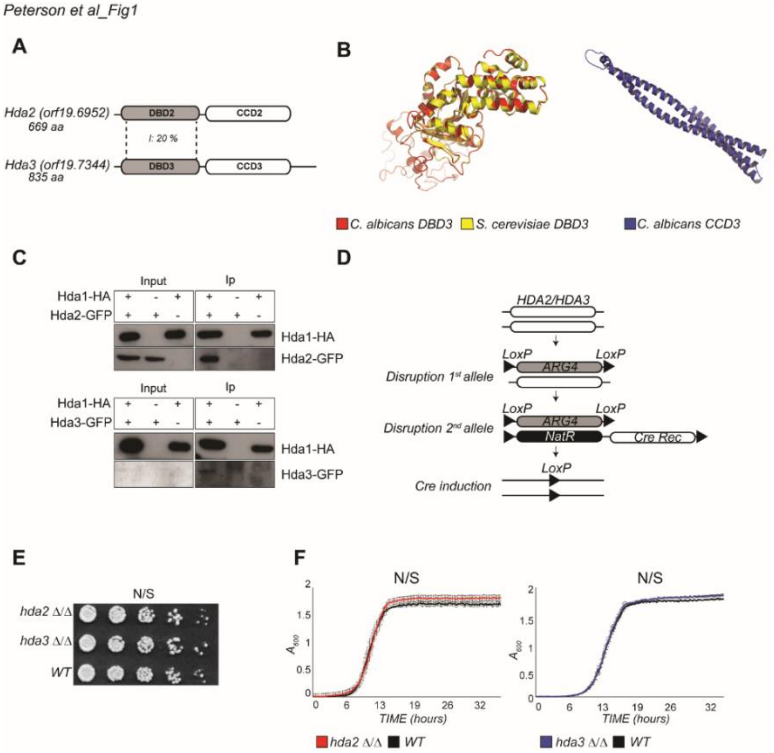

Peterson et al_Fig2

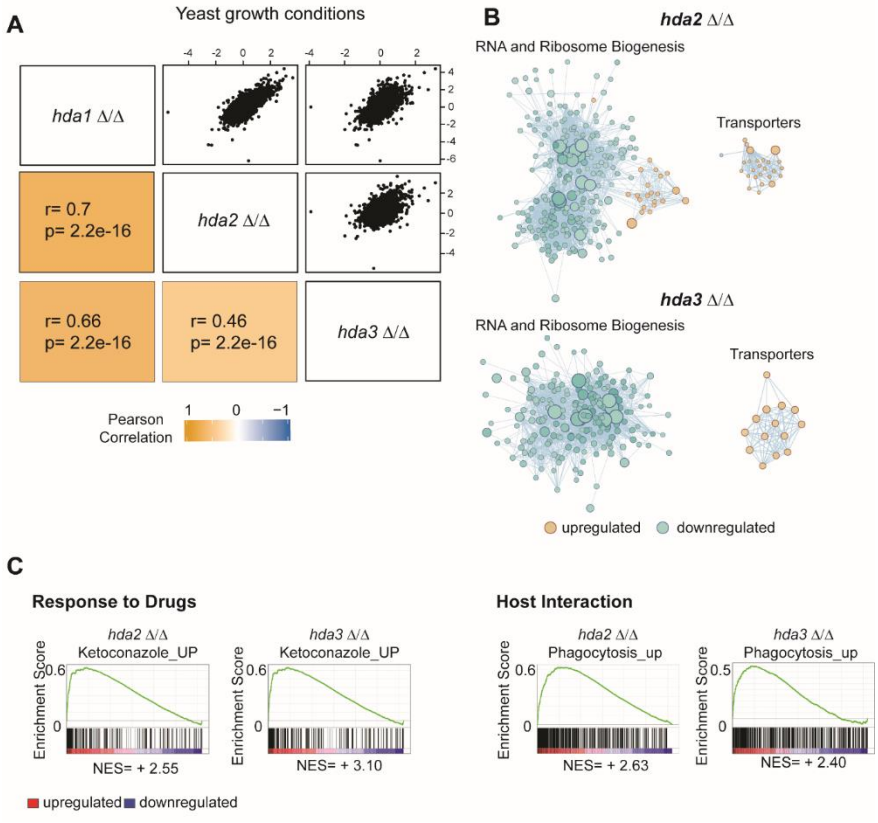

Peterson et al_Fig3

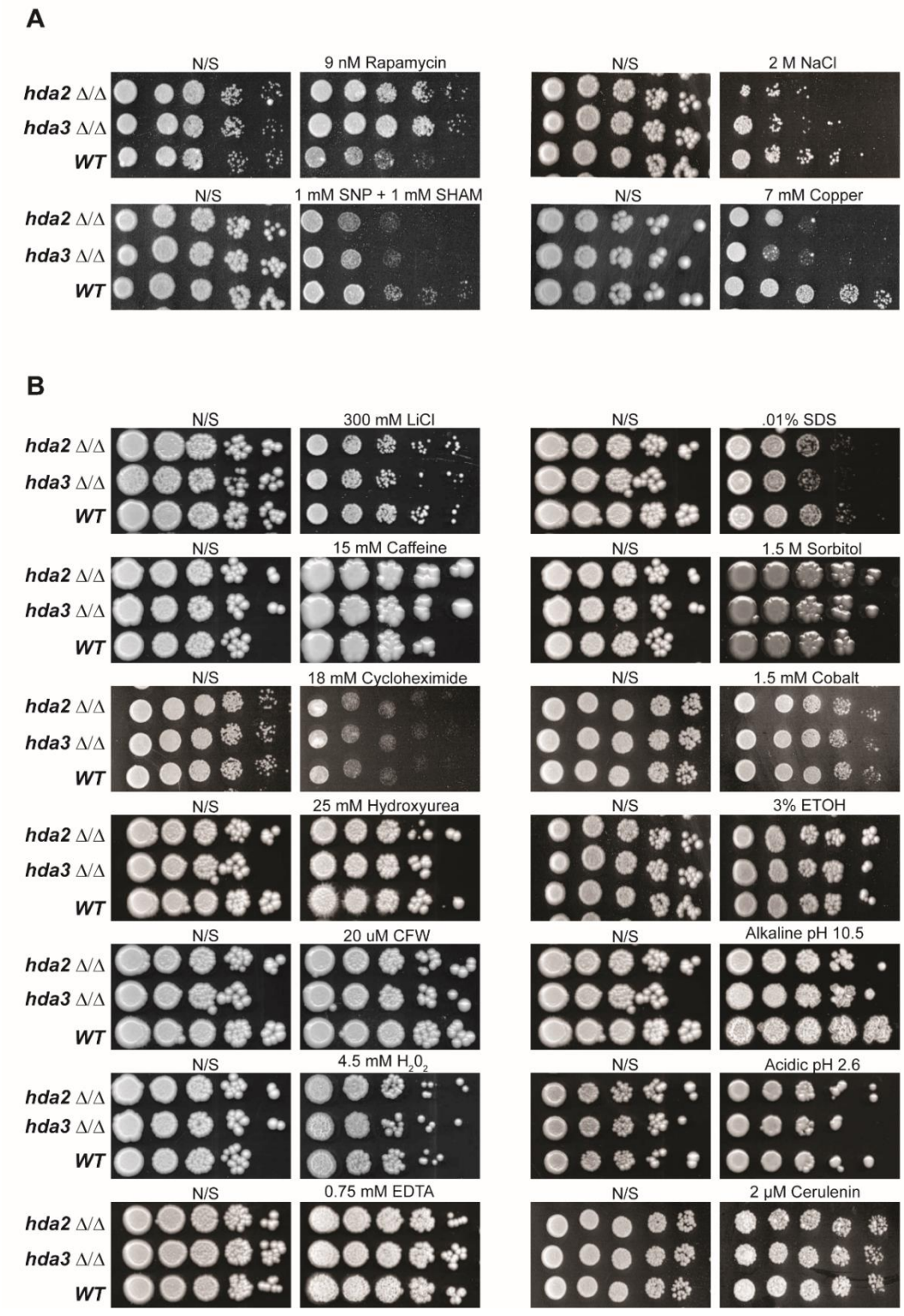

Peterson et al_Fig4

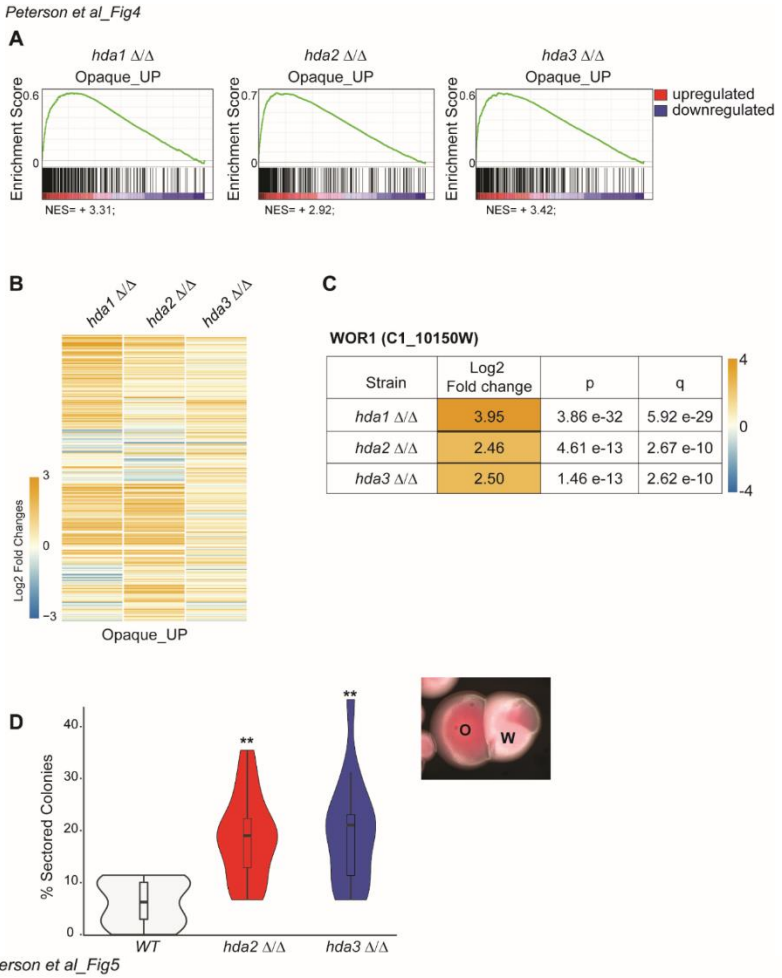

Peterson et al_Fig5

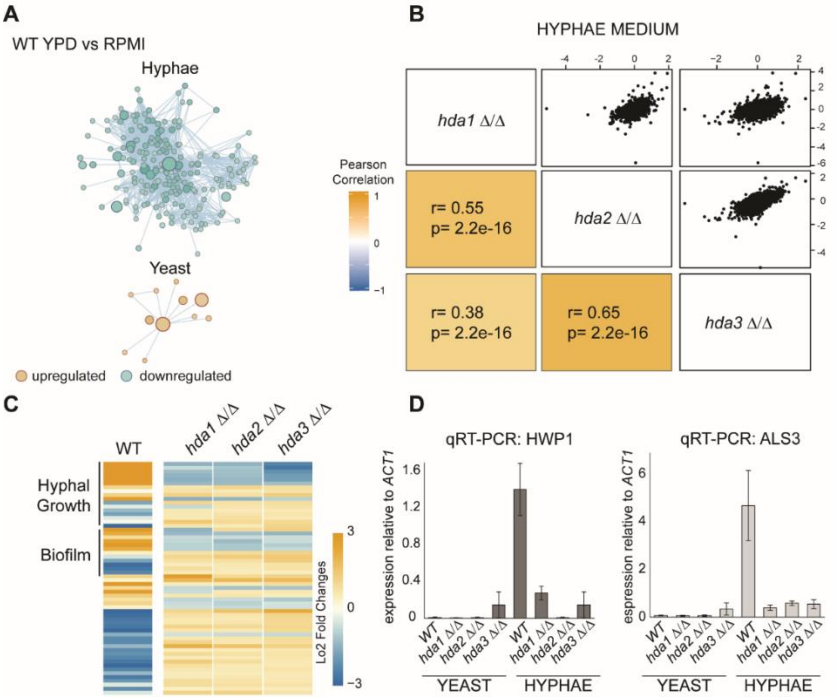

Peterson et al_Fig6

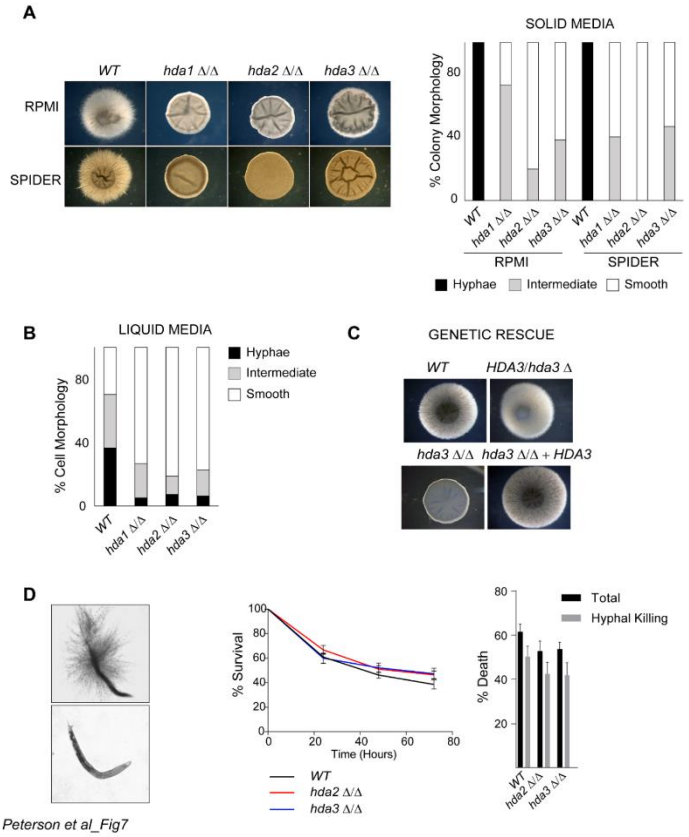

Peterson et al_Fig7